Design and development of probes for studying cannabinoid and related orphan G protein-coupled receptors and their signaling

Kumulative Dissertation

zur

Erlangung des Doktorgrades (Dr. rer. nat)

der

Mathemathisch-Naturwissenschaftlichen Fakultät

der

Rheinischen Friedrich-Wilhelms-Universität Bonn

vorgelegt von

Andhika Bintang Mahardhika

aus

Bandung, Indonesien

Bonn 2025

Angefertigt mit Genehmigung der Mathematisch-Naturwissenschaftlichen Fakultät
der Rheinischen Friedrich-Wilhelms-Universität Bonn

Gutachterin/Betreuerin: Prof. Dr. Christa E. Müller

Gutachterin: PD Dr. Anke C. Schiedel

Tag der Promotion: 14.05.2025

Erscheinungsjahr: 2025

ABSTRACT

G protein-coupled receptors (GPCRs) are the largest family of human membrane proteins and represent one of the most important classes of pharmacological targets for drugs. Among these, the cannabinoid (CB) receptor subtypes CB_1 and CB_2 have emerged as attractive targets due to their roles in various pathophysiological processes. Growing evidence indicates that cannabinoids can additionally interact with other GPCRs beyond CB_1 and CB_2 receptors, in particular with the orphan receptors GPR18 and GPR55. Both receptors have potential as drug targets, but conflicting findings have presented significant challenges in their validation for therapeutic application.

The present study aimed to design, synthesize, evaluate, and characterize tool compounds, for GPR18, CB_1 and CB_2 receptors. Through screening campaigns, structure–activity relationship (SAR) analysis, and broad pharmacological evaluation, several potent and reliable tools were developed.

For GPR18, the initial hit compounds **PSB-KD107** (EC_{50} = 0.562 µM) and **PSB-KD477** (EC_{50} = 0.454 µM) were used as starting points to yield more potent and selective agonists, including **PSB-KK1415** (EC_{50} = 0.0191 µM), **PSB-KK1445** (EC_{50} = 0.0454 µM), and **PSB-KK1418** (EC_{50} = 0.0711 µM). These compounds present the most potent (**PSB-KK1415)**, most selective (**PSB-KK1445**) and most efficacious (**PSB-KK1418**) GPR18 agonists known to date. Additionally, **PSB-KK1846** was identified as the most potent antagonist for GPR55, with an IC_{50} of 0.884 µM. The new agonists were found to display minimal species differences. In contrast, Δ^9-tetrahydrocannabinol (THC) – a standard tool compound for this receptor, acted as a weak partial agonist at the mouse GPR18 receptor, and therefore cannot be used for mouse studies of GPR18.

For CB_2 receptors, a fluorinated indole derivative, demonstrated high selectivity over other CB and CB-like receptors and exhibited a favorable profile in metabolic stability assays, making it a promising candidate for radiotracer development for positron emission tomography (PET). Diindolylmethane (DIM) and its derivatives were optimized to generate tool compounds for CB_2 receptors with distinct

pharmacological properties. **PSB-19837** (EC_{50} = 0.0144 μM) was identified as the most potent CB_2 agonist in the present series. **PSB-19571** exhibited biased agonism toward β-arrestin (6-fold preference for β-arrestin-2 over G-protein signaling), while **PSB-18691** showed a $G\alpha_i$-protein bias (20-fold preference for G-protein over β-arrestin-2 signaling).

A further study focused on the adenosine A_{2A} receptor, presenting the crystal structure of the receptor bound to the partial agonist LUF5834, with an atomic resolution of 2.3 Å. Structural studies revealed previously unobserved binding interactions, including the interaction of the phenolic group of LUF5834 with transmembrane helix III, and an ionic lock between the extracellular loops. Pharmacological studies confirmed that LUF5834 acts as a partial agonist, likely stabilizing an equilibrium between active and inactive receptor states.

In conclusion, the present work identified, optimized and broadly characterized small molecules that serve as potent tool compounds for GPR18 and CB_2 receptors. In addition, structural and pharmacological studies on the adenosine A_{2A} receptor provided valuable insights into the mechanism of partial agonism at this prototypic GPCR.

TABLE OF CONTENTS

1. OVERVIEW AND SUMMARY

G protein-coupled receptors (GPCRs) are involved in numerous physiological and pathophysiological processes. They represent one of the most targeted protein families in drug discovery, with over 30% of approved drugs acting on GPCRs. Despite their importance, many GPCRs remain underexplored.

One of these receptors is the orphan cannabinoid-like GPR18, which has been associated with immune regulation, cancer, and inflammatory diseases, making it a promising drug target. However, the exploration of GPR18 is hindered by the lack of reliable and selective tool compounds. The phytocannabinoid Δ^9-tetrahydrocannabinol (THC) has been proposed to activate GPR18, but it exhibits much higher potency at cannabinoid (CB) receptors which limits its utility for GPR18 research. In the past years, two lipids - *N*-arachidonylglycine (NAGly), an arachidonic acid metabolite, and Resolvin D2 (RvD2), a metabolite of docosahexaenoic acid (DHA) - were proposed as GPR18 agonists. However, these findings have proven impossible to reproduce, and the stability issues of RvD2 further complicate its use.

Another GPCR relevant to immune regulation, cancer, and inflammatory processes is the CB_2 receptor. Unlike GPR18, the CB_2 receptor has been extensively studied, and many ligands have been developed. However, no drugs targeting CB_2 receptors have reached the market, primarily due to off-target side effects. To address this challenge, alternative strategies to modulate CB_2 receptors need to be explored, potentially through new pathways or mechanisms such as the development of biased ligands or allosteric modulators.

This work aims to address the following key questions:

i) Can **reliable and selective tool compounds** for the enigmatic GPR18 receptor be developed and characterized?
ii) Can **novel ligands for targeting the CB_2 receptor** be identified, and how do they interact with CB_2 receptor?

To answer these questions, the present work focuses on the design, synthesis, and evaluation of small molecules as reliable tool compounds to modulate GPCRs,

particularly the CB receptors and the CB-like receptor GPR18. Initial steps include screening campaigns using a proprietary compound library, followed by structure–activity relationship (SAR) studies, and a variety of pharmacological studies to elucidate and validate the mechanisms of action of the optimized compounds. This work consists of five interconnected publications presented in chapters 3.1 to 3.5.

Chapter 3.1, "*Discovery of tricyclic xanthines as agonists of the cannabinoid-activated orphan G protein-coupled receptor GPR18*," lays the groundwork for GPR18 research by identifying tricyclic xanthine derivatives as the first potent and selective agonists for exploring GPR18. These findings provide a novel scaffold for further optimization and drug development, paving the way for exploring GPR18 as a therapeutic target in immune diseases and cancer.

Studies to further explore GPR18 and to develop agonists with improved properties is continued in **chapter 3.2**. This chapter, "*Potent, selective agonists for the cannabinoid-like orphan G protein-coupled receptor GPR18: a promising drug target for cancer and immunity*," introduces novel, bicyclic xanthine derivatives designed on the basis of the tricyclic xanthine scaffold. The newly developed agonists show high potency and selectivity for GPR18. These new compounds were evaluated against both human and mouse GPR18, addressing species differences that had previously been a limitation in the study of this receptor. Comprehensive pharmacological in vitro evaluation was conducted to validate these GPR18 agonists as excellent tool compounds. Additionally, selectivity evaluation identified a compound capable of blocking GPR55, another orphan cannabinoid-like receptor. The development of these tool compounds may help in advancing GPR18 (and GPR55) research and validate them as a potential drug targets for cancer and immune disorders.

The work described in chapter 3.3 and 3.4 focuses on the development of novel tool compounds for CB receptors, especially the CB_2 receptor, a validated target in immune regulation. **Chapter 3.3** "*Development of high-affinity fluorinated ligands for the cannabinoid subtype 2 (CB_2) receptor and the in vitro evaluation of a radioactive tracer for imaging*" explores the development and characterization of high-affinity fluoro-substituted indole derivatives to study CB_2 receptors. The SARs of these indole derivatives were investigated, and the best compound was radiolabeled for use as

imaging agents in positron emission tomography (PET) studies. In vitro evaluation of the new radiotracer in autoradiography studies confirmed that it is a valuable tool for CB_2 receptor imaging.

Further exploration of CB_2 receptor modulation is presented in **chapter 3.4** *"Design, synthesis, and structure–activity relationships of diindolylmethane (DIM) derivatives as cannabinoid CB_2 receptor agonists."* DIM, a naturally occurring compound and a partial agonist at CB_2 receptors, served as a starting compound. Systematic modifications of DIM identified key structural elements that enhanced CB_2 receptor affinity and selectivity, enabling the modulation of the efficacy of DIM derivatives from partial to full agonistic activity. The developed compounds exhibited diverse signaling profiles, including biased agonism and presumed allosteric binding. Thus, they represent versatile tools for studying CB_2 receptor signaling.

Finally, **chapter 3.5**, shifted the focus to the well-established adenosine A_{2A} receptor (A_{2A}AR). This study on "*Structural and functional insights into the partial agonism of LUF5834 at the adenosine A_{2A} receptor*," utilized an optimized receptor construct to elucidate previously unobserved interactions of the partial agonist LUF5834. Structural studies revealed interactions, e.g. that of the phenolic group of LUF5834 with transmembrane helix III, and an ionic lock between extracellular loops, while pharmacological evaluation demonstrated LUF5834's partial agonism. These findings suggest that LUF5834 can bind to the inactive state of the adenosine A_{2A} receptor and may induce a distinct receptor conformation, in contrast to full agonists that favor the active state. This work provides insights into receptor stabilization and describes a combined structural-functional approach, thereby advancing our understanding of partial agonism in GPCR pharmacology.

The main findings of the present work are summarized as follows:

i) **The development of potent and selective agonists for GPR18** resulted in the introduction of novel tool compounds, including the first potent and selective agonists, which provide are and reliable tools for exploring the receptor's physiological roles and therapeutic potential (**chapter 3.1** and **chapter 3.2**)

ii) **CB_2 receptor activity can be modulated by different classes of compounds** such as fluorinated indole derivatives (**chapter 3.3**) and diindolylmethane derivatives (**chapter 3.4**). The developed ^{18}F-labeled PET ligand serves as a tool for CB_2 receptor imaging. DIM derivatives allow for the investigation of biased signaling and allosteric modulation. The tunability of DIM and its derivatives, from partial agonists to full agonists with biased signaling profiles, highlights their potential as novel tool compounds for CB_2 receptors.

iii) Finally, the **crystal structure of the adenosine A_{2A} receptor bound to the partial agonist LUF5834** (**chapter 3.5**) revealed previously unobserved binding interactions and provided insights how partial agonists may act.

Together, these publications contribute significantly to the development of tool compounds for GPCR research, that are required to investigate receptor modulation and to advance our understanding of cannabinoid receptors, cannabinoid-like GPR18, and adenosine receptors all of which have great potential as drug targets. The combined structural and functional approaches presented in this work offer a framework for future GPCR-targeted drug discovery.

2. INTRODUCTION

2.1. G protein-coupled receptors

Cells in multicellular organisms communicate with their environment through a complex signal transduction system that enables the exchange of information between the extracellular and intracellular environments. Plasma membrane proteins are the first responders to extracellular signals. They bridge the communication between the external environment and the machinery of the cell.[1] Among these membrane proteins, G protein-coupled receptors (GPCRs), also known as 7 transmembrane (7TM) domain receptors, represent the largest family of plasma membrane proteins involved in signal transduction.[2]

GPCRs play an important role in detecting and transmitting external signals to initiate cellular responses. They constitute the largest human protein family, with over 830 members identified in the human genome.[3-5] Given their large number, it is not surprising that GPCRs are ubiquitously expressed throughout the human body, modulating diverse essential physiological processes such as vision, taste, olfaction, and the regulation of hormones and neurotransmitters.[6-8] As they modulate various biological functions, these receptors are activated by physically and chemically diverse extracellular signals. These include photons, ions (such as H^+, Zn^{2+}, Ca^{2+}), odorants, amino acids, peptides/proteins (e.g. chemokines), nucleotides, hormones (e.g. estrogen, angiotensin), lipids, and various small molecules (e.g. neurotransmitters, natural products).[9] This diversity makes GPCRs the largest druggable protein family in humans. Remarkably, more than 30% of all approved drugs target GPCRs, underscoring their significance for therapeutic interventions.[10]

According to the canonical model, the binding of an agonist to a 7TM receptor induces a conformational change of the receptor, facilitating the recruitment of effector proteins such as heterotrimeric guanine nucleotide-binding proteins (G proteins) or β-arrestins (Figure 2.1). While the terms 7TM and GPCR are sometimes used interchangeably, cellular and structural studies have proposed that 7TM receptors may be able to transmit signals independently of G proteins activation. The proposed alternative signaling pathway, mediated by β-arrestins, has led to the designation of such receptors as arrestin-coupled receptors.[11-13]

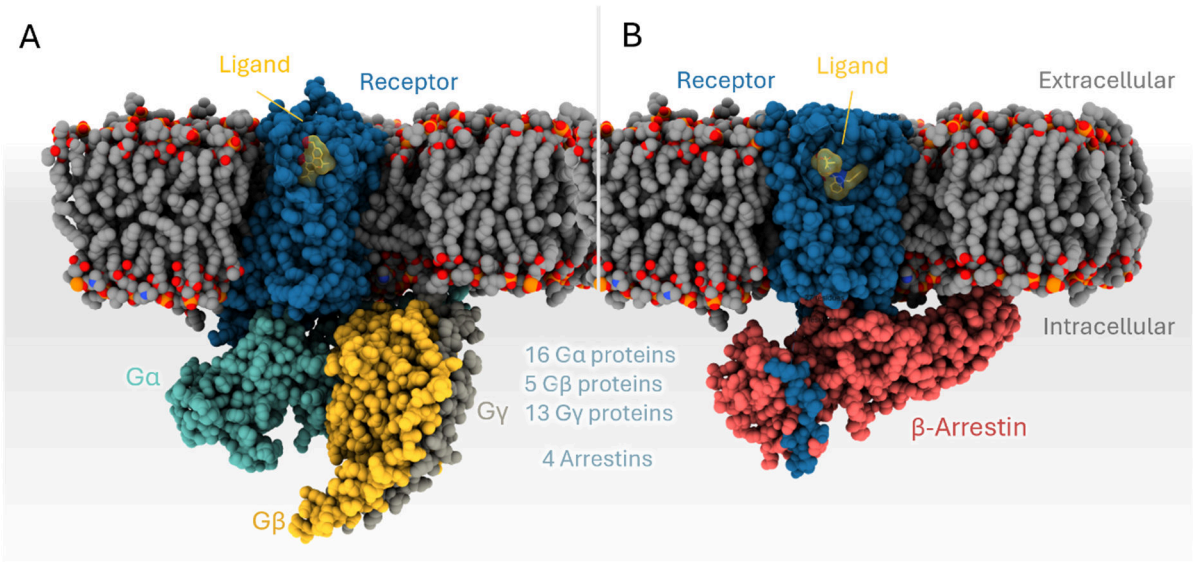

*Figure 2.1 Structural representation of a G protein-coupled receptor (GPCR) coupled to a heterotrimeric G protein (**A**) and to β-arrestin (**B**) embedded in a lipid bilayer. A small molecule ligand (yellow) interacts with the receptor (blue) at its binding site, inducing the coupling of heterotrimeric G protein subunits consisting of Gα (cyan) and Gβγ (yellow gray) to the receptor In humans, there are 16 Gα proteins, 5 Gβ proteins, and 13 Gγ proteins involved in GPCR signal transduction. A ligand can also promote the recruitment of β-arrestin (red) to the receptor. Four different arrestins are known to modulate GPCR signaling, namely arrestin-1, arrestin-2 (or β-arrestin-1) , arrestin-3 (or β-arrestin-2) and arrestin-4. The cannabinoid type 1 (CB_1) receptor is used to illustrate the model (PDB ID 9erx (CB_1 receptor bound to HU210 in complex with $G\alpha i_1\beta_1\gamma_2$)[14] and 8wu1 ($CB_1$ in complex with β-arrestin1).[15] The lipid bilayer was modelled using MemProtMD.[16]*

All GPCRs consist of extracellular regions comprising the N-terminus and three extracellular loops (ECL, ECL1-ECL3) , the transmembrane region that consists of seven transmembrane α-helices (TM1-TM7), intracellular regions that contains three intracellular loops (ICL, ICL1-ICL3) and the C-terminus (Figure 2.2). The pocket formed by the 7TM bundles of class A GPCRs serves as a binding site for orthosteric ligands – the site where the endogenous ligand binds, while the intracellular region is responsible for coupling with downstream effector proteins such as G proteins and arrestins. The 7TM bundle may also serve as a binding site for allosteric ligands – distinct sites on the receptor other than the orthosteric binding site to which ligands can bind.

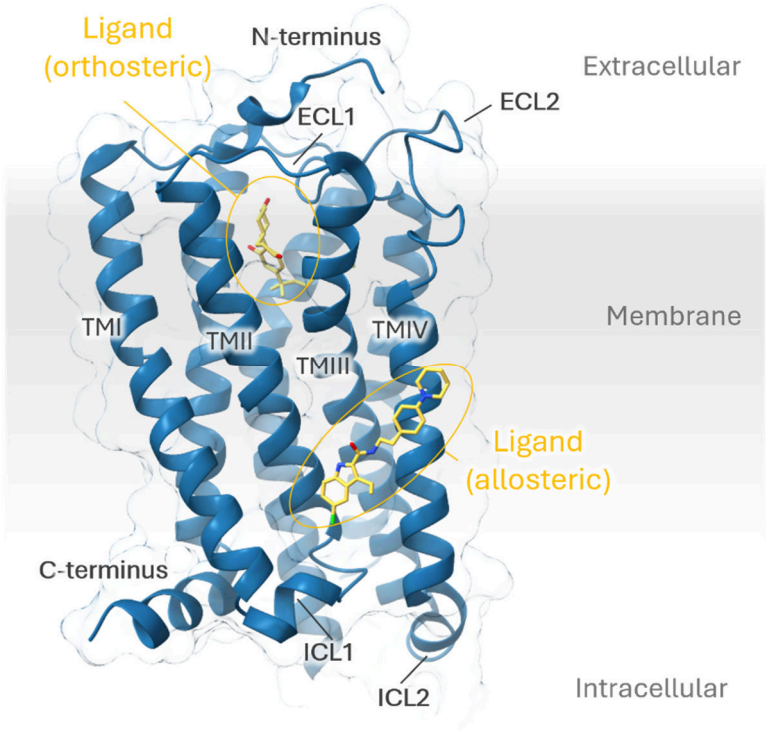

Figure 2.2 Representation of the secondary structural characteristics of GPCRs. All GPCRs contain an amino terminus (N-terminus) and seven transmembrane α-helices (TM1–TM7) connected by extracellular loops (ECLs) and intracellular loops (ICLs). The transmembrane regions are located within the lipid bilayer. Ligands (yellow) can interact with GPCRs at various binding sites. If a ligand binds at the same site as the endogenous ligand, referred to as the orthosteric site and it is a competitive ligand, whereas if a ligand binds at a different site, an allosteric binding site is observed for allosteric modulators. CP55,940 (orthosteric agonist) and ORG27569 (allosteric modulator) bound to the CB_1 receptor is used to illustrate the model (PDB ID 6kqi).[17] TM: transmembrane, ICL: and intracellular loops, ECL: extracellular loops.

GPCRs are classified using the two following criteria: a) based on sequence similarity and ligand types (A-F classification) [18, 19] and b) based on chromosomal positions and evolutionary relationships (GRAFS classification).[5, 20] These classification methods often overlap; they are widely used to categorize and characterize GPCRs.

On the basis of sequence similarity and ligand type, GPCRs are categorized into six major classes: Class A (rhodopsin-like), Class B (secretin-adhesion receptor family), Class C (metabotropic glutamate), Class D (fungal mating pheromone receptors), Class E (cyclic AMP receptors), and Class F (frizzled/smoothened). Classes D and E are not found in vertebrates. Class A is the largest and most diverse group, encompassing receptors that bind small ligands such as biogenic amines, small peptides, and chemokines. For these receptors, the ligand-binding site is typically located within the transmembrane domains. Class B is the second largest group.

Receptors in this class that bind larger molecules, such as peptides or proteins, often have ligand-binding sites in their extracellular loops or long N-terminal regions. Class C is the smallest group of GPCRs and is characterized by a long N-terminal region. Activation of these receptors involves dimerization, a unique feature compared to other classes. Class F includes the Frizzled and Smoothened receptors, which exhibit complex mechanisms of agonist activation. These receptors are primarily involved in developmental signaling pathways and play critical roles in cellular differentiation and growth.[1, 21] The representation of this classification system is depicted in Figure 2.3.

In the GRAFS classification system, GPCRs are divided into five categories based on chromosomal position and evolutionary relationships: glutamate, rhodopsin, adhesion, frizzled, and secretin (Figure 2.3). This classification aligns with the A-F system, where the glutamate family corresponds to Class C, the rhodopsin family to Class A, the secretin and adhesion families to Class B, and the frizzled family to Class F. This approach also allows for the construction of phylogenetic trees to explore evolutionary relationships. Among these, the rhodopsin family is the largest GPCR family, characterized by conserved motifs such as the NSxxNPxxY motif in TM7 and the DRY motif (or D(E)-R-Y(F)) at the boundary between TM3 and the intracellular loop (ICL2).

Within the rhodopsin family, further sub-classification is based on receptor-ligand relationships, dividing it into four main groups: α-branch (mostly amine-binding GPCRs), β-branch (GPCRs binding known peptides), γ-branch (peptide-and neuropeptide-binding receptors (but also other types of ligands)), and δ-branch (olfactory receptors, purine receptors, lipid receptors, and glycoprotein receptors, and many orphan receptors).[5, 20]

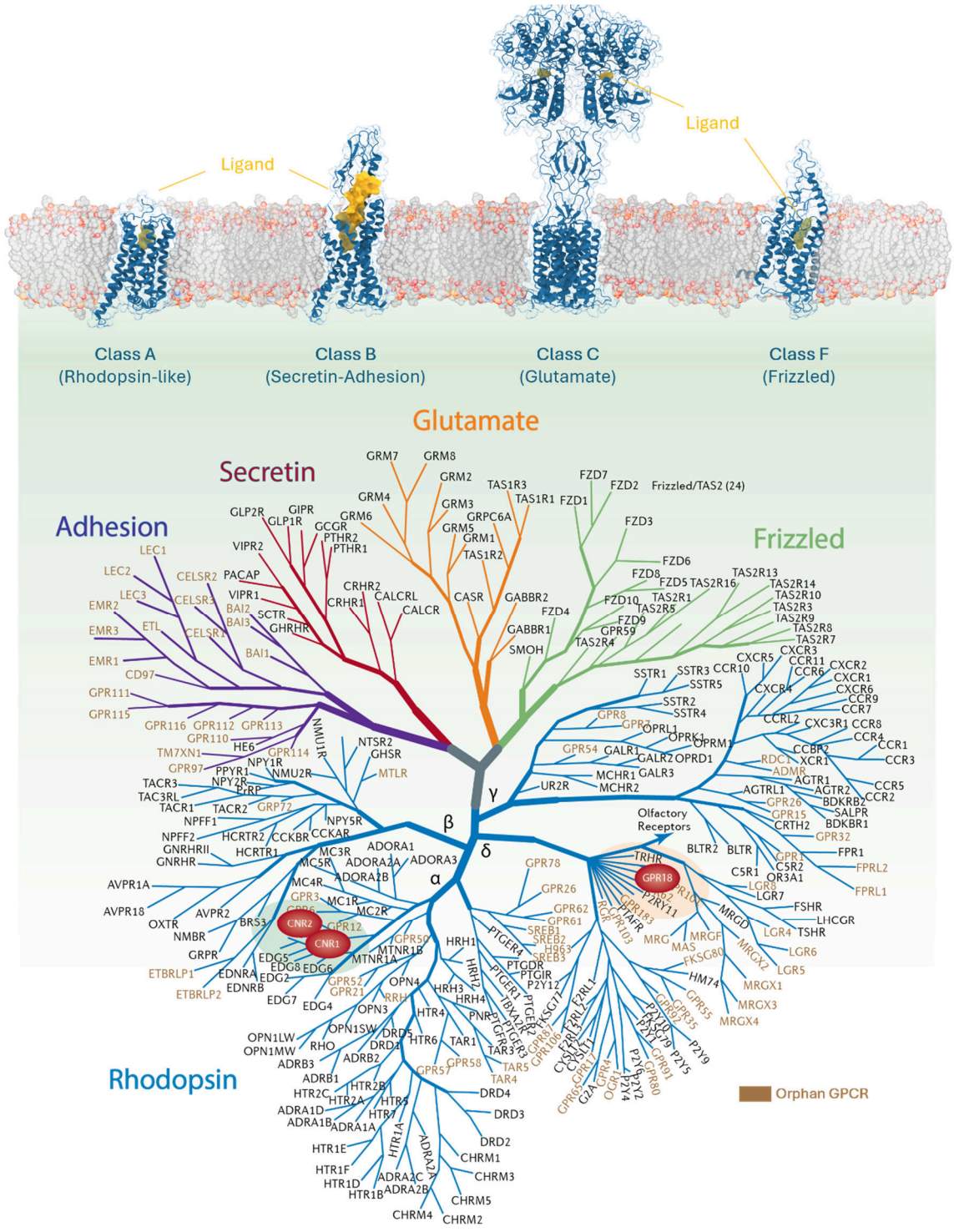

Figure 2.3 Classification of GPCRs according to the A-F classification system (top) and the GRAFS classification system (bottom). Representative structures of GPCRs are shown for Class A (rhodopsin-like – HU210 bound to the CB_1 receptor, PDB ID: 9erx)[14], Class B (secretin/adhesion – Glucagon-like peptide 1 (GLP-1) bound to GLP-1R, PDB ID: 5vai)[22], Class C (glutamate – quisqualate bound to the metabotropic glutamate 5 (mGlu5) receptor, PDB ID: 6n51)[23], and Class F (Frizzled – 24(S),25-epoxycholesterol bound to the smoothened receptor, PDB ID: 6oT0)[24]. Receptors are shown as cartoons (blue), with ligands bound to their orthosteric binding sites depicted in yellow. The phylogenetic tree of the GRAFS is adapted from Stevens et al.[25] with modifications and permission (order number 5778260708718). GPCRs are named according to their Uniprot entry name. Orphan GPCRs are highlighted in brown on the phylogenetic tree, while GPCRs explored in this thesis are highlighted in red (GPR18 is an orphan receptor). Data of orphan receptors were taken from Alexander et. al.[21] and Joost et al.[26]

Many class A GPCRs are orphan receptors (Figure 2.3, indicated with brown color), meaning their endogenous ligands have yet to be identified. Despite the lack of knowledge about their natural ligands, these receptors are known to play significant roles in various pathophysiological processes.[27] For instance, GPR18, a class A orphan receptor, has been found to be overexpressed in human melanoma. Silencing its expression using small interfering RNA (siRNA) was shown to enhance apoptosis in melanoma cells.[28]

Traditionally, identifying the endogenous ligand(s) of a GPCR has been considered essential for understanding its function and mechanisms. This knowledge is often viewed as a prerequisite for developing therapeutic agents targeting these receptors.[7] However, studying endogenous ligands presents several challenges. These ligands are typically present at very low concentrations, sometimes lack selectivity, and are metabolically unstable, making experimental studies difficult and hard to interpret. In such cases, developing surrogate ligands as tool compounds offers an alternative approach.[29, 30] These synthetic ligands could mimic the properties and function of endogenous ligand, and can be used to probe the functions and pathophysiological roles of orphan receptors.

2.2. Signal transduction of GPCRs

Signal transduction via GPCRs begins when a ligand, acting as an agonist, binds to the receptor. This interaction induces a conformational change in the receptor, causing outward movement of the transmembrane helices and rearrangement of microswitches within the transmembrane region. These structural shifts create a cytoplasmic interface, enabling engagement with intracellular transducers such as heterotrimeric G proteins, β-arrestins, and GPCR kinases (GRKs) (Figure 2.1 and Figure 2.4). The heterotrimeric G protein consists of three subunits: Gα, Gβ, and Gγ. Gβ and Gγ form stable heterodimers, with five known Gβ subtypes and 12 Gγ subtypes. Gα subunits are divided into 4 (four) subfamilies: $G\alpha_s$ ($G\alpha_s$ and $G\alpha_{olf}$), $G\alpha_i$ ($G\alpha_{i1\text{-}i3}$, $G\alpha_o$, $G\alpha_z$, and $G\alpha_t$), Gαq ($G\alpha_q$, $G\alpha_{11}$, and $G\alpha_{14–15}$), and $G\alpha_{12/13}$ ($G\alpha_{12}$ and $G\alpha_{13}$). In humans, there are four arrestins: two visual arrestins (arrestin-1 and arrestin-4)

expressed exclusively in photoreceptor cells, and two non-visual arrestins (arrestin-2 or β-arrestin-1 and arrestin-3 or β-arrestin-2), which are ubiquitously expressed. Similarly, there are seven GRKs (GRK1-7) expressed in the human body. GRK1 and GRK7 are specific to the retina, GRK4 is primarily found in the brain, kidneys, and testes, while GRKs 2, 3, 5, and 6 are expressed throughout the body.

When heterotrimeric G proteins engage with an activated receptor, the receptor catalyzes the exchange of guanosine diphosphate (GDP) for guanosine triphosphate (GTP) in the Gα subunit (Figure 2.4). This exchange causes the GTP-bound Gα subunit to dissociate from the Gβγ dimer. Both Gα-GTP and Gβγ can independently modulate effector proteins such as adenylyl cyclase (AC) and phospholipase C (PLC), leading to changes in the levels of second messengers like cyclic adenosine monophosphate (cAMP) or inositol 1,4,5-trisphosphate (IP_3). These messengers, subsequently, activate downstream signaling pathways to elicit diverse cellular responses.

In the canonical signaling pathway, Gβγ, after dissociation, recruits GRKs from the cytosol to phosphorylate the intracellular loops and C-terminal tail of the receptor. This phosphorylation facilitates the recruitment of β-arrestins, which play dual roles in signal modulation. Firstly, β-arrestins sterically hinder further G protein coupling, effectively "arresting" G protein signaling. Secondly, they were proposed to inhibit downstream signaling by scaffolding components like cyclic nucleotide phosphodiesterases (PDEs - which degrade the second messenger cAMP), or extracellular-signal regulated kinases (ERK). Following β-arrestin recruitment, the receptor undergoes internalization, leading to desensitization. Internalized receptors may be directed to lysosomes for degradation, transported to the Golgi apparatus for processing, or recycled back to the cell surface for resensitization.

Recent studies have proposed two distinct mechanisms by which β-arrestins are recruited to the activated GPCRs. [31-34] The first proposed mechanism involves the interaction of the phosphorylated carboxyl terminus of GPCRs with the N-terminal domain of β-arrestins, resulting in a "partially engaged" or "tail" binding mode. In the second mechanism, β-arrestins bind to both the phosphorylated C-terminus and the intracellular loop (ICL3) within the transmembrane bundle of the receptor, forming a "fully engaged" or "core" binding mode.[33] Interestingly, these two binding modes lead

to different cellular outcomes. The “tail” binding mode primarily facilitates receptor internalization and subsequent signaling or modulation of signaling mediated by the β-arrestin-receptor complex (proposed as β-arrestin-dependent modulation of signaling). In contrast, the “core” binding mode, while less critical for receptor internalization, plays a significant role in receptor desensitization (β-arrestin protein binds to phosphorylated GPCRs, thereby blocking the binding of G proteins or causing "uncoupling" from G-proteins).[31, 32, 35-38]

β-Arrestin and G protein binding to GPCRs were thought to be mutually exclusive, as seen with the core binding mode. However, the discovery of the tail binding mode introduces the possibility of simultaneous β-arrestin and G protein engagement. This allows for the formation of a "supercomplex," where the receptor simultaneously interacts with a β-arrestin in the tail conformation and a heterotrimeric Gα protein (Figure 2.4).[32, 39-42] This “supercomplex” enables the receptor to exhibit both G protein signaling and β-arrestin-dependent modulation of signaling, providing a layer of complexity in GPCR signaling.

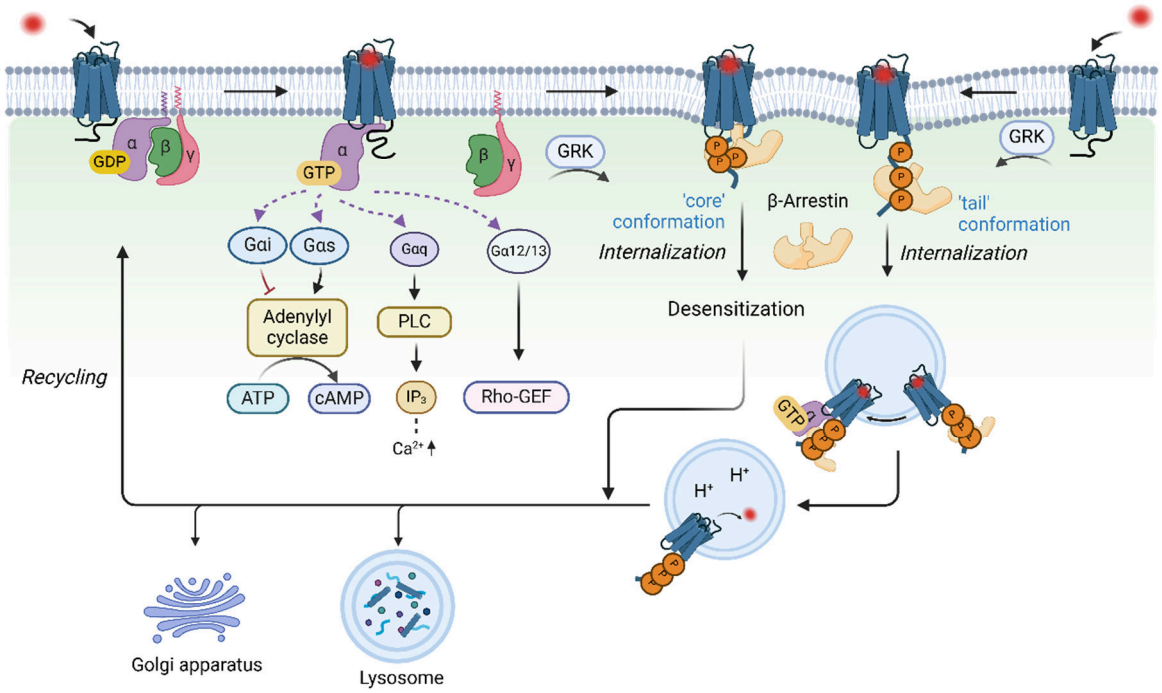

Figure 2.4 GPCRs' life cycle and signal transduction mechanism. Upon ligand binding, the GPCR undergoes conformational changes that enable interactions with intracellular transducers such as heterotrimeric G proteins, β-arrestins, and GPCR kinases (GRKs). The heterotrimeric G protein, consisting of Gα, Gβ, and Gγ subunits, is activated when the receptor facilitates GDP-to-GTP exchange in the Gα subunit. This activation causes the dissociation of Gα-GTP from the Gβγ dimer, allowing both Gα-GTP and Gβγ to regulate downstream effectors, such as adenylyl cyclase (AC) and phospholipase C (PLC), which modulate second messengers like cyclic adenosine monophosphate (cAMP) and inositol 1,4,5-trisphosphate (IP_3). IP_3 will induce the calcium ions (Ca^{2+}) release from intracellular stores such as the endoplasmic reticulum. Subsequently, The Gβγ dimer recruits GRKs to phosphorylate the receptor, promoting β-arrestin recruitment. β-Arrestins desensitize GPCRs by preventing further G protein coupling and facilitate receptor internalization. Internalized receptors may undergo lysosomal degradation, be trafficked to the Golgi apparatus, or be recycled back to the plasma membrane. β-Arrestins can adopt two distinct binding modes when engaging phosphorylated GPCRs: the "tail" binding mode, involving the receptor's C-terminal tail, and the "core" binding mode, which additionally engages intracellular loops (ICL3). The "tail" binding mode promotes receptor internalization and β-arrestin-dependent modulation of signaling, whereas the "core" binding mode primarily mediates receptor desensitization. In some cases, a supercomplex is formed, where the receptor interacts with both β-arrestins (in the tail binding mode) and a heterotrimeric G protein, enabling simultaneous G protein and β-arrestin-dependent modulation. AC: adenylyl cyclase; ATP: adenosine triphosphate; cAMP: cyclic adenosine monophosphate; GDP: guanosine diphosphate; Gα: G protein alpha subunit; Gβ: G protein beta subunit; Gγ: G protein gamma subunit; GTP: guanosine triphosphate; GRK: G protein-coupled receptor kinase; ICL3: intracellular loop 3; IP_3: inositol 1,4,5-trisphosphate; PLC: phospholipase C. The figure is created with Biorender.

2.3. Ligands acting at GPCRs: Orthosteric and allosteric ligands

Traditional concepts describe GPCRs as existing in a dynamic equilibrium between "off" (inactive) and "on" (active) conformational states with ligands influencing this equilibrium to trigger downstream signaling. Accordingly, ligands are classified as full agonists if they elicit a maximal response (maximum efficacy, induced 100% receptor activation, E_{max}), partial agonists if they generate a submaximal response even at saturating concentrations (<100% receptor activation), and antagonists if they lack intrinsic efficacy but competitively inhibit the effects of agonists.[43, 44] As research methods advanced, it became evident that GPCRs can exhibit varying levels of basal or constitutive activity, where they can adopt active signaling states even in the absence of ligands. This discovery highlighted the fact that GPCRs are not simple on–off switches but are versatile systems capable of adopting multiple conformations in response to different ligands. Antagonists, in this context, are further classified into neutral antagonists, which block agonist effects without affecting constitutive activity, and inverse agonists, which reduce constitutive activity.[45]

Agonists, partial agonists, and antagonists typically interact with the orthosteric site, the primary binding site for endogenous agonists that activate GPCRs (see Figure 2.2). In addition to orthosteric modulation, it is known that GPCRs can also be regulated allosterically by molecules that bind to distinct allosteric sites (allosteric binding site).

Table 2-1. Several types of allosteric modulators. Data is taken from Kenakin et al.[46]

Ligand	***Definition***	***Pharmacological effect***
Allosteric agonist	Molecule that binds to a site on the receptor distinct from the orthosteric binding site	Produces a cellular response which may be modulated by orthosteric agonism (potentiation, additivity, or inhibition)
PAM (Positive allosteric modulator)	Molecule that binds to a site on the receptor distinct from the orthosteric binding site to potentiate the orthosteric agonist response	No direct effect on its own; enhances the response of the orthosteric agonist when present

Ligand	***Definition***	***Pharmacological effect***
PAM-agonist (positive ago-allosteric modulator)	A PAM with additional efficacy to produce a response even without orthosteric agonist	Produces a direct agonist response in sensitive tissues; enhances the orthosteric agonist response when the agonist is present
NAM (Negative Allosteric Modulator)	Molecule that binds to a site on the receptor distinct from the orthosteric binding site to inhibit the orthosteric agonist response	No direct effect on its own; blocks the response of the orthosteric agonist when present
NAM-agonist	A NAM with additional efficacy to produce a response even without orthosteric agonist	Produces a direct agonist response in sensitive tissues; blocks the natural agonist response when the orthosteric agonist is present
PAM-antagonist	A NAM that increases receptor affinity for the agonist in its presence	Increases the agonist's affinity for the receptor but reduces its efficacy (in functional assays)

Allosteric modulators are distinct from orthosteric agonists and antagonists; they exhibit unique pharmacological characteristics. The orthosteric binding pocket of many GPCRs is highly conserved across receptor subtypes, making it challenging to develop highly selective ligands. In contrast, allosteric binding sites tend to be less conserved, offering a greater opportunity to design receptor-specific molecules that could selectively bind to this site. This allows for precise modulation of GPCR signaling, typically in the presence of the endogenous ligand. An example is the positive allosteric modulator (PAM) LY3154207, developed for the dopamine type 1 receptor (D_1R), which underwent clinical trials for the treatment of Parkinson's disease and schizophrenia.[47] Current Parkinson's disease treatments, such as levodopa and dopamine, and synthetic agonists like pramipexole, are associated with significant limitations, including low safety margins, cognitive impairment, and seizure risks at high doses. LY3154207, as a D_1R PAM, enhances GPCR–G protein coupling with high selectivity and favorable a pharmacokinetic and pharmacodynamic profile. In both animal and human studies, LY3154207 demonstrated reduced adverse effects compared to traditional therapies and

avoided the bell-shaped dose–response relationships typical of many D_1R agonists.[47] These advantages suggest its potential as a safer and more effective alternative for managing Parkinson's disease and schizophrenia.

Another example of an allosteric modulator is ORG27569, a PAM antagonist at the CB_1 receptor. ORG27569 has been shown to increase the binding affinity of CP55,940, a CB_1 receptor agonist, while simultaneously reducing its efficacy.[48] The CB_1 receptor inverse agonist Rimonabant (binding to the orthosteric site) was initially used as an appetite suppressant but was withdrawn from the market due to severe adverse effects. ORG27569 has been found to reduce food intake without affecting the analgesic and cataleptic effects mediated by orthosteric CB_1 agonists.[49, 50]

2.4. Cannabinoid receptors

The term "cannabinoids" originally referred to the collective chemical name for a group of terpenoids containing a C_{21} aromatic hydrocarbon, which are naturally found in the *Cannabis sativa* plant.[51] However, today, the term is used not only for naturally occurring compounds, but also for synthetic compounds or endogenous ligands that can mimic the actions of plant-derived cannabinoids.[52-54] The naturally occurring compounds are referred to as "phytocannabinoids," the synthetic compounds are called "synthetic cannabinoids," and the endogenous ligands are known as "endocannabinoids".[53, 55]

The first phytocannabinoid isolated from *Cannabis* was cannabinol (CBN) .[56] Interestingly, pure CBN was not initially tested for biological activity. Instead, its activity was assumed based on observations from crude cannabis extracts, leading to the conclusion that CBN was the active component of the plant. Subsequently, other phytocannabinoids, cannabidiol (CBD) and Δ^9-tetrahydrocannabinol (THC) were isolated, and their chemical structures were elucidated.[57, 58] CBN was later identified as a degradation product of other phytocannabinoids, formed under heat and acidic conditions, which is present only in minor amounts in the plant extract. In contrast, THC and CBD are the main components of cannabis extracts [56, 57, 59] Further studies revealed that these compounds primarily exist in the plant as carboxylates,

known as cannabinoid acids, which serve as precursors to the neutral cannabinoids.[60-62] Cannabinoid acids undergo decarboxylation with age or heating, forming neutral cannabinoids responsible for most pharmacological effect. To date, more than 140 phytocannabinoids have been identified in *Cannabis*.[61]

Despite the recognition of THC and CBD as the most active components of *Cannabis*, their cellular targets initially remained unknown. However, it was clear that cannabis extracts exert significant physiological effects in vivo.[63] The initial studies on the cellular target of cannabinoids were made by Howlett et al. by incubating neuroblastoma (C1300) cells with cannabinoids. These studies demonstrated that cannabinoids, particularly Δ^9-THC, reduced cAMP accumulation.[64] This reduction as attributed to the inhibition of adenylyl cyclase activity in cell-derived membranes.[65] This response was further shown to be modulated by guanine nucleotide,[66] suggesting the presence of a membrane-bound receptor (GPCR) coupled to $G\alpha_i$-proteins responsible for the observed effects.

Due to the high lipophilicity and challenges in isolating phytocannabinoids, efforts were made to develop better tool compounds. This led to the synthesis of CP55940, a potent and efficacious cannabinoid receptor agonist developed through a collaboration of Howlett's lab and scientists at Pfizer.[67, 68] Using tritiated CP55940 and radioligand binding studies, the primary cellular target of cannabinoids was identified, with the highest expression found in the brain. This receptor was termed "cannabinoid receptor." Independent cloning efforts confirmed the presence of this receptor in both rat and human tissues.[69, 70]

Three years later, a second GPCR responsive to cannabinoids was discovered, predominantly expressed in macrophages rather than the brain. This receptor was cloned using HL-60 promyeloblast cells and identified primarily in peripheral immune cells.[71] The first receptor was subsequently named cannabinoid type 1 (CB_1) receptor, while the second one was named cannabinoid type 2 (CB_2) receptor.[72] Since these discoveries, the term "cannabinoid" has been expanded to include any molecule capable of binding to one of the cannabinoid receptors.[73]

Advancements in cannabinoid receptor research and the development of tool compounds facilitated the discovery of endogenous ligands for cannabinoid receptors. Using organs with high receptor expression, deorphanization of the receptors was conducted. Porcine brains were extracted to isolate lipids, and radioligand binding assays were employed to assess their interactions with CB receptors. Through labor-intensive isolation procedures, a lipid from the brain extract was identified that activated CB receptors. This lipid, named anandamide (arachidonoylethanolamide, AEA), is a metabolite of arachidonic acid. When injected into rodents, AEA mimicked the behavioral effects of THC.[67]

Following a similar methodology, lipid molecules were extracted from canine gut and mouse tissues, with radioligand binding assays used to study their interactions with CB receptors. After extensive isolation and structural elucidation, this approach led to the identification of 2-arachidonoylglycerol (2-AG) as a second endogenous ligand for CB receptors.[74, 75] Both AEA and 2-AG are now recognized as endocannabinoids, the endogenous ligands of cannabinoid receptors.

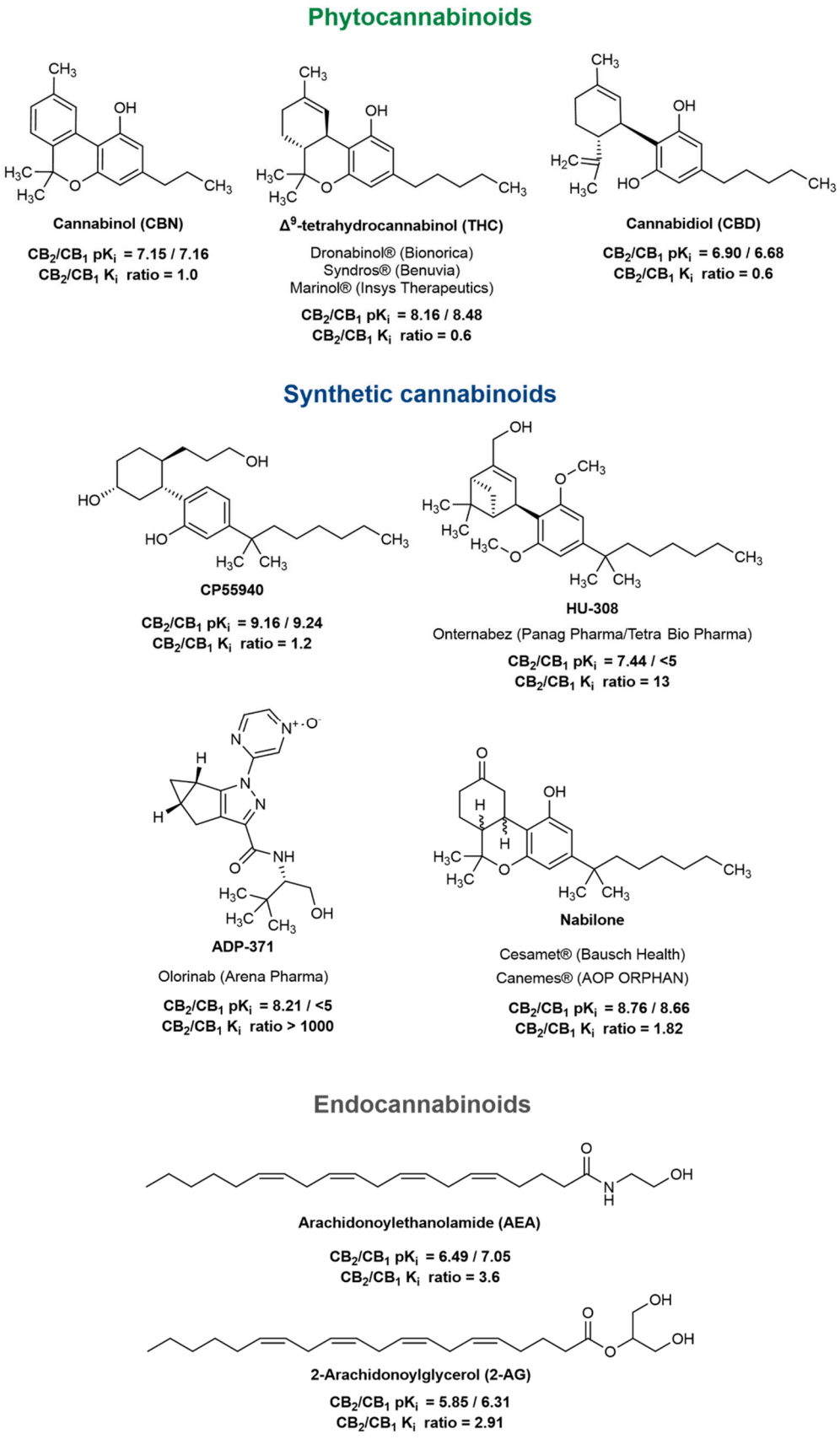

Figure 2.5 Structures of phytocannabinoids, synthetic cannabinoids, and endocannabinoids acting at human cannabinoid type 1 (CB_1) and human cannabinoid type 2 (CB_2) receptors. Selected compounds investigated in clinical trials are depicted. Data adapted from Naikoo et al.[76], Pertwee et al.[77], Howart et al.[53], and Kosar et al.[78]

CB_1 and CB_2 receptors are GPCRs belonging to the δ-branch of the class A, rhodopsin-like family. Both receptors are primarily coupled to the $G\alpha_i$ protein family.[53] The CB_1 receptor is predominantly expressed in the brain and other parts of the central nervous system (CNS) , where it plays a role in learning, memory, motor control, sensation, and CNS repair mechanisms.[52, 79-82] It has been suggested that the CB_1 receptor plays important role in various pathophysiological conditions, such as Alzheimer's disease, schizophrenia, and Huntington's disease. Furthermore, the CB_1 receptor is involved in modulating physiological functions that are relevant to treat conditions like obesity, cardiovascular disorders, hepatic disorders, neuropsychiatric disorders, and neuropathic or inflammatory pain.[52, 79-82] In contrast, the CB_2 receptor is mainly expressed on immune cells and in the periphery, including the cardiovascular, respiratory, and gastrointestinal systems. It is also expressed in the CNS, though to a lesser extent as compared to the CB_1 receptor. The CB_2 receptor is increasingly recognized as a promising drug target for inflammatory and autoimmune diseases, as well as liver and kidney fibrosis and osteoporosis.[83, 84] Activation of the CB_2 receptor in immune cells mediates immunosuppressive effects, such as inhibiting cell proliferation, inducing apoptosis, and suppressing cytokine and chemokine production. These effects contribute to tissue repair and limit tissue injury in various pathological conditions.[78, 85]

Inverse agonists or antagonists targeting CB_2 receptor may offer therapeutic benefits. While CB_2 activation is generally protective of tissue injury or inflammation, it can have detrimental effects in certain pathological conditions, such as specific cancers and infections. In these cases, the protective activation of CB_2 receptor may exacerbate tissue damage. [78, 85] For instance, during infections with live pathogens, immune system suppression may promote secondary infections, leading to further tissue injury. Similarly, in certain cancers, where the immune system plays an important protective role for controlling cancer growth, CB_2 activation may be counterproductive. [78, 85]

In the past years, numerous CB receptor ligands have been developed. However, despite this progress, no drug targeting CB receptors has been approved for clinical use (Table 2-2 and Figure 2.5). Several clinical trials focusing on CB_2-selective ligands

have been launched but were terminated after phase 1 or phase 2 due to lack of efficacy. More recently, clinical trials have focused on inflammatory and immunomodulatory targets rather than specific diseases. One highly selective CB_2 receptor antagonist has entered clinical trials for the treatment of solid tumors. All those drugs are targeting the orthosteric binding site. Although much is still unknown about allosteric modulators of CB_2 receptors, the possibility that different ligand-dependent CB_2 receptor conformations can lead to distinct pharmacological responses suggests that there is potential for new therapeutic strategies.

Table 2-2 Selected compounds investigated in clinical trials that target cannabinoid receptors. Data are taken from Naikoo et al.[76] and Kosar et al.[78]

Drug	***Indication***	***Target***
Δ^9-THC (Dronabinol®, Syndros®, Marinol®)	Appetite loss, chemotherapy induced nausea and vomiting (CNIV), anorexia, cancer pain	Unselective CB_2/CB_1 receptor agonist, possibly interacts with further receptors.[61]
Nabilone (Cesamet®, Canemes®)	Chemotherapy induced nausea and vomiting (CNIV)	Unselective CB_2/CB_1 receptor, might be interact with other receptors
ADP-371 (Olorinab)	Irritable Bowel Syndrome	Selective CB_2 receptor agonist, low brain penetration in rat[86] (phase I clinical trial)
TT-816	Advanced cancer (lung, renal cell and ovarian cancer)	Selective CB_2 receptor agonist (phase II clinical trial)
HU-308 (Onternabez)	Dry eyes, Uveitis	Selective CB_2 receptor agonist, exhibit brain penetration in mice[87] (phase I clinical trial)
CNTX-6016	Neuropathic and general pain	Selective CB_2 receptor antagonist (phase II clinical trial)

2.5. G protein-coupled receptor 18 (GPR18)

G protein-coupled receptor 18 (GPR18) is an orphan 7TM receptor belonging to the class A, rhodopsin-like GPCR family. It is composed of 331 amino acids and is expressed across various species in addition to humans, such as mouse (UniProt ID: Q8K1Z6), rats (UniProt ID: A1A5S3), Cynomolgus monkeys (UniProt ID: Q4R613), and cattle (UniProt ID: Q3T0E9). Comparative analysis reveals a high degree of similarity across species (>80%), with the highest similarity observed in monkeys (99.1%), as shown in Table 2-3. This suggests a conserved binding sites across these GPR18 orthologues.

Table 2-3 Protein similarity (identity) of GPR18 across species.

	HUMAN	MONKEY	BOVINE	MOUSE	RAT
HUMAN		99.1 *(97.3)*	94.6 *(89.2)*	93.4 *(85.8)*	92.4 *(84.9)*
MONKEY	99.1 *(97.3)*		94.9 *(88)*	93.7 *(85.2)*	92.7 *(84.3)*
BOVINE	94.9 *(89.4)*	95.2 *(88.2)*		92.7 *(85.5)*	92.7 *(84.9)*
MOUSE	93.4 *(85.8)*	93.7 *(85.2)*	92.5 *(85.2)*		97.0 *(95.2)*
RAT	92.4 *(84.9)*	92.7 *(84.3)*	92.5 *(84.6)*	97.0 *(95.2)*	

Percent similarity is shown above, while percent identity is indicated in parentheses "( )".

GPR18 was first described by Samuelson et al., who identified the mouse GPR18 (mGPR18). It shares significant nucleotide similarity with the rat μ-opioid receptor (44.5% nucleotide sequence identity). Subsequently, Gantz et al. identified human GPR18 (hGPR18) in canine gastric mucosa cells and the human colon cancer cell line Colo 320 DM.[88, 89]

In humans, GPR18 is located on chromosome 13q32, near GPR183 (13q32.3), a GPCR known to be activated by 7α,25-dihydroxycholesterol. [90-93] Sequence alignment on the protein level shows a 37% similarity between GPR18 and GPR183, the highest among GPCRs. Furthermore, GPR18 and GPR183 share overlapping expression patterns, with high expression in peripheral blood mononuclear cells and moderate

expression in lung tissue.[90, 94] These observations suggest potential functional and evolutionary links between the two receptors.

GPR18 is widely expressed across various organs (Table 2-4). It is abundantly expressed in lymphocytes[95] but shows minimal or no expression in several major organs, including the heart, lung, liver, kidney, pancreas, colon, skeletal muscle, ovary, placenta, prostate, adrenal medulla, and adrenal cortex.[88] A more detailed expression profiling study revealed high expression of GPR18 in peripheral blood leukocytes, the brainstem, cerebellum, striatum, ovary, testis, thymus, and thyroid. Moderate or low expression was observed in most brain regions (e.g., amygdala, cerebral cortex, frontal cortex, hippocampus, and thalamus) and other tissues such as the adrenal gland, colon, intestine, kidney, liver, muscle, prostate, skin, spleen, and stomach.[8]

Table 2-4 Expression level of GPR18 in various human tissues and organs. Data are taken from Vassilatis et al.,[8] Wang et al.,[96] and Gantz et al.[88]

EXPRESSION LEVEL	ORGANS
HIGH	Brainstem, cerebellum, striatum, thyroid, thymus, lymphoid tissues, lymphocytes, peripheral blood leukocytes, ovary, and testis
MEDIUM TO LOW	Most brain regions, skin, adrenal gland, liver, stomach, intestine, colon, spleen, kidney, muscle, and prostate.
NO EXPRESSION	Heart, lung, adrenal cortex, adrenal medulla, pancreas, kidney, colon, skeletal muscle, ovary, placenta, prostate.

GPR18 has been implicated in pathological conditions, including overexpression during melanoma metastasis[97] and in the blood of osteoarthritis patients.[98] Additionally, recent studies suggest that GPR18 may serve as a versatile B-cell marker for prognosis in human cancers such as sarcoma, head and neck squamous cell carcinoma, lung adenocarcinoma, liver hepatocellular carcinoma, cervical squamous cell carcinoma and endocervical adenocarcinoma, adrenocortical carcinoma, breast invasive carcinoma, brain lower grade glioma, and uveal melanoma.[99] High expression of GPR18 in immunological and hematological tissues, led to the hypothesis that GPR18 might play a physiological role in immunological or hematological functions.[88, 89] The human genome-wide association studies (GWAS)

have linked GPR18 with three diseases namely Crohn's disease, ulcerative colitis, and inflammatory bowel disease.[100] No natural variants of GPR18 have been identified to date.

Several ligands have been proposed as agonists for GPR18 (Figure 2.6), including lipid-derived compounds like *N*-arachidonoylglycine (NAGly)[101] and Resolvin D2[102], as well as various cannabinoids such as O-1602, THC, and AEA.[103-108] The latter finding has led to speculations that GPR18 might represent another type of cannabinoid receptor, similar to GPR55.[109-111] However, findings regarding these interactions have been contradictory. Among the proposed ligands, only THC has consistently demonstrated activity in our experiments and produced reproducible results across laboratories, making it a suitable candidate for pharmacological in vitro assessments. However, in vivo studies pose greater challenges, as THC exhibits much higher affinity and activity at classical cannabinoid receptors. Moreover, THC is only a weak partial agonist at mouse GPR18, as shown in the next chapter of this study. Therefore, the development of reliable tool compounds that are specific to GPR18 is essential for further investigation. These compounds will be discussed in greater detail in the subsequent chapters.

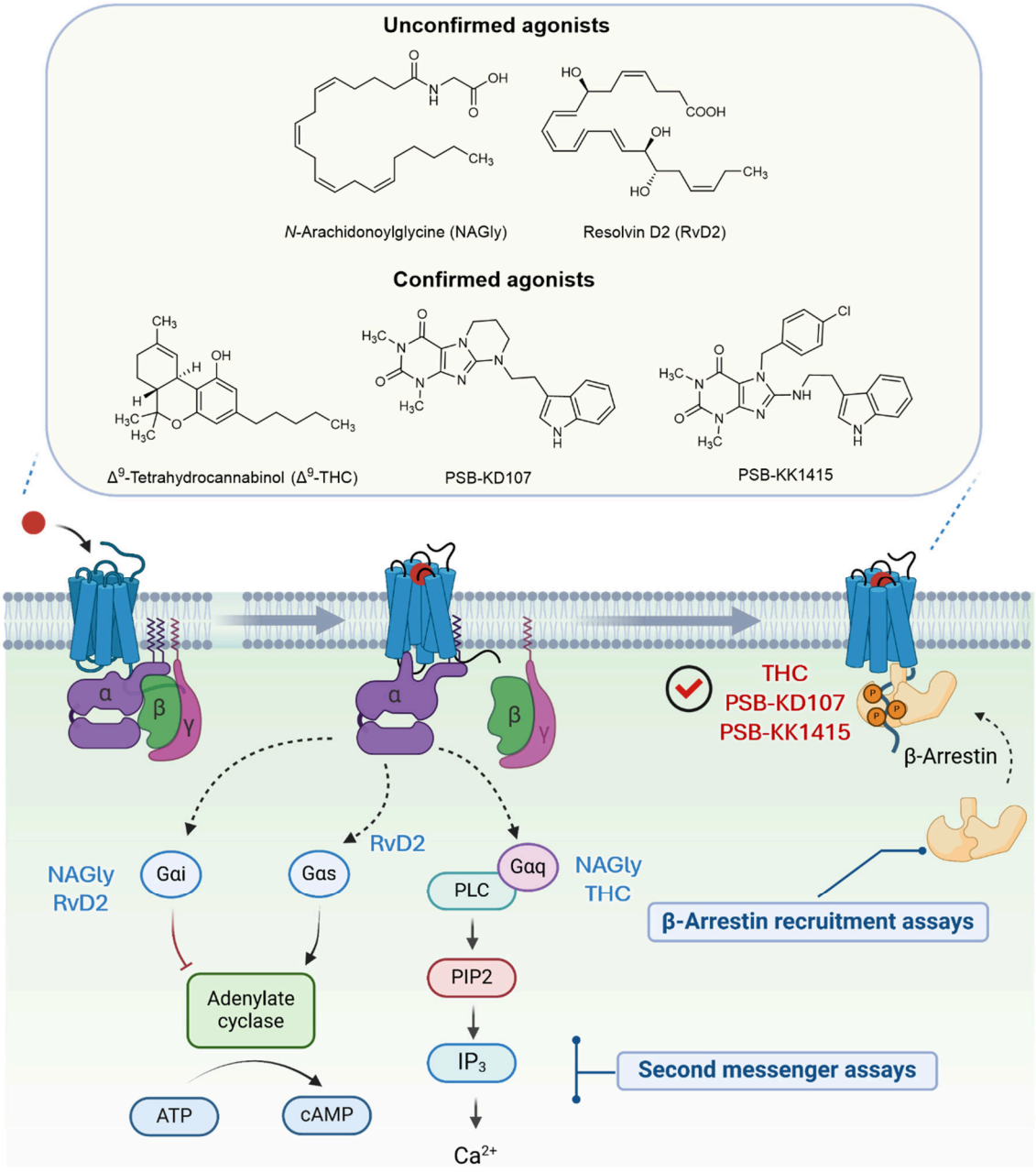

Figure 2.6 Ligands proposed to activate GPR18 through various signaling pathways. While several ligands, such as NAGly and RvD2, have been reported to modulate GPR18 via different G proteins, these findings remain unconfirmed due to conflicting results. Gα: G protein alpha subunit; β: G protein beta subunit; γ: G protein gamma subunit; AC: adenylyl cyclase; ATP: adenosine triphosphate; cAMP: cyclic adenosine monophosphate; IP_3: inositol 1,4,5-trisphosphate; NAGly: N-Arachidonoylglycine; PLC: phospholipase C; RvD2: Resolvin D2; THC: Δ9-tetrahydrocannabinol. The figure is created with Biorender.

The signaling pathways regulated by GPR18 are not well understood, leaving a significant gap between its activation and the resulting physiological effects. Several studies suggest GPR18 may be coupled to the $G\alpha_{i/o}$,[101, 106] $G\alpha_{q}$,[101, 110] and $G\alpha_{s}$,[102, 112]

protein families. However, other studies have failed to replicate these findings. Lu et al. showed that GPR18 does not couple with $G\alpha_{i/o}$, $G\alpha_s$, $G\alpha_z$, and $G\alpha_{15}$ when stimulated by NAGly.[113] Similarly, Finlay et al. observed a lack of response of GPR18 upon NAGly stimulation in human embryonic kidney (HEK293) and Chinese hamster ovary (CHO) cell lines across multiple assay systems.[114] Yin, et al. found no β-arrestin recruitment following NAGly stimulation of GPR18.[115] Inoue et al. utilized a transforming growth factor-α (TGF-α)shedding assay to detect GPCR activation and found that GPR18 remained unresponsive to NAGly stimulation.[116] Further studies by Lu et al.[117] and Wonjo et al.[118] using guanine nucleotide exchange supported by nucleotide-decoupled G proteins (denoted as Gα-4A), demonstrated that GPR18 showed low constitutive activity and does not couple with any G protein ($G\alpha_i$, $G\alpha_s$, $G\alpha_{13}$, $G\alpha_{15}$, and G_q) during nucleotide exchange.

Given these inconsistencies, any conclusions regarding the physiological outcomes of GPR18 activation should be made with caution, as the link between GPR18 and its proposed agonists remains inconsistent and elusive. A more comprehensive understanding of the pathways involved is crucial for determining the therapeutic potential of GPR18.

3. RESULTS AND DISCUSSION

3.1. Publication I: Discovery of tricyclic xanthines as agonists of the cannabinoid-activated orphan G protein-coupled receptor GPR18

Clara T. Schoeder,‡ **Andhika B Mahardhika**,‡ Anna Drabczyńska, Katarzyna Kieć-Kononowicz, and Christa E. Müller

‡authors contributed equally to this work

The article is reprinted with permission from Schoeder, C. T.; **Mahardhika, A. B.**; Drabczyńska, A.; Kieć-Kononowicz, K.; Müller, C. E. Discovery of tricyclic xanthines as agonists of the cannabinoid-activated orphan G protein coupled receptor GPR18. *ACS Med. Chem. Lett.* **2020**, *11*, 2024–2031. DOI: 10.1021/acsmedchemlett.0c00208. Copyright 2020 American Chemical Society.

Supplementary information for this work can be found in the **Appendix I**.

Publication summary and contributions

The G protein-coupled receptor 18 (GPR18) is classified as an orphan G protein-coupled receptor (GPCR).[21] It exhibits prominent expression in immune cells and tissues, such as spleen, thymus, lymphocytes, pro-inflammatory macrophages, and microglia.[88, 96, 101, 102, 112, 119] Its expression pattern suggests potential involvement in various pathological processes, immune responses, inflammation, wound healing, and cancer.[99, 102, 120, 121] Consequently, GPR18 has emerged as potential therapeutic target.

Despite their great potential as novel drugs, only very few agonists and antagonists for GPR18 have been described so far. Several lipidic and lipid-like compounds have been proposed as putative agonists for GPR18. *N*-Arachidonoylglycine (NAGly), an analog of anandamide, was proposed as an endogenous agonist for GPR18.[101] However, several research groups failed to observe NAGly-induced GPR18 activation, leaving GPR18 still an orphan receptor.[114-116] Resolvin D2 (RvD2), a docosahexaenoic acid metabolite, was later proposed as another endogenous agonist for GPR18.[102] However, again, this could not be confirmed independently. Thus, reliable tool compounds to study GPR18 are urgently needed. A screening campaign on several orphan receptors revealed that the cannabinoid Δ^9-tetrahydrocannabinol (THC) could induce β-arrestin recruitment via human GPR18, which suggested a connection

between GPR18 and cannabinoid (CB) receptors, and thus GPR18 was proposed as the third cannabinoid receptor subtype, besides CB_1 and CB_2.[107, 110, 115]

THC is the only proposed GPR18 agonist that could be confirmed in our laboratory.[122-124] However, THC has limited solubility, and is much more potent at the CB receptor subtypes, CB_1 and CB_2, than at GPR18.[61, 125] Moreover, it also interacts with the lipid-activated orphan receptor GPR55,[126, 127] making THC not well suitable as a tool compound for exploring GPR18.

In order to identify a new class of GPR18 agonists, a screening campaign was conducted in our group using a β-arrestin-2 recruitment assay. The screening campaign yielded a solitary hit, the tricyclic xanthine derivative **5** (PSB-KD107, 6,7,8,9-tetrahydro-9-[2-(1*H*-indol-3-yl)ethyl]-1,3-dimethylpyrimido[2,1-*f*]purine-2,4 (1*H*,3*H*)-dione), which had previously been characterized as a moderately potent A_{2A} adenosine receptor antagonist.[128] Concentration-dependent activation of GPR18 by compound **5** yielded an EC_{50} value of 0.562 ± 0.113 μM.

Further characterization of **5** showed a superior profile compared to THC in efficacy (191% of the efficacy observed with THC, set as 100%). This implies that THC exhibits partial agonistic activity relative to the novel GPR18 agonist **5** and has lower potency. We further characterized the selectivity profile of **5** versus the related orphan receptor GPR55 (using the identical β-arrestin assay system), and versus cannabinoid receptors (using radioligand binding). Compound **5** showed neither an ability to promote β-arrestin-2 recruitment via GPR55 nor binding to either CB_1 and CB_2 receptors.

Subsequently, the structure-activity relationships (SARs) were studied (Figure 3.1): The presence of an indole moiety was found to be essential. The substitution of the methyl groups in agonist **5** with the larger ethyl residue resulted in a significant decrease in GPR18 activity, suggesting limited size of the binding pocket of GPR18. Most modifications on the annelated six-membered tetrahydropyrimidine resulted in decreased potency and/or decreased selectivity for GPR18, except for the expansion of the 6-membered annelated ring to a 7-membered ring (compound **16**, PSB-KD477).

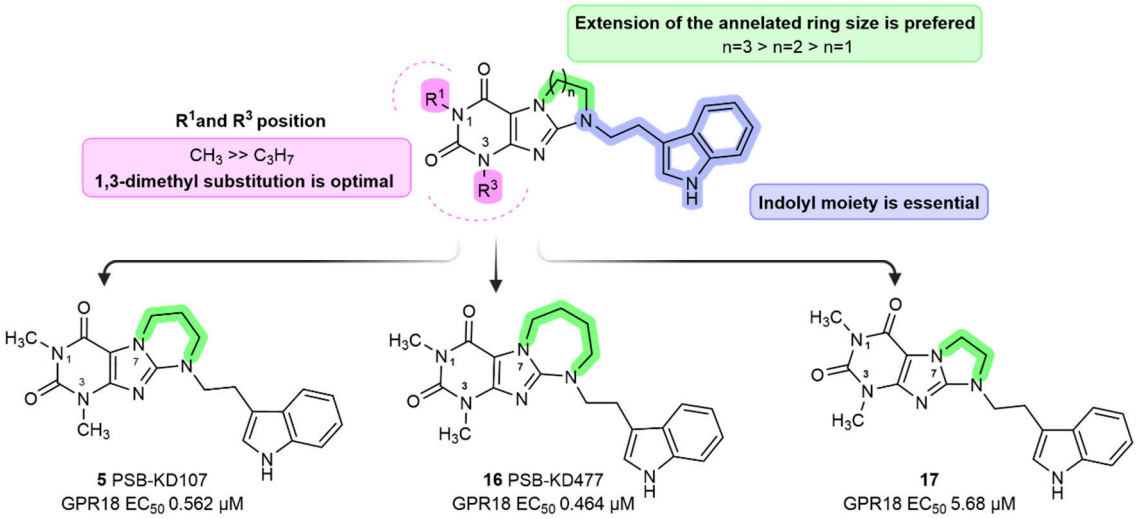

Figure 3.1 Structure-activity relationship of tricyclic xanthines derivatives as GPR18 agonists (top) and the structures of PSB-KD107, PSB-KD477 and compound 17 as GPR18 agonists.

Dr. Schoeder and I previously showed that PSB-CB27 could block THC-induced GPR18 in a dose-dependent manner with a competitive mechanism of inhibiton.[129] Thus, we investigated if PSB-CB27 could also block **5**-induced GPR18 activation. Interestingly, the GPR18 activation curves of **5** in the presence of PSB-CB27 showed that PSB-CB27 did not inhibit **5**-induced GPR18 activation. This may suggest the presence of distinct binding sites or receptor conformations that are targeted by the structurally diverse GPR18 agonists, namely the lipid-like THC and the heterotricyclic xanthine derivative **5**, and it is unlikely that the xanthine-based agonist shares the same binding site with THC.

To further investigate agonist **5**, GPR18 was activated with both the “partial” GPR18 agonist THC and the xanthine-type “full” agonist **5** at the same time. In the presence of the "full" agonist **5**, THC behaved as an antagonist in a dose-dependent manner, indicating that THC is indeed a partial agonist at GPR18. Interestingly, the presence of a fixed concentration of THC on the concentration–response curve of agonist **5**, showed an indication of allosterism between these two agonists. This suggests that the two agonists may indeed have different binding sites.

The newly discovered GPR18 agonists showed superior characteristics compared to the standard GPR18 agonist THC. These compounds represent the first selective

surrogate ligands for GPR18. These GPR18 agonists will be further optimized to obtain better agonists in terms of potency and selectivity. They will enable further studies and validation of the (patho)-physiological roles of GPR18.

In this article, the data from the screening campaign was obtained by Dr. Schoeder, while I performed all the additional experiments together with Dr. Schoeder. I also conducted the structure-activity relationship analysis, analyzed the data, and wrote the paper in cooperation with Prof. Christa Müller.

ACS Medicinal Chemistry Letters

pubs.acs.org/acsmedchemlett Letter

Discovery of Tricyclic Xanthines as Agonists of the Cannabinoid-Activated Orphan G-Protein-Coupled Receptor GPR18

Clara T. Schoeder,[‖] Andhika B. Mahardhika,[‖] Anna Drabczyńska, Katarzyna Kieć-Kononowicz,* and Christa E. Müller*

Cite This: *ACS Med. Chem. Lett.* 2020, 11, 2024−2031 Read Online

ACCESS | Metrics & More | Article Recommendations | Supporting Information

ABSTRACT: GPR18 is a rhodopsin-like orphan G-protein-coupled receptor (GPCR) that is activated by the natural cannabinoid (CB) Δ^9-tetrahydrocannabinol (THC). It is highly expressed in immune cells and represents a promising new drug target. However, THC is much more potent in activating CB receptors than GPR18, and several other proposed lipidic agonists for GPR18 have not been independently confirmed. Herein we describe the first non-lipid-like agonists for GPR18 based on a tricyclic xanthine-derived scaffold, along with initial structure−activity relationships. PSB-KD107 (**5**) and PSB-KD477 (**16**) displayed significantly higher potency and efficacy than THC, determined in a GPR18-dependent β-arrestin recruitment assay, and were found to be selective versus the CB-sensitive receptors CB_1, CB_2, and GPR55. Structure−activity relationships were steep, and indole substitution was crucial for biological activity. These first selective agonists, which are structurally distinct from the lipidic agonist(s), will allow target validation studies and may eventually contribute to the deorphanization of GPR18.

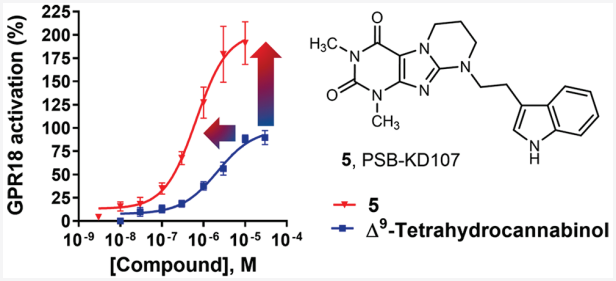

KEYWORDS: *Agonist, β-Arrestin, GPR18, Orphan receptor, Tetrahydrocannabinol, Xanthine*

First described in 1997, GPR18 is an orphan G-protein-coupled receptor (GPCR) that is located in the δ-branch of class-A, rhodopsin-like GPCRs.[1] The receptor is predominantly expressed in cells and tissues of the immune system including the spleen, thymus, lymphocytes, pro-inflammatory macrophages,[2−9] and microglia.[10,11] Furthermore, expression in the testis[5,12] and cancer cells[13,14] has been reported. Recent findings showed that GPR18 is also expressed in the eye and upregulated upon corneal damage, where it contributes to wound healing.[15,16] Thus GPR18 expression suggests its involvement in immunomodulatory and inflammatory processes, wound healing, and cancer progression, which makes it a promising new drug target.

In the past years, various lipidic and lipid-like physiological compounds have been proposed as agonists for GPR18. In 2006, Kohno et al. suggested *N*-arachidonoylglycine (Figure 1, NAGly, **1**), a metabolite of anandamide, to act as an endogenous ligand of GPR18 based on its effects in Ca^{2+} mobilization and cAMP accumulation assays in several cell lines expressing GPR18.[2] The cAMP-mediated signal by NAGly was abolished by pertussis toxin pretreatment, implying that NAGly activates GPR18 via $G\alpha_{i/0}$ proteins. These findings were supported by McHugh et al., who performed experiments using the microglial cell line BV-2 and the endometrial cell line HEC1b.[11,17] According to their results, GPR18 appeared to be activated by abnormal cannabidiol (**2**) and Δ^9-tetrahydrocan-

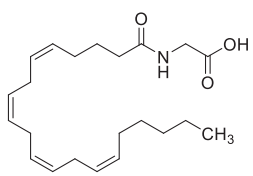

1 *N*-Arachidonoylglycine (NAGly)

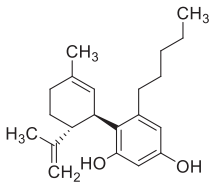

2 Abnormal cannabidiol (Abn-CBD)

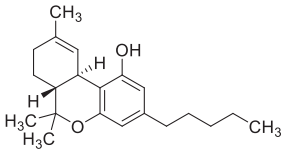

3 Δ^9-Tetrahydrocannabinol (Δ^9-THC)

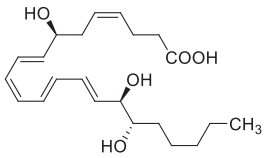

4 Resolvin D2 (RvD2)

Figure 1. Structures of proposed GPR18 agonists.

Special Issue: Medicinal Chemistry: From Targets to Therapies

Received: April 20, 2020
Accepted: June 11, 2020
Published: June 17, 2020

ACS Medicinal Chemistry Letters pubs.acs.org/acsmedchemlett Letter

Table 1. Agonistic Potencies of Xanthine Derivatives at GPR18 and GPR55 Determined in β-Arrestin Recruitment Assays

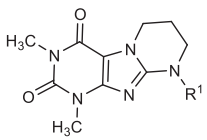

5-15

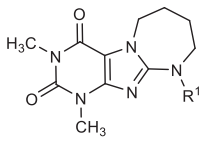

16

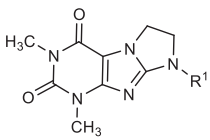

17-18

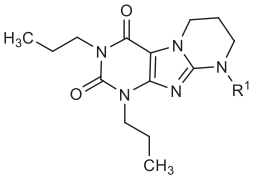

19

	Compound	R^1	Human GPR18		Human GPR55	
			Agonistic activity (% activation)[a] *[Efficacy][b]*	Antagonistic activity (% inhibition)[c]	Agonistic activity (% activation)[a] *[Efficacy][b]*	Antagonistic activity (% inhibition)[c]
			EC_{50} ± SEM (μM)	IC_{50} ± SEM (μM)	EC_{50} ± SEM (μM)	IC_{50} ± SEM (μM)
Previously proposed GPR18 agonists						
1	NAGly	For structure see Fig. 1	**>10** (10%)	**>10** (15%)	n.d.[d]	n.d.
2	Abnormal cannabidiol	For structure see Fig. 1	**>10** (-50%)	**>10** (42%)	**>10** (7%)	**>10** (33%)
3	THC	For structure see Fig. 1	**3.37** ± 1.19[e] *[100%]*	n.d.	**>10** (-4%)	**14.2** ± 5.2[27]
4	Resolvin D2	For structure see Fig. 1	**>10** (20%)	n.d.	n.d.	n.d.
Tricyclic xanthine derivatives						
5	PSB-KD107	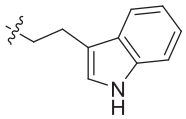	**0.562** ± 0.113 *[191%]*	n.d.	**>10** (-5%)	**>10** (20%)
6		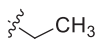	**>10** (2%)	**>10** (-4%)	**>10** (-16%)	**>10** (17%)
7		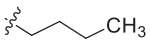	**>10** (26%)	**>10** (-18%)	**>10** (-4%)	**>10** (34%)
8		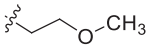	**>10** (40%)	**>10** (-13%)	**>10** (18%)	**>10** (-4%)
9		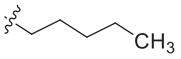	**>10** (-1%)	**>10** (19%)	**>10** (10%)	**>10** (-18%)
10		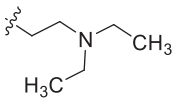	**>10** (39%)	**>10** (12%)	**>10** (4%)	**>10** (-3%)
11		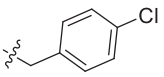	**>10** (6%)	**>10** (47%)	**>10** (-9%)	**>10** (1%)
12		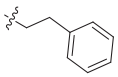	**>10** (2%)	**>10** (21%)	**>10** (16%)	**>10** (-10%)
13		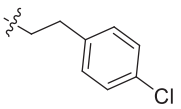	**>10** (14%)	**>10** (0%)	**>10** (10%)	**>10** (-29%)
14		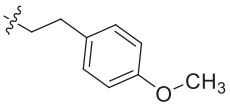	**>10** (-2%)	**>10** (-19%)	**>10** (-6%)	**>10** (-90%)
15		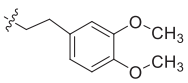	**>10** (-39%)	**>10** (-30%)	**>10** (15%)	**>10** (32%)
16	PSB-KD477	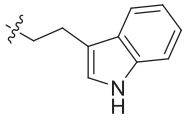	**0.454** ± 0.156 *[171%]*	n.d.	**>10** (38%)	**>10** (21%)

https://dx.doi.org/10.1021/acsmedchemlett.0c00208
ACS Med. Chem. Lett. 2020, 11, 2024−2031

Table 1. continued

Compound	R^1	Human GPR18		Human GPR55	
		Agonistic activity (% activation)[a] *[Efficacy][b]*	Antagonistic activity (% inhibition)[c]	Agonistic activity (% activation)[a] *[Efficacy][b]*	Antagonistic activity (% inhibition)[c]
		EC_{50} ± SEM (μM)	IC_{50} ± SEM (μM)	EC_{50} ± SEM (μM)	IC_{50} ± SEM (μM)
17	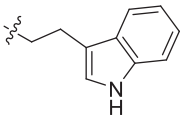	**5.68** ± 1.54 *[146%]*	n.d.	**>10** (20%)	**>10** (27%)
18	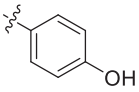	**>10** (22%)	**>10** (9%)	**>10** (13%)	**>10** (-40%)
19	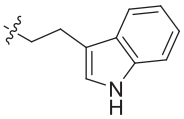	**>10** (-12)	**>10** (15)	**>10** (38%)	**>10** (-4%)

[a]Compounds were tested at a concentration of 10 μM. Effects were normalized to the signal induced by 10 μM THC (GPR18) or 1 μM LPI (GPR55). [b]Efficacy relative to the maximal effect of the standard agonist (GPR18, 30 μM THC; GPR55, 10 μM LPI) set at 100%. [c]Percent inhibition of agonist effect (GPR18, 10 μM THC; GPR55, 1 μM LPI) by test compound at 10 μM. [d]n.d., not determined. [e]Literature value: EC_{50} = 4.61 ± 0.50.[27]

nabinol (THC, **3**), both of which promoted cell migration.[17,18] These results suggested that GPR18 might be a novel type of cannabinoid (CB) receptor.[19,20] Console-Bram et al. supported these results with their findings that NAGly and THC produced increases in intracellular Ca^{2+} levels and induced mitogen-activated protein kinase (MAPK) activation. However, these authors reported that only THC, and not NAGly, was able to modulate GPR18 activity in β-arrestin recruitment assays.[21] Similar results were obtained by Yin et al.[22] and Rempel et al.,[23,24] who did not detect GPR18 activation in β-arrestin recruitment assays upon stimulation with NAGly. In fact, several groups failed to observe GPR18 activation by NAGly in a number of assays, including those measuring G-protein-dependent signaling.[22,25,26] Lu et al. reported the lack of GPR18 modulation by NAGly using electrophysiological experiments.[25] Finlay et al. performed a thoroughly controlled study reporting that in several functional assays under various conditions, GPR18-dependent effects on $G\alpha_{i/0}$ or G_s signaling by NAGly were observed in neither Chinese hamster ovary (CHO) nor human embryonic kidney (HEK) cells recombinantly expressing GPR18.[26] These findings are in agreement with results from our laboratory[24,27] (and unpublished results).

Besides NAGly, the polyunsaturated fatty acid metabolite resolvin D2 (RvD2, **4**) was proposed to act as an endogenous GPR18 agonist promoting the resolution of bacterial infections via GPR18.[3] However, this finding still awaits independent confirmation, and in our hands, **4** was not able to activate GPR18 (see Table 1).

Up to now, the only published GPR18 agonist that has been functional in our hands is THC. It allowed us to develop the first GPR18 antagonists, lipophilic heterocyclic compounds that were characterized to be competitive versus THC.[23,24,28] However, THC is lacking GPR18 selectivity due to its interaction with both CB receptor subtypes, CB_1 and CB_2, and with the lipid-activated orphan receptor GPR55.[27]

Contradictory reports and inconsistent results on GPR18 and its proposed ligands severely hamper the current GPR18 research. Moreover, the lack of selectivity of the confirmed agonist THC complicates the evaluation of GPR18 in biological systems. Thus, potent and selective agonists are urgently needed as tool compounds to explore the (patho)-physiological roles of GPR18 and to allow its validation as a drug target.

Here we describe the discovery and initial structure−activity relationships (SARs) of a novel class of GPR18 agonists that are derived from a non-lipid-like heterotricyclic xanthine scaffold.

Results and Discussion. To identify GPR18 agonists, we screened sublibraries of our proprietary compound collection (https://www.pharmchem1.uni-bonn.de/www-en/pharmchem1-en/mueller-laboratory/compound-library) using a β-arrestin recruitment assay that is based on enzyme complementation technology.[29] GPR18 and β-arrestin-2 were tagged with complementary parts of β-galactosidase. Upon β-arrestin recruitment to the tagged receptor, the enzyme is completed and can hydrolyze an added substrate, resulting in a luminescence signal. This assay thus detects GPCR activation regardless of the G-protein signaling pathway and is specific for the investigated GPCR.[29] Artifacts, such as false-positive signals, are rare and can be controlled by performing the same assay using cell lines that express different GPCRs. Our GPR18 agonist screening campaign provided a single hit, the tricyclic xanthine derivative **5** (Figure 2).

Xanthine **5** contains an annelated tetrahydropyrimidine ring that is substituted by an indolylethyl residue (Table 1). This compound had previously been identified as a moderately potent antagonist for the human adenosine A_{2A} receptor (K_i = 4.56 μM).[30] We subsequently determined the concentration-dependent activation of GPR18 by **5** and calculated an EC_{50} value of 0.562 ± 0.113 μM (Figure 3).

We observed a significantly higher maximal effect for agonist **5** as compared with the standard agonist THC, namely, 191% of THC efficacy (= 100%). This means that THC behaves as a partial agonist in comparison with the new agonist **5**. Thus **5** shows superior potency and efficacy.

To confirm that the effect observed for **5** was mediated by GPR18 activation and to study its selectivity, the compound was additionally tested at the related orphan GPCR GPR55

https://dx.doi.org/10.1021/acsmedchemlett.0c00208
ACS Med. Chem. Lett. 2020, 11, 2024−2031

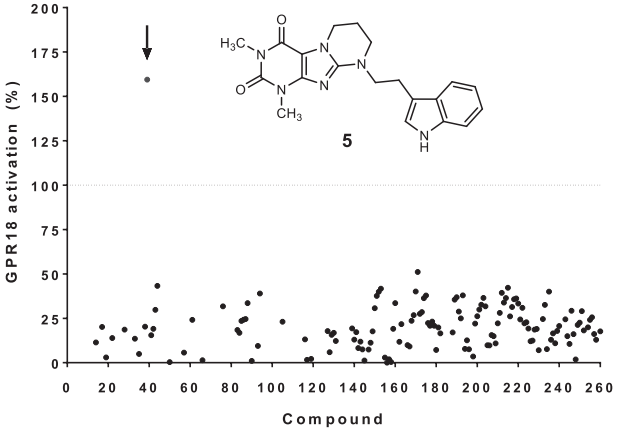

Figure 2. Screening of a compound sublibrary for GPR18 agonistic activity using a β-arrestin enzyme complementation assay. The human GPR18 was recombinantly expressed in CHO cells. Compound **5** was identified as a hit. Data were normalized to the effect observed for GPR18 activation by 10 μM Δ^9-THC (corresponding to its EC_{80}) set at 100%.

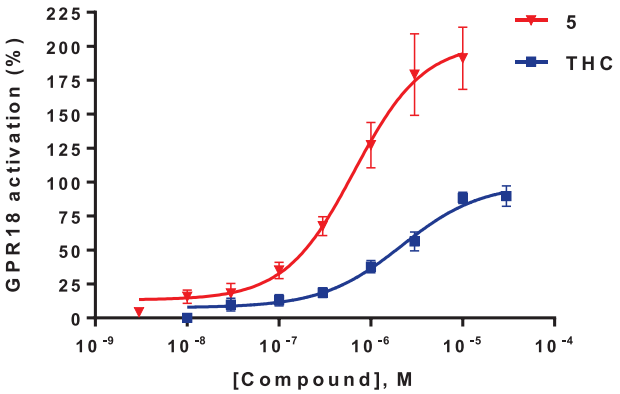

Figure 3. Concentration−response curves of hit compound **5** (EC_{50} = 0.562 ± 0.113 μM) and Δ^9-THC (EC_{50} = 3.37 ± 1.19 μM) determined in a β-arrestin enzyme complementation assay using CHO cells stably expressing the human GPR18. Data were normalized to the maximum effect of Δ^9-THC (set at 100%). Data points shown are mean values of three independent experiments, each performed in duplicate.

using the same assay system. GPR55 was chosen because it shares with GPR18 the ability to interact with cannabinoids. Compound **5**, tested at a high concentration of 10 μM, neither induced β-arrestin recruitment in CHO cells stably expressing GPR55 nor blocked GPR55 activation by its agonist lysophosphatidylinositol (LPI) (Table 1). This is a strong indication that **5** is selective for GPR18 over GPR55. However, because we measured β_2-arrestin recruitment only, which is well described for GPR55,[31] and not β_1-arrestin recruitment, it cannot be fully excluded at present that the compound might interact with GPR55 when differently assayed. The same applies to a potential bias toward G-protein signaling.[32−34]

When tested in radioligand binding studies at CB receptors, GPR18 agonist **5**, tested at a high concentration of 10 μM, showed no significant displacement of the CB receptor-specific radioligand at either CB_1 or at CB_2 receptors. It also did not show any increase in radioligand binding that could have been indicative of positive allosteric CB receptor modulation. This implies that **5** is also selective versus both CB receptor subtypes, although an allosteric modulation of the CB receptor function cannot be fully excluded.

Encouraged by these findings, we further studied the SARs of this new class of GPR18 agonists.

Chemistry. Tricyclic xanthines **5**−**9**, **11**−**15**, **18**, and **19** were synthesized as previously described.[30,35−37] The new compounds **10**, **16**, and **17** were obtained according to the following procedure (Scheme 1): Theophylline (**I**) was

Scheme 1. Synthesis of Tricyclic Xanthine Derivatives 11, 16, and 17[a]

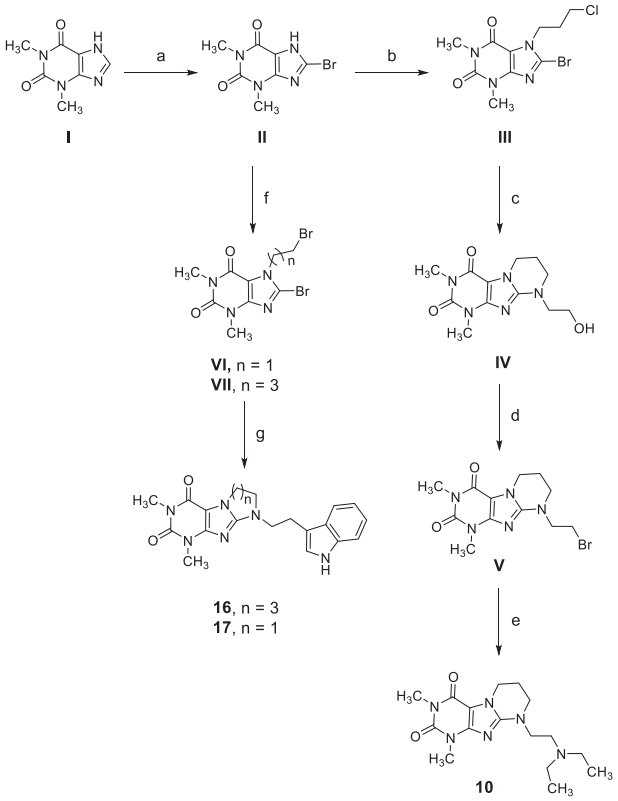

[a]Reagents and conditions: (a) HBr, $NaClO_3$, CH_3COOH, 60°C; (b) 1-bromo-3-chloropropane, benzyltriethylammonium chloride (BTEAC), K_2CO_3, acetone, reflux; (c) 2-aminoethanol, reflux; (d) PBr_3, $CHCl_3$, reflux; (e) diethylamine, propanol, reflux; (f) 1,4-dibromobutane for **16**, 1,2-dibromoethane for **17**, BTEAC, K_2CO_3, acetone, reflux; (g) 3-(2-aminoethyl)-indole, 2-methoxyethanol, reflux.

brominated with HBr in the presence of $NaOCl_3$, yielding 8-bromotheophylline (**II**) according to a previously described procedure.[35] Compound **II** was then alkylated at N7 with 1-bromo-3-chloropropane and *N*,*N*-diisopropylethylamine (DIPEA) as a base, resulting in 8-bromo-7-(3-chloropropyl)-1,3-dimethyl-3,7-dihydro-1*H*-purine-2,6-dione (**III**). Xanthine **III** was then cyclized by the reaction with 2-aminoethanol, yielding the tricyclic compound 9-(2-hydoxyethyl)-1,3-dimethylpyrimido[2,1-*f*]purine-2,4-dione (**IV**), which was subsequently brominated using PBr_3 yielding **V**. The final product **10** was obtained by the nucleophilic substitution of **V** with excess diethylamine. For the synthesis of products **16** and **17**, 8-bromotheophylline (**II**) was alkylated either with 1,4-dibromobutane or with 1,2-dibromoethane using benzyltri-

https://dx.doi.org/10.1021/acsmedchemlett.0c00208
ACS Med. Chem. Lett. 2020, 11, 2024−2031

ACS Medicinal Chemistry Letters pubs.acs.org/acsmedchemlett Letter

ethylammonium chloride (BTEAC) as a phase-transfer catalyst, resulting in 7-(2-bromoethyl)-8-bromotheophylline (**VI**) or 7-(4-bromobutyl)-8-bromotheophylline (**VII**), respectively. Compounds **VI** and **VII** were then cyclized with 3-(2-aminoethyl)indole in dimethylformamide (DMF) or 2-methoxyethanol, yielding diazepino- and imidazo-[2,1-*f*]-purine-2,4-diones **16** and **17**. The structures of the synthesized compounds were confirmed by MS, UV, IR, and ^{1}H NMR spectra. The purity of all compounds was confirmed to be >95%.

Structure–Activity Relationships. To study initial SARs, we modified the indolylethyl substituent on the xanthine core. Any replacement of the indolyl residue with other aromatic or aliphatic substituents (see **6**–**15** and **18**) abolished the GPR18 activity. (See Table 1.) This indicates the importance of the indole residue attached to the tricyclic xanthine scaffold for GPR18 agonistic activity.

Previously, we had reported on several natural products bearing indole moieties, which were able to inhibit THC-induced GPR18 activation.[38,39] In fact, these compounds had been the first antagonists described for GPR18. In light of the present findings, the observed requirement of an indole moiety not only for agonists but also for various antagonists suggests that the reported antagonists and the newly discovered agonists may share the same binding site on GPR18.

Next, we studied the tricyclic xanthine core itself. Extension of the annelated six-membered tetrahydropyrimidine ring present in agonist **5** to a seven-membered ring appeared to slightly increase the activity (**16**, PSB-KD477, EC_{50} 0.454 ± 0.156 μM). However, decreasing the ring size to a five-membered imidazolidine ring significantly reduced the activity by about 10-fold (**17**, EC_{50} = 5.68 ± 1.54 μM).

Agonist **16** was also somewhat more potent at GPR55 (38% activation at 10 μM) and at the CB_2 receptor (46% inhibition of radioligand binding at 10 μM) than lead structure **5**. (See Table 1 and Table S1.) Therefore, we continued modifying the more selective derivative, the six-ring-annelated xanthine derivative **5**.

In a subsequent step, we investigated the substituents in the N1- and N3-positions of the xanthine core. Replacement of the methyl groups in agonist **5** (which are also present in the naturally occurring xanthine alkaloids caffeine and theophylline) by the longer propyl residues (compound **19**) drastically reduced the GPR18 activity. These steep SARs indicate limited space in the binding pocket of GPR18.

None of the compounds evaluated in this study, including those that showed no GPR18-agonistic activity, inhibited THC-induced β-arrestin recruitment in GPR18-expressing cells (Table 1). This shows that the investigated tricyclic compounds that failed to activate GPR18 also did not block the receptor.

Finally, we characterized the new agonist **5** by trying to block its effect by the THC-competitive GPR18 antagonist PSB-CB-27 (**20**; see Figure 4).[24] In our previous study, we had shown that **20** was able to completely block THC-induced GPR18 activation in a β-arrestin recruitment assay, displaying an IC_{50} value of 0.650 μM. Agonist **5** was employed at a concentration of 1 μM, which corresponds to its EC_{80} value, and inhibition of its effect by GPR18 antagonist **20** was studied (Figure 4). Surprisingly, antagonist **20** was not able to fully inhibit GPR18 activation induced by the tricyclic xanthine agonist **5** (IC_{50} value of 0.944 μM, 65% maximal inhibition; see Figure 4).

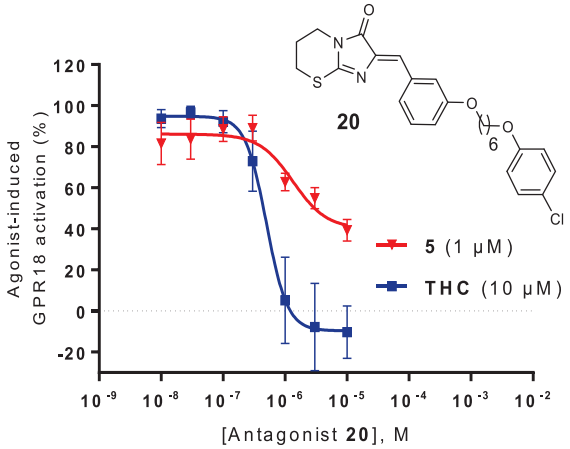

Figure 4. Concentration-dependent inhibition of GPR18 activation by an EC_{80} concentration of the GPR18 agonist THC (blue curve) and the GPR18 agonist **5** (red curve). IC_{50} values were 0.650 μM (vs THC, complete inhibition) and 0.944 μM (vs **5**, 64% maximal inhibition), determined in a β-arrestin enzyme complementation assay using CHO cells stably expressing the human GPR18 receptor. Data points are means of three independent experiments, each performed in duplicate.

These results may be indicative of different binding sites or receptor conformations to which the structurally very different GPR18 agonists, the lipid-like THC, on the one hand, and the heterotricyclic xanthine derivative **5**, on the other hand, are binding. Whereas the lipophilic antagonist **20** appears to bind to the same binding site as the lipid-like agonist THC, this is probably not the case for the xanthine-based agonist.

To confirm this hypothesis, we studied the concentration-dependent activation of GPR18 by xanthine agonist **5** in the absence and in the presence of different concentrations of the lipidic antagonist **20**. In fact, increasing concentrations of **20** led to a lowering of the maximal effect induced by agonist **5**. No significant rightward shift of the concentration–response curve could be observed (Figure 5), and the EC_{50} values were not significantly different from each other. (See Table S2.) This is consonant with an allosteric mechanism of inhibition

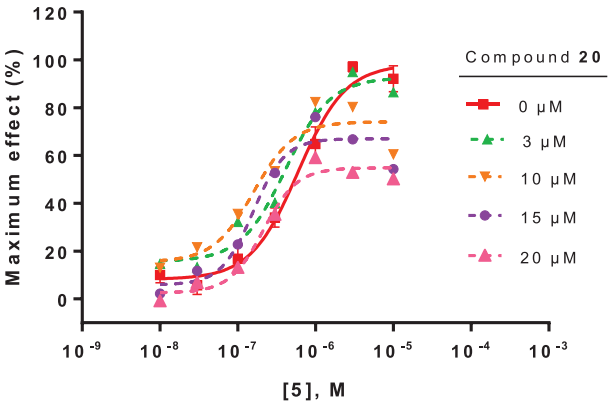

Figure 5. Activation of GPR18 by **5** in the absence and presence of different concentrations of **20**. EC_{50} values and maximum effects are collected in Table S2. Determined by the β-arrestin enzyme complementation assay using CHO stably expressing the human GPR18 receptor. Data points shown are means of three independent experiments performed in duplicate.

https://dx.doi.org/10.1021/acsmedchemlett.0c00208
ACS Med. Chem. Lett. 2020, 11, 2024–2031

ACS Medicinal Chemistry Letters pubs.acs.org/acsmedchemlett Letter

for antagonist **20** versus the xanthine-type agonist **5**. In contrast, antagonist **20** had previously been shown to block GPR18 activation by the lipidic GPR18 agonist THC in a competitive manner.[24]

As a next step, we studied the effects of combining the lipid-like "partial" GPR18 agonist THC with the xanthine-type "full" agonist **5** in the β-arrestin recruitment assay. In Figure 6A, the

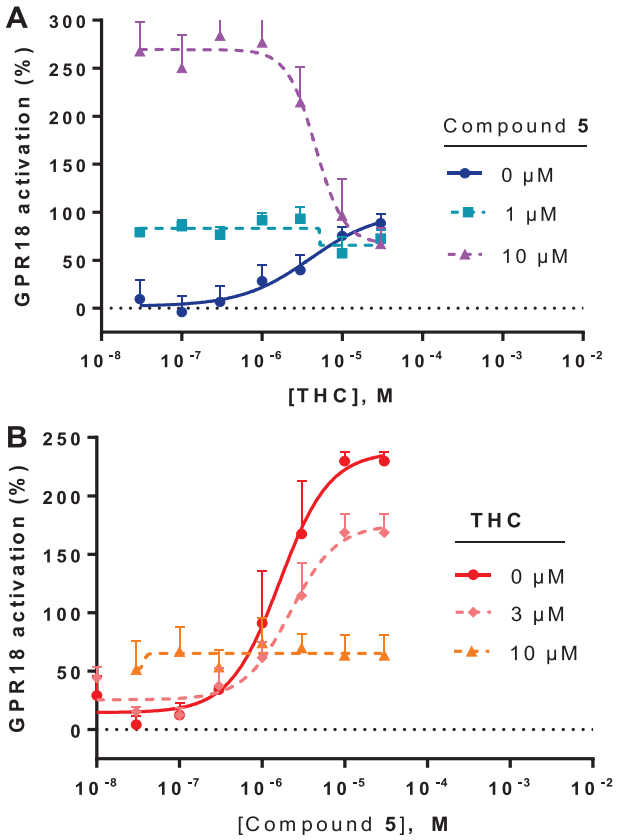

Figure 6. (A) Effects of fixed concentrations of xanthine agonist **5** on the concentration–response curve of THC. (B) Effects of fixed concentrations of THC on the concentration–response curve of xanthine-derived agonist **5**. Activation of the human GPR18 expressed in CHO cells was determined in β-arrestin recruitment assays. Data points shown are means of three independent experiments performed in duplicate.

effects of fixed concentrations of xanthine agonist **5** on the concentration–response curve of THC are shown. In Figure 6B, results of the reverse experiment are shown, in which the effects of fixed concentrations of THC on concentration-dependent GPR18 activation by xanthine agonist **5** were studied. Xanthine agonist **5**, used at its EC_{50} value of 1 μM, was able to increase the basal response of low concentrations of THC. However, at high concentrations of the xanthine agonist **5**, at which it showed maximal GPR18 activation, its effect was inhibited by THC in a concentration-dependent manner (Figure 6A). This behavior is typical for partial agonists. Along the same lines, concentration-dependent activation of GPR18 by the xanthine agonist **5** was partly inhibited by 3 μM of THC and inhibited by >70% at a high concentration of 10 μM THC (Figure 6B). Unfortunately, we could not add even higher concentrations of THC due to its limited water solubility. These observations clearly indicate that THC is a partial agonist at GPR18 in comparison with the novel xanthine-derived agonist **5**, and THC can even act as a GPR18 antagonist in the presence of the more efficacious agonist. These results highlight the superior properties of the newly discovered GPR18 agonist scaffold. It is interesting to note in this context that THC also behaves as a partial agonist at both CB receptor subtypes.[40−44]

In conclusion, we discovered a novel class of surrogate agonists for the orphan GPCR GPR18 and investigated preliminary SARs, which were found to be steep. The new scaffold is characterized by a tricyclic dimethylxanthine core substituted by an indole ring attached via an ethylene bridge. Agonist **5**, which showed a submicromolar EC_{50} value, was more potent and much more efficacious that the standard GPR18 agonist THC. These new GPR18 agonists represent suitable lead structures for further optimization to obtain potent and selective tool compounds. They will likely contribute to a breakthrough in the field of GPR18 research, allowing future target validation studies.

■ ASSOCIATED CONTENT

Supporting Information

The Supporting Information is available free of charge at https://pubs.acs.org/doi/10.1021/acsmedchemlett.0c00208.

Synthetic procedures, analytical data, assay procedures, and additional selectivity data (PDF)

■ AUTHOR INFORMATION

Corresponding Authors

Christa E. Müller − *Pharmaceutical Institute, Department of Pharmaceutical & Medicinal Chemistry, University of Bonn, Bonn 53121, Germany;* orcid.org/0000-0002-0013-6624; Phone: +49-228-73-2301; Email: christa.mueller@uni-bonn.de; Fax: +49-228-73-2567

Katarzyna Kieć-Kononowicz − *Department of Technology and Biotechnology of Drugs, Faculty of Pharmacy, Jagiellonian University Medical College, 30-688 Kraków, Poland;* Phone: +12-620-55-80; Email: mfkonono@cyf-kr.edu.pl

Authors

Clara T. Schoeder − *Pharmaceutical Institute, Department of Pharmaceutical & Medicinal Chemistry and Research Training Group 1873, University of Bonn, Bonn 53121, Germany*

Andhika B. Mahardhika − *Pharmaceutical Institute, Department of Pharmaceutical & Medicinal Chemistry and Research Training Group 1873, University of Bonn, Bonn 53121, Germany;* orcid.org/0000-0002-0456-1353

Anna Drabczyńska − *Department of Technology and Biotechnology of Drugs, Faculty of Pharmacy, Jagiellonian University Medical College, 30-688 Kraków, Poland*

Complete contact information is available at: https://pubs.acs.org/10.1021/acsmedchemlett.0c00208

Author Contributions

‖C.T.S. and A.B.M. contributed equally. The manuscript was mainly written by C.E.M. and A.B.M. with contributions from all authors. All authors (C.T.S., A.B.M., A.D., K.K.-K., and C.E.M.) have given approval to the final version of the manuscript.

Funding

C.T.S., A.B.M., and C.E.M. were supported by the Deutsche Forschungsgemeinschaft (DFG) within the Research Training

Group GRK 1873 "Pharmacology of 7TM-receptors and downstream signaling pathways" and the BMBF-funded Bonn International Graduate School Drug Sciences (BIGS DrugS). K.K.-K. was supported by the Jagiellonian University statutory funds (N42/DBS/000039). K.K.-K. and C.E.M. were supported by the EU COST Action ERNEST CA18133. C.T.S. received a BAYER Ph.D. fellowship through BIGS DrugS. A.B.M. was funded by the Ministry of Finance of Indonesia in the scheme of the Indonesia Endowment Fund for Education (Lembaga Pengelola Dana Pendidikan (LPDP).

Notes

The authors declare no competing financial interest.

■ ACKNOWLEDGMENTS

We thank Marion Schneider for the expert measurement of LCMS and NMR spectra.

■ ABBREVIATIONS

Abn-CBD, abnormal cannabidiol; BTEAC, benzyltriethylammonium chloride; BV-2, mouse microglial cell line BV-2; CB, cannabinoid receptor; CB_1, cannabinoid receptor type 1; CB_2, cannabinoid receptor type 2; CHO, Chinese hamster ovary; DIPEA, *N*,*N*-diisopropylethylamine; DMF, dimethylformamide; GPCR, G-protein-coupled receptor; GPR18, G-protein-coupled receptor 18; GPR55, G-protein-coupled receptor 55; HEC-1B, human endometrial cell line 1-B; HEK, human embryonic kidney; LPI, lysophosphatidylinositol; MAPK, mitogen-activated protein kinase; NAGly, *N*-arachidonoylglycine; RvD2, resolvin D2; SAR, structure−activity relationship; THC, Δ^9-tetrahydrocannabinol

■ REFERENCES

(1) Fredriksson, R.; Lagerström, M. C.; Lundin, L.-G.; Schiöth, H. B. The G-protein-coupled receptors in the human genome form five main families. Phylogenetic analysis, paralogon groups, and fingerprints. *Mol. Pharmacol.* **2003**, *63*, 1256−1272.

(2) Kohno, M.; Hasegawa, H.; Inoue, A.; Muraoka, M.; Miyazaki, T.; Oka, K.; Yasukawa, M. Identification of N-arachidonylglycine as the endogenous ligand for orphan G-protein-coupled receptor GPR18. *Biochem. Biophys. Res. Commun.* **2006**, *347*, 827−832.

(3) Chiang, N.; Dalli, J.; Colas, R. A.; Serhan, C. N. Identification of resolvin D2 receptor mediating resolution of infections and organ protection. *J. Exp. Med.* **2015**, *212*, 1203.

(4) Wang, X.; Sumida, H.; Cyster, J. G. GPR18 is required for a normal CD8$\alpha\alpha$ intestinal intraepithelial lymphocyte compartment. *J. Exp. Med.* **2014**, *211*, 2351−2359.

(5) Gantz, I.; Muraoka, A.; Yang, Y. K.; Samuelson, L. C.; Zimmerman, E. M.; Cook, H.; Yamada, T. Cloning and chromosomal localization of a gene (GPR18) encoding a novel seven transmembrane receptor highly expressed in spleen and testis. *Genomics* **1997**, *42*, 462−6.

(6) Regard, J. B.; Sato, I. T.; Coughlin, S. R. Anatomical profiling of G protein-coupled receptor expression. *Cell* **2008**, *135*, 561−571.

(7) Becker, A. M.; Callahan, D. J.; Richner, J. M.; Choi, J.; DiPersio, J. F.; Diamond, M. S.; Bhattacharya, D. GPR18 controls reconstitution of mouse small intestine intraepithelial lymphocytes following bone marrow transplantation. *PLoS One* **2015**, *10*, No. e0133854.

(8) Takenouchi, R.; Inoue, K.; Kambe, Y.; Miyata, A. N-arachidonoyl glycine induces macrophage apoptosis via GPR18. *Biochem. Biophys. Res. Commun.* **2012**, *418*, 366−71.

(9) Jablonski, K. A.; Amici, S. A.; Webb, L. M.; Ruiz-Rosado, J. d. D.; Popovich, P. G.; Partida-Sanchez, S.; Guerau-De-Arellano, M. Novel markers to delineate murine M1 and M2 macrophages. *PLoS One* **2015**, *10*, No. e0145342.

(10) McHugh, D. GPR18 in microglia: implications for the CNS and endocannabinoid system signalling. *Br. J. Pharmacol.* **2012**, *167*, 1575−82.

(11) McHugh, D.; Wager-Miller, J.; Page, J.; Bradshaw, H. B. siRNA knockdown of GPR18 receptors in BV-2 microglia attenuates N-arachidonoyl glycine-induced cell migration. *J. Mol. Signaling* **2014**, *7*, 10.

(12) Flegel, C.; Vogel, F.; Hofreuter, A.; Wojcik, S.; Schoeder, C.; Kiec-Kononowicz, K.; Brockmeyer, N. H.; Müller, C. E.; Becker, C.; Altmüller, J.; Hatt, H.; Gisselmann, G. Characterization of non-olfactory GPCRs in human sperm with a focus on GPR18. *Sci. Rep.* **2016**, *6*, 32255.

(13) Qin, Y.; Verdegaal, E. M. E.; Siderius, M.; Bebelman, J. P.; Smit, M. J.; Leurs, R.; Willemze, R.; Tensen, C. P.; Osanto, S. Quantitative expression profiling of G-protein-coupled receptors (GPCRs) in metastatic melanoma: the constitutively active orphan GPCR GPR18 as novel drug target. *Pigm. Cell Melanoma Res.* **2011**, *24*, 207−218.

(14) Qiao, G.-J.; Chen, L.; Wu, J.-C.; Li, Z.-R. Identification of an eight-gene signature for survival prediction for patients with hepatocellular carcinoma based on integrated bioinformatics analysis. *PeerJ* **2019**, *7*, No. e6548.

(15) Murataeva, N.; Daily, L.; Taylor, X.; Dhopeshwarkar, A.; Hu, S. S.-J.; Miller, S.; McHugh, D.; Oehler, O.; Li, S.; Bonanno, J. A.; Mackie, K.; Straiker, A. Evidence for a GPR18 role in chemotaxis, proliferation, and the course of wound closure in the cornea. *Cornea* **2019**, *38*, 905−913.

(16) Caldwell, M. D.; Hu, S. S.-J.; Viswanathan, S.; Bradshaw, H.; Kelly, M. E. M.; Straiker, A. A GPR18-based signalling system regulates IOP in murine eye. *Br. J. Pharmacol.* **2013**, *169*, 834−843.

(17) McHugh, D.; Hu, S. S.; Rimmerman, N.; Juknat, A.; Vogel, Z.; Walker, J. M.; Bradshaw, H. B. N-arachidonoyl glycine, an abundant endogenous lipid, potently drives directed cellular migration through GPR18, the putative abnormal cannabidiol receptor. *BMC Neurosci.* **2010**, *11*, 44.

(18) McHugh, D.; Page, J.; Dunn, E.; Bradshaw, H. B. Δ^9-Tetrahydrocannabinol and N-arachidonyl glycine are full agonists at GPR18 receptors and induce migration in human endometrial HEC-1B cells. *Br. J. Pharmacol.* **2012**, *165*, 2414−24.

(19) Alexander, S. P. So what do we call GPR18 now? *Br. J. Pharmacol.* **2012**, *165*, 2411−3.

(20) Alexander, S. P.; Christopoulos, A.; Davenport, A. P.; Kelly, E.; Marrion, N. V.; Peters, J. A.; Faccenda, E.; Harding, S. D.; Pawson, A. J.; Sharman, J. L.; Southan, C.; Davies, J. A.; CGTP Collaborators. The consice guide to pharmacology 2017/18: G protein-coupled receptors. *Br. J. Pharmacol.* **2017**, *174*, S17−S129.

(21) Console-Bram, L.; Brailoiu, E.; Brailoiu, G. C.; Sharir, H.; Abood, M. E. Activation of GPR18 by cannabinoid compounds: a tale of biased agonism. *Br. J. Pharmacol.* **2014**, *171*, 3908−3917.

(22) Yin, H.; Chu, A.; Li, W.; Wang, B.; Shelton, F.; Otero, F.; Nguyen, D. G.; Caldwell, J. S.; Chen, Y. A. Lipid G protein-coupled receptor ligand identification using beta-arrestin PathHunter assay. *J. Biol. Chem.* **2009**, *284*, 12328−38.

(23) Rempel, V.; Atzler, K.; Behrenswerth, A.; Karcz, T.; Schoeder, C.; Hinz, S.; Kaleta, M.; Thimm, D.; Kiec-Kononowicz, K.; Müller, C. E. Bicyclic imidazole-4-one derivatives: a new class of antagonists for the orphan G protein-coupled receptors GPR18 and GPR55. *MedChemComm* **2014**, *5*, 632−649.

(24) Schoeder, C. T.; Kaleta, M.; Mahardhika, A. B.; Olejarz-Maciej, A.; Łażewska, D.; Kieć-Kononowicz, K.; Müller, C. E. Structure-activity relationships of imidazothiazinones and analogs as antagonists of the cannabinoid-activated orphan G protein-coupled receptor GPR18. *Eur. J. Med. Chem.* **2018**, *155*, 381−397.

(25) Lu, V. B.; Puhl, H. L.; Ikeda, S. R. N-Arachidonyl glycine does not activate G-protein-coupled receptor 18 signaling via canonical pathways. *Mol. Pharmacol.* **2013**, *83*, 267.

(26) Finlay, D. B.; Joseph, W. R.; Grimsey, N. L.; Glass, M. GPR18 undergoes a high degree of constitutive trafficking but is unresponsive to N-arachidonoyl glycine. *PeerJ* **2016**, *4*, No. e1835.

https://dx.doi.org/10.1021/acsmedchemlett.0c00208
ACS Med. Chem. Lett. 2020, 11, 2024−2031

(27) Rempel, V.; Volz, N.; Gläser, F.; Nieger, M.; Bräse, S.; Müller, C. E. Antagonists for the orphan G-protein-coupled receptor GPR55 based on a coumarin scaffold. *J. Med. Chem.* **2013**, *56*, 4798−810.
(28) Neumann, A.; Engel, V.; Mahardhika, A. B.; Schoeder, C. T.; Namasivayam, V.; Kiec-Kononowicz, K.; Müller, C. E. Computational Investigations on the Binding Mode of Ligands for the Cannabinoid-Activated G Protein-Coupled Receptor GPR18. *Biomolecules* **2020**, *10*, 686.
(29) Bassoni, D. L.; Raab, W. J.; Achacoso, P. L.; Loh, C. Y.; Wehrman, T. S. Measurements of β-arrestin recruitment to activated seven transmembrane receptors using enzyme complementation. In *Receptor Binding Techniques*; Davenport, A. P., Ed.; Humana Press: Totowa, NJ, 2012; pp 181−203.
(30) Drabczyńska, A.; Müller, C. E.; Schiedel, A.; Schumacher, B.; Karolak-Wojciechowska, J.; Fruziński, A.; Zobnina, W.; Yuzlenko, O.; Kieć-Kononowicz, K. Phenylethyl-substituted pyrimido[2,1-f]-purinediones and related compounds: Structure-activity relationships as adenosine A_1 and A_{2A} receptor ligands. *Bioorg. Med. Chem.* **2007**, *15*, 6956−6974.
(31) Heynen-Genel, S.; Dahl, R.; Shi, S.; Milan, L.; Hariharan, S.; Bravo, Y.; Sergienko, E.; Hedrick, M.; Dad, S.; Stonich, D.; Su, Y.; Vicchiarelli, M.; Mangravita-Novo, A.; Smith, L. H.; Chung, T. D.; Sharir, H.; Barak, L. S.; Abood, M. E. Screening for selective ligands for GPR55-agonists. In *Probe Reports from the NIH Molecular Libraries Program [Internet]*; National Center for Biotechnology Information (US): 2011.
(32) Pertwee, R. G.; Howlett, A. C.; Abood, M. E.; Alexander, S. P.; Di Marzo, V.; Elphick, M. R.; Greasley, P. J.; Hansen, H. S.; Kunos, G.; Mackie, K.; Mechoulam, R.; Ross, R. A. International Union of Basic and Clinical Pharmacology. LXXIX. Cannabinoid receptors and their ligands: beyond CB(1) and CB(2). *Pharmacol. Rev.* **2010**, *62*, 588−631.
(33) Kapur, A.; Zhao, P.; Sharir, H.; Bai, Y.; Caron, M. G.; Barak, L. S.; Abood, M. E. Atypical responsiveness of the orphan receptor GPR55 to cannabinoid ligands. *J. Biol. Chem.* **2009**, *284*, 29817−29827.
(34) Fakhouri, L.; Cook, C. D.; Al-Huniti, M. H.; Console-Bram, L. M.; Hurst, D. P.; Spano, M. B. S.; Nasrallah, D. J.; Caron, M. G.; Barak, L. S.; Reggio, P. H.; Abood, M. E.; Croatt, M. P. Design, synthesis and biological evaluation of GPR55 agonists. *Bioorg. Med. Chem.* **2017**, *25*, 4355−4367.
(35) Drabczyńska, A.; Müller, C. E.; Lacher, S. K.; Schumacher, B.; Karolak-Wojciechowska, J.; Nasal, A.; Kawczak, P.; Yuzlenko, O.; Pękala, E.; Kieć-Kononowicz, K. Synthesis and biological activity of tricyclic aryloimidazo-, pyrimido-, and diazepinopurinediones. *Bioorg. Med. Chem.* **2006**, *14*, 7258−7281.
(36) Kieć-Kononowicz, K.; Drabczyńska, A.; Pękala, E.; Michalak, B.; Müller, C. E.; Schumacher, B.; Karolak-Wojciechowska, J.; Duddeck, H.; Rockitt, S.; Wartchow, R. New developments in A_1 and A_2 adenosine receptor antagonists. *Pure Appl. Chem.* **2001**, *73*, 1411.
(37) Drabczyńska, A.; Karcz, T.; Szymańska, E.; Köse, M.; Müller, C. E.; Paskaleva, M.; Karolak-Wojciechowska, J.; Handzlik, J.; Yuzlenko, O.; Kieć-Kononowicz, K. Synthesis, biological activity and molecular modelling studies of tricyclic alkylimidazo-, pyrimido- and diazepino-purinediones. *Purinergic Signalling* **2013**, *9*, 395−414.
(38) Nazir, M.; Harms, H.; Loef, I.; Kehraus, S.; El Maddah, F.; Arslan, I.; Rempel, V.; Müller, C. E.; König, G. M. GPR18 inhibiting Amauromine and the novel triterpene glycoside Auxarthonoside from the sponge-derived fungus Auxarthron reticulatum. *Planta Med.* **2015**, *81*, 1141−5.
(39) Harms, H.; Rempel, V.; Kehraus, S.; Kaiser, M.; Hufendiek, P.; Müller, C. E.; König, G. M. Indoloditerpenes from a marine-derived fungal strain of Dichotomomyces cejpii with antagonistic activity at GPR18 and cannabinoid receptors. *J. Nat. Prod.* **2014**, *77*, 673−7.
(40) Hess, C.; Schoeder, C. T.; Pillaiyar, T.; Madea, B.; Müller, C. E. Pharmacological evaluation of synthetic cannabinoids identified as constituents of spice. *Forensic Toxicol.* **2016**, *34*, 329−343.
(41) Rempel, V.; Volz, N.; Hinz, S.; Karcz, T.; Meliciani, I.; Nieger, M.; Wenzel, W.; Bräse, S.; Müller, C. E. 7-Alkyl-3-benzylcoumarins: A versatile scaffold for the development of potent and selective cannabinoid receptor agonists and antagonists. *J. Med. Chem.* **2012**, *55*, 7967−7977.
(42) Banister, S. D.; Arnold, J. C.; Connor, M.; Glass, M.; McGregor, I. S. Dark Classics in Chemical Neuroscience: Δ9-Tetrahydrocannabinol. *ACS Chem. Neurosci.* **2019**, *10*, 2160−2175.
(43) Banister, S. D.; Connor, M. The Chemistry and Pharmacology of Synthetic Cannabinoid Receptor Agonists as New Psychoactive Substances: Origins. In *New Psychoactive Substances: Pharmacology, Clinical, Forensic and Analytical Toxicology*; Maurer, H. H., Brandt, S. D., Eds.; Springer International Publishing: Cham, Switzerland, 2018; pp 165−190.
(44) Müller, C. E. Fortschritte in der Cannabis-Forschung aus pharmazeutisch-chemischer Sicht (Progress in cannabis research from a pharmaceutical chemist's point of view). *Bundesgesundheitsblatt - Gesundheitsforschung - Gesundheitsschutz* **2019**, *62*, 818−824.

https://dx.doi.org/10.1021/acsmedchemlett.0c00208
ACS Med. Chem. Lett. 2020, 11, 2024−2031

3.2. Publication II: Potent, selective agonists for the cannabinoid-like orphan G protein-coupled receptor GPR18: a promising drug target for cancer and immunity

Andhika B. Mahardhika, ‡ Michal Załuski, ‡ Clara T. Schoeder, ‡ Nader M. Boshta, ‡ Jakub Schabikowski, Filomena Perri, Dorota Łażewska, Alexander Neumann, Sarah E. Kremers, Angelo Oneto, Anastasiia Ressemann, Gniewomir Latacz, Vigneshwaran Namasivayam, Katarzyna Kieć-Kononowicz, Christa E. Müller

‡authors contribute equally to this work

The article is reprinted with permission from Mahardhika, A. B.; Załuski, M.; Schoeder, C. T.; Boshta, N. M.; Schabikowski, J.; Perri, F.; Łażewska, D.; Neumann, A.; Kremers, S.; Oneto, A.; Ressemann, A.; Latacz, G.; Namasivayam, V.; Kieć-Kononowicz, K.; Müller, C. E. Potent, selective agonists for the cannabinoid-like orphan G protein-coupled receptor GPR18: A promising drug target for cancer and immunity. *J. Med. Chem.* **2024**, *67*, 9896-9926. DOI: 10.1021/acs.jmedchem.3c02423. Copyright 2024 American Chemical Society.

Supplementary information for this work can be found in the **Appendix II**.

Publication summary and contributions

The orphan G protein-coupled receptor GPR18 was initially discovered and characterized in 1996 by Samuelson and Gantz during the search for a novel gastrin-releasing hormone (novel bombesin) receptor.[88, 89] At the chromosome level, GPR18 closely clustered with the EBI2 receptor (GPR183) and the lipid receptors for cysteinyl leukotriene receptor 1 and 2 (CysL1 and CysL2 receptors).[94] GPR18 is expressed in various tissues such as brain, heart, lungs, liver, and pancreas with its highest expression observed in the cells associated with the immune system such as spleen, thymus, peripheral blood leukocytes, and lymph nodes. Additionally, GPR18 is found in several cancer cell lines.[8, 88, 97, 99, 101] These expression patterns suggest that GPR18 may play a crucial role in cancer and immune diseases.

Several attempts have been made in recent years to identify the cognate ligand for GPR18, most of which have focused on lipid or lipid-like molecules. For example, *N*-arachidonoylglycine (NAGly) and Resolvin D2 (RvD2) have been proposed as endogenous agonists for GPR18.[101, 102] Additionally, cannabinoids such as Δ^9-tetrahydrocannabinol and cannabidiol were reported to activate GPR18.[106-108, 115] However, GPR18 still remains an orphan receptor because many of the published data could not be reproduced in other laboratories.

Previously, we reported on a new class of non-lipid-like compounds, tricyclic-xanthine derivatives, as potent and selective GPR18 agonists.[129] The tricyclic structure does not allow straightforward extensive exploration. Thus, in this manuscript, we further explored a novel scaffold, bicyclic xanthines, introducing substituents at the *N*1-, *N*3-, and *N*7-xanthine positions (Figure 3.2).

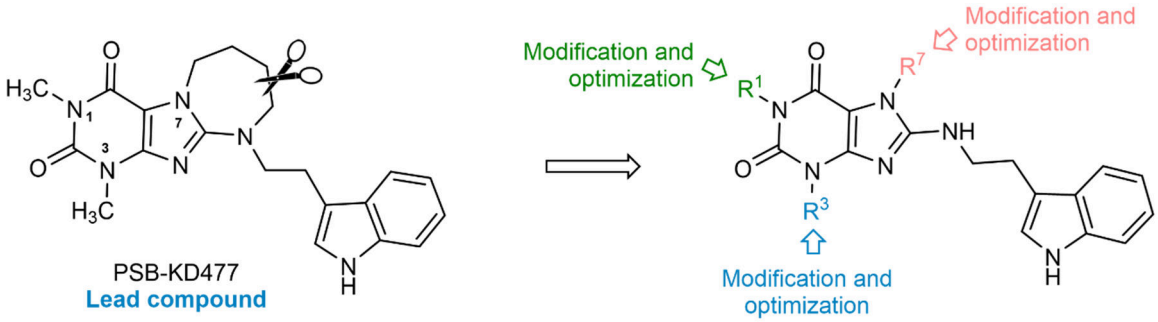

Figure 3.2 Strategy for the exploration and modification of the lead compound PSB-KD477. Reprinted (adapted) with permission from Mahardhika et. al.[130] Copyright © 2024 American Chemical Society.

In this manuscript, we extensively investigated 68 newly developed and synthesized compounds. These compounds were tested for activity at human GPR18 using the PathHunter β-arrestin-2 assay. Additionally, potential species differences were assessed by testing them at mouse GPR18. Selectivity studies were conducted versus cannabinoid (CB) receptors (CB_1 and CB_2 receptors) and the CB-like receptor, GPR55. Selected compounds were additionally tested at GPR183, which possesses the highest sequence identity with GPR18. Further confirmation of GPR18 activity was obtained using bioluminescent resonance energy transfer (BRET) assays, confirming that the compounds mediate their effects through GPR18.

Structure-activity relationship (SAR) studies at human GPR18 revealed steep SARs (Figure 3.3):

- At the *N*1- and *N*3-xanthine positions, methyl substituents were found to be the most favorable. Larger substituents were not tolerated, indicating limited space within the binding pocket of GPR18.
- The *N*7-xanthine moiety was divided into several categories: linear and branched aliphatic residues, unsaturated residues, and aromatic residues. Linear substituents such as methyl and ethyl showed an increase in potency

compared to PSB-KD107. However, increasing the alkyl chain length did not further increase GPR18 potency. Branched and unsaturated residues showed a slight increase in potency compared to PSB-KD107, while substituents with high electron density at this position were not preferred.

- The most significant potency difference was observed with aromatic residues at the *N*7-xanthine position. A halogenated benzyl substituent showed the highest potency at this position. Specifically, *p*-fluorobenzyl (**50**), *p*-chlorobenzyl (**51**), and *p*-bromobenzyl (**52**) derivatives exhibited a significant increase in potency at human GPR18 as compared to the unsubsituted benzyl moiety. However, disubstituted benzyl groups at the *N*7-xanthine position did not provide higher potency compared to the mono-substituted compounds. Substitution at this position with hydrophilic moieties resulted in a loss of activity at GPR18, highlighting the importance of lipophilic residues for GPR18 activity.

Some analogous observations were made at the bicyclic scaffold as with the tricyclic lead compound, PSB-KD107. An indolylethylamino residue at the xanthine core was essential for GPR18 agonistic activity, while substitution with other residues led to a complete loss of activity. This suggests that the presence of an indole moiety, connected to a xanthine moiety, is crucial for GPR18 activation.

At the human GPR18, we discovered compound **51** to be the most potent agonist with an EC_{50} of 0.0191 µM (>20-fold more potent compared to PSB-KD107), in fact, the most potent GPR18 agonist known to date.

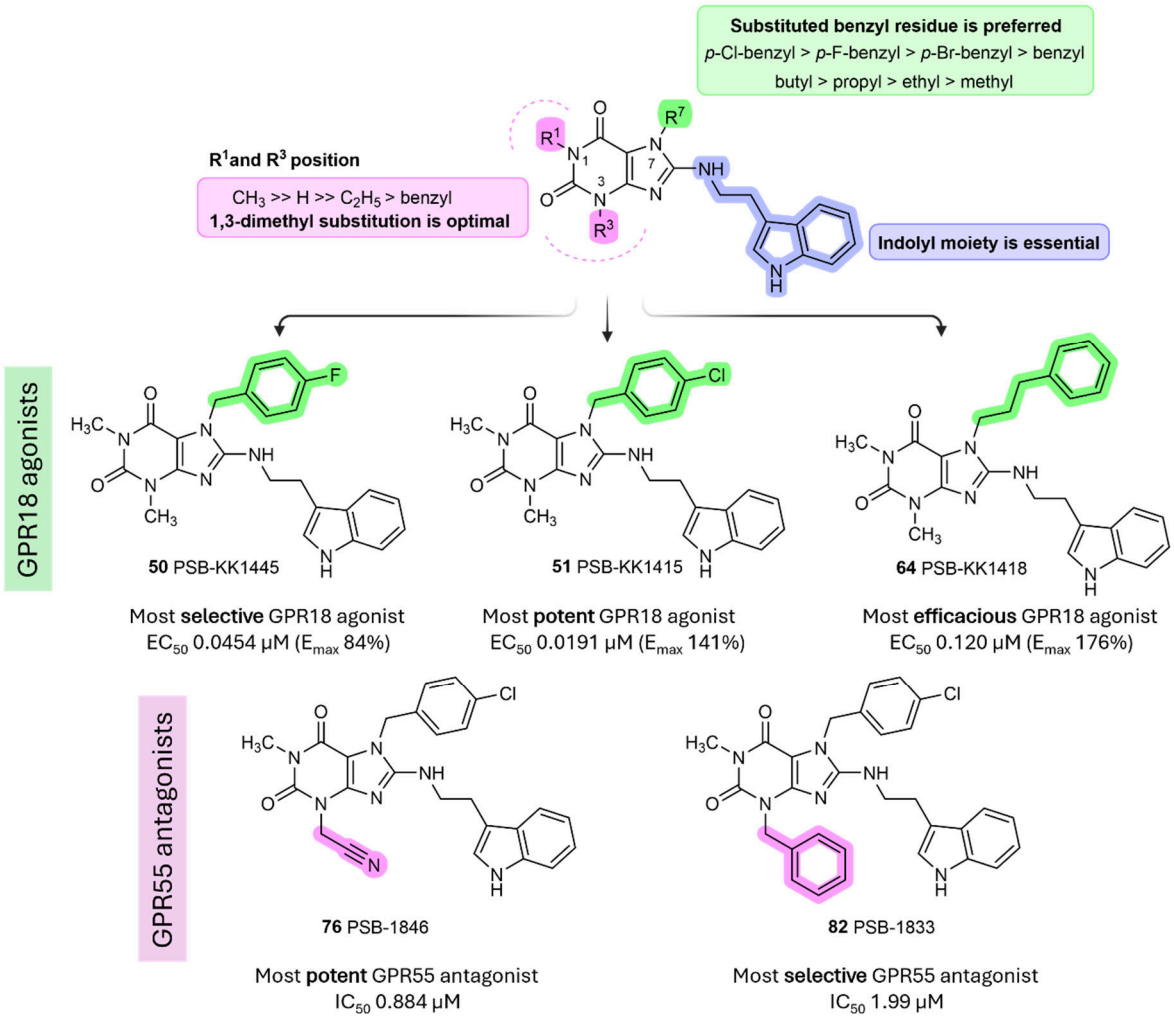

Figure 3.3 Structure-activity relationships of bicyclic xanthine derivatives as GPR18 agonists (top) and the structures of GPR18 agonists and GPR55 antagonists in the present paper (bottom). Efficacy (E_{max}) values compared to the maximum effect of THC in the assay system (set as 100%). Selectivity was assessed versus GPR55, CB_1, CB_2 and GPR183 receptors. Reprinted (adapted) with permission from Mahardhika et. al.[130] Copyright© 2024 American Chemical Society.

In the second part of the manuscript, we evaluated the relationship between human and mouse GPR18 activity of the newly developed agonists. As predicted, the potencies of these new agonists at human and mouse receptors were closely correlated, suggesting a virtually identical binding site for GPR18 in both species. Both species have high sequence similarity (90% sequence similarity) and sequence identity (86% sequence identity). Interestingly, THC, a cannabinoid which activates human GPR18,[115, 123, 129] only weakly activated mouse GPR18. This suggests that our newly developed compounds could serve as promising tool compounds for investigating GPR18 in mice which has, so far, not been possible.

In a subsequent part of the manuscript, the selectivity of the newly synthesized compounds was assessed. Assays were conducted at CB_1 and CB_2 receptors (using radioligand binding assays), at the CB-like receptor GPR55, and at the human GPR183 using β-arrestin-2 assays. We discovered that **50** (PSB-KK1445) is the most selective GPR18 agonist, while **51** (PSB-KK1415) is the most potent agonist, the latter showing micromolar affinity and partial agonistic activity at cannabinoid receptors. Compound **64** (PSB-KK1418) behaved as the most efficacious GPR18 agonist. Additionally, we discovered compound **82** (PSB-1833) to act as a selective GPR55 antagonist (IC_{50} 1.74 μM) while **76** (PSB-1846) is the most potent GPR55 antagonist with an IC_{50} of 0.884 μM.

Next, we attempted to block the effect of **51**-induced GPR18 activation with the published antagonist PSB-CB27.[124] Interestingly PSB-CB27 failed to block the effect of **51**-induced GPR18 activation, while it was able to inhibit THC-induced GPR18 activation. This indicates a different binding site for THC as compared to **51**, which was supported by docking studies using a homology model of GPR18.

Moreover, we demonstrated GPR18 activation-induced β-arrestin-2 recruitment by **51** using another assay system based on bioluminescence resonance energy transfer (BRET) in different cell line (HEK293), thereby confirming the GPR18 activity of **51** in an orthogonal assay. GPR18 acts as an atypical GPCR lacking any G protein activation.

In this manuscript, I performed biological experiments together with Dr. Schoeder. I developed the β-arrestin-2 assays for CB_1, CB_2, and GPR183 receptors and the BRET-based β-arrestin-2 assay for GPR18. I created all figures, analyzed structure-activity relationships, and wrote the manuscript together with Prof. Dr. Christa Müller with support by the other authors.

Journal of Medicinal Chemistry

Chapter 3.2

pubs.acs.org/jmc

Article

Potent, Selective Agonists for the Cannabinoid-like Orphan G Protein-Coupled Receptor GPR18: A Promising Drug Target for Cancer and Immunity

Andhika B. Mahardhika,[#] Michal Załuski,[#] Clara T. Schoeder,[#] Nader M. Boshta,[#] Jakub Schabikowski, Filomena Perri, Dorota Łażewska, Alexander Neumann, Sarah Kremers, Angelo Oneto, Anastasiia Ressemann, Gniewomir Latacz, Vigneshwaran Namasivayam, Katarzyna Kieć-Kononowicz,* and Christa E. Müller*

Cite This: *J. Med. Chem.* 2024, 67, 9896−9926

Read Online

ACCESS | Metrics & More | Article Recommendations | Supporting Information

ABSTRACT: The human orphan G protein-coupled receptor GPR18, activated by Δ^9-tetrahydrocannabinol (THC), constitutes a promising drug target in immunology and cancer. However, studies on GPR18 are hampered by the lack of suitable tool compounds. In the present study, potent and selective GPR18 agonists were developed showing low nanomolar potency at human and mouse GPR18, determined in β-arrestin recruitment assays. Structure−activity relationships were analyzed, and selectivity versus cannabinoid (CB) and CB-like receptors was assessed. Compound **51** (PSB-KK1415, EC_{50} 19.1 nM) was the most potent GPR18 agonist showing at least 25-fold selectivity versus CB receptors. The most selective GPR18 agonist **50** (PSB-KK1445, EC_{50} 45.4 nM) displayed >200-fold selectivity versus both CB receptor subtypes, GPR55, and GPR183. The new GPR18 agonists showed minimal species differences, while THC acted as a weak partial agonist at the mouse receptor. The newly discovered compounds represent the most potent and selective GPR18 agonists reported to date.

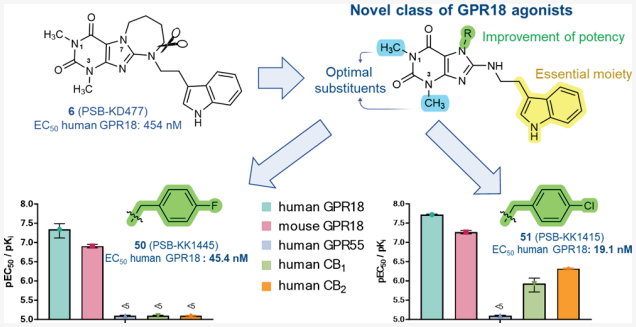

INTRODUCTION

G protein-coupled receptors (GPCRs) constitute the largest family in the human proteome, and approximately one-third of all approved drugs interact with GPCRs as their targets.[1] GPR18 is an orphan GPCR, first described in 1997, which was found in the search for a new gastrin-releasing peptide receptor using a relaxed stringency polymerase chain reaction.[2] The receptor is localized on chromosome 13q32, in close proximity to the related GPR183 (13q32.3),[3] which was recently found to be activated by 7α,25-dihydroxycholesterol.[4] GPR18 is predominantly expressed by cells and tissues associated with the immune system (e.g., spleen, thymus, peripheral blood leukocytes, and lymph nodes), and on cancer cells.[2,5−14] Therefore, it is of great interest as a novel potential drug target for immune diseases and cancer, including immuno-oncology. While agonists are expected to activate the immune system, antagonists may display anti-inflammatory and immunosuppressive effects.[8,15] However, due to the lack of potent pharmacological tool compounds, validation of GPR18 as a drug target has so far not been feasible.

In the past years, several attempts have been made to identify endogenous agonist(s) as well as surrogate ligands for GPR18. *N*-Arachidonoylglycine (NAGly, **1**, Figure 1) was proposed to be the cognate agonist of GPR18 based on calcium mobilization and cAMP accumulation assays in K562 and Chinese hamster ovary (CHO) cells recombinantly expressing GPR18, indicating G_q and $G_{i/o}$ protein coupling of GPR18.[6] Several years later, cannabinoids including abnormal-cannabidiol (Abn-CBD, **2**) and Δ^9-tetrahydrocannabinol (THC, **3**) were reported to activate GPR18, suggesting that it might be a novel type of cannabinoid (CB) receptor.[16−19] In 2015, a docosahexaenoic acid-derived lipid, the specialized pro-resolving mediator Resolvin D2 (RvD2, **4**), was proposed as an endogenous GPR18 agonist reported to display low nanomolar potency in CHO cells stably expressing GPR18.[7] Thus, an important role for GPR18 in the resolution of inflammation was suggested. The effect of RvD2 was found to be insensitive to pertussis toxin (PTX), but not to cholera toxin (CTX) pretreatment, suggesting the involvement of G_s protein coupling of

Received: December 22, 2023
Revised: March 27, 2024
Accepted: May 24, 2024
Published: June 17, 2024

Journal of Medicinal Chemistry pubs.acs.org/jmc Article

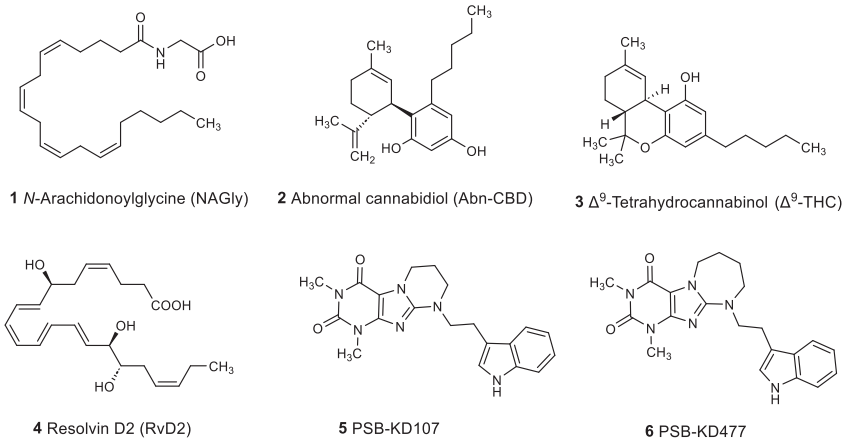

Figure 1. Structures of proposed GPR18 agonists. Only compound **3**, **5**, and **6** were confirmed in our hands to act as agonists of the human GPR18, while **1**, **2**, and **4** were found to be inactive.

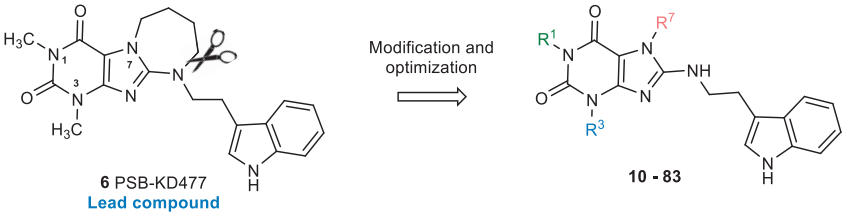

Figure 2. Design of novel GPR18 agonists based on the tricyclic lead structure **6** with a bicyclic xanthine core (see Table 1 for R^1, R^3 and R^7).

Scheme 1. Variation of the *N*1-Position, Synthesis of Compounds 10 and 12−18[a]

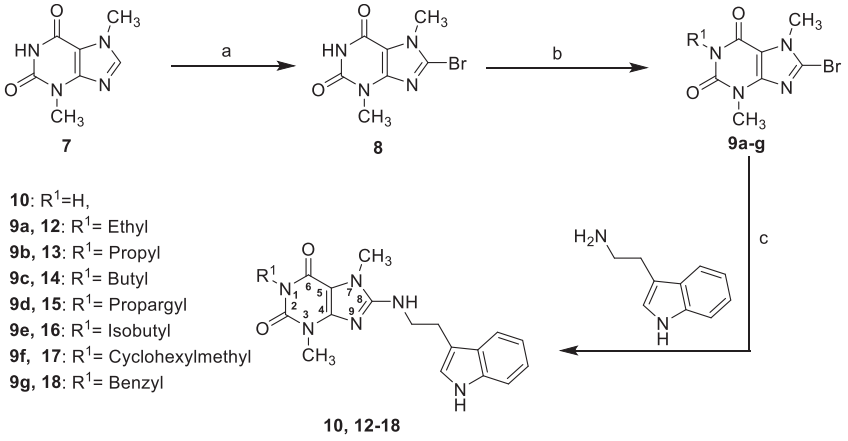

[a]Reagents and conditions: (a) 40% HBr, $NaClO_3$ (yield: 46%); (b) K_2CO_3, DMF, alkyl or arylalkyl halide, 70 °C, 4 h (yields: 33−62%); (c) tryptamine, triethylamine (TEA), propanol, microwave, 300 W, 140 °C, 10 bar, 1 h (yields: 28−66%).

GPR18.[7,20] Interestingly, the same research group had previously reported that RvD2 effects were sensitive to pertussis toxin in endothelial cells, indicating that RvD2 exerted its effects via G_i protein-coupled receptors.[21,22] In contrast, several research groups failed to observe any activation of GPR18 by physiological lipids, neither by NAGly nor by RvD2, using a variety of assays and cell lines.[23−28] Despite a multitude of studies conducted with the aim to elucidate the (patho)-physiological roles and signaling mechanisms of GPR18, and to identify its cognate agonist(s), the receptor still remains orphan, and its function is poorly understood.[29,30]

In our laboratory, we confirmed that out of the previously reported lipid-like agonists, only THC activates the human GPR18, inducing β-arrestin recruitment at micromolar concentrations (EC_{50} 3.37 μM).[23,24,31,32] However, due to its potent interaction with both CB receptor subtypes, CB_1 and CB_2,[33] and with another orphan receptor, GPR55,[34] pharmacological studies employing THC as a GPR18 agonist in more complex biological systems, such as native cell lines and tissues, or even in vivo, are difficult to interpret.

Recently, we discovered the first GPR18 agonists with submicromolar potency (EC_{50} values of around 500 nM), the indole-substituted tricyclic xanthine derivatives PSB-KD107 (**5**) and PSB-KD477 (**6**) (Figure 1) utilizing a β-arrestin recruitment assay based on enzyme (galactosidase) complementation.[32] These compounds showed selectivity for GPR18 versus CB receptors and the CB-like receptor GPR55. Here, we describe the discovery, optimization, and structure−activity relationships

https://doi.org/10.1021/acs.jmedchem.3c02423
J. Med. Chem. 2024, 67, 9896−9926

Journal of Medicinal Chemistry pubs.acs.org/jmc Article

Scheme 2. Synthesis of *N*7-Substituted Xanthine Derivatives 11, 21−28, 31−43, and 47−53, 56−66[a]

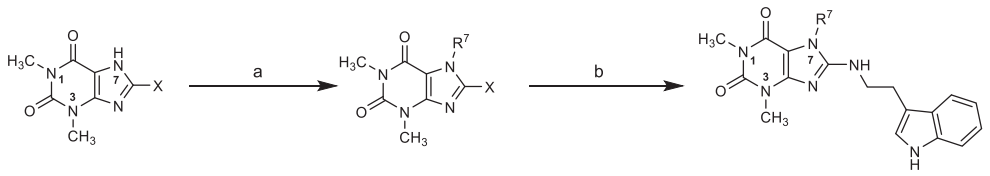

11, 20a: R^7= Methyl
20b, 21: R^7= Ethyl
20c, 22: R^7= Propyl
20d, 23: R^7= Butyl
20e, 24: R^7= Propenyl
20f, 25: R^7= Isopentyl
20g, 26: R^7= Butenyl
20h, 27: R^7= Proparagyl
20i, 28: R^7= Pent-3-ynyl
20j, 62: R^7= $(CH_2)_2$Cyclohexyl
20k, 63: R^7= $(CH_2)_2$Ph
20l, 64: R^7= $(CH_2)_3$Ph
20m, 65: R^7= $(CH_2)_3$-O-Ph
20n, 66: R^7= $(CH_2)_3$-O-(4-Cl)Ph
29a, 31: R^7= Benzyl
29b, 32: R^7= 2-F-Benzyl
29c, 33: R^7= 2-Cl-Benzyl
29d, 34: R^7= 2-Br-Benzyl
29e, 35: R^7= 3-F-Benzyl
29f, 36: R^7= 3-Cl-Benzyl
29g, 37: R^7= 3-Br-Benzyl
29h, 38: R^7= 3-OCH_3-Benzyl
29i, 39: R^7= 4-CH_3-Benzyl
29j, 40: R^7= 4-CF_3-Benzyl
29n, 41: R^7= 4-OCH_3-Benzyl
29o, 42: R^7= 4-$((CH_3)_2CH)$-Benzyl
29p, 43: R^7= 4-(CH_3CO_2)-Benzyl
29q, 47: R^7= 4-(NH_2SO_2)-Benzyl
29r, 48: R^7= 4-(CH_3NHSO_2)-Benzyl
29s, 49: R^7= 4-$(CH_3(CH_2)_2NHSO_2)$-Benzyl
29t, 50: R^7= 4-F-Benzyl
29u, 51: R^7= 4-Cl-Benzyl
29v, 52: R^7= 4-Br-Benzyl
29w, 53:R^7= 4-NO_2-Benzyl
29x, 56: R^7= 2-Cl,6-Cl-Benzyl
29y, 57: R^7= 2-Cl,4-Cl-Benzyl
29z, 58: R^7= 3-F,4-Cl-Benzyl
29aa, 59: R^7= 3-Cl,4-Cl-Benzyl
29ab, 60: R^7= 3-F,4-F-Benzyl
29ac, 61: R^7= 3-Cl,4-F-Benzyl

[a]Reagents and conditions: (a) K_2CO_3, DMF, alkyl or arylalkyl halide, room temperature (RT), 18 h; (b) tryptamine, TEA, propanol, microwave, 300 W, 140 °C, 10 bar, 1 h (compd. **11**, **21−28**, **31−42**, **50−53**, **56−57**, **59**, **62−66**), or tryptamine, DIPEA, NMP, 145 °C, 18 h (compd. **43**, **47−49**, **58**, **60−61**); yields 29−90%.

Scheme 3. Synthesis of *N*7-Substituted Xanthine Derivative 30[a]

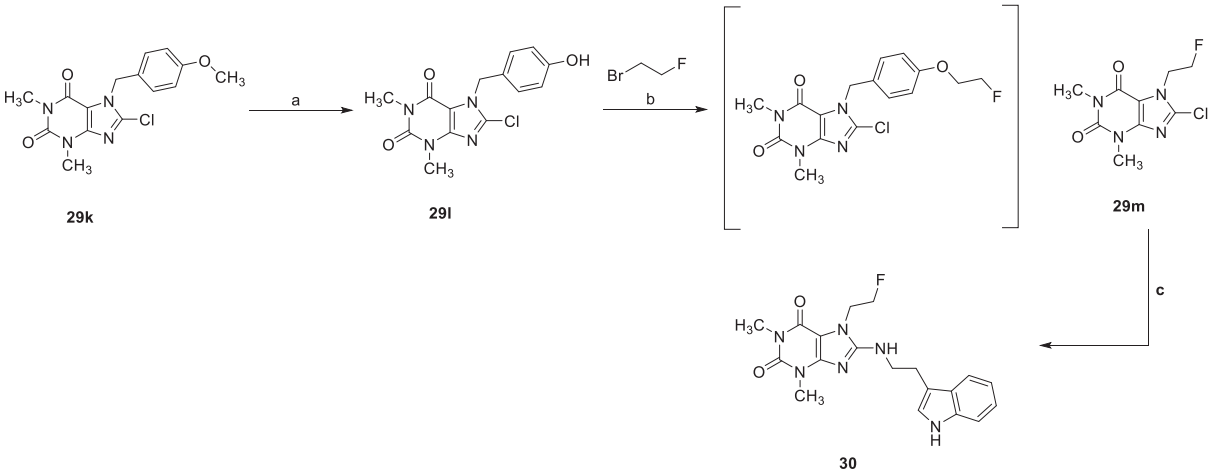

[a]Reagents and conditions: (a) BBr_3, DMF, 5 °C, 3 h (yield: 62%); (b) Cs_2CO_3, DMF, 60 °C, 2.5 h (yield: 32.5%); (c) tryptamine, DIPEA, NMP, 145 °C, 18 h (yield: 56%).

(SARs) of a novel, heterobicyclic class of GPR18 agonists based on our previous lead structures **5** and **6**. We obtained the first GPR18 agonists with potency in the low nanomolar range combined with high selectivity versus related receptors. The compounds showed only minor species differences between human and mouse GPR18. In contrast to THC, which acted as a very weak partial agonist at the mouse receptor, the new compounds displayed high efficacy at both human and mouse GPR18. Other previously proposed and disputed agonists, in particular NAGly (**1**), AbnCBD (**2**), and RvD2 (**4**) were inactive under a variety of conditions and in a range of concentrations, **2** even showing moderate inverse agonistic activity at GPR18.

RESULTS AND DISCUSSION

Design. In our previous study in which we discovered the tricyclic xanthine derivatives **5** and **6** as novel GPR18 agonists, an indolylethyl substitution was found to be important for GPR18 activation (see Figure 1). In the present study, we kept this residue but removed the third, saturated ring of the tricyclic core to allow higher flexibility and the possibility to easily introduce a variety of substituents into the *N*7-position of the xanthine scaffold (see Figure 2). This was inspired by the fact that a larger 7-membered ring (in **6**) had led to a somewhat more potent compound compared to a 6-membered ring (in **5**, see Table 1).

A series of indolylethylaminoxanthine derivatives **10−83** (Tables 1 and 2) was synthesized according to Scheme 1 (modifications at the *N*1-position of the xanthine core),

https://doi.org/10.1021/acs.jmedchem.3c02423
J. Med. Chem. 2024, 67, 9896−9926

Journal of Medicinal Chemistry pubs.acs.org/jmc Article

Scheme 4. Synthesis of *N*7-Substituted Xanthine Derivatives 43−46[a]

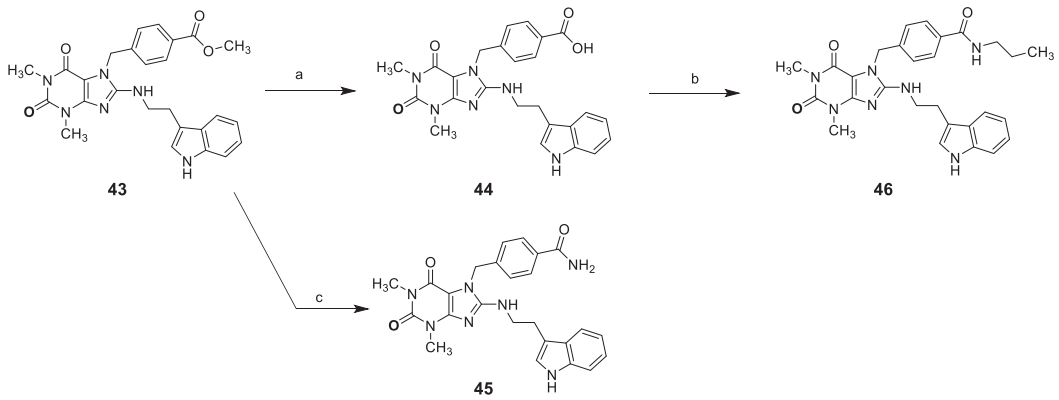

[a]Reagents and conditions: (a) LiOH·H_2O, THF, RT, overnight (yield: 64%); (b) 1-propylamine, TEA, T3P, DCM, RT, overnight (yield: 5%); (c) NH_4Cl, NH_4OH, 100 °C, 3 days (yield: 35%).

Scheme 5. Synthesis of *N*7-Substituted Xanthine Derivatives 54 and 55[a]

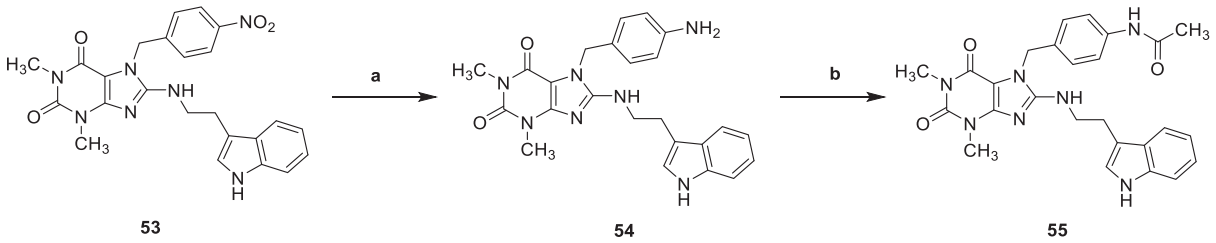

[a]Reagents and conditions: (a) Pd/C, H_2, methanol, RT, 7 h (yield: 39%); (b) acetic anhydride, DCM, RT, 1 h (yield 4%).

Scheme 6. Synthesis of the *N*3-Substituted Xanthine Derivatives 74−83[a]

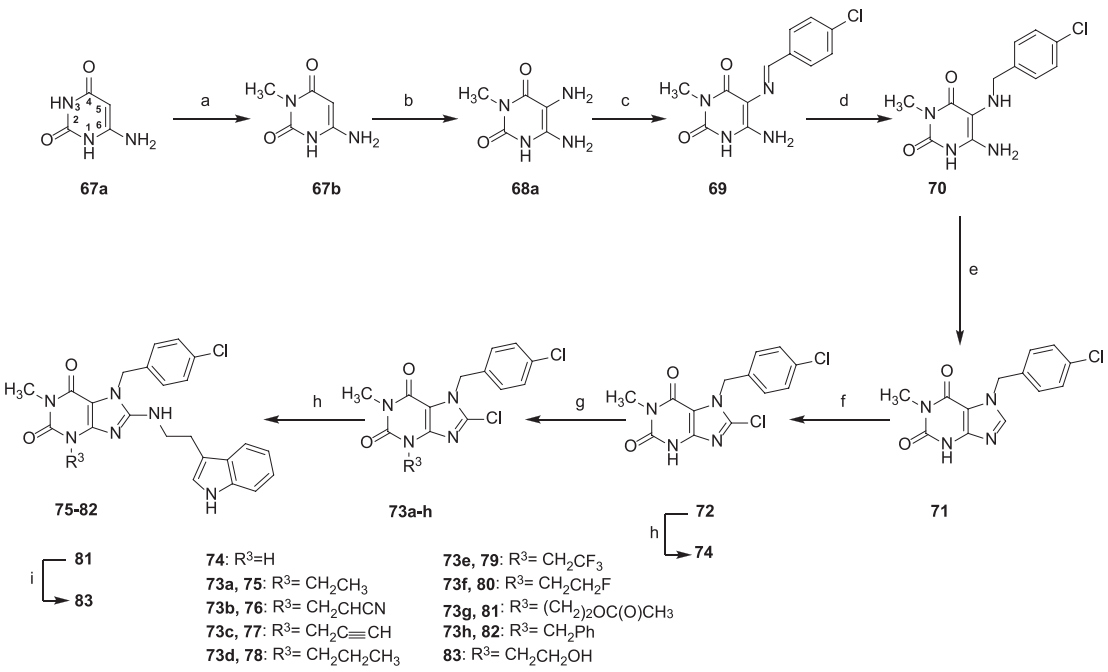

[a]Reagents and conditions: (a) Methyl iodide, $(NH_4)_2SO_4$, HMDS (yield: 71%); (b) (i) aq AcOH/$NaNO_2$, (ii) $Na_2S_2O_4$, NH_4OH (yield: 77%); (c) 4-chlorobenzaldehyde, CH_3CO_2H, H_2O (yield: 75%); (d) $NaBH_3CN$, CH_3CO_2H (yield: 70%); (e) triethyl orthoformate, 145 °C, 5 h (yield: 92%); (f) *N*-chlorosuccinimide, THF, RT, 16 h (yield: 81%); (g) K_2CO_3, DMF, alkyl or arylalkyl halide, RT, 18 h; (h) tryptamine, DIPEA, NMP, 145 °C, 18 h (yield: 12−65%); (i) KOH, MeOH, 65 °C, 18 h (yield: 63%).

Schemes 2−6 (modification at the *N*7-position), and Scheme 7 (modification at the *N*3-position). Moreover, to probe the

https://doi.org/10.1021/acs.jmedchem.3c02423
J. Med. Chem. 2024, 67, 9896−9926

Journal of Medicinal Chemistry pubs.acs.org/jmc Article

Scheme 7. Synthesis of the *N*3-Substituted Xanthine Derivative 75[a]

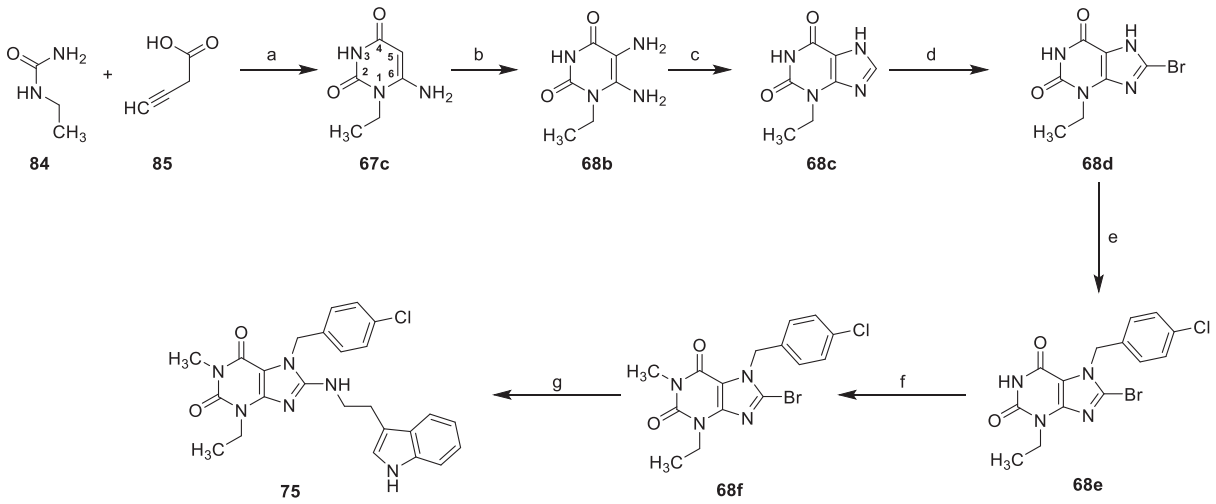

[a]Reagents and conditions: (a) $(CH_3CO)_2O$, AcOH (yield: 38%); (b) (i) $NaNO_2$, (ii) $Na_2S_2O_4$ (yield: 77%); (c) HCOOH, NaOH (yield: 79%); (d) HBr, $NaClO_3$ (yield: 82%); (e) 1-chloro-4-(chloromethyl)benzene, DIPEA (yield: 73%); (f) methyl iodide, K_2CO_3 (yield: 68%); (g) tryptamine, TEA, propanol, microwave, 300 W, 140 °C, 10 bar, 1 h (yield: 46%).

Scheme 8. Synthesis of Compounds 87−91[a]

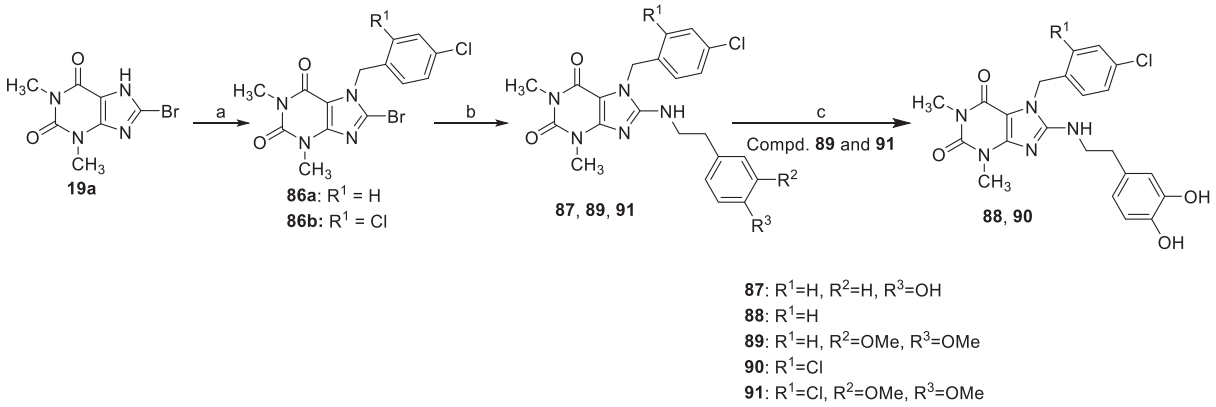

87: R^1=H, R^2=H, R^3=OH
88: R^1=H
89: R^1=H, R^2=OMe, R^3=OMe
90: R^1=Cl
91: R^1=Cl, R^2=OMe, R^3=OMe

[a]Reagents and conditions: (a) K_2CO_3, benzyltriethylammonium chloride (TEBA), benzyl chloride, acetone, 15 h reflux (yield: 51−68%); (b) phenylethylamine derivative, 2-methoxyethanol, reflux 11−16 h (yield: 23−35%); (c) 48% HBr, reflux, 30 min (yield: 24−43%).

necessity of the indolyl moiety in combination with the new bicyclic xanthine scaffold, we replaced the indolyl residue with different aromatic residues (see Scheme 8 and Table 2).

Syntheses. The target compounds were synthesized by multistep reaction sequences applying previously published procedures. Compounds **10** and **12−18** were prepared from commercially available theobromine (**7**) which was subjected to bromination at the 8-position.[35] The resulting 8-bromotheobromine (**8**) was alkylated at the *N*1-position using the appropriate alkyl or arylalkyl halide in dimethylformamide (DMF) in the presence of potassium carbonate, yielding **9a−g**. The final products **10** and **12−18** were prepared by substitution of the 8-bromotheobromine derivatives **8** and **9a−g** with the commercially available tryptamine in propanol under microwave irradiation in a closed vessel with controlled power, temperature, and pressure.

Next, we introduced a variety of substituents at the xanthine *N*7-position (Schemes 2−5). 8-Chlorotheophylline (**19a**) or 8-bromotheophylline (**19b**) was used as a starting material. *N*7-Alkylation was performed in DMF with various alkyl or arylalkyl bromides in the presence of potassium carbonate as a base. *N*7-Substituted 8-bromo- or 8-chloro-theophylline derivatives **20a−n** and **29a−ac** underwent a reaction with tryptamine in propanol in the presence of a base. This reaction was carried out using either microwave irradiation or conventional heating to yield the final products **11**, **21−28**, **31−43**, **47−60**, **61−66** (Scheme 2).

Demethylation of **29k** by BBr_3 in DMF led to the corresponding *p*-hydroxybenzyl derivative **29l** (Scheme 3). Initially, we were aiming to alkylate the *p*-hydroxy moiety of **29l**, based on literature.[36] Thus, **29l** was reacted with 1-bromo-2-fluoroethane in the presence of Cs_2CO_3 as a base in DMF. These turned out to be very harsh conditions since many undesired products were formed, the most abundant one being **29m**. This compound was formed by the alkylation of the debenzylated xanthine derivative with an excess of 1-bromo-2-fluoroethane. The side-product **29m** was isolated and further reacted with tryptamine to yield **30** (Scheme 3).

The benzoic acid methyl ester **43** was hydrolyzed by the addition of lithium hydroxide in tetrahydrofuran (THF) to obtain carboxylic acid **44** (Scheme 4). Compound **44** was subsequently treated with 1-propylamine in the presence of the coupling reagent propanephosphonic acid anhydride (T3P) and

https://doi.org/10.1021/acs.jmedchem.3c02423
J. Med. Chem. 2024, 67, 9896−9926

Journal of Medicinal Chemistry pubs.acs.org/jmc Article

triethylamine (TEA) in dichloromethane (DCM) furnishing amide **46**. Compound **43** was also directly reacted with ammonium hydroxide in the presence of ammonium chloride at 100 °C to yield carboxamide derivative **45** (Scheme 4).

The syntheses of the aniline derivative **54** and the anilide **55** (Scheme 5) were carried out starting from nitrobenzyl derivative **53**. Reductive hydrogenation of **53** in the presence of Pd on carbon yielded the *p*-aminobenzyl derivative **54**, which was subsequently acetylated with acetic anhydride in DCM furnishing **55** (Scheme 5).

The synthesis of xanthine derivatives bearing different *N*3-substituents was performed according to Scheme 6. Commercially available 6-aminouracil (**67a**) was subjected to selective methylation with methyl iodide at the *N*3-position after silylation with hexamethyldisilazane (HMDS) to provide **67b**.[37] Subsequent nitrosylation at C5 with sodium nitrite in aqueous acetic acid followed by reduction with sodium dithionite in the presence of ammonium hydroxide led to **68a**. The reaction of **68a** with 4-chlorobenzaldehyde in the presence of acetic acid yielded imine **69**, which was subsequently reduced using sodium cyanoborohydride to yield the 5-benzylaminouracil derivative **70.** Subsequently, ring closure reaction with triethyl orthoformate led to xanthine **71.** Chlorination at *C*8 was achieved with *N*-chlorosuccinimide (NCS) in THF resulting in the key intermediate **72**. For the synthesis of the target compounds **74**−**83**, compound **72** was alkylated at *N*3 with various (ar)alkyl halogenides in the presence of K_2CO_3 to afford 1,3,7,8-tetrasubstituted xanthine derivatives **73a**−**h**. Coupling of **72**, and **73a**−**h**, respectively, with tryptamine yielded the final products **74**−**83** (Scheme 6). Compound **83** was obtained by hydrolysis of **81** using potassium hydroxide in methanol at 65 °C for 18 h.

*N*3-Ethyl-substituted xanthine derivative **75** was obtained by an alternate reaction sequence (see Scheme 7). Condensation of *N*-ethylurea (**84**) and cyanoacetic acid (**85**) yielded uracil derivative **67c**. Nitrosation followed by reduction provided diaminouracil derivative **68b**. After ring closure by condensation with formic acid and subsequent condensation in the presence of sodium hydroxide, xanthine **68c** was isolated. Subsequent bromination at the 8-position afforded **68d**. Alkylation at *N*7 was performed with *p*-chlorobenzyl bromide to provide **68e,** which was subsequently methylated at *N*1 yielding the tetrasubstituted xanthine derivative **68f**. Finally, product **75** was obtained by a reaction of **68f** with tryptamine under microwave irradiation.

Next, we replaced the indolyl moiety with aromatic residues, which were introduced as depicted in Scheme 8. The intermediate 8-bromo-7-(4-chlorobenzyl)-1,3-dimethylxanthine derivatives **86a**−**86b** were obtained by alkylation reaction of the commercially available 8-bromotheophylline (**19a**) with the appropriate benzyl bromide derivatives. The target compounds **87**, **89**, and **91** were synthesized by the substitution of **86a**−**86b** with the appropriate phenylethylamine derivative in 2-methoxyethanol as a solvent. Demethylation of **89** and **91** using an aqueous hydrogen bromide solution afforded the corresponding catechol derivatives **88** and **90**.

Altogether, 68 new final products were prepared by multistep reactions. The structures and purities were confirmed by ^{1}H and ^{13}C NMR spectroscopy, in addition to HPLC-UV/MS analysis. Purities of all products were determined by HPLC-UV at 220−400 nm and confirmed to be at least 95% for all final products.

Biological Evaluation. The new 8-(indolylethylamino)-xanthine and 8-(phenylethylamino)xanthine derivatives were investigated to assess their agonistic activity at human GPR18 and to study their structure−activity relationships. In our previous study, we had reported on the first nonlipid-like GPR18 agonists, tricyclic xanthine derivatives (compounds **5** and **6**) representing novel agonists of the human GPR18 with EC_{50} values of 0.562 μM and 0.454 μM, respectively.[32] In the present study, we investigated a newly designed indolylethylamino-xanthine scaffold. The employed β-arrestin recruitment assay, based on a β-galactosidase complementation assay, was shown to be highly specific for GPR18.[38] This is because GPR18 was C-terminally fused with a small part of β-galactosidase (termed ProLink), while the complementary part of the β-galactosidase was fused with β-arrestin-2. Upon GPR18 activation, β-arrestin is recruited to the C-terminal domain of GPR18, and the β-galactosidase reassembles to become functional resulting in a luminescence signal in the presence of a suitable substrate (Figure S1). This assay is robust and reliable, while false positives are rare.[26,38−40] All compounds were initially screened at a concentration of 10 μM. For the test compounds that showed receptor activation of greater than 50%, full concentration−response curves were determined to calculate EC_{50} values. For this purpose, THC was used as a standard GPR18 agonist, and data were normalized to its effect at a high concentration of 10 μM. For the compounds that showed less than 50% activation, potential antagonistic activity was measured. To confirm that the effect observed by the compounds was mediated by GPR18 activation, all compounds were additionally tested at the related orphan receptor GPR55, activated by lysophosphatidylinositol (LPI), in the same assay system.[41] Selectivity versus cannabinoid receptors was assessed by radioligand binding assays using membrane preparations of Chinese hamster ovary cells (CHO-K1) stably expressing either human CB_1 or CB_2 receptors. Subsequently, selected potent compounds were additionally tested in CHO-β-arrestin cell lines stably expressing human GPR183, human CB_1, or human CB_2 receptors, respectively. GPR183 was selected due to its close phylogenetic relationship with GPR18, which is demonstrated by the shared chromosomal origin and similar expression patterns.[3,42] Furthermore, GPR183 exhibits the highest amino acid similarity with GPR18 (37% sequence similarity) among class A GPCRs. The activation of GPR183 using the established cell line was confirmed using its cognate agonist 7α,25-dihydroxycholesterol.[43] Potency (EC_{50}) and efficacy (maximum response compared to the standard agonist at the corresponding receptor) of each potent compound was determined. In order to study potential species differences, we additionally examined all compounds at mouse GPR18 (mGPR18) using the same assay system.

Standard Compounds Previously Published as GPR18 Agonists. Initially, we tested several previously published GPR18 agonists in our test system for comparison. In addition to the tricyclic xanthine derivatives PSB-KD107 (**5**) and PSB-KD477 (**6**), the physiological lipids NAGly (**1**) and resolvin D2 (**3**), and the cannabinoids THC (**3**) Abn-CBD (**2**) were studied. Besides **5** and **6,** only THC (**3**) was confirmed to activate human GPR18, while Abn-CBD and resolvin D2 did not significantly activate the receptor at concentrations ranging from 0.0001 to 10 μM. Abn-CBD (**2**), which had previously been reported to stimulate GPR18 and to promote cell migration[18,44] was unable to activate GPR18, which is in agreement with findings reported by another research group.[44] Interestingly, we observed that **2** reduced the basal activity of human GPR18, an effect that was less pronounced at mouse GPR18, and which was not seen at other related orphan GPCRs, namely GPR55 (see Table S1)

https://doi.org/10.1021/acs.jmedchem.3c02423
J. Med. Chem. 2024, 67, 9896−9926

Journal of Medicinal Chemistry pubs.acs.org/jmc Article

Table 1. Potencies of 8-(Indolylethylamino)xanthine Derivatives as Agonists of Human and Mouse GPR18

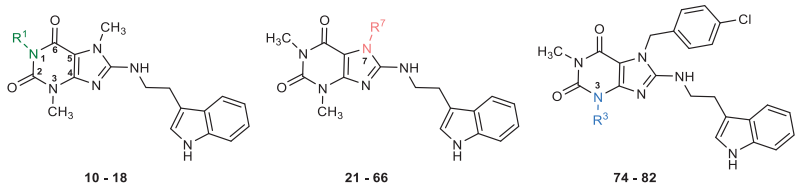

10 - 18 21 - 66 74 - 82

	R^1 or R^7 or R^3		β-Arrestin recruitment assay	
			Human GPR18 Agonistic activity (% activation)[a] *[Efficacy][b]*	Mouse GPR18 Agonistic activity (% activation)[a] *[Efficacy][b]*
			EC_{50} ± SEM (μM)	EC_{50} ± SEM (μM)
	Previously proposed and published GPR18 agonists			
1	**NAGly (1)**	For structure see Fig. 1	**>10** (10%)[c]	**>10** (4%)
2	**Abnormal cannabidiol (2)**	For structure see Fig. 1	**>10** (-50%)[c]	**>10** (-5%)
3	**THC (3)**	For structure see Fig. 1	**3.37** ± 1.19[c] *[100%]*	**>10** (10%)
4	**Resolvin D2 (4)**	For structure see Fig. 1	**>10** (26%)	**>10** (4%)
5	**PSB-KD107 (5)**	For structure see Fig. 1	**0.562** ± 0.113[c] *[191%]*	**1.78** ± 0.62 *[104%]*
6	**PSB-KD477 (6)**	For structure see Fig. 1	**0.454** ± 0.156[c] *[171%]*	**0.583** ± 0.214 *[111%]*
	Substitution of the *N*1-position (R^1)			
10		H	**>10** (14%)	**>10** (12%)
11			**0.902** ± 0.148 *[132%]*	**2.97** ± 1.02 *[132%]*
12			**>10** (30%)	**>10** (35%)
13		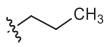	**>10** (15%)	**>10** (23%)
14		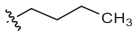	**>10** (11%)	**>10** (11%)
15			**>10** (18%)	**>10** (19%)
16		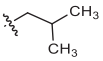	**>10** (5%)	**>10** (16%)
17		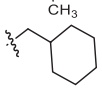	**>10** (13%)	**>10** (24%)
18		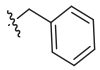	**>10** (37%)	**>10** (24%)
	Substitution of the *N*7-position (R^7)			
21			**0.190** ± 0.043 *[113%]*	**0.379** ± 0.055 *[85%]*
22			**0.196** ± 0.059 *[127%]*	**0.299** ± 0.109 *[81%]*
23		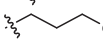	**0.151** ± 0.045 *[103%]*	**0.207** ± 0.038 *[111%]*
24		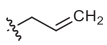	**0.169** ± 0.041 *[80%]*	**0.379** ± 0.079 *[84%]*
25		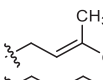	**>10** (30%)	**>10** (37%)
26		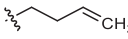	**0.111** ± 0.015 *[89%]*	**0.447** ± 0.119 *[80%]*
27		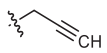	**0.247** ± 0.036 *[90%]*	**0.318** ± 0.033 *[108%]*
28		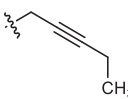	**0.254** ± 0.010 *[90%]*	**0.371** ± 0.102 *[102%]*

https://doi.org/10.1021/acs.jmedchem.3c02423
J. Med. Chem. 2024, 67, 9896−9926

Journal of Medicinal Chemistry pubs.acs.org/jmc Article

Table 1. continued

	R^1 or R^7 or R^3		β-Arrestin recruitment assay	
			Human GPR18 Agonistic activity (% activation)[a] *[Efficacy][b]*	Mouse GPR18 Agonistic activity (% activation)[a] *[Efficacy][b]*
			EC_{50} ± SEM (μM)	EC_{50} ± SEM (μM)
	Substitution of the *N*7-position (R^7)			
30			**1.39** ± 0.60 *[43%]*	**2.64** ± 0.05 *[85%]*
31		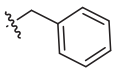	**0.149** ± 0.056 *[134%]*	**0.194** ± 0.053 *[116%]*
32		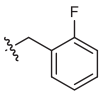	**0.137** ± 0.032 *[123%]*	**0.128** ± 0.018 *[106%]*
33		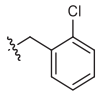	**0.0604** ± 0.0122 *[169%]*	**0.157** ± 0.007 *[96%]*
34		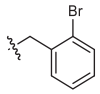	**0.189** ± 0.027 *[148%]*	**0.156** ± 0.013 *[92%]*
35		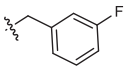	**0.115** ± 0.046 *[139%]*	**0.301** ± 0.046 *[106%]*
36	**(PSB-KK1448)**	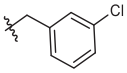	**0.0711** ± 0.0174 *[85%]*	**0.220** ± 0.062 *[134%]*
37		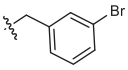	**0.101** ± 0.013 *[134%]*	**0.180** ± 0.033 *[101%]*
38		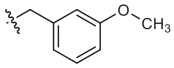	**0.166** ± 0.024 *[122%]*	**0.245** ± 0.030 *[108%]*
39		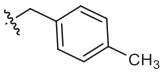	**0.0246** ± 0.051 *[117%]*	**0.0463** ± 0.0058 *[95%]*
40		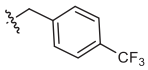	**0.136** ± 0.017 *[111%]*	**0.216** ± 0.066 *[112%]*
41		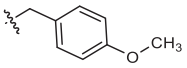	**0.138** ± 0.013 *[121%]*	**0.171** ± 0.013 *[96%]*
42		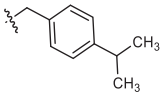	**0.352** ± 0.096 *[111%]*	**0.150** ± 0.019 *[87%]*
43		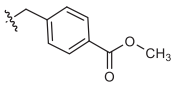	**0.469** ± 0.074 *[125%]*	**0.488** ± 0.083 *[93%]*
44		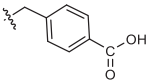	**>10** (8%)	**>10** (7%)
45		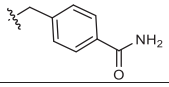	**3.60** ± 0.19 *[88%]*	**4.00** ± 0.611 *[87%]*

https://doi.org/10.1021/acs.jmedchem.3c02423
J. Med. Chem. 2024, 67, 9896−9926

Journal of Medicinal Chemistry pubs.acs.org/jmc Article

Table 1. continued

	R^1 or R^7 or R^3		β-Arrestin recruitment assay	
			Human GPR18 Agonistic activity (% activation)[a] *[Efficacy][b]*	Mouse GPR18 Agonistic activity (% activation)[a] *[Efficacy][b]*
			EC_{50} ± SEM (μM)	EC_{50} ± SEM (μM)
	Substitution of the *N*7-position (R^7)			
46		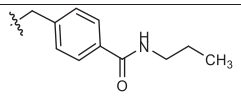	**1.41** ± 0.29 *[98%]*	**1.27** ± 0.31 *[147%]*
47		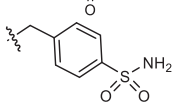	**6.64** ± 2.68 *[70%]*	**10.9** ± 0.8 *[95%]*
48		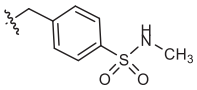	**3.67** ± 1.07 *[116%]*	**3.63** ± 0.24 *[99%]*
49		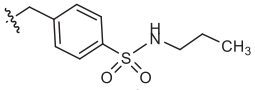	**0.584** ± 0.150 *[50%]*	**1.30** ± 0.05 *[80%]*
50	**(PSB-KK1445)**	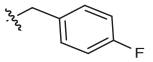	**0.0454** ± 0.081 *[84%]*	**0.124** ± 0.056 *[79%]*
51	**(PSB-KK1415)**	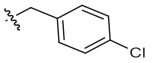	**0.0191** ± 0.0034 *[141%]*	**0.0541** ± 0.0241 *[100%]*
52		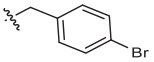	**0.0724** ± 0.547 *[65%]*	**0.058** ± 0.008 *[105%]*
53		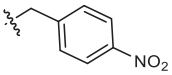	**0.0426** ± 0.0155 *[98%]*	**0.280** ± 0.194 *[155%]*
54		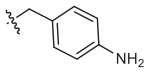	**0.261** ± 0.041 *[112%]*	**0.241** ± 0.032 *[110%]*
55		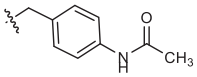	**0.218** ± 0.008 *[109%]*	**0.281**± 0.025 *[124%]*
56			**0.347** ± 0.0136 *[45%]*	**0.559** ± 0.050 *[101%]*
57		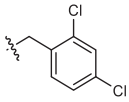	**0.0642** ± 0.0308 *[72%]*	**0.244** ± 0.026 *[104%]*
58		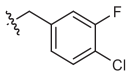	**0.0801** ± 0.0131 *[110%]*	**0.121** ± 0.029 *[102%]*
59		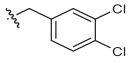	**0.0741** ± 0.023 *[82%]*	**0.0900** ± 0.0301 *[102%]*
60		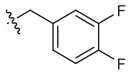	**0.142** ± 0.019 *[113%]*	**0.161** ± 0.039 *[122%]*
61		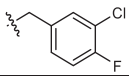	**0.193** ± 0.028 *[110%]*	**0.251**± 0.042 *[122%]*

https://doi.org/10.1021/acs.jmedchem.3c02423
J. Med. Chem. 2024, 67, 9896−9926

Journal of Medicinal Chemistry pubs.acs.org/jmc Article

Table 1. continued

	R^1 or R^7 or R^3		β-Arrestin recruitment assay	
			Human GPR18 Agonistic activity (% activation)[a] *[Efficacy][b]*	Mouse GPR18 Agonistic activity (% activation)[a] *[Efficacy][b]*
			EC_{50} ± SEM (μM)	EC_{50} ± SEM (μM)
	Substitution of the *N*7-position (R^7)			
62		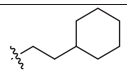	**0.102** ± 0.024 *[103%]*	**0.127** ± 0.013 *[100%]*
63		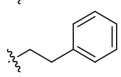	**0.442** ± 0.152 *[155%]*	**0.288** ± 0.071 *[108%]*
64	(PSB-KK1418)	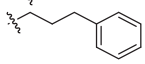	**0.120** ± 0.027 *[176%]*	**0.223** ± 0.043 *[104%]*
65		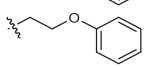	**0.229** ± 0.048 *[64%]*	**0.334** ± 0.080 *[88%]*
66		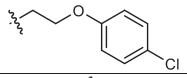	**0.417** ± 0.173 *[64%]*	**0.444** ± 0.084 *[84%]*
	Substitution of the *N*3-position (R^3)			
74		H	**0.206** ± 0.023 *[100%]*	**0.290** ± 0.019 *[93%]*
75			**0.0950** ± 0.0069 *[85%]*	**0.297** ± 0.037 *[91%]*
76	(PSB-1846)		**1.22** ± 0.17 *[70%]*	**0.981** ± 0.242 *[97%]*
77		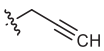	**>10** (18%)	**>10** (14%)
78		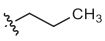	**>10** (45%)	**>10** (46%)
79			**0.486** ± 0.072 *[75%]*	**0.711** ± 0.101 *[83%]*
80			**0.351** ± 0.017 *[78%]*	**0.398** ± 0.089 *[93%]*
82	(PSB-1833)		**>10** (4%)	**>10** (4%)
83		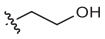	**1.63** ± 0.13 *[80%]*	**1.20** ± 0.54 *[103%]*

[a]Compounds were initially tested at a concentration of 10 μM. Effects were normalized to the signal induced by 10 μM THC (EC_{80} for human GPR18) or 0.3 μM of **51** (EC_{80} for mouse GPR18) set as 100%. For compounds that activated GPR18 by more than 50%, dose−response curves were recorded. EC_{50} values are shown in bold. [b]Efficacy relative to the maximal effect of the standard agonist (30 μM THC for human GPR18; 3 μM of **51** for mouse GPR18) set at 100%. [c]Data from Schoeder et al.[32]

and GPR183 (no effect at 10 μM, data not shown). This implies that the decrease in basal activity induced by **2** was specific for GPR18. When tested as an antagonist, **2** was able to inhibit THC-induced GPR18 activation by up to 42% (at 10 μM). These results imply that Abn-CBD may act as an inverse agonist at GPR18.

Moreover, we assessed GPR18 activation by RvD2 (**4**) (Figure S2A,B). Chiang et al. had reported activation of the human GPR18 by **4** with a significant effect at 10 nM in a β-arrestin recruitment assay, and a subnanomolar EC_{50} value.[7] In our hands, RvD2 did not show GPR18 activation in concentrations up to 10 μM.[32] An explanation could be that activation might only be observed at low concentrations, and not at high concentrations due to potential interfering effects.[45] However, we could not observe any effects of RvD2 on GPR18 tested in concentrations ranging from 0.1 nM to 10,000 nM, neither at the human nor the mouse receptor, using stock solutions of RvD2 either in DMSO or in ethanol (Figure S2A). Since RvD2 may be rapidly degraded, we assessed its purity by LC-MS analysis, which was confirmed to be >95% (Figures S3 and S4).

In Table S1 all determined activities are collected, and Hill slopes for concentration-activation curves were calculated, which ranged from 1.0 to 2.2 for mouse GPR18, and from 0.9 to 2.3 for the human receptor. Apart from a few exceptions, mostly for compounds showing moderate potency, the Hill slope did not significantly differ from unity (see Table S1).

Structure−Activity Relationships at Human GPR18. The focus of the present study was on investigating the substitution pattern of the xanthine core, since we assumed, based on previous studies, that an indolyl substituent may be important for interaction with GPR18.[31,32,46] Extension of the 6-membered tetrahydropyrimidine ring in the previously published tricyclic xanthine derivative **5** (EC_{50} 0.562 μM) to a 7-membered ring in compound **6** had slightly increased potency (EC_{50} 0.454 μM). Thus, there might be space in the pocket where that part of the molecule binds. The tricyclic structure is rather rigid and does not provide straightforward opportunities for substitution. Instead, we extensively varied the substitution

https://doi.org/10.1021/acs.jmedchem.3c02423
J. Med. Chem. 2024, 67, 9896−9926

Journal of Medicinal Chemistry pubs.acs.org/jmc Article

Table 2. Potencies of 8-(Phenylethylamino)-Substituted Xanthine Derivatives at GPR18 and GPR55 in Comparison to Corresponding 8-(Indoylethylamino)-Substituted Xanthines, Determined in β-Arrestin Recruitment Assays

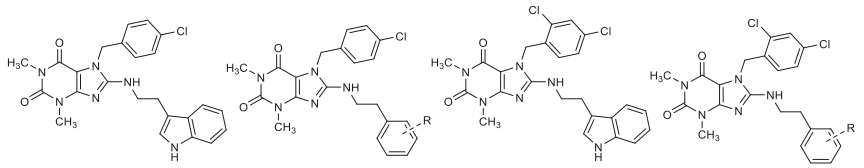

51 87-89 57 90-91

		R	Human GPR18		Human GPR55	
			Agonistic activity (% activation)[a] *[Efficacy]*[b]	**Antagonistic activity** (% inhibition)[c]	**Agonistic activity** (% activation)[a] *[Efficacy]*[b]	**Antagonistic activity** (% inhibition)[c]
			EC_{50} ± SEM (μM)	**IC_{50}** ± SEM (μM)	**EC_{50}** ± SEM (μM)	**IC_{50}** ± SEM (μM)
51		See structure above	**0.0191** ± 0.0034 *[141%]*	n.d[d]	**>10** (8%)	**>10** (43%)
87		4-OH	**>10** (3%)	**>10** (19%)	**>10** (15%)	**>10** (22%)
88		3,4-OH	**>10** (4%)	**>10** (32%)	**>10** (3%)	**>10** (31%)
89		3,4-OCH_3	**>10** (4%)	**>10** (7%)	**>10** (-1%)	**>10** (-4%)
57		See structure above	**0.0642** ± 0.0308 *[72%]*	n.d	**>10** (-5%)	**>10** (-4%)
90		3,4-OH	**>10** (-10%)	**>10** (31%)	**>10** (-14%)	**>10** (38%)
91		3,4-OCH_3	**>10** (1%)	**>10** (13 %)	**>10** (2%)	**>10** (29%)

[a]Compounds were tested at a concentration of 10 μM. Effects were normalized to the signal induced by 10 μM THC (EC_{80} for human GPR18) or 1 μM of LPI (EC_{80} for human GPR55) set as 100%. EC_{50} values are shown in bold. [b]Efficacy relative to the maximal effect of the standard agonist (human GPR18, 30 μM THC; GPR55, 10 μM LPI) set at 100%. [c]Percent inhibition of agonist effect (human GPR18, 10 μM THC; GPR55, 1 μM LPI) by test compound at 10 μM. [d]n.d = not determined.

pattern of the xanthine core at the *N*7-position. Additionally, we performed modifications at the *N*1- and the *N*3-position, respectively) to explore the structure−activity relationships of this new bicyclic class of GPR18 agonists based on a xanthine scaffold (see Table 1). The optimal residues in the tricyclic series had been methyl in the *N*1- as well as in the *N*3- position.[32]

As a first series of derivatives, we investigated compounds substituted at the *N*1-position either with different alkyl residues (**10**−**17**) or with a benzyl group (**18**). The *N*1-unsubstituted 3,7-dimethyl derivative **10** was inactive, while the 1-methyl derivative, 8-(3-indoylethylamino)caffeine (**11**), showed an EC_{50} value of 0.902 μM. This indicated that substitution is required at the *N*1-xanthine position, as in the tricyclic lead compound **5**, which is also methyl-substituted at the corresponding position. Replacement of the methyl group by larger substituents such as ethyl (**12**), propyl (**13**), or butyl (**14**) abolished GPR18 activity (EC_{50} > 10 μM), indicating a limited size of the binding pocket at this position. These inactive compounds were further tested as antagonists but did not inhibit THC-induced GPR18 activation, proving that they are too large to bind to the receptor.

Next, we explored the *N*7-position of the xanthine scaffold while retaining methyl groups at the *N*1- and *N*3-position. First, we investigated the effects of linear and branched aliphatic residues. Ethyl substitution (in **21**, EC_{50} 0.190 μM) showed increased potency compared to the 7-methyl-substituted compound **11** (EC_{50} 0.902 μM), and was also more potent than the tricyclic lead compound **5** (EC_{50} 0.562 μM). However, increasing the length of the alkyl chain did not further increase agonistic activity (propyl derivative **22**, EC_{50} 0.196 μM), or at least not significantly (butyl derivative **23**, EC_{50} 0.151 μM). We then investigated the effects of branched aliphatic and unsaturated substituents at this position. Allyl-substituted derivative **24** (EC_{50} 0.169 μM) and butenyl derivative **26** (EC_{50} 0.111 μM) showed potency comparable to that of the propyl derivative **22** (EC_{50} 0.196 μM) while the propargyl derivative **27** was slightly less potent (EC_{50} 0.247 μM). Interestingly, the introduction of a terminal double bond (in **24** and **26**) or a triple bond (in **27**), resulting in an increased electron density, led to reduced efficacy (80 and 90% for **24** and **27**, respectively, as compared to 127% for the propyl derivatives **22**). If the propargyl group (in **27**) was extended to a pent-3-ynyl residue (in **28**), potency and efficacy were unaltered. The fluoroethyl derivative **30** was 7-fold less potent compared to the nonfluorinated ethyl derivative **21**. This may indicate that high electron density close to the *N*7-xanthine position is not well tolerated. A branched 3-methyl-2-butenyl residue (in **25**) led to an almost inactive compound.

In the next step, the effects of introducing aromatic residues were evaluated. Benzyl substitution (in **31**, EC_{50} 0.149 μM) led to increased potency compared to methyl substitution in **11** (EC_{50} 0.902 μM) resulting in a similarly potent agonist as the butyl-substituted derivative **23** (EC_{50} 0.151 μM), but endowed with higher efficacy (134% vs 103%). Since benzyl derivative **31** showed relatively high potency as well as efficacy, it was selected as a new lead compound, and various substituents on the benzyl residue were explored.

The introduction of a fluorine atom at the *ortho*-position of the phenyl ring **32** (EC_{50} 0.137 μM) did not have a significant impact on potency compared to the unsubstituted benzyl derivative **31** (EC_{50} 0.149 μM). However, 2-chlorobenzyl substitution (**33**) resulted in increased potency as well as efficacy (EC_{50} value of 0.0604 μM, 169% maximal activation). Replacement by the larger bromine in **34** reduced potency (EC_{50} 0.189 μM). Various substituents at the *meta*-position, namely *m*-F (**35**, EC_{50} 0.115 μM), *m*-Br (**37**, EC_{50} 0.101 μM), or *m*-OCH_3 (**38**, EC_{50} 0.166 μM), resulted in potencies comparable to that of unsubstituted benzyl derivative **31**

https://doi.org/10.1021/acs.jmedchem.3c02423
J. Med. Chem. 2024, 67, 9896−9926

Journal of Medicinal Chemistry pubs.acs.org/jmc Article

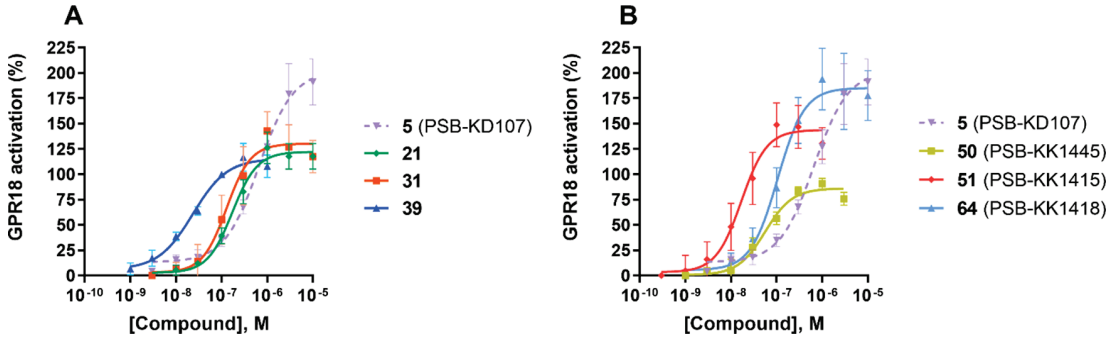

Figure 3. (A) Concentration-dependent activation of human GPR18 by **5** (EC_{50} 0.562 μM), **21** (EC_{50} 0.190 μM), **31** (EC_{50} 0.149 μM) and **39** (EC_{50} 0.0246 μM). (B) Concentration-dependent activation of human GPR18 by **5** (EC_{50} 0.562 μM), **50** (EC_{50} 0.0454 μM), **51** (EC_{50} 0.0191 μM) and **64** (EC_{50} 0.120 μM). CHO-K1 cells recombinantly expressing human GPR18 were used for β-arrestin enzyme complementation assays. Data points represent means ± SEM of at least three independent experiments. In the absence of a physiological agonist, data were normalized to the maximum activation of GPR18 induced by THC (at 30 μM, set as 100%).

(EC_{50} 0.149 μM). An exception was for the *meta*-chloro-substituted derivative **36** (EC_{50} 0.0711 μM, which showed similar potency as the so far most potent *o*-Cl-benzyl derivative **33**. However, its efficacy was slightly lower (85% maximal effect) compared to the other *meta*-substituted 7-benzylxanthine derivatives (122−135%).

Next, we investigated substitution in the *para*-position of the phenyl ring. The introduction of a methyl group (**39**, EC_{50} 0.0246 μM) increased potency by 6-fold compared to the unsubstituted **31** (EC_{50} 0.149 μM). Bioisosteric replacement of the methyl group by trifluoromethyl in **40** (EC_{50} 0.136 μM) was less beneficial showing comparable potency to the unsubstituted benzyl derivative **31**. Increasing the size of the substituent in the *p*-methoxybenzyl derivative **41** (EC_{50} 0.138 μM), the 4-isopropylbenzyl derivative **42** (EC_{50} 0.352 μM), the 4-amidobenzyl derivative **45** (EC_{50} 3.60 μM), the 4-propylamidobenzyl derivative **46** (EC_{50} 1.41 μM) and the 4-sulfonamidobenzyl derivative **47** (EC_{50} 6.64 μM) reduced the potency.

Introducing a highly polar carboxylate function (**44**, EC_{50} > 10 μM) or an amide (**45**, EC_{50} 3.60 μM) into the *para*-position of the benzyl substituent led to a large decrease in potency. Interestingly, the substitution of the sulfonamide of **47** (EC_{50} 6.64 μM) with a propyl residue (**49**, EC_{50} 0.584 μM) partially restored potency, but decreased efficacy.

Subsequently, we investigated substitution in the *para*-position with halogen atoms, namely *p*-fluorobenzyl (**50**), *p*-chlorobenzyl (**51**), and *p*-bromobenzyl (**52**) derivatives. This resulted in a significant increase in potency at GPR18. In fact, *p*-chlorobenzyl derivative **51** (PSB-KK1415) was the most potent GPR18 agonist of the present series with an EC_{50} value of 0.0191 μM (Figure 3). The *p*-fluorobenzyl derivative **50** and the *p*-bromobenzyl derivative **52** were slightly less potent with EC_{50} values of 0.0454 and 0.0724 μM, respectively. The rank order of potency, as well as efficacy, was *p*-Cl > *p*-F > *p*-Br. The *p*-halogen-substituted benzylxanthine derivatives showed significant differences in efficacy: *p*-Cl (141% maximal effect compared to the maximal effect of THC) > *p*-F (84%) > *p*-Br (65%). A *p*-nitro-substitution was also well tolerated (**53**, EC_{50} 0.0426 μM, 98%), while an amino residue (in **54**) reduced potency by 6-fold (EC_{50} 0.261 μM, 112% efficacy). Acetylation of **54** resulting in the *p*-acetylaminobenzylxanthine derivative **55** did not alter the potency or efficacy of the compound (EC_{50} 0.218 μM, 109%).

At this point, we concluded that chloro-substitution was superior in all positions on the benzyl group, *ortho* (**33**, EC_{50} 0.0604 μM), *meta* (**36**, EC_{50} 0.0711 μM), as well as *para* (**51**, EC_{50} 0.0191 μM). Therefore, our next strategy was to combine substituents. We focused on halogen substitution since they had so far provided the highest potency. 2,6-Dichlorobenzyl substitution in compound **56** (EC_{50} 0.347 μM) reduced potency (by 6-fold) compared to the monosubstituted **33** (EC_{50} 0.0604 μM). 2,4-Dichlorobenzyl substitution in **57** was also not additive, but showed similar potency (EC_{50} 0.0642 μM) as the *ortho*-chloro derivative **33** (EC_{50} 0.0604 μM) and even reduced potency compared to the *p*-substituted compound **51** (EC_{50} 0.0191 μM). Further combinations (*p*-Cl, *m*-F; EC_{50} 0.0801, **58**), *m*, *p*-di-Cl (**59**, EC_{50} 0.0741 μM) or *m*, *p*-di-F (**60**, EC_{50} 0.142 μM), all led to reduced potency compared to the mono-*p*-chloro-substituted front-runner **51**. This indicates that the benzyl group is flexible and, for example, the *m*-Cl-benzyl derivative **36** may bind in a slightly different conformation compared to the *p*-Cl-benzyl derivative **51**, to optimally interact with the binding pocket for the chlorine atom.

Next, we explored the effects of different linkers between the xanthine core and the phenyl ring (in compounds **63**−**66**), and of a replacement of the phenyl ring. Exchange of the phenyl ring in **63** by a nonaromatic cyclohexyl ring, (**62**, EC_{50} 0.102 μM, 103% efficacy), improved potency but not efficacy. Phenylethyl (**63**, EC_{50} 0.442 μM, 155%), phenylpropyl (**64**, EC_{50} 0.120 μM, 176%) or phenoxyethyl (**65**, EC_{50} 0.229 μM, 64%) and *p*-chloro-phenoxyethyl (**66**, EC_{50} 0.417 μM, 64%) residues all maintained similar potency as the unsubstituted benzyl derivative, but different efficacies were observed. The following rank order of efficacy was phenylpropyl (**64**, 176%) > phenylethyl (**63**, 155%) > cyclohexyl (**62**, 103%) > phenoxyethyl (**65**, 64%) ≈ *p*-chlorophenoxyethyl (**66**, 64%). While the *p*-chlorobenzyl derivative **51** (PSB-KK1415) displayed the highest agonistic potency at human GPR18, the phenylpropyl derivative **64** (PSB-KK1418) behaved as the most efficacious agonist. This implies that at the *N*7-position of the xanthine core, a lipophilic residue is important for high potency, and the nature of the substituent has a significant effect on the compound's efficacy. Some flexibility seems to be required (see, for example, **62** and **63**), and also electronic effects appear to play an important role (see, for example, **64** and **65**).

After settling on the 4-chlorobenzyl residue (see compound **51**) as the optimal substituent at the *N*7-position, we next modified the *N*3-position by introducing various aliphatic and

https://doi.org/10.1021/acs.jmedchem.3c02423
J. Med. Chem. 2024, 67, 9896−9926

Journal of Medicinal Chemistry pubs.acs.org/jmc Article

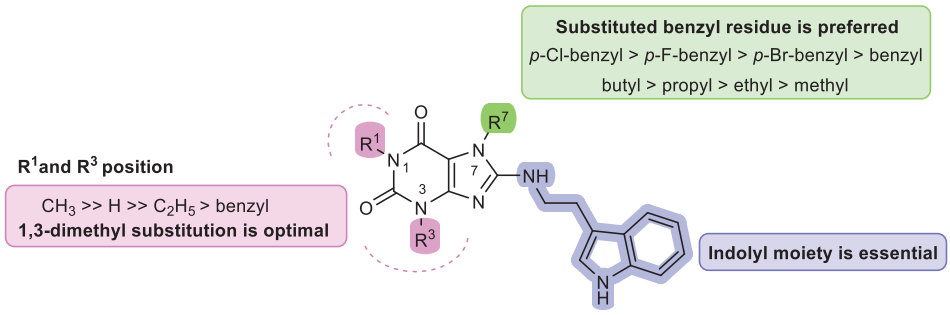

Figure 4. Structure–activity relationships of 8-substituted xanthine derivatives as GPR18 agonists.

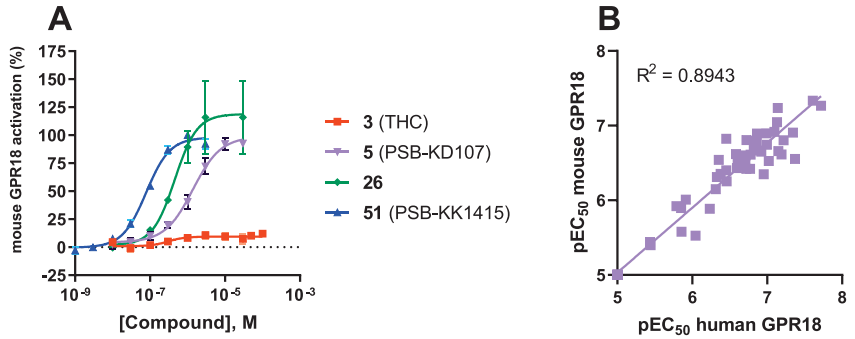

Figure 5. (A) Concentration-dependent activation of mouse GPR18 by **3** (THC), **5** (PSB-KD107, EC_{50} 1.78 μM), **26** (EC_{50} 0.447 μM), and **51** (EC_{50} 0.0541 μM) in CHO-K1 cells recombinantly expressing mouse GPR18, determined in β-arrestin enzyme complementation assays (see Table S1 for details). Data points represent means ± SEM of at least three independent experiments. All data were normalized to the maximum activation of GPR18 by **51** (at 3 μM). (B) Correlation plot between pEC_{50} values of indolylethylaminoxanthine derivatives at human GPR18 and at mouse GPR18 (R^2 = 0.8943).

aromatic residues (in **74**–**82**). Replacing the methyl group at the *N*3-position by hydrogen (in **74**, EC_{50} 0.206 μM, 100%) decreased potency by 11-fold compared to **51** (EC_{50} 0.0191 μM, 141%). Introducing longer residues such as ethyl (**75**, EC_{50} 0.0950 μM, 85%) or propyl (**78**, EC_{50} > 10 μM) also reduced potency. Both, the introduction of more polar residues, for example, propionitrile **76** (EC_{50} 1.22 μM, 70%) or hydroxypropyl (**83**, EC_{50} 1.63 μM, 80%), and an increase in the size of the substituent leading to benzyl derivative (**82**, EC_{50} > 10 μM) were not well tolerated by GPR18. Introducing a small halogen-substituted alkyl group, difluoroethyl (**71**) or fluoroethyl (**80**), neither improved potency nor efficacy compared to the *N*3-methyl-substituted xanthine derivative **51**. Thus, the small and lipophilic methyl group is superior compared to other substituents at the *N*3-position.

In the next step, we investigated the role of the indolylethylamino moiety by replacing it with different aromatic rings (compounds **87**–**91**). Interestingly, none of the compounds was able to activate the human GPR18 suggesting that the indolylethylamino moiety is indeed essential for GPR18-agonistic activity. We had observed a similar phenomenon with the previous tricyclic lead compound **5**, where the replacement of the indolylethyl moiety by other aromatic rings abolished GPR18 activity. Our results indicate a similar binding mode of bi- and tricyclic xanthine derivatives confirming our design concept for novel GPR18 agonists.

Figure 4 summarizes the structure–activity relationships of the investigated class of xanthine derivatives that were developed based on the rational design and optimization of a novel lead structure, leading to highly efficacious compounds with low nanomolar potency.

Structure–Activity Relationships at Mouse GPR18. Next, we investigated the new GPR18 agonists at mouse GPR18 (mGPR18) to study potential species differences. The mouse receptor was selected because the majority of preclinical studies are performed in mice. In addition to the new agonists, we tested several standard compounds previously claimed to activate the human GPR18 (hGPR18), at the mouse ortholog mGPR18 utilizing β-arrestin recruitment assays (Tables 1 and S1). NAGly (**4**) was not able to induce mGPR18 activation, consistent with its lack of activity at hGPR18. THC (**3**), which acts as an agonist at the human hGPR18 (EC_{50} **3.37** μM Table 1) and serves as a standard GPR18 agonist, only showed very weak maximal activation of β-arrestin recruitment at mGPR18 (see Figure 5A). Thus, we further tested the behavior of THC, which appeared to act as a partial agonist at mGPR18 as compared to the highly efficacious agonist **51**. A partial agonist will behave as an antagonist in the presence of a full agonist, reducing the maximum effect of the full agonist. Thus, the effects of a range of THC concentrations were tested vs the EC_{80} concentration of the new GPR18 agonist **51** (Figure S5). In fact, THC inhibited **51**-induced GPR18 activation in a dose-dependent manner with an IC_{50} value of 6.93 μM. This confirms that THC acts as a moderately potent partial agonist at mGPR18 with extremely low intrinsic activity.

The original tricyclic lead structures, **5** and **6**, were able to induce β-arrestin recruitment via mGPR18 activation (EC_{50} mGPR18 1.78 μM, and 0.583 μM, respectively, Table 1, Figure 5A) with similar potency as compared to the hGPR18 (EC_{50}, hGPR18, 0.562 μM, and 0.454 μM, respectively). Moreover, the most potent compound of the present series, **51**, displayed high potency at the mGPR18 (EC_{50} mGPR18 0.0541 μM, similar to

https://doi.org/10.1021/acs.jmedchem.3c02423
J. Med. Chem. 2024, 67, 9896–9926

Journal of Medicinal Chemistry pubs.acs.org/jmc Article

its EC_{50} at hGPR18 of 0.0191 μM). Since the efficacy of THC at the mGPR18 was very weak, and in the absence of a physiological GPR18 agonist, we subsequently used **51** as a reference agonist in experiments at the mGPR18 (Tables 1, S1 and Figure 5B).

As depicted in Figure 5B, the correlation of the pEC_{50} values at hGPR18 and mGPR18 was high (R^2 0.89), indicating a high similarity between the binding sites of GPR18 in both species. This is not surprising since there is a high sequence similarity and identity between hGPR18 and mGPR18 (90% sequence similarity and 86% sequence identity, see Figure S6). On the other hand, THC, which activated hGPR18, behaved only as a weak partial agonist at mGPR18. Thus, the novel indolylethyl-aminoxanthine derivatives will serve as valuable tool compounds for preclinical studies in mice. They are, in fact, the first class of agonists with proven potency on mGPR18, and are thus available for studies in mice.

Selectivity. Since GPR18 is considered a putative cannabinoid receptor, along with GPR55, we investigated whether the present series of compounds also interacted with GPR55, CB_1, and CB_2 receptors in order to assess the compounds' selectivity using the same assay system. A comparison of all data is depicted in Figure 6 as a heatmap. Data are collected in Tables 1 and S1.

The majority of the tested compounds displayed activity at GPR18, although certain compounds exhibited (additional) interaction with the CB_2 receptor, while only a few compounds interacted with the CB_1 receptor. No agonistic activity was observed at GPR55 for any of the compounds, but some compounds were able to block GPR55 at high, micromolar concentrations. This data indicates that most of the newly developed compounds exhibit selectivity for GPR18 as compared to the CB receptors and the CB-like receptor, GPR55. Most of the compounds that showed antagonistic activity at GPR55 belong to the group of xanthine derivatives with various substituents at the *N*3-position. Compound **76** bearing a cyanoethyl residue at *N*3 displayed an IC_{50} value of 0.884 μM at GPR55. Replacement by a propynyl residue, having a terminal triple bond, in compound **77** led to an only slightly less potent compound at GPR55 (IC_{50} of 1.99 μM). Larger substituents such as benzyl **82** were also tolerated by GPR55. In fact, compound **82** (PSB-1833) was the most selective GPR55 antagonist of the present series, with an IC_{50} value of 1.74 μM, while **76** (PSB-1846) was the most potent GPR55 antagonist (IC_{50} 0.884 μM). The most potent GPR18 agonist of the present series, **51** (GPR18, EC_{50} 0.0191 μM), did not show any effect on GPR55, neither agonistic nor antagonistic activity.

Additionally, we tested the best GPR18 agonist of the present series, **51**, at GPR183, a GPCR that is phylogenetically most closely related to GPR18[3,47] using a β-arrestin recruitment assay (Figure S7). 7α,25-Dihydroxycholesterol was employed as the cognate agonist of GPR183, showing an EC_{50} value of 0.0244 μM (see Figure S7, literature EC_{50} value: 0.0381−0.0794 μM (β-arrestin assay)).[48,49] Compound **51** did not activate GPR183 (1% activation at 10 μM), even at a high concentration of 30 μM (3% activation at 30 μM), demonstrating its GPR18-selectivity over GPR55 as well as GPR183.

Most of the compounds that were binding to CB receptors possess a large, lipophilic substituent at the xanthine *N*7-position (R^7) or the xanthine *N*3-position (R^3), respectively. The *N*7-substituted 2-chlorobenzyl derivative **33** that showed nanomolar potency at GPR18 (EC_{50} GPR18 0.0604 μM), displayed high selectivity versus the cannabinoid receptors (CB_1 and CB_2, K_i >

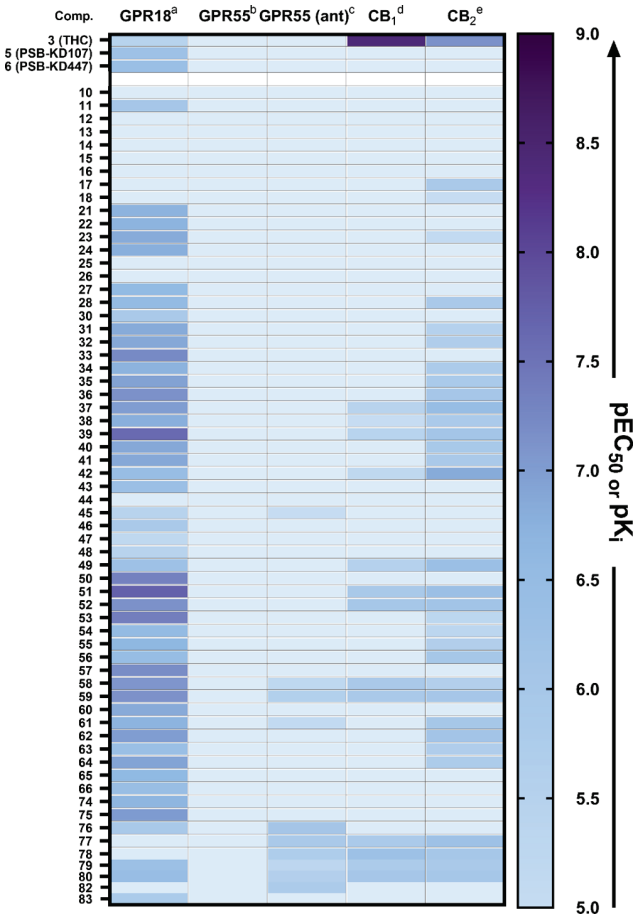

Figure 6. Heatmap of the pEC_{50} values (for GPR18 and GPR55) or pK_i values (for CB_1 and CB_2) at human GPCRs. Data represent means of at least three independent experiments (Tables 1 and S1). [a]Tested as agonist at human GPR18 (β-arrestin recruitment assay). [b]Tested as agonist at human GPR55 (β-arrestin recruitment assay). [c]Tested as antagonist at GPR55 (β-arrestin recruitment assay). [d]Tested at CB_1 receptor (radioligand binding assays). [e]Tested at CB_2 receptor (radioligand binding assays).

10 μM, Table S1). The replacement of chlorine by bromine in **34** or shifting of the halogen to the *meta*-position resulting in the 3-chlorobenzyl derivative **35** and the 3-bromobenzyl derivative **37** resulted in somewhat increased binding to the CB_2 receptor (CB_2 K_i values of 1.69, 0.896, and 0.344 μM for **34**, **36** and **37**, respectively).

Compound **39**, bearing a 4-methylbenzyl moiety at the xanthine *N*7-position, exhibited low micromolar binding affinity for the CB_1 receptor (K_i 3.48 μM, 55% maximal displacement of radioligand binding) and for the CB_2 receptor (K_i 0.827 μM, 87% maximal displacement of radioligand binding), still possessing >30-fold selectivity for GPR18 (EC_{50} 0.0246 μM) versus CB receptors.

Introducing even larger *N*7-substituents such as 4-methoxy-benzyl (**41**) abolished CB_1 binding but retained CB_2 receptor affinity (CB_2 K_i 1.41 μM). Similarly, a *p*-isopropylbenzyl residue (**42**) resulted in high-affinity binding at the CB_2 receptor but low affinity for the CB_1 receptor (K_i 6.28 μM and 0.150 μM for CB_1 and CB_2 receptors, respectively, see Figure 7 and Table S1).

The most potent GPR18 agonist of the present series, **51** (GPR18 EC_{50} 0.0191 μM), also displayed (moderate) binding affinity for CB_1 (K_i 1.18 μM) and CB_2 receptors (K_i 0.481 μM),

https://doi.org/10.1021/acs.jmedchem.3c02423
J. Med. Chem. 2024, 67, 9896−9926

Journal of Medicinal Chemistry pubs.acs.org/jmc Article

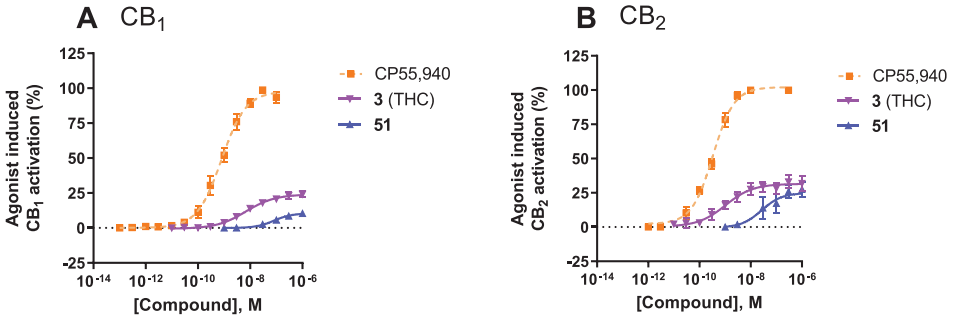

Figure 7. Concentration-dependent effects of **51** at the human CB_1 (A) and the human CB_2 receptor (B), determined in CHO-K1 β-arrestin enzyme complementation assays. CP55,940 and THC were used as standard agonists to induce β-arrestin recruitment by CB_1 (A, CP55,940, EC_{50} 0.00100 ± 0.00026 μM (100% max. activation); THC, EC_{50} 0.00673 ± 0.00174 μM (22% max. activation) and CB_2 receptors (B, CP55,940, EC_{50} 0.000315 ± 0.000048 μM (100% max. activation); THC, EC_{50} 0.00142 ± 0.00028 μM (35% max. activation compared to the maximal effect of the full agonist CP55,940 (0.1 μM set at 100%). Data points represent means ± SEM of at least three independent experiments.

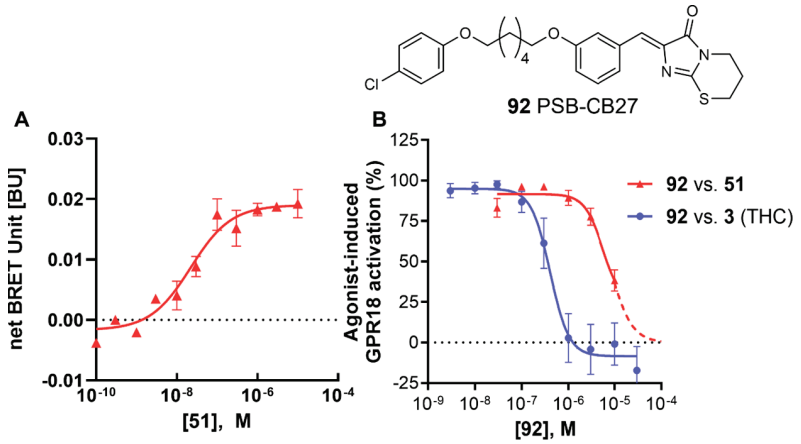

Figure 8. (A) Concentration-dependent activation of GPR18 by **51** in HEK293 cells recombinantly expressing GPR18-eYFP (enhanced Yellow Fluorescent Protein) and Rluc-βarrestin-2, determined in $BRET^1$ β-arrestin-2 enzyme complementation assays. An EC_{50} value of 0.0384 ± 0.011 μM was determined. Data points represent means ± SEM of at least three independent experiments. (B) Concentration-dependent inhibition of THC-induced GPR18 at its EC_{80} concentration by the GPR18 antagonist **92** (PSB-CB27)[24] (blue curve, IC_{50} PSB-CB27 vs THC: 0.487 ± 0.142 μM), and by **51**-induced GPR18 activation at its EC_{80} concentration (red curve; IC_{50} PSB-CB27 vs **51**: 9.91 ± 2.60 μM, extrapolated values are depicted as red dashed line).

but still exhibited at least 25-fold selectivity (Table S1). Interestingly, replacing the 4-chlorobenzyl for a 4-fluorobenzyl residue (in **50**) abolished binding to both cannabinoid receptor subtypes. GPR18 agonist **50** is therefore the most selective compound of this series with high agonistic potency at GPR18 and >100-fold selectivity.

Since the compounds had so far only been tested in radioligand binding assays at the cannabinoid receptors, we further investigated the functional effects of the most potent compound **51** at the G_i protein-coupled cannabinoid receptors. To this end, we tested **51** in cyclic adenosine monophosphate (cAMP) assays and in β-arrestin recruitment assays. In β-arrestin assays, **51** demonstrated a maximum activation of the cannabinoid receptors of approximately 12% (CB_1) and 27% (CB_2) (Figure 7). As a reference, we utilized the potent CB_1/CB_2 agonist CP55,940, and the partial agonist THC (compound **3**). Compound **3** (THC), which is known to be a partial agonist at cannabinoid receptors, exhibited a maximum activation of about 22% (at CB_1, see Figure 7A) and 35% (at CB_2, see Figure 7B), relative to the full agonist CP55,940 at a concentration of 10 μM. This finding is in close agreement with literature data.[50−52] Additional cAMP experiments (Tables S2 and S3) confirmed weak partial activation of human CB_1 by **51** (30% max. activation of the receptor) and CB_2 receptors (30% max. activation of the receptor), whereas THC, which acts as a partial agonist at CB receptors, showed a maximal activation of 49 and 51% at CB_1 and CB_2 receptor, respectively (Tables S2 and S3). We conclude that the best GPR18 agonist of the present series can interact with cannabinoid receptors only at high concentrations showing just weak partial activation.

Confirmation of GPR18 Activation. To confirm that the observed luminescence was in fact mediated by specific activation of GPR18, we pursued two strategies: (i) investigation of GPR18 activation in an orthogonal assay, and (ii) testing of the compounds at another class A GPCR using the same assay system (see selectivity results above).

As an alternative to the enzyme complementation assay in CHO cells (DiscoverX PathHunter), a bioluminescence resonance energy transfer type 1 ($BRET^1$) assay was employed to measure β-arrestin-2 recruitment by GPR18 in human embryonic kidney (HEK293) cells. For this assay, the human GPR18 was C-terminally fused with enhanced Yellow Fluorescent Protein (eYFP), while Renilla luciferase (Rluc) was fused to the N-terminus of β-arrestin-2. Upon stimulation of GPR18 with an agonist, β-arrestin will be translocated to the C-terminus of GPR18, bringing eYFP and Rluc in close proximity.

https://doi.org/10.1021/acs.jmedchem.3c02423
J. Med. Chem. 2024, 67, 9896−9926

Journal of Medicinal Chemistry pubs.acs.org/jmc Article

The addition of coelenterazine as a substrate for Rluc allows the calculation of BRET ratios by comparing the luminescence (from Rluc) to the fluorescence values (from eYFP). An increase in the BRET ratio is observed when Rluc-β-arrestin-2 is in close proximity to GPR18-eYFP due to the activation of GPR18. Since only the receptor and β-arrestin-2 are tagged, the signal specifically indicates the interaction between GPR18 and β-arrestin-2 (Figure S1). We selected the potent agonist **51** for testing in this orthogonal assay. As expected, **51** induced β-arrestin recruitment in a dose-dependent manner (Figure 8A, EC_{50} 0.0384 μM) with comparable potency as that determined in the enzyme complementation assay (Table 1). Thus, the recruitment of β-arrestin by **51** was not cell-type or assay-dependent and is clearly due to GPR18 activation.

In contrast, and in agreement with several previous studies, we could not detect any G protein coupling of GPR18.[25,27,32,53−55] Several 7-transmembrane (7TM) proteins share similarities with GPCRs but function differently, primarily by recruiting arrestin upon agonist stimulation. These are termed atypical GPCRs or arrestin-biased receptors.[56] Our findings suggest that GPR18 may belong to this receptor family, like, e.g., GPR27,[57] and GPR173.[58] Although these receptors lack typical GPCR signaling, they have been shown to play roles in (patho)-physiological processes, especially in cancer and immunological diseases. For instance, activation of GPR27 has been associated with an increase in cytosolic lactate levels and modulation of hepatocellular carcinoma progression,[59,60] while GPR173 activation has been linked to cell migration.[58]

Blockade of GPR18 Activation by Antagonists. Only a few GPR18 antagonists have been described to date. We recently reported the first GPR18 antagonists based on an imidazothiazinone core structure and optimized them to reach submicromolar potency.[24] PSB-CB27 (**92**) inhibited THC-induced GPR18 activation in β-arrestin enzyme complementation assays in a concentration-dependent manner (IC_{50} 0.650 μM, see Figure 8B).[24,61] Based on molecular modeling studies, and supported by experimental results, we hypothesized that GPR18 harbors two different agonist binding sites: a lipid-like site that is targeted by THC (blocked by the antagonist **92**), and a peptide- or nucleotide-like binding site occupied by the tricyclic xanthine derivatives.[32,61]

Antagonist **92** (PSB-CB27) showed moderate inhibition of GPR18 activation induced by the xanthine-derived agonist **51** (IC_{50} 9.89 μM vs **51**, extrapolated value due to limited solubility, see Figure 8B), while it was 20-fold more potent in blocking THC-induced GPR18 activation (IC_{50} 0.487 μM). In both cases, an agonist concentration corresponding to its EC_{80} value was employed. Thus, the xanthine agonist **51**, similar to the tricyclic lead structure **5**, likely binds to a different binding site on GPR18 than the lipid-like agonist THC.[32,61]

Physicochemical and Pharmacokinetic Properties − A Preliminary Assessment. We further assessed selected agonists with regard to their physicochemical and pharmacokinetic properties. The computational tool pkCSM (https://biosig.lab.uq.edu.au/pkcsm)[62] was employed to predict the compounds' properties (see Table 3). The molecular weight of the compounds is below 500 g/mol which characterizes them as small, drug-like molecules. They were predicted to display high permeability and intestinal absorption, although they may be P-glycoprotein (P-gp) substrates and therefore subject to efflux transport. Low brain permeability is suspected.

The most potent agonist, **51**, was experimentally evaluated for its metabolic stability in human and rat liver microsomes. The compound was metabolized during the incubation period of 120 min resulting in a number of metabolites that were detected by LC-MS (Figure S8). After 2 h of incubation in human liver microsomes, 32.8% of **51** remained intact, while 62.9% remained intact when incubated with rat liver microsomes. Verapamil, a therapeutic drug used for the treatment of cardiovascular diseases, and known to undergo hepatic metabolism,[63] was used as a control under the same conditions. For comparison, 30.8% (human) and 37.3% (rat) of verapamil remained intact (see Figure S8A,B). The metabolic pathways of **51** observed in both species mainly resulted in mono- and dihydroxylated derivatives, consistent with CYP450-induced metabolism[64] (Figure S8). Hydroxylation of the main metabolite of **51** likely occurred at the indole moiety (see Figure S8C). This indicates some stability of **51**, particularly in rats, but there will also be the need for further structural optimization, e.g., reducing lipophilicity and increasing metabolic stability.

Table 3. Prediction of Physicochemical and Pharmacokinetic Properties of Selected Compounds[a]

Compound No.	26	36	50	51	64	76
MW (g/mol)	392	463	446	463	457	488
log P[b]	2.21	3.52	3.12	3.52	3.66	3.22
Caco2 permeability[c] log $P_{app} \times 10^{-6}$	0.94	0.96	1.0	1.1	0.91	0.26
intestinal absorption[d] (% absorbed)	93	92	92	91	91	91
P-glycoprotein (P-gp) substrate	YES	YES	YES	YES	YES	YES
BBB permeability[e] (log BB)	−0.43	−0.35	−0.37	−0.35	−0.16	−0.47

[a]Computed using pkCSM (https://biosig.lab.uq.edu.au/pkcsm). [b]Calculated using Chemdraw. [c]Log P_{app}: Logarithm of the apparent permeability. Log P_{app} > 0.90 means high permeability. [d]Intestinal absorption <30% poorly absorbed. [e]BBB: Blood brain barrier, log BB > 0.3 readily crosses BB; < −1 poor distributed to the brain.

Molecular Modeling Studies. To provide a rationale for the observed structure−activity relationships, binding poses were predicted using our recently published homology model of the human GPR18.[61] The homology model was generated by a multitemplate approach based on the X-ray crystal structures of the murine μ-opioid receptor, the human $P2Y_1$ receptor, and the zebrafish lysophosphatidic acid receptor LPA6 as templates (PDB-IDs: 5C1M, 4XNV, and 5XSZ, respectively).[65−67] Agonists were docked into the equilibrated apo receptor form, and final docking positions were selected based on the best induced-fit docking (IFD) score. The putative binding mode of the most potent agonist **51** is presented in Figure 9.

Compound **51** is predicted to bind in the upper portion of the receptor directed toward the extracellular lumen, which is a common binding site for class A GPCRs.[68] The xanthine core is proposed to bind in a binding pocket formed by polar ($Arg78^{2.60}$, $Lys174^{ECL2}$, $Arg191^{5.42}$) and lipophilic ($Val102^{3.33}$, $Leu156^{4.60}$, $Phe248^{6.51}$, $Met275^{7.42}$) residues, as well as residues with mixed properties ($Thr101^{3.32}$, $Thr272^{7.79}$, $Asn276^{7.43}$). The methyl group at *N*1 is proposed to be directed toward a subpocket formed by $Met275^{7.42}$ and $Asn276^{7.43}$. H-bond interactions between the oxygen atom at the 2-position of the xanthine core and $Arg191^{5.42}$, and of the oxygen at the 6-position with $Arg78^{2.60}$ and $Asn276^{7.43}$ are feasible. The methyl group at *N*3 was placed close to $Phe248^{6.51}$ which may engage in additional interactions with the xanthine core structure. The *p*-chlorobenzyl group binds in a subpocket containing several

https://doi.org/10.1021/acs.jmedchem.3c02423
J. Med. Chem. 2024, 67, 9896−9926

Journal of Medicinal Chemistry pubs.acs.org/jmc Article

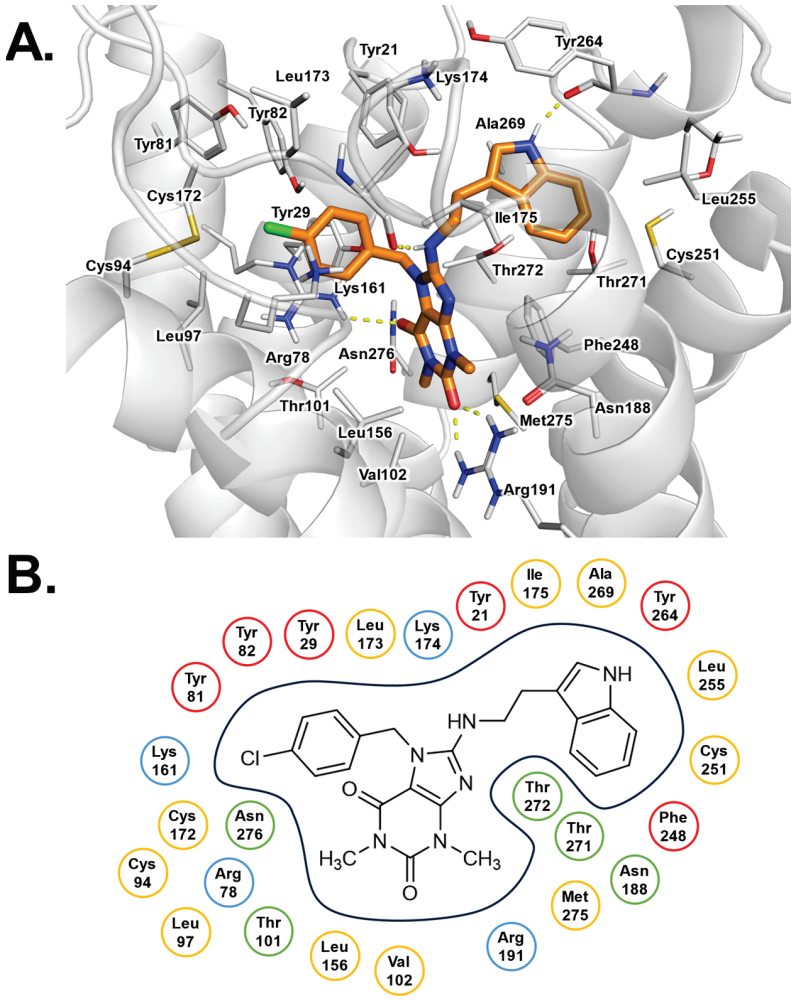

Figure 9. Proposed binding mode of agonist **51**. (A) Docked pose of **51** in complex with the homology model of the human GPR18 shown with residues suggested to form the binding pocket. The receptor is displayed in cartoon representation, the amino acid residues (white) and compound **51** (orange) are represented as stick models. Oxygen atoms are colored in red, nitrogen atoms in blue, and chlorine in green. (B) Schematic 2D representation of the binding pocket. Lipophilic amino acids are colored in yellow, hydrophilic ones in blue, aromatic ones in red, and amino acid residues with mixed properties are shown in green. The homology model of GPR18 was generated by a multitemplate approach based on the X-ray crystal structures of the murine μ-opioid receptor (PDB-ID: 5C1M),[65] the human $P2Y_1$ receptor (PDB-ID: 4XNV),[67] and the zebrafish lysophosphatidic acid receptor LPA6 (PDB-ID: 5XSZ)[66] as templates.

aromatic residues (Tyr21$^{1.31}$, Tyr29$^{1.39}$, Tyr81$^{2.63}$, Tyr82$^{2.64}$) that may engage in $\pi-\pi$ interactions with the ring system. Additional cation$-\pi$ interactions with Lys161^{ECL2} are plausible for the phenyl moiety. The chloro substituent of the *p*-chlorobenzyl group likely points toward a lipophilic surface formed by the side chains of Leu97$^{3.28}$ and Cys172^{ECL2}. The indole moiety was placed in a lipophilic binding cavity formed by Tyr21$^{1.31}$, Ile175^{ECL2}, Phe248$^{6.51}$, Cys251$^{6.54}$, Leu255$^{6.58}$, Tyr264$^{7.31}$, Ala269$^{7.36}$, and Thr271$^{7.38}$, where it forms an H-bond interaction with the backbone of Tyr264$^{7.31}$. Furthermore, $\pi-\pi$ stacking with Phe248$^{6.51}$ and Tyr264$^{7.31}$ may stabilize the binding of the moiety in this region.

The proposed interaction motif of agonist **51** differs from the presumed binding mode and binding site of THC and antagonist **92** (PSB-CB27),[61] which are likely interacting with the so-called "lipid binding site", confirming our previous experimental results.[32] According to our docking study, compound **51** exhibits only limited partial overlap with the proposed binding site of THC at GPR18, the xanthine core of **51**, and the alkyl chain of THC occupying the same volume (Figure 10).

Compounds **50** and **51** only differ in the *para*-benzyl substituent (*p*-fluoro in **50** and *p*-chloro in **51**), yet they exhibit different selectivity vs cannabinoid receptors. To explore this further, we overlaid **51** in its proposed binding mode at GPR18 with the published crystal structures of the CB_1 (in complex with AM11542, PDB ID: 5XRA)[69] and CB_2 receptor (complexed with AM10257, PDB ID: 5ZTY, Figure S9).[70] The structure of CB_1 bound to AM11542 closely resembles that of CB_2 bound to AM10257. The adamantyl group of AM10257 extends toward a hydrophobic site formed by Phe170$^{2.57}$, Phe174$^{2.61}$, Phe177$^{2.64}$, and His178$^{2.65}$. Similarly, the tricyclic tetrahydrocannabinol ring system of AM11542 interacts with Phe87$^{2.57}$, Phe91$^{2.61}$, Phe94$^{2.64}$, and His95$^{2.65}$. Interestingly, the *p*-chlorobenzyl moiety of **51** also appears to extend into this hydrophobic region, suggesting that lipophilicity at this position may play an important role in the binding of the compound to the CB receptors. Indeed, reducing the lipophilicity of this substituent to *p*-fluorobenzyl in **50** resulted in reduced affinity to CB

https://doi.org/10.1021/acs.jmedchem.3c02423
J. Med. Chem. 2024, 67, 9896−9926

Journal of Medicinal Chemistry pubs.acs.org/jmc Article

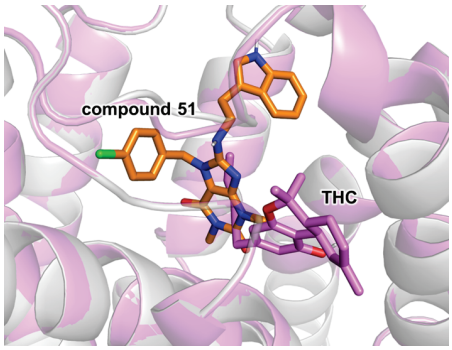

Figure 10. Overlay of proposed binding modes of agonist **51** (orange) and THC (violet). The receptor conformations are displayed in cartoon representation according to the color of their respective ligands (stick models). Oxygen atoms are colored in red, nitrogen atoms in blue, and chlorine in green.

receptors, while increasing the lipophilicity to *p*-bromobenzyl in **52** maintained affinity for the CB receptors.

Based on the docking studies, we investigated the structure–activity relationships (SARs) of the xanthine derivatives. To this end, we computationally assessed the quality of the ligand-target interactions using the drug discovery dashboard SeeSAR.[71,72] SeeSAR allows the editing and redocking of ligands with a subsequent assessment of their overall estimated affinity, as well as contributions of individual atoms using the HYDE algorithm.[73] Individual contributions are visualized as green (representing good binding) and red spheres (representing bad binding) together with a numerical value for the binding free energy, which, in turn, allows us to derive the effects of molecule modifications on potency. Furthermore, SeeSAR can be used to detect inter- and intramolecular clashes. The observations are summarized in Table S4.

In the series of derivatives modified in position *N*1, only methyl substitution (**11**, EC_{50} 0.902 μM) was tolerated, whereas other substituents (in compounds **10**, **12**–**18**) resulted in a >10-fold decrease in potency (EC_{50} > 10 μM). We observed limited space for *N*1-substituents in the proposed binding pocket due to Thr101$^{3.32}$ and Met275$^{7.42}$. The preference for the methyl substitution in comparison to the unsubstituted nitrogen atom may be due to lipophilic interactions with Met275$^{7.42}$.

The putative binding site for substituents in position *N*7 is characterized by several aromatic and lipophilic residues. The most potent compounds bear substituted benzyl groups. Compounds containing a lipophilic *meta*- (**35**–**38**) or *para*-substituted benzyl group (**39**, **50**–**53**, **57**–**59**) in position *N*7 were the most active ones in the present series. The distances between the *para*-chlorine of **51** and the lipophilic residues Tyr81$^{2.63}$, Leu97$^{3.28}$, and Cys172^{ECL2} amount to 3.9, 3.3, and 4.0 Å, respectively, according to the model, which is in the range for van der Waals contacts.[74] The superiority of chlorine over fluorine (**60**, **61**) and bromine may be explained by its optimal occupation of the binding pocket due to its size and its propensity to interact with the above-mentioned residues.[75] Similar interactions for *meta*-substituted derivatives are likely, as vacant volume is available in the unoccupied subpocket formed by Arg78$^{2.60}$, Leu97$^{3.28}$, and Gly98$^{3.29}$. Replacement of lipophilic groups by a hydrophilic amino group (**54**) led to an approximately 10-fold decrease in potency which can be rationalized by the lack of optimal H-bond interaction partners in the binding environment. Compounds bearing bulky *para*-substituents (**40**–**49**, and **55**) were more than 10-fold less potent than **51**, likely due to steric clashes with Tyr81$^{2.63}$, Leu97$^{3.28}$, and Cys172^{ECL2}. Interestingly, increasing the lipophilic part of the terminal substituent resulted in enhanced agonistic potency, likely due to an induced conformational shift for the sulfonamide-containing benzyl moiety. Redocking with SeeSAR proposed H-bond interactions between the nitrogen of the sulfonamide group and the backbone of Cys172^{ECL2}, and lipophilic interactions between the propyl group and Tyr21$^{1.31}$, Tyr82$^{2.64}$, and the alkyl chain of Lys174^{ECL2}. The unsubstituted compound **31** and the *ortho*-substituted derivatives (**32**–**36**) were somewhat less potent than their *para*-substituted analogs (~3-fold). In the case of the *ortho*-substituted derivatives (**32**–**34**, **56**, **57**), interactions between the halogen substituent and Arg78$^{2.60}$ and the backbone of Gly98$^{3.29}$, and Thr101$^{3.32}$ are feasible. Compounds containing a larger linker between the phenyl ring and the xanthine core (**63**, **64**) exhibited similar potency as **31**, indicating conformational adaptation in the binding pocket. A nonaromatic cyclohexylethyl group was also well tolerated, which can be explained by the overall high lipophilicity of the binding pocket. The introduction of an ether group in the linker resulted in **65** and **66** which were slightly less potent than compound **64**, likely due to the hydrophilic properties of the oxygen atom. It is expected that the terminal phenyl ring of compounds containing a larger linker reaches a different binding position than those with a methylene linker because the introduction of chlorine in compound **66** did not lead to increased potency as it was observed for benzyl-substituted compounds.

Compounds lacking an aromatic group at *N*7 were approximately 10-fold less potent (**21**–**24**, **26**–**28**) compared to **51**, or even more (**25**), possibly because of missing π–π-interactions with Tyr21$^{1.31}$, Tyr29$^{1.39}$, Tyr81$^{2.63}$, and Tyr82$^{2.64}$.

The *N*3-methylated **51** exhibited the highest agonistic potency (EC_{50} 0.0191 μM) in the series of *N*3-substituted derivatives. Removal of the methyl group led to a 10-fold decrease in potency (**74**, EC_{50} 0.206 μM likely due to a loss of lipophilic interactions between the *N*3 methyl group of **51** and Phe248$^{6.51}$). Introduction of ethyl, 2-fluoroethyl, or 2,2,2-trifluoroethyl substitution (in **75**, **79**–**80**) resulted in derivatives with 5-, 25-, and 18-fold decreased potency compared to **51** (EC_{50} 0.0950 μM, 0.486 μM, 0.351 μM, respectively). Further introduction of larger substituents in position *N*3 greatly diminished the agonistic potency of the derivatives with a more than 50-fold decrease in potency (**76**–**78**, **81**–**83**). These results suggest that the binding cavity accommodating the *N*3-substituent of the xanthine derivatives provides limited space which is best occupied by a methyl group. This is supported by the fact, that the nonfluorinated ethyl group was somewhat tolerated, while its potency decreased upon additional introduction of fluorine or oxygen atoms. Compound **82**, containing a bulky benzyl group at *N*3, was the least potent derivative of the series showing negligible activation at 10 μM. Figure 11 summarizes the analysis of the structure–activity relationship and the derived binding pocket interactions.

CONCLUSIONS

We designed a new class of GPR18 agonists, synthesized 68 novel indolylethylaminoxanthine derivates, and tested their activity as agonist at GPR18. Steep structure–activity relationships were observed. Systematic optimization based on SAR analysis yielded potent GPR18 agonists with nanomolar potency. Compound **51** (PSB-KK1415), EC_{50} 0.0191 μM, is

https://doi.org/10.1021/acs.jmedchem.3c02423
J. Med. Chem. 2024, 67, 9896–9926

Journal of Medicinal Chemistry pubs.acs.org/jmc Article

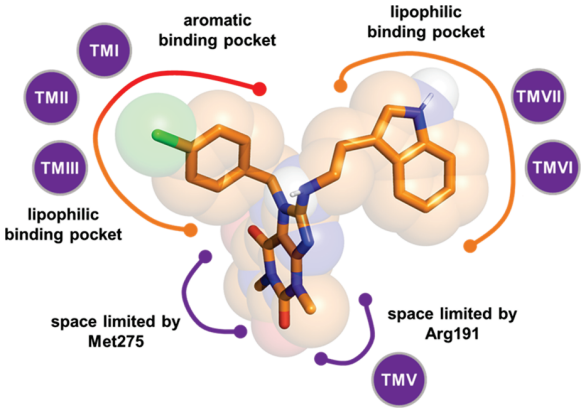

Figure 11. Schematic representation of the proposed binding mode of the xanthine derivatives, represented by the most potent agonist **51**.

the most potent agonist described so far, displaying >25-fold selectivity versus cannabinoid receptors. Compound **50** (PSB-KK1445, EC_{50} 0.0454 μM) is the most selective GPR18 agonist of the present series (determined vs cannabinoid receptors CB_1 and CB_2 and vs the cannabinoid-like receptor, GPR55). These compounds are the most potent GPR18 agonists described to date and the first ones that show high selectivity versus related GPCRs. Investigation of the indolylethylaminoxanthine derivatives at mouse GPR18 showed a close correlation between both species, human GPR18 and mouse GPR18 (R^2= 0.8943). In contrast, THC which activates the human GPR18, showed extremely low efficacy at the mouse GPR18.

Substitution of indolylethylaminoxanthine at the *N*3-position increases the antagonistic potency at GPR55. Compound **82** bearing a benzyl moiety at the xanthine *N*3-position (PSB-1833) was the most selective GPR55 antagonist with an IC_{50} value of 1.74 μM, while the cyanoethyl-substituted **76** (PSB-1846) was found to be the most potent GPR55 antagonist in this class of compounds with an IC_{50} of 0.884 μM.

These novel GPR18 agonists will be useful tool compounds to investigate the roles of GPR18 in health and disease. Moreover, they may serve as lead structures for the development of multitarget drugs, especially those with activity at GPR18 and CB_2 receptors, which might be useful for treating inflammatory and immune diseases.

EXPERIMENTAL SECTION

Synthesis. Starting materials, reagents, and solvents were used as purchased from ABCR, Alfa Aesar, Sigma-Aldrich, Activate Scientific, or Fluorochem. The progress of the reactions was monitored by thin-layer chromatography (TLC, Merck, 0,2 mm silica gel 60 F254) followed by analytical LC-MS. Column chromatography was performed on silica gel, 0.060−0.200 mm, pore diameter ca. 6 nm. All synthesized compounds were finally dried in a vacuum at 8−12 Pa (0.08−0.12 mbar). ^{1}H and ^{13}C NMR data were collected either on a Varian-Mercury-VX 300 MHz, Bruker Avance 400 or 500 MHz NMR spectrometer or JEOL FT-NMR 500 at 500 MHz (^{1}H) or 126 MHz (^{13}C) or on a Bruker Ascend 600 MHz NMR spectrometer at 600 MHz (^{1}H) or 151 MHz (^{13}C). DMSO-d_6 was employed as a solvent at 303 K, unless otherwise noted. Chemical shifts are reported in parts per million in relation to the deuterated solvent: DMSO, δ (^{1}H) 2.50 ppm; δ (^{13}C) 39.52 ppm; $CDCl_3$, δ (^{1}H) 7.26 ppm; δ (^{13}C) 77.16 ppm. Coupling constants *J* are given in Hertz, and spin multiplicities are given as singlet (s), doublet (d), doublet of doublet (dd), triplet (t), quartet (q), multiplet (m), and broad signal (br). The purities of isolated final products were determined by HPLC coupled to a diode array detector (DAD) measuring UV absorption from 200 to 950 nm, and electrospray ionization (ESI) mass spectrometer (Applied Biosystems API 2000 LC-MS/MS, HPLC Agilent 1100) using a Phenomenex Luna 3 μ C18 column (50 × 2.00 mm) (HPLC UV/ESI-MS) or a Waters TQD mass spectrometer coupled with a Waters ACQUITY UPLC (UPLC-MS). The compounds were dissolved at a concentration of 1.0 mg/mL in acetonitrile containing 2 mM ammonium acetate. Then, 10 μL of the sample was injected into an HPLC column, and elution was performed with a gradient of water/acetonitrile (containing 2 mM ammonium acetate) from 90:10 to 0:100 for 20 min at a flow rate of 300 μL/min, starting the gradient after 10 min. The purity of the compounds was in almost all cases >95%, unless otherwise noted.

High-resolution mass spectra (HR-MS) were recorded on a UPLC-MS/MS system consisting of a Waters Acquity I-Class Plus UPLC (Waters Corporation, Milford, MA, USA) coupled to a Waters Synapt XS mass spectrometer (electrospray ionization mode). Chromatographic separations were carried out using the Acquity UPLC BEH (bridged ethylene hybrid) C18 column; 2.1 × 100 mm, and 1.7 μm particle size, equipped with an Acquity UPLC BEH C18 VanGuard precolumn; 2.1 × 5 mm, 1.7 μm particle size. The column temperature was maintained at 40 °C, and the samples were eluted applying a gradient from 95 to 0% of eluent A and 5 to 100% of eluent B over 10 min at a flow rate of 0.3 mL min^{-1} (eluent A: water/formic acid (0.1%, v/v); eluent B: acetonitrile/formic acid (0.1%, v/v)). Chromatograms were recorded using a Waters eλ PDA detector. Spectra were analyzed from 200 to 700 nm with 1.2 nm resolution and a sampling rate of 20 points/s. MS detection settings of the Waters Synapt XS mass spectrometer were as follows: source temperature 150 °C, desolvation temperature 250 °C, desolvation gas flow rate 600 L h^{-1}, cone gas flow 100 L h^{-1}, capillary potential 3.00 kV, cone potential 30 V. Nitrogen was used for both nebulizing and drying gas. The data were obtained in a scan mode ranging from 50 to 1000 *m*/*z* in 0.2 s intervals. Leu-enkephalin was used as a mass reference. The data acquisition software was MassLynx V 4.2 (Waters).

General method 1 (GP1) and general method 2 (GP2) are reported in the SI (for **9a−g**, **10**, and **12−18**, respectively).

*General Method 3 (GP3): Synthesis of 8-Chloro-7-alkyl/arylalkyl-1,3-dimethyl-3,7-dihydro-1H-purine-2,6-dione (**20a−n**).* In a 100 mL flask containing 8-chlorotheophylline or 8-bromotheophylline (1 equiv), K_2CO_3 (2 equiv) and DMF were added, and the mixture was stirred for 30 min. Then, the appropriate alkyl or arylalkyl bromide (1.5 equiv) was added to the reaction mixture, which was vigorously stirred at room temperature for 18 h. The reaction mixture was poured onto ice-cold water (0 °C) and acidified with 2N aq. HCl solution. The precipitate was collected by filtration, then washed twice with 5 mL water, and the obtained products were used for the next reaction without further purification.

*General Method 4 (GP4): Synthesis of 8-((2-(1H-Indol-3-yl)ethyl)-amino)-7-alkyl/arylalkyl-1,3-dimethyl-3,7-dihydro-1H-purine-2,6-diones (**11**,**21−28**, **30−43**, **47−53**, **56−66**).* A mixture of the appropriate 8-chloro-7-alkyl/arylalkyl-1,3-dimethyl-3,7-dihydro-*1H*-purine-2,6-dione (**20a−n**) (1 equiv), tryptamine (2 equiv), and DIPEA (3.6 equiv) in NMP was added into a sealed tube, and the mixture was heated at 145 °C overnight. The reaction was monitored by TLC, using the eluent DCM: methanol (9.5:0.5) until completion of the reaction was indicated. The solvent was evaporated, followed by the addition of water. The resulting mixture was extracted three times using ethyl acetate and then washed twice with water and brine. Finally, it was dried over anhydrous $MgSO_4$. The solution was filtered and subsequently evaporated. The compound was purified by column chromatography or by recrystallization to yield the target compounds.

*8-((2-(1H-Indol-3-yl)ethyl)amino)-1,3,7-trimethyl-3,7-dihydro-1H-purine-2,6-dione (**11**).* Synthesized according to GP4; purification by column chromatography with a gradient of DCM: methanol (100:0 to 80:20); yield 62%; m.p.: 262−263 °C; **^{1}H NMR** (400 MHz, DMSO-d_6) δ 10.82 (br, 1H, NH_{indole}), 7.65 (d, *J* = 7.8 Hz, 1H, Ar−H), 7.33−7.36 (m, 1H, Ar−H), 7.16−7.21 (m, 2H, *NHCH*$_2$ and Ar−H), 7.07 (td, *J* = 7.4, 1.2 Hz, 1H, Ar−H), 6.96−7.01 (m, 1H, Ar−H), 3.57−3.62 (m, 2H, NHC*H*$_2$), 3.55 (s, 3H, N3CH_3), 3.39 (s, 3H, N1CH_3), 3.18 (s, 3H, N7CH_3), 2.98−3.03 (m, 2H, NHCH_2*CH*$_2$); **^{13}C NMR** (DMSO-d_6) δ ppm: 154.6, 153.3, 151.5, 149.0, 136.7, 127.8, 123.2, 121.4, 118.8,

https://doi.org/10.1021/acs.jmedchem.3c02423
J. Med. Chem. 2024, 67, 9896−9926

Journal of Medicinal Chemistry pubs.acs.org/jmc Article

118.7, 112.1, 111.8, 102.3, 43.9, 30.2, 29.7, 27.6, 26.0. UPLC-MS (*m/z*): 353.09 $[M + H]^+$; $C_{18}H_{20}N_6O_2$ (calculated MW: 352.40). Purity (UPLC-MS): 100%; t_R = 4.97.

*8-((2-(1H-Indol-3-yl)ethyl)amino)-7-ethyl-1,3-dimethyl-3,7-dihydro-1H-purine-2,6-dione (**21**).* Synthesized according to GP4; purification by column chromatography with a gradient of DCM: methanol (100:0 to 80:20); yield 65%; m.p.: 234−235 °C; **^{1}H NMR** (500 MHz, DMSO-d_6) δ 10.78 (br, 1H, NH_{indole}), 7.61 (d, *J* = 7.4 Hz, 1H, Ar−H), 7.30 (d, *J* = 8.0 Hz, 1H, Ar−H), 7.17 (t, *J* = 5.4 Hz, 1H, Ar−H), 7.13 (d, *J* = 1.7 Hz, 1H, Ar−H), 7.03 (t, *J* = 7.5 Hz, 1H, *NH*CH_2), 6.92−6.96 (m, 1H, Ar−H), 4.00 (q, *J* = 6.9 Hz, 2H, N7CH_2), 3.52−3.57 (m, 2H, NH*CH_2*), 3.35 (s, 3H, N3CH_3), 3.14 (s, 3H, N1CH_3), 2.96 (t, *J* = 7.5 Hz, 2H, NHCH$_2$*CH_2*), 1.13 (t, *J* = 7.2 Hz, 3H, N7CH_2*CH_3*); **^{13}C NMR** (DMSO-d_6) δ ppm: 153.7, 153.1, 151.6, 149.3, 136.8, 127.9, 123.3, 121.4, 118.9, 118.7, 112.2, 111.9, 101.6, 43.9, 38.0, 29.8, 27.7, 26.0, 15.3. UPLC-MS (*m/z*): 367.18 $[M + H]^+$; $C_{19}H_{22}N_6O_2$ (calculated MW: 366.43). Purity (UPLC-MS): 97.4%; t_R = 5.38.

*8-((2-(1H-Indol-3-yl)ethyl)amino)-1,3-dimethyl-7-propyl-3,7-dihydro-1H-purine-2,6-dione (**22**).* Synthesized according to GP4; purification by column chromatography with a gradient of DCM: methanol (100:0 to 80:20); yield 58%; m.p.: 206−207 °C; **^{1}H NMR** (400 MHz, $CDCl_3$) δ 8.23 (br, 1H, NH_{indole}), 7.66 (d, *J* = 7.8 Hz, 1H, Ar−H), 7.42 (d, *J* = 8.2 Hz, 1H, Ar−H), 7.25 (td, *J* = 7.6, 1.17 Hz, 1H, Ar−H), 7.14−7.19 (m, 1H, Ar−H), 7.07 (d, *J* = 2.3 Hz, 1H, Ar−H), 3.80−3.87 (m, 4H, N7CH_2, NH*CH_2*), 3.58 (s, 3H, N3CH_3), 3.39 (s, 3H, N1CH_3), 3.16 (t, *J* = 6.5 Hz, 2H, NHCH$_2$*CH_2*), 1.55−1.66 (m, 2H, N7CH_2*CH_2*), 0.82 (t, *J* = 7.4 Hz, 3H, N7CH_2CH$_2$*CH_3*); **^{13}C NMR** ($CDCl_3$) δ ppm: 153.9, 152.6, 151.8, 136.5, 127.3, 122.5, 122.2, 119.7, 118.6, 112.7, 111.4, 102.9, 44.8, 43.9, 29.8, 27.7, 25.4, 22.7, 10.8. UPLC-MS (*m/z*): 381.04 $[M + H]^+$; $C_{20}H_{24}N_6O_2$ (calculated MW: 380.45). Purity (UPLC-MS): 97.4%; t_R = 5.77.

*8-((2-(1H-Indol-3-yl)ethyl)amino)-7-butyl-1,3-dimethyl-3,7-dihydro-1H-purine-2,6-dione (**23**).* Synthesized according to GP4; purification by column chromatography with a gradient of DCM: methanol (100:0 to 80:20); yield 59%; m.p.: 160−161 °C; **^{1}H NMR** (500 MHz, DMSO-d6) δ 10.78 (br, 1H, NH_{indole}), 7.61 (d, *J* = 7.5 Hz, 1H, Ar−H), 7.30 (d, *J* = 8.0 Hz, 1H, Ar−H), 7.09−7.14 (m, 2H, *NH*CH_2 and Ar−H), 7.03 (t, *J* = 7.5 Hz, 1H, Ar−H), 6.92−6.96 (m, 1H, Ar−H), 3.95 (t, *J* = 6.9 Hz, 2H, N7CH_2), 3.52−3.58 (m, 2H, NH*CH_2*), 3.35 (s, 3H, N3CH_3), 3.14 (s, 3H, N1CH_3), 2.96 (t, *J* = 7.2 Hz, 2H, NHCH$_2$*CH_2*), 1.51 (dt, *J* = 14.3, 7.2 Hz, 2H, N7CH_2*CH_2*), 1.20 (dq, *J* = 14.8, 7.1 Hz, 2H, N7CH_2CH$_2$*CH_2*), 0.82 (t, *J* = 7.2 Hz, 3H, N7CH_2CH$_2$CH$_2$*CH_3*); **^{13}C NMR** (DMSO-d_6) δ 153.9, 153.1, 151.6, 149.2, 136.8, 127.9, 123.3, 121.4, 118.9, 118.7, 112.2, 111.9, 101.9, 43.9, 42.7, 31.8, 29.8, 27.7, 26.0, 19.6, 14.2. UPLC-MS (*m/z*): 395.16 $[M + H]^+$; $C_{21}H_{26}N_6O_2$ (calculated MW: 394.48). Purity (UPLC-MS): 99.3%; t_R = 6.25.

*8-((2-(1H-Indol-3-yl)ethyl)amino)-7-allyl-1,3-dimethyl-3,7-dihydro-1H-purine-2,6-dione (**24**).* Synthesized according to GP4; purification by column chromatography with a gradient of DCM: methanol (100:0 to 80:20); yield 44%; m.p.: 139−142 °C; **^{1}H NMR** (500 MHz, DMSO-d6) δ 10.81 (br, 1H, NH_{indole}), 7.64 (d, *J* = 7.6 Hz, 1H, Ar−H), 7.32 (d, *J* = 7.6 Hz, 1H, Ar−H), 7.13−7.18 (m, 2H, *NH*CH_2 and Ar−H), 7.05 (td, *J* = 7.5, 1.5 Hz, 1H, Ar−H), 6.94−7.00 (m, 1H, Ar−H), 5.78−5.92 (m, 1H, N7CH_2*CH*), 5.09 (dd, *J* = 10.3, 1.47 Hz, 1H, N7CH_2CH*CH_2*), 4.93 (dd, *J* = 17.0, 1.2 Hz, 1H, N7CH_2CH*CH_2*), 4.66 (d, *J* = 4.7 Hz, 2H, N7CH_2), 3.53−3.63 (m, 2H, NH*CH_2*), 3.39 (s, 3H, N3CH_3), 3.16 (s, 3H, N1CH_3), 2.97 (t, *J* = 7.6 Hz, 2H, NHCH$_2$*CH_2*); **^{13}C NMR** (DMSO-d_6) δ ppm: 154.0, 153.1, 151.8, 149.2, 136.7, 133.4, 127.7, 123.3, 121.4, 118.8, 118.7, 116.9, 112.0, 111.8, 101.6, 44.7, 43.8, 29.7, 27.6, 25.9. UPLC-MS (*m/z*): 379.21 $[M + H]^+$; $C_{20}H_{22}N_6O_2$ (calculated MW: 378.44). Purity (UPLC-MS): 97.4%; t_R = 5.88. HR-MS (ESI-QTOF) calcd for $C_{20}H_{23}N_6O_2$ $[M + H]^+$: 379.1882; found: 379.1873.

*8-((2-(1H-Indol-3-yl)ethyl)amino)-1,3-dimethyl-7-(prop-2-yn-1-yl)-3,7-dihydro-1H-purine-2,6-dione (**27**).* Synthesized according to GP4; purification by column chromatography with a gradient of DCM: methanol (100:0 to 80:20); yield 39%; m.p.: 167−168 °C; **^{1}H NMR** (300 MHz, DMSO-d_6) δ 10.79 (br, 1H, NH_{indole}), 7.65 (d, *J* = 7.6 Hz, 1H, Ar−H), 7.44 (t, *J* = 5.6 Hz, 1H, *NH*CH_2), 7.33 (d, *J* = 8.2 Hz, 1H, Ar−H), 7.18 (d, *J* = 1.8 Hz, 1H, Ar−H), 7.02−7.09 (m, 1H, Ar−H), 6.95−7.01 (m, 1H, Ar−H), 4.91 (d, *J* = 2.3 Hz, 2H, N7CH_2), 3.56−3.64 (m, 2H, NH*CH_2*), 3.37 (s, 3H, N3CH_3), 3.29 (t, *J* = 2.1 Hz, 1H, N7CH_2C*CH*), 3.17 (s, 3H, N1CH_3), 2.99 (t, *J* = 7.3 Hz, 2H, NHCH$_2$*CH_2*); **^{13}C NMR** (DMSO-d_6) δ ppm: 154.3, 153.2, 151.4, 149.5, 136.7, 127.7, 123.3, 121.4, 118.8, 118.7, 111.9, 111.8, 101.1, 78.9, 75.8, 43.8, 32.8, 29.7, 27.6, 25.9. UPLC-MS (*m/z*): 377.22 $[M + H]^+$; $C_{20}H_{20}N_6O_2$ (calculated MW: 376.42). Purity (UPLC-MS): 95.3%; t_R = 5.48.

*8-((2-(1H-Indol-3-yl)ethyl)amino)-1,3-dimethyl-7-(pent-2-yn-1-yl)-3,7-dihydro-1H-purine-2,6-dione (**28**).* Synthesized according to GP4; purification by column chromatography with a gradient of DCM:methanol (100:0 to 80:20); yield 90%; m.p.: 202−203 °C; **^{1}H NMR** (300 MHz, DMSO-d_6) δ 10.81 (br, 1H, NH_{indole}), 7.64 (d, *J* = 7.6 Hz, 1H, Ar−H), 7.30−7.37 (m, 2 H, *NH*CH_2 and Ar−H), 7.17 (d, *J* = 2.3 Hz, 1H, Ar−H), 7.05 (td, *J* = 7.6, 1.2 Hz, 1H, Ar−H), 6.94−7.00 (m, 1H, Ar−H), 4.87 (s, 2H, N7CH_2), 3.55−3.64 (m, 2H, NH*CH_2*), 3.36 (s, 3H, N3CH_3), 3.16 (s, 3H, N1*CH_3*), 2.98 (t, *J* = 7.6 Hz, 2H, NHCH$_2$*CH_2*), 2.08−2.18 (m, 2H, N7CH_2CC*CH_2*), 0.99 (t, *J* = 7.6 Hz, 3H, N7CH_2CCCH$_2$*CH_3*); **^{13}C NMR** (DMSO-d_6) δ ppm: 154.1, 153.1, 151.4, 149.3, 136.7, 127.7, 123.2, 121.4, 118.8, 118.7, 112.0, 111.8, 101.1, 86.4, 74.4, 43.7, 33.0, 29.7, 27.6, 25.9, 14.0, 12.1. UPLC-MS (*m/z*): 405.13 $[M + H]^+$; $C_{22}H_{24}N_6O_2$ (calculated MW: 404.47). Purity (UPLC-MS): 100.0%; t_R = 6.27.

*8-Chloro-7-(4-methoxybenzyl)-1,3-dimethyl-3,7-dihydro-1H-purine-2,6-dione (**29k**).* Synthesized according to GP3; yield 86%; m.p.: 179 °C; **^{1}H NMR** (600 MHz, DMSO-d_6): δ 7.28 (d, *J* = 8.7 Hz, 2H, Ar−H), 6.91 (d, *J* = 8.7 Hz, 2H, Ar−H), 5.45 (s, 2H, N7H_2), 3.72 (s, 3H, -OCH_3), 3.39 (s, 3H, N3CH_3), 3.24 (s, 3H, N1CH_3); **^{13}C NMR** (151 MHz, DMSO): δ 159.0, 153.9, 150.6, 146.8, 137.6, 129.0, 127.4, 114.1, 107.1, 55.1, 47.9, 29.5, 27.7; LC-MS (*m/z*): 334.9 $[M + H]^+$; $C_{15}H_{15}ClN_4O_3$ (calculated MW: 334.7). Purity (HPLC UV (254 nm)-ESI-MS): 96.3%.

*8-Chloro-7-(4-hydroxybenzyl)-1,3-dimethyl-3,7-dihydro-1H-purine-2,6-dione (**29l**).* **29k** (50 mg, 0.15 mmol) was given into a 50 mL round-bottomed flask and dissolved in DCM (1.5 mL). The mixture was stirred and cooled to 5 °C in an ice bath. Then, a 1 M solution of BBr_3 in DCM (0.6 mL) was added dropwise over 10 min. The reaction was kept stirring for 3h. Then, it was quenched by dropwise addition of 2 mL methanol and the solution was extracted with 20 mL DCM three times. The combined organic phases were further washed once with 20 mL of a saturated aq. solution of $NaHCO_3$ and dried over $MgSO_4$. After filtration, the solution was evaporated and the product was purified by column chromatography (DCM: methanol, 9.5:0.5); yield 62%; m.p.: 196 °C; **^{1}H NMR** (600 MHz, DMSO-d_6): δ 9.49 (s, 1H, −OH), 7.16 (d, *J* = 8.5 Hz, 2H, Ar−H), 6.72 (d, *J* = 8.5 Hz, 2H, Ar−H), 5.39 (s, 2H, N7H_2), 3.38 (s, 3H, N3CH_3), 3.24 (s, 3H, N1-CH_3); **^{13}C NMR** (151 MHz, DMSO) δ 157.1, 153.7, 150.7, 146.6, 137.4, 128.9, 125.5, 115.2, 106.9, 47.9, 29.3, 27.5; LC-MS (*m/z*): 321.0 $[M + H]^+$; $C_{14}H_{13}ClN_4O_3$ (calculated MW: 320.7). Purity (HPLC UV (254 nm)-ESI-MS): 93.7%.

*8-Chloro-7-(2-fluoroethyl)-1,3-dimethyl-3,7-dihydro-1H-purine-2,6-dione (**29m**).* **29l** (25 mg, 0.075 mmol) and Cs_2CO_3 (73 mg, 0.23 mmol) were given into a sealed tube and dissolved in DMF (1 mL) upon stirring for 15 min. Then, 1-bromo-2-fluoroethane (0.01 mL, 0.113 mmol) was added, and the mixture was stirred and heated at 60 °C for 2.5h. When no further reaction progress was detected, the reaction was quenched with 10 mL of ice-cold water to precipitate the product, which was subsequently filtered off. Yield 32.5%; LC-MS (*m/z*): 261.1 $[M + H]^+$; $C_9H_{10}ClFN_4O_2$ (calculated MW: 260.6). The crude was used without further purification for the next step.

*8-((2-(1H-Indol-3-yl)ethyl)amino)-7-(2-fluoroethyl)-1,3-dimethyl-3,7-dihydro-1H-purine-2,6-dione (**30**).* Synthesized according to GP4; purification by flash column chromatography (DCM: methanol, 9.5:0.5); yield 56%; m.p.: decomposition at 230 °C; **^{1}H NMR** (600 MHz, DMSO-d_6) δ 10.81 (br, 1H, NH_{indole}), 7.64 (d, *J* = 7.8 Hz, 1H, Ar−H), 7.35−7.29 (m, 2H, Ar−H and *NH*CH_2), 7.16 (d, *J* = 2.4 Hz, 1H, Ar−H), 7.06 (t, *J* = 7.5 Hz, 1H, Ar−H), 6.98 (t, *J* = 7.4 Hz, 1H, Ar−H), 4.63 (dt, *J* = 5.0, 47.2 Hz, 2H, *CH_2*F), 4.36 (dt, *J* = 5.1, 24.5 Hz, 2H,

https://doi.org/10.1021/acs.jmedchem.3c02423
J. Med. Chem. 2024, 67, 9896−9926

CH_2CH_2F), 3.61−3.56 (m, 2H, $NHCH_2CH_2$), 3.40 (s, 3H, N3-CH_3), 3.30 (s, 3H, N1-CH_3), 2.99 (t, J = 7.5 Hz, 2H, $NHCH_2CH_2$); **^{13}C NMR** (151 MHz, DMSO) δ 154.2, 151.15, 149.0, 136.3, 127.4, 122.9, 121.0, 118.4, 118.3, 111.7, 111.5, 101.5, 82.3, 81.2, 43.5, 43.0, 42.8, 29.4, 27.3, 25.5; LC-MS (m/z): 385.1 $[M + H]^+$; $C_{19}H_{21}FN_6O_2$ (calculated MW: 384.4). Purity (HPLC UV (254 nm)-ESI-MS): 98.5%. HR-MS (ESI-QTOF) calcd for $C_{19}H_{21}FN_6O_2Na$ $[M + Na]^+$: 407.1608; found: 407.1602.

*8-((2-(1H-Indol-3-yl)ethyl)amino)-7-benzyl-1,3-dimethyl-3,7-dihydro-1H-purine-2,6-dione (**31**).* Synthesized according to GP4; purification by column chromatography with a gradient of DCM: methanol (100:0 to 80:20); yield 59%; m.p.: 183−184 °C; **^{1}H NMR** (300 MHz, $CDCl_3$) δ 8.05 (br, 1H, NH_{indole}), 7.61 (d, J = 7.82 Hz, 1H, Ar−H), 7.40 (d, J = 8.2 Hz, 1H, Ar−H), 7.20−7.27 (m, 4H, Ar−H), 7.12−7.17 (m, 1H, Ar−H), 7.01 (dd, J = 7.8, 1.6 Hz, 2H, Ar−H), 6.75 (d, J = 1.2 Hz, 1H, Ar−H), 5.19 (s, 2H, N7CH_2), 4.28−4.35 (m, 1H, $NHCH_2$), 3.76 (q, J = 6.3 Hz, 2H, $NHCH_2$), 3.60 (s, 3H, N3CH_3), 3.41 (s, 3H, N1CH_3), 3.02 (t, J = 6.5 Hz, 2H, $NHCH_2CH_2$); **^{13}C NMR** ($CDCl_3$) δ ppm: 154.1, 152.9, 151.7, 136.4, 135.2, 129.0, 128.0, 127.2, 127.1, 122.4, 122.1, 119.6, 118.6, 112.2, 111.3, 102.9, 46.6, 43.4, 29.9, 27.7, 25.2. UPLC-MS (m/z): 429.12 $[M + H]^+$; $C_{24}H_{24}N_6O_2$ (calculated MW 428.50). Purity (UPLC-MS): 100.0%; t_R = 6.32.

*8-((2-(1H-Indol-3-yl)ethyl)amino)-7-(2-fluorobenzyl)-1,3-dimethyl-3,7-dihydro-1H-purine-2,6-dione (**32**).* Synthesized according to GP4; purification by column chromatography with a gradient of DCM: methanol (100:0 to 80:20); yield 34%; m.p.: 202−203 °C; **^{1}H NMR** (500 MHz, DMSO-d_6) δ 10.76 (br, 1H, NH_{indole}), 7.60 (d, J = 8.0 Hz, 1H, Ar−H), 7.33 (t, J = 5.6 Hz, 1H, $NHCH_2$), 7.25−7.31 (m, 2 H, Ar−H), 7.16−7.21 (m, 1H, Ar−H), 7.00−7.08 (m, 3H, Ar−H), 6.92−6.95 (m, 1H, Ar−H), 6.66−6.70 (m, 1H, Ar−H), 5.33 (s, 2H, N7CH_2), 3.54−3.59 (m, 2H, $NHCH_2$), 3.40 (s, 3H, N3CH_3), 3.09 (s, 3H, N1CH_3), 2.94 (t, J = 7.5 Hz, 2H, $NHCH_2CH_2$). UPLC-MS (m/z): 447.42 $[M + H]^+$; $C_{24}H_{23}FN_6O_2$ (calculated MW 446,49). Purity (UPLC-MS): 100.00%; t_R = 6.45. HR-MS (ESI-QTOF) calcd for $C_{24}H_{24}FN_6O_2$ $[M + H]^+$: 447.1945; found: 447.1946.

*8-((2-(1H-Indol-3-yl)ethyl)amino)-7-(2-chlorobenzyl)-1,3-dimethyl-3,7-dihydro-1H-purine-2,6-dione (**33**).* Synthesized according to GP4; purification by column chromatography with a gradient of DCM: methanol (100:0 to 80:20); yield 52%; m.p.: 209−210 °C; **^{1}H NMR** (300 MHz, DMSO-d_6) δ 10.77 (br, 1H, NH_{indole}), 7.62 (d, J = 7.6 Hz, 1H, Ar−H), 7.48 (dd, J = 7.6, 1.8 Hz, 1H, Ar−H), 7.39 (t, J = 5.6 Hz, 1H, $NHCH_2$), 7.19−7.33 (m, 3H, Ar−H), 7.10 (d, J = 2.3 Hz, 1H, Ar−H), 7.01−7.07 (m, 1H, Ar−H), 6.92−6.99 (m, 1H, Ar−H), 6.49 (dd, J = 7.3, 1.5 Hz, 1H, Ar−H), 5.34 (s, 2H, N7CH_2), 3.54−3.62 (m, 2H, $NHCH_2$), 3.43 (s, 3H, N3CH_3), 3.09 (s, 3H, N1CH_3), 2.96 (t, J = 7.3 Hz, 2H, $NHCH_2CH_2$); **^{13}C NMR** (DMSO-d_6) δ ppm: 154.6, 153.1, 151.5, 149.5, 136.7, 135.0, 131.5, 129.7, 129.1, 128.0, 127.7, 126.2, 123.3, 121.3, 118.8, 118.7, 112.0, 111.8, 101.6, 44.3, 43.7, 29.8, 27.5, 25.8. UPLC-MS (m/z): 463.38 $[M + H]^+$; $C_{24}H_{23}ClN_6O_2$ (calculated MW: 462.94). Purity (UPLC-MS): 100.00%; t_R = 6.51. HR-MS (ESI-QTOF) calcd for $C_{24}H_{24}ClN_6O_2$ $[M + H]^+$: 463.1649; found: 463.1646.

*8-((2-(1H-Indol-3-yl)ethyl)amino)-7-(2-bromobenzyl)-1,3-dimethyl-3,7-dihydro-1H-purine-2,6-dione (**34**).* Synthesized according to GP4; purification by column chromatography with a gradient of DCM: methanol (100:0 to 80:20); yield 43%; m.p.: 222−223 °C; **^{1}H NMR** (300 MHz, DMSO-d_6) δ 10.77 (br, 1H, NH_{indole}), 7.59−7.67 (m, 2H, Ar−H), 7.41 (t, J = 5.6 Hz, 1H, $NHCH_2$), 7.16−7.33 (m, 3H, Ar−H), 7.10 (d, J = 1.8 Hz, 1H, Ar−H), 7.01−7.07 (m, 1H, Ar−H), 6.92−6.99 (m, 1H, Ar−H), 6.41−6.46 (m, 1H, Ar−H), 5.28 (s, 2H, N7CH_2), 3.54−3.62 (m, 2H, $NHCH_2$), 3.43 (s, 3H, N3CH_3), 3.09 (s, 3H, N1CH_3), 2.96 (t, J = 7.3 Hz, 2H, $NHCH_2CH_2$); **^{13}C NMR** (DMSO-d_6) δ ppm: 154.6, 153.1, 151.5, 149.5, 136.7, 136.4, 133.3, 129.4, 128.5, 127.7, 126.3, 123.3, 121.6, 121.3, 118.8, 118.7, 112.0, 111.8, 101.5, 46.7, 43.7, 29.8, 27.5, 25.8. UPLC-MS (m/z): 509.38 $[M + H]^+$; $C_{24}H_{23}BrN_6O_2$ (calculated MW: 507.39). Purity (UPLC-MS): 96.5%; t_R = 6.89.

*8-((2-(1H-Indol-3-yl)ethyl)amino)-7-(3-fluorobenzyl)-1,3-dimethyl-3,7-dihydro-1H-purine-2,6-dione (**35**).* Synthesized according to GP4; purification by column chromatography (DCM: methanol, 9.3:0.7); yield 30%; mp 95.3 °C; **^{1}H NMR** (600 MHz, DMSO-d_6) δ 10.78 (br, 1H, NH_{indole}), 7.37 (t, J = 5.7 Hz, 1H, Ar−H), 7.36−7.32 (m, 2H, Ar−H and $NHCH_2$), 7.10 (d, J = 2.3 Hz, 1H, Ar−H), 7.09 (d, J = 2.6 Hz, 1H, Ar−H), 7.08−7.04 (m, 2H, Ar−H), 7.01 (d, J = 7.9 Hz, 1H, Ar−H), 6.98 (ddd, J = 8.0, 7.0, 1.0 Hz, 1H, Ar−H), 5.30 (s, 2H, N7CH_2), 3.63−3.59 (m, 2H,, $NHCH_2CH_2$), 3.41 (s, 3H, N3-CH_3), 3.17 (s, 3H,, N1-CH_3), 2.98 (t, J = 7.5 Hz, 2H, $NHCH_2CH_2$); **^{13}C NMR** (151 MHz, DMSO) δ 163.1, 161.4, 153.9, 152.9, 151.1, 149.1, 140.03, 139.98, 136.4, 130.7, 130.6, 127.4, 123.14, 123.11, 122.9, 121.0, 118.4, 118.3, 114.4, 114.2, 114.1, 114.0, 111.6, 111.5, 101.3, 44.9, 43.5, 29.4, 27.3, 25.5; LC-MS (m/z): 447.3 $[M + H]^+$; $C_{24}H_{23}FN_6O_2$ (calculated MW: 446.4). Purity (HPLC UV (254 nm)-ESI-MS): 97.7%. HR-MS (ESI-QTOF) calcd for $C_{24}H_{24}FN_6O_2$ $[M + H]^+$: 447.1945; found: 447.1937.

*8-((2-(1H-Indol-3-yl)ethyl)amino)-7-(3-chlorobenzyl)-1,3-dimethyl-3,7-dihydro-1H-purine-2,6-dione (**36**).* Synthesized according to GP4; purification by column chromatography with gradient of DCM: methanol (100:0 to 80:20); yield 59%; m.p.: 152−153 °C; **^{1}H NMR** (500 MHz, DMSO-d_6) δ 10.76 (s, 1H, NH_{indole}), 7.60 (d, J = 8.0 Hz, 1H, Ar−H), 7.38 (t, J = 5.7 Hz, 1H, $NHCH_2$), 7.28−7.32 (m, 4H, Ar−H), 7.06−7.09 (m, 2H, Ar−H), 7.00−7.04 (m, 1H, Ar−H), 6.92−6.96 (m, 1H, Ar−H), 5.25 (s, 2H, N7CH_2), 3.54−3.59 (m, 2H, $NHCH_2$), 3.36 (s, 3H, N3CH_3), 3.13 (s, 3H, N1CH_3), 2.94 (t, J = 7.5 Hz, 2H, $NHCH_2CH_2$); **^{13}C NMR** (DMSO-d_6) δ ppm: 43.8, 45.2, 101.6, 111.8, 112.0, 118.7, 118.8, 121.4, 122.1, 123.2, 126.4, 127.7, 130.3, 130.7, 131.2, 136.7, 140.2, 149.4, 151.4, 153.2, 154.2. UPLC-MS (m/z): 463.44 $[M + H]^+$; $C_{24}H_{23}ClN_6O_2$ (calculated MW: 462.94). Purity (UPLC-MS): 100.0%; t_R = 6.83. HR-MS (ESI-QTOF) calcd for $C_{24}H_{24}ClN_6O_2$ $[M + H]^+$: 463.1649, found: 463.1645.

*8-((2-(1H-Indol-3-yl)ethyl)amino)-7-(3-bromobenzyl)-1,3-dimethyl-3,7-dihydro-1H-purine-2,6-dione (**37**).* Synthesized according to GP4; purification by column chromatography with gradient of DCM: methanol (100:0 to 80:20); yield 41%; m.p.: 162−163 °C; **^{1}H NMR** (300 MHz, DMSO- d_6) δ 10.78 (br, 1H, NH_{indole}), 7.62 (d, J = 7.62 Hz, 1H, Ar−H), 7.38−7.48 (m, 3H; $NHCH_2$ and Ar−H), 7.32 (d, J = 7.62 Hz, 1H, Ar−H), 7.24 (m, J = 7.62, 7.62 Hz, 1H, Ar−H), 7.09−7.16 (m, 2H, Ar−H), 7.05 (td, J = 7.6, 1.2 Hz, 1H, Ar−H), 6.93−6.99 (m, 1H, Ar−H), 5.27 (s, 2H, Ar−H), 3.55−3.64 (m, 2H, $NHCH_2$), 3.39 (s, 3H, N3CH_3), 3.15 (s, 3H, N1CH_3), 2.96 (t, J = 7.3 Hz, 2H, $NHCH_2CH_2$); **^{13}C NMR** (DMSO-d_6) δ ppm: 154.2, 153.2, 151.4, 149.4, 140.2, 136.7, 131.2, 130.7, 130.3, 127.7, 126.4, 123.2, 122.1, 121.4, 118.8, 118.7, 112.0, 111.8, 101.6, 45.2, 43.8, 29.8, 27.7, 25.9. UPLC-MS (m/z): 509.38 $[M + H]^+$; $C_{24}H_{23}BrN_6O_2$ (calculated MW: 507.39). Purity (UPLC-MS): 99.4%; t_R = 6.93.

*8-((2-(1H-Indol-3-yl)ethyl)amino)-7-(3-methoxybenzyl)-1,3-dimethyl-3,7-dihydro-1H-purine-2,6-dione (**38**).* Synthesized according to GP4; purification by column chromatography with gradient of DCM: methanol (100:0 to 80:20); yield 57%; m.p.: 158−159 °C; **^{1}H NMR** (300 MHz, DMSO-d_6) δ 10.78 (s, 1H, NH_{indole}), 7.63 (d, J = 7.6 Hz, 1H, Ar−H), 7.30−7.38 (m, 2H, Ar−H and $NHCH_2$), 7.20 (t, J = 7.9 Hz, 1H, Ar−H), 7.10 (d, J = 2.3 Hz, 1H, Ar−H), 7.05 (td, J = 7.6, 1.2 Hz, 1H, Ar−H), 6.93−7.00 (m, 1H, Ar−H), 6.78−6.84 m, 2H, Ar−H), 6.73 (d, J = 7.6 Hz, 1H, Ar−H), 5.24 (s, 2H, N7CH_2), 3.68 (s, 3H, OCH_3), 3.55−3.63 (m, 2H, $NHCH_2$), 3.39 (s, 3H, N3CH_3), 3.15 (s, 3H, N1CH_3), 2.96 (t, J = 7.6 Hz, 2H, $NHCH_2CH_2$); **^{13}C NMR** (DMSO-d_6) δ ppm: 159.7, 154.3, 153.2, 151.5, 149.4, 139.0, 136.7, 130.1, 127.7, 123.3, 121.4, 119.5, 118.8, 118.7, 113.6, 112.9, 112.0, 111.8, 101.7, 55.4, 45.6, 43.8, 29.7, 27.7, 25.9. UPLC-MS (m/z): 459.45 $[M + H]^+$; $C_{25}H_{26}N_6O_3$ (calculated MW: 458.52). Purity (UPLC-MS): 100.0%; t_R = 6.36.

*8-((2-(1H-Indol-3-yl)ethyl)amino)-1,3-dimethyl-7-(4-methylbenzyl)-3,7-dihydro-1H-purine-2,6-dione (**39**).* Synthesized according to GP4; purification by column chromatography with a gradient of DCM: methanol (100:0 to 80:20); yield 41%; m.p.: 181−182 °C; **^{1}H NMR** (300 MHz, $CDCl_3$) δ 8.09 (br, 1H, NH_{indole}), 7.60 (d, J = 8.2 Hz, 1H, Ar−H), 7.39 (d, J = 8.2 Hz, 1H, Ar−H), 7.20−7.26 (m, 1H, Ar−H), 7.09−7.16 (m, 1H, Ar−H), 6.96−7.01 (m, 2H, Ar−H), 6.85−6.90 (m, 2H, Ar−H), 6.79 (d, J = 2.3 Hz, 1H, Ar−H), 5.11 (s, 2H, N7CH_2), 4.19 (t, J = 5.6 Hz, 1H, $NHCH_2$), 3.71 (q, J = 6.5 Hz, 2H, $NHCH_2$), 3.56 (s, 3H, N3CH_3), 3.39 (s, 3H, N1CH_3), 3.00 (t, J = 6.5 Hz, 2H,

Journal of Medicinal Chemistry pubs.acs.org/jmc Article

$NHCH_2CH_2$), 2.29 (s, 3 H, CH_3); **^{13}C NMR** ($CDCl_3$) δ ppm: 154.1, 153.3, 151.8, 148.7, 137.7, 136.4, 132.2, 129.6, 127.2, 127.0, 122.4, 122.1, 119.6, 118.7, 112.4, 111.3, 102.9, 46.3, 43.3, 29.7, 27.7, 25.3, 21.1. UPLC-MS (m/z): 443.43 $[M + H]^+$; $C_{25}H_{26}N_6O_2$ (calculated MW: 442.52). Purity (UPLC-MS): 100.0%; t_R = 6.73.

*8-((2-(1H-Indol-3-yl)ethyl)amino)-1,3-dimethyl-7-(4-(trifluoromethyl)benzyl)-3,7-dihydro-1H-purine-2,6-dione (**40**).* Synthesized according to GP4; purification by column chromatography with gradient of DCM: methanol (100:0 to 80:20); yield 51%; m.p.: 237−238 °C; **^{1}H NMR** (500 MHz, DMSO-d_6) δ 10.79 (br, 1H, NH_{indole}), 7.57−7.63 (m, 3H, Ar−H), 7.40 (t, J = 5.2 Hz, 1H, $NHCH_2$), 7.28−7.33 (m, 3H, Ar−H), 7.10 (br, 1H, Ar−H), 7.02 (t, J = 7.2 Hz, 1H, Ar−H), 6.91−6.96 (m, 1H, Ar−H), 5.33 (br, 2H, N7CH_2), 3.55−3.61 (m, 2H, $NHCH_2$), 3.37 (s, 3H, N3CH_3), 3.11 (s, 3H, N1CH_3), 2.95 (t, J = 7.2 Hz, 2H, $NHCH_2CH_2$); **^{13}C NMR** (DMSO-d_6) δ ppm: 154.4, 153.3, 151.5, 149.5, 142.4, 136.7, 128.1, 127.8, 126.0, 125.9, 123.4, 123.3, 121.4, 118.9, 118.7, 112.0, 111.9, 101.7, 45.4, 43.8, 29.8, 27.7, 25.8. UPLC-MS (m/z): 497.41 $[M + H]^+$; $C_{25}H_{23}F_3N_6O_2$ (MW 496.49). Purity (UPLC-MS): 97.4%; t_R = 6.85.

*8-((2-(1H-Indol-3-yl)ethyl)amino)-7-(4-methoxybenzyl)-1,3-dimethyl-3,7-dihydro-1H-purine-2,6-dione (**41**).* Synthesized according to GP4; purification by column chromatography with a gradient of DCM: methanol (100:0 to 80:20); yield 61%; m.p.: 114−115 °C; **^{1}H NMR** (500 MHz, DMSO-d_6) δ 10.79 (s, 1H, NH_{indole}), 7.61 (d, J = 8.0 Hz, 1H, Ar−H), 7.29−7.33 (m, 2 H, Ar−H and $NHCH_2$), 7.13−7.16 (m, 2H, Ar−H), 7.10 (d, J = 2.3 Hz, 1H, Ar−H), 7.03 (ddd, J = 8.0, 6.9, 1.2 Hz, 1H, Ar−H), 6.95 (ddd, J = 8.0, 6.9, 1.2 Hz, 1H, Ar−H), 6.77−6.80 (m, 2H, Ar−H), 5.16 (s, 2H, N7CH_2), 3.66 (s, 3H, OCH_3), 3.55−3.60 (m, 2H, $NHCH_2$), 3.35 (s, 3H, N3CH_3), 3.14 (s, 3H, N1CH_3), 2.95 (t, J = 7.5 Hz, 2H, $NHCH_2CH_2$); **^{13}C NMR** (DMSO-d_6) δ ppm: 159.2, 154.2, 153.3, 151.5, 149.5, 136.8, 129.6, 129.3, 127.8, 123.4, 121.5, 118.9, 118.8, 114.4, 112.1, 111.9, 101.7, 55.6, 45.2, 43.8, 29.8, 27.8, 25.9. UPLC-MS (m/z): 459.45 $[M + H]^+$; $C_{25}H_{26}N_6O_3$ (calculated MW: 458.52). Purity (UPLC-MS): 96.8%; t_R = 6.08.

*8-((2-(1H-Indol-3-yl)ethyl)amino)-7-(4-isopropylbenzyl)-1,3-dimethyl-3,7-dihydro-1H-purine-2,6-dione (**42**).* Synthesized according to GP4; purification by column chromatography with a gradient of DCM: methanol (100:0 to 80:20); yield 47%; m.p.: 209−210 °C;**^{1}H NMR** (500 MHz, DMSO-d_6) δ 10.78 (s, 1H, NH_{indole}), 7.61 (d, J = 8.0 Hz, 1H, Ar−H), 7.29−7.33 (m, 2H, $NHCH_2$ and Ar−H), 7.06−7.11 (m, 5H, Ar−H), 7.03 (s, 1H, Ar−H), 6.92−6.96 (m, 1H, Ar−H), 5.20 (s, 2H, N7CH_2 and Ar−H), 3.55−3.60 (m, 2H, $NHCH_2$), 3.36 (s, 3H, N3CH_3), 3.13 (s, 3H, N1CH_3), 2.95 (t, J = 7.5 Hz, 2H, $NHCH_2CH_2$), 2.75−2.81 (m, 1H, $CH(CH_3)_2$), 1.11 (d, J = 7.2 Hz, 6H, $CH(CH_3)_2$). UPLC-MS (m/z): 471.42 $[M + H]^+$; $C_{27}H_{30}N_6O_2$ (calculated MW: 470.58). Purity (UPLC-MS): 98.6%; t_R = 7.12. HR-MS (ESI-QTOF) calcd for $C_{27}H_{31}N_6O_2$ $[M + H]^+$: 471.2508, found: 471.2517.

*Methyl 4-((8-((2-(1H-Indol-3-yl)ethyl)amino)-1,3-dimethyl-2,6-dioxo-1,2,3,6-tetrahydro-7H-purin-7-yl)methyl)benzoate (**43**).* Synthesized according to GP4; purification by column chromatography (DCM: methanol, 9.8:0.2); yield 63%; m.p.: 194−195 °C; **^{1}H NMR** (500 MHz, DMSO-d_6) δ 10.78 (s, 1H, NH_{indole}), 7.88 (d, J = 8.4 Hz, 2H, Ar−H), 7.62 (d, J = 7.9 Hz, 1H, Ar−H), 7.39−7.32 (m, 2H, $NHCH_2$ and Ar−H), 7.27 (d, J = 8.4 Hz, 2H, Ar−H), 7.11 (d, J = 2.3 Hz, 1H, Ar−H), 7.06 (t, J = 8.1 Hz, 1H, Ar−H), 6.97 (t, J = 7.9 Hz, 1H, Ar−H), 5.36 (s, 2H, N7CH_2), 3.83 (s, 3H, OCH_3), 3.65−3.56 (m, 2H, $HNCH_2$), 3.41 (s, 3H, N3CH_3), 3.15 (s, 3H, N1CH_3), 2.98 (t, J = 7.4 Hz, 2H, $NHCH_2CH_2$); **^{13}C NMR** (126 MHz, DMSO-d_6) δ 165.9, 153.9, 152.7, 151.0, 148.9, 142.5, 136.2, 122.8, 120.9, 118.3, 118.2, 111.5, 111.3, 101.2, 94.5, 52.1, 45.2, 43.3, 29.3, 27.1, 25.3; LC-MS (m/z): 487.1 $[M + H]^+$; $C_{26}H_{26}N_6O_4$ (calculated MW: 486.5). Purity (HPLC UV (254 nm)-ESI-MS): 98.2%.

*4-((8-((2-(1H-Indol-3-yl)ethyl)amino)-1,3-dimethyl-2,6-dioxo-1,2,3,6-tetrahydro-7H-purin-7-yl)methyl)benzamide (**45**).* A mixture of **43** (0.03 g, 0.062 mmol) and NH_4Cl (0.013 g, 0.25 mmol) was suspended in NH_4OH (0.2 mL). The mixture was heated to 100 °C and stirred for 3 days at this temperature. During this time a precipitate formed, which was filtered off and washed with water (3 × 20 mL), then crystallized from methanol to yield the product as a white solid. Yield 35%; m.p.: 267−268 °C; **^{1}H NMR** (600 MHz, DMSO-d_6) δ 10.79 (s, 1H, NH_{indole}), 7.88 (s, 1H, Ar−H), 7.79 (d, J = 8.4 Hz, 2H, NH_2), 7.64 (d, J = 7.9 Hz, 1H, Ar−H), 7.38 (m, 1H, Ar−H), 7.35−7.30 (m, 2H, $NHCH_2$ and Ar−H), 7.24 (d, J = 8.3 Hz, 2H, Ar−H), 7.11 (s, 1H, Ar−H), 7.06−7.05 (m, 1H, Ar−H), 6.98 (t, J = 7.4 Hz, 1H, Ar−H), 5.33 (s, 2H, N7CH_2), 3.66−3.52 (m, 2H, $HNCH_2$), 3.41 (s, 3H, N3CH_3), 3.16 (s, 3H, N1CH_3), 3.02−2.94 (t, J = 7.4 Hz, 2H, $NHCH_2CH_2$); LC-MS (m/z): 472.2 $[M + H]^+$; $C_{25}H_{25}N_7O_3$ (calculated MW: 471.5). Purity (HPLC UV (254 nm)-ESI-MS): 96.8%.

*4-((8-((2-(1H-Indol-3-yl)ethyl)amino)-1,3-dimethyl-2,6-dioxo-1,2,3,6-tetrahydro-7H-purin-7-yl)methyl)-N-propylbenzamide (**46**).* Compound **44** (0.2 g, 0.42 mmol) and T3P (266 mg, 0.42 mmol, as a 50% solution in DCM) were dissolved in 1 mL of DCM. Then, a solution of propylamine (0.03 mL, 0.378 mmol) and TEA (0.1 mL, 0.76 mmol) in DCM (1 mL) was added dropwise cooling the mixture in a water/ice bath. The reaction mixture was kept stirring overnight at RT. Then, an extraction was performed with 20 mL of ethyl acetate and 20 mL of a saturated aq. solution of $NaHCO_3$ three times. The organic phase was dried over $MgSO_4$ and then concentrated by rotary evaporation. Purification by column chromatography (DCM: methanol, 9.5:0.5) led to the title product as a white solid; yield 5%; m.p.: 259−263 °C; **^{1}H NMR** (600 MHz, DMSO-d_6) δ 10.80 (s, 1H, NH_{indole}), 8.35 (t, J = 5.7 Hz, 1H, CONH), 7.75 (d, J = 8.3 Hz, 2H, Ar−H), 7.64 (d, J = 7.8 Hz, 1H, Ar−H), 7.40 (t, J = 5.7 Hz, 1H, $NHCH_2$), 7.34 (d, J = 8.1 Hz, 1H, Ar−H), 7.24 (d, J = 8.0 Hz, 2H, Ar−H), 7.13−7.11 (m, 1H, Ar−H), 7.06 (t, J = 6.9 Hz, 1H, Ar−H), 6.98 (t, J = 7.4 Hz, 1H, Ar−H), 5.33 (s, 2H, N7CH_2), 3.64−3.57 (m, 2H, $HNCH_2$), 3.41 (s, 3H, N3CH_3), 3.20 (q, J = 6.9 Hz, 2H,, $CH_2CH_2CH_3$), 3.16 (s, 3H, N1CH_3), 2.98 (t, J = 7.5 Hz, 2H, $NHCH_2CH_2$), 1.51 (dt, J = 7.3 Hz, 2H, $CH_2CH_2CH_3$), 0.87 (t, J = 7.4 Hz, 3H, CH_2CH_3); **^{13}C NMR** (151 MHz, DMSO-d_6) δ 165.9, 153.8, 152.7, 150.9, 148.9, 139.9, 136.2, 133.9, 127.3, 127.2, 126.7, 122.8, 120.9, 118.3, 118.2, 111.5, 111.4, 101.2, 45.1, 43.4, 40.9, 29.3, 27.2, 25.4, 22.3, 11.4; LC-MS (m/z): 514.2 $[M + H]^+$; $C_{28}H_{31}N_7O_3$ (calculated MW: 513.6). Purity: 95.0%. HR-MS (ESI-QTOF) calcd for $C_{28}H_{31}N_7O_3Na$ $[M + Na]^+$: 536.2381, found: 536.2360.

*4-((8-((2-(1H-Indol-3-yl)ethyl)amino)-1,3-dimethyl-2,6-dioxo-1,2,3,6-tetrahydro-7H-purin-7-yl)methyl)benzenesulfonamide (**47**).* Synthesized according to GP4; purification by column chromatography (DCM: methanol, 9.5:0.5); yield 37%; m.p.: 243−244 °C; **^{1}H NMR** (600 MHz, DMSO-d_6) δ 10.78 (s, 1H, NH_{indole}), 7.76 (d, J = 8.3 Hz, 2H, Ar−H), 7.65 (d, J = 7.9 Hz, 1H, Ar−H), 7.42 (t, J = 5.6 Hz, 1H, Ar−H), 7.35−7.32 (m, 3H, $NHCH_2$ and Ar−H), 7.31 (s, 2H, NH_2), 7.13 (d, J = 2.0 Hz, 1H, Ar−H), 7.07 (t, J = 7.5 Hz, 1H, Ar−H), 6.98 (t, J = 7.4 Hz, 1H, Ar−H), 5.36 (s, 2H, N7CH_2), 3.64−3.58 (m, 2H, $HNCH_2$), 3.42 (s, 3H, N3CH_3), 3.16 (s, 3H, N1CH_3), 3.01−2.97 (m, 2 H, $NHCH_2CH_2$); **^{13}C NMR** (151 MHz, DMSO-d_6) δ 153.8, 152.7, 150.9, 148.9, 143.0, 141.0, 136.2, 127.3, 127.2, 125.9, 122. 8, 120.9, 118.3, 118.2, 111.5, 111.4, 101.2, 45.0, 43.4, 29.3, 27.2, 25.4; LC-MS (m/z): 508.2 $[M + H]^+$; $C_{24}H_{25}N_7O_4S$ (calculated MW: 507.5). Purity (HPLC UV (254 nm)-ESI-MS): 99.3%.

*4-((8-((2-(1H-Indol-3-yl)ethyl)amino)-1,3-dimethyl-2,6-dioxo-1,2,3,6-tetrahydro-7H-purin-7-yl)methyl)-N-methylbenzenesulfonamide (**48**).* Synthesized according to GP4; purification by column chromatography (DCM: methanol, 9.5:0.5); yield 29%; m.p.: 169−170 °C; **^{1}H NMR** (600 MHz, DMSO-d_6) δ 10.78 (s, 1H, NH_{indole}), 7.71 (d, J = 8.3 Hz, 2H, Ar−H), 7.63 (d, J = 7.9 Hz, 1H, Ar−H), 7.41−7.38 (m, 2H, Ar−H and SO_2NH−), 7.36−7.33 (m, 3H, $NHCH_2$ and Ar−H), 7.13 (d, J = 2.0 Hz, 1H, Ar−H), 7.06 (t, J = 7.4 Hz, 1H, Ar−H), 6.97 (t, J = 7.4 Hz, 1H, Ar−H), 5.37 (s, 2H, N7CH_2), 3.65−3.55 (m, 2H, $HNCH_2$), 3.42 (s, 3H, N3CH_3), 3.15 (s, 3H, N1CH_3), 2.98 (t, J = 7.4 Hz, 2H, $NHCH_2CH_2$), 2.39 (d, J = 5.0 Hz, 3H, SO_2NHCH_3); **^{13}C NMR** (151 MHz, DMSO-d_6) δ 153.8, 152.8, 151.0, 149.9, 141.7, 138.3, 136.3, 127.4, 127.3, 126.9, 122.8, 120.9, 118.3, 118.2, 111.5, 111.4, 101.2, 45.0, 43.3, 28.6, 27.2, 25.3; LC-MS (m/z): 522.5 $[M + H]^+$; $C_{25}H_{27}N_7O_4S$ (calculated MW: 521.5). Purity (HPLC UV (254 nm)-ESI-MS): 93.6%.

*4-((8-((2-(1H-Indol-3-yl)ethyl)amino)-1,3-dimethyl-2,6-dioxo-1,2,3,6-tetrahydro-7H-purin-7-yl)methyl)-N-propylbenzenesulfonamide (**49**).* Synthesized according to GP4; purification by column chromatography (DCM: methanol, 9.8:0.2); yield: 38%; m.p.: 240.3−

https://doi.org/10.1021/acs.jmedchem.3c02423
J. Med. Chem. 2024, 67, 9896−9926

241.5 °C; **^{1}H NMR** (600 MHz, DMSO-d_6) δ 10.82 (s, 1H, NH_{indole}), 7.72 (d, J = 8.29 Hz, 2H, Ar−H), 7.63 (d, J = 7.86 Hz, 1H (Ar−H), 7.53 (t, J = 5.06 Hz, SO_2NH), 7.40 (t, J = 5.66 Hz, 1H, *NH*CH_2), 7.34 (d, J = 8.28 Hz, 3H, Ar−H), 7.13 (d, J = 2.36 Hz, 1H, Ar−H), 7.06 (t, J = 7.58 Hz, 1H Ar−H), 6.98 (t, J = 7.44 Hz, 1H, Ar−H), 5.37 (s, 2H, N7CH_2), 3.61 (dt, J = 6.19, 8.23 Hz, 2H, NH*CH_2*CH_2), 3.42 (s, 3H, N3-CH_3), 3.16 (s, 3H, N1-CH_3), 2.98 (t, J = 7.52 Hz, 2H, NHCH$_2$*CH_2*), 2.66 (q, J = 6.36 Hz, 2H, *CH_2*CH_2CH_3), 1.36 (h, J = 7.31 Hz, 2H, CH_2*CH_2*CH_3), 0.78 (t, J = 7.36 Hz, 3H, CH_2*CH_3*); **^{13}C NMR** (151 MHz, DMSO-d_6) δ 154.0, 152.9, 151.2, 149.2, 141.7, 139.8, 136.4, 127.6, 127.4, 126.9, 123.0, 121.1, 118.5, 118.4, 111.7, 111.5, 101.4, 45.2, 44.5, 43.5, 29.6, 27.4, 25.5, 22.6, 11.3; LC-MS (m/z): 550.5 $[M + H]^+$; $C_{27}H_{31}N_7O_4S$ (calculated MW: 549.6). Purity (HPLC UV (254 nm)-ESI-MS): 97.6%. HR-MS (ESI-QTOF) calcd for $C_{27}H_{31}N_7O_4SNa$ $[M + Na]^+$: 572.2050, found: 572.1957.

*8-((2-(1H-Indol-3-yl)ethyl)amino)-7-(4-fluorobenzyl)-1,3-dimethyl-3,7-dihydro-1H-purine-2,6-dione (**50**).* Synthesized according to GP4; purification by column chromatography with a gradient of DCM: methanol (100:0 to 80:20); yield 32%; m.p.: 176−178 °C; **^{1}H NMR** (300 MHz, DMSO-d_6) δ 10.79 (s, 1H, NH_{indole}), 7.62 (d, J = 7.6 Hz, 1H, Ar−H), 7.31−7.39 (m, 2H, Ar−H), 7.21−7.28 (m, 2 H, Ar−H), 7.02−7.13 (m, 4H, *NH*CH_2 and Ar−H), 6.93−6.99 (m, 1H, Ar−H), 5.24 (s, 2H, N7CH_2), 3.60 (q, J = 6.5 Hz, 2H, NH*CH_2*), 3.38 (s, 3H, N3CH_3), 3.16 (s, 3H, N1CH_3), 2.97 (t, J = 7.3 Hz, 2H, NHCH$_2$*CH_2*); **^{13}C NMR** (DMSO-d_6) δ ppm: 161.9, 154.1, 153.2, 151.4, 149.4, 136.7, 133.7, 129.8, 127.7, 123.3, 121.4, 118.8, 118.7, 115.7, 112.0, 111.8, 110.0, 101.5, 45.0, 43.7, 29.7, 27.7, 25.8. UPLC-MS (m/z): 447.14 $[M + H]^+$; $C_{24}H_{23}FN_6O_2$ (calculated MW: 446.49). Purity (UPLC-MS): 98.9%; t_R = 6.46. HR-MS (ESI-QTOF) calcd for $C_{24}H_{24}FN_6O_2$ $[M + H]^+$: 447.1945, found: 447.1945.

*8-((2-(1H-Indol-3-yl)ethyl)amino)-7-(4-chlorobenzyl)-1,3-dimethyl-3,7-dihydro-1H-purine-2,6-dione (**51**).* Synthesized according to GP4; purification by column chromatography with a gradient of DCM: methanol (100:0 to 80:20); yield 62%; m.p.: 217−218 °C; **^{1}H NMR** (400 MHz, $CDCl_3$) δ 8.07 (br, 1H, NH_{indole}), 7.61 (d, J = 7.8 Hz, 1H, Ar−H), 7.44 (d, J = 8.2 Hz, 1H, Ar−H), 7.25−7.28 (m, 1H, Ar−H), 7.11−7.18 (m, 3H, C5H, Ar−H), 6.86−6.90 (m, 2H, Ar−H), 6.78 (d, J = 2.4 Hz, 1H, Ar−H), 5.11 (s, 2H, N7CH_2), 4.11 (br, 1H, *NH*CH_2), 3.75 (q, J = 6.1 Hz, 2H, NH*CH_2*), 3.59 (s, 3H, N3CH_3), 3.40 (s, 3H, N1CH_3), 3.05 (t, J = 6.26 Hz, 2H, NHCH$_2$*CH_2*); **^{13}C NMR** ($CDCl_3$) δ ppm: 154.2, 151.7, 136.4, 133.8, 133.7, 129.1, 128.4, 127.2, 122.5, 122.1, 119.7, 118.6, 112.1, 111.4, 102.8, 45.9, 43.4, 29.8, 27.7, 25.0. UPLC-MS (m/z): 463.22 $[M + H]^+$; $C_{24}H_{23}ClN_6O_2$ (calculated MW: 462.94). Purity (UPLC-MS): 98.5%; t_R = 6.87. HR-MS (ESI-QTOF) calcd for $C_{24}H_{24}ClN_6O_2$ $[M + H]^+$: 463.1649, found: 463.1646.

*8-((2-(1H-Indol-3-yl)ethyl)amino)-7-(4-bromobenzyl)-1,3-dimethyl-3,7-dihydro-1H-purine-2,6-dione (**52**).* Synthesized according to GP4; purification by column chromatography with a gradient of DCM: methanol (100:0 to 80:20); yield 45%; m.p.: 155−156 °C; **^{1}H NMR** (300 MHz, DMSO-d_6) δ 10.80 (s, 1H, NH_{indole}), 7.62 (d, J = 8.2 Hz, 1H, Ar−H), 7.43−7.48 (m, 2H, Ar−H), 7.40 (t, J = 5.6 Hz, 1H, *NH*CH_2), 7.33 (d, J = 7.6 Hz, 1H, Ar−H), 7.10−7.15 (m, 3H, Ar−H), 7.02−7.08 (m, 1H, Ar−H), 6.92−6.99 (m, 1H, Ar−H), 5.24 (s, 2H, N7CH_2), 3.59 (q, J = 6.6 Hz, 2H, NH*CH_2*), 3.38 (s, 3H, N3CH_3), 3.14 (s, 3H, N1CH_3), 2.97 (t, J = 7.3 Hz, 2 H, NHCH$_2$*CH_2*); **^{13}C NMR** (DMSO-d_6) δ ppm: 154.2, 153.2, 151.4, 149.4, 137.0, 136.7, 131.8, 129.8, 127.7, 123.3, 121.4, 121.0, 118.8, 118.7, 112.0, 111.8, 101.5, 45.2, 43.7, 29.7, 27.7, 25.8. UPLC-MS (m/z): 509.08 $[M + H]^+$; $C_{24}H_{23}BrN_6O_2$ (calculated MW: 507.39). Purity (UPLC-MS): 98.2%; t_R = 6.98. HR-MS (ESI-QTOF) calcd for $C_{24}H_{24}BrN_6O_2$ $[M + H]^+$: 507.1144, found: 507.1143.

*8-((2-(1H-Indol-3-yl)ethyl)amino)-1,3-dimethyl-7-(4-nitrobenzyl)-3,7-dihydro-1H-purine-2,6-dione (**53**).* Synthesized according to GP4; purification by column chromatography with a gradient of DCM: methanol (100:0 to 80:20); yield 41%; m.p.: 198−199 °C; **^{1}H NMR** (500 MHz, DMSO-d_6) δ 10.78 (d, J = 1.2 Hz, 1H, NH_{indole}), 8.09−8.12 (m, 2H, Ar−H), 7.59 (d, J = 8.0 Hz, 1H, Ar−H), 7.41 (t, J = 5.58 Hz, 1H, *NH*CH_2), 7.34 (d, J = 8.88 Hz, 2H, Ar−H), 7.30 (d, J = 8.0 Hz, 1H, Ar−H), 7.08 (d, J = 2.3 Hz, 1H, Ar−H), 7.00−7.05 (m, 1H, Ar−H), 6.91−6.95 (m, 1H, Ar−H), 5.37 (s, 2H, N7CH_2), 3.56−3.61 (m, 2H, NH*CH_2*), 3.37 (s, 3H, N3CH_3), 3.11 (s, 3H, N1CH_3), 2.96 (t, J = 7.2 Hz, 2H, NHCH$_2$*CH_2*). UPLC-MS (m/z): 474.12 $[M + H]^+$; $C_{24}H_{23}N_7O_4$ (calculated MW: 473.49). Purity (UPLC-MS): 98.3%; t_R = 6.32.

*8-((2-(1H-Indol-3-yl)ethyl)amino)-7-(4-aminobenzyl)-1,3-dimethyl-3,7-dihydro-1H-purine-2,6-dione (**54**).* Compound **53** (0.223 g, 0.47 mmol) was dissolved in methanol and Pd/C (27.88 mg) was added. Argon was flushed into the flask before hydrogen gas was introduced. The reaction was kept stirring under H_2 for 7h. Then it was stopped, and the solution was diluted with 50 mL ethyl acetate, to completely dissolve the product, and the solution was filtered through Celite under reduced pressure, followed by purification by column chromatography (DCM: methanol, 9.5:0.5 to 8.5:1.5); yield 39%; m.p.: 137 °C; **^{1}H NMR** (600 MHz, DMSO-d_6) δ 10.79 (s, 1H, NH_{indole}), 7.66 (d, J = 6.8 Hz, 1H, Ar−H), 7.35 (d, J = 8.1 Hz, 1H, Ar−H), 7.20 (t, J = 5.7 Hz, 1H, *NH*CH_2), 7.13 (d, J = 2.3 Hz, 1H, Ar−H), 7.07 (ddd, J = 1.1, 7.0, 8.1 Hz, 1H, Ar−H), 7.00−6.95 (m, Ar−H), 6.47 (d, J = 8.5 Hz, 2H, Ar−H), 5.08 (s, 2H, N7CH_2), 4.98 (s, 2H, -NH_2), 3.60 (m, 2H, NH*CH_2*), 3.38 (s, 3H, N3-CH_3), 3.19 (s, 3H, N1-CH_3), 2.98 (t, J = 7.3, 7.8 Hz, 2H, NHCH$_2$*CH_2*);**^{13}C NMR** (151 MHz, DMSO) δ 153.6, 152.8, 151.0, 148.8, 148.0, 136.3, 128.4, 127.3, 124.0, 122.8, 120.9, 118.3, 118.2, 113.7, 111.6, 111.4, 101.2, 45.0, 43.4, 29.2, 27.2, 25.5; LC-MS (m/z): 444.2 $[M + H]^+$; $C_{24}H_{25}N_7O_2$ (calculated MW: 443.5). Purity (HPLC UV (254 nm)-ESI-MS): 100%. HR-MS (ESI-QTOF) calcd for $C_{24}H_{25}N_7O_2Na$ $[M + Na]^+$: 466.1962, found: 466.1926.

*N-(4-((8-((2-(1H-Indol-3-yl)ethyl)amino)-1,3-dimethyl-2,6-dioxo-1,2,3,6-tetrahydro-7H-purin-7-yl)methyl)phenyl)acetamide (**55**).* Compound **54** (0.062 g, 0.14 mmol, 1 equiv) was suspended in DCM (10 mL). Acetic anhydride (0.026 mL, 0.28 mmol, 1.2 equiv) was added and the mixture was stirred at RT for 1 h. The solvent was removed under reduced pressure and the crude product was partitioned between 20 mL of a saturated aq. Na_2CO_3 solution and 20 mL of ethyl acetate and extraction was performed three times. The organic phase was dried over $MgSO_4$ and concentrated by evaporation. Purification was achieved by column chromatography (DCM: methanol, 9.5:0.5); yield: 4%; m.p.: 167 °C; **^{1}H NMR** (600 MHz, DMSO-d_6) δ 10.77 (s, 1H, NH_{indole}), 9.89 (s, 1H, NHCO), 7.65 (d, J = 6.7 Hz, 1 H, Ar−H), 7.47 (d, J = 8.5 Hz, 2H, Ar−H), 7.34 (d, J = 8.2 Hz, Ar−H), 7.31 (t, J = 5.7 Hz, 1H, *NH*CH_2), 7.15 (d, J = 8.5 Hz, 2H, Ar−H), 7.11 (d, J = 2.2 Hz, 1H, Ar−H), 7.06 (ddd, J = 1.2, 7.0, 8.2 Hz, 1H, Ar−H), 6.98 (ddd, J = 1.0, 7.0, 8.0 Hz, 1H, Ar−H), 5.22 (s, 2H, N7CH_2), 3.61−3.57 (m, 2H, NH*CH_2*), 3.40 (s, 3H, N3-CH_3), 3.17 (s, 3H, N1-CH_3), 2.97 (t, J = 7.3 Hz, 2H, NHCH$_2$*CH_2*), 2.01 (s, 3H, $COCH_3$). **^{13}C NMR** (151 MHz, DMSO) δ 167.8, 153.3, 152.3, 150.6, 148.5, 138.0, 135.8, 131.2, 127.1, 126.8, 122.3, 120.5, 118.8, 117.9, 117.8, 111.1, 110.9, 100.8, 44.5, 43.0, 28.8, 26.8, 25.0, 23.5; LC-MS (m/z): 486.3 $[M + H]^+$; $C_{26}H_{27}N_7O_3$ (calculated MW: 485.5). Purity (HPLC UV (254 nm)-ESI-MS): 95.9%. HR-MS (ESI-QTOF) calcd for $C_{26}H_{27}N_7O_3Na$ $[M + Na]^+$: 508.2024; found: 508.2068.

*8-((2-(1H-Indol-3-yl)ethyl)amino)-7-(2,6-dichlorobenzyl)-1,3-dimethyl-3,7-dihydro-1H-purine-2,6-dione (**56**).* Synthesized according to GP4; purification by column chromatography with a gradient of DCM: methanol (100:0 to 80:20); yield 61%; m.p.: 190−191 °C; **^{1}H NMR** (300 MHz, $CDCl_3$) δ 8.13 (br, 1H, NH_{indole}), 7.49 (d, J = 7.6 Hz, 1H, Ar−H), 7.34−7.39 (m, 1H, Ar−H), 7.21 (td, J = 7.6, 1.2 Hz, 1H, Ar−H), 7.05−7.13 (m, 3H, Ar−H), 6.96−7.03 (m, 1H, Ar−H), 6.85 (d, J = 2.3 Hz, 1H, Ar−H), 5.64 (s, 2H, N7CH_2), 4.18 (t, J = 5.9 Hz, 1H, *NH*CH_2), 3.71 (q, J = 6.5 Hz, 2H, NH*CH_2*), 3.56 (s, 3H, N3CH_3), 3.41 (s, 3H, N1CH_3), 2.92 (t, J = 6.5 Hz, 2H, NHCH$_2$*CH_2*); **^{13}C NMR** ($CDCl_3$) δ ppm: 154.2, 153.2, 151.8, 148.2, 136.5, 135.9, 130.2, 129.4, 128.9, 127.4, 122.3, 121.8, 119.4, 118.7, 112.3, 111.1, 103.9,43.3, 42.7, 29.7, 27.8, 25.2. UPLC-MS (m/z): 497.12 $[M + H]^+$; $C_{24}H_{22}Cl_2N_6O_2$ (calculated MW: 497.38). Purity (UPLC-MS): 96.6%; t_R = 6.95.

*8-((2-(1H-Indol-3-yl)ethyl)amino)-7-(2,4-dichlorobenzyl)-1,3-dimethyl-3,7-dihydro-1H-purine-2,6-dione (**57**).* Synthesized according to GP4; purification by column chromatography with a gradient of DCM: methanol (100:0 to 80:20); yield 56%; m.p.: 188−189 °C; **^{1}H NMR** (500 MHz, DMSO-d_6) δ 10.77 (d, J = 1.43 Hz, 1H, NH_{indole}), 7.64 (d, J = 2.29 Hz, 1H, Ar−H), 7.59 (d, J = 7.7 Hz, 1H, Ar−H), 7.38

Journal of Medicinal Chemistry pubs.acs.org/jmc Article

(t, J = 5.7 Hz, 1H, $NHCH_2$), 7.25−7.31 (m, 2H, Ar−H), 7.09 (d, J = 2.3 Hz, 1H, Ar−H), 7.00−7.04 (m, 1H, Ar−H), 6.91−6.95 (m, 1H, Ar−H), 6.47 (d, J = 8.3 Hz, 1H, Ar−H), 5.27 (s, 2H, N7CH_2), 3.53−3.58 (m, 2H, NHCH_2), 3.41 (s, 3H, N3CH_3), 3.07 (s, 3H, N1CH_3), 2.94 (t, J = 7.5 Hz, 2H, NHCH$_2$$CH_2$). UPLC-MS ($m/z$): 497.19 $[M + H]^+$; $C_{24}H_{22}Cl_2N_6O_2$ (calculated MW: 497.38). Purity (UPLC-MS): 100.0%; t_R = 7.33. HR-MS (ESI-QTOF) calcd for $C_{24}H_{23}Cl_2N_6O_2$ $[M + H]^+$: 497.1260, found: 497.1256.

*8-((2-(1H-Indol-3-yl)ethyl)amino)-7-(4-chloro-3-fluorobenzyl)-1,3-dimethyl-3,7-dihydro-1H-purine-2,6-dione (**58**).* Synthesized according to GP4; purification by column chromatography (DCM: methanol, 9.8:0.2); yield 52%; m.p.: 139−140 °C; **^{1}H NMR** (600 MHz, DMSO-d_6) δ 10.79 (s, 1H, NH_{indole}), 7.62 (d, J = 7.9 Hz, 1H, Ar−H), 7.49 (t, J = 8.1 Hz, 1H, Ar−H), 7.38 (t, J = 5.6 Hz, 1H, $NHCH_2$), 7.34 (d, J = 8.1 Hz, 1H, Ar−H), 7.28 (dd, J = 10.2, 1.6 Hz, 1H, Ar−H), 7.12 (d, J = 2.0 Hz, 1H, Ar−H), 7.06 (t, J = 7.5 Hz, 1H, Ar−H), 7.00 (d, J = 8.5 Hz, 1H, Ar−H), 6.97 (t, J = 7.4 Hz, 1H, Ar−H), 5.27 (s, 2H, 2H, N7CH_2), 3.61 (q, J = 6.4 Hz, 2H, HNCH_2), 3.40 (s, 3H, N3CH_3), 3.16 (s, 3H, N1CH_3), 2.98 (t, J = 7.4 Hz, 2H, NHCH$_2$$CH_2$); **^{13}C NMR** (151 MHz, DMSO-d_6) δ 157.8, 156.2, 153.7, 152.8, 151.0, 149.0, 138.8, 138.7, 136.3, 130.7, 127.3, 124.2, 124.2, 122.8, 120.9, 118.5, 118.4, 118.3, 118.2, 115.7, 115.6, 111.5, 111.4, 101.1, 44.5, 43.3, 29.3, 27.2, 25.4; LC-MS (m/z): 481.1 $[M + H]^+$; $C_{24}H_{22}ClFN_6O_2$ (calculated MW: 480.9). Purity (HPLC UV (254 nm)-ESI-MS): 96.9%.

*8-((2-(1H-Indol-3-yl)ethyl)amino)-7-(3,4-dichlorobenzyl)-1,3-dimethyl-3,7-dihydro-1H-purine-2,6-dione (**59**).* Synthesized according to GP4; purification by column chromatography with a gradient of DCM: methanol (100:0 to 80:20); yield 57%; m.p.: 203−204 °C; **^{1}H NMR** (300 MHz, DMSO-d_6) δ 10.79 (s, 1H, NH_{indole}), 7.61 (d, J = 7.6 Hz, 1H, Ar−H), 7.50−7.54 (m, 2H, Ar−H), 7.40 (t, J = 5.6 Hz, 1H, $NHCH_2$), 7.33 (d, J = 8.2 Hz, 1H, Ar−H), 7.01−7.14 (m, 3H, Ar−H), 6.92−6.99 (m, 1H, Ar−H), 5.25 (s, 2H, N7CH_2), 3.56−3.64 (m, 2H, NHCH_2), 3.38 (s, 3H, N3CH_3), 3.15 (s, 3H, N1CH_3), 2.97 (t, J = 7.3 Hz, 2H, NHCH$_2$$CH_2$); **^{13}C NMR** (DMSO-$d_6$) δ ppm: 154.1, 153.2, 151.4, 149.5, 138.6, 136.7, 131.5, 131.2, 130.5, 129.7, 127.8, 127.7, 123.2, 121.4, 118.8, 118.7, 112.0, 111.8, 101.5, 44.8, 43.8, 29.8, 27.7, 25.8. UPLC-MS (m/z): 497.12 $[M + H]^+$; $C_{24}H_{22}Cl_2N_6O_2$ (calculated MW: 497.38). Purity (UPLC-MS): 100.0%; t_R = 7.32. HR-MS (ESI-QTOF) calcd for $C_{24}H_{23}Cl_2N_6O_2$ $[M + H]^+$: 497.1260, found: 497.1256.

*8-((2-(1H-Indol-3-yl)ethyl)amino)-7-(3,4-difluorobenzyl)-1,3-dimethyl-3,7-dihydro-1H-purine-2,6-dione (**60**).* Synthesized according to GP4; recrystallization from methanol; yield 47%; m.p.: 171−172 °C; **^{1}H NMR** (500 MHz, DMSO-d_6) δ 10.77 (s, 1H, NH_{indole}), 7.62 (d, J = 7.9 Hz, 1H, Ar−H), 7.38−7.28 (m, 4H, $NHCH_2$ and Ar−H), 7.11 (d, J = 2.3 Hz, 1H, Ar−H), 7.06 (t, J = 7.5 Hz, 1H, Ar−H), 7.03−7.00 (m, 1H, Ar−H), 6.99−6.95 (m, 1H, Ar−H), 5.25 (s, 2H, N7CH_2), 3.67−3.54 (m, 2H, HNCH_2), 3.40 (s, 3H, N3CH_3), 3.17 (s, 3H, N1CH_3), 2.98 (t, J = 7.4 Hz, 2H, NHCH$_2$$CH_2$); **^{13}C NMR** (126 MHz, DMSO-d_6) δ 153.7, 152.8, 151.0, 149.0, 136.3, 134.7 (t, J = 4.5 Hz), 127.2, 124.0 (dd, J = 6.9, 3.4 Hz), 122.8, 120.9, 118.3, 118.2, 117.6, 117.5, 116.5, 116.4, 111.5, 111.4, 101.1, 44.3, 43.3, 29.3, 27.2, 25.3; LC-MS (m/z): 464.18 $[M + H]^+$; $C_{24}H_{22}F_2N_6O_2$ (calculated MW: 464.4). Purity (HPLC UV (254 nm)-ESI-MS): 98.1%.

*8-((2-(1H-Indol-3-yl)ethyl)amino)-7-(3-chloro-4-fluorobenzyl)-1,3-dimethyl-3,7-dihydro-1H-purine-2,6-dione (**61**).* Synthesized according to GP4; recrystallization from methanol; yield 53%; m.p.: 193−194 °C; **^{1}H NMR** (500 MHz, DMSO-d_6) δ 10.77 (s, 1H, NH_{indole}), 7.62 (d, J = 7.9 Hz, 1H, Ar−H), 7.50 (dd, J = 7.2, 2.2 Hz, 1H, Ar−H), 7.38 (t, J = 5.6 Hz, 1H, $NHCH_2$), 7.35−7.28 (m, 2H, Ar−H), 7.19−7.14 (m, 1H, Ar−H), 7.12 (d, J = 2.3 Hz, 1H, Ar−H), 7.06 (t, J = 7.5 Hz, 1H, Ar−H), 6.97 (t, J = 7.9 Hz, 1H, Ar−H), 5.25 (s, 2H, N7CH_2), 3.67−3.55 (m, 2H, HNCH_2), 3.40 (s, 3H, N3CH_3), 3.17 (s, 3H, N1CH_3), 2.98 (t, J = 7.4 Hz, 2H, CH_2); **^{13}C NMR** (126 MHz, DMSO-d_6) δ 157.5, 155.5, 153.6, 152.8, 151.0, 149.0, 136.3, 134.9 (d, J = 3.7 Hz), 129.4, 127.9, 127.8, 127.2, 122.8, 120.9, 119.4, 119.3, 118.3, 118.2, 117.1, 116.9, 111.5, 111.4, 101.0, 44.2, 43.3, 29.3, 27.2, 25.3; LC-MS (m/z): 480.15 $[M + H]^+$; $C_{24}H_{22}ClFN_6O_2$ (calculated MW: 480.9). Purity (HPLC UV (254 nm)-ESI-MS): 97.5%.

*8-((2-(1H-Indol-3-yl)ethyl)amino)-7-(2-cyclohexylethyl)-1,3-dimethyl-3,7-dihydro-1H-purine-2,6-dione (**62**).* Synthesized according to GP4; purification by column chromatography with a gradient of DCM: methanol (100:0 to 80:20); yield 56%; m.p.: 215−216 °C; **^{1}H NMR** (300 MHz, $CDCl_3$) δ 8.21 (br, 1H, NH_{indole}), 7.64 (d, J = 8.2 Hz, 1H, Ar−H), 7.40 (d, J = 8.2 Hz, 1H, Ar−H), 7.23 (td, J = 7.6, 1.2 Hz, 1H, Ar−H), 7.10−7.17 (m, 1H, Ar−H), 7.06 (d, J = 2.3 Hz, 1H, Ar−H), 4.22 (t, J = 5.3 Hz, 1H, $NHCH_2$), 3.78−3.87 (m, 4H, NHCH_2 and N7CH_2), 3.56 (s, 3H, N3CH_3), 3.37 (s, 3H, N1CH_3), 3.13 (t, J = 6.5 Hz, 2H, NHCH$_2$$CH_2$), 1.52−1.68 (m, 6 H, N7CH$_2$$CH_2$ and cyclohexane), 1.34−1.44 (m, 2H, cyclohexane), 1.09−1.16 (m, 3H, cyclohexane), 0.75−0.86 (m, 2H, cyclohexane); **^{13}C NMR** ($CDCl_3$) δ ppm: 153.9, 152.5, 151.8, 148.5, 136.5, 127.3, 122.5, 122.2, 119.7, 118.6, 112.6, 111.4, 102.7, 43.7, 41.3, 36.7, 35.2, 32.8, 29.8, 27.7, 26.3, 26.0, 25.3. UPLC-MS (m/z): 449.48 $[M + H]^+$; $C_{25}H_{32}N_6O_2$ (calculated MW: 448.57). Purity (UPLC-MS): 100.0%; t_R = 7.73.

*8-((2-(1H-Indol-3-yl)ethyl)amino)-1,3-dimethyl-7-phenethyl-3,7-dihydro-1H-purine-2,6-dione (**63**).* Synthesized according to GP4; purification by column chromatography with a gradient of DCM: methanol (100:0 to 80:20); yield 48%; m.p.: 189−190 °C; **^{1}H NMR** (400 MHz, $CDCl_3$) δ 8.18 (br, 1H, NH_{indole}), 7.62 (d, J = 8.2 Hz, 1H, Ar−H), 7.42 (d, J = 7.8 Hz, 1H, Ar−H), 7.25 (td, J = 7.5, 1.0 Hz, 1H, Ar−H), 7.13−7.18 (m, 4H, Ar−H), 7.01 (d, J = 2.4 Hz, 1H, Ar−H), 6.95 (dd, J = 6.5, 2.9 Hz, 2H, Ar−H), 4.12 (t, J = 6.7 Hz, 2H, N7CH_2), 3.58−3.60 (m, 3H, N3CH_3), 3.51−3.56 (m, 2H, NHCH_2), 3.43 (s, 3H, N1CH_3), 2.96 (t, J = 6.7 Hz, 2H, NHCH$_2$$CH_2$), 2.88 (t, J = 6.9 Hz, 2H, N7CH$_2$$CH_2$); **^{13}C NMR** ($CDCl_3$) δ ppm: 153.9, 151.7, 138.0, 136.7, 128.9, 128.8, 127.3, 127.0, 122.4, 122.0, 119.6, 118.7, 112.6, 111.3, 102.4, 45.7, 43.8, 36.3, 30.1, 27.8, 25.8. UPLC-MS (m/z): 443.15 $[M + H]^+$; $C_{25}H_{26}N_6O_2$ (calculated MW: 442.52). Purity (UPLC-MS): 97.2%; t_R = 6.61.

*8-((2-(1H-Indol-3-yl)ethyl)amino)-1,3-dimethyl-7-(3-phenylpropyl)-3,7-dihydro-1H-purine-2,6-dione (**64**).* Synthesized according to GP4; purification by column chromatography with a gradient of DCM: methanol (100:0 to 80:20); yield 52%; m.p.: 128−129 °C; **^{1}H NMR** (400 MHz, CDCl3) δ 8.06 (br, 1H, NH_{indole}), 7.63 (d, J = 7.8 Hz, 1H, Ar−H), 7.36−7.39 (m, 1H, Ar−H), 7.18−7.27 (m, 4H, Ar−H), 7.12−7.17 (m, 1H, Ar−H), 7.03−7.07 (m, 2H, Ar−H), 6.97 (d, J = 2.4 Hz, 1H, Ar−H), 3.88−3.93 (m, 2H, N7CH_2), 3.75−3.80 (m, 2H, NHCH_2), 3.58 (s, 3H, N3CH_3), 3.40 (s, 3H, N1CH_3), 3.10 (t, J = 6.5 Hz, 2H, NHCH$_2$$CH_2$), 2.56 (t, J = 7.6 Hz, 2H, N7CH$_2$CH$_2$$CH_2$), 1.93 (dt, J = 15.0, 7.6 Hz, 2H, N7CH$_2$$CH_2CH_2$); **^{13}C NMR** ($CDCl_3$) δ ppm: 153.9, 151.7, 140.6, 136.4, 128.5, 128.2, 127.2, 126.2, 122.4, 122.2, 119.7, 118.6, 112.5, 111.4, 102.7, 43.6, 42.7, 32.4, 30.3, 30.0, 27.7, 25.3. UPLC-MS (m/z): 457.17 $[M + H]^+$; $C_{26}H_{28}N_6O_2$ (calculated MW: 456.55). Purity (UPLC-MS): 100.0%; t_R = 6.89. HR-MS (ESI-QTOF) calcd for $C_{26}H_{29}N_6O_2$ $[M + H]^+$: 457.2352, found: 457.2360.

*8-((2-(1H-Indol-3-yl)ethyl)amino)-1,3-dimethyl-7-(2-phenoxyethyl)-3,7-dihydro-1H-purine-2,6-dione (**65**).* Synthesized according to GP4; purification by column chromatography with a gradient of DCM: methanol (100:0 to 80:20); yield 43%; m.p.: 135−136 °C; **^{1}H NMR** (300 MHz, $CDCl_3$) δ NMR (300 MHz, CDCl3) δ 8.04 (br, 1H, NH_{indole}), 7.70 (d, J = 7.6 Hz, 1H, Ar−H), 7.34−7.38 (m, 1H, Ar−H), 7.05−7.24 (m, 5H, Ar−H), 6.87−6.94 (m, 1H, Ar−H), 6.40 (d, J = 8.2 Hz, 2H, Ar−H), 5.37 (t, J = 5.6 Hz, 1H, $NHCH_2$), 4.35−4.40 (m, 2H, N7CH_2), 4.20 (t, J = 4.4 Hz, 2H, N7CH$_2$$CH_2$), 3.84 (q, J = 6.5 Hz, 2H, NHCH_2), 3.55 (s, 3H, N3CH_3), 3.37 (s, 3H, N1CH_3), 3.17 (t, J = 6.5 Hz, 2H, NHCH$_2$$CH_2$); **^{13}C NMR** ($CDCl_3$) δ ppm: 157.4, 154.8, 154.2, 151.8, 148.9, 136.5, 129.5, 127.3, 122.4, 122.0, 121.6, 119.6, 118.8, 114.1, 112.8, 111.4, 102.7, 68.4, 43.7, 43.4, 29.7, 27.6, 25.7. UPLC-MS (m/z): 459.17 $[M + H]^+$; $C_{25}H_{26}N_6O_3$ (calculated MW: 458.52); Purity (UPLC-MS): 99.3%; t_R = 6.63.

*8-((2-(1H-Indol-3-yl)ethyl)amino)-7-(2-(4-chlorophenoxy)ethyl)-1,3-dimethyl-3,7-dihydro-1H-purine-2,6-dione (**66**).* Synthesized according to GP4; purification by column chromatography with a gradient of DCM: methanol (100:0 to 80:20); yield 53%; m.p.: 191−192 °C; **^{1}H NMR** (300 MHz, DMSO-d_6) δ 10.82 (s, 1H, NH_{indole}), 7.63 (d, J = 7.6 Hz, 1H, Ar−H), 7.33 (d, J = 8.2 Hz, 1H, Ar−H), 7.17−7.30 (m, 4H, Ar−H and $NHCH_2$), 7.02−7.09 (m, 1H, Ar−H), 6.94−

https://doi.org/10.1021/acs.jmedchem.3c02423
J. Med. Chem. 2024, 67, 9896−9926

Journal of Medicinal Chemistry pubs.acs.org/jmc Article

7.00 (m, 1H, Ar−H), 6.76−6.81 (m, 2H, Ar−H), 4.34−4.39 (m, 2H, N7CH$_2$), 4.14 (t, J = 5.6 Hz, 2H, N7CH$_2$*CH$_2$*), 3.61 (q, J = 6.5 Hz, 2H, NHC*H$_2$*), 3.37 (s, 3H, N3CH$_3$), 3.16 (s, 3H, N1CH$_3$), 3.00 (t, J = 7.0 Hz, 2H, NHCH$_2$*CH$_2$*); **^{13}C NMR** (DMSO-d_6) δ ppm: 157.3, 154.6, 153.1, 151.4, 149.3, 136.7, 129.6, 127.8, 124.9, 123.2, 121.4, 118.8, 118.7, 116.5, 112.1, 111.8, 101.8, 66.7, 43.8, 42.2, 29.7, 27.7, 25.8. UPLC-MS (m/z): 493.13 [M + H]$^+$; $C_{25}H_{25}ClN_6O_3$ (calculated MW: 492.96); Purity (UPLC-MS): 100.0%; t_R = 7.14.

*8-((2-(1H-Indol-3-yl)ethyl)amino)-7-(4-chlorobenzyl)-1-methyl-1H-purine-2,6(3H,7H)-dione (**74**).* Synthesized according to GP4 using 8-chloro-7-(4-chlorobenzyl)-1-methyl-3,7-dihydro-1*H*-purine-2,6-dione (**72**) as starting material.; purification by column chromatography (DCM: methanol, 9.8:0.2); yield 64%; m.p.: 261−262 °C; **^{1}H NMR** (500 MHz, DMSO-d_6) δ 11.65 (s, 1H, N3H), 10.79 (s, 1H, NH$_{indole}$), 7.55 (d, J = 7.9 Hz, 1H, Ar−H), 7.36−7.31 (m, 3H, Ar−H and *NH*CH$_2$), 7.26 (t, J = 5.6 Hz, 1H, Ar−H), 7.19 (d, J = 8.6 Hz, 2H, Ar−H), 7.10 (d, J = 2.3 Hz, 1H, Ar−H), 7.09−7.04 (m, 1H, Ar−H), 7.00−6.95 (m, 1H, Ar−H), 5.23 (s, 2H, N7CH$_2$), 3.58 (q, J = 7.1 Hz, 2H, HNC*H$_2$*), 3.11 (s, 3H, NCH$_3$), 2.96 (t, J = 7.2 Hz, 2H, NHCH$_2$*CH$_2$*); **^{13}C NMR** (126 MHz, DMSO-d_6) δ 154.0, 153.6, 151.0, 148.3, 136.3, 136.2, 132.0, 129.0, 128.4, 127.2, 122.7, 120.9, 118.31, 118.25, 111.5, 111.3, 101.1, 44.5, 43.2, 26.4, 25.2; LC-MS (m/z): 449.1 [M + H]$^+$; $C_{23}H_{21}ClN_6O_2$ (calculated MW: 448.9). Purity (HPLC UV (254 nm)-ESI-MS): 99.1%.

*General Method 5 (GP5): Synthesis of 8-Bromo-1-alkyl/arylalkyl-3,7-dimethyl-3,7-dihydro-1H-purine-2,6-diones (**76**−**82**).* Step A: In a 100 mL flask containing **72** (1 equiv), K_2CO_3 (2 equiv) and DMF were added, and the mixture was stirred for 30 min. Then, the appropriate alkylating reagent (1.5 equiv) was added, and the reaction mixture was vigorously stirred for 18 h. The reaction mixture was poured onto ice-cold water and acidified by the addition of 2N aq. HCl solution (pH ≈ 6). The formed precipitate was collected by filtration and the products (**73a**−**h**) were used for the subsequent reaction step without further purification.

Step B: A mixture of the appropriate 8-chloro-7-(4-chlorobenzyl)-3-alkyl/arylalkyl −1-methyl-3,7-dihydro-1*H*-purine-2,6-dione (**73a**−**h**) (1 equiv), tryptamine (2 equiv), and DIPEA (3.6 equiv) in NMP was added into a sealed tube, and the mixture was heated at 145 °C overnight. The reaction was monitored by TLC, using the eluent DCM: methanol (9.5:0.5) until completion of the reaction was indicated. The solvent was evaporated, followed by the addition of water. The resulting mixture was extracted three times using ethyl acetate and washed two times with water and brine. Finally, it was dried over anhydrous $MgSO_4$. The solution was filtered and subsequently evaporated. The compound was purified by column chromatography or by recrystallization to yield the target compounds.

*2-(8-((2-(1H-Indol-3-yl)ethyl)amino)-7-(4-chlorobenzyl)-1-methyl-2,6-dioxo-1,2,6,7-tetrahydro-3H-purin-3-yl)acetonitrile (**76**).* Synthesized according to GP5; purification by column chromatography (DCM: methanol, 9.0:1.0), yield 65%; m.p.: 205−206 °C; **^{1}H NMR** (600 MHz, DMSO-d_6) δ 10.81 (s, 1H, NH$_{indole}$), 7.62 (d, J = 7.9 Hz, 1H, Ar−H), 7.52 (t, J = 5.6 Hz, 1H, Ar−H), 7.35−7.34 (m, 3H, Ar−H and *NH*CH$_2$), 7.21 (d, J = 8.4 Hz, 2H, Ar−H), 7.13 (d, J = 2.1 Hz, 1H, Ar−H), 7.07 (t, J = 7.4 Hz, 1H, Ar−H), 6.99 (t, J = 7.4 Hz, 1H, Ar−H), 5.26 (s, 2H, N7CH$_2$), 4.98 (s, 2H, N3CH$_2$), 3.62 (q, J = 6.5 Hz, 2H, HNC*H$_2$*), 3.18 (s, 3H, N1CH$_3$), 3.01 (t, J = 7.4 Hz, 2H, NHCH$_2$*CH$_2$*); **^{13}C NMR** (151 MHz, DMSO-d_6) δ 153.7, 152.5, 150.1, 147.1, 136.3, 135.8, 132.1, 129.0, 128.5, 127.3, 122.9, 120.9, 118.31, 118.26, 115.7, 111.43, 111.36, 101.3, 44.8, 43.4, 30.6, 27.4, 25.2; LC-MS (m/z): 488.2 [M + H]$^+$; $C_{25}H_{22}ClN_7O_2$ (calculated MW: 487.9). Purity (HPLC UV (254 nm)-ESI-MS): 98.2%.

*8-((2-(1H-Indol-3-yl)ethyl)amino)-7-(4-chlorobenzyl)-1-methyl-3-(2,2,2-trifluoroethyl)-3,7-dihydro-1H-purine-2,6-dione (**79**).* Synthesized according to GP5; purification by column chromatography with a gradient of DCM: methanol (9.2:0.8), yield 12%; m.p.: 226−227 °C; **^{1}H NMR** (500 MHz, DMSO-d_6) δ 10.79 (s, 1H, NH$_{indole}$), 7.62 (d, J = 7.8 Hz, 1H, Ar−H), 7.49 (t, J = 5.6 Hz, 1H, Ar−H), 7.35 (m, 3H, Ar−H and *NH*CH$_2$), 7.22 (d, J = 8.5 Hz, 2H, Ar−H), 7.11 (d, J = 2.3 Hz, 1H, Ar−H), 7.09−7.05 (m, 1H, Ar−H), 6.96 (t, J = 7.9 Hz, 1H, Ar−H), 5.26 (s, 2H, N7CH$_2$), 4.75 (q, J = 9.0 Hz, 2H, N3C*H$_2$*), 3.63−3.54 (m, 2H, HNC*H$_2$*), 3.19 (s, 3H, N1CH$_3$), 3.01−2.96 (m, 2H, NHCH$_2$*CH$_2$*); **^{13}C NMR** (126 MHz, DMSO-d_6) δ 153.5, 152.6, 150.6, 148.0, 136.3, 135.8, 132.1, 129.0, 128.5, 127.3, 125.2, 122.8, 120.9, 118.2, 118.1, 111.42, 111.35, 101.1, 44.8, 43.3, 27.5, 25.2; LC-MS (m/z): 531.1 [M + H]$^+$; $C_{25}H_{22}ClF_3N_6O_2$ (calculated MW: 530.9). Purity (HPLC UV (254 nm)-ESI-MS): 96.7%.

*8-((2-(1H-Indol-3-yl)ethyl)amino)-7-(4-chlorobenzyl)-3-(2-fluoroethyl)-1-methyl-3,7-dihydro-1H-purine-2,6-dione (**80**).* Synthesized according to GP5; crystallization from methanol; yield 35%; m.p.: 196−197 °C; **^{1}H NMR** (600 MHz, DMSO-d_6) δ 10.80 (s, 1H, NH$_{indole}$), 7.62 (d, J = 7.9 Hz, 1H, Ar−H), 7.40 (t, J = 5.6 Hz, 1H, Ar−H), 7.35−7.34 (m, 3H, Ar−H and *NH*CH$_2$), 7.22 (d, J = 8.5 Hz, 2H, Ar−H), 7.12 (d, J = 2.0 Hz, 1H, Ar−H), 7.07 (s, 1H, Ar−H), 6.98 (d, J = 14.8 Hz, 1H, Ar−H), 5.26 (s, 2H, N7CH$_2$), 4.81−4.62 (m, 2H, N3C*H$_2$*CH$_2$), 4.38−4.18 (m, 2H, N3CH$_2$*CH$_2$*), 3.65−3.54 (m, 2H, CH$_2$, HNC*H$_2$*), 3.17 (s, 3H, CH$_3$, N1CH$_3$), 2.99 (d, J = 7.5 Hz, 2H, NHCH$_2$*CH$_2$*); **^{13}C NMR** (151 MHz, DMSO-d_6) δ 153.6, 152.7, 150.8, 148.6, 136.3, 136.0, 129.1, 128.5, 127.3, 122.8, 120.9, 118.3, 118.2, 111.5, 111.4, 101.2, 81.0, 79.9, 44.7, 43.3, 42.9, 42.7, 27.2, 25.3; LC-MS (m/z): 495.0 [M + H]$^+$; $C_{25}H_{24}ClFN_6O_2$ (calculated MW: 494.9). Purity (HPLC UV (254 nm)-ESI-MS): 95.8%.

*8-((2-(1H-Indol-3-yl)ethyl)amino)-3-benzyl-7-(4-chlorobenzyl)-1-methyl-3,7-dihydro-1H-purine-2,6-dione (**82**).* Synthesized according to GP5; purification by column chromatography (DCM: methanol, 9.5:0.5), yield 42%; m.p.: 182−183 °C; **^{1}H NMR** (600 MHz, DMSO-d_6) δ 10.79 (s, 1H, NH$_{indole}$), 7.57 (d, J = 7.9 Hz, 1H, Ar−H), 7.44−7.41 (m, 3H, Ar−H), 7.35−7.33 (m, 3H, Ar−H and *NH*CH$_2$), 7.30 (t, J = 7.4 Hz, 2H, Ar−H), 7.26−7.22 (m, 3H, Ar−H), 7.10 (d, J = 2.2 Hz, 1H, Ar−H), 7.05 (t, J = 8.0 Hz, 1H, Ar−H), 6.89 (t, J = 7.8 Hz, 1H, Ar−H), 5.26 (s, 2H, N7CH$_2$), 5.14 (s, 2H, N3C*H$_2$*), 3.65−3.54 (m, 2H, HNC*H$_2$*), 3.17 (s, 3H, N1CH$_3$), 3.02−2.95 (m, 2H, NHCH$_2$*CH$_2$*); **^{13}C NMR** (151 MHz, DMSO-d_6) δ 153.7, 152.7, 148.6, 137.1, 136.2, 136.0, 132.0, 129.1, 128.4, 128.3, 127.9, 127.34, 127.26, 122.8, 120.9, 118.2, 118.1, 111.5, 111.3, 101.1, 45.6, 44.7, 43.3, 27.2, 25.2; LC-MS (m/z): 539.4 [M + H]$^+$; $C_{30}H_{27}ClN_6O_2$ (calculated MW: 539.0). Purity (HPLC UV (254 nm)-ESI-MS): 95.1%.

*8-((2-(1H-Indol-3-yl)ethyl)amino)-7-(4-chlorobenzyl)-3-(2-hydroxyethyl)-1-methyl-3,7-dihydro-1H-purine-2,6-dione (**83**).* Compound **81** was synthesized according to GP4 followed by hydrolysis to give **83**. To a solution of **81** (0.04 g, 0.075 mmol) in methanol (5 mL), potassium hydroxide (0.1 g, 1.80 mmol) was added at RT, and the mixture was stirred at 65 °C for 18h. The reaction mixture was evaporated to dryness, and the residue was redissolved in DCM (50 mL) and washed with a saturated aq. solution of $NaHCO_3$ (3 × 30 mL), and then with water (2 × 30 mL). The organic layer was dried over anhydrous magnesium sulfate, and the solvent was removed in vacuo. The residue was purified by silica gel column chromatography (DCM: methanol, 9.0:1.0); yield 63%; m.p.: 169−171 °C; **^{1}H NMR** (500 MHz, DMSO-d_6) δ 10.79 (s, 1H, NH$_{indole}$), 7.62 (d, J = 7.8 Hz, 1H, Ar−H), 7.35−7.33 (m, 4H, Ar−H and *NH*CH$_2$), 7.22 (d, J = 8.6 Hz, 2H, Ar−H), 7.13 (s, 1H, Ar−H), 7.07 (t, J = 7.5 Hz, 1H, Ar−H), 6.99 (t, J = 7.4 Hz, 1H, Ar−H), 5.26 (s, 2H, N7CH$_2$), 4.80 (s, 1H, OH), 4.05 (t, J = 6.5 Hz, 2H, N3C*H$_2$*CH$_2$), 3.68 (t, J = 6.4 Hz, 2H, HN-C*H$_2$*), 3.60 (q, J = 6.6, 5.8 Hz, 2H, N3CH$_2$*CH$_2$*), 3.16 (s, 3H, N1CH$_3$), 2.99 (t, J = 7.4 Hz, 2H, NHCH$_2$*CH$_2$*). **^{13}C NMR** (126 MHz, DMSO-d_6) δ 153.6, 152.8, 150.8, 148.8, 136.2, 136.0, 129.1, 128.4, 127.3, 122.8, 120.9, 118.31, 118.25, 111.5, 111.3, 101.1, 57.8, 44.7, 44.6, 43.3, 27.2, 25.20; LC-MS (m/z): 493.1 [M + H]$^+$; $C_{25}H_{25}ClN_6O_3$ (calculated MW: 492.9). Purity (HPLC UV (254 nm)-ESI-MS): 95.8%.

***β*-Arrestin Recruitment Assay (Enzyme Complementation Assay).** Recruitment of β-arrestin-2 to the respective receptor was detected by using the β-galactosidase enzyme fragment complementation technology (β-arrestin PathHunter assay, DiscoverX, Fremont, CA, USA) according to previously published procedures.[23,24,32,76] In brief, CHO cells stably expressing the respective receptor were seeded in a volume of 90 μL into a 96-well plate at a density of 25,000−30,000 cells/well in a suitable growth medium (cell plating reagent 2, DiscoverX, or OptiMEM, Thermo Fisher) supplemented with 2% fetal calf serum, 100 U/mL penicillin, 100 μg/mL streptomycin, 800 μg/mL geneticin and 300 μg/mL hygromycin, and incubated for 24 h at

https://doi.org/10.1021/acs.jmedchem.3c02423
J. Med. Chem. 2024, 67, 9896−9926

37 °C. All test compounds were dissolved in DMSO (except for resolvin D2 (RvD2) which was dissolved either in DMSO or in ethanol, respectively).

For agonist assays, test compounds were diluted in phosphate-buffered saline (PBS) containing 10% DMSO and 0.1% bovine serum albumin, and added to the cells in a volume of 10 μL, followed by incubation for 90 min at 37 °C. For the determination of baseline luminescence, PBS buffer (containing 10% DMSO and 0.1% BSA) in the absence of the test compound was used. For the measurement of RvD2, RvD2 dissolved in ethanol (Cayman Bioscience) was stored at −80 °C. Stock solutions of RvD2 were either prepared in DMSO or in ethanol, and the results were compared. Suitable amounts of RvD2 were taken out to obtain final concentrations in the assay ranging from 0.1 to 10,000 nM. The solution was subjected to gentle evaporation under a stream of nitrogen, followed by the addition of DMSO or absolute ethanol, and predissolution in assay buffer prior to the experiments. The experiments were carried out according to the procedure described above for the determination of GPR18 activation (testing of agonists).

An agonist concentration corresponding to the respective EC_{80} concentration (hGPR18: 10 μM THC, mGPR18: 0.3 μM PSB-KK1415, GPR55: 1 μM lysophosphatidylinositol, CB_1: 0.003 μM CP55,940, CB_2: 0.001 μM CP55,940) was used as a positive control (set at 100%) to activate each receptor. For test compounds that showed at least 50% receptor activation, dose−response curves were recorded. A suitable control agonist was used at a concentration at which it showed maximum receptor activation (hGPR18: 30 μM THC, mGPR18: 3 μM PSB-KK1415, GPR55: 10 μM lysophosphatidylinositol, CB_1: 0.1 μM CP55,940, CB_2: 0.1 μM CP55,940) was used for determination of efficacy (E_{max}). During the incubation period, the detection reagent was prepared according to the supplier's protocol and previously published literature.[24,33,77] After the addition of 50 μL/well of detection reagent to the cells, the plate was incubated for a further 60 min at room temperature. Finally, luminescence was determined in a luminometer (TopCount NXT, Packard/Perkin-Elmer).

For the determination of antagonistic properties of the test compound, the assay was performed as described for agonists, except that the test compounds were added to the cells in a volume of 5 μL/well 60 min prior to the addition of the agonist. An agonist concentration corresponding to its EC_{80} concentration was used to activate the receptor (hGPR18: 10 μM THC, mGPR18: 0.3 μM PSB-KK1415, GPR55: 1 μM lysophosphatidylinositol, CB_1: 0.003 μM CP55,940, CB_2: 0.001 μM CP55,940). Data were obtained from at least three independent experiments, performed in duplicates. Data were analyzed using Graph Pad Prism version 10.1.0 (San Diego, CA, USA).

Radioligand Binding Assays at CB_1 and CB_2 Receptors. Competition binding assays were performed as described using the CB_1/CB_2 agonist radioligand [^{3}H](-)-*cis*-3-[2-hydroxy-4-(1,1-dimethylheptyl)phenyl]-*trans*-4-(3-hydroxypropyl)cyclohexanol ([^{3}H]CP55,940, ARC, American Radiolabeled Chemicals, St. Louis, MO, USA) in a final concentration of 0.1 nM.[76,78,79] As a source for human CB_1 and CB_2 receptors, membrane preparations of CHO cells stably expressing the respective receptor subtype were employed (30 μg of protein per vial for CB_1 assays, 16 μg of protein per vial for CB_2 receptor assays). Stock solutions of the test compounds were prepared in DMSO. The final DMSO concentration in the assays was 2.5%. Data were obtained from three independent experiments, performed in duplicates. Data were analyzed using Graph Pad Prism version 10.1.0 (San Diego, CA, USA). For the calculation of K_i values, the Cheng−Prusoff equation and a K_D value of 2.4 nM ([^{3}H]CP55,940 at hCB_1) and 0.7 nM ([^{3}H]CP55,940 at hCB_1) were used.[80]

cAMP Accumulation Assays at Human CB_1 and CB_2 Receptors. cAMP accumulation at human CB_1 and CB_2 receptors was determined according to a previously described procedure.[76,81,82] In brief, cells were seeded into a 24-well plate at a density of 200,000 cells per well and incubated for 24 h at at 37 °C. Then, the medium was replaced with Hank's buffered saline solution (HBSS, Gibco) and the cells were further incubated for an additional 2 h (37 °C, 5% CO_2). The phosphodiesterase inhibitor Ro-20-1724 (4-(3-butoxy-4-methoxybenzyl)-2-imodazolidinone) was added at a concentration of 40 μM (20 μL/well), followed by a 10 min incubation period. Subsequently, 15 μL of the test compound (diluted in HBSS) was added to each well, and the cells were further incubated for 5 min. Forskolin, an adenylate cyclase activator, was then added at a final concentration of 10 μM, and incubation continued for 15 min. The final concentration of DMSO in the assay was 1.9%. The reaction was stopped by adding hot lysis buffer (100 °C, containing 4 mM EDTA and 0.01% Triton X-100). Quantification of cAMP was carried out by mixing 50 μL of cell suspension with 30 μL of [^{3}H]cAMP (3 nM in Tris buffer) and 40 μL of cAMP-binding protein (50 μg of protein per well in Tris buffer),[83] followed by a 1 h incubation on ice. Bound and free radioligand was separated using GF/B glass fiber filters, and radioactivity was measured after 9 h of preincubation with a scintillation cocktail (ProSafe PFC+, Meridian Ltd.). Data were obtained in three independent experiments, each performed in duplicate.

Human and Rat Liver Microsomal Assays. The in vitro evaluation of metabolic stability was conducted using human (adult male and female, M0317, Sigma-Aldrich, St. Louis, MO, USA), or rat liver microsomes (Sprague−Dawley, male, M9066, Sigma-Aldrich, St. Louis, MO, USA). The test compound (50 μM) or verapamil (50 μM) was added to the microsome preparation (1 mg/mL) in 10 mM Tris-HCl buffer (pH 7.4), followed by 5 min of incubation. The reaction was initiated by adding 50 μL of the NADPH regeneration system (Promega, Madison, WI, USA) to the mixture, and incubation was performed for 120 min at 37 °C. The reaction was stopped by the addition of 200 μL of cold methanol, followed by 15 min of centrifugation at 14,000 rpm. The supernatant was taken and subjected to analysis using LC/MS (Waters ACQUITY 8482 TQD). Fragmentation analysis was conducted on both the starting compound and the products to determine the structures of major metabolites.

Molecular Modeling. For molecular modeling and docking studies, the previously published homology model of the human GPR18 based on the X-ray crystal structures of the murine μ-opioid receptor (PDB-ID: 5C1M),[65] the human $P2Y_1$ receptor (PDB-ID: 4XNV),[67] and the zebrafish lysophosphatidic acid receptor LPA6 (PDB-ID: 5XSZ),[66] was used.[61] The sequence identities of the template receptors amount to 24.8, 25.5, and 27.3%, respectively. Homology models were generated using MODELER (version 9.16, University of California, San Francisco, CA, USA).[84] The equilibrated apo form receptor model after 50 ns of molecular dynamics simulation was selected for docking studies.

The IFD module implemented in Maestro Schrödinger (package release 2016) was selected as the docking method for this study to address the high conformational flexibility of GPCRs.[85,86] Ligands and protein were prepared at a physiological pH of 7.4 following the standard protocol.[61,87−89] The standard IFD protocol begins with Glide ligand docking in which the side chains of the amino acids in the binding pocket are removed after initial docking.[90] The second step involves Prime to refine the nearby residues and subsequent optimization of the side chains.[91] In the final docking phase, the ligand is redocked into all induced fit protein structures that were within 30 kcal/mol of the lowest energy structure by using the Glide XP scoring function. The conformations of the docked ligands within an energy window of 2.5 kcal/mol were considered. For Glide docking, the following standard parameters were selected: receptor van der Waals scaling, 0.50, ligand van der Waals scaling, 0.50, and a maximum of 20 poses per ligand. Residues within 5.0 Å of the ligand poses were refined, and the side chains were optimized. The best docking pose was selected based on the IFD score.

Assessment of SARs was performed utilizing the drug discovery dashboard SeeSAR (version 13.0.4).[71] Molecules were edited with the Molecule Editor Mode and were redocked template-based on the best scoring pose of compound **51** from the previous section. If required, compounds were transferred to the Docking Mode and redocked template-based using the standard settings. The derivatives were analyzed using the labeling functionality of SeeSAR to assess potential interactions at the binding site with the target structure to elucidate the individual contributions of single atoms to the overall binding affinity of the ligands based on the calculated HYDE scores (indicated as spheres) as well as potential clashes with the binding site.[72,73]

■ ASSOCIATED CONTENT

Supporting Information

The Supporting Information is available free of charge at https://pubs.acs.org/doi/10.1021/acs.jmedchem.3c02423.

Detailed synthetic procedures and characterization of compounds; overview of the compounds' potencies at human and mouse GPR18, human GPR55, and human CB_1 and CB_2 receptors; potency and activity of compound **51** at CB_1 and CB_2 receptors; principle of β-arrestin recruitment assays used for measuring GPR18 activation; concentration-dependent effects of RvD2 on human GPR18 and mouse GPR18; concentration-dependent inhibition of agonist **51**-induced mouse GPR18 activation by THC; sequence alignment of human GPR18 and mouse GPR18; concentration-dependent activation of GPR183 by THC and agonist **51**; metabolic stability of **51**; ^{1}H and ^{13}C NMR spectral data for synthesized compounds; and LC-MS assessment of purity of selected compounds (PDF)

Coordinates of THC docked into the homology model (PDB)

Coordinates of compound **51** docked into the homology model (PDB)

Molecular formula strings (CSV)

■ AUTHOR INFORMATION

Corresponding Authors

Katarzyna Kieć-Kononowicz − *Department of Technology and Biotechnology of Drugs, Faculty of Pharmacy, Jagiellonian University Medical College, Pl 30-688 Kraków, Poland*; Phone: +12-620-55-80; Email: mfkonono@cyf-kr.edu.pl

Christa E. Müller − *Pharmaceutical Institute, Department of Pharmaceutical and Medicinal Chemistry, University of Bonn, D-53121 Bonn, Germany; Research Training Group 1873, University of Bonn, 53127 Bonn, Germany; Research Training Group 2873, University of Bonn, 53121 Bonn, Germany;* orcid.org/0000-0002-0013-6624; Phone: +49-228-73-2301; Email: christa.mueller@uni-bonn.de; Fax: +49-228-73-2567

Authors

Andhika B. Mahardhika − *Pharmaceutical Institute, Department of Pharmaceutical and Medicinal Chemistry, University of Bonn, D-53121 Bonn, Germany; Research Training Group 1873, University of Bonn, 53127 Bonn, Germany; Research Training Group 2873, University of Bonn, 53121 Bonn, Germany;* orcid.org/0000-0002-0456-1353

Michal Załuski − *Department of Technology and Biotechnology of Drugs, Faculty of Pharmacy, Jagiellonian University Medical College, Pl 30-688 Kraków, Poland*

Clara T. Schoeder − *Pharmaceutical Institute, Department of Pharmaceutical and Medicinal Chemistry, University of Bonn, D-53121 Bonn, Germany; Research Training Group 1873, University of Bonn, 53127 Bonn, Germany;* Present Address: Institute for Drug Discovery, Faculty of Medicine, Leipzig University, Liebigstr. 19, D-04103 Leipzig, Germany

Nader M. Boshta − *Pharmaceutical Institute, Department of Pharmaceutical and Medicinal Chemistry, University of Bonn, D-53121 Bonn, Germany;* Present Address: Chemistry Department, Faculty of Science, Manoufia University, Gamal Abdel-Nasser Street, Shebin El-Kom 32511, Egypt.

Jakub Schabikowski − *Department of Technology and Biotechnology of Drugs, Faculty of Pharmacy, Jagiellonian University Medical College, Pl 30-688 Kraków, Poland*

Filomena Perri − *Pharmaceutical Institute, Department of Pharmaceutical and Medicinal Chemistry, University of Bonn, D-53121 Bonn, Germany; Research Training Group 1873, University of Bonn, 53127 Bonn, Germany*

Dorota Łażewska − *Department of Technology and Biotechnology of Drugs, Faculty of Pharmacy, Jagiellonian University Medical College, Pl 30-688 Kraków, Poland;* orcid.org/0000-0001-8454-4440

Alexander Neumann − *Pharmaceutical Institute, Department of Pharmaceutical and Medicinal Chemistry, University of Bonn, D-53121 Bonn, Germany; Research Training Group 1873, University of Bonn, 53127 Bonn, Germany;* Present Address: BioSolveIT, An der Ziegelei 79, 53757 Sankt Augustin, Germany.

Sarah Kremers − *Pharmaceutical Institute, Department of Pharmaceutical and Medicinal Chemistry, University of Bonn, D-53121 Bonn, Germany*

Angelo Oneto − *Pharmaceutical Institute, Department of Pharmaceutical and Medicinal Chemistry, University of Bonn, D-53121 Bonn, Germany*

Anastasiia Ressemann − *Pharmaceutical Institute, Department of Pharmaceutical and Medicinal Chemistry, University of Bonn, D-53121 Bonn, Germany*

Gniewomir Latacz − *Department of Technology and Biotechnology of Drugs, Faculty of Pharmacy, Jagiellonian University Medical College, Pl 30-688 Kraków, Poland*

Vigneshwaran Namasivayam − *Pharmaceutical Institute, Department of Pharmaceutical and Medicinal Chemistry, University of Bonn, D-53121 Bonn, Germany*

Complete contact information is available at: https://pubs.acs.org/10.1021/acs.jmedchem.3c02423

Author Contributions

#A.B.M., M.Z., C.T.S., and N.M.B. contributed equally. The manuscript was written through contributions of all authors. All authors have given approval to the final version of the manuscript.

Notes

The authors declare no competing financial interest.

■ ACKNOWLEDGMENTS

A.B.M., C.T.S., A.N., F.P., and C.E.M. gratefully acknowledge support for the Deutsche Forschungsgemeinschaft (DFG): GRK 1873 "Pharmacology of 7TM-receptors and downstream signaling pathways". A.B.M. and C.E.M. acknowledge the support of GRK 2873 "Tools and drugs of the future−innovative methods and new modalities in medicinal chemistry". A.B.M. was funded by the Ministry of Finance Indonesia in the scheme of the Indonesia Endowment Fund for Education (Lembaga Pengelola Dana Pendidikan (LPDP)). C.T.S. was supported by a Bayer AG PhD fellowship. K.K.-K. gratefully acknowledges the support of the National Science Center, Poland (grant: DEC-2021/43/B/NZ7/01938). Some of the experiments were carried out utilizing research infrastructure financed by the Polish Operating Programme for Intelligent Development POIR 4.2 project no. POIR.04.02.00-00-D023/20 and equipment cofinanced by the qLIFE Priority Research Area under the program "Excellence Initiative − Research University" at the Jagiellonian University.

Journal of Medicinal Chemistry pubs.acs.org/jmc Article

■ ABBREVIATIONS

Abn-CBD	abnormal-cannabidiol
BSA	bovine serum albumin
cAMP	cyclic adenosine monophosphate
CB_1	cannabinoid receptor type 1
CB_2	cannabinoid receptor type 2
CHO cell	Chinese hamster ovary cell
CTX	cholera toxin
DMEM	Dulbecco's modified Eagle's medium
DCM	dichloromethane
DIPEA	*N*,*N*-diisopropylethylamine
DMF	*N*,*N*-dimethylformamide
DMSO	dimethyl sulfoxide
EC_{50}	half-maximal effective concentration
ECL2	extracellular loop 2
EDTA	ethylenediamine tetraacetic acid
eYFP	enhanced yellow fluorescent protein
FCS	fetal calf serum
GPCRs	G protein-coupled receptors
GPR18	G protein-coupled receptor 18
GPR183	G protein-coupled receptor 183
GPR55	G protein-coupled receptor 55
HBSS	Hanks' balanced salt solution
IC_{50}	half-maximal inhibitory concentration
HMDS	hexamethyldisilazane
IFD	induced-fit docking
LPA6	lysophosphatidic acid receptor 6
LPI	lysophosphatidylinositol
MAPK	mitogen-activated protein kinase
M.p.	melting point
NAGly	*N*-arachidonoylglycine
NCS	*N*-chlorosuccinimide
NMP	*N*-methyl-2-pyrrolidone
$P2Y_1$	P2Y purinoceptor 1
PBS	phosphate-bufferd saline
PSB	Pharmaceutical Sciences Bonn
PTX	pertussis toxin
Rluc	*Renilla* luciferase
RvD2	Resolvin D2
SAR	structure−activity relationship
T3P	propanephosphonic anhydride
TEA	triethylamine
THC	Δ^9-tetrahydrocannabinol
THF	tetrahydrofuran
TLC	thin-layer chromatography
TMX	transmembrane region X
TRIS	tris(hydroxymethyl)aminomethane

■ REFERENCES

(1) Hauser, A. S.; Attwood, M. M.; Rask-Andersen, M.; Schiöth, H. B.; Gloriam, D. E. Trends in GPCR drug discovery: new agents, targets and indications. *Nat. Rev. Drug Discovery* **2017**, *16* (12), 829−842.

(2) Gantz, I.; Muraoka, A.; Yang, Y. K.; Samuelson, L. C.; Zimmerman, E. M.; Cook, H.; Yamada, T. Cloning and chromosomal localization of a gene (GPR18) encoding a novel seven transmembrane receptor highly expressed in spleen and testis. *Genomics* **1997**, *42* (3), 462−466.

(3) Norregaard, K.; Benned-Jensen, T.; Rosenkilde, M. M. EBI2, GPR18, and GPR17 − Three structurally related but biologically distinct 7TM receptors. *Curr. Top. Med. Chem.* **2011**, *11* (6), 618−628.

(4) Hannedouche, S.; Zhang, J.; Yi, T.; Shen, W.; Nguyen, D.; Pereira, J. P.; Guerini, D.; Baumgarten, B. U.; Roggo, S.; Wen, B.; Knochenmuss, R.; Noël, S.; Gessier, F.; Kelly, L. M.; Vanek, M.; Laurent, S.; Preuss, I.; Miault, C.; Christen, I.; Karuna, R.; Li, W.; Koo, D.-I.; Suply, T.; Schmedt, C.; Peters, E. C.; Falchetto, R.; Katopodis, A.; Spanka, C.; Roy, M.-O.; Detheux, M.; Chen, Y. A.; Schultz, P. G.; Cho, C. Y.; Seuwen, K.; Cyster, J. G.; Sailer, A. W. Oxysterols direct immune cell migration via EBI2. *Nature* **2011**, *475* (7357), 524−527.

(5) Liu, Y.; Wang, L.; Lo, K.-W.; Lui, V. W. Y. Omics-wide quantitative B-cell infiltration analyses identify GPR18 for human cancer prognosis with superiority over CD20. *Commun. Biol.* **2020**, *3* (1), 234.

(6) Kohno, M.; Hasegawa, H.; Inoue, A.; Muraoka, M.; Miyazaki, T.; Oka, K.; Yasukawa, M. Identification of N-arachidonylglycine as the endogenous ligand for orphan G-protein-coupled receptor GPR18. *Biochem. Biophys. Res. Commun.* **2006**, *347* (3), 827−832.

(7) Chiang, N.; Dalli, J.; Colas, R. A.; Serhan, C. N. Identification of resolvin D2 receptor mediating resolution of infections and organ protection. *J. Exp. Med.* **2015**, *212* (8), 1203.

(8) Wang, X.; Sumida, H.; Cyster, J. G. GPR18 is required for a normal CD8$\alpha\alpha$ intestinal intraepithelial lymphocyte compartment. *J. Exp. Med.* **2014**, *211* (12), 2351−2359.

(9) Regard, J. B.; Sato, I. T.; Coughlin, S. R. Anatomical profiling of G protein-coupled receptor expression. *Cell* **2008**, *135* (3), 561−571.

(10) Becker, A. M.; Callahan, D. J.; Richner, J. M.; Choi, J.; DiPersio, J. F.; Diamond, M. S.; Bhattacharya, D. GPR18 controls reconstitution of mouse small intestine intraepithelial lymphocytes following bone marrow transplantation. *PLoS One* **2015**, *10* (7), No. e0133854.

(11) Takenouchi, R.; Inoue, K.; Kambe, Y.; Miyata, A. N-arachidonoyl glycine induces macrophage apoptosis via GPR18. *Biochem. Biophys. Res. Commun.* **2012**, *418* (2), 366−371.

(12) Jablonski, K. A.; Amici, S. A.; Webb, L. M.; Ruiz-Rosado, J. D. D.; Popovich, P. G.; Partida-Sanchez, S.; Guerau-de-Arellano, M. Novel markers to delineate murine M1 and M2 macrophages. *PLoS One* **2015**, *10* (12), No. e0145342.

(13) Ren, H.; Hu, D.; Mao, Y.; Su, X. Identification of Genes with Prognostic Value in the Breast Cancer Microenvironment Using Bioinformatics Analysis. *Med. Sci. Monit.* **2020**, *26*, No. e920212.

(14) Sun, Y.; Zhang, Q.; Yao, L.; Wang, S.; Zhang, Z. Comprehensive analysis reveals novel gene signature in head and neck squamous cell carcinoma: predicting is associated with poor prognosis in patients. *Transl. Cancer Res.* **2020**, *9* (10), 5882−5892.

(15) Sumida, H.; Cyster, J. G. G-Protein coupled receptor 18 contributes to establishment of the CD8 effector T cell compartment. *Front. Immunol.* **2018**, *9*, 660.

(16) Alexander, S. P. So what do we call GPR18 now? *Br. J. Pharmacol.* **2012**, *165* (8), 2411−2413.

(17) Alexander, S. P.; Christopoulos, A.; Davenport, A. P.; Kelly, E.; Marrion, N. V.; Peters, J. A.; Faccenda, E.; Harding, S. D.; Pawson, A. J.; Sharman, J. L.; Southan, C.; Davies, J. A.; CGTP Collaborators. The consice guide to pharmacology 2017/18: G protein-coupled receptors. *Br. J. Pharmacol.* **2017**, *174* (S1), S17−S129.

(18) McHugh, D.; Hu, S. S.; Rimmerman, N.; Juknat, A.; Vogel, Z.; Walker, J. M.; Bradshaw, H. B. N-arachidonoyl glycine, an abundant endogenous lipid, potently drives directed cellular migration through GPR18, the putative abnormal cannabidiol receptor. *BMC Neurosci.* **2010**, *11*, 44.

(19) McHugh, D.; Wager-Miller, J.; Page, J.; Bradshaw, H. B. siRNA knockdown of GPR18 receptors in BV-2 microglia attenuates N-arachidonoyl glycine-induced cell migration. *J. Mol. Signal.* **2014**, *7* (1), 10.

(20) Chiang, N.; de la Rosa, X.; Libreros, S.; Serhan, C. N. Novel Resolvin D2 Receptor Axis in Infectious Inflammation. *J. Immunol.* **2017**, *198* (2), 842−851.

(21) Spite, M.; Norling, L. V.; Summers, L.; Yang, R.; Cooper, D.; Petasis, N. A.; Flower, R. J.; Perretti, M.; Serhan, C. N. Resolvin D2 is a potent regulator of leukocytes and controls microbial sepsis. *Nature* **2009**, *461* (7268), 1287−1291.

(22) Perna, E.; Aguilera-Lizarraga, J.; Florens, M. V.; Jain, P.; Theofanous, S. A.; Hanning, N.; De Man, J. G.; Berg, M.; De Winter, B.; Alpizar, Y. A.; Talavera, K.; Vanden Berghe, P.; Wouters, M.; Boeckxstaens, G. Effect of resolvins on sensitisation of TRPV1 and visceral hypersensitivity in IBS. *Gut* **2021**, *70* (7), 1275−1286.

https://doi.org/10.1021/acs.jmedchem.3c02423
J. Med. Chem. 2024, 67, 9896−9926

(23) Rempel, V.; Atzler, K.; Behrenswerth, A.; Karcz, T.; Schoeder, C.; Hinz, S.; Kaleta, M.; Thimm, D.; Kieć-Kononowicz, K.; Müller, C. E. Bicyclic imidazole-4-one derivatives: a new class of antagonists for the orphan G protein-coupled receptors GPR18 and GPR55. *MedChemComm* **2014**, *5* (5), 632−649.
(24) Schoeder, C. T.; Kaleta, M.; Mahardhika, A. B.; Olejarz-Maciej, A.; Łażewska, D.; Kieć-Kononowicz, K.; Müller, C. E. Structure-activity relationships of imidazothiazinones and analogs as antagonists of the cannabinoid-activated orphan G protein-coupled receptor GPR18. *Eur. J. Med. Chem.* **2018**, *155*, 381−397.
(25) Lu, V. B.; Puhl, H. L.; Ikeda, S. R. N-Arachidonyl glycine does not activate G-protein−coupled receptor 18 signaling via canonical pathways. *Mol. Pharmacol.* **2013**, *83* (1), 267.
(26) Yin, H.; Chu, A.; Li, W.; Wang, B.; Shelton, F.; Otero, F.; Nguyen, D. G.; Caldwell, J. S.; Chen, Y. A. Lipid G protein-coupled receptor ligand identification using beta-arrestin PathHunter assay. *J. Biol. Chem.* **2009**, *284* (18), 12328−12338.
(27) Finlay, D. B.; Joseph, W. R.; Grimsey, N. L.; Glass, M. GPR18 undergoes a high degree of constitutive trafficking but is unresponsive to N-Arachidonoyl Glycine. *PeerJ.* **2016**, *4*, No. e1835.
(28) Inoue, A.; Raimondi, F.; Kadji, F. M. N.; Singh, G.; Kishi, T.; Uwamizu, A.; Ono, Y.; Shinjo, Y.; Ishida, S.; Arang, N.; Kawakami, K.; Gutkind, J. S.; Aoki, J.; Russell, R. B. Illuminating G-protein-coupling selectivity of GPCRs. *Cell* **2019**, *177* (7), 1933−1947.e25.
(29) Alexander, S. P. H.; Christopoulos, A.; Davenport, A. P.; Kelly, E.; Mathie, A.; Peters, J. A.; Veale, E. L.; Armstrong, J. F.; Faccenda, E.; Harding, S. D.; Pawson, A. J.; Sharman, J. L.; Southan, C.; Davies, J. A.; CGTP Collaborators. The concise guide to pharmacology 2019/20: G protein-coupled receptors. *Br. J. Pharmacol.* **2019**, *176* (S1), S21−S141.
(30) Alexander, S. P.; Christopoulos, A.; Davenport, A. P.; Kelly, E.; Mathie, A.; Peters, J. A.; Veale, E. L.; Armstrong, J. F.; Faccenda, E.; Harding, S. D.; Pawson, A. J.; Southan, C.; Davies, J. A.; Abbracchio, M. P.; Alexander, W.; Al-hosaini, K.; Bäck, M.; Barnes, N. M.; Bathgate, R.; Beaulieu, J.-M.; Bernstein, K. E.; Bettler, B.; Birdsall, N. J. M.; Blaho, V.; Boulay, F.; Bousquet, C.; Bräuner-Osborne, H.; Burnstock, G.; Caló, G.; Castaño, J. P.; Catt, K. J.; Ceruti, S.; Chazot, P.; Chiang, N.; Chini, B.; Chun, J.; Cianciulli, A.; Civelli, O.; Clapp, L. H.; Couture, R.; Csaba, Z.; Dahlgren, C.; Dent, G.; Singh, K. D.; Douglas, S. D.; Dournaud, P.; Eguchi, S.; Escher, E.; Filardo, E. J.; Fong, T.; Fumagalli, M.; Gainetdinov, R. R.; Gasparo, M. D.; Gerard, C.; Gershengorn, M.; Gobeil, F.; Goodfriend, T. L.; Goudet, C.; Gregory, K. J.; Gundlach, A. L.; Hamann, J.; Hanson, J.; Hauger, R. L.; Hay, D. L.; Heinemann, A.; Hollenberg, M. D.; Holliday, N. D.; Horiuchi, M.; Hoyer, D.; Hunyady, L.; Husain, A.; IJzerman, A. P.; Inagami, T.; Jacobson, K. A.; Jensen, R. T.; Jockers, R.; Jonnalagadda, D.; Karnik, S.; Kaupmann, K.; Kemp, J.; Kennedy, C.; Kihara, Y.; Kitazawa, T.; Kozielewicz, P.; Kreienkamp, H.-J.; Kukkonen, J. P.; Langenhan, T.; Leach, K.; Lecca, D.; Lee, J. D.; Leeman, S. E.; Leprince, J.; Li, X. X.; Williams, T. L.; Lolait, S. J.; Lupp, A.; Macrae, R.; Maguire, J.; Mazella, J.; McArdle, C. A.; Melmed, S.; Michel, M. C.; Miller, L. J.; Mitolo, V.; Mouillac, B.; Müller, C. E.; Murphy, P.; Nahon, J.-L.; Ngo, T.; Norel, X.; Nyimanu, D.; O'Carroll, A.-M.; Offermanns, S.; Panaro, M. A.; Parmentier, M.; Pertwee, R. G.; Pin, J.-P.; Prossnitz, E. R.; Quinn, M.; Ramachandran, R.; Ray, M.; Reinscheid, R. K.; Rondard, P.; Rovati, G. E.; Ruzza, C.; Sanger, G. J.; Schöneberg, T.; Schulte, G.; Schulz, S.; Segaloff, D. L.; Serhan, C. N.; Stoddart, L. A.; Sugimoto, Y.; Summers, R.; Tan, V. P.; Thal, D.; Thomas, W.; Timmermans, P. B. M. W. M.; Tirupula, K.; Tulipano, G.; Unal, H.; Unger, T.; Valant, C.; Vanderheyden, P.; Vaudry, D.; Vaudry, H.; Vilardaga, J.-P.; Walker, C. S.; Wang, J. M.; Ward, D. T.; Wester, H.-J.; Willars, G. B.; Woodruff, T. M.; Yao, C.; Ye, R. D. The consise guide to pharmacology 2021/22: G protein-coupled receptors. *Br. J. Pharmacol.* **2021**, *178* (S1), S27−S156.
(31) Nazir, M.; Harms, H.; Loef, I.; Kehraus, S.; El Maddah, F.; Arslan, I.; Rempel, V.; Müller, C. E.; König, G. M. GPR18 inhibiting Amauromine and the novel triterpene glycoside Auxarthonoside from the sponge-derived fungus Auxarthron reticulatum. *Planta Med.* **2015**, *81* (12−13), 1141−1145.
(32) Schoeder, C. T.; Mahardhika, A. B.; Drabczyńska, A.; Kieć-Kononowicz, K.; Müller, C. E. Discovery of tricyclic xanthines as agonists of the cannabinoid-activated orphan G-protein-coupled receptor GPR18. *ACS Med. Chem. Lett.* **2020**, *11* (10), 2024−2031.
(33) Rempel, V.; Volz, N.; Glaser, F.; Nieger, M.; Brase, S.; Müller, C. E. Antagonists for the orphan G-protein-coupled receptor GPR55 based on a coumarin scaffold. *J. Med. Chem.* **2013**, *56* (11), 4798−4810.
(34) Banister, S. D.; Arnold, J. C.; Connor, M.; Glass, M.; McGregor, I. S. Dark classics in chemical neuroscience: Δ^9-Tetrahydrocannabinol. *ACS Chem. Neurosci.* **2019**, *10* (5), 2160−2175.
(35) Jansen, K.; De Winter, H.; Heirbaut, L.; Cheng, J. D.; Joossens, J.; Lambeir, A.-M.; De Meester, I.; Augustyns, K.; Van der Veken, P. Selective inhibitors of fibroblast activation protein (FAP) with a xanthine scaffold. *MedChemComm* **2014**, *5* (11), 1700−1707.
(36) Szardenings, A. K.; Gordeev, M. F.; Patel, D. V. A general and convenient synthesis of novel phosphotyrosine mimetics. *Tetrahedron Lett.* **1996**, *37* (21), 3635−3638.
(37) Müller, C. E. Synthesis of 3-substituted 6-aminouracils. *Tetrahedron Lett.* **1991**, *32* (45), 6539−6540.
(38) Bassoni, D. L.; Raab, W. J.; Achacoso, P. L.; Loh, C. Y.; Wehrman, T. S. Measurements of β-arrestin recruitment to activated seven transmembrane receptors using enzyme complementation. In *Receptor Binding Techniques*; Davenport, A. P. Ed.; Humana Press: 2012; pp 181−203.
(39) Soethoudt, M.; van Gils, N.; van der Stelt, M.; Heitman, L. H. Protocol to study β-arrestin recruitment by CB_1 and CB_2 cannabinoid receptors. In *Endocannabinoid Signaling: Methods and Protocols*; Maccarrone, M., Ed.; Springer: New York, 2016; pp 103−111.
(40) Southern, C.; Cook, J. M.; Neetoo-Isseljee, Z.; Taylor, D. L.; Kettleborough, C. A.; Merritt, A.; Bassoni, D. L.; Raab, W. J.; Quinn, E.; Wehrman, T. S.; Davenport, A. P.; Brown, A. J.; Green, A.; Wigglesworth, M. J.; Rees, S. Screening β-arrestin recruitment for the identification of natural ligands for orphan G-protein−coupled receptors. *J. Biomol. Screen.* **2013**, *18* (5), 599−609.
(41) Oka, S.; Nakajima, K.; Yamashita, A.; Kishimoto, S.; Sugiura, T. Identification of GPR55 as a lysophosphatidylinositol receptor. *Biochem. Biophys. Res. Commun.* **2007**, *362* (4), 928−934.
(42) Rosenkilde, M. M.; Benned-Jensen, T.; Andersen, H.; Holst, P. J.; Kledal, T. N.; Lüttichau, H. R.; Larsen, J. K.; Christensen, J. P.; Schwartz, T. W. Molecular pharmacological phenotyping of EBI2: An orphan seven-transmembrane receptor with constitutive activity. *J. Biol. Chem.* **2006**, *281* (19), 13199−13208.
(43) Liu, C.; Yang, X. V.; Wu, J.; Kuei, C.; Mani, N. S.; Zhang, L.; Yu, J.; Sutton, S. W.; Qin, N.; Banie, H.; Karlsson, L.; Sun, S.; Lovenberg, T. W. Oxysterols direct B-cell migration through EBI2. *Nature* **2011**, *475* (7357), 519−523.
(44) Console-Bram, L.; Brailoiu, E.; Brailoiu, G. C.; Sharir, H.; Abood, M. E. Activation of GPR18 by cannabinoid compounds: a tale of biased agonism. *Br. J. Pharmacol.* **2014**, *171* (16), 3908−3917.
(45) Spite, M.; Fredman, G.. Chapter Seven - Insights into the role of the resolvin D2-GPR18 signaling axis in cardiovascular physiology and disease. In *Adv. Pharmacol.*; Zeldin, D. C.; Seubert, J. M. Eds.; Academic Press, 2023; Vol. *97*, pp 257−281.
(46) Harms, H.; Rempel, V.; Kehraus, S.; Kaiser, M.; Hufendiek, P.; Müller, C. E.; König, G. M. Indoloditerpenes from a marine-derived fungal strain of *Dichotomomyces cejpii* with antagonistic activity at GPR18 and cannabinoid receptors. *J. Nat. Prod.* **2014**, *77* (3), 673−677.
(47) Gessier, F.; Preuss, I.; Yin, H.; Rosenkilde, M. M.; Laurent, S.; Endres, R.; Chen, Y. A.; Marsilje, T. H.; Seuwen, K.; Nguyen, D. G.; Sailer, A. W. Identification and characterization of small molecule modulators of the Epstein−Barr Virus-Induced Gene 2 (EBI2) receptor. *J. Med. Chem.* **2014**, *57* (8), 3358−3368.
(48) Benned-Jensen, T.; Norn, C.; Laurent, S.; Madsen, C. M.; Larsen, H. M.; Arfelt, K. N.; Wolf, R. M.; Frimurer, T.; Sailer, A. W.; Rosenkilde, M. M. Molecular characterization of oxysterol binding to the Epstein-Barr Virus-induced gene 2 (GPR183). *J. Biol. Chem.* **2012**, *287* (42), 35470−35483.
(49) Daugvilaite, V.; Madsen, C. M.; Lückmann, M.; Echeverria, C. C.; Sailer, A. W.; Frimurer, T. M.; Rosenkilde, M. M.; Benned-Jensen, T. Biased agonism and allosteric modulation of G protein-coupled

receptor 183 − a 7TM receptor also known as Epstein−Barr virus-induced gene 2. *Br. J. Pharmacol.* **2017**, *174* (13), 2031−2042.
(50) Soethoudt, M.; Grether, U.; Fingerle, J.; Grim, T. W.; Fezza, F.; de Petrocellis, L.; Ullmer, C.; Rothenhäusler, B.; Perret, C.; van Gils, N.; Finlay, D.; MacDonald, C.; Chicca, A.; Gens, M. D.; Stuart, J.; de Vries, H.; Mastrangelo, N.; Xia, L.; Alachouzos, G.; Baggelaar, M. P.; Martella, A.; Mock, E. D.; Deng, H.; Heitman, L. H.; Connor, M.; Di Marzo, V.; Gertsch, J.; Lichtman, A. H.; Maccarrone, M.; Pacher, P.; Glass, M.; van der Stelt, M. Cannabinoid CB_2 receptor ligand profiling reveals biased signalling and off-target activity. *Nat. Commun.* **2017**, *8* (1), 13958.
(51) Patel, M.; Manning, J. J.; Finlay, D. B.; Javitch, J. A.; Banister, S. D.; Grimsey, N. L.; Glass, M. Signalling profiles of a structurally diverse panel of synthetic cannabinoid receptor agonists. *Biochem. Pharmacol.* **2020**, *175*, No. 113871.
(52) Miljuš, T.; Heydenreich, F. M.; Gazzi, T.; Kimbara, A.; Rogers-Evans, M.; Nettekoven, M.; Zirwes, E.; Osterwald, A.; Rufer, A. C.; Ullmer, C.; Guba, W.; Le Gouill, C.; Fingerle, J.; Nazaré, M.; Grether, U.; Bouvier, M.; Veprintsev, D. B. Diverse chemotypes drive biased signaling by cannabinoid receptors. *bioRxiv* **2020**, No. 375162.
(53) Lu, S.; Jang, W.; Inoue, A.; Lambert, N. A. Constitutive G protein coupling profiles of understudied orphan GPCRs. *PLoS One* **2021**, *16* (4), No. e0247743.
(54) Jang, W.; Lu, S.; Xu, X.; Wu, G.; Lambert, N. A. The role of G protein conformation in receptor−G protein selectivity. *Nat. Chem. Biol.* **2023**, *19* (6), 687−694.
(55) Inoue, A.; Ishiguro, J.; Kitamura, H.; Arima, N.; Okutani, M.; Shuto, A.; Higashiyama, S.; Ohwada, T.; Arai, H.; Makide, K.; Aoki, J. TGFα shedding assay: an accurate and versatile method for detecting GPCR activation. *Nat. Methods* **2012**, *9* (10), 1021−1029.
(56) Pandey, S.; Kumari, P.; Baidya, M.; Kise, R.; Cao, Y.; Dwivedi-Agnihotri, H.; Banerjee, R.; Li, X. X.; Cui, C. S.; Lee, J. D.; Kawakami, K.; Maharana, J.; Ranjan, A.; Chaturvedi, M.; Jhingan, G. D.; Laporte, S. A.; Woodruff, T. M.; Inoue, A.; Shukla, A. K. Intrinsic bias at non-canonical, β-arrestin-coupled seven transmembrane receptors. *Mol. Cell* **2021**, *81* (22), 4605−4621.e11.
(57) Nadine, D.; Céline, L.; Delphine, F.; Martyna, S.; Julie, G.; Pierre, G.; Arvind, S.; Anne-Simone, P.; Bernard, P.; Andy, C.; Jean-Claude, T.; Julien, H. Activation of the orphan G protein−coupled receptor GPR27 by surrogate ligands promotes beta-arrestin 2 recruitment. *Mol. Pharmacol.* **2017**, *91* (6), 595.
(58) Larco, D. O.; Semsarzadeh, N. N.; Cho-Clark, M.; Mani, S. K.; Wu, T. J. β-Arrestin 2 is a mediator of GnRH-(1−5) signaling in immortalized GnRH neurons. *Endocrinology* **2013**, *154* (12), 4726−4736.
(59) Dolanc, D.; Zorec, T. M.; Smole, Z.; Maver, A.; Horvat, A.; Pillaiyar, T.; Trkov Bobnar, S.; Vardjan, N.; Kreft, M.; Chowdhury, H. H.; Zorec, R. The activation of GPR27 increases cytosolic L-lactate in 3T3 embryonic cells and astrocytes. *Cells* **2022**, *11* (6), 1009.
(60) Wang, H.; Du, D.; Huang, J.; Wang, S.; He, X.; Yuan, S.; Xiao, J. GPR27 regulates hepatocellular carcinoma progression via MAPK/ERK pathway. *Cancer Manag. Res.* **2022**, *14*, 1165−1177.
(61) Neumann, A.; Engel, V.; Mahardhika, A. B.; Schoeder, C. T.; Namasivayam, V.; Kieć-Kononowicz, K.; Müller, C. E. Computational investigations on the binding mode of ligands for the cannabinoid-activated G protein-coupled receptor GPR18. *Biomolecules* **2020**, *10* (5), 686.
(62) Pires, D. E. V.; Blundell, T. L.; Ascher, D. B. pkCSM: Predicting small-molecule pharmacokinetic and toxicity properties using graph-based signatures. *J. Med. Chem.* **2015**, *58* (9), 4066−4072.
(63) Nicolaï, J.; De Bruyn, T.; Van Veldhoven, P. P.; Keemink, J.; Augustijns, P.; Annaert, P. Verapamil hepatic clearance in four preclinical rat models: towards activity-based scaling. *Biopharm. Drug Dispos.* **2015**, *36* (7), 462−480.
(64) Guengerich, F. P. A history of the roles of cytochrome P450 enzymes in the toxicity of drugs. *Toxicological Res.* **2021**, *37* (1), 1−23.
(65) Huang, W.; Manglik, A.; Venkatakrishnan, A. J.; Laeremans, T.; Feinberg, E. N.; Sanborn, A. L.; Kato, H. E.; Livingston, K. E.; Thorsen, T. S.; Kling, R. C.; Granier, S.; Gmeiner, P.; Husbands, S. M.; Traynor, J. R.; Weis, W. I.; Steyaert, J.; Dror, R. O.; Kobilka, B. K. Structural insights into μ-opioid receptor activation. *Nature* **2015**, *524* (7565), 315−321.
(66) Taniguchi, R.; Inoue, A.; Sayama, M.; Uwamizu, A.; Yamashita, K.; Hirata, K.; Yoshida, M.; Tanaka, Y.; Kato, H. E.; Nakada-Nakura, Y.; Otani, Y.; Nishizawa, T.; Doi, T.; Ohwada, T.; Ishitani, R.; Aoki, J.; Nureki, O. Structural insights into ligand recognition by the lysophosphatidic acid receptor LPA6. *Nature* **2017**, *548* (7667), 356−360.
(67) Zhang, D.; Gao, Z.-G.; Zhang, K.; Kiselev, E.; Crane, S.; Wang, J.; Paoletta, S.; Yi, C.; Ma, L.; Zhang, W.; Han, G. W.; Liu, H.; Cherezov, V.; Katritch, V.; Jiang, H.; Stevens, R. C.; Jacobson, K. A.; Zhao, Q.; Wu, B. Two disparate ligand-binding sites in the human $P2Y_1$ receptor. *Nature* **2015**, *520* (7547), 317−321.
(68) Zhou, Q.; Yang, D.; Wu, M.; Guo, Y.; Guo, W.; Zhong, L.; Cai, X.; Dai, A.; Jang, W.; Shakhnovich, E. I.; Liu, Z.-J.; Stevens, R. C.; Lambert, N. A.; Babu, M. M.; Wang, M.-W.; Zhao, S. Common activation mechanism of class A GPCRs. *eLife* **2019**, *8*, No. e50279.
(69) Hua, T.; Vemuri, K.; Nikas, S. P.; Laprairie, R. B.; Wu, Y.; Qu, L.; Pu, M.; Korde, A.; Jiang, S.; Ho, J.-H.; Han, G. W.; Ding, K.; Li, X.; Liu, H.; Hanson, M. A.; Zhao, S.; Bohn, L. M.; Makriyannis, A.; Stevens, R. C.; Liu, Z.-J. Crystal structures of agonist-bound human cannabinoid receptor CB_1. *Nature* **2017**, *547* (7664), 468−471.
(70) Li, X.; Hua, T.; Vemuri, K.; Ho, J.-H.; Wu, Y.; Wu, L.; Popov, P.; Benchama, O.; Zvonok, N.; Locke, K. a.; Qu, L.; Han, G. W.; Iyer, M. R.; Cinar, R.; Coffey, N. J.; Wang, J.; Wu, M.; Katritch, V.; Zhao, S.; Kunos, G.; Bohn, L. M.; Makriyannis, A.; Stevens, R. C.; Liu, Z.-J Crystal structure of the human cannabinoid receptor CB_2. *Cell* **2019**, *176* (3), 459−467.e13.
(71) *SeeSAR version 13.0.4*; BioSolveIT GmbH, Sankt Augustin: Germany. www.biosolveit.de/SeeSAR (accessed Dec 10, 2023).
(72) Reulecke, I.; Lange, G.; Albrecht, J.; Klein, R.; Rarey, M. Towards an Integrated Description of Hydrogen Bonding and Dehydration: Decreasing False Positives in Virtual Screening with the HYDE Scoring Function. *ChemMedChem.* **2008**, *3* (6), 885−897.
(73) Schneider, N.; Lange, G.; Hindle, S.; Klein, R.; Rarey, M. A consistent description of HYdrogen bond and DEhydration energies in protein−ligand complexes: methods behind the HYDE scoring function. *J. Comput. Aided Mol. Des.* **2013**, *27* (1), 15−29.
(74) Bissantz, C.; Kuhn, B.; Stahl, M. A medicinal chemist's guide to molecular interactions. *J. Med. Chem.* **2010**, *53* (14), 5061−5084.
(75) Kortagere, S.; Ekins, S.; Welsh, W. J. Halogenated ligands and their interactions with amino acids: Implications for structure−activity and structure−toxicity relationships. *J. Mol. Graphics Modell.* **2008**, *27* (2), 170−177.
(76) Mahardhika, A. B.; Ressemann, A.; Kremers, S. E.; Gregório Castanheira, M. S.; Schoeder, C. T.; Müller, C. E.; Pillaiyar, T. Design, synthesis, and structure−activity relationships of diindolylmethane derivatives as cannabinoid CB2 receptor agonists. *Arch. Pharm.* **2023**, *356* (3), No. e2200493.
(77) Rempel, V.; Fuchs, A.; Hinz, S.; Karcz, T.; Lehr, M.; Koetter, U.; Müller, C. E. Magnolia extract, magnolol, and metabolites: activation of cannabinoid CB_2 receptors and blockade of the related GPR55. *ACS Med. Chem. Lett.* **2013**, *4* (1), 41−45.
(78) Rempel, V.; Volz, N.; Hinz, S.; Karcz, T.; Meliciani, I.; Nieger, M.; Wenzel, W.; Bräse, S.; Müller, C. E. 7-Alkyl-3-benzylcoumarins: A versatile scaffold for the development of potent and selective cannabinoid receptor agonists and antagonists. *J. Med. Chem.* **2012**, *55* (18), 7967−7977.
(79) Modemann, D. J.; Mahardhika, A. B.; Yamoune, S.; Kreyenschmidt, A.-K.; Maaß, F.; Kremers, S.; Breunig, C.; Sahlmann, C.-O.; Bucerius, J.; Stalke, D.; Wiltfang, J.; Bouter, Y.; Müller, C. E.; Bouter, C.; Meller, B. Development of high-affinity fluorinated ligands for cannabinoid subtype 2 receptor, and in vitro evaluation of a radioactive tracer for imaging. *Eur. J. Med. Chem.* **2022**, *232*, No. 114138.
(80) Behrenswerth, A.; Volz, N.; Toräng, J.; Hinz, S.; Bräse, S.; Müller, C. E. Synthesis and pharmacological evaluation of coumarin derivatives as cannabinoid receptor antagonists and inverse agonists. *Bioorg. Med. Chem.* **2009**, *17* (7), 2842−2851.

(81) Hess, C.; Schoeder, C. T.; Pillaiyar, T.; Madea, B.; Muller, C. E. Pharmacological evaluation of synthetic cannabinoids identified as constituents of spice. *Forensic Toxicol.* **2016**, *34* (2), 329−343.
(82) Schoeder, C. T.; Hess, C.; Madea, B.; Meiler, J.; Müller, C. E. Pharmacological evaluation of new constituents of "Spice": synthetic cannabinoids based on indole, indazole, benzimidazole and carbazole scaffolds. *Forensic Toxicol.* **2018**, *36* (2), 385−403.
(83) Nordstedt, C.; Fredholm, B. B. A modification of a protein-binding method for rapid quantification of cAMP in cell-culture supernatants and body fluid. *Anal. Biochem.* **1990**, *189* (2), 231−234.
(84) Webb, B.; Sali, A. Protein structure modeling with MODELLER. In *Protein Structure Prediction*; Kihara, D., Ed.; Springer: New York, 2014; pp 1−15.
(85) Clark, A. J.; Tiwary, P.; Borrelli, K.; Feng, S.; Miller, E. B.; Abel, R.; Friesner, R. A.; Berne, B. J. Prediction of protein−ligand binding poses via a combination of induced fit docking and metadynamics simulations. *J. Chem. Theory Comput.* **2016**, *12* (6), 2990−2998.
(86) Sherman, W.; Day, T.; Jacobson, M. P.; Friesner, R. A.; Farid, R. Novel procedure for modeling ligand/receptor induced fit effects. *J. Med. Chem.* **2006**, *49* (2), 534−553.
(87) Attah, I. Y.; Neumann, A.; Al-Hroub, H.; Rafehi, M.; Baqi, Y.; Namasivayam, V.; Müller, C. E. Ligand binding and activation of UTP-activated G protein-coupled $P2Y_2$ and $P2Y_4$ receptors elucidated by mutagenesis, pharmacological and computational studies. *Biochim. Biophys. Acta, Gen. Subj.* **2020**, *1864* (3), No. 129501.
(88) Rafehi, M.; Malik, E. M.; Neumann, A.; Abdelrahman, A.; Hanck, T.; Namasivayam, V.; Müller, C. E.; Baqi, Y. Development of potent and selective antagonists for the UTP-activated $P2Y_4$ receptor. *J. Med. Chem.* **2017**, *60* (7), 3020−3038.
(89) Rafehi, M.; Neumann, A.; Baqi, Y.; Malik, E. M.; Wiese, M.; Namasivayam, V.; Müller, C. E. Molecular recognition of agonists and antagonists by the nucleotide-activated G protein-coupled $P2Y_2$ receptor. *J. Med. Chem.* **2017**, *60* (20), 8425−8440.
(90) Friesner, R. A.; Murphy, R. B.; Repasky, M. P.; Frye, L. L.; Greenwood, J. R.; Halgren, T. A.; Sanschagrin, P. C.; Mainz, D. T. Extra precision Glide: Docking and scoring Incorporating a model of hydrophobic enclosure for protein−ligand complexes. *J. Med. Chem.* **2006**, *49* (21), 6177−6196.
(91) Jacobson, M. P.; Pincus, D. L.; Rapp, C. S.; Day, T. J. F.; Honig, B.; Shaw, D. E.; Friesner, R. A. A hierarchical approach to all-atom protein loop prediction. *Proteins: Struct. Funct. Genet.* **2004**, *55* (2), 351−367.

https://doi.org/10.1021/acs.jmedchem.3c02423
J. Med. Chem. 2024, 67, 9896−9926

3.3. Publication III: Development of high-affinity fluorinated ligands for cannabinoid subtype 2 receptor, and in vitro evaluation of a radioactive tracer for imaging

Daniel J. Modemann, **Andhika B. Mahardhika**, Sabrina Yamoune, Anne-Katrin Kreyenschmid, Frederike Maaß, Sarah Kremers, Christian Breunig, Carsten-Oliver Sahlmann, Jan A. Bucerius, Dietmar Stalke, Jens Wiltfang, Yvonne Bouter, Christa E. Müller, Caroline Bouter, and Birgit Meller

Published in: *European Journal of Medicinal Chemistry* ***2002****, (232) 114138.*
DOI: 10.1016/j.ejmech.2022.114138

Supplementary information for this work can be found in the **Appendix III**.

Publication summary and contributions

Cannabinoid (CB) receptors are G protein-coupled receptors that are a part of the endocannabinoid system (ECS).[84] The ECS plays an essential role in neuromodulation and immune modulation.[52, 131, 132] CB receptors are divided into two subtypes: Cannabinoid type 1 (CB_1) receptor and cannabinoid type 2 (CB_2) receptor.[77] They share only 44% sequence similarity and 30% sequence identity at the protein level.[133] CB_1 receptors are mainly expressed in neurons, brain, skeletal muscle, and pancreatic islets, while CB_2 receptors are mainly expressed in immune and endocrine organs such as spleen and testis.[80, 134, 135] The CB_2 receptor was believed not to be expressed in the brain (hence the CB_2 receptor is referred to be the "peripheral CB receptor"). However, due to advances in detection methods, CB_2 receptors has also been shown to be expressed in the brain, albeit to a lower extent than the CB_1 receptor.[136-140]

Due to its expression, the CB_1 receptor plays an essential role in pain, energy metabolism, appetite, and musculoskeletal disorders, while the CB_2 receptor plays a vital role in inflammation. The CB_2 receptor is expressed in microglia, and is upregulated during neuroinflammation.[136, 137, 141] Activation of CB_2 receptors with agonists causes a switch of microglia from a pro-inflammatory state to an anti-

inflammatory state, hence reducing the inflammation processes. Due to the essential role of the CB_2 receptor in neuroinflammation, it has become an attractive drug target.[142] In order to detect neuroinflammation, several tracer molecules targeting CB_2 receptors have been developed. However, the low expression of CB_2 receptors in the brain, metabolic instability of the tracers, the higher expression of the CB_2 receptor in the peripheral system, and lacking selectivity of the tracers versus CB_1 receptors have hampered the detection of CB_2 recepors in the brain.

In this manuscript, a new series of compounds based on an indole-3-yl-tetramethylcylopropylketone scaffold bearing fluorine atoms was developed, and the compound's binding affinity and pharmacological activity at CB_1 and CB_2 receptors was evaluated. The best compound was further labeled with ^{18}F to obtain a positron emission tomography (PET) radiotracer, and autoradiography measurements were employed to investigate the distribution of the tracer in mouse organs.

A total of 11 optimized compounds was synthesized by Dr. Daniel Modemann under supervision of Prof. Dr. Birgit Meller (Göttingen University). Subsequently, their binding to CB_1 and CB_2 receptors was evaluated in radioligand binding experiments. Additionally, their interaction with the CB-like orphan receptors GPR18 and GPR55 was investigated. (1-(2-Fluoroethyl)-1*H*-indole-3-yl)(2,2,3,3-tetramethyl-cyclopropyl)methanone (**5**) was chosen as the lead compound because of high selectivity for the CB_2 receptor (>207-fold) over the CB_1 receptor subtype. Further optimization was carried out to achieve better CB_2 receptor affinity and selectivity. Several modifications were performed, such as extending the aliphatic chain at the *N*1-indole position and/or introducing a methyl moiety at the *C*2 indole position.

Compound **7** (Figure 3.4, DM102 (1-(3-fluoropropyl)-1*H*-indole-3-yl)(2,2,3,3-tetramethyl-cyclopropyl)methanone) was the most selective compound of the present series (435-fold selective *vs.* CB_1 receptor). Thus, further pharmacological characterization was performed to evaluate the functional properties of **7**. Bioluminescent resonance energy transfer (BRET) measuring G protein dissociation (Trupath BRET^2) was used to evaluate the $G\alpha_i$-protein dissociation pathway, and a galactosidase enzyme complementation assay (PathHunter) was employed to

measure β-arrestin-2 recruitment. Compound **7** displayed agonistic activity in both assays, $G\alpha_i$ protein dissociation assay and β-arrestin recruitment assay, being equally active in both pathways. It showed comparable potency and efficacy (EC_{50} $G\alpha_i$-protein pathway 12.9 nM, EC_{50} β-arrestin pathway 0.396 nM) to the full standard CB_2 agonist CP55,940 (EC_{50} $G\alpha_i$-protein pathway 8.53 nM, EC_{50} β-arrestin pathway 0.588 nM). Additionally, it showed high selectivity for the CB_2 over the CB_1 receptor – in agreement with the radioligand binding results.

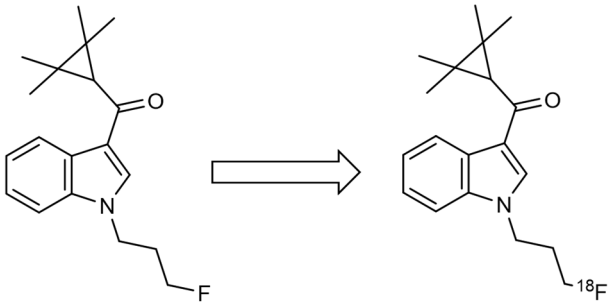

7 **[^{18}F]7**

CB_2/CB_1 K_i ratio : 435-fold
CB_2 EC_{50} 0.0129 µM (G protein dissociation assay)
CB_2 EC_{50} 0.000396 µM (β-arrestin assay)

Figure 3.4 Structure of compound 7 as the most selective CB_2 receptor ligand at the present series. The radioligand [^{18}F]7 was synthesized for further characterization.

One of the requirements for a tracer to detect CB_2 receptors in brain cells is the ability of the compound to penetrate the blood-brain barrier (BBB). Thus, we evaluated the logP value and performed central nervous system multiparameter optimization to evaluate BBB permeability. Compound **7** demonstrated favorably high binding affinity and selectivity comparable to all other published CB_2 tracers described to date, in addition to predicted penetration of the BBB.

The radiosynthesis of **7** yielding [^{18}F]**7** was achieved (34% within 2 hours), with a purity >99% and a specific radioactivity of up to 1500 GBq/µmol. We further evaluated the metabolic stability and identified a metabolite of the radiotracer by using LC/MS. The fluorine-18 was found to be substituted by hydroxyl during stability tests, yielding **18** (1-(3-hydroxypropyl)-1*H*-indole-3-yl)(2,2,3,3-tetramethyl-cyclopropyl)methanone).

Compound **18** was able to bind to CB_2 receptors, albeit with lower affinity as compared to **7** (4.6-fold lower affinity), while still maintaining selectivity against the CB_1 receptor (>270-fold). This metabolite could compete with the tracer in binding to the CB_2 receptor. However, the metabolite's lower binding affinity will result in its lower to bind to the CB_2 receptor. Further characterization revealed that [^{18}F]**7** has a half-life of 30 minutes. This half-life is within the acceptable range for PET examinations thus making [^{18}F]**7** a suitable candidate. Autoradiography measurements using rat spleen tissue revealed that [^{18}F]**7** was able to bind to CB_2 receptors, with significantly lower binding observed when known agonists were employed to block the CB_2 receptor binding site. This demonstrates the potential of the compound as a new, highly potent PET tracer.

For this manuscript, I performed radioligand binding experiments and functional assays for all compounds. I developed and established the β-arrestin assays and tested selected compounds in this assay. Additionally, I suggested several compounds to be synthesized to achieve better affinity and selectivity for the CB_2 receptor. I prepared figures for the manuscript and wrote the manuscript in cooperation with Dr. Daniel Modemann, Prof. Dr. Christa E. Müller, Prof. Dr. Birgit Meller and all other authors.

European Journal of Medicinal Chemistry 232 (2022) 114138

Contents lists available at ScienceDirect

European Journal of Medicinal Chemistry

journal homepage: http://www.elsevier.com/locate/ejmech

Development of high-affinity fluorinated ligands for cannabinoid subtype 2 receptor, and *in vitro* evaluation of a radioactive tracer for imaging

Daniel J. Modemann [a], Andhika B. Mahardhika [b, c], Sabrina Yamoune [d, e], Anne-Katrin Kreyenschmidt [f], Frederike Maaß [g], Sarah Kremers [b], Christian Breunig [a], Carsten-Oliver Sahlmann [a], Jan Bucerius [a], Dietmar Stalke [f], Jens Wiltfang [h, i, j], Yvonne Bouter [h], Christa E. Müller [b, c], Caroline Bouter [a], Birgit Meller [a, *]

[a] *Clinic of Nuclear Medicine, University Medicine Göttingen (UMG), Germany*
[b] *Pharmaceutical Institute, Department of Pharmaceutical & Medicinal Chemistry, University of Bonn, Germany*
[c] *Research Training Group GRK1873, University of Bonn, Germany*
[d] *Federal Institute for Drugs and Medical Devises, Research Division, BfArM Bonn, Germany*
[e] *Institute of Clinical Pharmacology, University Hospital RWTH Aachen, Germany*
[f] *Institute of Inorganic Chemistry, Georg-August-University Göttingen, Germany*
[g] *Max-Planck-Institute for Experimental Medicine, Göttingen, Germany*
[h] *Department of Psychiatry and Psychotherapy, University Medical Center Göttingen, Göttingen, Germany*
[i] *German Center for Neurodegenerative Diseases (DZNE), Research Site Göttingen, Germany*
[j] *Neurosciences and Signaling Group, Institute of Biomedicine (iBiMED), Department of Medical Sciences, University of Aveiro, Aveiro, Portugal*

ARTICLE INFO

Article history:
Received 4 November 2021
Received in revised form
12 January 2022
Accepted 14 January 2022
Available online 28 January 2022

Keywords:
CB_2R
PET-Tracer
Diagnostic of neurodegenerative diseases
Microglia

ABSTRACT

The development of neurodegenerative diseases is associated with cerebral inflammation, which activates resident immune cells of the central nervous system (CNS), namely microglial cells that show an up-regulation of the cannabinoid subtype 2 receptor (CB_2R) expression. Therefore our work aimed to design and synthesize a radiotracer for the detection of CB_2R expression by positron emission tomography (PET) allowing an early diagnosis of neurodegenerative diseases. For the development of such a PET tracer, *N*-alkyl-substituted indole-3-yl-tetramethylcyclopropylketones served as lead structures due to their high CB_2R potency and selectivity, allowing radiolabeling on the *N*-alkyl chain. To this end, eight novel fluorinated *N*-alkyl-indole-3-yl-tetramethylcyclopropylketones were synthesized, investigated in radioligand binding studies, and structure-activity relationships were evaluated. The most promising candidate was (1-(4-fluoropropyl)-1*H*-indole-3-yl)(2,2,3,3-tetramethyl-cyclopropyl)methanone (K_i: 7.88 nM at the CB_2R, 3430 nM at cannabinoid subtype 1 receptor (CB_1R)). A precursor was synthesized, radiofluorinated with no-carrier-added [$^{18}F]F^-$ by nucleophilic substitution of a tosyl group, and the resulting PET ligand was purified, all being performed on a fully automated synthesis module. The tracer was produced in 34 ± 6% radiochemical yield within 2 h and with molar activities of up to 1500 GBq/μmol. A first preclinical evaluation was carried out including determination of logP, metabolic stability by liver microsomes, and autoradiography. The novel PET tracer for imaging CB_2R showed promising results warranting subsequent clinical evaluation.

1. Introduction

The incidence of neurodegenerative diseases increases continuously with the rise in life expectancy and is most prominent in industrialized countries. Common neurodegenerative diseases include Alzheimer's disease (AD), Parkinson's disease, amyotrophic lateral sclerosis and Huntington's disease [1]. The main commonality of these diseases is the irreversible loss of neurons. Therefore,

Abbreviations: CB_2R, cannabinoid subtype 2 receptor; PET, positron emission tomography.

* Corresponding author.
E-mail address: birgit.meller@med.uni-goettingen.de (B. Meller).

https://doi.org/10.1016/j.ejmech.2022.114138
0223-5234/

the diagnosis of neurodegenerative disease in the early stages of the disease progression is essential to treat the advancing neuron loss as early as possible [2].

More than 20 years ago, it was shown that neurodegeneration is associated with cerebral inflammatory processes. This is represented by the activation of primary immune cells (microglia) in the surrounding tissue [3]. Activation of microglia has been shown to be associated with the overexpression of different receptors. One of them being the peripheral benzodiazepine receptor, also known as the translocator protein (TSPO). In order to detect neuroinflammation, several tracer molecules which bind to TSPO have been developed for PET imaging. However, TSPO exhibits two separate binding sites for these tracers with different binding affinities. As a consequence, the differential expression of both binding sites leads to a tri-modal distribution of the binding affinities which makes the interpretation of PET images difficult. In addition, the permeability of the blood brain barrier (BBB) poses a problem and high non-specific binding interferes with imaging [4–7], but other options for possible tracers should be explored.

Several studies have shown that the activation of microglia in the context of inflammatory reactions also leads to an upregulation of the expression of a cannabinoid receptor (CBR), namely CB_2R. In general, the expression of CB_2R is very low in the CNS under physiological conditions [8–10]. In addition, independent studies have shown the expression of CB_2R in the brain and its involvement in neurodegenerative diseases such as Alzheimer's [11,12], Schizophrenia [13,14], and Parkinson's disease [15,16]. Furthermore, there have been many attempts to treat neurodegenerative diseases with CB_2R agonists, intending to inhibit the progress of neurodegenerative disorder [17].

The cannabinoid system contains two classical receptors, which belong to the superfamily of G protein-coupled receptors. The CB_1R is primarily expressed in the brain, but also in peripheral organs [18]. The CB_2R is mainly found on peripheral immune cells and is enriched in immune system-associated tissues, e.g. spleen [19]. Besides CB_1R and CB_2R, further CB-like receptors, including GPR18 [20], GPR55 [21] and GPR119 [22] have been described, to interact with cannabinoids, but are phylogenetically not closely related to the classical CBR [23].

Due to its prominent role in neuroinflammation, the CB_2R is a potential target for tracer development in positron emission tomography (PET) imaging aimed at performing early *in vivo* diagnostic studies of neurodegenerative diseases. A variety of lead structures have been evaluated, e.g. those containing oxoquinoline, pyridine, triazine, oxadiazole, or indole scaffolds, to synthesize fluorine-18 or carbon-11 radiolabeled tracers with high binding affinities and selectivity towards CB_2R [24–26].

Still, tracer development for CB_2R imaging in nuclear medicine is a difficult task since the tracer needs to fulfill several of criteria [25,27]: high CB_2R affinity and high selectivity over the closely related CB_1R are required, a considerable crossing of the blood-brain barrier (BBB), and the non-specific binding in brain tissue should be minimal [28]. High lipophilicity will result in high non-specific binding of the tracer in the surrounding brain tissue and the periphery [27]. This behavior causes problems in imaging. Unfortunately, the majority of CBR ligands display very high lipophilicity, e.g. the natural cannabinoid (−)-Δ^9-*trans*-tetrahydrocannabinol (Δ^9-THC) has a $logD_{7.4}$ value of 7.7, and the potent synthetic agonist CP55,940 displays a value of 6.0 [29]. Furthermore, the tracer needs to be stable towards metabolic degradation, especially the generation of radioactive metabolites that would disturb imaging of the brain should be prevented. Finally, the tracer must be produced with high molar radioactivity and without any relevant impurities, which could disturb the binding of the tracer to the receptor and thereby lead to low PET image quality. Increased receptor expression outside the brain (e.g. spleen) binds the tracer to a greater extent, but this does not affect imaging if the distances between the organs are large enough.

Frost et al. developed a series of indole-3-yl-tetramethylcyclopropylketone derivatives, which showed high CB_2R binding affinity and selectivity [30,31]. Examples (I, II) with high CB_2R affinity and selectivity are given in Scheme 1. Here we report the development of a new radiotracer based on an indole-3-yl-tetramethylcyclopropylketone scaffold as a PET tracer for CB_2R imaging. This work includes the development and synthesis of new fluorine-containing ligands and their evaluation in binding studies at CB_1R and CB_2R. The most promising candidate should be obtained in the fluorine-18-labeled form and the new PET tracer should be subsequently evaluated in preclinical *in vitro* studies.

2. Results and discussion

2.1. Synthesis and evaluation of ligands

For the development of new radiopharmaceuticals that could enable the diagnosis of neurodegenerative disease in the early stages with PET scans, a variety of different fluorinated molecules were designed considering binding affinity for CB_1R and CB_2R. The synthesis of the target molecules is shown in Scheme 2.

The syntheses of compounds **1** and **2** (see Scheme 2) started from 1*H*-indole, or 2-methyl-1*H*-indole, respectively, using diethyl aluminum chloride [32]. In comparison to the synthetic approach by Frost et al. using EtMgBr and $ZnCl_2$, we could increase the yield from 42% to 87% for **1**. Compounds **5**–**10** were synthesized by N-alkylation of **1** and **2**. Sodium hydride was used for deprotonation of the indoles and different fluoroalkyl moieties were introduced using the appropriate bromides or tosylates with very good yields. Compounds **12** and **13** were synthesized by the introduction of a tetrahydropyranyl-protected (THP) alcohol, which was subsequently hydrolyzed by *p*-toluenesulfonic acid. Williamson ether synthesis was performed to obtain the *N*-(2-fluoroethoxy)ethyl-substituted indole derivatives **14** and **15**.

We subsequently investigated the eight fluorinated indole-3-yl-tetramethylcyclopropylketones (**5**–**10**, **14** and **15,** Table 1) and three additional known compounds (**12**, **16** and **18**) for their interaction with CB_1R and CB_2R in radioligand binding assays. Additionally, all newly synthesized compounds were evaluated on the cannabinoid-like orphan receptors GPR18 and GPR55.

Compound **5,** which contains a fluoroethyl residue on *N1* of the indole moiety, displayed affinity in nanomolar range for the CB_2R

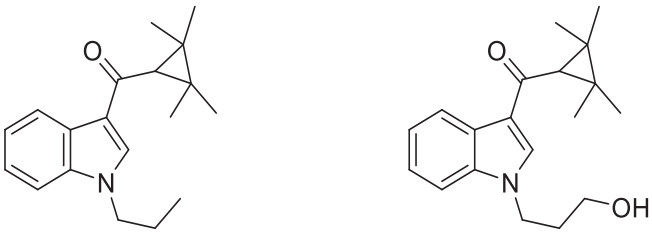

I
Ki: 9.2 nM (CB_2R)
Ki: 4,300 nM (CB_1R)

II
Ki: 2.1 nM (CB_2R)
Ki: 2,200 nM (CB_1R)

Scheme 1. Examples of Indole-3-yl-tetramethylcyclopropylketone derivatives by Frost et al. inclouding CB_1R and CB_2R affinities [30].

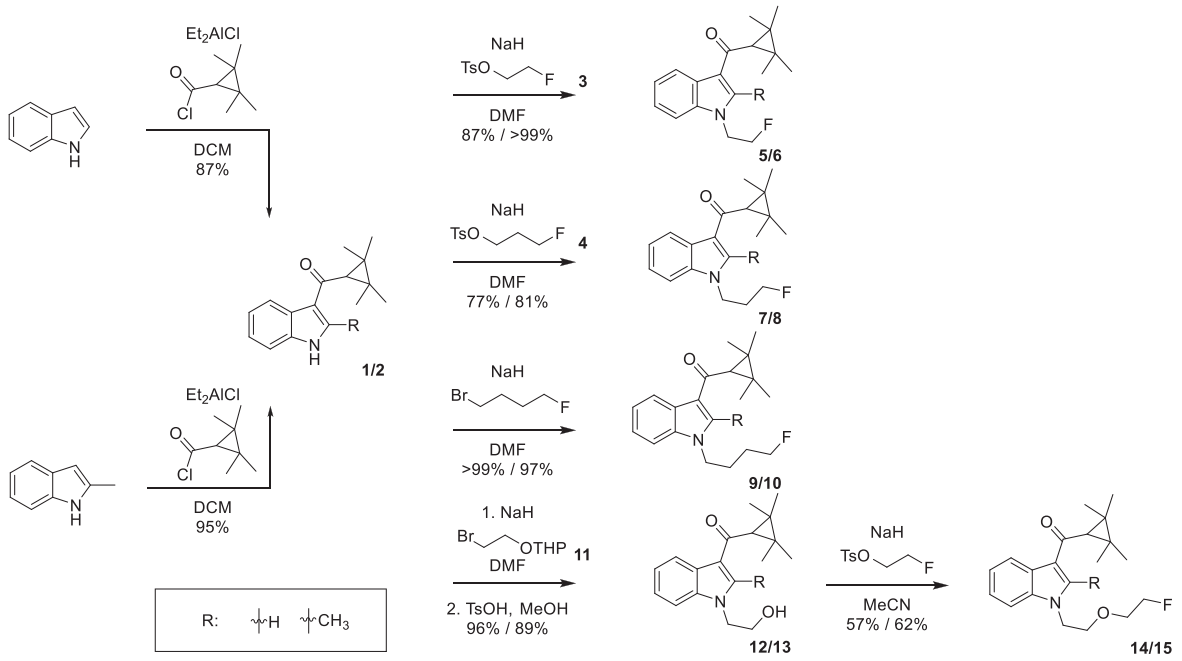

Scheme 2. Synthetic scheme of the investigated compounds according to binding to CBR. Syntheses were performed according to the experimental Section.

Table 1
Affinities and selectivity of investigated compounds for human CB_1R and CB_2R.

Comp.	R R′	Radioligand binding assay[a]		CB_1R/CB_2R selectivity ratio	CNS MPO[d]
		Human CB_2R $K_i \pm$ SEM (nM)	Human CB_1R $K_i \pm$ SEM (nM) (or percent inhibition at 10 μM)		
CP55,940		1.42 ± 0.75[b]	1.28 ± 0.44[b]		1.5
5	H F	48.3 ± 16.1	>10,000 (14%)	>207	3.0
6	CH_3 F	2,530 ± 290	>10,000 (32%)	>4	2.7
7 (**DM102**)	H F	7.88 ± 2.59	3,430 ± 290	435	2.8
8	CH_3 F	81.9 ± 38.6	>10,000 nM (43%)	>22	2.6
9	H F	1.14 ± 0.20	214 ± 59	188	2.6
10	CH_3 F	19.8 ± 6.3	374 ± 113	19	2.4
14	H O F	17.3 ± 1.9	931 ± 247	54	3.5
15	CH_3 O F	10.8 ± 6.2	1,290 ± 52	119	3.2
12	H OH	663 ± 127 [56 nM][c]	>10,000 (4%) [>10,000][c]	>15	4.6
16	H CH_3	25.8 ± 16.3 [9.2 nM][c]	4200 ± 440 [4,300 nM][c]	161	2.4
18	H OH	37.2 ± 5.0 nM [2.1 nM][c]	>10,000 nM (38%) [2,200 nM][c]	>270	4.2

[a] Affinities were determined in competition binding experiment versus 0.1 nM [^{3}H]CP55,940 as described in the experimental section. K_i values represent means ± SEM from three independent experiments. Literature values are given in square brackets for comparison.
[b] Data from Schoeder et al. from our laboratory, obtained under the same conditions [33,37].
[c] Frost et al. [30], radioligand binding studies versus [^{3}H]CP55,940.
[d] Central nervous system multiparameter optimization (CNS MPO) calculated [42] with data from ChemDraw (v.16.0).

(K_i = 48.3 nM) combined with high selectivity versus the CB_1R (>200 fold). This compound displays a similar structure to compound **12**, which had previously been published as a selective CB_2R agonist [30]. In our radioligand binding assays, we could reproduce and confirm the binding affinities for these compounds, as well as other known ligands, all of which showed comparable binding

affinities as already reported (see Table 1 for details). Next, we tried to further optimize CB_2R potency and selectivity.

Extension of the fluoroethyl to a fluoropropyl chain at the *N*1-indole moiety resulted in compound **7**, which showed an increased affinity for the CB_2R (K_i = 7.88 nM) compared to a micromolar affinity for the CB_1R (K_i = 3427 nM). Thus, we observed an increase in selectivity (435 fold) compared to compound **5** (207-fold). A lipophilic and flexible side chain at the *N*1-indole moiety is known to have a beneficial effect on CBR affinity, preferably with respect to the CB_1R [33–35]. As we anticipated, replacement of the fluoropropyl by a fluorobutyl residue (compound **9**) increased the affinity for CB_2R as well as at CB_1R (CB_2R K_i 1.14 nM, CB_1R K_i 214 nM; CB_1R/CB_2R ratio 188, Fig. 1). Thus, compound **9** shows excellent CB_2R affinity, still combined with high selectivity. Replacing the fluoroalkyl residue with a fluoroethoxyethyl residue (compound **14**) neither improved CB_2R affinity nor selectivity.

In 2000, Aung et al. had investigated the effects of various alkyl chains on a naphthoylindole scaffold showing that methyl substitution at the C2 of the indole could lead to an increase in CB_2R selectivity versus CB_1R [36]. Thus, in the next set of experiments, we studied the effects of methyl substitution at the indole C2 position. The 2-methyl-substituted indole derivatives **6**, **8**, **10,** and **15** were obtained (Table 1). Most of the resulting compounds exhibited comparable selectivity or even a decrease in selectivity compared to the unsubstituted analogs. This indicates that a 2-unmethylated indole ring is beneficial for CB_2R selectivity.

Based on these results, we further continued with compound **7**, which displayed the highest selectivity ratio of all compounds of the present series (435 fold). As a next step, we performed a functional characterization of compound **7** utilizing a novel G protein activation assay, the Trupath $BRET^2$ (bioluminescence resonance energy transfer) G protein dissociation technology [38].

CBR are G_i protein-coupled receptors. Agonists activate the receptors leading to a dissociation of the heterotrimeric G proteins. In the applied Trupath assay, this is visualized by a decrease in the BRET signal. As depicted in Fig. 2 A and B, compound **7** displayed agonistic behavior at both CBR subtypes with EC_{50} of 12.9 nM (CB_2R) and 2,960 nM (extrapolated value) at CB_1R. These results correlate well with the radioligand binding data (Table 1). At the CB_2R, compound **7** acted as a full agonist with comparable efficacy to the full standard CB_1R/CB_2R agonist CP55,940 (EC_{50} 8.53 nM). In contrast, at the CB_1R, compound **7** showed very weak agonistic activity. A full concentration-response curve could not be performed due to solubility limitations, therefore, the EC_{50} value had to be extrapolated. These results confirm the high CB_2R-selectivity of compound **7**.

Encouraged by these results, we further investigated the ability of compound **7** to induce β-arrestin recruitment, in addition to G_i protein activation, via the CB_2R using an enzyme complementation assay (Fig. 2 C and D). Compound **7** induced the recruitment of β-arrestin-2 in a concentration-dependent manner in CHO cells transfected with the human CB_2R displaying an EC_{50} value of 0.396 nM. In contrast, and as expected, only marginal β-arrestin recruitment was induced by **7** via CB_1R even at a high concentration (EC_{50} > 10,000 nM) again indicating the high selectivity of compound **7** for CB_2R over CB_1R. Compound **7** showed comparable potency as the standard agonist CP 55,940 in this assay (EC_{50} 0.588 nM). These results showed that compound **7** behaves as a non-biased, CB_2R-selective agonist that activates both pathways, G_i protein dissociation and β-arrestin recruitment.

The orphan receptors GPR18 and GPR55 have been shown to interact with CBR ligands, and thus, these receptors might be novel types of cannabinoid receptors [39,40]. Therefore, we investigated the possibility that our compounds might interact with these receptors (Table S1). We could show that none of the compounds of the present series was able to activate or inhibit GPR18 or GPR55 at a high concentration of 10 μM. This clearly shows that these compounds are also selective versus GPR18 and GPR55.

In summary, compound **7** exhibits the highest selectivity for the CB_2R with a concomitant high binding affinity. Compound **9** displays a higher binding affinity, but at the same time shows lower selectivity versus the CB_1R. The central nervous system multiparameter optimization (MPO) is a tool for evaluating CNS drugs in terms of their permeability by the BBB, among other factors. Lipophilicity, molecular mass, topological polar surface area, hydrogen bond donor and acidity are used for this evaluation. The score ranges from 0 to 6 where 6 is the best score for the drug [41]. The scores for the compounds in Table 1 were determined from calculated values. It shows the relationship between CNS MPO score and structure. An increase in lipophilicity results in a lower score (**5** – **10**) whereas more hydrophilic groups perform significantly better (**12**, **14**, **15**, and **18**). Based on the CNS MPO rating, compound **7** is preferable to **9** because of its better properties. When comparing radiotracers described in the literature with compound **7**, our synthesized tracer exhibits high binding affinity and high selectivity for the CB_2R comparable to CB_2R ligands described so far.

2.2. Radiosynthesis and preclinical evaluation of the tracer

The targeted precursor **19** was synthesized for the projected radiosynthesis of compound **[^{18}F]7**. Therefore, compound **1** was coupled with the THP-protected alcohol **17**, and afterwards, the

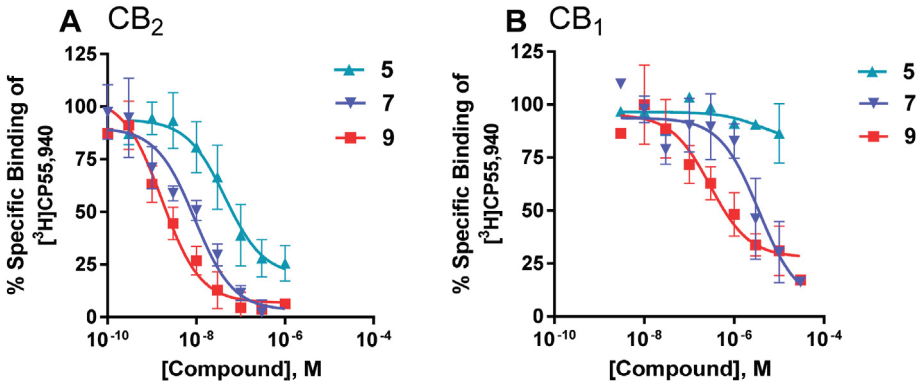

Fig. 1. Concentration-dependent inhibition of specific [^{3}H]CP55,940 binding by compounds **5**, **7**, and **9** at human CB_2R (A) and human CB_1R (B)..Concentration-dependent inhibition of specific [^{3}H]CP55,940 binding experiments were performed as described in the experimental section. Data points represent means ± standard error of the mean (SEM) of three independent experiments. See Table 1 for details.

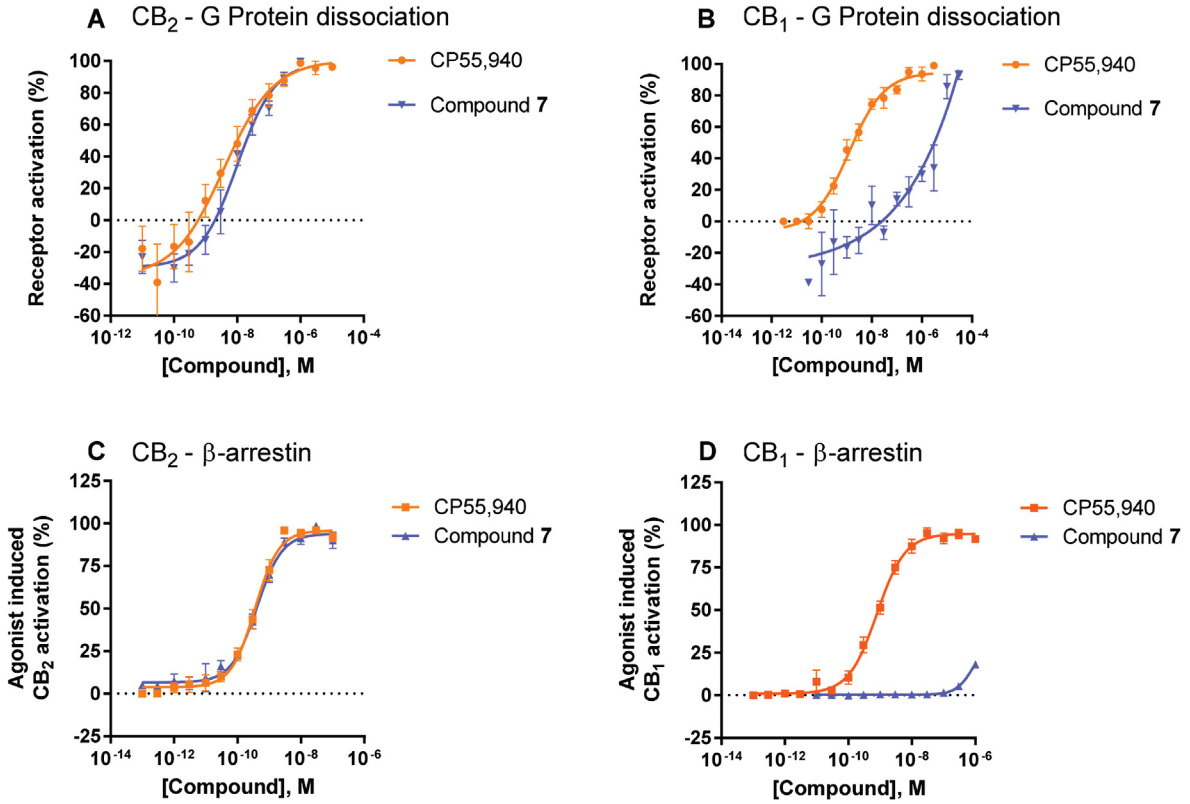

Fig. 2. Functional effects of compound **7** and CP55,940 at human CB_1R and CB_2R. 2A, 2B. determined in recombinant HEK293 cells using the TRUPATH $BRET^2$ assay [38]; 2C, 2D. determined in CHO K1 cells using a β-arrestin recruitment assay based on enzyme complementation. All data were normalized to the maximum effect of CP55,940 at the respective receptor subtype. The EC_{50} of CP55,940 in the TRUPATH $BRET^2$ assay is 8.53 ± 3.64 nM and 1.62 ± 0.51 nM for the CB_2R and CB_1R, respectively; the EC_{50} value of compound **7** is 12.9 ± 5.3 nM (for the CB_2R) and 2,960 ± 980 nM (for the CB_1R, extrapolated curve). The EC_{50} value of CP55,940 in the β-arrestin recruitment assay is 0.588 ± 0.216 nM (CB_2R) and 1.25 ± 0.34 nM (for CB_1R), and the EC_{50} value of compound **7** is 0.396 ± 0.061 nM (CB_2R). Data points represent means ± SEM of at least three independent experiments.

protection group was hydrolyzed. The obtained alcohol **18** was tosylated to yield the desired compound **19**. Thus, the precursor for the following radiosynthesis (**19**) was obtained in 75% total yield in a four-step synthesis starting from 1*H*-indole (see Scheme 3).

The radiosynthesis of **[^{18}F]DM102** (**[^{18}F]7**) (Scheme 4) was performed on a commercially and fully automated synthesis module (ORA Neptis Perform). In short, the radioactive fluoride was trapped by solid-phase extraction and eluted with tetrabutylammonium bicarbonate as aqueous solution. The fluoride was azeotropically dried by acetonitrile. Then, the precursor was dissolved in anhydrous acetonitrile and the radiofluorination was performed at 90 °C within 5 min. The radioactive tracer was purified by solid-phase extraction and semipreparative HPLC. In a final step, the tracer was reformulated to obtain an aqueous solution containing 10% ethanol (see Fig. 6).

Good radiochemical yields of 34 ± 6% (n = 4) were reached within 2 h. The radiochemical yield is isolated and decay corrected in accordance with the definition by Coenen et al. [42]. The radiochemical purity was determined by radio-HPLC (Fig. 3) to be greater than 99%, and molar activities of up to 1500 GBq/μmol were achieved.

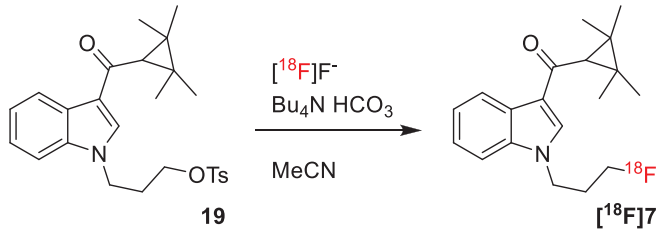

Scheme 4. Radiosynthesis of **[^{18}F]DM102 ([^{18}F]7).** Synthesis of compound [^{18}F]7 was performed as described in the experimental section.

The novel radioactive tracer was subsequently evaluated in a variety of different preclinical experiments. The calculated logP value of **7** was 3.74 (Chem Draw v.16.0). In a shake-flask experiment using 50 mM phosphate buffer (pH: 7.4) and octanol, an experimental value of 3.83 ± 0.04 was obtained confirming the calculated value (n = 3).

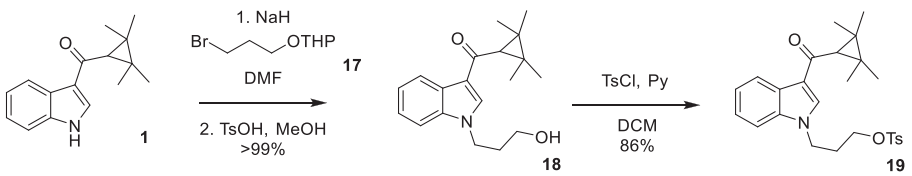

Scheme 3. Precursor synthesis for radiosynthesis of compound **[^{18}F]7.**

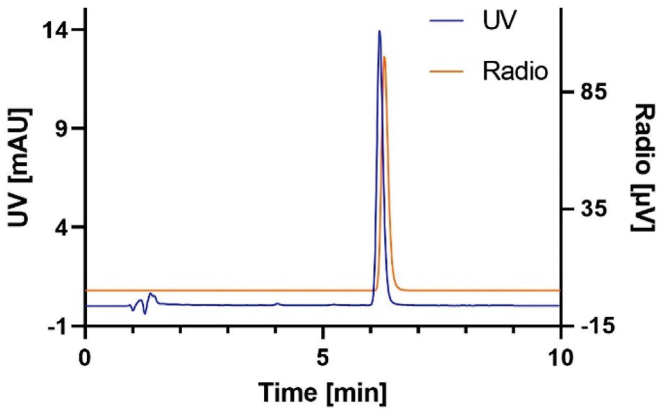

Fig. 3. HPLC chromatogram with radiodetection of compound **[^{18}F]7** with co-injection of non-radioactive **7** for identification. HPLC-conditions: M&N EC 150/3 Nucleodur 100-3 C18ec, 0.6 mL/min 70% MeCN *aq* + 0.1% trifluoroacetic acid (TFA), UV: 305 nm. Peaks: 6.194 min (UV detector), 6.292 min (radio detector). UV- and radiodetector are 0.1 min apart.

The metabolic stability of the tracer was studied *in vitro* in human liver microsomes (Fig. 4). The detection of non-radioactive metabolites by LC-MS was carried out using non-radioactive **7** in a separate assay. In another assay, radioactive metabolites were detected by thin-layer chromatography (Fig. 4A). The detection of radioactive metabolites is of great importance for imaging, as their biodistribution may visal overlay the specific uptake of the radioactive tracer, especially if their binding properties are unclear. Additionally, the most common metabolite of fluorinated compounds, fluoride, can be detected significantly better in a radioactive assay. The detection of non-radioactive metabolites by LC-MS serves as evidence for the complete metabolite detection in the radioactive assay. For imaging non-radioactive metabolites are only relevant because of their potential competition with the radioactive tracer, as far as these metabolites will pass the BBB.

During the metabolism of **[^{18}F]7** in the radioactive assay, the fluoride-18 is removed from the *n*-position of the alkyl chain and is presumably substituted by an −OH group. Further radioactive metabolites could not be detected The LC-MS analysis confirmed this assumption and verified the formation of the defluorinated hydroxypropyl derivative **18**(Fig. 4B).

The half-live of **[^{18}F]7** in the assay were interpolated to 110 min.In the complimentary LC-MS studies, the estimated half-life of 30 min was significantly shorter. This is not surprising, as the experiments could not be carried out under absolutely identical conditions. However, both half-lives are in a range that is potentially acceptable for PET examinations, especially since the released floride is accumulated in the bone and do not pass the BBB. Nevertheless, the half-life of the assays cannot be directly transferred to an *in vivo* experiment but indicates potential problems with the *in vivo* application of the substance. Taking this into account it can be assumed that during an *in vivo* PET scan, the radioactive fluoride, which is released from the tracer, will accumulate in the bones including the cranial bone.

The actual effects and the biological half-life have to be investigated in an *in vivo* PET scan. Wohlfarth et al. [43] investigated the human hepatocyte-mediated metabolism of XLR-11, which differs from compound **7** by the substituent on the indole *N*-atom, namely a fluoropentyl-group instead of a fluoropropyl residue. Most of the observed metabolites were due to defluorination, supporting our results.

Autoradiography of rat spleen tissue sections with known high CB_2R expression revealed the specific binding of compound **[^{18}F]7** to CB_2R and the degree of non-specific binding. This technique is frequently used to illustrate the imaging potential of CB_2R tracers. In the experiment, the first four tissue sections were incubated with compound **[^{18}F]7** without any receptor blocking which results in average intensity of 112 ± 26 Counts/Pixel (n = 4) (Fig. 5 A). The CB_2R in the next slices were blocked with GW405833 (B, 52 Counts/Pixel, −53%, n = 2), CP55,940 (C, 56 Counts/Pixel, −50%, n = 2) and the non-radioactive **7** (D, 63 Counts/Pixel, −44%, n = 2) at 10 µM (see Fig. 5 B to D).

The differential uptake of the tracer in the tissue illustrates its

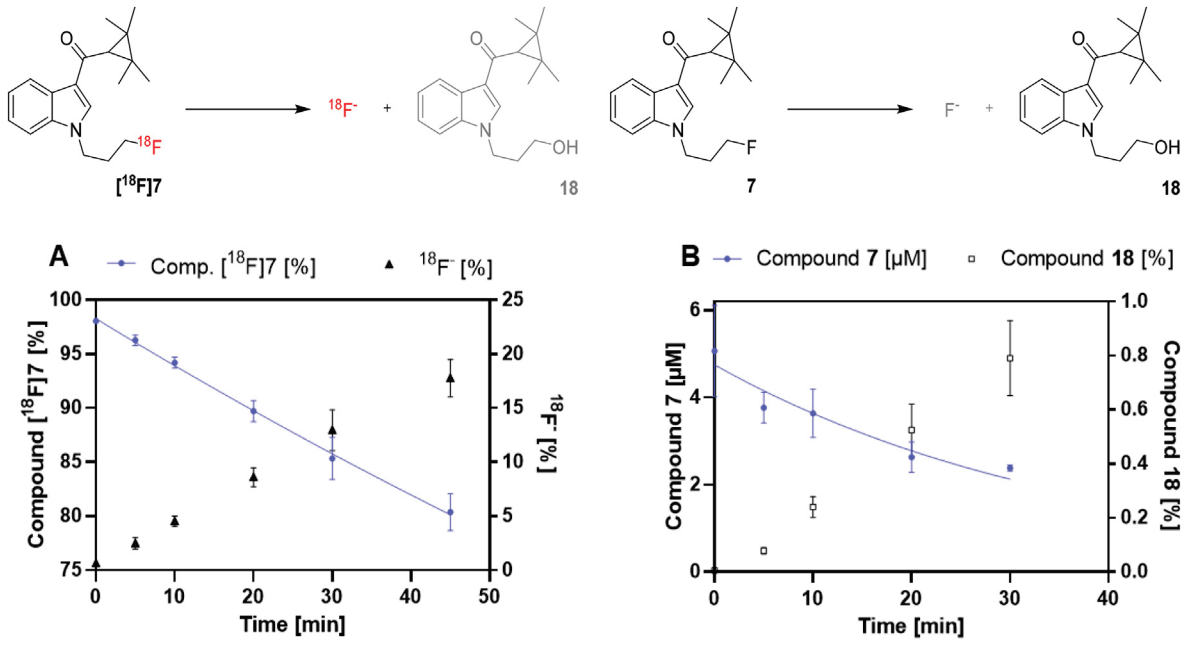

Fig. 4. Metabolite analysis of compound **[^{18}F]7** and **7. Metabolic analysis of [^{18}F]7 by radioactive (A) and non-radioactive (B) methods. In A the $^{18}F^-$ is measured and in B compound 18 is measured besides [^{18}F]7 respectively compound 7. In A 1–2% of radioactive impurities or artifacts were identified. In B the relative signal intensity of compound 18 is shown.**

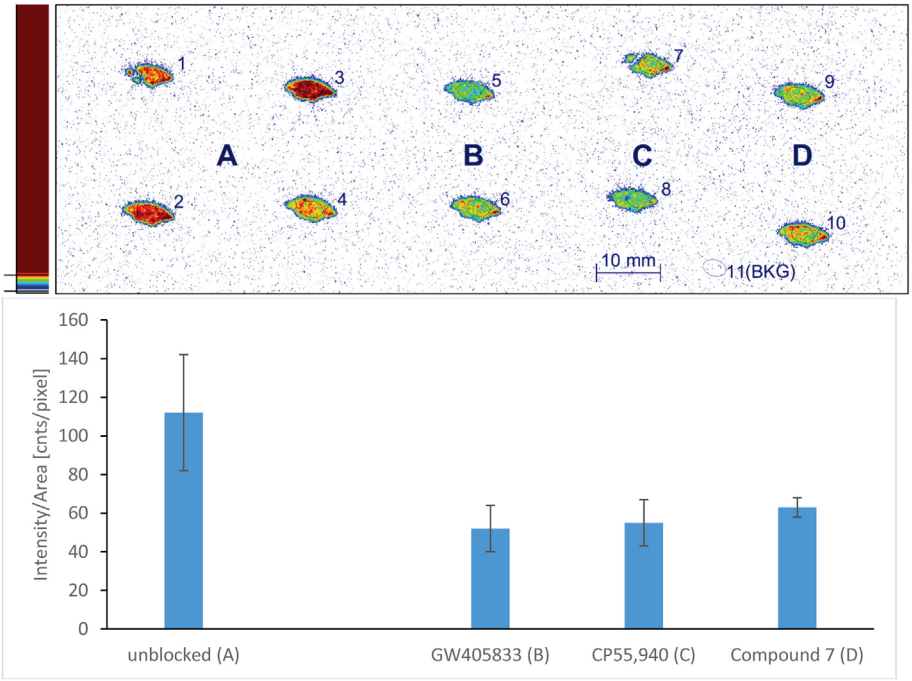

Fig. 5. Autoradiography of rat spleen slices in blocking experiments of compound **[^{18}F]7.** Autoradiography of compound [^{18}F]7 without blocking (A) and compound [^{18}F]7 after blocking with 10 μM GW405833 as CB_2R partial agonist (B), 10 μM CP55,940 as potent non-selective CBR agonist (C) and 10 μM non-radioactive Compound 7 (D). An oval region of interest was centered in the organic sections for quantification (Intensity/Area-BKG). The background (11 BKG) was subtracted from the measured values. In the diagram results of quantification is gives as means. Bars represent the standard deviations.

potential for imaging. Despite the blocking of CB_2R, the tracer binds to the tissue in a non-specific manner. This phenomenon is also described in the literature [27]. In general, the non-specific binding of CB_2R tracers might be a possible disadvantage for their application in PET-imaging. However, the degree of non-specific binding of our newly synthesized tracer is acceptable [44–48].

3. Conclusion

A series of new CB_2R ligands were designed and synthesized, and their binding affinity to CB_1R and CB_2R was investigated. The newly developed fluorinated indole-3-yl-tetramethylcyclopropylketone derivatives generally exhibited CB_2R selectivity. Compound **7** was selected as the most promising candidate due to its high CB_2R affinity, selectivity and high CNS MPO score. A suitable precursor for radiosynthesis was produced, and automated synthesis of compound **[^{18}F]DM102** (**[^{18}F]7**) was performed with a commercial synthesis module that allows sterile conditions according to GMP requirements. The radiosynthesis was carried out in high yield and delivered the novel tracer with high molar radioactivity. Preclinical experiments were performed to characterize the developed tracer. The calculated log P value could be confirmed by an shake-flask-experiment. Microsomal stability revealed a defluorination of the tracer by liver enzymes. The potential of the tracer could be demonstrated by autoradiography experiments. Future *in vivo* experiments to measure biodistribution and kinetics of the newly developed tracer are warranted.

4. Materials and methods

4.1. Chemistry

All chemicals and solvents were used directly as obtained commercially (Sigma Aldrich and Carl Roth) unless noted otherwise. 3-Fluoropropan-1-ol was purchased by Apollo Scientific. 3-Bromopropan-1-ol was purchased by Enamine. Indole and 1-Bromo-4-fluorobutane were purchased by ABCR. Reaction progress was monitored by thin-layer chromatography, silica gel 60 aluminum plates with F254 as indicator. Column chromatography was carried out on silica gel 60 (230–400 mesh).

All NMR spectra were recorded either on a Bruker AVANCE III 400 MHz spectrometer with a BBFO (BroadBandFlourineObservation) probe or on a Bruker AVANCE NEO 400 MHz spectrometer equipped with a CPP-BBO probe (CryoProbeProdigy-BroadBandObserve). The samples were prepared using 5 mm NMR tubes made of borosilicate glass. NMR spectra were measured at ambient temperature, if not indicated otherwise. Chemical shifts (δ) are given in ppm relative to TMS using the residual solvent signals as internal standards. Coupling constants (J) are reported in Hz and standard abbreviations indicating multiplicity are used as follows: s = singlet, d = doublet, t = triplet, quint = quintet, m = multiplet, br = broad signal. Combined abbreviations are derived from their components (e.g. dd = doublet of doublets).

4.2. General procedure 1 - 1H-indole acylation

The protocol is based on the literature [32]. 2,2,3,3-Tetramethylcyclopropanecarboxylic acid (1.5 equivalents (eq.)) was dissolved in 10 mL DCM and 2 drops of DMF were added. Thionyl chloride (2 eq.) was added and the mixture was refluxed for 2 h. Afterwards the solvents were removed *in vacuo* and the crude product was used without further purification.1 *H*-indole (1 eq.) was dissolved in DCM under Ar. The reaction mixture was cooled to 0 °C by an ice bath and diethylaluminium chloride (1.0 M in heptane, 1.5 eq.) was added dropwise. The mixture was stirred for 30 min and the crude acyl chloride dissolved in DCM was added. The reaction mixture was stirred for 2.5 h at 0 °C and afterwards quenched by the slow addition of 30 mL 1 M HCl *aq*. The aqueous Phase was extracted 3x by DCM, next the organic phase was

washed with saturated $NaHCO_3$ *aq* and brine. The organic phase was dried over Na_2SO_4 and filtered through a pad of silicate. Product was recrystallized from DCM/petroleum ether (bp. 40–60 °C; PE).

4.3. General procedure 2 - tosylation

The alcohol (1 eq.) was dissolved in DCM under Argon. The mixture was cooled to 0 °C and tosyl chloride (1.5 eq.) and pyridine (3 eq.) were added and the mixture was stirred for 10 min. Afterwards the reaction mixture was allowed to warm to room temperature and stirred for 3 h. The reaction was quenched by the addition of 30 mL 1 M HCl *aq* which was extracted 3x with DCM. The organic phase was washed with brine, dried over Na_2SO_4 and the solvent was removed *in vacuo*. The product was purified by flash-chromatography (SiO_2, reasonable mixture of EtOAc or acetone in PE according to R_f given in analytical data).

4.4. General procedure 3 - N-indole alkylation

Compound **1** (1 eq.) was dissolved in 8 mL DMF in a prior dried round bottom flask under Argon. The mixture was cooled to 0 °C with an ice bath and NaH (60% dispersion in mineral oil, 2 eq.) were added. The mixture was stirred for 10 min at 0 °C followed by 30 min at room temperature. The coupling compound (1.5 eq.) was added and the mixture was stirred at 0 °C for 10 min. Then reaction mixture was allowed to warm to room temperature and stirred overnight. The reaction was stopped by the addition of saturated NH_4Cl *aq*. The aqueous phase was extracted 3x with PE which was dried over Na_2SO_4. The crude product was purified by flash-chromatography (SiO_2, reasonable mixture of acetone in PE according to R_f given in analytical data).

4.5. General procedure 4 - THP-protection of alcohols

The alcohol (1 eq.) was dissolved in 5 mL DCM and 3,4-Dihydro-2*H*-pyran (1.2 eq.) was added, followed by the addition of $TsOH \cdot H_2O$ (0.05 eq.). The reaction mixture was stirred for 3 h and the organic phase was washed with saturated $NaHCO_3$ *aq* and brine, dried over Na_2SO_4. The crude product was dried *in vacuo* and used without further purification.

4.6. General procedure 5 - Williamson ether synthesis

The alcohol (1 eq.) was dissolved in 5 mL of anhydrous MeCN under Argon and NaH (60% dispersion in mineral oil, 2 eq.) and **3** (1.2 eq.) was added. Afterwards the reaction mixture was refluxed for 2.5 h. The reaction was quenched with water and cooled to room temperature. MeCN was removed *in vacuo* and the aqueous phase was extracted 3x with diethyl ether. The organic phase was washed with 2x water and brine, dried over Na_2SO_4. The crude product was purified by flash-chromatography (SiO_2, reasonable mixture of acetone in PE according to R_f given in analytical data).

(1*H*-Indole-3-yl)(2,2,3,3-tetramethylcyclopropyl)methanone (1). 1 was synthesized according to General procedure 1, starting with 1*H*-indole (1.50 g, 12.8 mmol). 2.69 g (11.2 mmol, 87% yield) clear crystals of **1** were obtained. The analytical-data is according to the literature [30]. R_f: 0.31 (20% acetone in hexane). ^{1}H NMR (400 MHz, $CDCl_3$) δ 9.20 (s, 1H), 8.51–8.38 (m, 1H), 7.78 (d, J = 3.0 Hz, 1H), 7.46–7.35 (m, 1H), 7.33–7.18 (m, 2H), 2.00 (s, 1H), 1.40 (s, 6H), 1.32 (s, 6H). ^{13}C NMR (101 MHz, $CDCl_3$) δ 195.78, 136.47, 130.70, 125.57, 123.51, 122.42, 121.18, 111.52, 41.91, 32.01, 24.15, 17.22. HRMS (ESI, *m/z*, $C_{16}H_{19}NO$): $[M+H]^+$ calcd. 242.1539, found 242.1541.

(2-Methyl-1*H*-indole-3-yl)(2,2,3,3-tetramethylcyclopropyl) methanone (2). 2 was synthesized according to general procedure 1, starting with 2-methylindole (1.50 g, 11.4 mmol). 2.79 g faint red crystals (10.9 mmol, 95% yield) were obtained. The analytical-data is according to the literature [31]. R_f: 0.38 (20% acetone in hexane). ^{1}H NMR (400 MHz, $CDCl_3$) δ 8.73 (s, 1H), 8.01 (d, J = 7.5 Hz, 1H), 7.34–7.15 (m, 3H), 2.67 (s, 3H), 2.25 (s, 1H), 1.42 (s, 6H), 1.39 (s, 6H). ^{13}C NMR (101 MHz, $CDCl_3$) δ 197.8, 141.3, 134.6, 127.0, 122.2, 121.5, 120.4, 117.7, 111.0, 44.5, 32.9, 24.4, 17.2, 14.9. HRMS (ESI, *m/z*, $C_{17}H_{21}NO$): $[M+H]^+$ calcd. 256.1696, found 256.1696.

2-Fluoroethyl 4-methylbenzenesulfonate (3). 3 was synthesized according to general procedure 2, starting with 2-fluorethanol (0.50 mL, 8.5 mmol). 1.68 g (7.7 mmol, 90% yield) of a colorless oil was obtained. R_f: 0.24 (20% acetone in hexane). ^{1}H NMR (400 MHz, $CDCl_3$) δ 7.87–7.76 (m, 2H), 7.40–7.31 (m, 2H), 4.66–4.47 (m, 2H), 4.33–4.19 (m, 2H), 2.45 (s, 3H). ^{13}C NMR (101 MHz, $CDCl_3$) δ 145.28, 132.77, 130.07, 128.09, 80.66 (d, J = 173.7 Hz), 68.58 (d, J = 20.9 Hz), 21.77. ^{19}F NMR (376 MHz, $CDCl_3$) δ 224.65 (tt, J = 47.1, 27.2 Hz). HRMS (ESI, *m/z*, $C_9H_{11}FO_3S$): undetected.

3-Fluoropropyl 4-methylbenzenesulfonate (4). 4 was synthesized according to general procedure 2, starting with 3-fluoropropanol (0.62 g, 8.0 mmol). **4** was obtained as 2.05 g of a yellow oil (7.6 mmol, 95% yield). R_f: 0.31 (20% acetone in hexane). ^{1}H NMR (400 MHz, CDCl3) δ 7.85–7.75 (m, 2H), 7.41–7.31 (m, 1H), 4.54 (t, J = 5.6 Hz, 1H), 4.42 (t, J = 5.6 Hz, 1H), 4.16 (t, J = 6.2 Hz, 2H), 2.45 (s, 3H), 2.04 (ddt, J = 25.8, 11.7, 6.0 Hz, 2H). ^{13}C NMR (101 MHz, $CDCl_3$) δ 145.09, 132.94, 130.05, 128.03, 79.66 (d, J = 166.0 Hz), 66.27 (d, J = 4.9 Hz), 30.15 (d, J = 20.2 Hz), 21.77. ^{19}F NMR (376 MHz, $CDCl_3$) δ −223.41 (tt, J = 46.9, 25.8 Hz). HRMS (ESI, *m/z*, $C_{10}H_{13}O_3FS$): $[M+Na]^+$ calcd. 255.0462, found 255.0466.

(1-(2-Fluoroethyl)-1*H*-indole-3-yl)(2,2,3,3-tetramethylcyclopropyl)methanone (5). Compound **5** was synthesized according to general procedure 2, starting with **1** (0.25 g, 1.0 mmol). 0.26 g of **5** (0.9 mmol, 87% yield) was received as white crystals. R_f: 0.38 (20% acetone in hexane). ^{1}H NMR (400 MHz, $CDCl_3$) δ 8.45–8.36 (m, 1H), 7.32–7.19 (m, 3H), 4.72 (dt, J = 46.9, 4.8 Hz, 2H), 4.40 (dt, J = 26.3, 4.8 Hz, 2H), 1.91 (s, 1H), 1.32 (s, 6H), 1.27 (s, 6H). ^{13}C NMR (101 MHz, $CDCl_3$) δ 194.84, 136.64, 133.97, 126.54, 123.38, 123.06, 122.48, 120.49, 109.26, 81.85 (d, J = 172.8 Hz), 47.09 (d, J = 21.4 Hz), 41.77, 31.92, 24.15, 17.12. ^{19}F NMR (377 MHz, $CDCl_3$) δ −219.70 (tt, J = 46.9, 26.3 Hz). HRMS (ESI, *m/z*, $C_{18}H_{22}NO$): $[M+H]^+$ calcd. 288.1758, found 288.1746.

(1-(2-Fluoroethyl)-2-methyl-1*H*-indole-3-yl)(2,2,3,3-tetramethylcyclopropyl)methanone (6). 6 was synthesized according to general procedure 2, starting with **2** (0.25 g, 1.0 mmol) which was reacted with **3** (0.32 g, 1.5 mmol, 1.5 eq.). **6** was obtained as 0.28 g of a faint yellow solid (1.0 mmol, >99% yield). R_f: 0.44 (20% acetone in hexane). ^{1}H NMR (400 MHz, $CDCl_3$) δ 8.05–7.90 (m, 1H), 7.36–7.20 (m, 3H), 4.73 (dt, J = 46.8, 5.1 Hz, 2H), 4.46 (dt, J = 23.9, 5.1 Hz, 2H), 2.73 (s, 3H), 2.24 (s, 1H), 1.42 (s, 6H), 1.39 (s, 6H). ^{13}C NMR (101 MHz, $CDCl_3$) δ 197.71, 141.93, 135.88, 126.69, 122.10, 121.65, 120.47, 118.33, 109.26, 81.68 (d, J = 173.4 Hz), 44.98, 43.28 (d, J = 22.3 Hz), 33.23, 24.40, 17.13, 12.24, 12.22. ^{19}F NMR (377 MHz, $CDCl_3$) δ −221.08 to −221.57 (m). HRMS (ESI, *m/z*, $C_{19}H_{24}NOF$): $[M+H]^+$ calcd. 302.1915, found 302.1912.

(1-(3-Fluoropropyl)-1*H*-indole-3-yl)(2,2,3,3-tetramethylcyclopropyl)methanone 7 (DM102). 7 was synthesized according to general procedure 2, starting with **1** (0.12 g, 0.5 mmol) which was reacted with **4**. 0.12 g of a faint orange solid (0.4 mmol, 77% yield) was received as the titled compound **7**. R_f: 0.48 (20% acetone in hexane). ^{1}H NMR (400 MHz, $CDCl_3$) δ 8.49–8.40 (m, 1H), 7.70 (s, 1H), 7.41–7.35 (m, 1H), 7.34–7.25 (m, 2H), 4.55–4.33 (m, 4H), 2.27 (dquint, J = 27.0, 6.1 Hz, 2H), 1.96 (s, 1H), 1.37 (s, 6H), 1.33 (s, 6H). ^{13}C NMR (101 MHz, $CDCl_3$) δ 194.75, 136.60, 133.76, 126.60, 123.32, 123.02, 122.40, 120.18, 109.55, 80.47

(d, J = 165.9 Hz), 42.80 (d, J = 4.2 Hz), 41.81, 31.85, 30.81 (d, J = 20.2 Hz), 24.17, 17.15. ^{19}F NMR (377 MHz, $CDCl_3$) δ −223.07 (tt, J = 47.0, 27.2 Hz). HRMS (ESI, *m/z*, $C_{19}H_{24}FNO$): $[M+H]^+$ calcd. 302.1915, found 302.1915.

(1-(3-Fluoropropyl)-2-methyl-1*H*-indole-3-yl)(2,2,3,3-tetramethylcyclopropyl)methanone (8). 8 was synthesized according to general procedure 2, starting with **2** (0.20 g, 0.8 mmol) which was reacted with **4** (0.27 g, 1.2 mmol, 1.5 eq.). **8** was obtained as 0.20 g of a faint orange solid (0.6 mmol, 81% yield). R_f: 0.37 (20% acetone in hexane). ^{1}H NMR (400 MHz, $CDCl_3$) δ 8.06−7.88 (m, 1H), 7.43−7.33 (m, 1H), 7.33−7.18 (m, 2H), 4.46 (dt, J = 47.0, 5.4 Hz, 1H), 4.32 (t, J = 6.9 Hz, 2H), 2.73 (s, 3H), 2.25 (s, 1H), 2.24−2.09 (m, 2H), 1.42 (s, 1H), 1.40 (s, 1H). ^{13}C NMR (101 MHz, $CDCl_3$) δ 197.65, 141.72, 135.85, 126.60, 121.98, 121.49, 120.34, 118.01, 109.52, 80.64 (d, J = 165.8 Hz), 44.90, 38.94 (d, J = 3.8 Hz), 33.07, 30.63 (d, J = 20.3 Hz), 24.40, 17.15, 12.10. ^{19}F NMR (376 MHz, $CDCl_3$) δ −220.89 (tt, J = 47.0, 28.2 Hz). HRMS (ESI, *m/z*, $C_{20}H_{26}NOF$): $[M+H]^+$ calcd. 316.2071, found 316.2074.

(1-(4-Fluorobutyl)-1*H*-indole-3-yl)(2,2,3,3-tetramethylcyclopropyl)methanone (9). 9 Compound **5** was synthesized according to general procedure 2, starting with **1** (0.25 g, 1.0 mmol) which was reacted with 1-bromo-4-fluorobutane (0.24 g, 1.6 mmol, 1.5 eq.). **9** was obtained as 0.33 g of white crystals (1.0 mmol, >99% yield). R_f: 0.37 (20% acetone in hexane). ^{1}H NMR (400 MHz, $CDCl_3$) δ 8.51−8.36 (m, 1H), 7.70 (s, 1H), 7.42−7.22 (m, 3H), 4.51 (dt, J = 47.2, 5.7 Hz, 2H), 4.25 (t, J = 7.1 Hz, 2H), 2.14−2.02 (m, 2H), 1.97 (s, 1H), 1.86−1.68 (m, 2H), 1.38 (s, 6H), 1.34 (s, 6H). ^{13}C NMR (101 MHz, $CDCl_3$) δ 194.75, 136.65, 133.45, 126.54, 123.15, 122.91, 122.29, 119.97, 109.65, 83.66 (d, J = 165.7 Hz), 46.64, 41.79, 31.84, 27.80 (d, J = 20.1 Hz), 26.43 (d, J = 4.0 Hz), 24.19, 17.13. ^{19}F NMR (377 MHz, $CDCl_3$) δ −218.58 (tt, J = 47.2, 26.7 Hz). HRMS (ESI, *m/z*, $C_{20}H_{26}NOF$): $[M+H]^+$ calcd. 316.2071, found 316.2072.

(1-(4-Fluorobutyl)-2-methyl-1*H*-indole-3-yl)(2,2,3,3-tetramethylcyclopropyl)methanone (10). 10 was synthesized according to general procedure 2, starting with **2** (0.25 g, 1.0 mmol) which was reacted with 1-bromo-4-fluorobutane (0.23 g, 1.5 mmol, 1.5 eq.). In addition after flash-chromatography the obtained product was further purified by RP-chromatography (90% MeCN *aq*). **9** was obtained as 0.30 g of white crystals (1.0 mmol, 97% yield). R_f: 0.42 (20% acetone in hexane). ^{1}H NMR (400 MHz, $CDCl_3$) δ 8.02−7.91 (m, 1H), 7.39−7.30 (m, 1H), 7.30−7.20 (m, 2H), 4.49 (dt, J = 47.3, 5.7 Hz, 2H), 4.20 (t, J = 7.4 Hz, 2H), 2.73 (s, 3H), 2.25 (s, 1H), 2.02−1.87 (m, 2H), 1.87−1.70 (m, 2H), 1.42 (s, 6H), 1.39 (s, 6H). ^{13}C NMR (101 MHz, $CDCl_3$) δ 197.66, 141.63, 135.82, 126.57, 121.83, 121.37, 120.32, 117.86, 109.60, 83.68 (d, J = 165.8 Hz), 44.86, 42.69, 33.01, 27.94 (d, J = 20.2 Hz), 26.17, 26.13, 24.41, 17.17, 12.32. ^{19}F NMR (377 MHz, $CDCl_3$) δ −218.71 (tt, J = 47.3, 26.2 Hz). HRMS (ESI, *m/z*, $C_{21}H_{28}FNO$): $[M+H]^+$ calcd. 330.2228, found 330.2230.

2-(2-Bromoethoxy)tetrahydro-2*H*-pyran (11). 11 was synthesized according to general procedure 4, starting with 0.50 mL 1-bromoethanol (7.0 mmol). 1.27 g crude product was obtained.

(1-(2-Hydroxyethyl)-1*H*-indole-3-yl)(2,2,3,3-tetramethylcyclopropyl)methanone (12). 12 was synthesized according to general procedure 2, starting with **1** (0.53 g, 2.2 mmol) which was reacted with **11** (0.69 g, 3.3 mmol, 1.5 eq.). Subsequently, the THP-ether was hydrolyzed with 10 mL 0.05 M $TsOH \cdot H_2O$ in MeOH within 3 h without prior purification. The reaction was quenched by the addition of saturated $NaHCO_3$ *aq*. The aqueous phase was 3x extracted by DCM and the organic phase was washed with brine and dried over Na_2SO_4. Flash-chromatography (SiO_2, 20% acetone in PE) was performed and **12** was received as 0.60 g of faint yellow crystals (2.1 mmol, 96% yield). The analytical-data is according to the literature [28]. R_f: 0.23 (20% acetone in hexane). ^{1}H NMR (400 MHz, $CDCl_3$) δ 8.48−8.35 (m, 1H), 7.74 (s, 1H), 7.45−7.23 (m, 3H), 4.31 (t, J = 5.0 Hz, 2H), 4.02 (t, J = 5.0 Hz, 2H), 2.36 (brs, 1H), 1.83 (s, 1H), 1.32 (s, 6H), 1.29 (s, 6H). ^{13}C NMR (101 MHz, $CDCl_3$) δ 195.06, 136.71, 134.67, 126.57, 123.23, 122.88, 122.39, 119.87, 109.67, 61.42, 49.34, 41.63, 31.58, 24.12, 17.20. HRMS (ESI, *m/z*, $C_{18}H_{23}NO_2$): $[M+H]^+$ calcd. 286.1802, found 286.1803.

(1-(2-Hydroxyethyl)-2-methyl-1*H*-indole-3-yl)(2,2,3,3-tetramethylcyclopropyl)methanone (13). 13 was synthesized according to general procedure 2 and compound **12**, starting with **2** (0.50 g, 2.0 mmol) which was reacted with **11** (0.61 g, 1.5 mmol, 1.5 eq.) followed by hydrolysis (0.05 M $TsOH \cdot H_2O$ in MeOH). **13** was obtained as 0.52 g of faint yellow crystals (1.7 mmol, 89% yield). R_f: 0.15 (20% acetone in hexane). ^{1}H NMR (400 MHz, $CDCl_3$) δ 7.98−7.89 (m, 1H), 7.38−7.29 (m, 1H), 7.25−7.16 (m, 2H), 4.28 (t, J = 5.6 Hz, 2H), 3.94 (t, J = 5.6 Hz, 2H), 2.69 (s, 3H), 2.18 (s, 1H), 1.84 (s, 1H), 1.38 (s, 6H), 1.36 (s, 6H). ^{13}C NMR (101 MHz, $CDCl_3$) δ 197.81, 142.30, 136.10, 126.64, 121.97, 121.54, 120.35, 118.07, 109.70, 61.45, 45.21, 44.96, 33.11, 24.40, 17.16, 12.45. HRMS (ESI, *m/z*, $C_{19}H_{25}NO_2$): $[M+H]^+$ calcd. 300.1958, found 300.1959.

(1-(2-(2-Fluoroethoxy)ethyl)-1*H*-indole-3-yl)(2,2,3,3-tetramethylcyclopropyl)methanone (14). 14 was synthesized according to general procedure 2, starting with **12** (0.10 g, 0.4 mmol). 0.08 g of **14** (0.2 mmol, 57% yield) was received as white crystals. R_f: 0.24 (20% acetone in hexane). ^{1}H NMR (400 MHz, $CDCl_3$) δ 8.41 (dt, J = 47.6, 4.0 Hz, 1H), 7.78 (s, 1H), 7.38−7.29 (m, 1H), 7.29−7.20 (m, 3H), 4.48 (dd, J = 47.6, 4.0 Hz, 2H), 4.33 (t, J = 5.3 Hz, 2H), 3.86 (t, J = 5.2 Hz, 2H), 3.62 (dd, J = 29.7, 4.0 Hz, 2H), 1.93 (s, 1H), 1.33 (s, 6H), 1.28 (s, 6H). ^{13}C NMR (101 MHz, $CDCl_3$) δ 194.95, 136.72, 134.72, 126.51, 123.10, 122.97, 122.31, 120.01, 109.44, 83.09 (d, J = 169.7 Hz), 70.65 (d, J = 19.4 Hz), 69.95, 46.80, 41.68, 31.72, 24.12, 17.16. ^{19}F NMR (376 MHz, $CDCl_3$) δ −222.79 (tt, J = 47.7, 29.7 Hz). HRMS (ESI, *m/z*, $C_{20}H_{26}FNO_2$): $[M+H]^+$ calcd. 332.2020, found 332.2023.

(1-(2-(2-Fluoroethoxy)ethyl)-2-methyl-1*H*-indole-3-yl)(2,2,3,3-tetramethylcyclopropyl)methanone (15). 15 was synthesized according to general procedure 5, starting with **13** (0.20 g, 0.7 mmol) which was reacted with **3** (0.18 g, 0.8 mmol, 1.2 eq.). **15** was obtained as 0.17 g of a faint yellow solid (0.5 mmol, 62% yield). R_f: 0.40 (20% acetone in hexane). ^{1}H NMR (400 MHz, $CDCl_3$) δ 8.01−7.87 (m, 1H), 7.38−7.28 (m, 1H), 7.25−7.14 (m, 2H), 4.47 (dt, J = 47.6, 4.1 Hz, 2H), 4.33 (t, J = 5.8 Hz, 2H), 3.81 (t, J = 5.8 Hz, 2H), 3.60 (dt, J = 29.6, 4.1 Hz, 2H), 2.72 (s, 3H), 2.21 (s, 1H), 1.39 (s, 6H), 1.36 (s, 6H). ^{13}C NMR (101 MHz, $CDCl_3$) δ 197.67, 142.41, 135.95, 126.64, 121.84, 121.44, 120.34, 117.94, 109.57, 83.17 (d, J = 169.5 Hz), 70.71 (d, J = 19.5 Hz), 69.83, 44.88, 43.14, 32.97, 24.40, 17.16, 12.38. ^{19}F NMR (377 MHz, $CDCl_3$) δ −222.97 (tt, J = 47.7, 29.6 Hz). HRMS (ESI, *m/z*, $C_{21}H_{28}FNO_2$): $[M+H]^+$ calcd. 346.2177, found 346.2180.

(1-Propyl-1*H*-indole-3-yl)(2,2,3,3-tetramethylcyclopropyl) methanone (16). 16 was synthesized according to general procedure 2, starting with **1** (0.23 g, 1.0 mmol) which was reacted with 1-bromopropane (0.13 mL, 1.4 mmol, 1.5 eq.). **16** was obtained as 0.18 g of a faint yellow solid (0.7 mmol, 70% yield). R_f: 0.60 (20% acetone in hexane). The analytical-data is according to the literature [30]. ^{1}H NMR (400 MHz, $CDCl_3$) δ 8.51−8.36 (m, 1H), 7.69 (s, 1H), 7.43−7.22 (m, 3H), 4.15 (t, J = 7.1 Hz, 2H), 2.04−1.87 (m, 3H), 1.38 (s, 6H), 1.33 (s, 6H), 1.01 (t, J = 7.4 Hz, 3H). ^{13}C NMR (101 MHz, $CDCl_3$) δ 194.74, 136.77, 133.65, 126.53, 122.98, 122.83, 122.17, 119.73, 109.77, 48.75, 41.76, 31.65, 24.18, 23.41, 17.16, 11.58. HRMS (ESI, *m/z*, $C_{19}H_{25}NO$): $[M+H]^+$ calcd. 284.2009, found 284.2009.

2-(3-Bromopropoxy)tetrahydro-2*H*-pyran (17). 17 was synthesized according to general procedure 4, starting with 1.00 mL 1-bromoethanol (11.1 mmol). 2.57 g crude product was obtained.

(1-(3-Hydroxypropyl)-1*H*-indole-3-yl)(2,2,3,3-tetramethylcyclopropyl)methanone (18). 18 was synthesized according to general procedure 1, starting with **1** (0.80 g, 3.3 mmol) which was reacted with **17** (1.16 g, 5.0 mmol, 1.5 eq.). The crude product was hydrolyzed without purification. Therefore, the crude product was dissolved in 10 mL, 0.05 M $TsOH \cdot H_2O$ in MeOH and the

reaction was stirred for 3 h at room temperature. The reaction was quenched by addition of saturated $NaHCO_3$ *aq* which was extracted 3x with DCM. The organic phase was washed with brine, dried over Na_2SO_4 and the product was isolated by flash-chromatography (SiO_2, 20% acetone in PE). 0.99 g (3.3 mmol, >99%) of **18** was received as clear crystals. The analytical-data is according to the literature [30]. R_f: 0.19 (20% acetone in hexane). ^{1}H NMR (400 MHz, $CDCl_3$) δ 8.49–8.35 (m, 1H), 7.73 (s, 1H), 7.46–7.35 (m, 1H), 7.35–7.21 (m, 2H), 4.35 (t, J = 6.8 Hz, 2H), 3.67 (t, J = 5.8 Hz, 2H), 2.19–2.07 (m, 2H), 1.98 (s, 1H), 1.83 (s, 1H), 1.37 (s, 6H), 1.33 (s, 6H). ^{13}C NMR (101 MHz, $CDCl_3$) δ 194.98, 136.75, 134.00, 126.50, 123.12, 122.80, 122.27, 119.89, 109.78, 59.17, 43.39, 41.83, 32.38, 31.88, 24.19, 17.16. HRMS (ESI, *m/z*, $C_{19}H_{25}NO_2$): $[M+H]^+$ calcd. 300.1958, found 300.1947.

3-(3-(2,2,3,3-tetramethylcyclopropane-1-carbonyl)-1H-indole-1-yl)propyl 4-methylbenzenesulfonate (19). 19 was synthesized according to general procedure 3, starting with **18** (0.60 g, 2.0 mmol). In contrast to general procedure 3; 3 eq. of tosyl chloride were used and the reaction time was prolonged to 24 h. 0.79 g of a clear oil (1.7 mmol, 86%) of **19** was received. R_f: 0.19 (20% acetone in hexane). ^{1}H NMR (400 MHz, $CDCl_3$) δ 8.51–8.34 (m, 1H), 7.82–7.68 (m, 3H), 7.39–7.20 (m, 5H), 4.30 (t, J = 6.5 Hz, 2H), 3.99 (t, J = 5.6 Hz, 2H), 2.44 (s, 3H), 2.22 (quint, J = 6.0 Hz, 2H), 1.98 (s, 1H), 1.36 (s, 6H), 1.32 (s, 6H). ^{13}C NMR (101 MHz, $CDCl_3$) δ 194.89, 145.33, 136.35, 133.93, 132.67, 130.13, 127.98, 126.62, 123.28, 123.06, 122.40, 120.17, 109.40, 66.84, 42.84, 41.73, 32.05, 29.29, 24.16, 21.79, 17.11. HRMS (ESI, *m/z*, $C_{26}H_{31}NO_4S$): $[M+H]^+$ calcd. 454.2047, found 454.2038.

Purity of all *in vitro* tested compounds was ≥95% as confirmed by HPLC measurements (see Supporting Information).

4.7. Radioligand binding studies at CBR

Radioligand binding studies were performed using membrane preparations from Chinese hamster ovary (CHO) stably expressing human CB_1R and the non-selective CBR agonist radioligand [^{3}H](−)-*cis*-3-[2-hydroxy-4-(1,1-dimethylheptyl)phenyl]-trans-4-(3-hydroxypropyl)-cyclohexanol (ARC American Radiolabeled Chemicals, St. Louis, Mo, USA). A final concentration of 0.1 nM was used for all of the experiments.

A mixture containing 465 μL of assay buffer (50 mM tris(hydroxymethyl)aminomethan (TRIS, Carl Roth GmbH & Co. KG, Karlsruhe, Gemany), 3 mM $MgCl_2$ (Carl Roth GmbH & Co. KG, Karlsruhe, Gemany), 0.1% BSA, pH 7.4), 15 μL of the test compound dissolved in DMSO, and 60 μL of [^{3}H]CP55,940 in assay buffer (final concentration: 0.1 nM), and 60 μL of membrane preparation (in 50 mM TRIS, pH 7.4) in a 96 well plate were incubated for 2 h at room temperature. DMSO without test compound was used to measure total binding while unlabeled CP55,940 was used to determine non-specific binding of the radioligand. The binding was terminated by rapid filtration through GF/C glass fiber filters (Perkin-Elmer, Waltham, MA, USA), presoaked for 0.5 h in 0.3% aq. polyethyleneimine (Fluka, Sigma Aldrich Corp., St. Louis, MO, USA) and subsequently dried for 1.5 h at 50 °C. The amount of radioactivity on the filters was measured in a liquid scintillation counter (Topcount NXT, Packard/Perkin-Elmer) after 10 h of preincubation with 50 μL of scintillation cocktail (Microscint20, Perkin-Elmer). For the calculation of K_i values, the Cheng-Prusoff equation and K_D values of 2.4 nM ([^{3}H]CP55,940 at CB_1R) and 0.7 nM ([^{3}H] CP55,940 at CB_2R) were used [49].

4.8. Functional assays at CB_1R and CB_2R

Functional assays at human CB_1R and CB_2R were performed using the TRUPATH BRET^2 assay system according to literature [38,50]. All the TRUPATH construct plasmids were a kind gift from Bryan Roth (Addgene kit #1000000163). HEK293 cells were seeded 4 h before the experiment in a 6-well-plate (700.000 cells/well). Transfection was performed using Lipofectamine 2000 (Thermo Fisher) according to the manufacturer's protocol (DNA mixtures consisted of $G\alpha_i$1-Rluc8, ß3 and γ9-GFP2 and either the human CB_1R or CB_2R in pcDNA3.1(+) in a 1:1:1:1 ratio). The cells were incubated overnight and seeded at a density of 40.000 cells/well in a 96-well-plate with full growth medium. About 24 h later (48 h after transfection), the full growth medium was replaced by 60 μL of HBSS-HEPES buffer subsequently with the addition of 10 μL of 50 μM coelenterazine 400a (Biomol) as substrate. The mixture was further incubated for 5 min at room temperature. The test compound was prediluted in DMSO and HBSS-HEPES buffer (final concentration of DMSO is 1%) and was added to the well in a volume of 30 μL. The mixture was further incubated for 5 min. The signal produced was measured using a Mitras LB940 plate reader according to previously published literature [51]. Data were obtained from minimal three independent experiments performed minimal in duplicates.

4.9. β-Arrestin recruitment assays at CB_1R, CB_2R, GPR18, and GPR55

ß-Arrestin recruitment assays were performed according to previously published procedures [37]. In brief, CHO cells stably expressing β-arrestin fused to a mutant of β-galactosidase (β-arrestin2-EA, DiscoverX, Fremont, CA, USA) and either the human CB_1R or CB_2R, GPR18 or the human GPR55 fused to a complementary part of β-galactosidase (ProLink1) were prepared according to the manufacturer's protocol. Cells were kept in full growth medium (F-12 (Nutri-Mix, Thermo Fisher Scientific, Waltham, MA, USA) supplemented with 10% fetal calf serum (PANBiotech GmbH, Germany), 100 U/mL penicillin, 100 μg/mL streptomycin (Thermo Fisher Scientific), 800 μg/mL geneticin (Thermo Fisher Scientific) and 300 μg of hygromycin (InvivoGen, San Diego, CA, USA). About 24 h prior to the experiment, the cells were seeded into 96-well plates (NUNClon™ Delta Surface, Thermo Fisher Scientific) at a density of 20.000–30.000 cells/well and kept at 37 °C. The test compound in assay buffer (PBS supplemented with 0.1% BSA) was then added to the cells in a volume of 10 μL/well (for agonistic activity) or 5 μL/well (for antagonistic activity) and incubated for further 90 min at 37 °C. Subsequently, 50 μL of detection reagent was added according to a previously described procedure, and the mixture was incubated for another 60 min. Luminescence signals were subsequently measured in a TopCount NXT, Packard, Perkin-Elmer. Three to four independent experiments were performed, each in duplicates. All pharmacological data were analysed using GraphPad Prism (GraphPad Inc., La Jolla, CA). The potent and selective GPR18 agonist PSB-KK1415 (0.1 μM, corresponding to EC_{80}) was used to stimulate GPR18, while LPI (1 μM, correspond to its EC_{80}) was used to stimulate GPR55. CP55,940 as unselective CB receptors ligand was used to stimulate the CB_1 and CB_2 receptor (0.1 μM, correspond to its maximal receptor activation).

4.10. Radiosynthesis and quality control

After manual pretests with low activities, the radio synthesis, purification and reformulation was performed fully automatic on ORA Neptis perform, a commercial synthesis cassette module. The synthesis sequence was self-assembled, just like the synthesis cassettes, which were assembled by parts of the Developer kits type 1 (see Fig. 6).

The [^{18}F]F$^-$ was trapped on a QMA-cartridge (Waters Sep-Pak Accell Plus QMA Carbonate Plus Light Cartridge, 46 mg) and eluted by 750 μL *tert*-Butylammonium bicarbonate solution. The water was evaporated and the fluoride was dried by azeotropic

distillation using acetonitrile. Next the precursor **19** (9 mg, 20 μmol in 0.5 mL of anhydrous acetonitrile) was added and the reaction was heated to 90 °C for 5 min. The reaction mixture was quenched with water and the tracer was separated by solid-phase extraction (Waters Sep-Pak Plus Light C18). The cartridge was washed with water and eluted with 1.5 mL MeCN. The eluate was diluted with 1.5 mL water, filtered and injected into the semi.-prep. HPLC (Waters SunFire C18 OBD Prep Column, 100 Å, 5 μm, 10 mm × 250 mm, 4.0 mL/min 65% MeCN *aq*, UV: 305 nm). Afterwards the purified tracer was reformulated to 10% EtOH *aq* by SPE (Waters Sep-Pak Plus Light C18).

The tracer analysis was performed on a radio HPLC by Agilent (Macherey-Nagel EC 150/3 Nucleodur 100-3 C18ec, 0.6 mL/min 70% MeCN *aq* + 0.1% TFA, UV: 305 nm) and a radiodetector (fLumo, Berthold) (Fig. 3). Molar activity was measured on HPLC, the calibration including the measured value for 1500 GBq/μmol is shown in the supporting information (Fig. S1).

4.11. Experimental logP measurement by shake-flask-method

A small amount of compound **[^{18}F]7** (0.5 MBq, 5 μL 10% EtOH *aq*) was mixed with 1.2 mL 50 mM Phosphate buffer (pH: 7.4) and 1.2 mL OcOH. The mixture was vigorously shaken for 30 min. Afterwards the phases were separated and the organic phase was diluted to 1%. 1 mL of the aqueous phase and 1 mL of the 1% organic phase were measured in a gamma counter (Automatic Gamma Counter, HIDEX). The obtained data was used to calculate the logP value of the produced tracer.

4.12. Radioactive microsomal metabolism assay

The time course of compound **[^{18}F]7** metabolism was determined in human liver microsomes (ThermoFisher). Compound **[^{18}F]7** was incubated in a total reaction volume of 500 μL. The reaction was conducted in 100 mM potassium phosphate buffer (pH 7.4) with 0,5 mg/mL human liver microsomal protein, 1 mM NADPH, 125 mM NaCl and 1 mM EDTA.

The reaction mixture was pre-incubated for 3 min at 37 °C. Afterwards the reaction was started by the addition of the radioactive tracer. At each time of measurement, an aliquot (80 μL) was removed and the reaction was stopped by adding 80 μL acetonitrile. After stopping the metabolic reactions of the aliquots, the reaction mixtures were centrifuged at 20,000×*g* for 10 min at 4 °C. 3 μL of each supernatant were applied to a silica TLC-plate and developed with 20% acetone in PE. The developed TLC-plate was exposed to a phosphor screen over night. The phosphor screen was read by Typhoon FLA 9500 (GE Healthcare).

4.13. Non-radioactive microsomal metabolism assay

Human liver microsomes (Thermo Fisher Scientific), were used at a final concentration of 0.5 mg/mL in a reaction mixture with 100 μM NADPH, 1 mM EDTA, 125 mM NaCl in 100 mM potassium phosphate buffer. The reaction was pre-incubated at 37 °C for 5 min before addition of 10 nmol/mL **7**. After 0 min, 5 min, 10 min, 20 min, and 30 min, 80 μL of the reaction were removed and quenched in 80 μL cold acetonitrile. The reaction was centrifuged at 4 °C, 3000×*g* for 30 min and the supernatant was analysed by LC-MS/MS.

The systems (LC-MS/MS) consisted of a triple quadrupole mass spectrometer QTRAP 6500 (AB Sciex, Darmstadt, Germany) coupled to a high performance liquid chromatography (Shimadzu, Duisburg, Germany). The chromatographic analytic separation was performed at room temperature on an Accucore C8 column 50 × 3 mm in size with a particle size of 2.6 μm (Thermo Fisher Scientific, Germany). Gradient elution was applied using mobile phases consisting of acetonitrile and 0.2% formic acid in water (v/v). The gradient ran for 10 min with a flow rate of 0.5 mL/min and a sample volume of 5 μL. Solvent flow starts with 40:60 acetonitrile:formic acid *aq*, constantly increased to 100% acetonitrile at 7 min. These solvent composition was hold to 8 min, followed by 2 min of 40:60 acetonitrile:formic acid *aq*. For subsequent MS analysis, ionisation

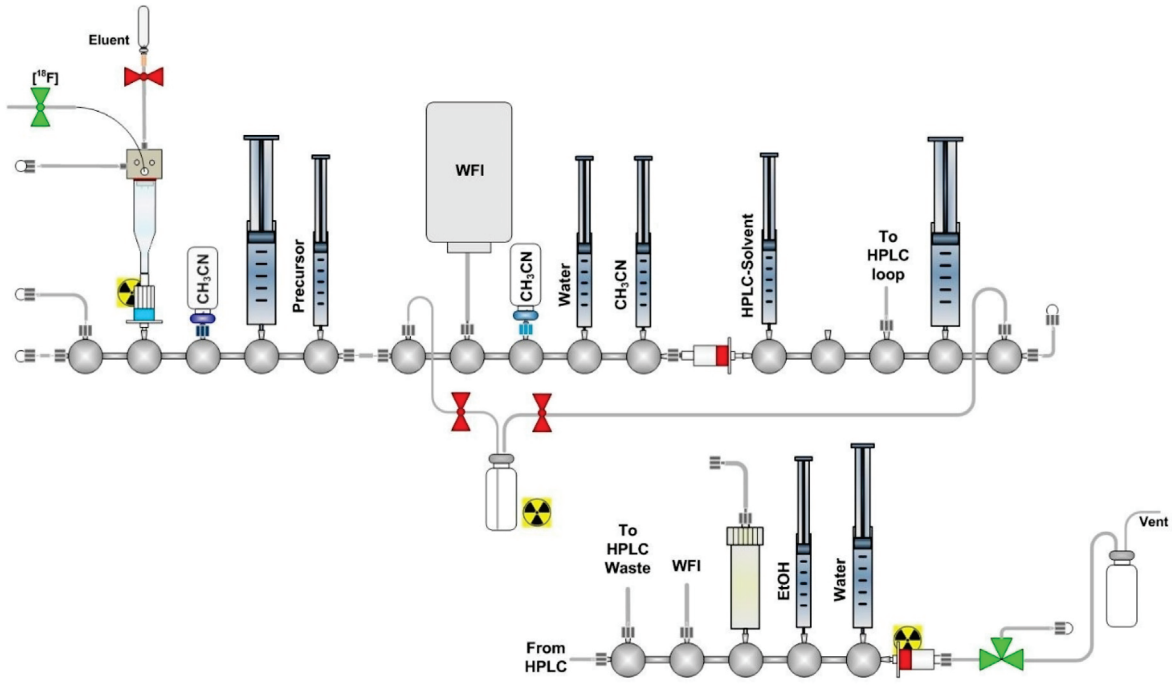

Fig. 6. Schematic illustration of the synthesis on the module ORA Neptis perform for the radiosynthesis and purification of compound **[^{18}F]7**.

was performed by electrospray, followed by selected reaction monitoring (SRM) using parameters specific to compound **7** and **18** determined prior.

Transitions of compound **7** and compound **18** precursor ions to product ions were determined to be *m/z* 302 to *m/z* 125 for compound **7** and *m/z* 300 to *m/z* 202 for compound **18**. Fragmentation was performed with a collision potential of 30 V for compound **7**, and 35 V for compound **18**. Acquisition data was visualized and analysed using the Sciex software Analyst version 1.6.2 and its companion software Multiquant. **18** was quantified as percentage of compound **7** based on the peak area (area %), calculated by Multiquant.

5. Autoradiography

Autoradiography was performed according to the tritium-autoradiography by Rühl et al. [52] Briefly, the spleen tissue was removed rapidly of a sacrificed male Wistar rat, frozen and cut on a cryostat to 12 μm thick slices. The cut slices were stored at −30 °C until use for autoradiography. For autoradiography the slides were brought to RT., dried and preincubated for 15 min with buffer A (50 mM TRIS·HCl + 5% BSA (pH 7.4) at rt.). The slides were completely dried before incubation for 2 h with compound **[^{18}F]7** in buffer A (+2% ethanol). CB_2R were blocked by GW405833, CP55,940 and compound **7** in 10,000 nM. Slides were washed twice for 30 min with buffer B (50 mM TRIS·HCl + 1% BSA (pH 7.4) at 4 °C), followed by a short dip into deionized water at 4 °C. The slides were dried and exposed to imaging plates over night. The imaging plates were measured by a phosphor screen. The phosphor screen was readout by Typhoon FLA 9500 (GE Healthcare).

Author contributions

The manuscript was written through contributions of all authors.

Funding sources

This study was supported by University Medicine, Georg-August-University Göttingen. ABM is grateful for a PhD scholarship from the Indonesian government (Ministry of Finance of Indonesia in the scheme of the Indonesia Endowment Fund for Education (Lembaga Pengelola Dana Pendidikan (LPDP)). CEM and ABM were supported by the Bonn International Graduate School Drug Sciences (BIGS-DrugS) with support by the German Federal Ministery of Research and Education (BMBF), Germany, and by the German Research Foundation (GRK1873), Germany. CB and YB were supported by the Alzheimer Stiftung Göttingen, Germany, and by the German Research Foundation (CNMPB), Germany, to YB.

Declaration of competing interest

The authors declare that they have no known competing financial interests or personal relationships that could have appeared to influence the work reported in this paper.

Acknowledgments

We would like to thank Mr H. Riedesel (experimental animal facility of the UMG) for his help in taking the rat spleens, Ms U. Ehbrecht and Ms M. Küffer (Institute of Pathology, UMG) for their support in preparing the cryosections and Mr D. Baranovski for introducing us to the use of microtomes. Ms G. Lehmann, Ms M. Franke-Klein and Mr. B. Kopka (Büsinger Institute, Laboratory for Radioisotopes, Georg-August University Göttingen) supported us in the measurement of the autoradiography with great effort. We would like to thank Mr. D. Janssen-Müller (Organic Chemistry, Georg-August University Göttingen) for the linguistic revision. We would also like to thank Mr. G. Villeret (ORA, Belgium) for his assistance and tips in programming the synthesis module. Additionally, we would like to thank Ms S. Walburg from our working group for her perfect assistance. The authors are grateful for the smart.servier.com (Servier Medical Art) for the generous icon pack to be used for graphical abstract.

Appendix A. Supplementary data

Supplementary data to this article can be found online at https://doi.org/10.1016/j.ejmech.2022.114138.

Abbreviations

AD	Alzheimer's disease
aq	aqueous
BBB	blood-brain barrier
BKG	Background
BRET	bioluminiscence resonance energy transfer
CBR	cannabinoid receptor
CB_1R	cannabinoid receptor subtype 1
CB_2R	cannabinoid subtype 2 receptor
CHO	Chinese hamster ovary,
CNS	central nervous system
Cnts	Counts
DCM	dichloromethane
DM102	Compound **7**
DMF	*N,N*-Dimethylformamide
DMSO	Dimethyl sulfoxide
eq.	equivalents
G_i	Guanine nucleotide-binding protein subunit alpha-1
LC-MS	Liquid Chromatigraphy Mass Spectrometry
MPO	multiparameter optimization
PE	Petroleum Ether
PET	positron emission tomography
RCY	radiochemical yields
SEM	standard error measurement
TFA	Trifluoroacetic acid
(Δ^9-[1]THC)	(−)-Δ^9-trans-tetrahydrocannabinol
THP	Tetrahydropyranyl
tPSA	topological polar surface area
TRIS	tris(hydroxymethyl)aminomethane.

References

[1] P.H. Reddy, Mitochondrial medicine for aging and neurodegenerative diseases, NeuroMolecular Med. 10 (2008) 291–315, https://doi.org/10.1007/s12017-008-8044-z.
[2] K.S. Sheinerman, S.R. Umansky, Early detection of neurodegenerative diseases: circulating brain-enriched microRNA, Cell Cycle (Georgetown, Tex.) 12 (2013) 1–2, https://doi.org/10.4161/cc.23067.
[3] Y.M. Arends, C. Duyckaerts, J.M. Rozemuller, P. Eikelenboom, J.J. Hauw, Microglia, amyloid and dementia in alzheimer disease. A correlative study, Neurobiol. Aging 21 (2000) 39–47, https://doi.org/10.1016/s0197-4580(00)00094-4.s.
[4] D.S. Albrecht, C. Granziera, J.M. Hooker, M.L. Loggia, In vivo imaging of human neuroinflammation, ACS Chem. Neurosci. 7 (2016) 470–483, https://doi.org/10.1021/acschemneuro.6b00056.
[5] S. Tiepolt, M. Patt, G. Aghakhanyan, P.M. Meyer, S. Hesse, H. Barthel, O. Sabri, Current radiotracers to image neurodegenerative diseases, EJNMMI Radiopharm. Chem. 4 (2019) 17, https://doi.org/10.1186/s41181-019-0070-7.
[6] E.L. Werry, F.M. Bright, O. Piguet, L.M. Ittner, G.M. Halliday, J.R. Hodges, M.C. Kiernan, C.T. Loy, J.J. Kril, M. Kassiou, Recent developments in TSPO PET imaging as A biomarker of neuroinflammation in neurodegenerative disorders, Int. J. Mol. Sci. 20 (2019) 3161, https://doi.org/10.3390/ijms20133161.
[7] B.J. Wolf, M. Brackhan, P. Bascuñana, I. Leiter, B.L.N. Langer, T.L. Ross, J.P. Bankstahl, M. Bankstahl, TSPO PET identifies different anti-inflammatory

minocycline treatment response in two rodent models of epileptogenesis, Neurotherapeutics 17 (2020) 1228–1238, https://doi.org/10.1007/s13311-020-00834-5.
[8] J.C. Ashton, M. Glass, The cannabinoid CB2 receptor as a target for inflammation-dependent neurodegeneration, Curr. Neuropharmacol. 5 (2007) 73–80, https://doi.org/10.2174/157015907780866884.
[9] N. Stella, Endocannabinoid signaling in microglial cells, Neuropharmacology 56 (Suppl 1) (2009) 244–253, https://doi.org/10.1016/j.neuropharm.2008.07.037.
[10] C. Benito, R.M. Tolón, M.R. Pazos, E. Núñez, A.I. Castillo, J. Romero, Cannabinoid CB2 receptors in human brain inflammation, Br. J. Pharmacol. 153 (2008) 277–285, https://doi.org/10.1038/sj.bjp.0707505.
[11] J. Ehrhart, D. Obregon, T. Mori, H. Hou, N. Sun, Y. Bai, T. Klein, F. Fernandez, J. Tan, R.D. Shytle, Stimulation of cannabinoid receptor 2 (CB2) suppresses microglial activation, J. Neuroinflammation 2 (2005) 29, https://doi.org/10.1186/1742-2094-2-29.
[12] A. Köfalvi, C. Lemos, A.M. Martín-Moreno, B.S. Pinheiro, L. García-García, M.A. Pozo, Á. Valério-Fernandes, R.O. Beleza, P. Agostinho, R.J. Rodrigues, S.J. Pasquaré, R.A. Cunha, M.L. de Ceballos, Stimulation of brain glucose uptake by cannabinoid CB2 receptors and its therapeutic potential in Alzheimer's disease, Neuropharmacology 110 (2016) 519–529, https://doi.org/10.1016/j.neuropharm.2016.03.015.
[13] H. Ishiguro, Y. Horiuchi, M. Ishikawa, M. Koga, K. Imai, Y. Suzuki, M. Morikawa, T. Inada, Y. Watanabe, M. Takahashi, T. Someya, H. Ujike, N. Iwata, N. Ozaki, E.S. Onaivi, H. Kunugi, T. Sasaki, M. Itokawa, M. Arai, K. Niizato, S. Iritani, I. Naka, J. Ohashi, A. Kakita, H. Takahashi, H. Nawa, T. Arinami, Brain cannabinoid CB2 receptor in schizophrenia, Biol. Psychiatr. 67 (2010) 974–982, https://doi.org/10.1016/j.biopsych.2009.09.024.
[14] N. De Marchi, L. De Petrocellis, P. Orlando, F. Daniele, F. Fezza, V. Di Marzo, Endocannabinoid signalling in the blood of patients with schizophrenia, Lipids Health Dis. 2 (2003) 5, https://doi.org/10.1186/1476-511X-2-5.
[15] P. Rentsch, S. Stayte, T. Egan, I. Clark, B. Vissel, Targeting the cannabinoid receptor CB2 in a mouse model of l-dopa induced dyskinesia, Neurobiol. Dis. 134 (2020) 104646, https://doi.org/10.1016/j.nbd.2019.104646.
[16] H. Javed, S. Azimullah, M.E. Haque, S.K. Ojha, Cannabinoid type 2 (CB2) receptors activation protects against oxidative stress and neuroinflammation associated dopaminergic neurodegeneration in rotenone model of Parkinson's disease, Front. Neurosci. 10 (2016), https://doi.org/10.3389/fnins.2016.00321.
[17] T. Cassano, S. Calcagnini, L. Pace, F.d. Marco, A. Romano, S. Gaetani, Cannabinoid receptor 2 signaling in neurodegenerative disorders: from pathogenesis to a promising therapeutic target, Front. Neurosci. 11 (2017) 30, https://doi.org/10.3389/fnins.2017.00030.
[18] W.A. Devane, F.A. Dysarz, M.R. Johnson, L.S. Melvin, A.C. Howlett, Determination and characterization of a cannabinoid receptor in rat brain, Mol. Pharmacol. 34 (1988) 605–613.
[19] S. Munro, K.L. Thomas, M. Abu-Shaar, Molecular characterization of a peripheral receptor for cannabinoids, Nature 365 (1993) 61–65, https://doi.org/10.1038/365061a0.
[20] R.G. Pertwee, A.C. Howlett, M.E. Abood, S.P. Alexander, V. Di Marzo, M.R. Elphick, P.J. Greasley, H.S. Hansen, G. Kunos, K. Mackie, R. Mechoulam, R.A. Ross, International union of basic and clinical pharmacology. LXXIX. Cannabinoid receptors and their ligands: beyond CB(1) and CB(2), Pharmacol. Rev. 62 (2010) 588–631, https://doi.org/10.1124/pr.110.003004.
[21] E. Ryberg, N. Larsson, S. Sjögren, S. Hjorth, N.-O. Hermansson, J. Leonova, T. Elebring, K. Nilsson, T. Drmota, P.J. Greasley, The orphan receptor GPR55 is a novel cannabinoid receptor, Br. J. Pharmacol. 152 (2007) 1092–1101, https://doi.org/10.1038/sj.bjp.0707460.
[22] R. Guerrero-Alba, P. Barragán-Iglesias, A. González-Hernández, E.E. Valdez-Moráles, V. Granados-Soto, M. Condés-Lara, M.G. Rodríguez, B.A. Marichal-Cancino, Some prospective alternatives for treating pain: the endocannabinoid system and its putative receptors GPR18 and GPR55, Front. Pharmacol. 9 (2019), https://doi.org/10.3389/fphar.2018.01496.
[23] A. Irving, G. Abdulrazzaq, S.L.F. Chan, J. Penman, J. Harvey, S.P.H. Alexander, Chapter seven - cannabinoid receptor-related orphan G protein-coupled receptors, in: D. Kendall, S.P.H. Alexander (Eds.), Advances in Pharmacology, Academic Press, 2017, pp. 223–247, https://doi.org/10.1016/bs.apha.2017.04.004.
[24] F. Spinelli, L. Mu, S.M. Ametamey, Radioligands for positron emission tomography imaging of cannabinoid type 2 receptor, J. Label. Compd. Radiopharm. 61 (2018) 299–308, https://doi.org/10.1002/jlcr.3579.
[25] R. Ni, L. Mu, S. Ametamey, Positron emission tomography of type 2 cannabinoid receptors for detecting inflammation in the central nervous system, Acta Pharmacol. Sin. 40 (2019) 351–357, https://doi.org/10.1038/s41401-018-0035-5.
[26] A. Martella, H. Sijben, A.C. Rufer, U. Grether, J. Fingerle, C. Ullmer, T. Hartung, A.P. Ijzerman, M. van der Stelt, L.H. Heitman, A novel selective inverse agonist of the CB2 receptor as a radiolabeled tool compound for kinetic binding studies, Mol. Pharmacol. 92 (2017) 389–400, https://doi.org/10.1124/mol.117.108605.
[27] V.W. Pike, PET radiotracers: crossing the blood-brain barrier and surviving metabolism, Trends Pharmacol. Sci. 30 (2009) 431–440, https://doi.org/10.1016/j.tips.2009.05.005.
[28] M. Willmann, J. Hegger, B. Neumaier, J. Ermert, Radiosynthesis and biological evaluation of [18F]R91150, a selective 5-HT2A receptor antagonist for PET-imaging, ACS Med. Chem. Lett. 12 (2021) 738–744, https://doi.org/10.1021/acsmedchemlett.0c00658.
[29] A.G. Horti, K. van Laere, Development of radioligands for in vivo imaging of type 1 cannabinoid receptors (CB1) in human brain, Curr. Pharmaceut. Des. 14 (2008) 3363–3383, https://doi.org/10.2174/138161208786549380.
[30] J.M. Frost, M.J. Dart, K.R. Tietje, T.R. Garrison, G.K. Grayson, A.V. Daza, O.F. El-Kouhen, B.B. Yao, G.C. Hsieh, M. Pai, C.Z. Zhu, P. Chandran, M.D. Meyer, Indol-3-ylcycloalkyl ketones: effects of N1 substituted indole side chain variations on CB2 cannabinoid receptor activity, J. Med. Chem. 53 (2010) 295–315, https://doi.org/10.1021/jm901214q.
[31] J.M. Frost, M.J. Dart, K.R. Tietje, T.R. Garrison, G.K. Grayson, A.V. Daza, O.F. El-Kouhen, L.N. Miller, L. Li, B.B. Yao, G.C. Hsieh, M. Pai, C.Z. Zhu, P. Chandran, M.D. Meyer, Indol-3-yl-tetramethylcyclopropyl ketones: effects of indole ring substitution on CB2 cannabinoid receptor activity, J. Med. Chem. 51 (2008) 1904–1912, https://doi.org/10.1021/jm7011613.
[32] T. Okauchi, M. Itonaga, T. Minami, T. Owa, K. Kitoh, H. Yoshino, A general method for acylation of indoles at the 3-position with acyl chlorides in the presence of dialkylaluminum chloride, Org. Lett. 2 (2000) 1485–1487, https://doi.org/10.1021/ol005841p.
[33] C.T. Schoeder, C. Hess, B. Madea, J. Meiler, C.E. Müller, Pharmacological evaluation of new constituents of "Spice": synthetic cannabinoids based on indole, indazole, benzimidazole and carbazole scaffolds, Forensic Toxicol. 36 (2018) 385–403, https://doi.org/10.1007/s11419-018-0415-z.
[34] J. Mella-Raipán, S. Hernández-Pino, C. Morales-Verdejo, D. Pessoa-Mahana, 3D-QSAR/CoMFA-Based structure-affinity/selectivity relationships of aminoalkylindoles in the cannabinoid CB1 and CB2 receptors, Molecules 19 (2014) 2842–2861, https://doi.org/10.3390/molecules19032842.
[35] G. Navarro, A. Gonzalez, A. Sánchez-Morales, N. Casajuana-Martin, M. Gómez-Ventura, A. Cordomí, F. Busqué, R. Alibés, L. Pardo, R. Franco, Design of negative and positive allosteric modulators of the cannabinoid CB2 receptor derived from the natural product cannabidiol, J. Med. Chem. 64 (2021) 9354–9364, https://doi.org/10.1021/acs.jmedchem.1c00561.
[36] M.M. Aung, G. Griffin, J.W. Huffman, M.-J. Wu, C. Keel, B. Yang, V.M. Showalter, M.E. Abood, B.R. Martin, Influence of the N-1 alkyl chain length of cannabimimetic indoles upon CB1 and CB2 receptor binding, Drug Alcohol Depend. 60 (2000) 133–140, https://doi.org/10.1016/S0376-8716(99)00152-0.
[37] C.T. Schoeder, A.B. Mahardhika, A. Drabczyńska, K. Kieć-Kononowicz, C.E. Müller, Discovery of tricyclic xanthines as agonists of the cannabinoid-activated orphan G-protein-coupled receptor GPR18, ACS Med. Chem. Lett. 11 (2020) 2024–2031, https://doi.org/10.1021/acsmedchemlett.0c00208.
[38] R.H.J. Olsen, J.F. DiBerto, J.G. English, A.M. Glaudin, B.E. Krumm, S.T. Slocum, T. Che, A.C. Gavin, J.D. McCorvy, B.L. Roth, R.T. Strachan, TRUPATH, an open-source biosensor platform for interrogating the GPCR transducerome, Nat. Chem. Biol. 16 (2020) 841–849, https://doi.org/10.1038/s41589-020-0535-8.
[39] S.P. Alexander, So what do we call GPR18 now? Br. J. Pharmacol. 165 (2012) 2411–2413, https://doi.org/10.1111/j.1476-5381.2011.01731.x.
[40] S.P. Alexander, A. Christopoulos, A.P. Davenport, E. Kelly, N.V. Marrion, J.A. Peters, E. Faccenda, S.D. Harding, A.J. Pawson, J.L. Sharman, C. Southan, J.A. Davies, C. Collaborators, The consice guide to pharmacology 2017/18: G protein-coupled receptors, Br. J. Pharmacol. 174 (2017) S17–S129, https://doi.org/10.1111/bph.13878.
[41] T.T. Wager, X. Hou, P.R. Verhoest, A. Villalobos, Central nervous system multiparameter optimization desirability: application in drug discovery, ACS Chem. Neurosci. 7 (2016) 767–775, https://doi.org/10.1021/acschemneuro.6b00029.
[42] H.H. Coenen, A.D. Gee, M. Adam, G. Antoni, C.S. Cutler, Y. Fujibayashi, J.M. Jeong, R.H. Mach, T.L. Mindt, V.W. Pike, A.D. Windhorst, Consensus nomenclature rules for radiopharmaceutical chemistry — setting the record straight, Nucl. Med. Biol. 55 (2017) v–xi, https://doi.org/10.1016/j.nucmedbio.2017.09.004.
[43] A. Wohlfarth, S. Pang, M. Zhu, A.S. Gandhi, K.B. Scheidweiler, H.-f. Liu, M.A. Huestis, First metabolic profile of XLR-11, a novel synthetic cannabinoid, obtained by using human hepatocytes and high-resolution mass spectrometry, Clin. Chem. 59 (2013) 1638–1648, https://doi.org/10.1373/clinchem.2013.209965.
[44] R.-P. Moldovan, R. Teodoro, Y. Gao, W. Deuther-Conrad, M. Kranz, Y. Wang, H. Kuwabara, M. Nakano, H. Valentine, S. Fischer, M.G. Pomper, D.F. Wong, R.F. Dannals, P. Brust, A.G. Horti, Development of a high-affinity PET radioligand for imaging cannabinoid subtype 2 receptor, J. Med. Chem. 59 (2016) 7840–7855, https://doi.org/10.1021/acs.jmedchem.6b00554.
[45] R. Slavik, A.M. Herde, D. Bieri, M. Weber, R. Schibli, S.D. Krämer, S.M. Ametamey, L. Mu, Synthesis, radiolabeling and evaluation of novel 4-oxo-quinoline derivatives as PET tracers for imaging cannabinoid type 2 receptor, Eur. J. Med. Chem. 92 (2015) 554–564, https://doi.org/10.1016/j.ejmech.2015.01.028.
[46] R. Slavik, U. Grether, A. Muller Herde, L. Gobbi, J. Fingerle, C. Ullmer, S.D. Kramer, R. Schibli, L. Mu, S.M. Ametamey, Discovery of a high affinity and selective pyridine analog as a potential positron emission tomography imaging agent for cannabinoid type 2 receptor, J. Med. Chem. 58 (2015) 4266–4277, https://doi.org/10.1021/acs.jmedchem.5b00283.
[47] A. Haider, A. Müller Herde, R. Slavik, M. Weber, C. Mugnaini, A. Ligresti, R. Schibli, L. Mu, S. Mensah Ametamey, Synthesis and biological evaluation of thiophene-based cannabinoid receptor type 2 radiotracers for PET imaging, Front. Neurosci. 10 (2016) 350, https://doi.org/10.3389/fnins.2016.00350.
[48] L. Mu, R. Slavik, A. Müller, K. Popaj, S. Cermak, M. Weber, R. Schibli, S.D. Krämer, S.M. Ametamey, Synthesis and preliminary evaluation of a 2-

oxoquinoline carboxylic acid derivative for PET imaging the cannabinoid type 2 receptor, Pharmaceuticals 7 (2014) 339–352, https://doi.org/10.3390/ph7030339.

[49] A. Behrenswerth, N. Volz, J. Toräng, S. Hinz, S. Bräse, C.E. Müller, Synthesis and pharmacological evaluation of coumarin derivatives as cannabinoid receptor antagonists and inverse agonists, Bioorg. Med. Chem. 17 (2009) 2842–2851, https://doi.org/10.1016/j.bmc.2009.02.027.

[50] T. Pillaiyar, M. Sedaghati, A.B. Mahardhika, L.L. Wendt, C.E. Müller, Iodine-catalyzed electrophilic substitution of indoles: synthesis of (un)symmetrical diindolylmethanes with a quaternary carbon center, Beilstein J. Org. Chem. 17 (2021) 1464–1475, https://doi.org/10.3762/bjoc.17.102.

[51] S. Hinz, G. Navarro, D. Borroto-Escuela, B.F. Seibt, Y.-C. Ammon, E. De Filippo, A. Danish, S.K. Lacher, B. Červinková, M. Rafehi, K. Fuxe, A.C. Schiedel, R. Franco, C.E. Müller, Adenosine A2A receptor ligand recognition and signaling is blocked by A2B receptors, Oncotarget 9 (2018) 13593–13611, https://doi.org/10.18632/oncotarget.24423.

[52] T. Rühl, W. Deuther-Conrad, S. Fischer, R. Günther, L. Hennig, H. Krautscheid, P. Brust, Cannabinoid receptor type 2 (CB2)-selective N-aryl-oxadiazolyl-propionamides: synthesis, radiolabelling, molecular modelling and biological evaluation, Org. Med. Chem. Lett. 2 (2012) 32, https://doi.org/10.1186/2191-2858-2-32.

3.4. Publication IV: Design, synthesis, and structure-activity relationships of diindolylmethane derivatives as cannabinoid CB_2 receptor agonists

Andhika B. Mahardhika, Anastasiia Ressemann, Sarah E. Kremers, Mariana S. Gregório Castanheira, Clara T. Schoeder, Christa E. Müller, Thanigaimalai Pillaiyar

Published in: *Archiv der Pharmazie* ***2023,*** *356: e2200493.*
DOI: 10.1002/ardp.202200493

Supplementary information for this work can be found in the **Appendix IV**.

Publication summary and contributions

Cannabinoid (CB) receptors are G protein-coupled receptors (GPCRs) that are part of the endocannabinoid system,[84] which plays a role in regulating various physiological processes such as pain, mood, appetite, and immune function.[132] CB receptors were originally discovered as membrane proteins that mediate the effects of the constitutents present in *Cannabis sativa* extracts, of which Δ^9-tetrahydrocannabinol (Δ^9-THC, classical cannabinoid) is the major bioactive compound.[67, 69, 74] THC acts as an agonist at CB_1 and CB_2 receptors, and was later found to be a partial agonist at both CB receptor subtypes, with respect to, (–)-CP 55,940, identified as a potent, highly efficacious, and non-selective CB receptor agonist.[68, 143, 144]

Two subtypes of CB receptors, CB_1 and CB_2 receptors exist. CB_1 receptors are primarily localized in the central nervous system, where they modulate various physiological functions, including pain perception, memory, and appetite.[134] In contrast, CB_2 receptors are mainly expressed by immune cells and peripheral tissues, where they play a critical role in regulating inflammation and immune responses.[71, 85, 145] Both, CB_1 and CB_2 receptors, belong to the class A (rhodopsin-like) GPCRs.[77] CB_1 receptors primarily couple with $G\alpha_{i/o}$ proteins, but are able to couple with $G\alpha_s$ and $G\alpha_q$ proteins under certain conditions as well, for example upon high receptor expression.[146] CB_2 receptors only (or mainly) couple to $G\alpha_{i/o}$ proteins.[77] Activation of CB receptors by agonists leads to a cascade of intracellular events. The initial step in this pathway involves the dissociation of $G\alpha_{i/o}$ proteins from the heterotrimeric $G\alpha\beta\gamma$

complex. $G\alpha_{i/o}$ proteins are inhibitory proteins that play a crucial role in reducing the activity of adenylate cyclase, an enzyme family that is responsible for catalyzing the production of cyclic AMP (cAMP) from ATP. When $G\alpha_{i/o}$ proteins dissociate from the $G\alpha\beta\gamma$ complex, adenylate cyclase activity is inhibited, leading to a decrease in the production of cAMP.[147]

Over the years, there have been extensive studies on the structure-activity relationships (SARs) of ligands that target cannabinoid receptors, focusing on the development of ligands that possess similar or distinct structures as compared to classical cannabinoids or nonclassical cannabinoids. The goal of this study has been to improve the selectivity of these ligands towards one of the cannabinoid receptor subtypes or to achieve dual targeting of both receptors.[148, 149] Nabiximol, nabilone, and dronabinol are example of nonselective CB_1/CB_2 receptor agonists that have been approved for clinical use.[150-152] Rimonabant, a selective CB_1 receptor antagonist/inverse agonist, was previously approved and marketed as anti-obesity drug, but was withdrawn due to severe central nervous system side effects, in particular, an increase in the rate of suicides.[153] Nevertheless, CB receptors are still attractive drug targets because of their critical roles in regulating important pathophysiological conditions.[148, 154, 155]

Plant-derived compounds including those from *Cannabis sativa*, have provided a rich source of CB_1 and CB_2 receptor ligands. 3,3'-Diindolylmethane (DIM) which is a naturally occurring compound that is found in cruciferous vegetables such as broccoli, cauliflower, and cabbage, has been found to interact with CB receptors.[115] DIM showed partial agonistic activity at the CB_2 receptor, while it interacted with the CB_1 receptor as an antagonist/inverse agonist.[115] Due to its intriguing characteristics at CB receptors, the structure-activity relationships of DIM and its analogs at CB receptors were studied in the present project, using 3,3'-diindolylmethane (DIM) as a lead structure.

In this manuscript, a total of 99 DIM derivatives and analogs were assessed for their ability to bind to membrane preparations of CHO cells recombinantly expressing human CB_1 or CB_2 receptors, using radioligand competition binding experiments. The nonspecific agonist radioligand [^{3}H]CP55,940 was used for the assays. Structure-

activity relationships were established for the test compounds, and functional assays (cAMP accumulation assays (G protein dependent pathway) and β-arrestin-2 recruitment (G protein-independent effect)) were subsequently performed for compounds with high affinity to assess their agonistic or antagonistic activity.

The investigated DIM derivatives are divided into three classes (Figure 3.5): a) substitution of the indole rings in various positions including symmetrical and unsymmetrical substitution patterns, b) replacement of the 3,3'-methylene linker (CH_2) by a carbonyl group, and oxidation and or reduction of the diindolylmethane ring system, c) monosubstitution or disubstitution of the 3,3'-methylene linker by alkyl and aryl residues. Analysis of the SARs revealed that many of the symmetrically substituted DIM derivatives display higher affinity for the CB_2 receptor than unsymmetrically substituted analogs: the presence of halogen or small substituents at position 4 of both indole rings improved binding affinity, while 5,5'-substituents on the indole rings resulted in a lower binding affinity. Similar to 5,5'-substituents, the substitution at either the 6,6'-positions or the 7,7'-positions of DIM did not improve affinity. In most cases, one unsubstituted indole (free NH) at the DIM core moiety is necessary for CB_2 receptor binding. Substitutions on the methylene bridge of 3,3'-diindolylmethane (DIM) derivatives were generally not well tolerated, resulting in only moderate potency when compared to unsubstituted analogs. Similar results were observed with the oxidation or reduction of the diindolylmethane ring system, and most of these derivatives were not tolerated by CB_2 receptors. The SARs of DIM and its analogs at the CB_1 receptor showed a different profile from the SARs at the CB_2 receptor. At the CB_1 receptor, large and lipophilic substituents are preferable, irrespective of the position.

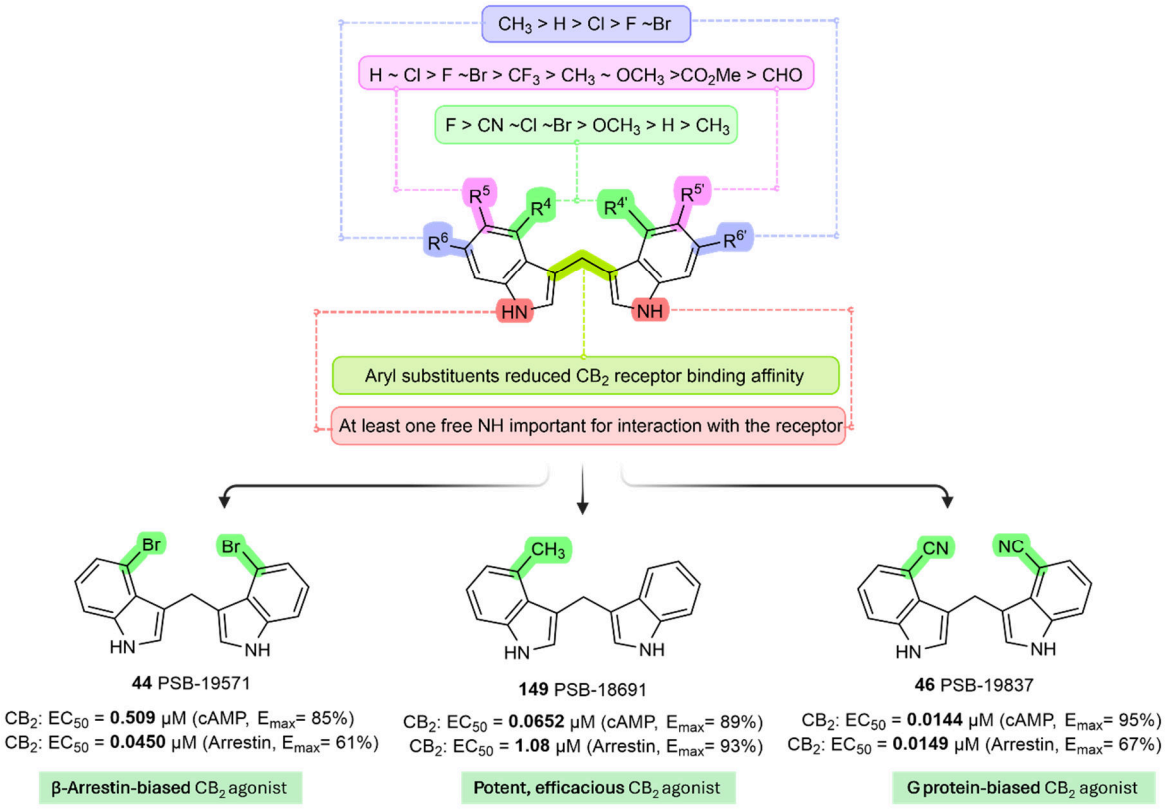

Figure 3.5 Structure-activity relationships of diindolylmethane derivatives as cannabinoid CB_2 receptor agonists (top) and the structures of CB_2 agonists in the present paper (bottom). The structure-activity relationships figure is reprinted (adapted) with permission from Mahardhika et. al.[156]

Several compounds showed higher binding affinity at the CB_2 receptor, as compared to the lead structure DIM. These compounds showed high CB_2 receptor affinity and were selective versus the CB_1 receptor. Interestingly, some of the DIM derivatives showed an incomplete displacement of [^{3}H]CP55,940 used as a radioligand at the CB_2 receptor. This might indicate that DIM derivatives bind to the CB receptors through a different binding site, possibly an allosteric site, rather than binding to the same orthosteric binding site as the radioligand. Another possible explanation is that these derivatives do bind to the orthosteric site, but to a different conformation than the one recognized by classical cannabinoids.

In order to investigate whether DIM and its derivatives and analogs are agonists or antagonists at CB receptors, we performed functional studies of selected compounds using G protein-dependent assays (measuring cAMP concentration), and determining β-arrestin recruitment. In agreement with earlier reports, the behavior of DIM was found to be similar to that of THC, acting as a partial agonist in both cAMP and β-arrestin assays.[115] A low correlation between affinity (in binding assays) and

potency (in functional assays) was observed indicating that DIM derivatives likely act as allosteric CB_2 receptor ligands. Several compounds showed biased signaling either for the G protein-dependent cAMP production pathway, or for β-arrestin recruitment. The most potent CB_2 receptor agonist was found to be di-(4-cyano-1*H*-indol-3-yl)methane (**46**, PSB-19837), displaying an unbiased signaling profile (EC_{50} [cAMP]: 0.0144 μM, EC_{50} [β-arrestin]: 0.0149 μM). In contrast, di-(4-bromo-1*H*-indol-3-yl)methane (**44**, PSB-19571) showed bias towards β-arrestin signaling (EC_{50} [cAMP]: 0.509 μM, EC_{50} [β-arrestin]: 0.0450 μM), while 3-((1*H*-indol-3-yl)methyl)-4-methyl-1*H*-indole (**149**, PSB-18691) exhibited a G protein signaling bias (EC_{50} [cAMP]: 0.0652 μM, EC_{50} [β-arrestin]: 1.08 μM). These compounds with varying pharmacological profiles are valuable tools for investigating CB_2 receptors. Additionally, a few derivatives of DIM showed moderate affinity and potency at the CB_1 receptor, inhibiting CB_1-mediated β-arrestin recruitment. The study's findings suggest an allosteric binding site for DIM derivatives at CB receptors, and the determined radioligand binding data may underestimate the compounds' potency. These DIM derivatives can be valuable tool compounds for investigating the signaling pathways of CB_2 receptors and the effects of biased signaling.

In this manuscript, I performed radioligand binding experiments and functional assays at the CB_1 and CB_2 receptors. I also developed and established the β-arrestin-2 assays for CB receptors and investigated the selected compounds in this assay. Additionally, I prepared all figures and the Supporting Information of the manuscript and wrote the manuscript in cooperation with all authors. The first draft was provided by myself and Dr. Thanigaimalai Pillaiyar. Prof. Dr. Christa E. Müller created the final version in cooperation with all authors.

Received: 19 September 2022 | Revised: 31 October 2022 | Accepted: 3 November 2022

DOI: 10.1002/ardp.202200493

FULL PAPER

ARCH PHARM DPhG
Archiv der Pharmazie

Design, synthesis, and structure–activity relationships of diindolylmethane derivatives as cannabinoid CB_2 receptor agonists

Andhika B. Mahardhika[1,2] | Anastasiia Ressemann[1] | Sarah E. Kremers[1] | Mariana S. Gregório Castanheira[1] | Clara T. Schoeder[1,2] | Christa E. Müller[1,2] | Thanigaimalai Pillaiyar[1,3]

[1]Department of Pharmaceutical & Medicinal Chemistry, PharmaCenter Bonn, Pharmaceutical Institute, University of Bonn, Bonn, Germany

[2]Research Training Group 1873, University of Bonn, Bonn, Germany

[3]Pharmaceutical/Medicinal Chemistry and Tübingen Center for Academic Drug Discovery, Institute of Pharmacy, Eberhard Karls University, Tübingen, Germany

Correspondence

Christa E. Müller, PharmaCenter Bonn, Pharmaceutical Institute, Pharmaceutical & Medicinal Chemistry, An der Immenburg 4, Bonn D-53121, Germany.
Email: christa.mueller@uni-bonn.de

Thanigaimalai Pillaiyar, Pharmaceutical/Medicinal Chemistry and Tübingen Center for Academic Drug Discovery, Institute of Pharmacy, Eberhard Karls University, Tübingen D-72076, Germany.
Email: thanigaimalai.pillaiyar@uni-tuebingen.de

Funding information

Deutsche Forschungsgemeinschaft (DFG): Research Training Group GRK1873, Germany; German Federal Ministry of Education and Research (BMBF); BIGS DrugS, Germany; Lembaga Pengelola Dana Pendidikan (LPDP), Indonesia

Abstract

3,3′-Diindolylmethane (DIM), a natural product-derived compound formed upon ingestion of cruciferous vegetables, was recently described to act as a partial agonist of the anti-inflammatory cannabinoid (CB) receptor subtype CB_2. In the present study, we synthesized and evaluated a series of DIM derivatives and determined their affinities for human CB receptor subtypes in radioligand binding studies. Potent compounds were additionally evaluated in functional cAMP accumulation and β-arrestin recruitment assays. Small substituents in the 4-position of both indole rings of DIM were beneficial for high CB_2 receptor affinity and efficacy. Di-(4-cyano-1*H*-indol-3-yl)methane (**46**, PSB-19837, EC_{50}: cAMP, 0.0144 μM, 95% efficacy compared to the full standard agonist CP55,940; β-arrestin, 0.0149 μM, 67% efficacy) was the most potent CB_2 receptor agonist of the present series. Di-(4-bromo-1*H*-indol-3-yl)methane (**44**, PSB-19571) showed higher potency in β-arrestin (EC_{50} 0.0450 μM, 61% efficacy) than in cAMP accumulation assays (EC_{50} 0.509 μM, 85% efficacy) while 3-((1*H*-indol-3-yl)methyl)−4-methyl-1*H*-indole (**149**, PSB-18691) displayed a 19-fold bias for the G protein pathway (EC_{50}: cAMP, 0.0652 μM; β-arrestin, 1.08 μM). DIM and its analogs act as allosteric CB_2 receptor agonists. These potent CB_2 receptor agonists have potential as novel drugs for the treatment of inflammatory diseases.

KEYWORDS

agonist, allosteric, cannabinoid receptors, DIM, structure–activity relationship

1 | INTRODUCTION

Cannabinoid (CB) receptors belong to the superfamily of G protein-coupled receptors (GPCRs)[1]; the CB_1 receptor is the most highly expressed GPCR in the brain.[2] In addition, it is also expressed in peripheral organs such as the lungs, liver, and kidneys.[3] The CB_1 receptor modulates neurotransmitter release and has been proposed as a potential drug target for the treatment of pain, neurodegenerative,[4,5] and metabolic diseases.[6,7] CB_2 receptors are predominantly expressed on immune cells, including macrophages and leukocytes,[8–10] and in organs associated with the immune system, for example, tonsils, spleen, and thymus.[10,11] Therefore, CB_2 receptors are potential therapeutic targets for the treatment of inflammatory diseases.[12] Both CB receptor subtypes couple to $G_{i/o}$ proteins,[13] and the activation of these receptors results in the inhibition of adenylate cyclase, which leads to reduced intracellular cAMP levels.

CBs that target CB receptors are subdivided into three classes: endocannabinoids, which are naturally produced in the body, phytocannabinoids, derived from plants, and synthetic CBs obtained by chemical synthesis.[12,14,15] The main psychoactive component of the herbal drug marijuana, *Cannabis sativa*, is Δ^9-tetrahydrocannabinol (Δ^9-THC, **1**, Figure 1), a balanced partial agonist of CB_1 and CB_2 receptors.[16,17] It is used for the therapy of muscle spasms, nausea, and cachexia, and has the potential for a number of further indications.[18,19] In recent years, a wide range of synthetic CB_1 or CB_2 receptor agonists has been developed (see examples **2** and **3** in Figure 1), and several approved nonselective CB_1/CB_2 receptor agonists such as nabiximol, nabilone, and dronabinol are in clinical use. Herbal products containing added synthetic CBs, known as "spice," have been found on the illicit drug market.[20,21] Due to their illegal use, many synthetic CBs are included in the list of controlled substances.

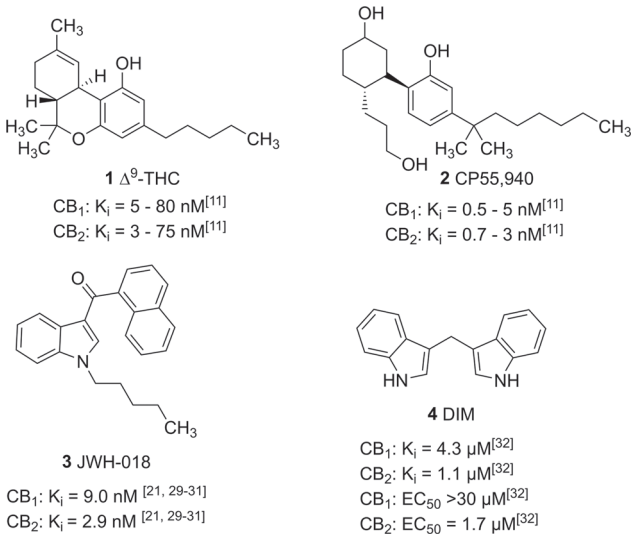

FIGURE 1 Structures and potencies of selected cannabinoid receptors agonists

It is well known that the psychoactive effects of CBs are mediated by activation of the CB_1 receptor expressed in the brain. Selective CB_2 receptor ligands are expected to be safer since they are not prone to drug abuse. CB_2 receptor agonists have been proposed for the treatment of neurodegenerative and neuroinflammatory diseases, including Alzheimer's, Huntington's, and Parkinson's disease, multiple sclerosis, and amyotrophic lateral sclerosis.[22–25] Moreover, CB_2 receptor agonists may be effective in the treatment of irritable bowel syndrome, myocardial infarction, bone disorders, and different types of cancer.[18,26,27] However, none of the CB_2 receptor ligands studied in clinical trials has thus far received approval as a drug, primarily because of side effects.[28,29]

Indole represents an important privileged core structure found in many biologically active natural products and synthetic drugs.[11,20] Indole constitutes an important scaffold among synthetic CBs (see, e.g., **3**, JWH-018).[21,30–32] 3,3′-Diindolylmethane (DIM, **4**), a metabolite of indole-3-carbinol, has been reported to exhibit various biological activities, including anticancer effects.[24,25] In addition to its CB receptor interaction, DIM has been linked to further biochemical targets: It has been shown to activate the arylhydrocarbon receptor (at 30 μM),[26,27,30] and the immunostimulatory orphan GPCR GPR84 (at submicromolar concentrations).[33] Furthermore, it was found to block the androgen receptor (at a concentration of ca. 50 μM), and the enzyme histone deacetylase-1 (HDAC-1) at a concentration of 100 μM, which is close to its solubility limit. In a previous study, Yin et al. identified DIM as a CB_2 receptor agonist upon screening of a compound library.[34] CB_2 receptor interaction and activation by DIM were confirmed in receptor radioligand binding and functional assays including β-arrestin recruitment, [^{35}S]GTPγS binding, and cAMP assays.[34] DIM was reported to display potency in all four assays, with K_i/IC_{50} values ranging from 0.42 to 1.7 μM. It was found to act as a partial CB_2 receptor agonist when compared to the full agonist CP55,940 (**2**, Figure 1). DIM was also able to bind to the human CB_1 receptor (K_i > 4.3 μM) but acted as an antagonist/inverse agonist at that receptor subtype (IC_{50} 11.1 μM).[34] Recently, we developed a synthetic method for the preparation of unsymmetrical 3,3′-DIM derivatives and analogs. Preliminary biological studies of some new DIM derivatives indicated structure-dependent interactions with CB receptors.[35] In the present study, we selected DIM (**4**) as a lead structure to perform an in-depth study of structure–activity relationships (SARs) at the human CB receptors, mainly with the aim of improving the compound's potency, efficacy, and selectivity for the CB_2 receptor subtype. Due to the CB_2 receptor selectivity of DIM and its expected allosteric nature, which might result in functional selectivity, this new class of CB receptor agonists appeared to be attractive.

2 | RESULTS AND DISCUSSION

2.1 | Chemistry

The synthesis of symmetrical DIM derivatives **40–73** (Table 1, Scheme 1) without a substituent on the methylene bridge was

TABLE 1 The binding affinity of 3,3′-diindolylmethane derivatives **4**, and **40–73** at human CB_1 and CB_2 receptors

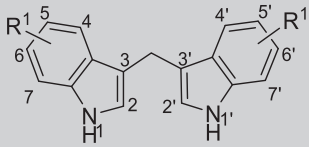

4, **40-70**

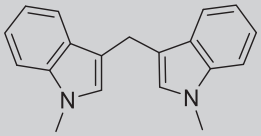

71

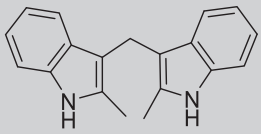

72

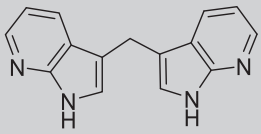

73

Compound[a]	R^1	Human CB_2 receptor Radioligand binding assay K_i ± SEM (μM) (or percent inhibition of [^{3}H]CP55,940 at 5 μM) *[Maximal inhibition (%)]*	Human CB_1 receptor K_i ± SEM (μM) (or percent inhibition of [^{3}H]CP55,940 at 5 μM) *[Maximal inhibition (%)]*
4 (DIM)	H	**0.690** ± 0.159 *[98%]* (**1.1**)[a]	**5.42** ± 1.00 *[86%]* (**4.3**)[a]
40	4-CH_3	**0.845** ± 0.086 *[81%]*	**>5** (4%)
41	4-OCH_3	**0.579** ± 0.157 *[94%]*	**5.03** ± 2.29 *[79%]*
42 (PSB-16357)	4-F	**0.279** ± 0.056 *[99%]*	**>5** (28%)
43	4-Cl	**0.332** ± 0.230 *[93%]*	**0.753** ± 0.048 *[61%]*
44 (PSB-19571)	4-Br	**0.374** ± 0.074 *[100%]*	**7.27** ± 0.45 *[99%]*
45	4-NO_2	**>5** (29%)	**>5** (6%)
46 (PSB-19837)	4-CN	**0.339** ± 0.061 *[99%]*	**≥10** (47%)
47	5-CH_3	**2.78** ± 1.36 *[86%]*	**>5** (26%)
48 (PSB-16105)	5-OCH_3	**2.84** ± 1.51 *[83%]*	**5.89** ± 1.28 *[62%]*
49 (PSB-15160)	5-F	**1.17** ± 0.33 *[100%]*	**4.08** ± 0.22 *[96%]*
50	5-CF_3	**1.98** ± 0.14 *[100%]*	**9.94** ± 3.86 *[100%]*
51	5-Cl	**0.747** ± 0.067 *[73%]*	**>5** (6%)
52	5-Br	**1.27** ± 0.23 *[100%]*	**>5** (34%)
53	5-CN	**>5** (30%)	**>5** (35%)
54	5-NO_2	**≥5** (45%)	**>5** (30%)
55	5-CO_2Me	**2.99** ± 0.03 *[71%]*	**>5** (19%)

(Continues)

TABLE 1 (Continued)

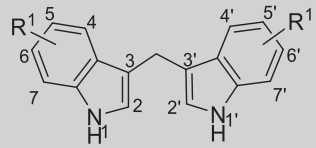

4, 40-70

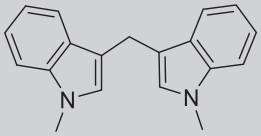

71

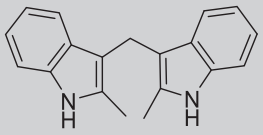

72

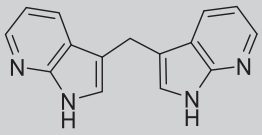

73

Compound[a]	R^1	Human CB_2 receptor Radioligand binding assay K_i ± SEM (μM) (or percent inhibition of [^{3}H]CP55,940 at 5 μM) *[Maximal inhibition (%)]*	Human CB_1 receptor K_i ± SEM (μM) (or percent inhibition of [^{3}H]CP55,940 at 5 μM) *[Maximal inhibition (%)]*
56	5-CHO	**7.25** ± 1.39 *[71%]*	**>5** (23%)
57	5-CO_2H	**>5** (34%)	**>5** (−17%)
58	5-OBn	**>5** (37%)	**2.95** ± 0.74 *[88%]*
59	6-CH_3	**0.504** ± 0.252 *[76%]*	**>5** (30%)
60	6-OCH_3	**>5** (32%)	**>5** (26%)
61 (PSB-16358)	6-F	**0.985** ± 0.094 *[90%]*	**>5** (27%)
62	6-Cl	**0.911** ± 0.105 *[84%]*	**0.820** ± 0.385 *[59%]*
63	6-Br	**3.44** ± 0.56 *[100%]*	**5.28** ± 2.02 *[100%]*
64 (PSB-16381)	7-F	**≥5** (49%)	**>5** (18%)
65	7-OCH_3	**≥5** (48%)	**>5** (30%)
66	4-Cl,6-Cl	**0.626** ± 0.219 *[90%]*	**1.68** ± 0.32 *[68%]*
67	5-F,6-Cl	**>5** (36%)	**>5** (25%)
68	4-F,5-F	**3.04** ± 0.78 *[90%]*	**5.34** ± 1.81 *[70%]*
69 (PSB-16586)	5-F,6-F	**≈5** (59%)	**>5** (39%)
70 (PSB-16671)	5-F,7-F	**1.10** ± 0.19 *[100%]*	**2.64** ± 0.28 *[100%]*
71	See structure above	**3.39** ± 1.14 *[68%]*	**>5** (35%)
72	See structure above	**≥5** (48%)	**>5** (45%)
73	See structure above	**>5** (3%)	**>5** (20%)

[a]Data were obtained from Yin et al.[34]

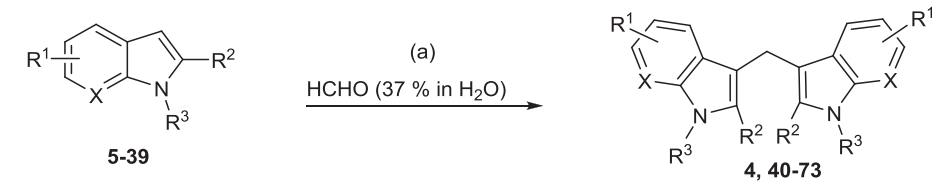

5-39

4, 40-73

5-37: $R^2 = R^3 = H$, X = CH

5, 4: R^1 = H, **6, 40**: R^1 = 4-CH_3
7, 41: R^1 = 4-OCH_3, **8, 42**: R^1 = 4-F
9, 43: R^1 = 4-Cl, **10, 44**: R^1 = 4-Br
11, 45: R^1 = 4-NO_2, **12, 46**: R^1 = 4-CN
13, 47: R^1 = 5-CH_3, **14, 48**: R^1 = 5-OCH_3
15, 49: R^1 = 5-F, **16, 50**: R^1 = 5-CF_3
17, 51: R^1 = 5-Cl, **18, 52**: R^1 = 5-Br
19, 53: R^1 = 5-CN, **20, 54**: R^1 = 5-NO_2
21, 55: R^1 = 5-CO_2Me, **22, 56**: R^1 = 5-CHO
23, 57: R^1 = 5-CO_2H, **24, 58**: R^1 = 5-OBn

4, 40-70: $R^2 = R^3 = H$, X = CH

25, 59: R^1 = 6-CH_3, **26, 60**: R^1 = 6-OCH_3
27, 61: R^1 = 6-F, **28, 62**: R^1 = 6-Cl
29, 63: R^1 = 6-Br, **30, 64**: R^1 = 7-F
31, 65: R^1 = 7-OCH_3, **32, 66**: R^1 = 4-Cl,6-Cl
33, 67: R^1 = 5-F,6-Cl, **34, 68**: R^1 = 4-F,5-F
35, 69: R^1 = 5-F,6-F, **36, 70**: R^1 = 5-F,7-F
37, 71: $R^1 = R^2 = H$, $R^3 = CH_3$, X= CH
38, 72: $R^1 = R^3 = H$, $R^2 = CH_3$, X= CH
39, 73: $R^1 = R^2 = R^3 = H$, X= N

SCHEME 1 Synthesis of diindolylmethane derivatives and analogs **40–73**. Reagents and conditions: (a) H_2O, 100°C, microwave, 20–180 min, yield 45%–98%. For R^1, R^2, and R^3, see Table 1 and experimental methods for details.

performed by reaction of indoles **5–39** with formaldehyde (37% in water) upon microwave irradiation, according to a previously developed optimized method.[33] Symmetrical DIMs (**100–136**, Table 2, Scheme 2) containing substituents on the bridging methylene group were synthesized by reaction of indoles **5**, **7**-**8**, **13–15**, **27**, **30**, and **32** with various aldehydes or ketones (**74–99**) in water in the presence of concentrated sulfuric acid.[35] Unsymmetrical DIMs **149–170** (Table 3, Scheme 3) were synthesized based on two different procedures: (i) reaction of (3-indolylmethyl) trimethylammonium iodides **137–140** with a range of substituted indole derivatives (**6**, **8**, **10**, **13–15**, **17**, **21**, **23**, **20**, **30**, **37**, **38**, **141**, **142**, or **143**) in water[36] or (ii) decarboxylative coupling of indoles **144–148** with various indolylacetic acid derivatives.[37] The synthesis of 2-oxoindole derivatives was performed according to reported procedures (Table 4, Scheme 4).[33]

2-Oxoindole derivatives **171** and **172** were reacted with the appropriate aldehyde (**173–174**) in ethanol in the presence of piperidine at 65°C to produce α,β-unsaturated indol-2-one derivatives **175–177**. These products were reduced by $NaBH_4$ to yield the corresponding saturated indole-2-one derivatives **178–180** (Table 4, Scheme 4).

The structures of the newly synthesized compounds were confirmed by ^{1}H- and ^{13}C-NMR spectra. In addition, HPLC analysis coupled to UV and electrospray ionization mass spectrometry (LC/UV-ESI-MS) was performed, which was also used to determine the purity of the compounds. For all compounds, the purity was above 95%.

2.2 | Pharmacology

All compounds were initially evaluated at a concentration of 5 μM for their binding affinity to membrane preparations of Chinese hamster ovary (CHO) cells recombinantly expressing either human CB_1 or CB_2 receptors. The nonspecific agonist radioligand [^{3}H]CP55,940 was used at a concentration of 0.1 nM for competition binding studies at both receptor subtypes.[21,30,38] For compounds that showed displacement of radioligand binding of more than 50%, full concentration-inhibition curves were determined, and K_i values were calculated. Functional assays for the compounds that showed low micromolar K_i values were performed to evaluate their agonistic (or antagonistic) activity. The compounds were evaluated in cAMP accumulation assays according to a described procedure.[21,30,39] In addition, agonist-induced β-arrestin recruitment was measured as a G protein-independent pathway using a β-galactosidase complementation assay.[38]

2.2.1 | Radioligand binding studies and SARs

A total of 99 DIM derivatives and analogs were evaluated for their binding affinities at the human CB_2 receptor. The K_i value of the lead structure DIM (**4**) in our assay system was 0.690 μM, which is comparable to the reported value of 1.1 μM (see Table 1). SAR analysis revealed that many of the symmetrically substituted indole derivatives displayed higher affinity at the CB_2 receptor when compared to the unsymmetrically substituted ones. Substitutions on the methylene bridge of the DIM derivatives were in general not well tolerated, leading to only moderate potency compared to the unsubstituted analogs (all results are collected in Tables 1–4).

The effects of substituents at the 4,4′-position of the indole rings were studied. The following substituents were introduced: 4,4′-dimethyl (**40**: K_i 0.845 μM), 4,4′-dimethoxy (**41**: K_i 0.579 μM), 4,4′-difluoro (**42**: K_i 0.279 μM), 4,4′-dichloro (**43**: K_i 0.332 μM), 4,4′-dibromo (**44**: K_i 0.374 μM), 4,4′-dinitro (**45**: K_i > 5.0 μM),

TABLE 2 The binding affinity of 3,3′-diindolylmethane derivatives **100**–**136** at the human CB_1 and CB_2 receptors

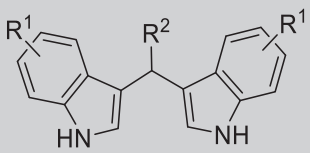

100-134

Structure I

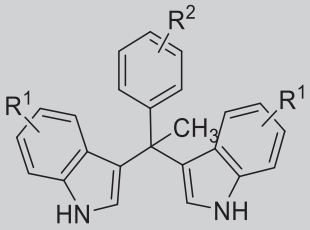

135-136

Structure II

Compound	R^1	R^2	Human CB_2 receptor Radioligand binding assay K_i ± SEM (μM) (or percent inhibition of [^{3}H]CP55,940 at 5 μM) *[Maximal inhibition (%)]*	Human CB_1 receptor K_i ± SEM (μM) (or percent inhibition of [^{3}H]CP55,940 at 5 μM) *[Maximal inhibition (%)]*
Structure I				
100	H	Me	**5.74** ± 0.30 *[77%]*	**8.15** ± 2.40 *[71%]*
101	H	Ethyl	**0.804** ± 0.249 *[97%]*	**2.70** ± 1.86 *[90%]*
102	H	Propyl	**>5** (33%)	**>5** (45%)
103	H	Butyl	**>5** (36%)	**>5** (−2%)
104	H	4-MePh	**2.55** ± 0.28 *[98%]*	**2.51** ± 0.40 *[100%]*
105	H	3-MePh	**1.79** ± 0.36 *[79%]*	**3.56** ± 1.47 *[74%]*
106	H	2-MePh	**4.55** ± 1.52 *[59%]*	**2.98** ± 1.76 *[58%]*
107	H	4-EthylPh	**1.35** ± 0.56 *[95%]*	**4.44** ± 2.16 *[100%]*
108	H	4-IsopropylPh	**1.55** ± 0.41 *[85%]*	**0.832** ± 0.281 *[82%]*
109	H	4-MeOPh	**2.41** ± 0.02 *[73%]*	**0.774** ± 0.169 *[71%]*
110	H	3-MeOPh	**2.07** ± 0.75 *[96%]*	**3.04** ± 1.16 *[91%]*
111	H	2-MeOPh	**2.72** ± 2.02 *[59%]*	**1.70** ± 0.41 *[84%]*
112	H	2,3-Methylenedioxy-Ph	**3.04** ± 0.22 *[84%]*	**1.19** ± 0.102 *[84%]*
113	H	4-PhenoxyPh	**>5** (41%)	**0.402** ± 0.306 *[80%]*
114	H	4-(OH)Ph	**7.13** ± 0.617 *[60%]*	**>5** (43%)

TABLE 2 (Continued)

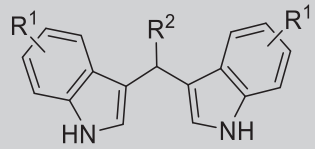

100-134

Structure I

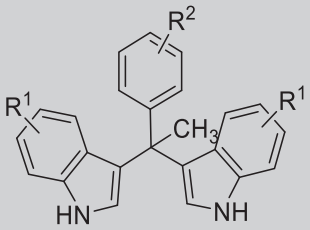

135-136

Structure II

Compound	R^1	R^2	Human CB_2 receptor Radioligand binding assay K_i ± SEM (μM) (or percent inhibition of [^{3}H]CP55,940 at 5 μM) *[Maximal inhibition (%)]*	Human CB_1 receptor K_i ± SEM (μM) (or percent inhibition of [^{3}H]CP55,940 at 5 μM) *[Maximal inhibition (%)]*
115	H	4-ClPh	**3.06** ± 0.90 *[94%]*	**1.24** ± 0.40 *[92%]*
116	H	4-FPh	**>5** (44%)	**3.54** ± 1.49 *[88%]*
117	H	4-NO_2Ph	**1.57** ± 0.04 *[80%]*	**0.596** ± 0.240 *[78%]*
118	H	Napth-1-yl	**>5** (9%)	**>5** (7%)
119	H	7-MeO-napth-1-yl	**>5** (36%)	**0.983** ± 0.463 *[69%]*
120	H	Indol-3-yl	**>5** (9%)	**>5** (18%)
121	4-OMe	Ph	**>5** (35%)	**>5** (44%)
122	4-OMe	4-MeOPh	**>5** (26%)	**0.541** ± 0.173 *[88%]*
123	5-OMe	4-MePh	**>5** (42%)	**0.414** ± 0.260 *[68%]*
124	5-OMe	4-FPh	**>5** (18%)	**>5** (34%)
125	5-OMe	4-MeOPh	**2.04** ± 0.37 *[91%]*	**0.176** ± 0.649 *[83%]*
126	5-Me	Ph	**>5** (−8%)	**>5** (−31%)
127	5-Me	4-MeOPh	**1.30** ± 0.45 *[79%]*	**2.34** ± 0.172 *[76%]*
128	5-Me	4-FPh	**2.18** ± 0.29 *[87%]*	**2.69** ± 0.60 *[92%]*
129	5-F	Napth-2-yl	**2.35** ± 0.19 *[71%]*	**2.79** ± 0.61 *[80%]*
130	4-F	Pyridin-4-yl	**5.42** ± 0.22 *[92%]*	**4.96** ± 0.17 *[82%]*
131	5-F	Pyridin-4-yl	**>5** (28%)	**>5** (47%)

(Continues)

TABLE 2 (Continued)

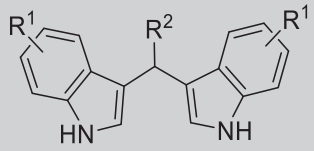

100-134

Structure I

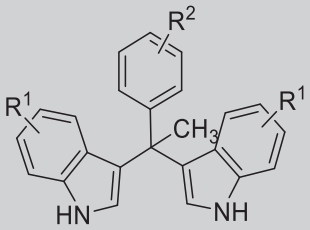

135-136

Structure II

Compound	R^1	R^2	Human CB_2 receptor Radioligand binding assay K_i ± SEM (μM) (or percent inhibition of [^{3}H]CP55,940 at 5 μM) *[Maximal inhibition (%)]*	Human CB_1 receptor K_i ± SEM (μM) (or percent inhibition of [^{3}H]CP55,940 at 5 μM) *[Maximal inhibition (%)]*
132	6-F	Pyridin-4-yl	**>5** (29%)	**5.03** ± 1.40 *[79%]*
133	7-F	Pyridin-4-yl	**>5** (14%)	**>5** (23%)
134	5-Cl	Pyridin-4-yl	**>5** (9%)	**>5** (9%)
Structure II				
135	H	4-CH_3	**0.674** ± 0.529 *[53%]*	**≥5** (44%)
136	H	4-OCH_3	**>5** (35%)	**2.84** ± 0.17 *[73%]*

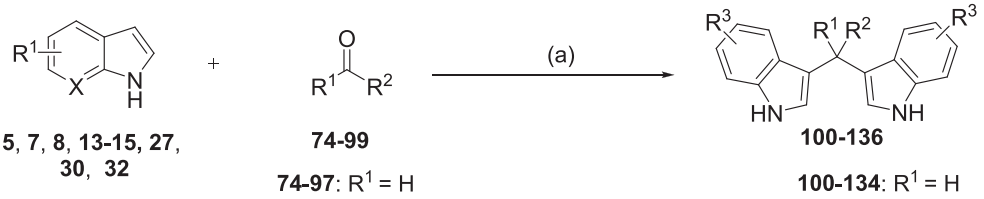

5, **7**, **8**, **13-15**, **27**, **30**, **32**

74-99

74-97: R^1 = H

100-136

100-134: R^1 = H

74, 100: R^2 = Me, **75, 101**: R^2 = Ethyl, **76, 102**: R^2 = Propyl,
77, 103: R^2 = Butyl, **78, 104**: R^2 = 4-MePh, **79, 105**: R^2 = 3-MePh,
80, 106: R^2 = 2-MePh, **81, 107**: R^2 = 4-EthylPh,
82, 108: R^2 = 4-IsopropylPh, **83, 109**: R^2 = 4-OMePh,
84, 110: R^2 = 3-OMePh, **85, 111**: R^2 = 2-OMePh,
86, 112: R^2 = 2,3-MethylenedioxyPh
87, 113: R^2 = 4-PhenoxyPh, **88, 114**: R^2 = 4-(OH)Ph
89, 115: R^2 = 4-ClPh, **90, 116**: R^2 = 4-FPh, **91, 117**: R^2 = 4-NO_2Ph
92, 118: R^2 = Naphthalen-1-yl, **93, 119**: R^2 = 7-OMe-naphthalen-1-yl
94, 120: R^2 = Indol-3-yl, **95**: R^2 = Ph, **96**: R^2 = Naphthalen-2-yl,
97: R^2 = Pyridin-4-yl; **98**: R^1 = CH_3, R^2 = 4-MePh,
99: R^1 = CH_3, R^2 = 4-OMePh,

121: R^2 = Ph, R^3 = 4-OMe
122: R^2 = 4-MeOPh, R^3 = 4-OMe
123: R^2 = 4-MePh, R^3 = 5-OMe
124: R^2 = 4-FPh, R^3 = 5-OMe
125: R^2 = 4-MeOPh, R^3 = 5-OMe
126: R^2 = Ph, R^3 = 5-Me
127: R^2 = 4-MeOPh, R^3 = 5-Me
128: R^2 = 4-FPh, R^3 = 5-Me
129: R^2 = Napth-2-yl, R^3 = 5-F
130: R^2 = Pyridin-4-yl, R^3 = 4-F
131: R^2 = Pyridin-4-yl, R^3 = 5-F
132: R^2 = Pyridin-4-yl, R^3 = 6-F
133: R^2 = Pyridin-4-yl, R^3 = 7-F
134: R^2 = Pyridin-4-yl, R^3 = 5-Cl
135: R^2 = 4MePh, R^3 = H
136: R^2 = 4MeOPh, R^3 = H

SCHEME 2 Synthesis of diindolylmethane derivatives and analogs **100–136**. Reagents and conditions: (a) H_2O, H_2SO_4, 5 min, 56%–97%. See Table 2 and experimental methods for details.

TABLE 3 The binding affinity of 3,3′-diindolylmethane derivatives **149**–**170** at the human CB_1 and the CB_2 receptors

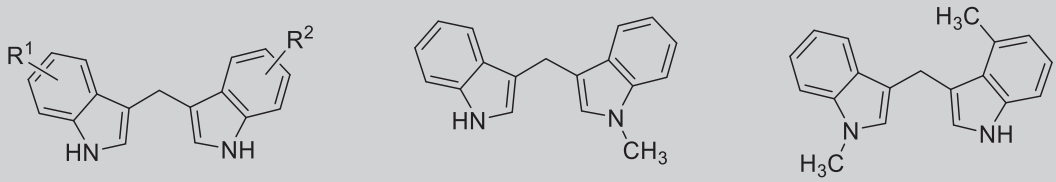

149-168 **169** **170**

Compound	R^1	R^2	Human CB_2 receptor Radioligand binding assay K_i ± SEM (μM) (or percent inhibition of [^{3}H]CP55,940 at 5 μM) *[Maximal inhibition (%)]*	Human CB_1 receptor K_i ± SEM (μM) (or percent inhibition of [^{3}H]CP55,940 at 5 μM) *[Maximal inhibition (%)]*
149 (PSB-18691)	H	4-Me	**0.498** ± 0.176 *[98%]*	**>10** (35%)
150	H	4-F	**0.758** ± 0.178 *[98%]*	**6.09** ± 1.78 *[100%]*
151	H	4-Br	**0.944** ± 0.106 *[99%]*	**31.1** ± 7.4 *[97%]*
152	H	5-OMe	**2.32** ± 0.71 *[87%]*	**>5** (33%)
153	H	5-F	**3.78** ± 0.30 *[85%]*	**>5** (20%)
154	H	5-Cl	**1.21** ± 0.05 *[93%]*	**4.40** ± 0.40 *[91%]*
155	H	5-CO_2Me	n.d[a]	**>5** (41%)
156	H	5-CO_2H	**>5** (20%)	**>5** (−7%)
157	4-Cl	4-Br	**0.237** ± 0.006 *[98%]*	**4.07** ± 1.36 *[92%]*
158	4-Cl	4-CH_3	**0.536** ± 0.058 *[96%]*	**7.13** ± 1.68 *[89%]*
159	5-OMe	4-F	**1.17** ± 0.14 *[97%]*	**>5** (39%)
160	5-OMe	5-F	**2.44** ± 0.27 *[88%]*	**>5** (49%)
161	5-OMe	7-F	**2.82** ± 0.09 *[91%]*	**>5** (31%)
162	5-OMe	4-F, 5-F	**3.74** ± 0.14 *[98%]*	**>5** (36%)
163	5-OMe	4-F, 6-F	**1.64** ± 0.15 *[98%]*	**>5** (44%)
164	5-OMe	5-Me	**1.20** ± 0.28 *[95%]*	**>5** (48%)

(Continues)

TABLE 3 (Continued)

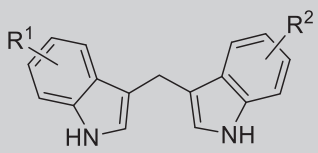

149-168

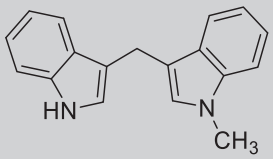

169

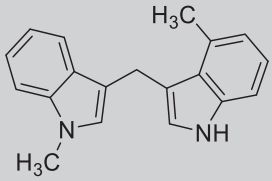

170

Compound	R^1	R^2	Human CB_2 receptor Radioligand binding assay K_i ± SEM (μM) (or percent inhibition of [^{3}H]CP55,940 at 5 μM) *[Maximal inhibition (%)]*	Human CB_1 receptor K_i ± SEM (μM) (or percent inhibition of [^{3}H]CP55,940 at 5 μM) *[Maximal inhibition (%)]*
165	5-OH	6-F	**12.0** ± 3.2 *[80%]*	**26.5** ± 12.4 *[82%]*
166	5-OMe	6-CF_3	**8.93** ± 1.10 *[82%]*	**>5** (44%)
167	5-OBn	6-F	**1.99** ± 0.39 *[96%]*	**1.40** ± 0.07 *[100%]*
168	5-OBn	6-CF_3	**4.12** ± 0.49 *[94%]*	**2.87** ± 0.93 *[100%]*
169	See above		**>5** (30%)	**>5** (16%)
170	See above		**0.716** ± 0.001 *[99%]*	**≈ 10** (53%)

[a]n.d, not determined.

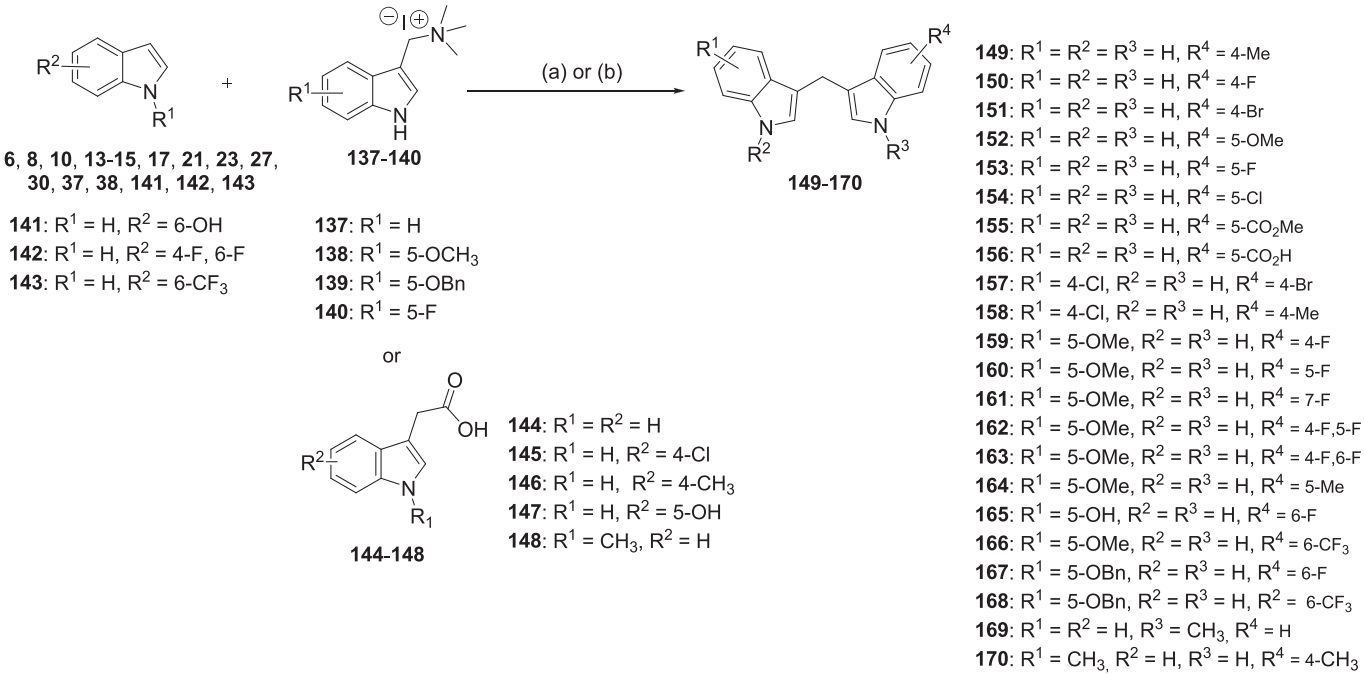

SCHEME 3 Synthesis of diindolylmethane derivatives and analogs **149–170**. Reagents and conditions: (a) H_2O, 53%–94%. (b) $Cu(OAc)_2 \cdot H_2O$, acetonitrile (ACN), 115°C, 2 h, 64%–83%. See Table 3 and experimental methods for details.

TABLE 4 The binding affinity of 2-oxyindole derivatives **175–180** at the human CB_1 and the CB_2 receptors

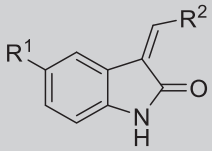

175-177

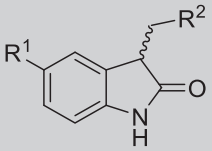

178-180

Compound	R^1	R^2	Human CB_2 receptor Radioligand binding assay K_i ± SEM (μM) (or percent inhibition of [^{3}H]CP55,940 at 5 μM) *[Maximal inhibition (%)]*	Human CB_1 receptor K_i ± SEM (μM) (or percent inhibition of [^{3}H]CP55,940 at 5 μM) *[Maximal inhibition (%)]*
175	H	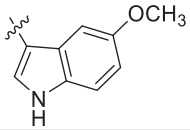	**>5** (28%)	**>5** (38%)
176	5-F	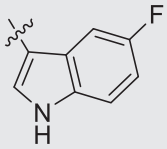	**3.42** ± 0.22 *[100%]*	**4.72** ± 0.14 *[100%]*
177	5-F	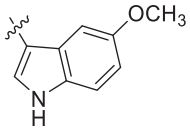	**>5** (39%)	**9.14** ± 0.87 *[100%]*
178	H	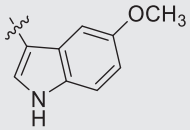	**>5** (33%)	**>5** (33%)
179	5-F	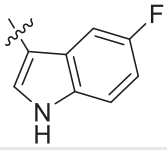	**>5** (20%)	**>5** (33%)
180	5-F	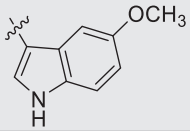	**>5** (41%)	**>5** (16%)

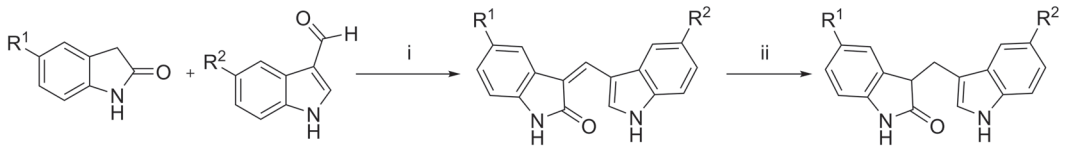

171-172
171: R^1 = H
172: R^1 = 5-F

173-174
173: R^1 = 5-OCH_3
174: R^1 = 5-F

175-177
175: R^1 = H, R^2 = 5-OCH_3
176: R^1 = 5-F, R^2 = 5-F
177: R^1 = 5-F, R^2 = 5-OCH_3

178-180
178: R^1 = H, R^2 = 5-OCH_3
179: R^1 = 5-F, R^2 = 5-F
180: R^1 = 5-F, R^2 = 5-OCH_3

SCHEME 4 Synthesis of unsaturated and saturated 2-oxoindole derivatives **175–177**, and **178–180**. Reagents and conditions: (i) (a) piperidine, ethanol, 65°C, 2 h; (b) $NaBH_4$, ethanol, 65°C, 2 h. See Table 4 and experimental methods for details.

and 4,4′-dicyano (**46**: K_i 0.339 μM). Substituents in that position could slightly improve potency as compared to the unsubstituted DIM. 4,4′-Difluoro, 4,4′-dichloro, and 4,4′-dicyano substitution was best tolerated.

Next, substituents were introduced at the 5,5′-positions of DIM-yielding compounds **47–58**. In general, compounds with 5,5′-substituents on the indole rings showed, in most cases, lower binding affinity compared to the 4,4′-substituted DIM derivatives. The 5,5′-dichloro-DIM (**51**: K_i 0.747 μM) exhibited the highest affinity among all derivatives of this series. Notably, it displayed only 73% maximum displacement of the radioligand in our assay system. 5,5′-Dimethyl-DIM (**47**: K_i 2.78 μM), 5,5′-dimethoxy-DIM (**48**: K_i 2.84 μM), 5,5′-difluoro-DIM (**49**: K_i 1.17 μM), 5,5′-dibromo-DIM (**52**: K_i 1.27 μM), 5,5′-ditrifluromethyl-DIM (**50**: K_i 1.98 μM), and 5,5′-dicarboxylic acid-DIM (**57**: K_i > 5.0 μM) showed moderate affinities, while 5,5′-diformyl-DIM (**56**: K_i 7.25 μM), 5,5′-dicyano-DIM (**53**: K_i > 5.0 μM) and 5,5′-dinitro-DIM (**54**: K_i > 5.0 μM) were only weakly potent or inactive at a concentration of 5 μM.

Substitution at the 6,6′-positions of DIM did not improve binding affinity (see compounds **59–63** in Table 1). Substituents such as 6,6′-dimethyl (**59**: K_i 0.524 μM), 6,6′-difluoro (**61**: K_i 0.985 μM), and 6,6′-dichloro (**62**: K_i 0.911 μM) were tolerated, showing similar affinity as lead compound **4**. Bulkier substituents, namely 6,6′-dimethoxy (**60**: K_i 5 μM) and 6,6′-dibromo (**63**: K_i 3.44 μM) reduced the binding affinity. This is probably caused by limited space in the binding site of the CB_2 receptor. We next studied 7,7′-substituted DIM derivatives (see Table 1). 7,7′-Difluoro-DIM (**64**: K_i > 5 μM) and 7,7′-dimethoxy-DIM (**65**: K_i > 5 μM) derivatives were inactive at 5 μM, indicating that substitutions at the 7,7′-positions are detrimental.

Our next effort was aimed at introducing multiple halogen substituents (compounds **66–70**). In general, this modification tended to reduce binding affinity irrespective of the positions of the halogen atoms. Chloro-substitution at the 4- and 6-positions (**66**: K_i 0.624 μM) was the best combination with equipotent binding affinity to lead compound **4**. It was interesting to note that compound **69** was less potent when compared to its 4,4′-dichloro-DIM analog **43** and slightly more potent than its 6,6′-dichloro-DIM derivative (**62**). Other combinations, as indicated in Table 1 (compounds **67–70**), reduced binding affinity. The 1,1′-dimethyl-DIM derivative **71** (K_i 3.39 μM) reduced binding affinity, confirming a role for NH in interacting with the CB_2 receptor. Substitution of the 2-position as in the 2,2′-dimethyl derivative **72** (K_i > 5 μM), or introduction of a nitrogen atom in the 7-position of the indole rings as in di-(7-azaindolyl)methane (**73**: K_i > 5 μM), led to a loss in CB_2 receptor binding affinity. These results indicated that substituents at the 4,4′- or 6,6′-positions were well tolerated, and in some cases, especially those substituted in the 4,4′-positions, could lead to an improvement in binding affinity compared to lead structure **4**. Concentration-inhibition curves for selected compounds are shown in Figure 2.

In the next set of experiments, we investigated the effects of substitution of the 3,3′-methylene bridge (C-10) of lead structure **4** (Table 2). A large variety of (aryl)alkyl substituents was introduced. Methyl substitution (**100**: K_i 5.74 μM) reduced binding affinity, while ethyl (**101**: K_i 0.804 μM) resulted in an affinity comparable to that of the lead compound. A further increase in the carbon chain length to propyl (**102**: K_i > 5 μM) and butyl (**103**: K_i > 5 μM) abolished affinity for the CB_2 receptor. Introducing aryl substituents at the 3,3′-methylene bridge either reduced or abolished CB_2 receptor affinity. Selected examples included *p*-tolyl (**104**: K_i 2.55 μM), *m*-tolyl (**105**: K_i 1.79 μM), *o*-tolyl (**106**: K_i 4.55 μM), *p*-anisyl (**109**: K_i 2.41 μM), *m*-anisyl (**110**: K_i 2.07 μM) and *o*-anisyl derivatives (**111**: K_i 2.72 μM), (4-phenoxy)phenyl (**113**: K_i > 5 μM), and a 4-hydroxyphenyl (**114**: K_i 7.13 μM)-substituted derivatives. The combination of substituents on the indole rings and on the methylene bridge of DIM did not improve binding affinity (see compounds **121–134**, Table 2). Interestingly, a DIM derivative with a quaternary center (**135**: K_i 0.674 μM) showed an equipotent binding affinity to DIM, although the maximal displacement of radioligand binding was limited to 53% (see Table 2 and Figure 2b). However, its methoxyl derivative (**136**: K_i > 5 μM) lost the affinity for the CB_2 receptor, indicating unfavorable interaction when a bulky substituent was present.

In summary, the substitution of the methylene bridge of DIM derivatives did not improve the compounds' binding affinity for the CB_2 receptor, but a few derivatives retained moderate affinity.

As a next step, we investigated a series of unsymmetrically substituted DIMs for their binding to the CB_2 receptor (see Table 3). Initially, only on one of both indole rings a substituent was introduced in the 4-position. The following rank order of potency was observed: 4-methyl-DIM (**149**: K_i 0.498 μM) > 4-F-DIM (**150**: K_i 0.758 μM) > 4-Br-DIM (**151**: K_i 0.944 μM). Thus, these compounds showed comparable binding affinity as the lead compound DIM. All of them were able to completely displace the radioligand in our experiments.

Next, mono-substitution at the 5-position of one of the indole rings was introduced. The following rank order of potency was observed: 5-Cl-DIM (**154**: K_i 1.21 μM) ≥ 5-methoxy-DIM (**152**: K_i 2.32 μM) ≥ 5-F-DIM (**153**: K_i3.78 μM). In general, mono-substitution at the 5-position appeared to be less advantageous than di-substitution on both indole rings in that position. We further investigated the behavior of unsymmetrical DIM derivatives with multiple substitutions, see compounds **157–170**. As expected, substituents in the 4-position were found to yield the best unsymmetrical DIM derivatives. The following rank order of potency was observed: 4-Cl,4′-Br-DIM (**157**: K_i 0.237 μM) > 4-Cl,4′-CH_3-DIM (**158**: K_i 0.536 μM). Both derivatives were able to nearly completely displace the radioligand. Compounds that have a 5-methoxy or 5-benzyloxy substituent combined with other substituents showed only moderate affinities (see compounds **159–168**). 5-OCH_3,4′-F-DIM (**159**: K_i 1.17 μM), and 5-OCH_3,5′-CH_3-DIM (**164**: K_i 1.20 μM) were among the most potent ligands in this series showing complete displacement of the radioligand. Introducing a polar hydroxyl group at position 5 of the indole ring (**165**: K_i 12.0 μM) reduced binding affinity. The *N*-methylated compound lost binding affinity (**169**: K_i > 5 μM), but introducing a methyl group at position 4′ of **170** restored affinity (**170**: K_i 0.716 μM).

We extended the SARs of DIM derivatives by preparing unsaturated (**175–177**) and saturated 2-oxyindole derivatives (**178–180**; Table 4). Among them, compound **176** showed moderate binding affinity, but the other compounds lost affinity.

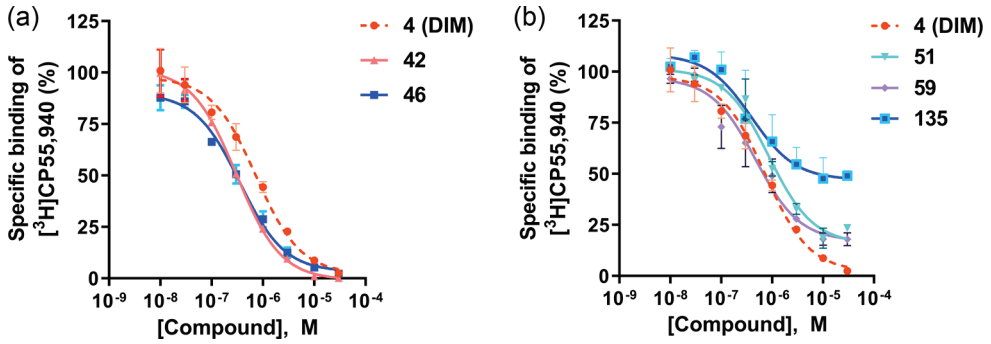

FIGURE 2 Concentration-dependent inhibition of specific [^{3}H]CP55,940 binding by lead structure **4** (K_i 0.690 ± 0.159 μM) and analogs **42** (K_i 0.279 ± 0.056 μM), **46** (K_i 0.339 ± 0.061 μM), **51** (K_i 0.747 ± 0.067 μM), **59** (K_i 0.504 ± 0.252 μM) and **135** (K_i 0.674 ± 0.529 μM) at the human CB_2 receptor. Data points represent means ± SEM of three independent experiments, performed in duplicates.

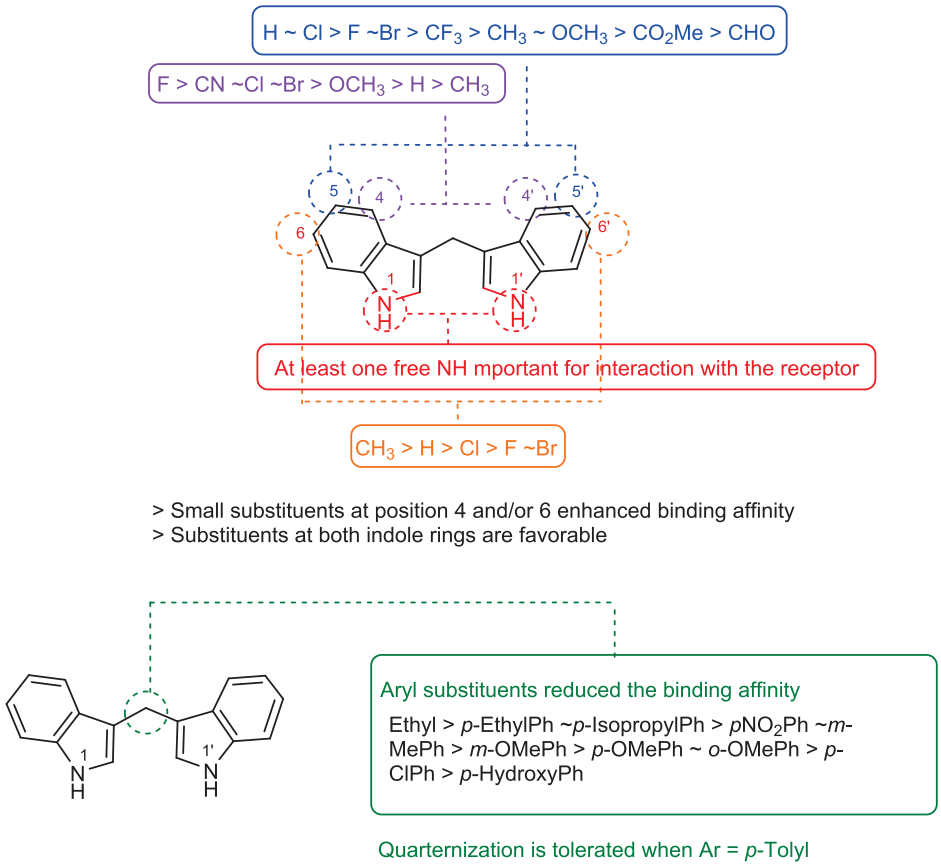

FIGURE 3 Structure–activity relationships of diindolylmethane (DIM) derivatives at CB_2 receptor. See text for details.

The SARs of DIM derivatives at the CB_2 receptor is summarized in Figure 3. DIM derivatives represent a new class of CB_2 receptor ligands with K_i values reaching the submicromolar concentration range. In general, symmetrically substituted DIMs without substitutions on the methylene bridge showed similar or higher affinities as compared to the lead compound DIM. In particular, the presence of halogen at position 4 of both indole rings improved the binding affinity, while aryl substituents at the methylene bridge reduced it. At least one unsubstituted indole-NH appears to be required for CB_2 receptor binding.

Some of the DIM derivatives, even very potent ones, showed incomplete inhibition of [^{3}H]CP55,940 binding, see, for example, **51**, **56**, **136** (Tables 1 and 2, Figure 2). This may indicate that the DIM derivatives do not bind to the same binding site as the radioligand, that is the orthosteric binding site, but act as allosteric agonists. Another explanation could be that they do bind—at least in part—to the orthosteric binding site, but to a conformation that differs from the conformation to which classical CBs are binding or which they are stabilizing.

2.2.2 | Functional assays at CB_2 receptors

Next, we studied the functional activity of selected ligands. First, we performed cAMP accumulation assays as well as β-arrestin recruitment assays for DIM at the CB_2 receptor to confirm previous results.[34] DIM behaved as a partial agonist in both cAMP and β-arrestin assays with EC_{50} values of 0.334 μM (E_{max} 65% compared to 1 μM full agonist of CP55,940) and 0.562 μM (E_{max} 63% compared to 0.1 μM full agonist of CP55,940) (see Figures 4 and 5, Table 5). Thus, DIM behaved similarly as the partial agonist THC, which displayed E_{max} values of 59% (cAMP) and 32% (β-arrestin assay), respectively.

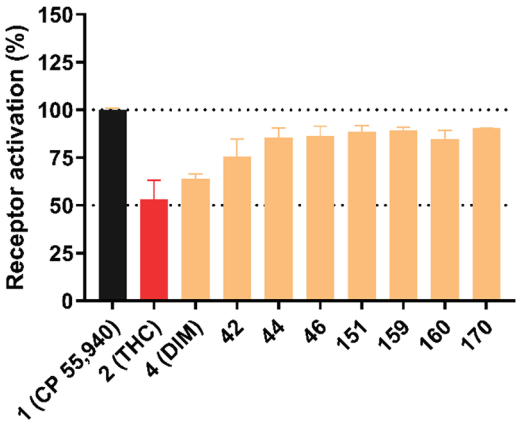

FIGURE 4 Functional properties of selected compounds determined in cAMP accumulation assays, in the presence of forskolin (10 μM). All results were normalized to the maximal receptor activation by the full agonist CP55,940 at 1 μM.

Results for compounds selected for cAMP accumulation studies are shown in Figure 4. Like DIM, all investigated DIM derivatives behaved as partial agonists at the CB_2 receptor, but their efficacy differed, some of the new compounds being more efficacious than DIM and significantly more efficacious than THC. Concentration-response curves were determined for compounds that showed more than 50% receptor activation at a concentration of 5 μM (see Figure 5). The results are collected in Table 5.

In the cAMP assay, the symmetrical substitution of DIM with 4,4′-difluoro-DIM (**42**: EC_{50} 0.0551 μM) led to an increase in agonistic activity. The larger substituents in 4,4′-dibromo-DIM (**44**: EC_{50} 0.509 μM) resulted in reduced activity at the CB_2 receptor. Surprisingly, the 4,4′-dicyano-DIM derivative **46** (EC_{50} 0.0144 μM) showed low nanomolar potency; in fact, compound **46** is the most potent agonist identified in the present series showing full intrinsic activity at the CB_2 receptor. The mono-substituted 4-methyl DIM (**149**) displayed slightly lower activity at the CB_2 receptor with an EC_{50} of 0.0652 μM. Reduced potency was found with unsymmetrically substituted DIM derivatives indicating that unsymmetrical substitution was not favorable for agonistic activity

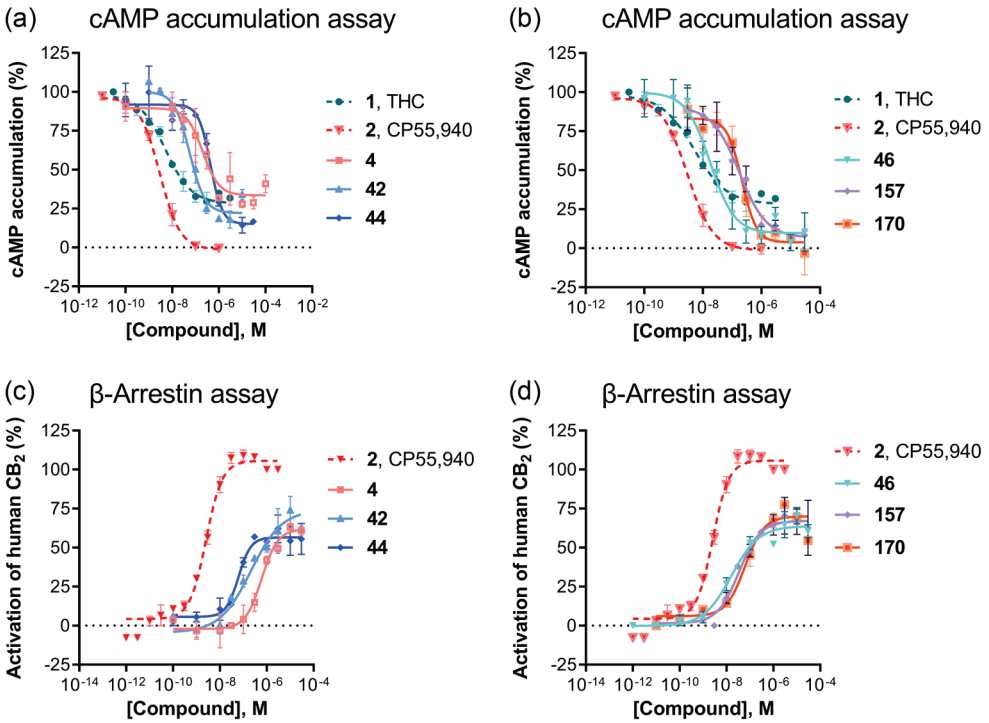

FIGURE 5 (a, b) Activation of the cannabinoid CB_2 receptor by **4** (EC_{50} 0.334 ± 0.174 μM), **42** (EC_{50} 0.0551 ± 0.0189 μM), **44** (EC_{50} 0.509 ± 0.100 μM), **46** (EC_{50} 0.0144 ± 0.0023 μM), **157** (EC_{50} 0.237 ± 0.081 μM), and **170** (EC_{50} 0.228 ± 0.030 μM) determined in cAMP accumulation assays. All data were normalized to the maximum effect of CP55,940 (1 μM). (c, d) Activation of the cannabinoid CB_2 receptor by **4** (EC_{50} 0.562 ± 0.195 μM), **42** (EC_{50} 0.290 ± 0.148 μM), **44** (EC_{50} 0.0450 ± 0.0189 μM), **46** (EC_{50} 0.0149 ± 0.0021 μM), **157** (EC_{50} 0.0385 ± 0.0125 μM), and **170** (EC_{50} 0.0803 ± 0.0340 μM) determined in β-arrestin recruitment assays. All data were normalized to the maximum effect of CP55,940 (0.1 μM). At least three independent experiments were performed in duplicates.

TABLE 5 The potency of diindolylmethane derivatives as agonists at the human CB_2 receptor

		Human CB_2 receptor			
		Radioligand binding assay K_i ± SEM (μM) (or percent inhibition of [^{3}H] CP55,940 at 5 μM)	cAMP assay EC_{50} ± SEM (μM) (or percent receptor activation at 10 μM)	β-Arrestin recruitment assay EC_{50} ± SEM (μM) (or percent receptor activation at 10 μM)	
Compound		*[Maximal inhibition (%)]*	*[efficacy]*[a]	*[efficacy]*[b]	ΔΔlog (E_{max}/EC_{50})[c]
1	THC	**0.00595** ± 0.00027	**0.00527** ± 0.00019	**0.00142** ± 0.00003	0.8
		[100%]	*[59%]*	*[32%]*	
2	CP55,940	**0.000293** ± 0.00008	**0.00320** ± 0.00068	**0.00262** ± 0.00003	0
		[100%]	*[100%]*	*[100%]*	
4 DIM	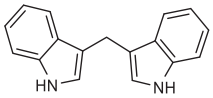	**0.690** ± 0.159	**0.334** ± 0.174	**0.562** ± 0.195	0.3
		[98%]	*[65%]*	*[63%]*	
42	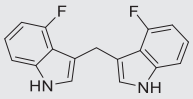	**0.279** ± 0.056	**0.0551** ± 0.0189	**0.290** ± 0.148	0.9
		[99%]	*[80%]*	*[70%]*	
44	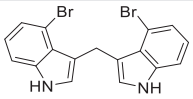	**0.374** ± 0.074	**0.509** ± 0.100	**0.0450** ± 0.0189	−0.8
		[100%]	*[85%]*	[61%]	
46	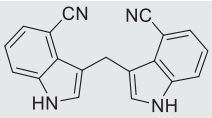	**0.339** ± 0.061	**0.0144** ± 0.0023	**0.0149** ± 0.0021	0.2
		[99%]	*[95%]*	*[67%]*	
149	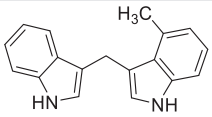	**0.498** ± 0.176	**0.0652** ± 0.0112	1.08 ± 0.37	1.3
		[98%]	*[89%]*	*[93%]*	
157	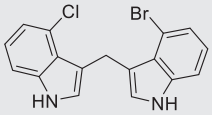	**0.237** ± 0.006	0.237 ± 0.081	**0.0385** ± 0.0125	−0.6
		[98%]	*[87%]*	*[69%]*	
158	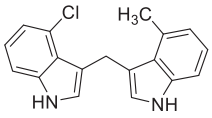	**0.536** ± 0.058	**0.281** ± 0.109	**0.120** ± 0.045	0.2
		[96%]	*[110%]*	*[51%]*	
170	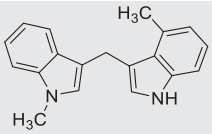	**0.716** ± 0.001	**0.228** ± 0.030	**0.0803** ± 0.0340	−0.3
		[99%]	*[89%]*	*[70%]*	

[a]Efficacy relative to the maximal effect of the standard agonist CP55,940 at 1 μM set at 100%.

[b]Efficacy relative to the maximal effect of the standard agonist CP55,940 at 0.1 μM set at 100%.

[c]Bias factor was calculated as described in experimental section. Negative numbers indicate β-arrestin-biased compounds; positive numbers indicate G protein-biased agonists. The bias factor is logarithmic: 1 corresponds to a 10-fold bias, and two corresponds to a 100-fold bias.

at the CB_2 receptor. Concentration-response curves for selected compounds are depicted in Figure 5.

We further evaluated these selected compounds in β-arrestin recruitment assays using an enzyme complementation assay. The standard agonist CP55,940 was used as a reference agonist. Like in the cAMP assays, our lead compound DIM (**4**) showed partial agonistic activity in the β-arrestin recruitment assays as well (EC_{50} 0.562 μM, 63% maximal activation). Thus, DIM showed nearly identical EC_{50} values in both the cAMP and the β-arrestin assays (Table 5). 4,4′-Difluoro-DIM (**42**: EC_{50} 0.290 μM) exhibited an increase in agonistic activity compared to lead compound **4** (Figure 5). Surprisingly, introducing larger substituents like 4,4′-dibromo (**44**) 4,4′-dicyano (**46**), or 4-chloro,4′-bromo (**157**) increased the potency of the DIM derivatives in the β-arrestin assays dramatically yielding EC_{50} values of 0.0450, 0.0149, and 0.0385 μM, respectively.

We calculated bias factors for the most potent agonists, comparing their effects in G_i-dependent cAMP assays with those determined in β-arrestin assays, as previously described.[40,41] CP55,940 was used as a reference compound (Table 5). A bias factor of 0 means no bias between two pathways, whereas a factor of 1 corresponds to a 10-fold preference, and a bias factor of two corresponds to a 100-fold preference for the G protein-dependent pathway. The partial agonist THC showed a slight preference for cAMP over β-arrestin signaling in our assay system (bias factor 0.8- or 6-fold preference for cAMP compared to β-arrestin signaling). This finding is well in agreement with published data.[42,43] DIM (**4**) displayed a two-fold preference (bias factor 0.3) for cAMP over β-arrestin signaling. Compound **42** (4,4′-difluoro-DIM) showed a seven-fold preference (bias factor 0.9) for inhibition of cAMP accumulation, while 4,4′-dibromo-DIM (**44**) had the opposite preference being biased toward the β-arrestin over the cAMP pathway (bias factor −0.8). 4,4′-Dicyano-DIM (**46**) was characterized as a virtually unbiased agonist (bias factor: 0.2). In fact, **46** was found to be the most potent non-biased CB_2 receptor agonist of the present series. The asymmetrical DIM-derivative **149** displayed the strongest bias towards cAMP over β-arrestin signaling, preferably activating G_i-dependent cAMP over β-arrestin signaling (bias factor: 1.3- or 19-fold preference). In contrast, unsymmetrically disubstituted DIM derivatives showed a preference for β-arrestin signaling over G_i-dependent cAMP signaling. This may result in functional antagonistic activity depending on the employed concentration since receptor internalization can be expected as a result of β-arrestin recruitment.

Next, we calculated the correlation of the results obtained in different experiments. The correlation between the potency of the DIM derivatives in cAMP and β-arrestin assays (Figure 6a) showed a low correlation. Some agonists are somewhat G_i protein-biased, which would result in longer-lasting activity because receptor internalization is less pronounced, while others are β-arrestin biased, which will lead to fast receptor internalization. Additionally, a comparison of functional and radioligand binding data revealed only a very low correlation (Figure 6b). This may be explained by the fact that DIM derivatives bind to a different binding site than the orthosteric agonist radioligand. Thus, DIM derivatives appear to act as allosteric CB_2 receptor agonists.

2.2.3 | Selectivity studies

Radioligand binding studies at the CB_1 receptor subtype were performed and compared with results at the CB_2 receptor (see Tables 1–4). The results showed that many of the compounds were able to bind to the CB_1 receptor as well. Among them, 6,6′-di-Cl-DIM (**62**, CB_1: K_i 0.820 μM; CB_2: K_i 0.911 μM) was found to display comparable binding affinity at both CB_1 and CB_2 receptors. However, only a few compounds displayed CB_1 receptor selectivity. Selected examples include **58** (K_i 2.95 μM), **119** (K_i 0.983 μM), **122** (K_i 0.541 μM), **123** (K_i > 0.414 μM), and **136** (K_i > 2.84 μM). Among these, compound **122** might be further developed in the future to

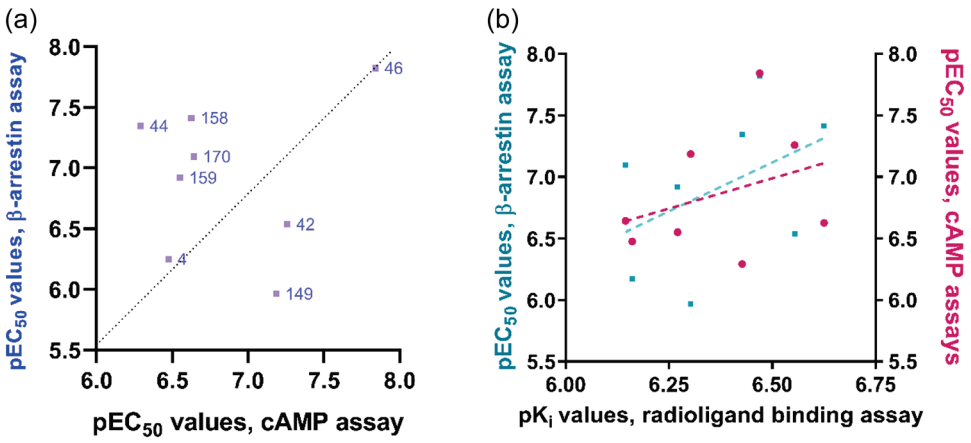

FIGURE 6 Correlation plots of radioligand binding data and data obtained in functional assays for diindolylmethane (DIM) derivatives. (a) Correlation of cAMP versus β-arrestin assays (r^2 < 0.1; p-value = 0.76). (b) Correlation plot between radioligand binding assays and β-arrestin assays (denoted in blue–green, r^2 = 0.193; p-value = 0.27), and correlation plot between radioligand binding assays and cAMP assays (denoted in red, r^2 = 0.112; p-value = 0.41).

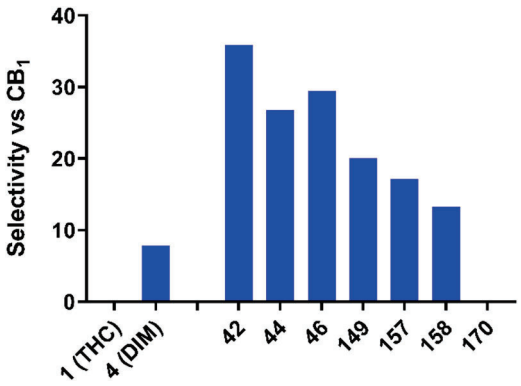

FIGURE 7 Selectivity index of selected compounds determined in radioligand binding assays. The lead structure diindolylmethane (DIM) and the nonselective THC are shown for comparison.

obtain potent, selective CB_1 receptor ligands. Importantly, the most potent CB_2 receptor ligands, including **4**, **42**, **44**, **46**, **149**, **157**, **158**, and **170**, were selective for the CB_2 versus the CB_1 receptor (Supporting Information: Table S2, Figure 7). In contrast to THC, which is nonselective (see Figure 7), potent, CB_2-selective agonists were discovered among the developed DIM derivatives. DIM (**4**) itself showed 8-fold selectivity for the CB_2 versus the CB_1 receptor. Compounds **42** (4,4′-di-F-DIM) and **46** (4,4′-di-CN-DIM) displayed the highest selectivity, being 36- and 30-fold selective for the CB_2 receptor, respectively. Unsymmetrically substituted DIMs such as **149**, **157**, **158**, and **170** showed a slightly lower CB_2-selectivity index.

It is important to note that compound **70** (PSB-16671), a potent GPR84 allosteric agonist (EC_{50} 0.043 μM) identified by our group, was shown to bind to both CB_1 (K_i 1.10 μM) and CB_2 receptors (K_i 2.64 μM) with comparable affinities. Mancini et al. recently reported that the ability of PSB-16671 to activate G proteins in mouse bone marrow-derived neutrophils was due to "off-target effects" and not mediated by GPR84.[44] This result was further supported by the inability of a GPR84 antagonist to block the effects of PSB-16671 on mouse GPR84 in both transfected cells and in the RAW264.7 cell line. Based on our results that PSB-16671 is able to interact with both CB receptor subtypes, we suggest that the observed effects of PSB-16671 could be due to its interaction with CB receptors natively expressed in the employed cell lines.

In native, nontransfected CHO cells DIM and its derivatives did not show any inhibition of cAMP accumulation. This clearly shows that the observed effects of DIM and its derivatives observed in the present study are due to the activation of the recombinantly expressed CB receptors in CHO cells. SARs at CB_2 receptors and GPR84 are quite different, and both, CB_2-selective or GPR84-selective agonists could be developed. However, one has to carefully choose concentrations—if high concentrations are employed, selectivity may not be given anymore.

We further investigated several DIM derivatives in functional assays at CB_1 receptors employing cAMP accumulation as well as β-arrestin recruitment assays (Table 6, Figure 8, Supporting Information: Table S3). Interestingly, none of the compounds was active in cAMP assays at concentrations up to 10 μM, neither as agonist nor as antagonist versus the standard agonist CP55,940 (see Supporting Information: Table S3). However, they showed antagonistic activity in β-arrestin assays at micromolar concentrations (Table 6, Figure 8). This indicates once more that DIM derivatives can act as allosteric modulators, not only of CB_2 but also of CB_1 receptors. Depending on their substitution pattern, they can, in fact, act as biased CB_1 receptor antagonists.

3 | CONCLUSIONS

In conclusion, a series of 99 symmetrical and unsymmetrical DIM derivatives and analogs were synthesized and evaluated with the aim to optimize their CB_2 receptor affinity, selectivity, and efficacy, of which **44–46**, **50**, **105**, **106**, **108**, **110**, **111**, **113**, **119**, **124**, **125**, **135**, **136**, and **165** are new compounds not previously reported in the literature. Compounds **42**, **44**, **46**, **149**, **157**, **158**, and **170** displayed high CB_2 receptor binding affinity and selectivity versus the CB_1 receptor. When they were investigated in functional assays, namely cAMP accumulation, and β-arrestin recruitment assays, the compounds behaved as CB_2 receptor agonists. However, only low correlations between affinity determined in binding assays and potency measured in functional assays were observed strongly hinting at allosteric interactions. Some of the compounds showed biased signaling either for G protein-dependent cAMP production or for β-arrestin recruitment. Di-(4-cyano-1*H*-indol-3-yl)methane (**46**, PSB-19837, EC_{50} [cAMP]: 0.0144 μM, EC_{50} [β-arrestin]: 0.0149 μM) was the most potent unbiased CB_2 receptor agonist. On the other hand, di-(4-bromo-1*H*-indol-3-yl)methane (**44**, PSB-19571, EC_{50} (cAMP): 0.509 μM, EC_{50} (β-arrestin): 0.0450 μM) is biased toward β-arrestin signaling, while 3-((1*H*-indol-3-yl)methyl)-4-methyl-1*H*-indole (**149**, PSB-18691, EC_{50} [cAMP]: 0.0652 μM, EC_{50} [β-arrestin]: 1.08 μM) is a G_i-protein biased CB_2 receptor agonist. These tool compounds possessing different pharmacological profiles will be useful for studying CB_2 receptors. Few DIM derivatives of the present series showed moderate affinity and potency at the CB_1 receptor, inhibiting CB_1-mediated β-arrestin recruitment (**109**, **113**, **122**, and **123**). Our results clearly point to an allosteric binding site for DIM derivatives at CB_1 and CB_2 receptors, and the determined radioligand binding data actually underestimate the compounds' potency in most cases. These DIM derivatives can serve as valuable tool compounds to elucidate the role of different signaling pathways activated by CB_2 receptors.

4 | EXPERIMENTAL

4.1 | Chemistry

4.1.1 | General

All commercially available reagents were used as purchased (Acros, Alfa Aesar, Sigma-Aldrich, ABCR or TCI). Solvents were used without

TABLE 6 Pharmacological evaluation of diindolylmethane derivatives at the human CB_1 receptor

Compound	Human CB_1 receptor		
	Radioligand binding assay K_i ± SEM (μM) (or percent inhibition of [^{3}H]CP55,940 at 5 μM) *[Maximal inhibition (%)]*	cAMP assay (agonistic activity) EC_{50} ± SEM (μM) (or percent receptor activation at 10 μM) *[efficacy]*[a]	β-Arrestin recruitment assay (antagonistic activity) IC_{50} ± SEM (μM) (or percent receptor inhibition at 10 μM) *[Maximal inhibition (%)]*[b]
THC	**0.00387** ± 0.00091	**0.00326** ± 0.00017 *[51%]*	n.d[c]
CP55,940	**0.00192** ± 0.00140 *[100%]*	**0.00336** ± 0.00057 *[100%]*	n.d
43	**0.753** ± 0.048 *[61%]*	**>10** (2%)	**≥10** (43%)
62	**0.820** ± 0.385 *[59%]*	**>10** (11%)	**>10** (35%)
109	**0.774** ± 0.169 *[71%]*	**>10** (1%)	**6.09** ± 0.50 *[91%]*
113	**0.402** ± 0.306 *[80%]*	**>10** (0%)	**4.43** ± 0.61 *[94%]*
122	**0.541** ± 0.173 [88%]	**>10** (0%)	**3.06** ± 0.29 *[91%]*
123	**0.414** ± 0.260 *[68%]*	**>10** (−10%)	**6.43** ± 0.45 *[95%]*

[a]Efficacy relative to the maximal effect of the standard agonist CP55,940 at 1 μM set at 100%.

[b]Inhibition compared to the EC_{80} of CP55,940 (0.001 μM) at the human CB_1 receptor, set at 100%.

[c]n.d, not determined.

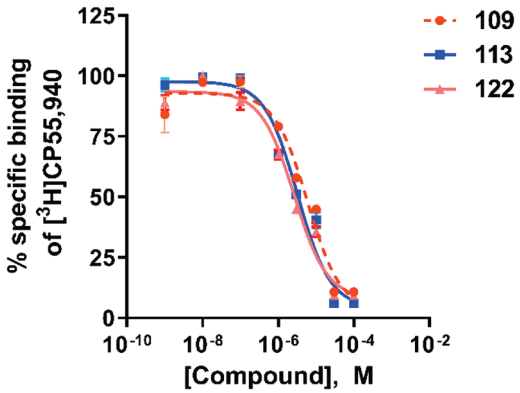

FIGURE 8 Concentration-inhibition curve of compound **109** (IC_{50} 6.09 ± 0.50 μM), **113** (IC_{50} 4.43 ± 0.61 μM), and **122** (IC_{50} 3.06 ± 0.29 μM) at the human CB_1 receptor, measured in β-arrestin assays. CP55,940 at its EC_{80} (0.001 μM) was used to activate the receptor. Data represent mean values ± standard error resulting from three independent experiments, performed in duplicates.

additional purification or drying except for dichloromethane, which was distilled over calcium hydride. Thin layer chromatography (TLC) using aluminum sheets with silica gel 60 F254 was employed to monitor the reactions (Merck). Column chromatography was performed with silica gel 0.060–0.200 mm, pore diameter ca. 6 nm. For microwave reactions, a CEM-Focused Microwave Synthesis type Discover apparatus was used. All synthesized compounds were finally dried in a vacuum at 8–12 Pa (0.08–0.12 mbar) using a sliding vane rotary vacuum pump (Vacuubrand GmbH). ^{1}H-, ^{13}C NMR, and $^{13}C_{apt}$ NMR data were collected on a Bruker Avance 500 MHz NMR spectrometer at 500 MHz (^{1}H), or 126 MHz (^{13}C), respectively. If indicated, NMR data were collected on a Bruker Ascend 600 MHz NMR spectrometer at 600 MHz (^{1}H), or 151 MHz (^{13}C), respectively. DMSO-d_6 was employed as a solvent at 303 K unless otherwise noted. Chemical shifts are reported in parts per million (ppm) relative to the deuterated solvent; that is, DMSO, δ ^{1}H: 2.49 ppm; ^{13}C: 39.7 ppm. Coupling constants J are given in Hertz and spin multiplicities are given as s (singlet), d (doublet), t (triplet), q (quartet),

sext. (sextet), m (multiplet), br (broad). Melting points were determined on a Büchi 530 melting point apparatus and are uncorrected. The purities of isolated products were determined by ESI-mass spectra obtained on an LCMS instrument (Applied Biosystems API 2000 LCMS/MS, HPLC Agilent 1100) using the following procedure: the compounds were dissolved at a concentration of 1.0 mg/ml in acetonitrile containing 2 mM ammonium acetate. Then, 10 µl of the sample were injected into an HPLC column (Macherey-Nagel Nucleodur® 3 µl C18, 50 × 2.00 mm). Elution was performed with a gradient of water/acetonitrile (containing 2 mM ammonium acetate) from 90:10 to 0:100 for 20 min at a flow rate of 300 µl/min, starting the gradient after 10 min. UV absorption was detected from 200 to 950 nm using a diode array detector. Purity of all compounds was determined at 254 nm. The purity of the compounds was generally ≥95%. Compounds **44–46**, **50**, **105**, **106**, **108**, **110**, **111**, **113**, **119**, **124**, **125**, **135**, **136**, and **165** are new, and not previously reported in the literature.

The InChI codes of the investigated compounds, together with some biological activity data, are provided as Supporting Information.

4.1.2 | General procedure for the synthesis of diindolylmethane derivatives

*General procedure for the preparation of **4**, **40–73**[33]*

The appropriate indole (**5–41**, 10 mmol) and formaldehyde (38%) (5 mmol) in water (5 ml) were microwave-irradiated for the required period of time at 100°C. The mixture was diluted with water (50 ml) and extracted with ethyl acetate (2 × 50 ml) after the reaction was completed. The combined organic layers were rinsed with brine, dried over $MgSO_4$, filtered, and evaporated to dryness under reduced pressure. The crude product was purified by silica gel column chromatography. Compounds **4**, **40–43**, **47–49**, **51–62**, **63**, **64–73** were previously reported.[33]

*Di[4-bromo-indol-3-yl]methane (**44**).* The compound was synthesized by reaction of 4-bromoindole (**10**, 10 mmol) with formaldehyde (38%) (5 mmol) in water (5 ml). The product was isolated as a brown solid (82% yield, 166 mg). ^{1}H NMR (600 MHz, DMSO-d_6) δ 11.31 (S, 2H, NH), 7.37 (dd, J = 8.1, 0.9 Hz, 2H, Ar), 7.13 (dd, J = 7.6, 0.8 Hz, 2H, Ar), 6.95 (t, J = 7.8 Hz, 2H, Ar), 6.85 (dd, J = 2.0, 0.9 Hz, 2H, Ar), 4.79–4.41 (m, 2H, CH_2). ^{13}C NMR (151 MHz, DMSO) δ 138.12 (C8), 125.71 (C7), 124.84 (C5), 122.58 (C6), 122.08 (C2), 115.55 (C4), 113.37 (C7), 111.38 (C3), 23.56 (CH_2). LC-MS (*m/z*): positive mode 405 $[M+H]^{1+}$; Purity by HPLC-UV(254 nm)-ESI-MS: 96.0%.

*Di[4-nitro-indol-3-yl]methane (**45**).* The compound was synthesized by reaction of 4-nitroindole (**11**, 10 mmol) with formaldehyde (38%) (5 mmol) in water (5 ml). The product was isolated as a brown solid (69% yield, 116 mg). ^{1}H NMR (500 MHz, DMSO-d_6) δ 8.09 (dd, J = 8.1, 6.3 Hz, 2H, Ar), 7.81 (d, J = 3.2 Hz, 2H, Ar), 7.37 (t, J = 8.0 Hz, 1H, Ar), 7.04 (d, J = 3.2 Hz, 1H, Ar), 6.65 (t, J = 7.3 Hz, 2H, Ar), 4.21 (d, J = 7.4 Hz, 2H, CH_2).^{13}Capt NMR (126 MHz, DMSO-d_6) δ 139.48 (C4), 137.73 (C8), 122.41 (C2), 120.69 (C6), 118.37 (C7), 117.52 (C5 and C7), 101.11 (C3), 29.33 (CH2). LC-MS (*m/z*): positive mode 337 $[M+H]^{1+}$; Purity by HPLC-UV(254 nm)-ESI-MS: 97.0%.

*Di[4-cyano-indol-3-yl]methane (**46**).* The compound was synthesized by reaction of 4-cyanoindole (**12**, 10 mmol) with formaldehyde (38%) (5 mmol) in water (5 ml). The product was isolated as a yellow solid (69% yield, 102 mg). ^{1}H NMR (600 MHz, DMSO-d_6) δ 11.62 (s, 2H, NH), 7.72 (dd, J = 8.2, 0.8 Hz, 2H, Ar), 7.47 (dd, J = 7.3, 0.8 Hz, 2H, Ar), 7.22 (dd, J = 8.2, 7.4 Hz, 2H, Ar), 7.14 (d, J = 2.1 Hz, 1H, Ar), 4.73 (s, 2H, CH_2). ^{13}C NMR (151 MHz, DMSO-d_6) δ 136.94 (C9), 127.22 (C7), 125.86 (C5), 121.03 (C2), 119.51 (C6), 117.19 (CN), 114.02 (C7), 100.69 (C3), 20.60. LC-MS (*m/z*): positive mode 297 $[M+H]^{1+}$; Purity by HPLC-UV(254 nm)-ESI-MS: 96.0%.

*Di[5-trifluoromethylindol-3-yl]methane (**50**).* The compound was synthesized by reaction of 5-trifluoromethylindole (**16**, 10 mmol) with formaldehyde (38%) (5 mmol) in water (5 ml). The product was isolated as a yellow solid (78% yield, 149 mg). ^{1}H NMR (600 MHz, DMSO-d_6) δ 10.82 (s, 2H, NH), 7.32–7.26 (m, 3H, Ar), 7.26 (d, J = 2.3 Hz, 2H, Ar), 7.21 (dd, J = 10.1, 2.5 Hz, 2H, Ar), 6.85 (dd, J = 9.2, 2.6 Hz, 2H, Ar), 4.05 (s, 2H, CH_2). ^{13}C NMR (151 MHz, DMSO-d_6) δ 133.20 (C9), 127.46 (C8), 127.40 (CF_3), 125.12 (C5), 118.37 (C2), 114.34 (C4), 112.38 (C6), 112.32 (C7), 108.88 (C3), 20.86 (CH_2). LC-MS (*m/z*): positive mode 383 $[M+H]^{1+}$; Purity by HPLC-UV(254 nm)-ESI-MS: 96.0%.

*General procedure for the synthesis of **100–136**[33,44]*

Concentrated sulfuric acid (1 equiv.) was added to a stirred mixture of the suitable indole (**5**, **7**, **8**, **13–15**, **27**, **30**, or **32**; 3.1–6.7 mmol) and the appropriate aldehyde or ketone (**74–99**; 1.5–3.3 mmol, 0.5 equiv.) diluted in water (5 ml). The aqueous suspension was dissolved in ethyl acetate and rinsed with brine once the reaction was completed. The organic layer was dried over $MgSO_4$, filtered, and evaporated to dryness under reduced pressure. Silica gel column chromatography was used to purify the crude product. Compounds **100–104**,[33] **107**,[45] **109**,[35] **112**, [33] **114-117**, [33] **118**,[45] **120**,[33] **121–122**,[45] **123**,[33] **126–134**[45] were previously reported.

*3,3'-(m-Tolylmethylene)di(indole) (**105**).* The compound was synthesized by reaction of indole (**5**, 3.1 mmol) with 3-methylbenzaldehyde (**79**, 1.5 mmol) in water (5 ml). The product was isolated as a brown solid (76% yield, 397 mg). ^{1}H NMR (500 MHz, DMSO-d_6) δ 10.75 (s, 2H), 7.36–7.31 (m, 2H, Ar), 7.27 (d, J = 7.9 Hz, 2H, Ar), 7.18 (s, 1H, Ar), 7.13 (dd, J = 4.0, 1.1 Hz, 2H), 7.02 (dd, J = 8.1, 7.1 Hz, 2H, Ar), 7.00–6.93 (m, 1H, Ar), 6.85 (dd, J = 8.0, 7.1 Hz, 2H, Ar), 6.80 (dd, J = 8.5, 6.7 Hz, 2H, Ar), 5.77 (s, 1H, CH-), 2.23 (s, 3H, CH_3). ^{13}C NMR (126 MHz, DMSO-d_6) δ 145.06 (C-3"), 137.01 (C-1"), 136.68 (C9), 129.04 (C8), 128.00 (C-2"), 126.77 (C-5"), 126.58 (C-4"), 125.49 (C-6"), 123.63 (C5), 120.94 (C6 and C4), 119.18 (C2), 111.53 (C3), 40.26 (C10), 21.16 (CH_3). LC-MS (*m/z*): positive mode 337 $[M+H]^{1+}$; Purity by HPLC-UV(254 nm)-ESI-MS: 97.0%.

*3,3′-(o-Tolylmethylene)di(indole) (**106**).* The compound was synthesized by reaction of indole (**5**, 3.1 mmol) with 2-methylbenzaldehyde (**80**, 1.5 mmol) in water (5 ml). The product was isolated as a brown solid (79% yield, 412 mg). ^{1}H NMR (500 MHz, DMSO-d_6) δ 10.75 (s, 2H, NH), 7.34 (dd, J = 8.1, 0.8 Hz, 2H, Ar), 7.21 (d, J = 7.9 Hz, 2H, Ar), 7.16 (dd, J = 7.3, 0.7 Hz, 1H, Ar), 7.07 (dd, J = 7.9, 6.5 Hz, 2H, Ar), 7.02 (dd, J = 8.1, 5.2 Hz, 3H, Ar), 6.84 (dd, J = 8.0, 7.1 Hz, 2H, Ar), 6.66 (d, J = 1.7 Hz, 2H, Ar), 5.94 (s, 1H, CH), 2.33 (s, 3H, CH_3). ^{13}C NMR (126 MHz, DMSO-d_6) δ 143.91 06 (C-2"), 136.77 06 (C-1"), 135.50 06 (C-9), 130.15 06 (C-8), 127.96 (C-5"), 126.84 (C-4"), 125.85 (C-6"), 125.62 (C-5), 124.03 (C-2), 120.97 (C-5), 119.02 (C-6), 118.29 (C-4), 111.58 (C-3), 40.29 (C10), 19.26 (CH_3). LC-MS (*m/z*): positive mode 337 $[M+H]^{1+}$; Purity by HPLC-UV(254 nm)-ESI-MS: 96.0%.

*3,3′-[(4-Isopropylphenyl)methylene]di(indole) (**108**).* The compound was synthesized by reaction of indole (**5**, 3.1 mmol) with 4-isopropylbenzaldehyde (**82**, 1.5 mmol) in water (5 ml). The product was obtained as a brown solid (68% yield, 385 mg). ^{1}H NMR (500 MHz, $CDCl_3$) δ 7.87 (s, 2H, NH), 7.39 (d, J = 8.0 Hz, 2H, Ar), 7.33 (d, J = 8.2 Hz, 2H, Ar), 7.25 (d, J = 7.6 Hz, 2H, Ar), 7.15 (d, J = 7.3 Hz, 2H, Ar), 7.14–7.08 (m, 2H, Ar), 6.99 (t, J = 7.5 Hz, 2H, Ar), 6.65 (s, 2H, Ar), 5.84 (s, 1H, CH-), 2.97–2.72 (m, 1H, CH), 1.22 (d, J = 6.9 Hz, 6H, 2CH3). ^{13}C NMR (126 MHz, $CDCl_3$) δ 146.44 (C-4"), 141.21 (C-9), 136.67 (C-8), 128.49 (C-2"), 127.13 (C-6"), 126.18 (C-3" and C-5"), 123.52 (C-2), 121.83 (C-6), 119.98 (C-5), 119.12 (C-4), 110.96 (C3, and C7), 39.74 (C10), 33.71 (CH), 20.63 (2 x CH_3). LC-MS (*m/z*): positive mode 365 $[M+H]^{1+}$; Purity by HPLC-UV(254 nm)-ESI-MS: 98.0%.

*3,3′-[(3-Methoxyphenyl)methylene]di(indole) (**110**).* The compound was synthesized by reaction of indole (**5**, 3.1 mmol) with 3-methoxybenzaldehyde (**84**, 1.5 mmol) in water (5 ml). The product was obtained as a brown solid (82% yield, 449 mg). ^{1}H NMR (500 MHz, DMSO) δ 10.77 (s, 2H, NH), 7.33 (d, J = 8.1 Hz, 2H, Ar), 7.28 (d, J = 7.9 Hz, 2H, Ar), 7.17 (t, J = 7.9 Hz, 1H, Ar), 7.02 (t, J = 7.5 Hz, 2H, Ar), 6.91 (dd, J = 12.5, 5.0 Hz, 2H, Ar), 6.88–6.80 (m, 4H, Ar), 6.74 (d, J = 2.6 Hz, 1H, Ar), 5.81 (d, J = 19.6 Hz, 1H, CH-), 3.66 (s, 3H, OCH_3). ^{13}C NMR (126 MHz, DMSO) δ 159.23 (C-3"), 146.77 (C-1"), 136.69 (C-5"), 129.08 (C-9), 126.77 (C8), 123.63 (C6), 120.96 (C2), 119.20 (C-6"), 118.43 (C4), 118.04 (C5), 114.63 (C-2"), 111.54 (C-4"), 110.79 (C3), 54.97 (CH, CH_3). LC-MS (*m/z*): positive mode 353 $[M+H]^{1+}$; Purity by HPLC-UV(254 nm)-ESI-MS: 96.0%.

*3,3′-[(2-Methoxyphenyl)methylene]di(indole) (**111**).* The compound was synthesized by reaction of indole (**5**, 3.1 mmol) with 2-methoxybenzaldehyde (**85**, 1.5 mmol) in water (5 ml). The product was obtained as a brown solid (79% yield, 432 mg). ^{1}H NMR (500 MHz, DMSO) δ 10.70 (s, 2H, NH), 7.32 (d, J = 8.1 Hz, 2H, Ar), 7.20 (d, J = 7.9 Hz, 2H, Ar), 7.18–7.05 (m, 2H, Ar), 7.04–6.95 (m, 3H, Ar), 6.83 (dd, J = 7.6, 0.9 Hz, 2H, Ar), 6.80 (dd, J = 7.4, 1.0 Hz, 1H, Ar), 6.71 (d, J = 1.7 Hz, 2H, Ar), 6.20 (s, 1H, CH-), 3.79 (s, 3H, OCH_3). ^{13}C NMR (126 MHz, DMSO) δ 156.42 (C-2"), 136.70 (C-9), 132.81 (C-6"), 129.24 (C-1"), 127.10 (C-4"), 126.88 (C-8), 123.67 (C-2), 120.88 (C-5"), 120.15 (C-4), 119.00 (C-6), 117.93 (C-5), 111.51 (C-3" and C-3), 55.72 (OCH_3). LC-MS (*m/z*): positive mode 353 $[M+H]^{1+}$; Purity by HPLC-UV(254 nm)-ESI-MS: 96.0%.

*3,3′-[(4-Phenoxyphenyl)methylene]di-(indole) (**113**).* The compound was synthesized by reaction of indole (**5**, 3.1 mmol) with 4-phenoxybenzaldehyde (**87**, 1.5 mmol) in water (5 ml). The product was obtained as a yellow solid (71% yield, 387 mg). ^{1}H NMR (500 MHz, $CDCl_3$) δ 7.89 (d, J = 2.4 Hz, 2H, Ar), 7.43–7.37 (m, 2H, Ar), 7.34 (dd, J = 8.2, 0.9 Hz, 2H, Ar), 7.32–7.26 (m, 4H, Ar), 7.17 (dd, J = 8.2, 7.0 Hz, 2H, Ar), 7.11–7.03 (m, 1H, Ar), 7.03–6.95 (m, 4H, Ar), 6.95–6.89 (m, 2H, Ar), 6.65 (dd, J = 2.4, 1.0 Hz, 2H, Ar), 5.86 (s, 1H, CH). ^{13}C NMR (126 MHz, $CDCl_3$) δ 157.48 (C-1‴), 155.30 (C-4"), 139.01 (C-9), 136.69 (C-1"), 129.90 (C-2"), 129.62 (C-6"), 127.00 (C-3‴ and 5‴), 123.52 (C2), 122.93 (C-3"), 121.95 (C-5"), 119.91 (C-6), 119.75 (C-2‴ and 6‴), 118.73 (C7), 118.61 (C4), 111.05 (C3), 60.40 (C10). LC-MS (*m/z*): positive mode 415 $[M+H]^{1+}$; Purity by HPLC-U (254 nm)-ESI-MS: 96.0%.

*3,3′-[(7-Methoxynaphth-1-yl)methylene]di(indole) (**119**).* The compound was synthesized by reaction of indole (**5**, 3.1 mmol) with 7-methoxy-1-naphthaldehyde (**93**, 1.5 mmol) in water (5 ml). The product was obtained as a brown solid (89% yield, 556 mg).^{1}H NMR (500 MHz, $CDCl_3$) δ 7.94–7.86 (s, 2H, NH), 7.70–7.61 (m, 2H, Ar), 7.59 (d, J = 8.9 Hz, 1H, Ar), 7.46 (dd, J = 8.4, 1.8 Hz, 1H, Ar), 7.42–7.37 (m, 2H, Ar), 7.34 (dd, J = 8.2, 0.8 Hz, 2H, Ar), 7.23 (s, 1H, Ar), 7.15 (dd, J = 8.2, 7.0 Hz, 2H, Ar), 7.10 (d, J = 2.6 Hz, 1H, Ar), 7.07 (dd, J = 8.9, 2.5 Hz, 1H, Ar), 6.97 (dd, J = 8.0, 7.1 Hz, 2H, Ar), 6.65 (dd, J = 2.2, 1.0 Hz, 2H, Ar), 6.01 (s, 1H, CH-), 3.89 (s, 3H, OCH_3). ^{13}C NMR (126 MHz, $CDCl_3$) δ 157.29 (C-OCH_3), 139.31 (C9), 136.70 (naphthyl), 133.32 (naphthyl), 129.37 (naphthyl), 129.03 (naphthyl), 128.22 (C8), 127.11 (naphthyl), 126.60 (naphthyl), 126.59 (naphthyl), 123.72 (C2), 121.92 (C6), 119.98 (C5), 119.96 (C4), 119.74 (naphthyl), 110.99 (C7), 105.64 (C3), 55.29 (C10), 40.08 (OCH_3). LC-MS (*m/z*): positive mode 403 $[M+H]^{1+}$; Purity by HPLC-UV(254 nm)-ESI-MS: 96.0%.

*3,3′-[(4-Fluorophenyl)methylene]di(5-methoxyindole) (**124**).* The compound was synthesized by reaction of 5-methoxyindole (**14**, 3.1 mmol) with 4-methoxybenzaldehyde (**83**, 1.5 mmol) in water (5 ml). The product was obtained as a brown solid (82% yield, 510 mg). ^{1}H NMR (500 MHz, DMSO-d_6) δ 10.66 (d, J = 2.4 Hz, 2H, NH), 7.28–7.12 (m, 2H, Ar), 6.63 (s, 1H, Ar), 6.52 (dd, J = 2.4, 0.8 Hz, 2H, Ar), 6.35 (dd, J = 6.3, 2.3 Hz, 2H, Ar), 5.89 (s, 1H, CH), 3.59 (s, 6H, 2 x OCH_3). ^{13}C NMR (126 MHz, DMSO-d_6) δ 161.55 (C-4‴, J = 257 Hz), 155.66 (C5), 138.11 (C-1"), 130.02 (C-2" and C-6"), 129.95 (C-9), 122.25 (C8), 121.75 (C2), 120.17 (C-3" and C-5"), 116.75 (C6), 114.28 (C7), 114.12 (C3), 104.89 (C4), 55.13 (2 x OCH_3). LC-MS (*m/z*): positive mode 401 $[M+H]^{1+}$; Purity by HPLC-UV(254 nm)-ESI-MS: 99.0%.

*3,3′-[(4-Methoxyphenyl)methylene]di(5-methoxyindole) (**125**).* The compound was obtained by reaction of 5-methoxyindole (**14**, 3.1 mmol) with

4-fluorobenzaldehyde (**90**, 1.5 mmol) in water (5 ml). The product was isolated as a brown solid (78% yield, 485 mg). ^{1}H NMR (500 MHz, DMSO-d_6) δ 10.58 (d, J = 2.5 Hz, 2H, NH), 7.23 (dd, J = 10.9, 8.7 Hz, 4H, Ar), 6.86–6.79 (m, 2H, Ar), 6.77 (dd, J = 2.4, 0.8 Hz, 2H, Ar), 6.71 (d, J = 2.5 Hz, 2H, Ar), 6.68 (dd, J = 8.7, 2.5 Hz, 2H, CH-), 3.70 (s, 3H, OCH_3), 3.59 (s, 6H, 2 x OCH_3). ^{13}C NMR (126 MHz, DMSO-d_6) δ 157.42 (C-4‴), 152.75 (C5), 137.12 (C-1"), 131.96 (C9), 129.32 (C8), 127.13 (C-2" and C-6"), 124.30 (C2), 118.17 (C-3" and C-5"), 113.48 (C5), 112.06 (C6), 110.58 (C3), 101.73 (C7), 55.42 (C10), 55.07 (3 x OCH_3). LC-MS (*m/z*): positive mode 413 $[M+H]^{1+}$; Purity by HPLC-UV(254 nm)-ESI-MS: 99.0%.

3,3′-[1-(p-Tolyl)ethane-1,1-diyl]di(indole) (***135***). The compound was synthesized by reaction of indole (**5**, 3.1 mmol) with 1-(*p*-tolyl) ethan-1-one (**98**, 1.5 mmol) in water (5 ml). The product was obtained as a brown solid (74% yield, 402 mg). ^{1}H NMR (500 MHz, DMSO-d_6) δ 10.73 (d, J = 1.8 Hz, 2H, Ar), 7.32 (s, 2H, Ar), 7.28–7.13 (m, 2H, Ar), 7.07 (d, J = 8.1 Hz, 2H, Ar), 7.02 (d, J = 8.0 Hz, 2H, 2H), 6.99–6.90 (m, 2H, Ar), 6.74 (dd, J = 8.0, 7.0 Hz, 2H, Ar), 6.65–6.63 (m, 1H, Ar), 3.30 (s, 3H, CH_3), 2.24 (s, 3H, CH_3). ^{13}C NMR (126 MHz, DMSO-d_6) δ 145.16 (C-1"), 137.19 (C9), 134.67 (C-4‴), 128.69 (C8), 127.87 (C-3‴ and C5‴), 126.32 (C-2‴ and C6‴), 123.44 (C2), 123.20 (C6), 121.40 (C5), 120.52 (C4), 117.81 (C7), 111.82 (C3), 42.94 (C10), 28.86 (CH_3). LC-MS (*m/z*): positive mode 351 $[M+H]^{1+}$; Purity by HPLC-UV(254 nm)-ESI-MS: 96.0%.

3,3′-[1-(4-Methoxyphenyl)ethane-1,1-diyl]di(indole) (***136***). The compound was synthesized by reaction of indole (**5**, 3.1 mmol) with 1-(*p*-anisyl)ethan-1-one (**99**, 1.5 mmol) in water (5 ml). The product was obtained as a brown solid (79% yield, 450 mg). ^{1}H NMR (500 MHz, DMSO-d_6) δ 10.72 (s, 2H, NH), 7.32 (d, J = 8.1 Hz, 2H, Ar), 7.27–7.15 (m, 2H, Ar), 7.07 (s, 2H, Ar), 7.00–6.91 (m, 2H, Ar), 6.83–6.76 (m, 2H, Ar), 6.75 (dd, J = 8.0, 0.9 Hz, 2H, Ar), 6.71 (dd, J = 8.6, 1.7 Hz, 3H, Ar), 165.3.70 (s, 3H, OCH_3), 2.19 (s, 3H, CH_3). ^{13}C NMR (126 MHz, DMSO-d_6) δ 157.13 (C-4‴), 140.57 (C9), 137.20 (C-1‴), 126.22 (C-2‴ and C6‴), 123.42 (C8), 123.30 (C2), 121.16 (C6), 120.53 (C5), 118.00 (C4), 112.96 (C-3‴ and C5‴), 111.65 (C3), 55.01 (OCH_3), 42.62 (C10), 29.33 (C10). LC-MS (*m/z*): positive mode 367 $[M+H]^{1+}$; Purity by HPLC-UV(254 nm)-ESI-MS: 97.0%.

General Procedure for the synthesis of ***149–170***[36]

Procedure A. (3-Indolylmethyl)trimethylammonium iodides (**137–140**, 1.6 mmol) and the appropriate indole derivative (**6–8**, **13–15**, **17**, **21**, **27**, **30**, **37**, **38**, **141**, **142**, or **143**; 3.2 mmol) were dissolved in H_2O (5 ml) in a 50 ml sealed tube. The reaction mixture was heated at 80°C upon stirring. After completion of the reaction, which was monitored by TLC, the mixture was allowed to cool to room temperature. The compound that precipitated on the tube wall was dissolved in ethyl acetate (10 ml), after the water had been decanted from the mixture. The resulting solution was dried over Na_2SO_4 and the product was purified by recrystallization or column chromatography.

Procedure B. In a 50 ml sealed tube, the appropriate indole derivative (**6–8**, **13–15**, **17**, **21**, **27**, **30**, **37**, **38**, **141**, **142**, or **143**; 1.14 mmol) and $Cu(OAc)_2{\cdot}H_2O$ (0.57 mmol) were given to a solution of a 2-(1*H*-indol-3-yl)acetic acid derivative (**144–148**; 0.57 mmol) in ACN (5 ml). The reaction mixture was stirred for 2 h at 115°C. The mixture was cooled to room temperature when the reaction was completed as monitored by TLC. The reaction mixture was poured into water and extracted with 2 × 25 ml of ethyl acetate. The mixed organic layers were washed with a brine solution (25 ml), dried over Na_2SO_4, and evaporated to dryness under reduced pressure. Recrystallization or column chromatography was used to purify the crude product.

Compounds **149–151**,[36] **152–153**,[36,37] **154**,[36] **155–156**,[33,36] **157–158**,[36] **159–164**,[37] **165–168**,[37] **169**,[36] and **170**,[33] have previously been reported.

3-[(6-Fluoroindol-3-yl)methyl]indole-5-ol (***165***). The compound was synthesized according to procedure B by reaction of 6-fluorolindole (**27**, 0.57 mmol) with 2-(5-hydroxy-1*H*-indol-3-yl) acetic acid (**147**, 0.57 mmol) in ACN (5 ml). The product was obtained as a brown solid (78% yield,125 mg). ^{1}H NMR (600 MHz, DMSO-d_6) δ 12.25 (s, 1H, NH), 11.09 (s, 1H, NH), 10.73 (s, 1H, OH), 7.66 (d, J = 8.4 Hz, 2H, Ar), 7.50 (d, J = 7.8 Hz, 1H, Ar), 7.36 (d, J = 8.5 Hz, 1H, Ar), 7.31 (d, J = 8.1 Hz, 1H Ar), 7.24 (s, 1H, Ar), 7.09 (s, 1H, Ar), 7.02 (t, J = 7.4 Hz, 1H, Ar), 6.91 (t, J = 7.4 Hz, 1H, Ar), 4.16 (s, 2H, Ar). ^{13}C NMR (151 MHz, DMSO-d_6) δ 168.62 (C6, J = 287 Hz), 139.04 (C-5′), 136.56 (C-9′), 127.24 (C9), 126.86 (C8), 124.59 (C8′), 122.88 (C2), 122.28 (C-2′), 120.95 (C-4′), 118.74 (C3), 118.21 (C5), 115.75 (C6), 113.99 (C-3′), 111.47 (C-5′), 111.15 (C-7′), 20.95 (C10). LC-MS (*m/z*): positive mode 281$[M+H]^{1+}$; purity by HPLC-UV(254 nm)-ESI-MS: 96.0%.

General procedure for the synthesis of ***175–177***

2-Oxindole (**171–172**, 37 mmol) in absolute ethanol was treated with the appropriate indolecarboxaldehyde (**173–174**; 41 mmol) and piperidine (16 mmol). After heating the mixture at 65°C for 2 h, the solvent was evaporated under reduced pressure. The residue was dissolved in 50 ml of water and extracted with ethyl acetate (2 × 30 ml). The combined organic layer was washed with brine, dried over $MgSO_4$, and evaporated to dryness. The product was purified by silica gel column chromatography. Compounds **175–177** have previously been reported.[33]

General procedure for the synthesis of ***178–180***

$NaBH_4$ (12 mmol) was added portion-wise over a period of 5–10 min at room temperature to a solution of the appropriate 2-oxindole derivative (**175–177**, 10 mmol) in ethanol (20 ml), and the reaction mixture was heated at 65°C for 2 h. Once the reaction was completed, the mixture was cooled to rt, and the ethanol was evaporated under reduced pressure. The residue was dissolved in ice water and extracted with 2 × 50 ml of ethyl acetate. The organic layers were combined, washed with brine, dried over $MgSO_4$, filtered, and evaporated under reduced pressure. The resulting product was

purified by column chromatography using a mixture of petroleum ether and ethyl acetate. Compounds **178–180** have been described previously.[33]

4.2 | Pharmacological/biological assays

4.2.1 | Radioligand binding assays at CB_1 and CB_2 receptors

Competition binding assays were performed using the nonselective CB receptor agonist radioligand [^{3}H](−)-cis-3-[2-hydroxy-4-(1,1-dimethylheptyl)phenyl]-trans-4-(3-hydroxypropyl)cyclohexanol ([^{3}H]CP55,940, final concentration 0.1 nM) as previously described.[38,46,47] Membrane preparations of CHO cells stably expressing either human CB_1 or CB_2 receptor were used (CB_1: 30 µg of protein/well and CB_2: 16 µg of protein/well) for all of the radioligand binding experiments. Stock solutions of the DIM derivatives were prepared in DMSO. The mixture containing 15 µl of the test compound in DMSO, 60 µl of [^{3}H]CP55,940 solution in assay buffer (50 mM TRIS, 3 mM $MgCl_2$, 0.1% bovine serum albumin [BSA], pH 7.4), 60 µl of membrane preparation and 465 µl of assay buffer was incubated for 2 h at room temperature (final DMSO conc. in the assay was 2.5%). Incubation was terminated by filtration through GF/C glass fiber filters (presoaked for 0.5 h in 0.3% aq. polyethyleneimine solution). Total binding was determined by adding DMSO without test compound, while nonspecific binding was determined in the presence of 10 µM of unlabeled CP55,940. The filter was then dried for 1.5 h at 50°C. Radioactivity on the filters was determined in a liquid scintillation counter (Top count NXT, Packard/Perkin-Elmer) after 10 h of preincubation with 50 µl of scintillation cocktail (Multiscint 25, Perkin-Elmer). Data were obtained in minimum of three independent experiments, performed in duplicates. For the calculation of K_i values, the Cheng-Prusoff equation and K_D values of 2.4 nM ([^{3}H]CP55,940 at CB_1) and 0.7 nM ([^{3}H]CP55,940 at CB_2) were used.[48]

4.2.2 | cAMP accumulation assays at human CB_1 and CB_2 receptor

The inhibition of adenylate cyclase activity was determined according to a described procedure in the literature using a competition binding assay for cAMP quantification in CHO cells stably expressing the CB_1 or the CB_2 receptor subtype, respectively.[21,30] Briefly, cells were seeded into a 24-well plate (200,000 cells/well) and incubated for 24 h. On the day of the assay, the medium was exchanged for Hank's buffered saline solution (HBSS, Gibco) and the cells were further incubated for another 2 h. About 20 µl of 40 µM Ro-20-1724 (4-(3-butoxy-4-methoxybenzyl)-2-imodazolidinone) as phosphodiesterase inhibitor was added into each of the wells. After 10 min incubation, 15 µl of test compound (diluted in HBSS) was added to the mixture and the cells were further incubated for another 5 min. The adenylate cyclase activator, forskolin (final concentration 10 µM), was added to the mixture, and incubation was continued for a further 15 min. The final DMSO concentration was 1.9%. The reaction was stopped by lysis of the cells with hot lysis buffer (100°C; 4 mM EDTA, 0.01% Triton X-100). The cAMP quantification was performed by mixing 50 µl of cell suspension, 30 µl of [^{3}H]cAMP (3 nM in Tris buffer), and 40 µl of cAMP-binding protein (50 µg per well in Tris buffer). The mixture was incubated for 1 h on ice. Bound and free radioligand were separated through GF/B glass fiber filters, and the radioactivity was measured after 9 h of preincubation with a scintillation cocktail (LumaSafeplus, Perkin-Elmer). Data were obtained from three independent experiments, performed in duplicates.

4.2.3 | β-Arrestin assays at human CB_1 and CB_2 receptor

β-Arrestin recruitment assays based on galactosidase enzyme complementation assay (DiscoverX) were performed according to previously published.[38] Briefly, CHO β-arrestin2 cells stably transfected either human CB_1-prolink1 or human CB_2-prolink1 were seeded in the density of 30,000 cells/well (CB_1), or 20,000 cells/well (CB_2), and incubated for 24 h. On the day of the assay, about 10 µl of the test compound was added and the cells were further incubated for another 90 min. CP 55,940 (0.1 µM) was used as the standard agonist for maximal response. For antagonistic activity, the test compounds (5 µl) were added to the wells, and incubated for 60 min at 37°C, and then the agonist at its EC_{80} was added (5 µl) and the mixture was incubated for another 90 min at 37°C. The galactosidase activity was measured by lysis of the cells according to the manufacturing protocol. The luminescence was measured with an LBMitras 940 plate reader (Berthold, Bad Wildbad). A minimum of three independent experiments was performed, each in duplicate.

4.2.4 | Operational model to determine the bias factor of the agonists

The pathway bias was calculated as described by Winpenny et al.[41,49] and Pillaiyar et al.[40] The E_{max} (max activation in %) and the EC_{50} (in M) for each compound were used to obtain the transduction ratio (log (E_{max}/EC_{50}). The transduction ratio within a pathway ($\Delta\log(E_{max}/EC_{50})$) was calculated by subtracting the transduction ratio of the agonist (log (E_{max}/EC_{50}) of the test compound) from the transduction ratio of the reference compound CP55,940 (log(E_{max}/EC_{50}) of CP55,940 regarding the same pathway. Ligand bias (or bias factor) between two pathways ($\Delta\Delta\log(E_{max}/EC_{50})$) was determined by calculating the difference between the transduction ratio ($\Delta\log(E_{max}/EC_{50})$) of one pathway and

the transduction ratio of the other pathway ($\Delta\log(E_{max}/EC_{50})$ cAMP – $\Delta\log(E_{max}/EC_{50})$ β-arrestin).

ACKNOWLEDGMENTS

Andhika B. Mahardhika, Clara T. Schoeder, and Christa E. Müller gratefully acknowledge funding by the Deutsche Forschungsgemeinschaft (DFG) for the Research Training Group GRK1873 "Pharmacology of 7TM-receptors and downstream signaling pathways," and by the German Federal Ministry of Education and Research (BMBF, BIGS DrugS). Andhika B. Mahardhika was funded by the Ministry of Finance Indonesia in the scheme of the Indonesia Endowment Fund for Education (Lembaga Pengelola Dana Pendidikan [LPDP]). Clara T. Schoeder was supported by a Bayer PhD fellowship. Open Access funding enabled and organized by Projekt DEAL.

CONFLICT OF INTEREST

The authors declare no conflict of interest.

ORCID

Andhika B. Mahardhika http://orcid.org/0000-0002-0456-1353
Christa E. Müller http://orcid.org/0000-0002-0013-6624
Thanigaimalai Pillaiyar http://orcid.org/0000-0001-5575-8896

REFERENCES

[1] R. Fredriksson, M. C. Lagerström, L.-G. Lundin, H. B. Schiöth, *Mol. Pharmacol.* **2003**, *63*, 1256. https://doi.org/10.1124/mol.63.6.1256
[2] M. Glass, R. L. M. Faull, M. Dragunow, *Neuroscience* **1997**, *77*, 299. https://doi.org/10.1016/S0306-4522(96)00428-9
[3] S. Galiegue, S. Mary, J. Marchand, D. Dussossoy, D. Carriere, P. Carayon, M. Bouaboula, D. Shire, G. Fur, P. Casellas, *Eur. J. Biochem.* **1995**, *232*, 54. https://doi.org/10.1111/j.1432-1033.1995.tb20780.x
[4] A. Gowran, J. Noonan, V. A. Campbell, *CNS Neurosci. Ther.* **2011**, *17*, 637. https://doi.org/10.1111/j.1755-5949.2010.00195.x
[5] E. Scotter, C. Goodfellow, E. Graham, M. Dragunow, M. Glass, *Br. J. Pharmacol.* **2010**, *160*, 747. https://doi.org/10.1111/j.1476-5381.2010.00773.x
[6] L. O'Keefe, A. C. Simcocks, D. H. Hryciw, M. L. Mathai, A. J. McAinch, *Diabetes, Obes. Metab.* **2014**, *16*, 294. https://doi.org/10.1111/dom.12144
[7] P. Pacher, G. Kunos, *FEBS J.* **2013**, *280*, 1918. https://doi.org/10.1111/febs.12260
[8] M. Herkenham, A. Lynn, M. Johnson, L. Melvin, B. de Costa, K. Rice, *J. Neurosci.* **1991**, *11*, 563. https://doi.org/10.1523/jneurosci.11-02-00563.1991
[9] S. Munro, K. L. Thomas, M. Abu-Shaar, *Nature* **1993**, *365*, 61. https://doi.org/10.1038/365061a0
[10] P. Pacher, R. Mechoulam, *Prog. Lipid Res.* **2011**, *50*, 193. https://doi.org/10.1016/j.plipres.2011.01.001
[11] G. A. Cabral, E. S. Raborn, L. Griffin, J. Dennis, F. Marciano-Cabral, *Br. J. Pharmacol.* **2008**, *153*, 240. https://doi.org/10.1038/sj.bjp.0707584
[12] R. G. Pertwee, A. C. Howlett, M. E. Abood, S. P. H. Alexander, V. Di Marzo, M. R. Elphick, P. J. Greasley, H. S. Hansen, G. Kunos, K. Mackie, R. Mechoulam, R. A. Ross, *Pharmacol. Rev.* **2010**, *62*, 588. https://doi.org/10.1124/pr.110.003004
[13] A. C. Howlett, *Pharmacol. Rev.* **2002**, *54*, 161. https://doi.org/10.1124/pr.54.2.161
[14] R. G. Pertwee, *Br. J. Pharmacol.* **2008**, *153*, 199. https://doi.org/10.1038/sj.bjp.0707442
[15] J. Gertsch, R. G. Pertwee, V. Di Marzo, *Br. J. Pharmacol.* **2010**, *160*, 523. https://doi.org/10.1111/j.1476-5381.2010.00745.x
[16] R. G. Pertwee, in *Cannabinoids* (Ed.: R. G. Pertwee), Springer Berlin Heidelberg, Berlin, Heidelberg, **2005**, pp. 1, https://doi.org/10.1007/3-540-26573-2_1
[17] S. D. Banister, J. C. Arnold, M. Connor, M. Glass, I. S. McGregor, *ACS Chem. Neurosci.* **2019**, *10*, 2160. https://doi.org/10.1021/acschemneuro.8b00651
[18] S. Pisanti, P. Picardi, A. D'Alessandro, C. Laezza, M. Bifulco, *Trends Pharmacol. Sci.* **2013**, *34*, 273. https://doi.org/10.1016/j.tips.2013.03.003
[19] C. E. Müller, *Bundesgesundheitsblatt - Gesundheitsforschung - Gesundheitsschutz* **2019**, *62*, 818. https://doi.org/10.1007/s00103-019-02964-4
[20] M. E. Lynch, M. A. Ware, *J. Neuroimmune Pharmacol.* **2015**, *10*, 293. https://doi.org/10.1007/s11481-015-9600-6
[21] C. Hess, C. T. Schoeder, T. Pillaiyar, B. Madea, C. E. Müller, *Forensic Toxicol.* **2016**, *34*, 329. https://doi.org/10.1007/s11419-016-0320-2
[22] G. Navarro, P. Morales, C. Rodríguez-Cueto, J. Fernández-Ruiz, N. Jagerovic, R. Franco, *Front. Neurosci.* **2016**, *10*, 406. https://doi.org/10.3389/fnins.2016.00406
[23] T. Bisogno, V. Di Marzo, *CNS & Neurol Disorders Drug Targets* **2010**, *9*, 564. https://doi.org/10.2174/187152710793361568
[24] J. L. Shoemaker, K. A. Seely, R. L. Reed, J. P. Crow, P. L. Prather, *J. Neurochem.* **2007**, *101*, 87. https://doi.org/10.1111/j.1471-4159.2006.04346.x
[25] M. Aghazadeh Tabrizi, P. G. Baraldi, P. A. Borea, K. Varani, *Chem. Rev.* **2016**, *116*, 519. https://doi.org/10.1021/acs.chemrev.5b00411
[26] M. Maccarrone, I. Bab, T. Bíró, G. A. Cabral, S. K. Dey, V. Di Marzo, J. C. Konje, G. Kunos, R. Mechoulam, P. Pacher, K. A. Sharkey, A. Zimmer, *Trends Pharmacol. Sci.* **2015**, *36*, 277. https://doi.org/10.1016/j.tips.2015.02.008
[27] C. Blázquez, L. González-Feria, L. Álvarez, A. Haro, M. L. Casanova, M. Guzmán, *Cancer Res.* **2004**, *64*, 5617. https://doi.org/10.1158/0008-5472.Can-03-3927
[28] Z. M. Whiting, J. Yin, S. M. de la Harpe, A. J. Vernall, N. L. Grimsey, *Trends Pharmacol. Sci.* **2022**, *43*, 754. https://doi.org/10.1016/j.tips.2022.06.010
[29] D. An, S. Peigneur, L. A. Hendrickx, J. Tytgat, *Int. J. Mol. Sci.* **2020**, *21*, 5064. https://doi.org/10.3390/ijms21145064
[30] C. T. Schoeder, C. Hess, B. Madea, J. Meiler, C. E. Müller, *Forensic Toxicol.* **2018**, *36*, 385. https://doi.org/10.1007/s11419-018-0415-z
[31] J. L. Wiley, D. R. Compton, D. Dai, J. A. Lainton, M. Phillips, J. W. Huffman, B. R. Martin, *J. Pharmacol. Exp. Ther.* **1998**, *285*, 995.
[32] J. L. Wiley, J. A. Marusich, B. R. Martin, J. W. Huffman, *Drug Alcohol Depend.* **2012**, *123*, 148. https://doi.org/10.1016/j.drugalcdep.2011.11.001
[33] T. Pillaiyar, M. Köse, K. Sylvester, H. Weighardt, D. Thimm, G. Borges, I. Förster, I. von Kügelgen, C. E. Müller, *J. Med. Chem.* **2017**, *60*, 3636. https://doi.org/10.1021/acs.jmedchem.6b01593
[34] H. Yin, A. Chu, W. Li, B. Wang, F. Shelton, F. Otero, D. G. Nguyen, J. S. Caldwell, Y. A. Chen, *J. Biol. Chem.* **2009**, *284*, 12328. https://doi.org/10.1074/jbc.M806516200
[35] T. Pillaiyar, M. Dawood, H. Irum, C. E. Mäller, *ARKIVOC* **2017**, *2018*, 1. https://doi.org/10.24820/ark.5550190.p010.259
[36] T. Pillaiyar, E. Gorska, G. Schnakenburg, C. E. Müller, *J. Org. Chem.* **2018**, *83*, 9902. https://doi.org/10.1021/acs.joc.8b01349
[37] T. Pillaiyar, M. Uzair, S. Ullah, G. Schnakenburg, C. E. Müller, *Adv. Synth. Catal.* **2019**, *361*, 4286. https://doi.org/10.1002/adsc.201900688
[38] D. J. Modemann, A. B. Mahardhika, S. Yamoune, A.-K. Kreyenschmidt, F. Maaß, S. Kremers, C. Breunig, C.-O. Sahlmann, J. Bucerius, D. Stalke, J. Wiltfang, Y. Bouter, C. E. Müller, C. Bouter,

B. Meller, *Eur. J. Med. Chem.* **2022**, *232*, 114138. https://doi.org/10.1016/j.ejmech.2022.114138
[39] C. Nordstedt, B. B. Fredholm, *Anal. Biochem.* **1990**, *189*, 231. https://doi.org/10.1016/0003-2697(90)90113-N
[40] T. Pillaiyar, M. Köse, V. Namasivayam, K. Sylvester, G. Borges, D. Thimm, I. von Kügelgen, C. E. Müller, *ACS Omega* **2018**, *3*, 3365. https://doi.org/10.1021/acsomega.7b02092
[41] D. Winpenny, M. Clark, D. Cawkill, *Br. J. Pharmacol.* **2016**, *173*, 1393. https://doi.org/10.1111/bph.13441
[42] T. Miljuš, F. M. Heydenreich, T. Gazzi, A. Kimbara, M. Rogers-Evans, M. Nettekoven, E. Zirwes, A. Osterwald, A. C. Rufer, C. Ullmer, W. Guba, C. Le Gouill, J. Fingerle, M. Nazaré, U. Grether, M. Bouvier, D. B. Veprintsev, *bioRxiv* **2020**. https://doi.org/10.1101/2020.11.09.375162
[43] M. Soethoudt, U. Grether, J. Fingerle, T. W. Grim, F. Fezza, L. de Petrocellis, C. Ullmer, B. Rothenhäusler, C. Perret, N. van Gils, D. Finlay, C. MacDonald, A. Chicca, M. D. Gens, J. Stuart, H. de Vries, N. Mastrangelo, L. Xia, G. Alachouzos, M. P. Baggelaar, A. Martella, E. D. Mock, H. Deng, L. H. Heitman, M. Connor, V. Di Marzo, J. Gertsch, A. H. Lichtman, M. Maccarrone, P. Pacher, M. Glass, M. van der Stelt, *Nat. Commun.* **2017**, *8*, 13958. https://doi.org/10.1038/ncomms13958
[44] W. Qiang, X. Liu, T.-P. Loh, *ACS Sustain. Chem. Eng.* **2019**, *7*, 8429. https://doi.org/10.1021/acssuschemeng.9b00094
[45] Y. Cheng, X. Ou, J. Ma, L. Sun, Z.-H. Ma, *Eur. J. Org. Chem.* **2019**, *2019*, 66. https://doi.org/10.1002/ejoc.201801612
[46] T. Pillaiyar, M. Sedaghati, A. B. Mahardhika, L. L. Wendt, C. E. Müller, *Beilstein J. Org. Chem.* **2021**, *17*, 1464. https://doi.org/10.3762/bjoc.17.102
[47] C. T. Schoeder, A. B. Mahardhika, A. Drabczyńska, K. Kieć-Kononowicz, C. E. Müller, *ACS Med. Chem. Lett.* **2020**, *11*, 2024. https://doi.org/10.1021/acsmedchemlett.0c00208
[48] A. Behrenswerth, N. Volz, J. Toräng, S. Hinz, S. Bräse, C. E. Müller, *Bioorg. Med. Chem.* **2009**, *17*, 2842. https://doi.org/10.1016/j.bmc.2009.02.027
[49] E. T. van der Westhuizen, B. Breton, A. Christopoulos, M. Bouvier, *Mol. Pharmacol.* **2014**, *85*, 492. https://doi.org/10.1124/mol.113.088880

SUPPORTING INFORMATION

Additional supporting information can be found online in the Supporting Information section at the end of this article.

How to cite this article: A. B. Mahardhika, A. Ressemann, S. E. Kremers, M. S. Gregório Castanheira, C. T. Schoeder, C. E. Müller, T. Pillaiyar, *Arch. Pharm.* **2023**;356:e2200493. https://doi.org/10.1002/ardp.202200493

3.5. Publication V: Structural insights into partial activation of the prototypic G protein-coupled adenosine A_{2A} receptor

Tobias Claff,‡ Andhika B. Mahardika,‡ Victoria J. Vaaßen, Jonathan G. Schlegel, Christin Vielmuth, Renato H. Weiße, Norbert Sträter, and Christa E. Müller

‡authors contributed equally for this work

The article is reprinted with permission from Claff, T.; **Mahardhika, A. B.**; Vaaßen, V. J.; Schlegel, J. G.; Vielmuth, C.; Weiße, R. H.; Sträter, N.; Müller, C. E. Structural insights into partial activation of the prototypic G protein-coupled adenosine A_{2A} receptor. *ACS Pharmacol. Transl. Sci*. **2024**. DOI: 10.1021/acsptsci.4c00051. Copyright 2024 American Chemical Society.

Publication summary and contributions

Adenosine, a naturally occurring molecule in the body, plays a crucial role in transcellular signaling.[157, 158] It activates adenosine receptors, G protein-coupled receptors (GPCRs), and is involved in many physiological and pathological processes.[159, 160] There are four subtypes of adenosine receptors (ARs) : the A_1 and A_3 receptors, which primarily couple with $G\alpha_i$ proteins, and the A_{2A} and A_{2B} receptors, which couple with $G\alpha_s$ proteins.[161] The A_{2A}AR, is highly expressed in the central nervous system (CNS) and in smooth muscle, and has been shown to play an important role in Alzheimer's and Parkinsons's disease as well as in cardiovascular diseases.[162-164] A_{2A}ARs are abundantly expressed by immune cells and are upregulated in cancer cells. Thus, they are promising drug targets for immunotherapy of cancer.

Several nucleoside and non-nucleoside derivatives have been developed that activate A_{2A}AR, being full agonists (for example, *N*-ethylcarboxamidoadenosine, NECA) or antagonists (for example 3-(3-hydroxypropyl)-7-methyl-8-(*m*-methoxystyryl)-1-propargylxanthine, MSX-2).[165] In 2001, based on screening a campaign by Bayer, the first class of non-nucleosidic AR agonists was discovered which has partial agonistic activity at ARs.[166] Subsequent development by IJzerman et al. showed that LUF5833 (2-amino-6-[(1*H*-imidazol-2-ylmethyl)sulfanyl]-4-phenyl-3,5-pyridinedicarbonitrile) and LUF5834 (2-amino-4-(4-hydroxyphenyl)-6-[(1*H*-

imidazol-2-ylmethyl)sulfanyl]-3,5-pyridinedicarbonitrile were potent partial A_{2A}AR agonists.[167] Later on, in 2021, a crystal structure of LUF5833 bound to an inactive state of the human A_{2A}AR was published.[168] The "Stabilized Receptor" (StaR) crystallization construct A_{2A}-StaR2-bRIL which contains nine point mutations (A54$^{2.52}$L, T88$^{3.36}$A, R107$^{3.55}$A, K122$^{4.43}$A, L202$^{5.63}$A, L235$^{6.37}$A, V239$^{6.41}$A, S277$^{7.42}$A and N154 ^{ECL2}A), two of which are inside the orthosteric binding pocket (T88$^{3.36}$A and S277$^{7.42}$A), was employed. The authors were not able to obtain the co-crystal structure of LUF5384, featuring an additional phenolic group.

In the present paper, the crystal structure of LUF5834 bound to an optimized construct of the A_{2A}AR (A_{2A}-PSB2-bRIL; bRIL is thermostabilized apocytochrome b $_{562}$) and its pharmacological characterization was studied. The study provides insights on how a partial agonist may bind to the inactive state of a GPCR. The A_{2A}-PSB2-bRIL construct featuring only two mutations, S91$^{3.39}$K and N154^{ECL2}A, showed advantages over the A_{2A}-StaR2-bRIL construct. The crystal structure showed a resolution of 2.43 Å. Similar to LUF5833, LUF5834 binds to the orthosteric site of the A_{2A}AR. Interestingly, T88$^{3.36}$ showed an interaction with the phenolic group of LUF5834 – a feature which could not have been observed in the previously used construct of A_{2A}AR due to its T88$^{3.36}$A mutation. Additionally, an ionic lock between H264^{ECL3} and E169^{ECL2} was observed which was not present in the prior structure.

Radioligand binding evaluation of the partial agonist LUF5834 demonstrated its ability to displace both an agonist radioligand ([^{3}H]NECA) and an antagonist radioligand ([^{3}H]MSX-2) with a lower affinity value versus the agonist radioligand compared to the antagonist. LUF5834 was able to bind to the previously published inactive-state crystallization constructs, whereas full agonists for the A_{2A}AR were unable to bind to these constructs.

A G protein dissociation assay was used to investigate the functional activity LUF5834 at the A_{2A}AR. This assay measures the direct dissociation of heterotrimeric G proteins upon A_{2A}AR stimulation, providing a more upstream measurement compared to traditional second messenger assays. The $G\alpha_s\beta_3\gamma_9$ combination was used to monitor receptor activation. Similar to radioligand binding experiments, the full agonist NECA and the partial agonist LUF5834 were not able to activate the A_{2A}AR crystal constructs

since they are stabilized in their inactive state. Interestingly, LUF5834 was not able to activate the wild-type A_{2A}AR under standard experimental conditions. However, when a higher DNA amount was used to express a high level of the wild-type A_{2A}AR, LUF5834 was able to activate the A_{2A}AR in a dose-dependent manner. Since a a partial agonist will act as antagonist in the presence of a full agonist, LUF5834 in the presence of the full agonist NECA was tested at the wild-type A_{2A}AR. LUF5834 was found to inhibit NECA-induced A_{2A}AR activation, confirming that LUF5834 is indeed a partial agonist, the intrinsic activity of which is expression level dependent on the receptor.

In conclusion LUF5834 binds to inactive and active states of the A_{2A}AR, potentially stabilizing an equilibrium between these states or inducing a different conformation between the active and inactive states. In contrast, the full A_{2A}AR agonist NECA exhibits affinity only for the active state which it stabilizes.

In this manuscript, I performed the extensive pharmacological characterization of LUF5834 and NECA at the A_{2A}AR. The author wrote the manuscript in cooperation with Dr. Tobias Claff, Prof. Dr. Christa E. Müller, and all other authors.

ACS Pharmacology & Translational Science

pubs.acs.org/ptsci Article

Structural Insights into Partial Activation of the Prototypic G Protein-Coupled Adenosine A_{2A} Receptor

Tobias Claff,[#] Andhika B. Mahardhika,[#] Victoria J. Vaaßen, Jonathan G. Schlegel, Christin Vielmuth, Renato H. Weiße, Norbert Sträter, and Christa E. Müller*

Cite This: *ACS Pharmacol. Transl. Sci.* 2024, 7, 1415−1425 Read Online

ACCESS | Metrics & More | Article Recommendations

ABSTRACT: The adenosine A_{2A} receptor (A_{2A}AR) belongs to the rhodopsin-like G protein-coupled receptor (GPCR) family, which constitutes the largest class of GPCRs. Partial agonists show reduced efficacy as compared to physiological agonists and can even act as antagonists in the presence of a full agonist. Here, we determined an X-ray crystal structure of the partial A_{2A}AR agonist 2-amino-6-[(1*H*-imidazol-2-ylmethyl)sulfanyl]-4-*p*-hydroxyphenyl-3,5-pyridinedicarbonitrile (LUF5834) in complex with the A_{2A}AR construct A_{2A}-PSB2-bRIL, stabilized in its inactive conformation and being devoid of any mutations in the ligand binding pocket. The determined high-resolution structure (2.43 Å) resolved water networks and crucial binding pocket interactions. A direct hydrogen bond of the *p*-hydroxy group of LUF5834 with $T88^{3.36}$ was observed, an amino acid that was mutated to alanine in the most frequently used A_{2A}AR crystallization constructs thus preventing the discovery of its interactions in most of the previous A_{2A}AR co-crystal structures. G protein dissociation studies confirmed partial agonistic activity of LUF5834 as compared to that of the full agonist *N*-ethylcarboxamidoadenosine (NECA). In contrast to NECA, the partial agonist was still able to bind to the receptor construct locked in its inactive conformation by an $S91^{3.39}$K mutation, although with an affinity lower than that at the native receptor. This could explain the compound's partial agonistic activity: while full A_{2A}AR agonists bind exclusively to the active conformation, likely following conformational selection, partial agonists bind to active as well as inactive conformations, showing higher affinity for the active conformation. This might be a general mechanism of partial agonism also applicable to other GPCRs.

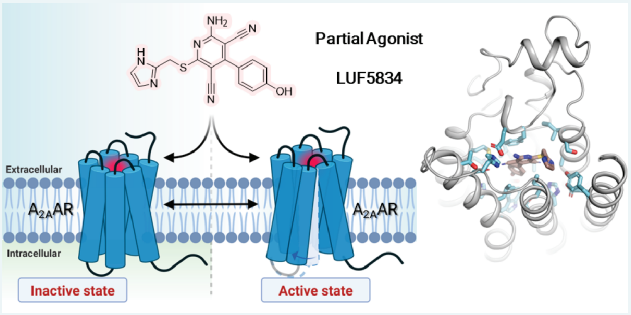

KEYWORDS: *adenosine receptors, G protein-coupled receptor, partial agonism, X-ray crystallography*

Adenosine receptors (ARs) are G protein-coupled receptors (GPCRs) involved in many physiological and pathological processes in the body.[1,2] They are subdivided into four subtypes, A_1, A_{2A}, A_{2B}, and A_3. The adenosine A_{2A} receptor (A_{2A}AR) is a drug target for cardiac imaging (agonists) and Parkinson's disease (antagonists).[3,4] Moreover, A_{2A}AR antagonists have potential for the treatment of Alzheimer's disease[5,6] and for the immunotherapy of cancer.[7] The latter indication is due to the fact that adenosine accumulates in the microenvironment of cancer cells leading to immune cell blockade, cancer cell proliferation, and metastasis.[8] In recent years, the A_{2A}AR has been intensively studied as a prototypic class A, rhodopsin-like GPCR by structural biology and computational approaches.[9,10]

ARs are activated by the nucleoside adenosine and its derivatives, e.g., NECA (Figure 1a). In a screening campaign in 2001, 2-amino-4-phenyl-3,5-pyridinedicarbonitrile derivatives were discovered as the first class of potent non-nucleoside-derived AR agonists.[11] Later on, it was found that most of them acted as partial agonists[12−14] showing lower efficacy than the cognate agonist adenosine, unless the receptors are massively overexpressed. Subsequently, derivatives with high selectivity for either the A_1AR, e.g., capadenoson, or the A_{2B}AR, e.g., BAY60−6583, were developed and pharmacologically evaluated (for structures see Figure 1a). Based on the original discovery, Beukers et al. (re)synthesized different partial agonists and analyzed their binding affinities and potencies at all four AR subtypes.[14] The most potent derivatives in their study were the phenyl-substituted 2-amino-6-[(1*H*-imidazol-2-ylmethyl)sulfanyl]-4-phenyl-3,5-pyridinedicarbonitrile (LUF5833) and the corresponding *p*-hydroxyphenyl derivative LUF5834 (Figure 1a). A crystal structure of the A_{2A}AR in complex with the partial agonist

Received: January 31, 2024
Revised: February 29, 2024
Accepted: March 1, 2024
Published: April 29, 2024

https://doi.org/10.1021/acsptsci.4c00051
ACS Pharmacol. Transl. Sci. 2024, 7, 1415−1425

ACS Pharmacology & Translational Science pubs.acs.org/ptsci Article

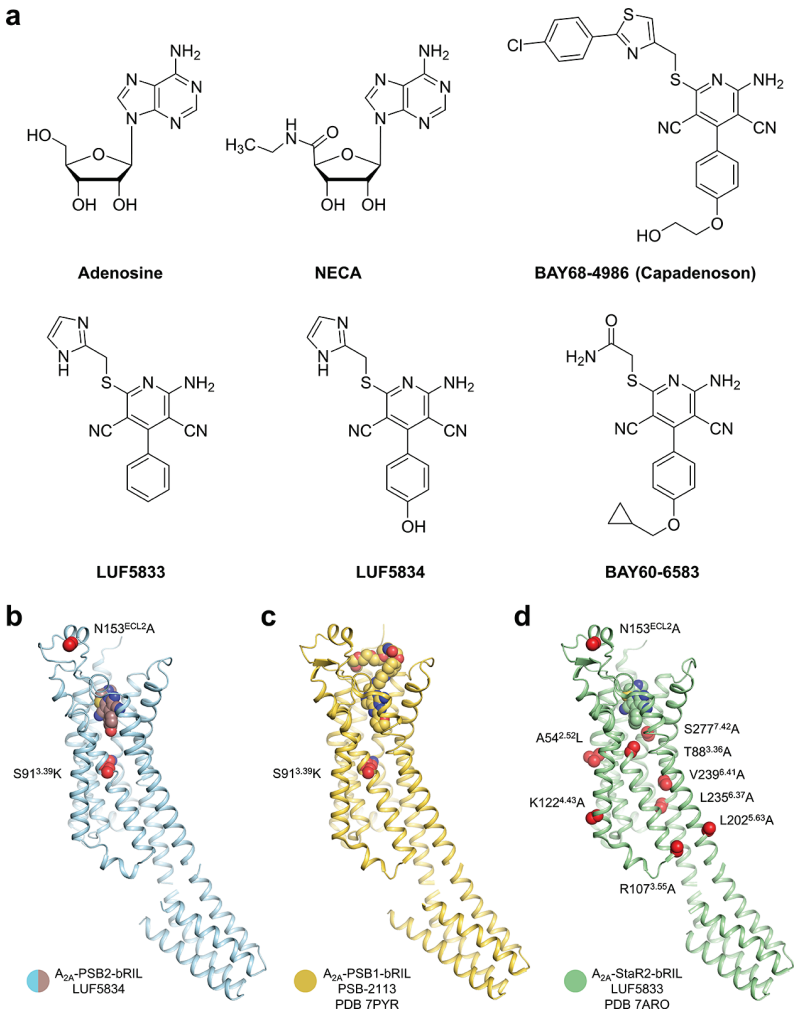

Figure 1. Overview of discussed AR agonists and crystallization constructs. (a) Chemical structure of full and partial AR agonists. (b–d) Architecture of selected A_{2A}AR crystallization constructs, highlighting the location of employed point mutations by red spheres.

LUF5833 (3.12 Å resolution) was previously obtained, but its moderate resolution did not allow to observe some details, such as water networks.[15] The *p*-hydroxyphenyl-substituted compound LUF5834 represents a generally utilized, commercially available tool compound for studying the A_{2A}AR in particular, and ARs in general.[16−19] The authors reported that they "also attempted to obtain a receptor crystal structure with LUF5834 but were unsuccessful".[15] Importantly, the "Stabilized Receptor" (StaR) crystallization construct A_{2A}-StaR2-bRIL[20] (bRIL refers to thermostabilized apocytochrome b_{562}RIL[21]) utilized in that study contains two mutations inside the orthosteric binding pocket ($T88^{3.36}$A and $S277^{7.42}$A, Figure 1b–d). Although the binding affinity (determined vs. the antagonist radioligand [^{3}H]ZM241385) of the hydroxyphenyl derivative LUF5834 was reported to be unaffected by the mutations, the $S277^{7.42}$A mutation was found to increase the compound's efficacy.[22]

In the present study, we determined the crystal structure of LUF5834 in complex with the recently developed optimized crystallization construct A_{2A}-PSB2-bRIL[23] (PSB refers to Pharmaceutical Sciences Bonn) that contains less mutations than other frequently used A_{2A}AR crystallization constructs and does not have any mutation in the orthosteric binding site. In addition, we aimed to improve the structural resolution to gain more insight into the interactions of this important partial agonistic scaffold. Herein, we describe the cocrystal structure of A_{2A}-PSB2-bRIL with LUF5834 at 2.43 Å resolution. The structural data are complemented by radioligand binding and G protein dissociation assays to characterize the mode of action of LUF5834 at the wild type (wt) A_{2A}AR and its crystallization construct.

RESULTS AND DISCUSSION

The crystal structure of the A_{2A}AR in complex with LUF5834 was determined at 2.43 Å resolution (Table 1) using the optimized crystallization construct A_{2A}-PSB2-bRIL[23] that contains two point mutations: (1) a thermostabilizing mutation in the sodium binding pocket ($S91^{3.39}$K)[9,24,25] and (2) a glycosylation site removal mutation ($N154^{ECL2}$A).[23] The $S91^{3.39}$K mutation constraints the A_{2A}AR in a constitutively inactive state with all common activation micoswitches unambiguously in the inactive conformation.[26] The partial A_{2A}AR agonist LUF5834 is bound to the orthosteric binding pocket with a refined occupancy of 0.7 (Figure 2a). The 3-cyano group of LUF5834 (for numbering, see Figure 2b) forms a direct hydrogen bond to $N253^{6.55}$ (Figure 2a). The interaction with $N253^{6.55}$ is further strengthened by a water-mediated hydrogen bond of the 2-amino group. The second

https://doi.org/10.1021/acsptsci.4c00051
ACS Pharmacol. Transl. Sci. 2024, 7, 1415−1425

ACS Pharmacology & Translational Science pubs.acs.org/ptsci Article

Table 1. Data Collection and Refinement Statistics[a]

A_{2A}-PSB2-bRIL-LUF5834 (PDB ID 8RLN)	
Data collection	
space group	$C222_1$
cell dimensions *a*, *b*, *c* (Å)	39.56, 179.69, 140.45
no. of unique reflections	16837 (843)
multiplicity	12.1 (12.9)
resolution (Å)	89.85−2.43 (2.59−2.43)
max. resolution aniso. (Å)	2.365, 2.568, 2.460
R_{meas}	0.264 (2.201)
R_{pim}	0.076 (0.609)
$CC_{1/2}$	0.997 (0.493)
mean $I/\sigma I$	7.9 (1.3)
completeness spherical	86.4 (25.0)
completeness ellipsoidal	90.8 (33.5)
Wilson B ($Å^2$)	43.05
Refinement	
resolution (Å)	70.23−2.43 (2.58−2.43)
no. reflections work/test set	16825/866
R_{work}	0.2029 (0.2301)
R_{free}	0.2813 (0.3715)
no. atoms (non-hydrogen)	
A_{2A}AR	2358
bRIL	697
LUF5834	37
lipids, polyethylene glycol (PEG), and waters	232
B-factors ($Å^2$)	
A_{2A}AR	43.05
bRIL	76.06
LUF5834	48.68
lipids, PEG, and waters	50.7
rmsd bonds (Å)	0.013
rmsd angles (deg)	1.422
Ramachandran favored (%)	96.88
Ramachandran allowed (%)	3.12
Ramachandran outliers (%)	0.00
rotamer outliers (%)	3.10
MolProbity clashscore	9.72

[a]Data from a single crystal was collected. The statistics for the highest resolution shell are shown in parentheses.

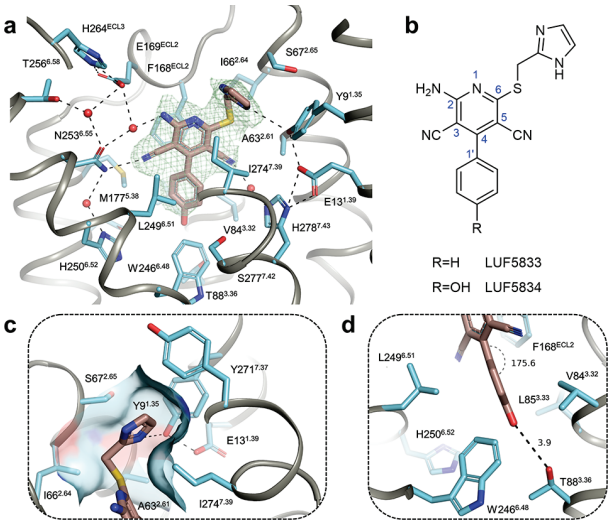

Figure 2. Ligand binding pocket of LUF5834 in the A_{2A}AR. (a) Overview of the LUF5834 binding pocket. The polder omit map of LUF5834 is shown in green mesh (contoured at 3σ). (b) Chemical structure of LUF5834. (c) Binding mode of the imidazole moiety of LUF5834 to a pocket represented by the protein surface (colored according to the nearby protein atom types). (d) Enlarged view of the interaction of the phenol moiety of LUF5834 with $T88^{3.36}$. The C4−C1′−O angle (175.6°) deviates by 4.4° from the linearity of a perfect aromatic system.

cyano group in position 5 is connected to $H278^{7.43}$ via a water molecule (Figure 2a). Aromatic $\pi-\pi$ stacking interaction between the pyridine moiety and $F168^{ECL2}$ is observed, similar to the binding of other structurally diverse A_{2A}AR ligands in previously reported A_{2A}AR structures.[20,27] The imidazole moiety of LUF5834 is located in a pocket shaped by $Y9^{1.35}$, $A63^{2.61}$, $S67^{2.65}$, $L267^{7.32}$, $Y271^{7.36}$, and $I274^{7.39}$. The basic imidazole (pK_a estimated to be 6.30 by the program Chemaxon, https://chemaxon.com/) is predominantly protonated under the crystallization conditions performed at pH 5.2 forming a weak direct hydrogen bond to $Y9^{1.35}$ (N−O distance 3.6 Å, Figure 2c). The phenolic group of LUF5834 faces toward the sodium binding pocket and is in contact with $W246^{6.48}$ of the CxWP motif and with $L249^{6.51}$ (Figure 2d).[28] It was previously reported that $L249^{6.51}$, present in the A_{2A}AR, is responsible for the A_{2B}AR selectivity of the structurally related BAY60-6583 over the A_{2A}AR.[29] This amino acid represents the only difference in the binding pocket of the A_{2A}AR compared to that of the A_{2B}ARs (A_{2A}AR: $L249^{6.51}$; A_{2B}AR: $V250^{6.51}$). An $L249^{6.51}V$ mutation in the A_{2A}AR transformed BAY60-6583 into a dual A_{2A}/A_{2B}AR partial agonist showing equal potency at both receptors.[29]

The close proximity of the phenolic OH group to $W246^{6.48}$ forces the aromatic ring into a bent structure. The C4−C1′−O angle (for numbering see Figure 2b) deviates by 4.1° from linearity; this deviation may in fact be even larger, considering that the stereochemical restraints enforce planarity of the phenolic ring in the crystallographic refinement. The OH group is located close to $T88^{3.36}$, likely participating in a weak hydrogen bond (O−O distance 3.9 Å) (Figure 2d). $T88^{3.36}$ is mutated to alanine in the A_{2A}-StaR2-bRIL construct which may contribute to the fact that cocrystallization trials of LUF5834 with that construct had previously failed.[15] $T88^{3.36}$ is conformationally restricted in the constitutively inactive conformation of A_{2A}-PSB2-bRIL, used in the present study, as a result of the introduced $S91^{3.39}K$ mutation that locks the receptor in its inactive state.[9] In fact, $T88^{3.36}$ had been observed in two distinct conformations when A_{2A}-ΔC-bRIL, the corresponding construct without any mutations, had been utilized to solve an A_{2A}AR cocrystal structure with the antagonist ZM241385 [Protein Data Bank (PDB) entry 4EIY].[27] These results imply somewhat greater flexibility of $T88^{3.36}$ in the wt receptor compared to the $S91^{3.39}K$ mutant. Hence, $T88^{3.36}$ might engage the phenolic OH group of LUF5834 in the wt receptor in an even more favorable way since it lacks the conformational restriction imposed by the $S91^{3.39}K$ mutation in the present structure.

The binding pose of LUF5833, lacking a phenolic OH group, in the previously published lower-resolution structure[15] (PDB ID 7ARO) is similar to the one that we determined for the phenolic analog LUF5834 (root-mean-square deviation 1.03 Å). However, a crucial difference represents the conformation of $H264^{ECL3}$ showing a unique position in the previous LUF5833 cocrystral structure, with $H264^{ECL3}$ pointing toward the extracellular surface (Figure 2a). This

https://doi.org/10.1021/acsptsci.4c00051
ACS Pharmacol. Transl. Sci. 2024, 7, 1415−1425

ACS Pharmacology & Translational Science pubs.acs.org/ptsci Article

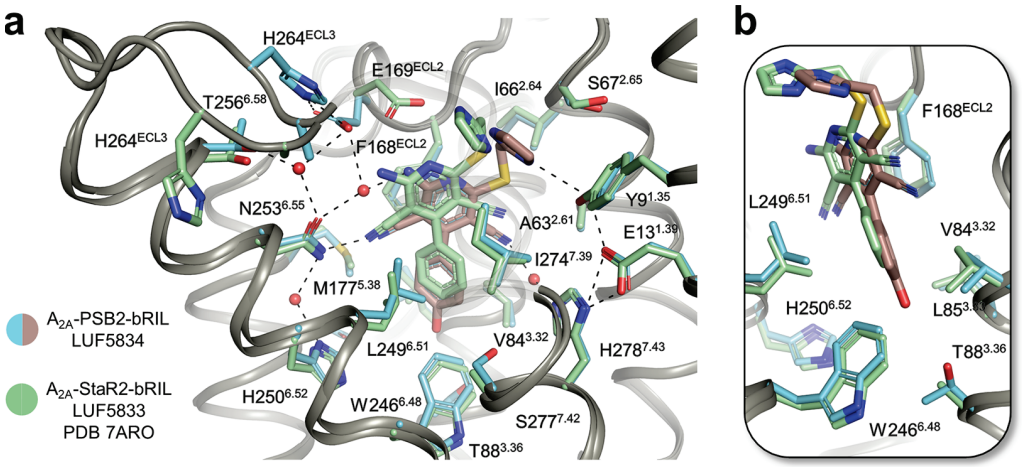

Figure 3. Comparison of the ligand binding pockets of LUF5833 (nonphenolic) and LUF5834 (phenolic). (a) Superposition of the ligand binding pocket of A_{2A}-PSB2-bRIL-LUF5834 (present study) with A_{2A}-StaR2-bRIL-LUF5833 (PDB 7ARO); (b) ligand binding poses and neighboring amino acids of LUF5833 and the phenolic LUF5834 forming a hydrogen bond with $T88^{3.36}$. Note that $T88^{3.36}$ is mutated to alanine in the A_{2A}-StaR2-bRIL construct.

Table 2. Affinities of NECA and LUF5834 Using Different A_{2A}AR Constructs[a]

			NECA	LUF5834
A_{2A}AR construct	radioligand	cell type	pK_i [K_i, *nM*]	pK_i ± SEM [K_i, *nM*]
	[^{3}H]NECA	CHO	**8.15**[b] [*7.06*]	**8.04** ± 0.04^{ns}[*9.12*]
A_{2A} wt	[^{3}H]MSX-2	CHO	**7.00**[c] [*99.2*]	**7.03** ± 0.10**[*93.3*]
	[^{3}H]MSX-2	*Sf9*	**6.25**[d] [*563*]	**7.75** ± 0.04[*17.8*]
A_{2A}-ΔC	[^{3}H]MSX-2	*Sf9*	**6.65**[d] [*223*]	n.d.
A_{2A}-PSB1-bRIL	[^{3}H]MSX-2	*Sf9*	>100,000[d]	**6.49** ± 0.14***[*324*]
A_{2A}-StaR2-bRIL	[^{3}H]MSX-2	*Sf9*	>100,000[d]	**7.16** ± 0.07*[*69.2*]

[a] pK_i values were determined as means ± standard error of the mean (SEM) from three independent experiments using radioligand binding assays with antagonist ([^{3}H]MSX-2) or agonist ([^{3}H]NECA) radioligand, respectively, performed with Sf9 insect or CHO cell membranes. A_{2A}-ΔC refers to the A_{2A}AR with truncated C-terminus (residues 1-316) which represents the length of the A_{2A}AR used for the crystallization constructs. n.d., not determined. Statistical analysis was performed to compare pK_i values of LUF5834 with its affinity to the wt A_{2A}AR (*Sf9*, [^{3}H]MSX-2) using the one-way-ANOVA (analysis of variance) with Dunnett's posthoc test: ns not significant, * $p < 0.05$, ** $p < 0.01$, *** $p < 0.001$. [b] see De Filippo et al.[35] [c] see De Filippo et al.[36] [d] see Claff et al.[9]

conformation has not been observed in any other A_{2A}AR structure so far, and the side chain position of $H264^{ECL3}$ is not clearly defined, indicating flexibility. In addition, the side chain of $E169^{ECL2}$ is rotated toward the ligand and interacts with the imidazole moiety of LUF5833 (Figure 3a). In the A_{2A}AR structure in complex with LUF5834, $H264^{ECL3}$ forms an ionic lock to $E169^{ECL2}$ instead (Figures 2a and 3a), which represents a frequent feature in A_{2A}AR crystal structures when crystals grew at acidic or neutral pH values.[9,23] The pK_a value of the $H264^{ECL3}$ side chain imidazole was calculated to 6.90 using the propKa[30,31] online tool. Thus, it is almost fully protonated at the pH value used for crystallization (pH 5.2) and is roughly 25% protonated at a physiological pH value of 7.4. This had, however, no effect on the conformation of the ECL3, which was found to be the same as in A_{2A}AR crystal structures determined at neutral pH value.[23,30]

In comparison to the phenolic LUF5834, LUF5833 is slightly rotated and shifted toward the extracellular space in the A_{2A}-StaR2-bRIL-LUF5833 structure (Figure 3a,b). The two crystal structures have been determined in the same crystal form, and a superposition did not indicate significant differences in crystal packing interactions that might be responsible for these differences (data not shown).

Information about the binding affinity of LUF5833 to the crystallization construct A_{2A}-StaR2-bRIL had not been provided in the respective publication of its A_{2A}AR cocrystal structure.[15] Herein, phenolic LUF5834 was thoroughly characterized in radioligand binding and G protein dissociation assays using wt A_{2A}AR as well as different crystallization constructs (Table 2). First, we determined the affinity of LUF5834 to the wt A_{2A}AR, recombinantly expressed in Chinese hamster ovary (CHO) cells, using cell membrane preparations and two different radioligands: (1) the antagonist [^{3}H]MSX-2 and (2) the agonist [^{3}H]*N*-ethylcarboxamidoadenosine ([^{3}H]NECA). When using the antagonist radioligand, the determined K_i value was ∼10-fold higher than that determined versus the agonist radioligand (93.3 nM vs 9.12 nM, $p = 0.0016$, two-tailed, unpaired *t* test), consistent with the (partial) agonistic nature of LUF5834. In *Spodoptera frugiperdia* (*Sf9*) insect cell membrane preparations, the affinity of LUF5834 to the wt A_{2A}AR, determined with the antagonist radioligand [^{3}H]MSX-2, was 17.8 nM (Table 2). Thus, the affinities were almost identical for the wt A_{2A}AR expressed in two different systems, CHO and *Sf9* insect cell membranes, respectively. As the next step, we validated the binding affinity of LUF5834 to the stabilized crystallization constructs. To this end, we used A_{2A}-PSB1-bRIL expressed in

https://doi.org/10.1021/acsptsci.4c00051
ACS Pharmacol. Transl. Sci. 2024, 7, 1415−1425

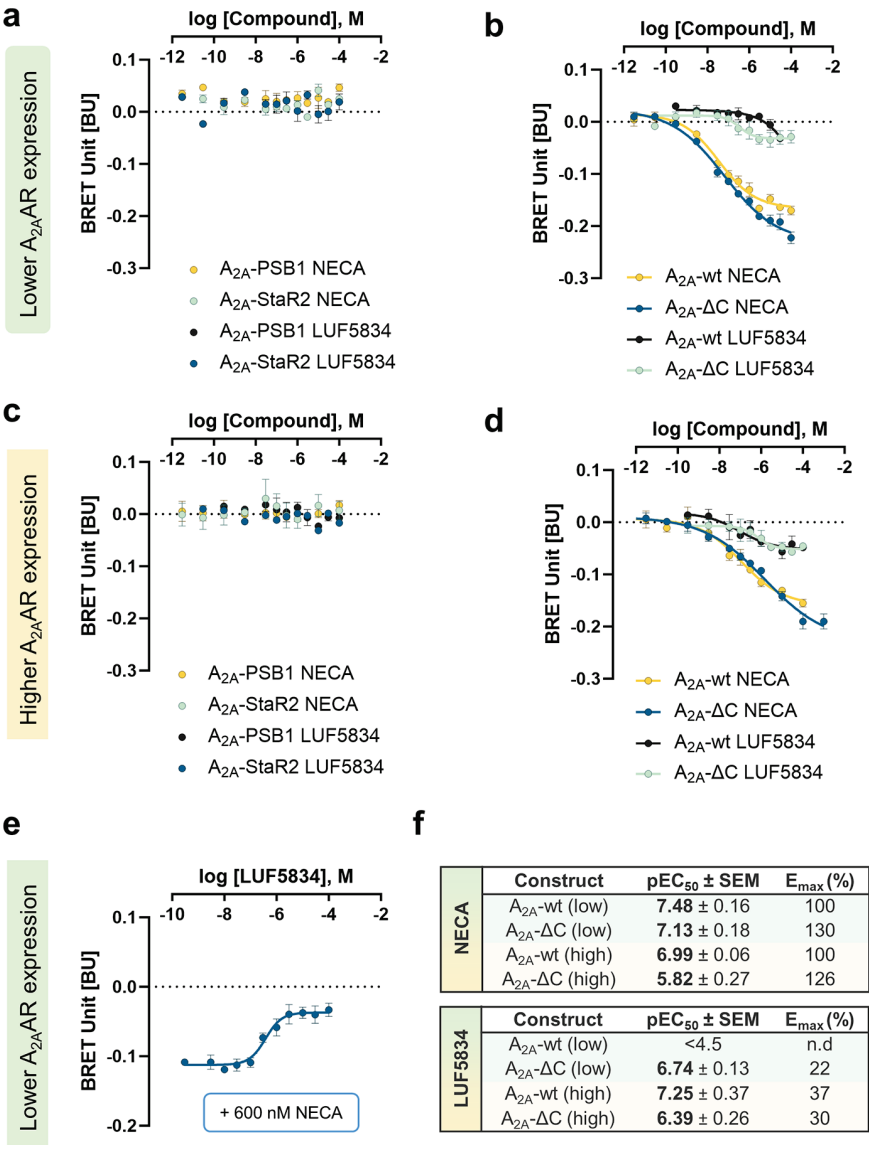

	Construct	pEC_{50} ± SEM	E_{max} (%)
NECA	A_{2A}-wt (low)	**7.48** ± 0.16	100
	A_{2A}-ΔC (low)	**7.13** ± 0.18	130
	A_{2A}-wt (high)	**6.99** ± 0.06	100
	A_{2A}-ΔC (high)	**5.82** ± 0.27	126

	Construct	pEC_{50} ± SEM	E_{max} (%)
LUF5834	A_{2A}-wt (low)	<4.5	n.d
	A_{2A}-ΔC (low)	**6.74** ± 0.13	22
	A_{2A}-wt (high)	**7.25** ± 0.37	37
	A_{2A}-ΔC (high)	**6.39** ± 0.26	30

Figure 4. BRET-based $G\alpha_s$ protein dissociation assays with NECA and LUF5834 at different A_{2A}AR constructs. Dose−response curves of NECA and LUF5834 as agonists at low (a) and (c) high A_{2A}AR expression levels of human A_{2A}AR crystallization constructs A_{2A}-PSB1 and A_{2A}-StaR2 with ICL3-bRIL fusions restored back to wt. Dose−response curves of NECA and LUF5834 as an agonist at low (b) and high (d) A_{2A}AR expression levels of human A_{2A}AR constructs, A_{2A}-wt and A_{2A}-ΔC. (e) LUF5834 in the presence of NECA-induced A_{2A}AR $G\alpha_s$-$G\beta\gamma$ dissociation. NECA at its EC_{80} (EC_{80} 600 nM) concentration was used to stimulate the A_{2A}AR. LUF5834 was able to inhibit the NECA-induced A_{2A}AR $G\alpha_s$-$G\beta\gamma$ dissociation with an IC_{50} value of 394 ± 62 nM. (f) Potency (pEC_{50}) and efficacy (E_{max}) of NECA and LUF5834 at different A_{2A}AR constructs. Efficacy relative to the maximal effect of NECA (100 μM) at the wt A_{2A}AR was set at 100%. All experiments were determined in G protein dissociation assay[39] with $G\alpha_s$-short-Rluc8-$G\beta_3$-$G\gamma_9$-GFP2 biosensors. Each of the A_{2A}AR constructs was transfected with the amount of 100 ng DNA per 10^6 cells (maintained at a ratio of 1:1 within the biosensors) for panel a, b, and e, whereas 250 ng DNA was used for panels c and d, respectively. Data represent means ± SEM of at least three independent experiments.

Sf9 insect cells,[9] which differs from the construct used for structure determination in this study, A_{2A}-PSB2-bRIL, only by a single peripheral mutation introduced to remove a glycosylation site ($N154^{ECL2}$A in the crystallized construct, Figure 1b,d).[23] In addition, we studied the affinity of LUF5834 for A_{2A}-StaR2-bRIL. The affinities of LUF5834 for both crystallization constructs were lower (18-fold and 4-fold, respectively, Table 2) than those for the wt A_{2A}AR expressed in *Sf9* insect cells (324 and 69.2 nM). Thus, although the A_{2A}-StaR2-bRIL construct contains two mutations inside the ligand binding pocket that prevent the binding of full agonists,[23] the affinity of the partial agonist LUF5834 was only moderately affected (Table 2). The general conformational changes required for agonist binding are likely not impeded by the mutations in the A_{2A}-StaR2-bRIL construct, i.e., both agonistic and antagonistic binding pocket conformations may still be possible. In contrast, the $S91^{3.39}$K mutation in the A_{2A}-PSB1-bRIL construct stabilizes a constitutively inactive state of the A_{2A}AR that provides a plausible explanation for the affinity reduction of LUF5834 in this construct. The full AR agonist NECA does not bind to either crystallization construct, whereas it displays submicromolar affinity to the wt A_{2A}AR and its *C*-terminally truncated analog (A_{2A}-ΔC) expressed in *Sf9* insect cells, determined versus the antagonist radioligand

ACS Pharmacology & Translational Science pubs.acs.org/ptsci Article

[^{3}H]MSX-2 (Table 2). The GPCR-G protein complex generally displays higher affinity for agonists than the GPCR alone.[32,33] Therefore, the lower affinity of NECA for the wt A_{2A}AR expressed in insect cells may originate from the fact that proper G proteins are lacking.[34]

Next, we determined the potency and efficacy of LUF5834 at the wt A_{2A}AR, A_{2A}-ΔC, A_{2A}-PSB1, and A_{2A}-StaR2 in functional assays (Figure 4). Due to steric inhibition of G protein binding, the bRIL fusion protein was removed, and the original intracellular loop 3 was restored. We employed a bioluminescence resonance energy transfer (BRET)-based G protein dissociation assay[37−39] by cotransfecting the respective A_{2A}AR gene (ADORA2A) together with a *Renilla* luciferase (Rluc8)-coupled Gα_s subunit, Gβ_3, and Gγ_9 (fused to Green Fluorescent Protein (GFP)). Two different amounts of A_{2A}AR plasmid were transfected (100 ng or 250 ng), in order to modify the expression level of the A_{2A}AR receptor.[40−42] In either setting, both constructs, A_{2A}-PSB1 and A_{2A}-StaR2, could not be activated by the full agonist NECA and did not show any signs of activation by the partial agonist LUF5834 (Figure 4a,c). In contrast, NECA showed a concentration-dependent activation of both the wt A_{2A}AR and A_{2A}-ΔC with nM potency (100 ng transfection) (Figure 4b). Upon the higher expression level (250 ng plasmid, Figure 4d), the potency of NECA appeard to slightly decrease for at wt A_{2A}AR (EC_{50} 33.1 nM vs 102 nM, $p = 0.0212$, two-tailed, unpaired t test), and by 20-fold for A_{2A}-ΔC (EC_{50} 74.1 nM vs 1513 nM, $p = 0.0393$, two-tailed, unpaired t test), in contrast to the concept of receptor reserve.[43,44] The partial agonist LUF5834 barely activated the wt A_{2A}AR in the cell line with the lower transfection level, but showed a concentration-dependent activation of the wt A_{2A}AR with an EC_{50} value of 56.2 nM and 37% efficacy in the high-expressing cells (compared to the maximal effect of NECA (at 100 μM) in the cell line with the high expression level of the wt A_{2A}AR, set at 100%, Figure 4b,d). LUF5834 activated A_{2A}-ΔC at both A_{2A}AR expression levels (EC_{50} 182 and 407 nM, $p = 0.105$, two-tailed, unpaired t test). Therefore, the *C*-terminally truncated A_{2A}AR construct likely shows higher expression levels than the wt A_{2A}AR. Our results confirm that LUF5834 is a partial A_{2A}AR agonist whose intrinsic activity depends on receptor density. The efficacies of LUF5834 in the cells with the higher expression level were consistent with partial agonism (∼30−37%) (Figure 4d). Next, we investigated the effect of LUF5834 on NECA-induced Gα_s activation employed at its EC_{80} value (EC_{80}, NECA: 600 nM) (Figure 4e). In this setting, LUF5834 acted as an antagonist (IC_{50} = 372 nM), reducing the maximal response of NECA by approximately 70% at the highest tested concentration of 100 μM LUF5834.

Despite growing knowledge about structures and interactions of partial agonists, the exact mechanism of partial activation of GPCRs is not fully understood and may vary between structurally diverse ligands and receptors.[45] A widely accepted theory for partial agonists assumes that they stabilize a conformational state which is different from that of a full agonist.[46,47] They are suggested to thereby induce a lower affinity state for the G protein and weaker G protein activation, ultimately leading to less effective nucleotide exchange. This hypothesis was supported by nuclear magnetic resonance (NMR) experiments,[16,18,48] and by allosteric nanobodies.[49] However, cryo-electron microscopy (cryo-EM) structures in complex with G proteins showed similar (nucleotide-free) G protein conformations for partial agonists and full agonists, e.g., for the A_{2B}AR[29,50] or for serotonin receptors.[51] While the new A_{2A}AR structure in complex with the potent partial agonist LUF5834 does not provide a direct understanding of partial agonism at the A_{2A}AR, we do show that LUF5834 still binds to a receptor construct that presents a constitutively inactive conformation (A_{2A}-PSB1-bRIL), albeit with lower affinity than to the wt A_{2A}AR. In contrast, we previously showed that the full agonist NECA does not show any binding to the A_{2A}-PSB1-bRIL construct (at concentrations of up to 3 mM, determined vs. the antagonist radioligand [^{3}H]MSX-2), whereas the affinity of antagonists and of the antagonist radioligand itself was unaffected.[9] It is worth noting that structures of NECA have been solved with[33,52] or without[53] G proteins. While intracellular rearrangements and especially the extent of the outward movement of helix VI are largely dependent on the presence of G proteins, the ligand binding pocket in these full agonist-bound structures is identical—independent of the presence of G proteins—and clearly distinct from the inactive receptor conformation. Hence, another explanation for the partial agonistic activity of LUF5834 may be that it originates from its binding to both inactive and active states of the A_{2A}AR, whereas full A_{2A}AR agonists only exhibit affinity for the active state, as supported by radioligand binding using the full agonist NECA.[9] Protein NMR experiments performed with the β_2-adrenergic receptor showed that partial agonists, in contrast to full agonists, indeed stabilized an equilibrium of both inactive and active conformations.[52] Therefore, the conformational selection of full A_{2A}AR agonists would be restricted to active states, thus resulting in greater efficacy, in contrast to partial agonists. Interestingly, NMR[18] and single-molecule Förster resonance energy transfer (smFRET) investigations of the A_{2A}AR in complex with LUF5834 revealed distinct conformations when compared to those found for NECA or the antagonist ZM241385.[53] However, the covalent β_2-adrenergic receptor agonist FAUC50[54] as well as β_1-adrenergic receptor agonists[55] were reported to stably bind to inactive conformations without G proteins present. Alternatively, the partial agonistic mechanism of action may also be explained by a combination of the above-mentioned principles[56] and may even be different for various GPCRs or ligands.

CONCLUSIONS

The present study offers a detailed elucidation of the interactions between the A_{2A}AR and the partial agonist LUF5834, as revealed through high-resolution cocrystal structure analysis using the optimized crystallization construct A_{2A}-PSB2-bRIL. LUF5834 was observed to be anchored by hydrogen bonding to $N253^{6.55}$ and aromatic stacking interactions to $F168^{ECL2}$ whereas its imidazole moiety is located in a subpocket between helices I and VII. Previous knowledge of partial agonist binding at the A_{2A}AR was solely based on a structure of moderate resolution (3.12 Å) in complex with the related partial agonist LUF5833 using the crystallization construct A_{2A}-StaR2-bRIL which contains mutations in the ligand binding pocket.[15] The new A_{2A}AR structure in complex with LUF5834, determined at a higher resolution of 2.43 Å, revealed similar interactions for LUF5834 but additionally resolved a tight water network within the binding pocket. $T88^{3.36}$ is directly involved in hydrogen bonding to the phenolic group of LUF5834; this amino acid was mutated to alanine in the A_{2A}-StaR2-bRIL construct used for the previous LUF5833 structure. Moreover, our structures

https://doi.org/10.1021/acsptsci.4c00051
ACS Pharmacol. Transl. Sci. 2024, 7, 1415−1425

ACS Pharmacology & Translational Science pubs.acs.org/ptsci Article

revealed a well-folded ECL3, similar to previous A_{2A}AR structures, whereas the A_{2A}-StaR2-bRIL-LUF5833 structures showed an unusually folded ECL3.[15] We showed that, in contrast to full A_{2A}AR agonists,[9] LUF5834 binds to a constitutively inactive conformation of the A_{2A}AR, albeit with lower affinity. While many hypotheses on the mechanism behind partial agonism exist, this dual affinity for both inactive and active states may explain the decreased efficacy of the partial agonist LUF5834 as compared to full agonists at the A_{2A}AR. Our findings are crucial for advancing knowledge on GPCR signaling and may have significant implications for developing new and more effective therapeutic agents targeting GPCRs.

METHODS

Expression, Purification, and Crystallization of A_{2A}-PSB2-bRIL. The A_{2A}-PSB2-bRIL construct was expressed in *Sf9* insect cells and purified as previously described for the A_{2A}-PSB2-bRIL-Etrumadenant complex.[23] Briefly, *Sf9* insect cell membranes were prepared by repeated washing with low- and high-osmotic buffers in the absence of any ligands. The purified membranes were incubated with 50 μM LUF5834 [obtained from Tocris, cat. no. 4603, and dissolved in dimethyl sulfoxide (DMSO)] and 2 mg per ml iodoacetamide for 1 h. Then, proteins were solubilized from the membranes for 3 h at 4 °C with a buffer consisting of 55 mM HEPES pH 7.5 (4 °C), 5 mM KCl, 5 mM $MgCl_2$, 800 mM NaCl, 15% glycerol, 0.75% (w/v) dodecyl-β-D-maltoside (DDM), and 0.15% (w/v) cholesteryl hemisuccinate (CHS). Solubilized proteins were separated from the membranes by centrifugation at 50,000 *g*. The supernatant was supplemented with 20 mM imidazole and incubated with Co^{2+}-based immobilized metal affinity chromatography resin (TALON Superflow, Cytiva), followed by overnight incubation at 4 °C. The next day, the A_{2A}-PSB2-bRIL-LUF5834 complex was purified using gravity flow chromatography with buffers containing 50 μM LUF5834 and varying imidazole concentrations, as previously described.[9,23] Then, the complex was eluted using the final protein buffer consisting of 25 mM HEPES pH 7.5 (4 °C), 800 mM NaCl, 10% (v/v) glycerol, 220 mM imidazole, 0.025% (w/v) DDM, 0.005% (w/v) CHS, and 50 μM LUF5834. The protein complex was concentrated to approximately 30 mg per ml in the same elution buffer using 100 kDa molecular weight cutoff concentrators (Vivaspin, Sartorius) and immediately used for lipidic cubic phase (LCP) crystallization. Monodispersity of the complex and purity were analyzed by analytical size-exclusion chromatography and sodium dodecyl sulfate−polyacrylamide gel electrophoresis. The LCP was produced by mixing protein with a molten lipid mixture [90% (w/v) 1-oleyl-*rac*-glycerin (Sigma), 10% (w/v) cholesterol (Sigma)] in a 2−3 ratio using the two-syringe method.[57] The automatic crystallization robot Formulatrix NT8 was used to overlay 50 nL of the resulting mesophase with 800 μL of precipitant solution on glass sandwich plates (Marienfeld). Crystallization plates were sealed and incubated at 20 °C using a Formulatrix RockImager54 until crystal harvesting. The A_{2A}-PSB2-bRIL-LUF5834 complex crystallized in the following precipitant solution: 23% (w/v) PEG400, 90 mM sodium thiocyanate, 100 mM sodium citrate (pH 5.2), and 2% (w/v) 2,5-hexandiol. Crystals were harvested using micromounts (MiTeGen) and flash-frozen in liquid nitrogen without further cryoprotection.

Crystal Structure Determination. X-ray diffraction data were collected at 100 K (X-ray wavelength 0.97621 Å) using the European Molecular Biology Laboratory (EMBL) beamline P14 of the German Electron Synchrotron (DESY, Hamburg). Reflections were collected using an EIGER2 16M detector, while the crystal was rotated for 360° at 0.25° increments with an exposure of 0.017 s. The data sets were indexed, integrated, scaled, and converted to structure factor amplitudes using ISPyB,[58] autoPROC,[59] XDS,[60] CCP4,[61] POINTLESS,[62] AIMLESS,[63] and STARANISO.[64] Data collection and refinement statistics are listed in Table 1. The model of PDB ID 5IU4 was used as the starting model for refinement with Phenix.[65] Coot[66] was used for further model building. The stereochemical restraints for LUF5834 were generated with the GRADE web server.[67]

As the electron density of the ligand was less well-defined than that of the surrounding amino acids, we refined the occupancy of the ligand to a value of 0.7. Two water molecules (residue numbers 59 and 61, shown in Figure 2A) are coordinated to the ligand and to protein residues. These water molecules have distances of only ∼2.4 Å to the ligand or protein, but we assume that they bind together with the ligand. The short distances likely result from the influence of alternatively occupied water positions in the absence of the ligand (i.e., with occupancy of max. ∼0.3) and limitations of the precision of the refined water positions.

Radioligand Binding Assays. CHO or *Sf9* insect cell preparations recombinantly expressing the desired AR construct were used for radioligand binding studies as previously described.[23,68] In order to determine A_{2A}AR binding, the radioligands [^{3}H]MSX-2 (antagonist, 1 nM) or [^{3}H]NECA (agonist, 10 nM) were employed, respectively. Assays were performed in 50 mM *Tris*(hydromethyl)-aminomethan (Tris) buffer pH 7.4 in a final volume of 400 μL. Assays with [^{3}H]NECA contained 10 mM $MgCl_2$ in the buffer. NECA and LUF5834 were dissolved in DMSO and incubated with the respective A_{2A}AR membrane preparation and radioligand at room temperature for 30 min ([^{3}H]MSX-2), or at 25 °C for 2 h ([^{3}H]NECA) with a final DMSO concentration of 1%. The membranes were separated from the free radioligand by filtration through GF/B glass fiber filters using a cell harvester (Brandel). Filters were presoaked in an aqueous solution of 0.3% (w/v) polyethylenimine for at least 30 min to reduce nonspecific binding. Radioactivity was counted after incubation for at least 9 h with a scintillation cocktail (Beckmann Coulter) using a scintillation counter (Tricarb 2700TR). Statistical evaluations were performed on pK_i values using ANOVA or Student's *t* test (two-tailed, unpaired) as indicated.

G Protein Dissociation Assays. G protein dissociation assays were performed with the TRUPATH BRET^2 assay [TRUPATH was a gift from Bryan Roth (Addgene kit #1000000163)].[39] All A_{2A}AR plasmids were cloned into the pcDNA3.1(+) plasmid: A_{2A}AR-wt, A_{2A}AR with 95 *C*-terminal amino acids truncated (A_{2A}-ΔC), A_{2A}-ΔC containing S91$^{3.39}$K and N154^{ECL2}A mutations (A_{2A}-PSB2), and A_{2A}-ΔC containing A54$^{2.52}$L, T88$^{3.36}$A, R107$^{3.55}$A, K122$^{4.43}$A, L202$^{5.63}$A, L235$^{6.37}$A, V239$^{6.41}$A, S277$^{7.42}$A, and N154 ^{ECL2}A mutations (A_{2A}-StaR2). The TRUPATH BRET^2 assays were performed according to previously described procedures in human embryonic kidney (HEK293) cells employing the combination of Gα_s-Rluc8, Gβ_3, and Gγ_9-GFP2 biosensors.[9,23,39,40] The agonists NECA (Santa Cruz Biotechnology) and LUF5834

https://doi.org/10.1021/acsptsci.4c00051
ACS Pharmacol. Transl. Sci. 2024, 7, 1415−1425

ACS Pharmacology & Translational Science pubs.acs.org/ptsci Article

(Tocris Bioscience) were dissolved in DMSO while coeleterazine400a (CTZ400a, Cayman Chemical), used as a Rluc8 substrate, was dissolved in ethanol. HEK293 cells were transfected in 6-well plates with Lipofectamine 2000, following the manufacturer's protocol. The cells were transfected with either a 1:1:1:1 DNA ratio (A_{2A} receptor construct: Gα_s-Rluc8, Gβ_3, and Gγ_9-GFP2)—for the lower expression level, or a 2.5:1:1:1 ratio (A_{2A} wt: Gα_s-Rluc8, Gβ_3, Gγ_9-GFP2)—for higher expression level. The cells were harvested and seeded into a white 96-well plate 24 h after transfection. All measurements were conducted approximately 48 h post-transfection. On the day of the experiment, the medium was carefully removed and exchanged for 60 μL of assay buffer (Hank's Balanced Salt Solution plus 20 mM HEPES, pH 7.4) and 5 μg of adenosine deaminase (ADA) per mL of assay buffer. Agonist solution (NECA or LUF5834) was further diluted in assay buffer to the desired concentrations and added to the cells (in a volume of 30 μL) 5 min after the addition of CTZ400a (final concentration of CTZ400a: 5 μM). For antagonist measurements, LUF5834 was added to the cells in a volume of 15 μL and incubated for 15 min before the addition of CTZ400a. NECA (15 μL) was then added 5 min after the addition of CTZ400a solution at its EC_{80} concentrations (NECA EC_{80}: 600 nM). $BRET^2$ measurements were performed using an LB Mitras940 instrument with a 395 nm emission filter for Rluc8 and a 515 nm emission filter for the GFP2 protein. The $BRET^2$ ratio was obtained by dividing the GFP2 fluorescence by the Rluc8 luminescence. The BRET Unit (BU) or NET BRET was calculated by subtracting the BRET ratio values from the test compounds with the vehicle's (DMSO) BRET ratio. Data normalization for LUF5834 was performed by normalizing data to the control (100% activation = NECA without LUF5834, 0% activation = no agonist). GraphPad PRISM v10 was used for generating nonlinear sigmoidal curves with variable slope for all data. Statistical evaluations were performed on pEC_{50} values using Student's *t* test (two-tailed, unpaired).

■ ASSOCIATED CONTENT

Data Availability Statement

The atomic coordinates of the A_{2A}-PSB2-bRIL-LUF5834 complex have been deposited in the PDB with accession code 8RLN.

■ AUTHOR INFORMATION

Corresponding Author

Christa E. Müller − *PharmaCenter Bonn & Pharmaceutical Institute, Department of Pharmaceutical & Medicinal Chemistry, University of Bonn, Bonn 53113, Germany; Research Training Group 2873, University of Bonn, Bonn 53121, Germany*; Email: christa.mueller@uni-bonn.de

Authors

Tobias Claff − *PharmaCenter Bonn & Pharmaceutical Institute, Department of Pharmaceutical & Medicinal Chemistry, University of Bonn, Bonn 53113, Germany*; orcid.org/0000-0001-8186-107X

Andhika B. Mahardhika − *PharmaCenter Bonn & Pharmaceutical Institute, Department of Pharmaceutical & Medicinal Chemistry, University of Bonn, Bonn 53113, Germany; Research Training Group 2873, University of Bonn, Bonn 53121, Germany*

Victoria J. Vaaßen − *PharmaCenter Bonn & Pharmaceutical Institute, Department of Pharmaceutical & Medicinal Chemistry, University of Bonn, Bonn 53113, Germany*

Jonathan G. Schlegel − *PharmaCenter Bonn & Pharmaceutical Institute, Department of Pharmaceutical & Medicinal Chemistry, University of Bonn, Bonn 53113, Germany*

Christin Vielmuth − *PharmaCenter Bonn & Pharmaceutical Institute, Department of Pharmaceutical & Medicinal Chemistry, University of Bonn, Bonn 53113, Germany*

Renato H. Weiße − *Institute of Bioanalytical Chemistry, Center for Biotechnology and Biomedicine, Leipzig University, Leipzig 04103, Germany*

Norbert Sträter − *Institute of Bioanalytical Chemistry, Center for Biotechnology and Biomedicine, Leipzig University, Leipzig 04103, Germany*; orcid.org/0000-0002-2001-0500

Complete contact information is available at: https://pubs.acs.org/10.1021/acsptsci.4c00051

Author Contributions

#T.C. and A.B.M. contributed equally to this work. T.C., A.B.M., and C.E.M. contributed to conceptualization. T.C., A.B.M., V.J.V., J.G.S., N.S., and C.E.M. contributed to validation. T.C., A.B.M., and N.S contributed to formal analysis. T.C., A.B.M., V.J.V., J.G.S., C.V., and R.H.W contributed to investigation. T.C. and A.B.M. contributed to visualization. N.S. and C.E.M. contributed to supervision. N.S. and C.E.M. contributed to funding acquisition. C.E.M. contributed to project administration. The manuscript was written through contributions of all authors. All authors have given approval to the final version of the manuscript.

Notes

The authors declare no competing financial interest.

■ ACKNOWLEDGMENTS

We thank Dr. Bryan Roth, University of North Carolina School of Medicine, Chapel Hill, NC, USA, for sharing the TRUPATH Biosensor Platform. T.C., A.B.M., V.J.V., and C.E.M. acknowledge support by the German Federal Ministry of Research and Technology (BMBF) for the project Bonn International Graduate School of Drug Sciences (BIGS-DrugS). A.B.M. and C.E.M. express their gratitude for the support from the Deutsche Forschungsgemeinschaft (DFG), in the scheme of GRK1873 (Pharmacology of 7TM-receptors and downstream signaling pathways, project number 214362475) and GRK2873 (Tools and drugs of the future—innovative methods and new modalities in medicinal chemistry, project number 494832089). A.B.M. has received funding from the Ministry of Finance Indonesia through the Indonesia Endowment Fund for Education (Lembaga Pengelola Dana Pendidikan (LPDP)). N.S. thanks the DFG for financial support (CRC 1423, project number 421152132, subproject A6). We acknowledge DESY (Hamburg, Germany), a member of the Helmholtz Association HGF, and the EMBL for the provision of experimental facilities at synchrotron beamlines P13 and P14. We thank Dr. Isabel Bento for assistance in using the EMBL beamlines. The abstract graphic was created with BioRender.com.

■ ABBREVIATIONS

AR adenosine receptor

BRET	bioluminescence resonance energy transfer
bRIL	thermostabilized apocytochrome b_{562}RIL
CHO	Chinese hamster ovary
cryo-EM	cryo-electron microscopy
GFP	green Fluorescent Protein
GPCR	G protein-coupled receptor
HEK	human embryonic kidney
NECA	*N*-ethylcarboxamidoadenosine
NMR	nuclear magnetic resonance
PDB	Protein Data Bank
PSB	Pharmaceutical Sciences Bonn
Rluc	*Renilla* luciferase
SEM	standard error of the mean
StaR	"stabilized receptor"

REFERENCES

(1) Borea, P. A.; Gessi, S.; Merighi, S.; Vincenzi, F.; Varani, K. Pharmacology of adenosine receptors: the state of the art. *Physiol. Rev.* **2018**, *98*, 1591−1625.
(2) IJzerman, A. P.; Jacobson, K. A.; Müller, C. E.; Cronstein, B. N.; Cunha, R. A.; Ohlstein, E. International union of basic and clinical pharmacology. CXII: adenosine receptors: a further update. *Pharmacol. Rev.* **2022**, *74*, 340−372.
(3) Jenner, P.; Mori, A.; Hauser, R.; Morelli, M.; Fredholm, B. B.; Chen, J. F. Adenosine, adenosine A_{2A} antagonists, and Parkinson's disease. *Parkinsonism Relat. Disord.* **2009**, *15*, 406−413.
(4) Müller, C. E.; Jacobson, K. A. Recent developments in adenosine receptor ligands and their potential as novel drugs. *Biochim. Biophys. Acta* **2011**, *1808*, 1290−1308.
(5) Launay, A.; Nebie, O.; Vijaya Shankara, J.; Lebouvier, T.; Buée, L.; Faivre, E.; Blum, D. The role of adenosine A_{2A} receptors in Alzheimer's disease and tauopathies. *Neuropharmacology* **2023**, *226*, 109379.
(6) Illes, P.; Ulrich, H.; Chen, J.-F.; Tang, Y. Purinergic receptors in cognitive disturbances. *Neurobiol. Dis.* **2023**, *185*, 106229.
(7) Ohta, A.; Gorelik, E.; Prasad, S. J.; Ronchese, F.; Lukashev, D.; Wong, M. K. K.; Huang, X.; Caldwell, S.; Liu, K.; Smith, P.; et al. A_{2A} adenosine receptor protects tumors from antitumor T cells. *Proc. Natl. Acad. Sci. U. S. A.* **2006**, *103*, 13132−13137.
(8) Fredholm, B. B.; IJzerman, A. P.; Jacobson, K. A.; Linden, J.; Müller, C. E. International Union of Basic and Clinical Pharmacology. LXXXI. Nomenclature and classification of adenosine receptors - an update. *Pharmacol. Rev.* **2011**, *63*, 1−34.
(9) Claff, T.; Klapschinski, T. A.; Subhramanyam, U. K. T.; Vaaßen, V. J.; Schlegel, J. G.; Vielmuth, C.; Voß, J. H.; Labahn, J.; Müller, C. E. Single stabilizing point mutation enables high-resolution co-crystal Structures of the adenosine A_{2A} receptor with preladenant conjugates. *Angew. Chem., Int. Ed.* **2022**, *61*, No. e202115545.
(10) Congreve, M.; Brown, G. A.; Borodovsky, A.; Lamb, M. L. Targeting adenosine A_{2A} receptor antagonism for treatment of cancer. *Expert Opinion Drug Discovery* **2018**, *13*, 997−1003.
(11) Rosentreter, U.; Henning, R.; Bauser, M.; Krämer, T.; Vaupel, A.; Hübsch, W.; Dembowsky, K.; Salcher-Schraufstätter, O.; Stasch, J.-P.; Krahn, T., et al. Substituted 2-thio-3,5-dicyano-4-aryl-6-amino-pyridines and the use thereof, WO 01/25210 A2, 2001.
(12) Hinz, S.; Lacher, S. K.; Seibt, B. F.; Müller, C. E. BAY60-6583 Acts as a Partial Agonist at Adenosine A $_{2B}$ Receptors. *J. Pharmacol. Exp. Ther.* **2014**, *349*, 427−436.
(13) Baltos, J.-A.; Vecchio, E. A.; Harris, M. A.; Qin, C. X.; Ritchie, R. H.; Christopoulos, A.; White, P. J.; May, L. T. Capadenoson, a clinically trialed partial adenosine A_1 receptor agonist, can stimulate adenosine A_{2B} receptor biased agonism. *Biochem. Pharmacol.* **2017**, *135*, 79−89.
(14) Beukers, M. W.; Chang, L. C. W.; von Frijtag Drabbe Künzel, J. K.; Mulder-Krieger, T.; Spanjersberg, R. F.; Brussee, J.; IJzerman, A. P. New, non-adenosine, high-potency agonists for the human adenosine A_{2B} receptor with an improved selectivity profile compared to the reference agonist N-ethylcarboxamidoadenosine. *J. Med. Chem.* **2004**, *47*, 3707−3709.
(15) Amelia, T.; van Veldhoven, J. P. D.; Falsini, M.; Liu, R.; Heitman, L. H.; van Westen, G. J. P.; Segala, E.; Verdon, G.; Cheng, R. K. Y.; Cooke, R. M.; et al. Crystal structure and subsequent ligand design of a nonriboside partial agonist bound to the adenosine A_{2A} receptor. *J. Med. Chem.* **2021**, *64*, 3827−3842.
(16) Ye, L.; van Eps, N.; Zimmer, M.; Ernst, O. P.; Prosser, R. S. Activation of the A_{2A} adenosine G-protein-coupled receptor by conformational selection. *Nature* **2016**, *533*, 265−268.
(17) Navarro, G.; Gonzalez, A.; Campanacci, S.; Rivas-Santisteban, R.; Reyes-Resina, I.; Casajuana-Martin, N.; Cordomí, A.; Pardo, L.; Franco, R. Experimental and computational analysis of biased agonism on full-length and a C-terminally truncated adenosine A_{2A} receptor. *Comput. Struct. Biotechnol. J.* **2020**, *18*, 2723−2732.
(18) Eddy, M. T.; Martin, B. T.; Wüthrich, K. A_{2A} adenosine receptor partial agonism related to structural rearrangements in an activation microswitch. *Structure* **2021**, *29*, 170−176.e3.
(19) Fernandes, D. D.; Neale, C.; Gomes, G.-N. W.; Li, Y.; Malik, A.; Pandey, A.; Orazietti, A. P.; Wang, X.; Ye, L.; Scott Prosser, R.; et al. Ligand modulation of the conformational dynamics of the A_{2A} adenosine receptor revealed by single-molecule fluorescence. *Sci. Rep.* **2021**, *11*, 5910.
(20) Doré, A. S.; Robertson, N.; Errey, J. C.; Ng, I.; Hollenstein, K.; Tehan, B.; Hurrell, E.; Bennett, K.; Congreve, M.; Magnani, F.; et al. Structure of the adenosine A_{2A} receptor in complex with ZM241385 and the xanthines XAC and caffeine. *Structure* **2011**, *19*, 1283−1293.
(21) Chu, R.; Takei, J.; Knowlton, J.; Andrykovitch, M.; Pei, W.; Kajava, A. V.; Steinbach, P. J.; Ji, X.; Bai, Y. Redesign of a four-helix bundle protein by phage display coupled with proteolysis and structural characterization by NMR and X-ray crystallography. *J. Mol. Biol.* **2002**, *323*, 253−262.
(22) Lane, J. R.; Klein Herenbrink, C.; van Westen, G. J. P.; Spoorendonk, J. A.; Hoffmann, C.; IJzerman, A. P. A novel nonribose agonist, LUF5834, engages residues that are distinct from those of adenosine-like ligands to activate the adenosine A_{2A} receptor. *Mol. Pharmacol.* **2012**, *81*, 475−487.
(23) Claff, T.; Schlegel, J. G.; Voss, J. H.; Vaaßen, V. J.; Weiße, R. H.; Cheng, R. K. Y.; Markovic-Mueller, S.; Bucher, D.; Sträter, N.; Müller, C. E. Crystal structure of adenosine A_{2A} receptor in complex with clinical candidate Etrumadenant reveals unprecedented antagonist interaction. *Commun. Chem.* **2023**, *6*, 106.
(24) Yasuda, S.; Kajiwara, Y.; Takamuku, Y.; Suzuki, N.; Murata, T.; Kinoshita, M. Identification of thermostabilizing mutations for membrane proteins: rapid method based on statistical thermodynamics. *J. Phys. Chem. B* **2016**, *120*, 3833−3843.
(25) Kimura, K. T.; Asada, H.; Inoue, A.; Kadji, F. M. N.; Im, D.; Mori, C.; Arakawa, T.; Hirata, K.; Nomura, Y.; Nomura, N.; et al. Structures of the 5-HT_{2A} receptor in complex with the antipsychotics risperidone and zotepine. *Nat. Struct. Mol. Biol.* **2019**, *26*, 121−128.
(26) White, K. L.; Eddy, M. T.; Gao, Z.-G.; Han, G. W.; Lian, T.; Deary, A.; Patel, N.; Jacobson, K. A.; Katritch, V.; Stevens, R. C. Structural connection between activation microswitch and allosteric sodium site in GPCR signaling. *Structure* **2018**, *26*, 259−269.e5.
(27) Liu, W.; Chun, E.; Thompson, A. A.; Chubukov, P.; Xu, F.; Katritch, V.; Han, G. W.; Roth, C. B.; Heitman, L. H.; IJzerman, A. P.; et al. Structural basis for allosteric regulation of GPCRs by sodium ions. *Science* **2012**, *337*, 232−236.
(28) Nygaard, R.; Frimurer, T. M.; Holst, B.; Rosenkilde, M. M.; Schwartz, T. W. Ligand binding and micro-switches in 7TM receptor structures. *Trends Pharmacol. Sci.* **2009**, *30*, 249−259.
(29) Cai, H.; Xu, Y.; Guo, S.; He, X.; Sun, J.; Li, X.; Li, C.; Yin, W.; Cheng, X.; Jiang, H.; et al. Structures of adenosine receptor A_{2B}R bound to endogenous and synthetic agonists. *Cell Discovery* **2022**, *8*, 140.
(30) Bas, D. C.; Rogers, D. M.; Jensen, J. H. Very fast prediction and rationalization of p K a values for protein−ligand complexes. *Proteins* **2008**, *73*, 765−783.

(31) Ohno, Y.; Suzuki, M.; Asada, H.; Kanda, T.; Saki, M.; Miyagi, H.; Yasunaga, M.; Suno, C.; Iwata, S.; Saito, J.-I.; et al. In vitro pharmacological profile of KW-6356, a novel adenosine A_{2A} receptor antagonist/inverse agonist. *Mol. Pharmacol.* **2023**, *103*, 311−324.
(32) Murphree, L. J.; Marshall, M. A.; Rieger, J. M.; MacDonald, T. L.; Linden, J. Human A_{2A} adenosine receptors: High-affinity agonist binding to receptor-G protein complexes containing $G\beta_4$. *Mol. Pharmacol.* **2002**, *61*, 455−462.
(33) Carpenter, B.; Nehmé, R.; Warne, T.; Leslie, A. G. W.; Tate, C. G. Structure of the adenosine A_{2A} receptor bound to an engineered G protein. *Nature* **2016**, *536*, 104−107.
(34) Schneider, E. H.; Seifert, R. Sf9 cells: a versatile model system to investigate the pharmacological properties of G protein-coupled receptors. *Pharmacol. Ther.* **2010**, *128*, 387−418.
(35) de Filippo, E.; Namasivayam, V.; Zappe, L.; El-Tayeb, A.; Schiedel, A. C.; Müller, C. E. Role of extracellular cysteine residues in the adenosine A_{2A} receptor. *Purinergic Signal.* **2016**, *12*, 313−329.
(36) de Filippo, E.; Hinz, S.; Pellizzari, V.; Deganutti, G.; El-Tayeb, A.; Navarro, G.; Franco, R.; Moro, S.; Schiedel, A. C.; Müller, C. E. A_{2A} and A_{2B} adenosine receptors: The extracellular loop 2 determines high A_{2A} or low affinity A_{2B} for adenosine. *Biochem. Pharmacol.* **2020**, *172*, 113718.
(37) Galés, C.; Rebois, R. V.; Hogue, M.; Trieu, P.; Breit, A.; Hébert, T. E.; Bouvier, M. Real-time monitoring of receptor and G-protein interactions in living cells. *Nat. Methods* **2005**, *2*, 177−184.
(38) Galés, C.; van Durm, J. J. J.; Schaak, S.; Pontier, S.; Percherancier, Y.; Audet, M.; Paris, H.; Bouvier, M. Probing the activation-promoted structural rearrangements in preassembled receptor-G protein complexes. *Nat. Struct. Mol. Biol.* **2006**, *13*, 778−786.
(39) Olsen, R. H. J.; Diberto, J. F.; English, J. G.; Glaudin, A. M.; Krumm, B. E.; Slocum, S. T.; Che, T.; Gavin, A. C.; McCorvy, J. D.; Roth, B. L.; et al. TRUPATH, an open-source biosensor platform for interrogating the GPCR transducerome. *Nat. Chem. Biol.* **2020**, *16*, 841−849.
(40) Voss, J. H.; Mahardhika, A. B.; Inoue, A.; Müller, C. E. Agonist-dependent coupling of the promiscuous adenosine A_{2B} receptor to $G\alpha$ protein subunits. *ACS Pharmacol. Transl. Sci.* **2022**, *5*, 373−386.
(41) Lin, C.-Y.; Huang, Z.; Wen, W.; Wu, A.; Wang, C.; Niu, L. Enhancing protein expression in HEK-293 cells by lowering culture temperature. *PLoS One* **2015**, *10*, No. e0123562.
(42) Mori, Y.; Yoshida, Y.; Satoh, A.; Moriya, H. Development of an experimental method of systematically estimating protein expression limits in HEK293 cells. *Sci. Rep.* **2020**, *10*, 4798.
(43) Hill, S. J. G-protein-coupled receptors: past, present and future. *Br. J. Pharmacol.* **2006**, *147*, 27−37.
(44) Jakubík, J.; Randáková, A.; Rudajev, V.; Zimčík, P.; El-Fakahany, E. E.; Doležal, V. Applications and limitations of fitting of the operational model to determine relative efficacies of agonists. *Sci. Rep.* **2019**, *9*, 4637.
(45) Weis, W. I.; Kobilka, B. K. The molecular basis of G protein-coupled receptor activation. *Annu. Rev. Biochem.* **2018**, *87*, 897−919.
(46) Wingler, L. M.; Lefkowitz, R. J. Conformational basis of G protein-coupled receptor signaling versatility. *Trends Cell Biol.* **2020**, *30*, 736−747.
(47) Kobilka, B. K.; Deupi, X. Conformational complexity of G-protein-coupled receptors. *Trends In Pharmacological Sciences* **2007**, *28*, 397−406.
(48) Gregorio, G. G.; Masureel, M.; Hilger, D.; Terry, D. S.; Juette, M.; Zhao, H.; Zhou, Z.; Perez-Aguilar, J. M.; Hauge, M.; Mathiasen, S.; et al. Single-molecule analysis of ligand efficacy in β_2AR−G-protein activation. *Nature* **2017**, *547*, 68−73.
(49) Staus, D. P.; Strachan, R. T.; Manglik, A.; Pani, B.; Kahsai, A. W.; Kim, T. H.; Wingler, L. M.; Ahn, S.; Chatterjee, A.; Masoudi, A.; et al.. Allosteric nanobodies reveal the dynamic range and diverse mechanisms of G-protein-coupled receptor activation. *Nature* **2016**, *535*, 448−452.
(50) Chen, Y.; Zhang, J.; Weng, Y.; Xu, Y.; Lu, W.; Liu, W.; Liu, M.; Hua, T.; Song, G. Cryo-EM structure of the human adenosine A_{2B} receptor−G s signaling complex. *Sci. Adv.* **2022**, *8*, No. eadd3709.
(51) Xu, P.; Huang, S.; Zhang, H.; Mao, C.; Zhou, X. E.; Cheng, X.; Simon, I. A.; Shen, D.-D.; Yen, H.-Y.; Robinson, C. V.; et al.. Structural insights into the lipid and ligand regulation of serotonin receptors. *Nature* **2021**, *592*, 469−473.
(52) Kofuku, Y.; Ueda, T.; Okude, J.; Shiraishi, Y.; Kondo, K.; Maeda, M.; Tsujishita, H.; Shimada, I. Efficacy of the β_2-adrenergic receptor is determined by conformational equilibrium in the transmembrane region. *Nat. Commun.* **2012**, *3*, 1045.
(53) Maslov, I.; Volkov, O.; Khorn, P.; Orekhov, P.; Gusach, A.; Kuzmichev, P.; Gerasimov, A.; Luginina, A.; Coucke, Q.; Bogorodskiy, A.; et al.. Sub-millisecond conformational dynamics of the A_{2A} adenosine receptor revealed by single-molecule FRET. *Commun. Biol.* **2023**, *6*, 362.
(54) Rosenbaum, D. M.; Zhang, C.; Lyons, J. A.; Holl, R.; Aragao, D.; Arlow, D. H.; Rasmussen, S. G. F.; Choi, H.-J.; Devree, B. T.; Sunahara, R. K.; et al.. Structure and function of an irreversible agonist-β_2 adrenoceptor complex. *Nature* **2011**, *469*, 236−240.
(55) Warne, T.; Moukhametzianov, R.; Baker, J. G.; Nehmé, R.; Edwards, P. C.; Leslie, A. G. W.; Schertler, G. F. X.; Tate, C. G. The structural basis for agonist and partial agonist action on a β_1-adrenergic receptor. *Nature* **2011**, *469*, 241−244.
(56) Solt, A. S.; Bostock, M. J.; Shrestha, B.; Kumar, P.; Warne, T.; Tate, C. G.; Nietlispach, D. Insight into partial agonism by observing multiple equilibria for ligand-bound and Gs-mimetic nanobody-bound β_1-adrenergic receptor. *Nat. Commun.* **2017**, *8*, 1795.
(57) Caffrey, M. Crystallizing membrane proteins for structure determination: use of lipidic mesophases. *Annu. Rev. Biophys.* **2009**, *38*, 29−51.
(58) Delagenière, S.; Brenchereau, P.; Launer, L.; Ashton, A. W.; Leal, R.; Veyrier, S.; Gabadinho, J.; Gordon, E. J.; Jones, S. D.; Levik, K. E.; et al.. ISPyB: an information management system for synchrotron macromolecular crystallography. *Bioinformatics* **2011**, *27*, 3186−3192.
(59) Vonrhein, C.; Flensburg, C.; Keller, P.; Sharff, A.; Smart, O.; Paciorek, W.; Womack, T.; Bricogne, G. Data processing and analysis with the autoPROC toolbox. *Acta Crystallogr. D Biol. Crystallogr.* **2011**, *67*, 293−302.
(60) Kabsch, W. XDS. *Acta Crystallogr. D Biol. Crystallogr.* **2010**, *66*, 125−132.
(61) Winn, M. D.; Ballard, C. C.; Cowtan, K. D.; Dodson, E. J.; Emsley, P.; Evans, P. R.; Keegan, R. M.; Krissinel, E. B.; Leslie, A. G. W.; McCoy, A.; et al.. Overview of the CCP4 suite and current developments. *Acta Crystallogr. D Biol. Crystallogr.* **2011**, *67*, 235−242.
(62) Evans, P. Scaling and assessment of data quality. *Acta Crystallogr. D Biol. Crystallogr.* **2006**, *62*, 72−82.
(63) Evans, P. R.; Murshudov, G. N. How good are my data and what is the resolution? *Acta Crystallogr. D Biol. Crystallogr.* **2013**, *69*, 1204−1214.
(64) Tickle, I. J.; Flensburg, C.; Keller, P.; Paciorek, W.; Sharff, A.; Vonrhein, C.; Bricogne, G. *STARANISO*; Global Phasing Ltd.: Cambridge, United Kingdom, 2018−2021.
(65) Afonine, P. V.; Grosse-Kunstleve, R. W.; Echols, N.; Headd, J. J.; Moriarty, N. W.; Mustyakimov, M.; Terwilliger, T. C.; Urzhumtsev, A.; Zwart, P. H.; Adams, P. D. Towards automated crystallographic structure refinement with phenix.refine. *Acta Crystallogr. D Biol. Crystallogr.* **2012**, *68*, 352−367.
(66) Emsley, P.; Lohkamp, B.; Scott, W. G.; Cowtan, K. Features and development of Coot. *Acta Crystallogr. D Biol. Crystallogr.* **2010**, *66*, 486−501.
(67) Smart, O.; Womack, T. O.; Sharff, A.; Flensburg, C.; Keller, P.; Paciorek, W.; Vonrhein, C.; Bricogne, G. Grade, version 1.2.20 Global Phasing Ltd.: Cambridge, United Kingdom, 2011. https://www.globalphasing.com.
(68) Alnouri, M. W.; Jepards, S.; Casari, A.; Schiedel, A. C.; Hinz, S.; Müller, C. E. Selectivity is species-dependent: characterization of

ACS Pharmacology & Translational Science pubs.acs.org/ptsci Article

standard agonists and antagonists at human, rat, and mouse adenosine receptors. *Purinergic Signal.* **2015**, *11*, 389−407.

https://doi.org/10.1021/acsptsci.4c00051
ACS Pharmacol. Transl. Sci. 2024, 7, 1415−1425

4. LIST OF ABBREVIATIONS

2-AG	2-Arachidonoylglycerol
7TM	7-Transmembrane
$A_{2A}AR$	Adenosine A_{2A} receptor
AC	Adenylyl cyclase
AEA	Arachidonoylethanolamide
AR	Adenosine receptor
BRET	Bioluminescent resonance energy transfer
bRIL	Thermostabilized apocytochrome b_{562}
cAMP	Cyclic adenosine monophosphate
CB	Cannabinoid
CB_1	Cannabinoid type1 receptor
CB_2	Cannabinoid type 2 receptor
CBD	Cannabidiol
CBN	Cannabinol
CHO	Chinese hamster ovary
CNS	Central nervous system
CysL1	Cysteinyl leukotriene receptor 1
CysL2	Cysteinyl leukotriene receptor
D_1R	Dopamine type 1 receptor
DHA	Docosahexaenoic acid
DIM	Diindoylmethane
ECL	Extracellular loops
ECS	Endocannabinoid system
ERK	Extracellular-signal regulated kinases
GDP	Guanosine diphosphate
GLP1	Glucagon-like peptide 1
GPCRs	G protein-coupled receptors
GPR18	G protein-coupled receptors 18
GPR183	G protein-coupled receptor 183
GRK	GPCR kinases
GTP	Guanosine triphosphate
HEK293	Human embryonic kidney 293 cells
hGPR18	Human GPR18
ICL	Intracellular loops
IP_3	Inositol 1,4,5-trisphosphate
mGlu5	Metabotropic glutamate 5
mGPR18	mouse GPR18
NAGly	*N*-Arachidonylglycine
NAM	Negative allosteric modulator
NECA	*N*-Ethylcarboxamidoadenosine
PAM	Positive allosteric modulator
PDB	Protein data ban
PDE	Phosphodiesterases
PET	Positron emission tomography

PLC	Phospholipase C
RvD2	Resolvin D2
SARs	Structure–activity relationships
siRNA	Small interfering RNA
TGF-α	Transforming growth factor-α
THC	Δ^9-Tetrahydrocannabinol

5. REFERENCES

(1) Heldin, C.-H.; Lu, B.; Evans, R.; Gutkind, J. S. Signals and receptors. *Cold Spring Harb. Perspect. Biol.* **2016**, *8*. DOI: 10.1101/cshperspect.a005900.

(2) G protein-coupled receptors. In *Encyclopedic Reference of Molecular Pharmacology*, Springer Berlin Heidelberg, 2004; pp 428-433. DOI: 10.1007/3-540-29832-0_720.

(3) Lander, E. S.; Linton, L. M.; Birren, B.; Nusbaum, C.; Zody, M. C.; Baldwin, J.; Devon, K.; Dewar, K.; Doyle, M.; FitzHugh, W.; Funke, R.; Gage, D.; Harris, K.; Heaford, A.; Howland, J.; et al. Initial sequencing and analysis of the human genome. *Nature* **2001**, *409*, 860-921. DOI: 10.1038/35057062.

(4) Bjarnadóttir, T. K.; Gloriam, D. E.; Hellstrand, S. H.; Kristiansson, H.; Fredriksson, R.; Schiöth, H. B. Comprehensive repertoire and phylogenetic analysis of the G protein-coupled receptors in human and mouse. *Genomics* **2006**, *88*, 263-273. DOI: 10.1016/j.ygeno.2006.04.001.

(5) Fredriksson, R.; Lagerström, M. C.; Lundin, L.-G.; Schiöth, H. B. The G-protein-coupled receptors in the human genome form five main families: Phylogenetic analysis, paralogon groups, and fingerprints. *Mol. Pharmacol.* **2003**, *63*, 1256-1272. DOI: 10.1124/mol.63.6.1256.

(6) Rosenbaum, D. M.; Rasmussen, S. G. F.; Kobilka, B. K. The structure and function of G protein-coupled receptors. *Nature* **2009**, *459*, 356-363. DOI: 10.1038/nature08144.

(7) Stockert, J. A.; Devi, L. A. Advancements in therapeutically targeting orphan GPCRs. *Front. Pharmacol.* **2015**, *6*, Review. DOI: 10.3389/fphar.2015.00100.

(8) Vassilatis, D. K.; Hohmann, J. G.; Zeng, H.; Li, F.; Ranchalis, J. E.; Mortrud, M. T.; Brown, A.; Rodriguez, S. S.; Weller, J. R.; Wright, A. C.; Bergmann, J. E.; Gaitanaris, G. A. The G protein-coupled receptor repertoires of human and mouse. *Proc Natl Acad Sci U S A* **2003**, *100*, 4903-4908. DOI: 10.1073/pnas.0230374100.

(9) Venkatakrishnan, A. J.; Deupi, X.; Lebon, G.; Tate, C. G.; Schertler, G. F.; Babu, M. M. Molecular signatures of G-protein-coupled receptors. *Nature* **2013**, *494*, 185-194. DOI: 10.1038/nature11896.

(10) Congreve, M.; de Graaf, C.; Swain, N. A.; Tate, C. G. Impact of GPCR structures on drug discovery. *Cell* **2020**, *181*, 81-91. DOI: 10.1016/j.cell.2020.03.003.

(11) Rajagopal, K.; Lefkowitz, R. J.; Rockman, H. A. When 7 transmembrane receptors are not G protein–coupled receptors. *J. Clin. Investig.* **2005**, *115*, 2971-2974. DOI: 10.1172/JCI26950.

(12) Pandey, S.; Kumari, P.; Baidya, M.; Kise, R.; Cao, Y.; Dwivedi-Agnihotri, H.; Banerjee, R.; Li, X. X.; Cui, C. S.; Lee, J. D.; Kawakami, K.; Maharana, J.; Ranjan, A.; Chaturvedi, M.; Jhingan, G. D.; et al. Intrinsic bias at non-canonical, β-arrestin-coupled seven transmembrane receptors. *Mol. Cell.* **2021**, *81*, 4605-4621.e4611. DOI: 10.1016/j.molcel.2021.09.007.

(13) Pandey, S.; Maharana, J.; Li, X. X.; Woodruff, T. M.; Shukla, A. K. Emerging insights into the structure and function of complement C5a receptors. *Trends Biochem. Sci* **2020**, *45*, 693-705. DOI: 10.1016/j.tibs.2020.04.004.

(14) Gloriam, D.; Thorsen, T.; Kulkarni, Y.; Sykes, D.; Boggild, A.; Drace, T.; Hompluem, P.; Iliopoulos-Tsoutsouvas, C.; Nikas, S.; Daver, H.; Makriyannis, A.; Nissen, P.; Gajhede, M.; Veprintsev, D.; Boesen, T.; et al. Structural basis of Delta(9)-THC analog activity at the Cannabinoid 1 receptor. *Research Square (Preprint)* **2024**. DOI: 10.21203/rs.3.rs-4277209/v1.

(15) Liao, Y.-Y.; Zhang, H.; Shen, Q.; Cai, C.; Ding, Y.; Shen, D.-D.; Guo, J.; Qin, J.; Dong, Y.; Zhang, Y.; Li, X.-M. Snapshot of the cannabinoid receptor 1-arrestin complex unravels the biased signaling mechanism. *Cell* **2023**, *186*, 5784-5797.e5717. DOI: 10.1016/j.cell.2023.11.017.

(16) Newport, T. D.; Sansom, M. S P.; Stansfeld, P. J. The MemProtMD database: a resource for membrane-embedded protein structures and their lipid interactions. *Nucleic Acids Res.* **2019**, *47*, D390-D397. DOI: 10.1093/nar/gky1047.

(17) Shao, Z.; Yan, W.; Chapman, K.; Ramesh, K.; Ferrell, A. J.; Yin, J.; Wang, X.; Xu, Q.; Rosenbaum, D. M. Structure of an allosteric modulator bound to the CB_1 cannabinoid receptor. *Nat. Chem. Biol.* **2019**, *15*, 1199-1205. DOI: 10.1038/s41589-019-0387-2.

(18) Attwood, T. K.; Findlay, J. B. C. Fingerprinting G protein-coupled receptors. *Protein Eng. Des. Sel.* **1994**, *7*, 195-203. DOI: 10.1093/protein/7.2.195.

(19) Kolakowski, L. F. GCRDb: a G-protein-coupled receptor database. *Recept. Channels* **1994**, *2*, 1-7.

(20) Schiöth, H. B.; Fredriksson, R. The GRAFS classification system of G-protein coupled receptors in comparative perspective. *Gen. Comp. Endocrinol.* **2005**, *142*, 94-101. DOI: 10.1016/j.ygcen.2004.12.018.

(21) Alexander, S. P.; Christopoulos, A.; Davenport, A. P.; Kelly, E.; Mathie, A.; Peters, J. A.; Veale, E. L.; Armstrong, J. F.; Faccenda, E.; Harding, S. D.; Pawson, A. J.; Southan, C.; Davies, J. A.; Abbracchio, M. P.; Alexander, W.; et al. The consise guide to pharmacology 2021/22: G protein-coupled receptors. *Br. J. Pharmacol.* **2021**, *178*, S27-S156. DOI: 10.1111/bph.15538.

(22) Zhang, Y.; Sun, B.; Feng, D.; Hu, H.; Chu, M.; Qu, Q.; Tarrasch, J. T.; Li, S.; Sun Kobilka, T.; Kobilka, B. K.; Skiniotis, G. Cryo-EM structure of the activated GLP-1 receptor in complex with a G protein. *Nature* **2017**, *546*, 248-253. DOI: 10.1038/nature22394.

(23) Koehl, A.; Hu, H.; Feng, D.; Sun, B.; Zhang, Y.; Robertson, M. J.; Chu, M.; Kobilka, T. S.; Laeremans, T.; Steyaert, J.; Tarrasch, J.; Dutta, S.; Fonseca, R.; Weis, W. I.; Mathiesen, J. M.; et al. Structural insights into the activation of metabotropic glutamate receptors. *Nature* **2019**, *566*, 79-84. DOI: 10.1038/s41586-019-0881-4.

(24) Qi, X.; Liu, H.; Thompson, B.; McDonald, J.; Zhang, C.; Li, X. Cryo-EM structure of oxysterol-bound human Smoothened coupled to a heterotrimeric Gi. *Nature* **2019**, *571*, 279-283. DOI: 10.1038/s41586-019-1286-0.

(25) Stevens, R. C.; Cherezov, V.; Katritch, V.; Abagyan, R.; Kuhn, P.; Rosen, H.; Wüthrich, K. The GPCR Network: a large-scale collaboration to determine human GPCR structure and function. *Nat. Rev. Drug Discovery* **2013**, *12*, 25-34. DOI: 10.1038/nrd3859.

(26) Joost, P.; Methner, A. Phylogenetic analysis of 277 human G-protein-coupled receptors as a tool for the prediction of orphan receptor ligands. *Genome Biol.* **2002**, *3*, research0063.0061. DOI: 10.1186/gb-2002-3-11-research0063.

(27) Jobe, A.; Vijayan, R. Orphan G protein-coupled receptors: the ongoing search for a home. *Front. Pharmacol.* **2024**, *15*, Review. DOI: 10.3389/fphar.2024.1349097.

(28) Takenouchi, R.; Inoue, K.; Kambe, Y.; Miyata, A. N-arachidonoyl glycine induces macrophage apoptosis via GPR18. *Biochem. Biophys. Res. Commun.* **2012**, *418*, 366-371. DOI: 10.1016/j.bbrc.2012.01.027.

(29) Howard, A. D.; McAllister, G.; Feighner, S. D.; Liu, Q.; Nargund, R. P.; Van der Ploeg, L. H. T.; Patchett, A. A. Orphan G protein-coupled receptors and natural ligand discovery. *Trends Pharmacol. Sci.* **2001**, *22*, 132-140. DOI: 10.1016/S0165-6147(00)01636-9.

(30) Takeda, S.; Yamamoto, A.; Okada, T.; Matsumura, E.; Nose, E.; Kogure, K.; Kojima, S.; Haga, T. Identification of surrogate ligands for orphan G protein-coupled receptors. *Life Sci.* **2003**, *74*, 367-377. DOI: 10.1016/j.lfs.2003.09.030.

(31) Cahill, T. J.; Thomsen, A. R. B.; Tarrasch, J. T.; Plouffe, B.; Nguyen, A. H.; Yang, F.; Huang, L.-Y.; Kahsai, A. W.; Bassoni, D. L.; Gavino, B. J.; Lamerdin, J. E.; Triest, S.; Shukla, A. K.; Berger, B.; Little, J.; et al. Distinct conformations of GPCR–β-arrestin complexes mediate desensitization, signaling, and endocytosis. *Proc. Natl. Acad. Sci. U. S. A.* **2017**, *114*, 2562-2567. DOI: 10.1073/pnas.1701529114.

(32) Kumari, P.; Srivastava, A.; Ghosh, E.; Ranjan, R.; Dogra, S.; Yadav, P. N.; Shukla, A. K. Core engagement with β-arrestin is dispensable for agonist-induced vasopressin receptor endocytosis and ERK activation. *Mol. Biol. Cell* **2017**, *28*, 1003-1010. DOI: 10.1091/mbc.e16-12-0818.

(33) Shukla, A. K.; Westfield, G. H.; Xiao, K.; Reis, R. I.; Huang, L.-Y.; Tripathi-Shukla, P.; Qian, J.; Li, S.; Blanc, A.; Oleskie, A. N.; Dosey, A. M.; Su, M.; Liang, C.-R.; Gu, L.-L.; Shan, J.-M.; et al. Visualization of arrestin recruitment by a G protein-coupled receptor. *Nature* **2014**, *512*, 218-222. DOI: 10.1038/nature13430.

(34) Eiger, D. S.; Hicks, C.; Gardner, J.; Pham, U.; Rajagopal, S. Location bias: A "hidden variable" in GPCR pharmacology. *Bioessays* **2023**. DOI: 10.1002/bies.202300123.

(35) Chen, K.; Zhang, C.; Lin, S.; Yan, X.; Cai, H.; Yi, C.; Ma, L.; Chu, X.; Liu, Y.; Zhu, Y.; Han, S.; Zhao, Q.; Wu, B. Tail engagement of arrestin at the glucagon receptor. *Nature* **2023**, *620*, 904-910. DOI: 10.1038/s41586-023-06420-x.

(36) Gutkind, J. S.; Kostenis, E. Arrestins as rheostats of GPCR signalling. *Nat. Rev. Mol. Cell Biol.* **2018**, *19*, 615-616. DOI: 10.1038/s41580-018-0041-y.

(37) Grundmann, M.; Merten, N.; Malfacini, D.; Inoue, A.; Preis, P.; Simon, K.; Rüttiger, N.; Ziegler, N.; Benkel, T.; Schmitt, N. K.; Ishida, S.; Müller, I.; Reher, R.; Kawakami, K.; Inoue, A.; et al. Lack of beta-arrestin signaling in the absence of active G proteins. *Nat. Commun.* **2018**, *9*, 341. DOI: 10.1038/s41467-017-02661-3.

(38) Lohse, M. J.; Bock, A.; Zaccolo, M. G protein–coupled receptor signaling: New insights define cellular nanodomains. *Annu. Rev. Pharmacool. Toxicol.* **2024**, *64*, 387-415. DOI: 10.1146/annurev-pharmtox-040623-115054.

(39) Nguyen, A. H.; Thomsen, A. R. B.; Cahill, T. J.; Huang, R.; Huang, L.-Y.; Marcink, T.; Clarke, O. B.; Heissel, S.; Masoudi, A.; Ben-Hail, D.; Samaan, F.; Dandey, V. P.; Tan, Y. Z.; Hong, C.; Mahoney, J. P.; et al. Structure of an endosomal signaling GPCR–G protein–β-arrestin megacomplex. *Nat. Struct. Mol. Biol.* **2019**, *26*, 1123-1131. DOI: 10.1038/s41594-019-0330-y.

(40) Thomsen, A. R. B.; Plouffe, B.; Cahill, T. J., III; Shukla, A. K.; Tarrasch, J. T.; Dosey, A. M.; Kahsai, A. W.; Strachan, R. T.; Pani, B.; Mahoney, J. P.; Huang, L.; Breton, B.; Heydenreich, F. M.; Sunahara, R. K.; Skiniotis, G.; et al. GPCR-G protein-β-arrestin super-complex mediates sustained G protein signaling. *Cell* **2016**, *166*, 907-919. DOI: 10.1016/j.cell.2016.07.004.

(41) Gilliland, C. T.; Salanga, C. L.; Kawamura, T.; Trejo, J.; Handel, T. M. The chemokine receptor CCR1 is constitutively active, which leads to G protein-independent, beta-arrestin-mediated internalization. *J. Biol. Chem.* **2013**, *288*, 32194-32210. DOI: 10.1074/jbc.M113.503797.

(42) Sutkeviciute, I.; Vilardaga, J.-P. Structural insights into emergent signaling modes of G protein coupled receptors. *J. Biol. Chem.* **2020**, *295*, 11626-11642. DOI: 10.1074/jbc.REV120.009348.

(43) Takeda, S.; Ikeda, E.; Okazaki, H.; Watanabe, K.; Aramaki, H. Chapter 74 - Effects of Δ^9-Tetrahydrocannabinol in Human Breast Cancer. In *Handbook of Cannabis and Related Pathologies*, Preedy, V. R. Ed.; Academic Press, 2017; pp 722-728. DOI: 10.1016/B978-0-12-800756-3.00085-5.

(44) Wacker, D.; Stevens, R. C.; Roth, B. L. How ligands illuminate GPCR molecular pharmacology. *Cell* **2017**, *170*, 414-427. DOI: 10.1016/j.cell.2017.07.009.

(45) Kenakin, T. Inverse, protean, and ligand-selective agonism: matters of receptor conformation. *FASEB J.* **2001**, *15*, 598-611. DOI: 10.1096/fj.00-0438rev.

(46) Kenakin, T. Allostery: The good, the bad, and the ugly. *J. Pharmacol. Exp. Ther.* **2024**, *388*, 110-120. DOI: 10.1124/jpet.123.001838.

(47) Bruns, R. F.; Mitchell, S. N.; Wafford, K. A.; Harper, A. J.; Shanks, E. A.; Carter, G.; O'Neill, M. J.; Murray, T. K.; Eastwood, B. J.; Schaus, J. M.; Beck, J. P.; Hao, J.; Witkin, J. M.; Li, X.; Chernet, E.; et al. Preclinical profile of a dopamine D_1 potentiator suggests therapeutic utility in neurological and psychiatric disorders. *Neuropharmacol.* **2018**, *128*, 351-365. DOI: 10.1016/j.neuropharm.2017.10.032.

(48) Price, M. R.; Baillie, G. L.; Thomas, A.; Stevenson, L. A.; Easson, M.; Goodwin, R.; McLean, A.; McIntosh, L.; Goodwin, G.; Walker, G.; Westwood, P.; Marrs, J.; Thomson, F.; Cowley, P.; Christopoulos, A.; et al. Allosteric modulation of the cannabinoid CB_1 receptor. *Mol. Pharmacol.* **2005**, *68*, 1484-1495. DOI: 10.1124/mol.105.016162.

(49) Ding, Y.; Qiu, Y.; Jing, L.; Thorn, D. A.; Zhang, Y.; Li, J.-X. Behavioral effects of the cannabinoid CB_1 receptor allosteric modulator ORG27569 in rats. *Pharmacol. Res. Perspect.* **2014**, *2*, e00069. DOI: 10.1002/prp2.69.

(50) Gamage, T. F.; Ignatowska-Jankowska, B. M.; Wiley, J. L.; Abdelrahman, M.; Trembleau, L.; Greig, I. R.; Thakur, G. A.; Tichkule, R.; Poklis, J.; Ross, R. A.; Pertwee, R. G.; Lichtman, A. H. In vivo pharmacological evaluation of the CB_1-receptor allosteric modulator ORG27569. *Behav. Pharmacol.* **2014**, *25*.

(51) Mechoulam, R.; Gaoni, Y. Recent advances in the chemistry of hashish. In *Fortschritte der Chemie Organischer Naturstoffe / Progress in the Chemistry of Organic Natural Products / Progrès dans la Chimie des Substances Organiques Naturelles*, Ashurst, P. R., Bohlmann, F., Farkas, L., Gaoni, Y., Kling, H., Mechoulam, R., Morrison, G. A., Pallos, L., Romo, J., De Vivar, A. R., et al. Eds.; Springer Vienna, 1967; pp 175-213. DOI: 10.1007/978-3-7091-8164-5_6.

(52) Pertwee, R. G. Pharmacological actions of cannabinoids. In *Cannabinoids*, Pertwee, R. G. Ed.; Springer Berlin Heidelberg, 2005; pp 1-51. DOI: 10.1007/3-540-26573-2_1.

(53) Howlett, A. C.; Barth, F.; Bonner, T. I.; Cabral, G.; Casellas, P.; Devane, W. A.; Felder, C. C.; Herkenham, M.; Mackie, K.; Martin, B. R.; Mechoulam, R.; Pertwee, R. G. International Union of Pharmacology. XXVII. Classification of cannabinoid receptors. *Pharmacol. Rev.* **2002**, *54*, 161-202. DOI: 10.1124/pr.54.2.161.

(54) Mechoulam, R.; Hanuš, L. r. A historical overview of chemical research on cannabinoids. *Chem. Phys. Lipids* **2000**, *108*, 1-13. DOI: 10.1016/S0009-3084(00)00184-5.

(55) Banister, S. D.; Connor, M. The chemistry and pharmacology of synthetic cannabinoid receptor agonists as new psychoactive substances: Origins. In *New psychoactive substances : Pharmacology, clinical, forensic and analytical toxicology*,

Maurer, H. H., Brandt, S. D. Eds.; Springer International Publishing, 2018; pp 165-190. DOI: 10.1007/164_2018_143.

(56) Wood, T. B.; Spivey, W. T. N.; Easterfield, T. H. XL.—Charas. The resin of Indian hemp. *J. Chem. Soc., Trans.* **1896**, *69*, 539-546, 10.1039/CT8966900539. DOI: 10.1039/CT8966900539.

(57) Adams, R.; Baker, B. R.; Wearn, R. B. Structure of cannabinol. III. Synthesis of cannabinol, 1-hydroxy-3-*N*-amyl-6,6,9-trimethyl-6-dibenzopyran. *J. Am. Chem. Soc.* **1940**, *62*, 2204-2207. DOI: 10.1021/ja01865a083.

(58) Mechoulam, R.; Gaoni, Y. The absolute configuration of Δ^1-tetrahydrocannabinol, the major active constituent of hashish. *Tetrahedron Lett.* **1967**, *8*, 1109-1111. DOI: 10.1016/S0040-4039(00)90646-4.

(59) Cahn, R. S. 326. Cannabis indica resin. Part IV. The synthesis of some 2 : 2-dimethyldibenzopyrans, and confirmation of the structure of cannabinol. *J. Chem. Soc.* **1933**, 1400-1405, 10.1039/JR9330001400. DOI: 10.1039/JR9330001400.

(60) Wang, Y.-H.; Avula, B.; ElSohly, M. A.; Radwan, M. M.; Wang, M.; Wanas, A. S.; Mehmedic, Z.; Khan, I. A. Quantitative determination of Δ^9-THC, CBG, CBD, their acid precursors and five other neutral cannabinoids by UHPLC-UV-MS. *Planta Med.* **2018**, *84*, 260-266. DOI: 10.1055/s-0043-124873.

(61) Banister, S. D.; Arnold, J. C.; Connor, M.; Glass, M.; McGregor, I. S. Dark classics in chemical neuroscience: Δ^9-Tetrahydrocannabinol. *ACS Chem. Neurosci.* **2019**, *10*, 2160-2175. DOI: 10.1021/acschemneuro.8b00651.

(62) Müller, C. E. Fortschritte in der Cannabis-Forschung aus Pharmazeutisch-chemischer Sicht (Progress in cannabis research from a pharmaceutical chemist's point of view). *Bundesgesundheitsblatt - Gesundheitsforschung - Gesundheitsschutz* **2019**, *62*, 818-824. DOI: 10.1007/s00103-019-02964-4.

(63) Edery, H.; Grunfeld, Y.; Ben-Zvi, Z.; Mechoulam, R. Structural requirements for cannabinoid activity. *Ann. N.Y. Acad. Sci.* **1971**, *191*, 40-53. DOI: 10.1111/j.1749-6632.1971.tb13985.x.

(64) Howlett, A. C. Inhibition of neuroblastoma adenylate cyclase by cannabinoid and nantradol compounds. *Life Sci.* **1984**, *35*, 1803-1810. DOI: 10.1016/0024-3205(84)90278-9.

(65) Howlett, A. C. Cannabinoid inhibition of adenylate cyclase: Relative activity of constituents and metabolites of marihuana. *Neuropharmacol.* **1987**, *26*, 507-512. DOI: 10.1016/0028-3908(87)90035-9.

(66) Howlett, A. C.; Qualy, J. M.; Khachatrian, L. L. Involvement of G_i in the inhibition of adenylate cyclase by cannabimimetic drugs. *Mol. Pharmacol.* **1986**, *29*, 307-313.

(67) Devane, W. A.; Dysarz, F. A.; Johnson, M. R.; Melvin, L. S.; Howlett, A. C. Determination and characterization of a cannabinoid receptor in rat brain. *Mol. Pharmacol.* **1988**, *34*, 605–613.

(68) Howlett, A. C.; Johnson, M. R.; Melvin, L. S.; Milne, G. M. Nonclassical cannabinoid analgetics inhibit adenylate cyclase: development of a cannabinoid receptor model. *Mol. Pharmacol.* **1988**, *33*, 297-302.

(69) Matsuda, L. A.; Lolait, S. J.; Brownstein, M. J.; Young, A. C.; Bonner, T. I. Structure of a cannabinoid receptor and functional expression of the cloned cDNA. *Nature* **1990**, *346*, 561-564. DOI: 10.1038/346561a0.

(70) Gérard, C. M.; Mollereau, C.; Vassart, G.; Parmentier, M. Molecular cloning of a human cannabinoid receptor which is also expressed in testis. *Biochem. J* **1991**, *279*, 129-134. DOI: 10.1042/bj2790129.

(71) Munro, S.; Thomas, K. L.; Abu-Shaar, M. Molecular characterization of a peripheral receptor for cannabinoids. *Nature* **1993**, *365*, 61-65. DOI: 10.1038/365061a0.

(72) Davenport, A. P.; Alexander, S. P. H.; Sharman, J. L.; Pawson, A. J.; Benson, H. E.; Monaghan, A. E.; Liew, W. C.; Mpamhanga, C. P.; Bonner, T. I.; Neubig, R. R.; Pin, J. P.; Spedding, M.; Harmar, A. J. International Union of Basic and Clinical Pharmacology. LXXXVIII. G protein-coupled receptor list: Recommendations for new pairings with cognate ligands. *Pharmacol. Rev.* **2013**, *65*, 967-986. DOI: 10.1124/pr.112.007179.

(73) Lambert, D. M.; Fowler, C. J. The endocannabinoid system: Drug targets, lead compounds, and potential therapeutic applications. *J. Med. Chem.* **2005**, *48*, 5059-5087. DOI: 10.1021/jm058183t.

(74) Devane, W. A.; Hanus, L.; Breuer, A.; Pertwee, R. G.; Stevenson, L. A.; Griffin, G.; Gibson, D.; Mandelbaum, A.; Etinger, A.; Mechoulam, R. Isolation and structure of a brain constituent that binds to the cannabinoid receptor. *Science* **1992**, *258*, 1946-1949. DOI: 10.1126/science.1470919.

(75) Sugiura, T.; Kondo, S.; Sukagawa, A.; Nakane, S.; Shinoda, A.; Itoh, K.; Yamashita, A.; Waku, K. 2-Arachidonoylglycerol: A possible endogenous cannabinoid receptor ligand in brain. *Biochem. Biophys. Res. Commun.* **1995**, *215*, 89-97. DOI: 10.1006/bbrc.1995.2437.

(76) Naikoo, R. A.; Painuli, R.; Akhter, Z.; Singh, P. P. Cannabinoid receptor 2 (CB_2) modulators: A patent review (2016–2024). *Bioorg. Chem.* **2024**, *153*, 107775. DOI: 10.1016/j.bioorg.2024.107775.

(77) Pertwee, R. G.; Howlett, A. C.; Abood, M. E.; Alexander, S. P.; Di Marzo, V.; Elphick, M. R.; Greasley, P. J.; Hansen, H. S.; Kunos, G.; Mackie, K.; Mechoulam, R.; Ross, R. A. International Union of Basic and Clinical Pharmacology. LXXIX. Cannabinoid receptors and their ligands: beyond CB_1 and CB_2. *Pharmacol. Rev.* **2010**, *62*, 588-631. DOI: 10.1124/pr.110.003004.

(78) Kosar, M.; Mach, L.; Carreira, E. M.; Nazaré, M.; Pacher, P.; Grether, U. Patent review of cannabinoid receptor type 2 (CB_2R) modulators (2016-present). *Expert Opin. Ther. Pat.* **2024**, *34*, 665-700. DOI: 10.1080/13543776.2024.2368745.

(79) Adam, J. M.; Cairns, J.; Caulfield, W.; Cowley, P.; Cumming, I.; Easson, M.; Edwards, D.; Ferguson, M.; Goodwin, R.; Jeremiah, F.; Kiyoi, T.; Mistry, A.; Moir, E.; Morphy, R.; Tierney, J.; et al. Design, synthesis, and structure–activity relationships of indole-3-carboxamides as novel water soluble cannabinoid CB_1 receptor agonists. *MedChemComm.* **2010**, *1*, 54. DOI: 10.1039/c0md00022a.

(80) Oyagawa, C. R. M.; Grimsey, N. L. Cannabinoid receptor CB_1 and CB_2 interacting proteins: Techniques, progress and perspectives. In *Methods in Cell Biology*, Academic Press, 2021. DOI: 10.1016/bs.mcb.2021.06.011.

(81) Ramesh, K.; Rosenbaum, D. M. Molecular basis for ligand modulation of the cannabinoid CB_1 receptor. *Br. J. Pharmacol.* **2022**, *179*, 3487-3495. DOI: 10.1111/bph.15627.

(82) Rech, G. R.; Narouze, S. N. Cannabinoid Receptor 1 (CB_1). In *Cannabinoids and Pain*, Springer International Publishing, 2021; pp 47-54. DOI: 10.1007/978-3-030-69186-8_7.

(83) De Marchi, N.; De Petrocellis, L.; Orlando, P.; Daniele, F.; Fezza, F.; Di Marzo, V. Endocannabinoid signalling in the blood of patients with schizophrenia. *Lipids Health Dis.* **2003**, *2*, 5. DOI: 10.1186/1476-511X-2-5.

(84) Di Marzo, V. The endocannabinoid system: Its general strategy of action, tools for its pharmacological manipulation and potential therapeutic exploitation. *Pharmacol. Res.* **2009**, *60*, 77-84. DOI: 10.1016/j.phrs.2009.02.010.

(85) Pacher, P.; Mechoulam, R. Is lipid signaling through cannabinoid 2 receptors part of a protective system? *Prog. Lipid Res.* **2011**, *50*, 193-211. DOI: 10.1016/j.plipres.2011.01.001.

(86) Han, S.; Thoresen, L.; Jung, J.-K.; Zhu, X.; Thatte, J.; Solomon, M.; Gaidarov, I.; Unett, D. J.; Yoon, W. H.; Barden, J.; Sadeque, A.; Usmani, A.; Chen, C.; Semple, G.; Grottick, A. J.; et al. Discovery of APD371: Identification of a highly potent and selective CB_2 agonist for the treatment of chronic pain. *ACS Med. Chem. Lett.* **2017**, *8*, 1309-1313. DOI: 10.1021/acsmedchemlett.7b00396.

(87) Gómez-Gálvez, Y.; Palomo-Garo, C.; Fernández-Ruiz, J.; García, C. Potential of the cannabinoid CB_2 receptor as a pharmacological target against inflammation in Parkinson's disease. *Prog. Neuro-Psychopharmacol. Biol. Psychiatry* **2016**, *64*, 200-208. DOI: 10.1016/j.pnpbp.2015.03.017.

(88) Gantz, I.; Muraoka, A.; Yang, Y. K.; Samuelson, L. C.; Zimmerman, E. M.; Cook, H.; Yamada, T. Cloning and chromosomal localization of a gene (GPR18) encoding a novel seven transmembrane receptor highly expressed in spleen and testis. *Genomics* **1997**, *42*, 462-466. DOI: 10.1006/geno.1997.4752.

(89) Samuelson, L. C.; Swanberg, L. J.; Gantz, I. Mapping of the novel G protein-coupled receptor Gprl8 to distal mouse chromosome 14. *Mamm. Genome* **1996**, *7*, 920-921. DOI: 10.1007/s003359900272.

(90) Norregaard, K.; Benned-Jensen, T.; Rosenkilde, M. M. EBI2, GPR18, and GPR17 – Three structurally related but biologically distinct 7TM receptors. *Curr. Top. Med. Chem.* **2011**, *11*, 618-628. DOI: 10.2174/1568026611109060618.

(91) Hannedouche, S.; Zhang, J.; Yi, T.; Shen, W.; Nguyen, D.; Pereira, J. P.; Guerini, D.; Baumgarten, B. U.; Roggo, S.; Wen, B.; Knochenmuss, R.; Noël, S.; Gessier, F.; Kelly, L. M.; Vanek, M.; et al. Oxysterols direct immune cell migration via EBI2. *Nature* **2011**, *475*, 524-527. DOI: 10.1038/nature10280.

(92) Liu, C.; Yang, X. V.; Wu, J.; Kuei, C.; Mani, N. S.; Zhang, L.; Yu, J.; Sutton, S. W.; Qin, N.; Banie, H.; Karlsson, L.; Sun, S.; Lovenberg, T. W. Oxysterols direct B-cell migration through EBI2. *Nature* **2011**, *475*, 519-523. DOI: 10.1038/nature10226.

(93) Sun, S.; Liu, C. 7α, 25-dihydroxycholesterol-mediated activation of EBI2 in immune regulation and diseases. *Front. Pharmacol.* **2015**, *6*, Review.

(94) Rosenkilde, M. M.; Benned-Jensen, T.; Andersen, H.; Holst, P. J.; Kledal, T. N.; Lüttichau, H. R.; Larsen, J. K.; Christensen, J. P.; Schwartz, T. W. Molecular pharmacological phenotyping of EBI2: An orphan seven-transmembrane receptor with constitutive activity. *J. Biol. Chem.* **2006**, *281*, 13199-13208. DOI: 10.1074/jbc.M602245200.

(95) Sumida, H.; Cyster, J. G. G protein-coupled receptor 18 contributes to establishment of the CD8 effector T cell compartment. *Front. immunol.* **2018**, *9*, Original Research. DOI: 10.3389/fimmu.2018.00660.

(96) Wang, X.; Sumida, H.; Cyster, J. G. GPR18 is required for a normal CD8αα intestinal intraepithelial lymphocyte compartment. *J. Exp. Med.* **2014**, *211*, 2351-2359. DOI: 10.1084/jem.20140646.

(97) Qin, Y.; Verdegaal, E. M. E.; Siderius, M.; Bebelman, J. P.; Smit, M. J.; Leurs, R.; Willemze, R.; Tensen, C. P.; Osanto, S. Quantitative expression profiling of G protein-coupled receptors (GPCRs) in metastatic melanoma: The constitutively active orphan GPCR GPR18 as novel drug target. *Pigment Cell Melanoma Res.* **2011**, *24*, 207-218. DOI: 10.1111/j.1755-148X.2010.00781.x.

(98) Ramos, Y. F. M.; Bos, S. D.; Lakenberg, N.; Böhringer, S.; den Hollander, W. J.; Kloppenburg, M.; Slagboom, P. E.; Meulenbelt, I. Genes expressed in blood link osteoarthritis with apoptotic pathways. *Ann. Rheum. Dis.* **2014**, *73*, 1844-1853. DOI: 10.1136/annrheumdis-2013-203405.

(99) Liu, Y.; Wang, L.; Lo, K.-W.; Lui, V. W. Y. Omics-wide quantitative B-cell infiltration analyses identify GPR18 for human cancer prognosis with superiority over CD20. *Commun. Biol.* **2020**, *3*, 234. DOI: 10.1038/s42003-020-0964-7.

(100) Cerezo, M.; Sollis, E.; Ji, Y.; Lewis, E.; Abid, A.; Bircan, Karatuğ O.; Hall, P.; Hayhurst, J.; John, S.; Mosaku, A.; Ramachandran, S.; Foreman, A.; Ibrahim, A.; McLaughlin, J.; Pendlington, Z.; et al. The NHGRI-EBI GWAS catalog: standards for reusability, sustainability and diversity. *Nucleic Acids Res.* **2025**, *53*, D998-D1005. DOI: 10.1093/nar/gkae1070.

(101) Kohno, M.; Hasegawa, H.; Inoue, A.; Muraoka, M.; Miyazaki, T.; Oka, K.; Yasukawa, M. Identification of *N*-arachidonylglycine as the endogenous ligand for orphan G-protein-coupled receptor GPR18. *Biochem. Biophys. Res. Commun.* **2006**, *347*, 827-832. DOI: 10.1016/j.bbrc.2006.06.175.

(102) Chiang, N.; Dalli, J.; Colas, R. A.; Serhan, C. N. Identification of resolvin D2 receptor mediating resolution of infections and organ protection. *J. Exp. Med.* **2015**, *212*, 1203, 10.1084/jem.20150225. DOI: 10.1084/jem.20150225.

(103) Bradshaw, H. B.; Lee, S. H.; McHugh, D. Orphan endogenous lipids and orphan GPCRs: a good match. *Prostaglandins Other Lipid Mediat.* **2009**, *89*, 131-134. DOI: 10.1016/j.prostaglandins.2009.04.006.

(104) McHugh, D. GPR18 in microglia: implications for the CNS and endocannabinoid system signalling. *Br. J. Pharmacol.* **2012**, *167*, 1575-1582. DOI: 10.1111/j.1476-5381.2012.02019.x.

(105) McHugh, D.; Bradshaw, H. B. GPR18 and NAGly signaling: New members of the endocannabinoid family or distant cousins? In *endoCANNABINOIDS: Actions at Non-CB_1/CB_2 Cannabinoid Receptors*, Abood, M. E., Sorensen, R. G., Stella, N. Eds.; Springer New York, 2013; pp 135-142. DOI: 10.1007/978-1-4614-4669-9_6.

(106) McHugh, D.; Hu, S. S.; Rimmerman, N.; Juknat, A.; Vogel, Z.; Walker, J. M.; Bradshaw, H. B. *N*-Arachidonoyl glycine, an abundant endogenous lipid, potently drives directed cellular migration through GPR18, the putative abnormal cannabidiol receptor. *BMC Neurosci.* **2010**, *11*, 44. DOI: 10.1186/1471-2202-11-44.

(107) McHugh, D.; Page, J.; Dunn, E.; Bradshaw, H. B. Delta(9)-Tetrahydrocannabinol and *N*-arachidonylglycine are full agonists at GPR18 receptors and induce migration in human endometrial HEC-1B cells. *Br. J. Pharmacol.* **2012**, *165*, 2414-2424. DOI: 10.1111/j.1476-5381.2011.01497.x.

(108) McHugh, D.; Wager-Miller, J.; Page, J.; Bradshaw, H. B. siRNA knockdown of GPR18 receptors in BV-2 microglia attenuates N-arachidonoyl glycine-induced cell migration. *J. Mol. Signal.* **2012**, *7*, 10. DOI: 10.1186/1750-2187-7-10.

(109) Alexander, S. P. So what do we call GPR18 now? *Br. J. Pharmacol.* **2012**, *165*, 2411-2413. DOI: 10.1111/j.1476-5381.2011.01731.x.

(110) Console-Bram, L.; Brailoiu, E.; Brailoiu, G. C.; Sharir, H.; Abood, M. E. Activation of GPR18 by cannabinoid compounds: A tale of biased agonism. *Br. J. Pharmacol.* **2014**, *171*, 3908-3917. DOI: 10.1111/bph.12746.

(111) Morales, P.; Lago-Fernandez, A.; Hurst, D. P.; Sotudeh, N.; Brailoiu, E.; Reggio, P. H.; Abood, M. E.; Jagerovic, N. Therapeutic exploitation of GPR18: Beyond the cannabinoids? *J. Med. Chem.* **2020**, *63*, 14216-14227. DOI: 10.1021/acs.jmedchem.0c00926.

(112) Chiang, N.; de la Rosa, X.; Libreros, S.; Serhan, C. N. Novel resolvin D2 receptor axis in infectious inflammation. *J. Immunol.* **2017**, *198*, 842-851. DOI: 10.4049/jimmunol.1601650.

(113) Lu, V. B.; Puhl, H. L.; Ikeda, S. R. *N*-Arachidonyl glycine does not activate G protein–coupled receptor 18 signaling via canonical pathways. *Mol. Pharmacol.* **2012**, *83*, 267, 10.1124/mol.112.081182.

(114) Finlay, D. B.; Joseph, W. R.; Grimsey, N. L.; Glass, M. GPR18 undergoes a high degree of constitutive trafficking but is unresponsive to *N*-arachidonoylglycine. *PeerJ* **2016**, *4*, e1835. DOI: 10.7717/peerj.1835.

(115) Yin, H.; Chu, A.; Li, W.; Wang, B.; Shelton, F.; Otero, F.; Nguyen, D. G.; Caldwell, J. S.; Chen, Y. A. Lipid G protein-coupled receptor ligand identification using beta-arrestin PathHunter assay. *J. Biol. Chem.* **2009**, *284*, 12328-12338. DOI: 10.1074/jbc.M806516200.

(116) Inoue, A.; Ishiguro, J.; Kitamura, H.; Arima, N.; Okutani, M.; Shuto, A.; Higashiyama, S.; Ohwada, T.; Arai, H.; Makide, K.; Aoki, J. TGFα shedding assay: an accurate and versatile method for detecting GPCR activation. *Nat. Methods* **2012**, *9*, 1021-1029. DOI: 10.1038/nmeth.2172.

(117) Lu, S.; Jang, W.; Inoue, A.; Lambert, N. A. Constitutive G protein coupling profiles of understudied orphan GPCRs. *PLOS ONE* **2021**, *16*, e0247743. DOI: 10.1371/journal.pone.0247743.

(118) Jang, W.; Lu, S.; Xu, X.; Wu, G.; Lambert, N. A. The role of G protein conformation in receptor–G protein selectivity. *Nat. Chem. Biol.* **2023**, *19*, 687-694. DOI: 10.1038/s41589-022-01231-z.

(119) Becker, A. M.; Callahan, D. J.; Richner, J. M.; Choi, J.; DiPersio, J. F.; Diamond, M. S.; Bhattacharya, D. GPR18 controls reconstitution of mouse small intestine intraepithelial lymphocytes following bone marrow transplantation. *PLoS One* **2015**, *10*, e0133854. DOI: 10.1371/journal.pone.0133854.

(120) Murataeva, N.; Daily, L.; Taylor, X.; Dhopeshwarkar, A.; Hu, S. S.-J.; Miller, S.; McHugh, D.; Oehler, O.; Li, S.; Bonanno, J. A.; Mackie, K.; Straiker, A. Evidence for a GPR18 role in chemotaxis, proliferation, and the course of wound closure in the cornea. *Cornea* **2019**, *38*, 905-913. DOI: 10.1097/ico.0000000000001934.

(121) Park, J.; Langmead, C. J.; Riddy, D. M. New advances in targeting the resolution of inflammation: Implications for specialized pro-resolving mediator GPCR drug discovery. *ACS Pharmacol. Transl. Sci.* **2020**, *3*, 88-106. DOI: 10.1021/acsptsci.9b00075.

(122) Nazir, M.; Harms, H.; Loef, I.; Kehraus, S.; El Maddah, F.; Arslan, I.; Rempel, V.; Müller, C. E.; König, G. M. GPR18 inhibiting Amauromine and the novel triterpene glycoside Auxarthonoside from the sponge-derived fungus *Auxarthron reticulatum*. *Planta Med.* **2015**, *81*, 1141-1145. DOI: 10.1055/s-0035-1545979.

(123) Rempel, V.; Atzler, K.; Behrenswerth, A.; Karcz, T.; Schoeder, C.; Hinz, S.; Kaleta, M.; Thimm, D.; Kieć-Kononowicz, K.; Müller, C. E. Bicyclic imidazole-4-one derivatives: a new class of antagonists for the orphan G protein-coupled receptors GPR18 and GPR55. *MedChemComm.* **2014**, *5*, 632-649. DOI: 10.1039/c3md00394a.

(124) Schoeder, C. T.; Kaleta, M.; Mahardhika, A. B.; Olejarz-Maciej, A.; Łażewska, D.; Kieć-Kononowicz, K.; Müller, C. E. Structure-activity relationships of imidazothiazinones and analogs as antagonists of the cannabinoid-activated orphan G protein-coupled receptor GPR18. *Eur. J. Med. Chem.* **2018**, *155*, 381-397. DOI: 10.1016/j.ejmech.2018.05.050.

(125) Adel, Y.; Alexander, S. P. H. Neuromolecular mechanisms of cannabis action. In *Cannabinoids and Neuropsychiatric Disorders*, Murillo-Rodriguez, E., Pandi-Perumal, S. R., Monti, J. M. Eds.; Springer International Publishing, 2021; pp 15-28. DOI: 10.1007/978-3-030-57369-0_2.

(126) Rempel, V.; Volz, N.; Glaser, F.; Nieger, M.; Brase, S.; Müller, C. E. Antagonists for the orphan G protein-coupled receptor GPR55 based on a coumarin scaffold. *J. Med. Chem.* **2013**, *56*, 4798-4810. DOI: 10.1021/jm4005175.

(127) Lauckner, J. E.; Jensen, J. B.; Chen, H.-Y.; Lu, H.-C.; Hille, B.; Mackie, K. GPR55 is a cannabinoid receptor that increases intracellular calcium and inhibits M current. *Proc. Natl. Acad. Sci. U. S. A.* **2008**, *105*, 2699-2704. DOI: 10.1073/pnas.0711278105.

(128) Drabczyńska, A.; Müller, C. E.; Schiedel, A.; Schumacher, B.; Karolak-Wojciechowska, J.; Fruziński, A.; Zobnina, W.; Yuzlenko, O.; Kieć-Kononowicz, K. Phenylethyl-substituted pyrimido[2,1-*f*]purinediones and related compounds: Structure–activity relationships as adenosine A_1 and A_{2A} receptor ligands. *Bioorg. Med. Chem.* **2007**, *15*, 6956-6974. DOI: 10.1016/j.bmc.2007.07.051.

(129) Schoeder, C. T.; Mahardhika, A. B.; Drabczyńska, A.; Kieć-Kononowicz, K.; Müller, C. E. Discovery of tricyclic xanthines as agonists of the cannabinoid-activated orphan G protein-coupled receptor GPR18. *ACS Med. Chem. Lett.* **2020**, *11*, 2024-2031. DOI: 10.1021/acsmedchemlett.0c00208.

(130) Mahardhika, A. B.; Załuski, M.; Schoeder, C. T.; Boshta, N. M.; Schabikowski, J.; Perri, F.; Łażewska, D.; Neumann, A.; Kremers, S.; Oneto, A.; Ressemann, A.; Latacz, G.; Namasivayam, V.; Kieć-Kononowicz, K.; Müller, C. E. Potent, selective agonists for the cannabinoid-like orphan G protein-coupled receptor GPR18: A promising drug target for cancer and immunity. *J. Med. Chem.* **2024**, *67*, 9896-9926. DOI: 10.1021/acs.jmedchem.3c02423.

(131) Pertwee, R. G. The diverse CB_1 and CB_2 receptor pharmacology of three plant cannabinoids: Δ^9-tetrahydrocannabinol, cannabidiol and Δ^9-tetrahydrocannabivarin. *Br. J. Pharmacol.* **2008**, *153*, 199-215. DOI: 10.1038/sj.bjp.0707442.

(132) Pertwee, R. G. The pharmacology of cannabinoid receptors and their ligands: an overview. *Int. J. Obes.* **2006**, *30*, S13-S18. DOI: 10.1038/sj.ijo.0803272.

(133) Zou, S.; Kumar, U. Cannabinoid receptors and the endocannabinoid system: Signaling and function in the central nervous system. *Int. J. Mol. Sci.* **2018**, *19*, 833.

(134) Glass, M.; Faull, R. L. M.; Dragunow, M. Cannabinoid receptors in the human brain: a detailed anatomical and quantitative autoradiographic study in the fetal, neonatal and adult human brain. *Neurosci.* **1997**, *77*, 299-318. DOI: 10.1016/S0306-4522(96)00428-9.

(135) Tiziana, B.; Vincenzo Di, M. Cannabinoid receptors and endocannabinoids: Role in neuroinflammatory and neurodegenerative disorders. *CNS Neurol. Disord. Drug Targets* **2010**, *9*, 564-573. DOI: 10.2174/187152710793361568.

(136) Ashton, J. C.; Glass, M. The cannabinoid CB_2 receptor as a target for inflammation-dependent neurodegeneration. *Curr. Neuropharmacol.* **2007**, *5*, 73–80. DOI: 10.2174/157015907780866884.

(137) Benito, C.; Tolón, R. M.; Pazos, M. R.; Núñez, E.; Castillo, A. I.; Romero, J. Cannabinoid CB_2 receptors in human brain inflammation. *Br. J. Pharmacol.* **2008**, *153*, 277–285. DOI: 10.1038/sj.bjp.0707505.

(138) Cabral, G. A.; Raborn, E. S.; Griffin, L.; Dennis, J.; Marciano-Cabral, F. CB_2 receptors in the brain: role in central immune function. *Br. J. Pharmacol.* **2008**, *153*, 240-251. DOI: 10.1038/sj.bjp.0707584.

(139) Galiègue, S.; Mary, S.; Marchand, J.; Dussossoy, D.; Carrière, D.; Carayon, P.; Bouaboula, M.; Shire, D.; LE Fur, G.; Casellas, P. Expression of central and peripheral cannabinoid receptors in human immune tissues and leukocyte subpopulations. *Eur. J. Biochem.* **1995**, *232*, 54-61. DOI: 10.1111/j.1432-1033.1995.tb20780.x.

(140) Gowran, A.; Noonan, J.; Campbell, V. A. The multiplicity of action of cannabinoids: Implications for treating neurodegeneration. *CNS Neurosci. Ther.* **2011**, *17*, 637-644. DOI: 10.1111/j.1755-5949.2010.00195.x.

(141) Stella, N. Endocannabinoid signaling in microglial cells. *Neuropharmacol.* **2009**, *56 Suppl 1*, 244–253. DOI: 10.1016/j.neuropharm.2008.07.037.

(142) Cassano, T.; Calcagnini, S.; Pace, L.; Marco, F. d.; Romano, A.; Gaetani, S. Cannabinoid receptor 2 signaling in neurodegenerative disorders: From pathogenesis to a promising therapeutic target. *Front. Neurosci.* **2017**, *11*, 30. DOI: 10.3389/fnins.2017.00030.

(143) Johnson, M. R.; Melvin, L. S. The discovery of nonclassical cannabinoid analgetics. In *Cannabinoids as therapeutic agents*, Chapman and Hall/CRC, 2019; pp 121-146.

(144) Melvin, L. S.; Johnson, M. R. Structure-activity relationships of tricyclic and nonclassical bicyclic cannabinoids. *NIDA Res. Monogr.* **1987**, *79*, 31-47.

(145) Herkenham, M.; Lynn, A.; Johnson, M.; Melvin, L.; de Costa, B.; Rice, K. Characterization and localization of cannabinoid receptors in rat brain: a quantitative in vitro autoradiographic study. *J. Neurosci.* **1991**, *11*, 563-583. DOI: 10.1523/jneurosci.11-02-00563.1991.

(146) Finlay, D. B.; Cawston, E. E.; Grimsey, N. L.; Hunter, M. R.; Korde, A.; Vemuri, V. K.; Makriyannis, A.; Glass, M. $G\alpha_s$ signalling of the CB_1 receptor and the influence of receptor number. *Br. J. Pharmacol.* **2017**, *174*, 2545-2562. DOI: 10.1111/bph.13866.

(147) Bockaert, J. G protein-coupled receptors. In *Encyclopedia of Life Sciences*, John Wiley & Sons, Ltd (Ed.). DOI: 10.1002/9780470015902.a0000118.pub3.

(148) Pagano, C.; Navarra, G.; Coppola, L.; Avilia, G.; Bifulco, M.; Laezza, C. Cannabinoids: Therapeutic use in clinical practice. *Int. J. Mol. Sci.* **2022**, *23*, 3344. DOI: 10.3390/ijms23063344.

(149) Coelho, M. P.; Duarte, P.; Calado, M.; Almeida, A. J.; Reis, C. P.; Gaspar, M. M. The current role of cannabis and cannabinoids in health: A comprehensive review of their therapeutic potential. *Life Sci.* **2023**, *329*, 121838. DOI: 10.1016/j.lfs.2023.121838.

(150) Gaisey, J.; Narouze, S. N. Dronabinol (Marinol®). In *Cannabinoids and Pain*, Springer International Publishing, 2021; pp 105-107. DOI: 10.1007/978-3-030-69186-8_14.

(151) Harrison, N. J.; Simpson, H. Nabilone (Cesamet). In *Cannabinoids and Pain*, Springer International Publishing, 2021; pp 109-112. DOI: 10.1007/978-3-030-69186-8_15.

(152) Boivin, M. Nabiximols (Sativex®). In *Cannabinoids and Pain*, Springer International Publishing, 2021; pp 119-126. DOI: 10.1007/978-3-030-69186-8_17.

(153) Howard, P.; Twycross, R.; Shuster, J.; Mihalyo, M.; Wilcock, A. Cannabinoids. *J. Pain Symptom Manag.* **2013**, *46*, 142-149. DOI: 10.1016/j.jpainsymman.2013.05.002.

(154) Dos Santos, N. A.; Romão, W. Cannabis – A state of the art about the millenary plant: Part I. *Forensic Chem.* **2023**, *32*, 100470. DOI: 10.1016/j.forc.2023.100470.

(155) Malach, M.; Kovalchuk, I.; Kovalchuk, O. Medical cannabis in pediatric oncology: friend or foe? *Pharmaceuticals.* **2022**, *15*, 359. DOI: 10.3390/ph15030359.

(156) Mahardhika, A. B.; Ressemann, A.; Kremers, S. E.; Gregório Castanheira, M. S.; Schoeder, C. T.; Müller, C. E.; Pillaiyar, T. Design, synthesis, and structure–activity relationships of diindolylmethane derivatives as cannabinoid CB_2 receptor agonists. *Arch. Pharm.* **2023**, *356*, e2200493. DOI: 10.1002/ardp.202200493.

(157) Ijzerman, A. P.; Jacobson, K. A.; Müller, C. E.; Cronstein, B. N.; Cunha, R. A. International Union of Basic and Clinical Pharmacology. CXII: Adenosine receptors: A further update. *Pharmacol. Rev.* **2022**, *74*, 340. DOI: 10.1124/pharmrev.121.000445.

(158) Burnstock, G. Purinergic signalling and disorders of the central nervous system. *Nat. Rev. Drug Discovery* **2008**, *7*, 575-590. DOI: 10.1038/nrd2605.

(159) Borea, P. A.; Gessi, S.; Merighi, S.; Vincenzi, F.; Varani, K. Pharmacology of adenosine receptors: The state of the art. *Physiol. Rev.* **2018**, *98*, 1591-1625. DOI: 10.1152/physrev.00049.2017.

(160) Müller, C. E.; Jacobson, K. A. Recent developments in adenosine receptor ligands and their potential as novel drugs. *Biochim. Biophys. Acta, Biomembr.* **2011**, *1808*, 1290-1308. DOI: 10.1016/j.bbamem.2010.12.017.

(161) Alexander, S. P. H. Adenosine Receptors. In *xPharm: The comprehensive pharmacology reference*, Enna, S. J., Bylund, D. B. Eds.; Elsevier, 2007; pp 1-3. DOI: 10.1016/B978-008055232-3.60215-6.

(162) Launay, A.; Nebie, O.; Vijaya Shankara, J.; Lebouvier, T.; Buée, L.; Faivre, E.; Blum, D. The role of adenosine A_{2A} receptors in Alzheimer's disease and tauopathies. *Neuropharmacol.* **2023**, *226*, 109379. DOI: 10.1016/j.neuropharm.2022.109379.

(163) Chen, J.-F.; Cunha, R. A. The belated US FDA approval of the adenosine A_{2A} receptor antagonist istradefylline for treatment of Parkinson's disease. *Purinergic Signal.* **2020**, *16*, 167-174. DOI: 10.1007/s11302-020-09694-2.

(164) Bahreyni, A.; Avan, A.; Shabani, M.; Ryzhikov, M.; Fiuji, H.; Soleimanpour, S.; Khazaei, M.; Hassanian, S. M. Therapeutic potential of A2 adenosine receptor pharmacological regulators in the treatment of cardiovascular diseases, recent progress, and prospective. *J. Cell. Physiol.* **2019**, *234*, 1295-1299. DOI: 10.1002/jcp.27161.

(165) Müller, C. E.; Maurinsh, J.; Sauer, R. Binding of [^{3}H]MSX-2 (3-(3-hydroxypropyl)-7-methyl-8-(*m*-methoxystyryl)-1-propargylxanthine) to rat striatal membranes — a new, selective antagonist radioligand for A_{2A} adenosine receptors. *Eur. J. Pharm. Sci.* **2000**, *10*, 259-265. DOI: 10.1016/S0928-0987(00)00064-6.

(166) Bayer-Aktiengesellschaft. WO0125210. 2001.

(167) Beukers, M. W.; Chang, L. C. W.; von Frijtag Drabbe Künzel, J. K.; Mulder-Krieger, T.; Spanjersberg, R. F.; Brussee, J.; Ijzerman, A. P. New, non-adenosine, high-potency agonists for the human adenosine A_{2B} receptor with an improved selectivity profile

compared to the reference agonist *N*-ethylcarboxamidoadenosine. *J. Med. Chem.* **2004**, *47*, 3707-3709. DOI: 10.1021/jm049947s.

(168) Amelia, T.; van Veldhoven, J. P. D.; Falsini, M.; Liu, R.; Heitman, L. H.; van Westen, G. J. P.; Segala, E.; Verdon, G.; Cheng, R. K. Y.; Cooke, R. M.; van der Es, D.; Ijzerman, A. P. Crystal structure and subsequent ligand design of a nonriboside partial agonist bound to the adenosine A_{2A} receptor. *J. Med. Chem.* **2021**, *64*, 3827-3842. DOI: 10.1021/acs.jmedchem.0c01856.

6. LIST OF PUBLICATIONS

(1) **Mahardhika, A. B**.; Załuski, M.; Schoeder, C. T.; Boshta, N. M.; Schabikowski, J.; Perri, F.; Łażewska, D.; Neumann, A.; Kremers, S.; Oneto, A.; Ressemann, A.; Latacz, G.; Namasivayam, V.; Kieć-Kononowicz, K.; Müller, C. E. Potent, selective agonists for the cannabinoid-like orphan G protein-coupled receptor gpr18: A promising drug target for cancer and immunity. *J. Med. Chem.* **2024**, *67* (12), 9896-9926. DOI: 10.1021/acs.jmedchem.3c02423.

(2) Claff, T.; **Mahardhika, A. B**.; Vaaßen, V. J.; Schlegel, J. G.; Vielmuth, C.; Weiße, R. H.; Sträter, N.; Müller, C. E. Structural insights into partial activation of the prototypic G protein-coupled adenosine A_{2A} receptor. *ACS Pharmacol. Transl. Sci*. **2024**. DOI: 10.1021/acsptsci.4c00051. **(Claff and Mahardhika contributed equally).**

(3) **Mahardhika, A. B**.; Ressemann, A.; Kremers, S. E.; Gregório Castanheira, M. S.; Schoeder, C. T.; Müller, C. E.; Pillaiyar, T. Design, synthesis, and structure–activity relationships of diindolylmethane derivatives as cannabinoid CB_2 receptor agonists. *Arch. Pharm*. **2023**, 356 (3), e2200493. DOI: 10.1002/ardp.202200493.

(4) Modemann, D. J.; **Mahardhika, A. B**.; Yamoune, S.; Kreyenschmidt, A.-K.; Maaß, F.; Kremers, S.; Breunig, C.; Sahlmann, C.-O.; Bucerius, J.; Stalke, D.; Wiltfang, J.; Bouter, Y.; Müller, C. E.; Bouter, C.; Meller, B. Development of high-affinity fluorinated ligands for cannabinoid subtype 2 receptor, and in vitro evaluation of a radioactive tracer for imaging. *Eur. J. Med. Chem*. **2022**, 232, 114138. DOI: 10.1016/j.ejmech.2022.114138.

(5) Voss, J. H.; **Mahardhika, A. B.**; Inoue, A.; Müller, C. E. Agonist-dependent coupling of the promiscuous adenosine A_{2B} receptor to Gα protein subunits. *ACS Pharmacol. Transl. Sci.* **2022**, 5 (5), 373-386. DOI: 10.1021/acsptsci.2c00020.

(6) Pillaiyar, T.; Sedaghati, M.; **Mahardhika, A.B**; L. Wendt, L.; Müller, C. E. Iodine-catalyzed electrophilic substitution of indoles: Synthesis of (un)symmetrical diindolylmethanes with a quaternary carbon center. *Beilstein J. Org. Chem.* **2021**, 17, 1464-1475. DOI: 10.3762/bjoc.17.102.

(7) Schoeder, C. T.; **Mahardhika, A. B**.; Drabczyńska, A.; Kieć-Kononowicz, K.; Müller, C. E. Discovery of tricyclic xanthines as agonists of the cannabinoid-activated orphan G-protein-coupled receptor GPR18. *ACS Med. Chem. Lett.* **2020**, 11 (10), 2024-2031. DOI: 10.1021/acsmedchemlett.0c00208. **(Schoeder and Mahardhika contributed equally)**

(8) Neumann, A.; Engel, V.; **Mahardhika, A. B**.; Schoeder, C. T.; Namasivayam, V.; Kiec-Kononowicz, K.; Müller, C. E. Computational investigations on the binding mode of ligands for the cannabinoid-activated G protein-coupled receptor GPR18. *Biomolecules* **2020**, 10 (5), 686. DOI: 10.3390/biom10050686.

(9) Schoeder, C. T.; Meyer, A.; **Mahardhika, A. B.**; Thimm, D.; Blaschke, T.; Funke, M.; Müller, C. E. Development of chromen-4-one derivatives as (ant)agonists for the lipid-activated g protein-coupled receptor GPR55 with tunable efficacy. *ACS Omega* **2019**, 4 (2), 4276-4295. DOI: 10.1021/acsomega.8b03695.

(10) Schoeder, C. T.; Kaleta, M.; **Mahardhika, A. B.;** Olejarz-Maciej, A.; Łażewska, D.; Kieć-Kononowicz, K.; Müller, C. E. Structure-activity relationships of imidazothiazinones and analogs as antagonists of the cannabinoid-activated orphan G protein-coupled receptor GPR18. *Eur. J. Med. Chem.* **2018**, 155, 381-397. DOI: 10.1016/j.ejmech.2018.05.050.

7. APPENDICES

7.1. Appendix I
Supplementary information from publication I: Discovery of tricyclic xanthines as agonists of the cannabinoid-activated orphan G protein-coupled receptor GPR18

The supplementary information of this publication is also available online at:

https://pubs.acs.org/doi/suppl/10.1021/acsmedchemlett.0c00208/suppl_file/ml0c00208_si_001.pdf

Discovery of tricyclic xanthines as agonists of the cannabinoid-activated orphan G protein-coupled receptor GPR18

Clara T. Schoeder,[a,c]‡ Andhika B Mahardhika,[a,c]‡ Anna Drabczyńska,[b] Katarzyna Kieć-Kononowicz,[b]* and Christa E. Müller[a]*

[a] Pharmaceutical Institute, Department of Pharmaceutical & Medicinal Chemistry, University of Bonn, Bonn, Germany.

[b] Department of Technology and Biotechnology of Drugs, Faculty of Pharmacy, Jagiellonian University, Medical College, 9 Medyczna St., 30-688 Kraków, Poland.

[c] Research Training Group 1873, University of Bonn, 53127 Bonn, Germany.

*Address correspondence to:

Christa Müller, Pharmazeutisches Institut, An der Immenburg 4, D-53121 Bonn, Germany, phone: +49-228-73-2301, Fax: +49-228-73-2567, e-mail: christa.mueller@uni-bonn.de

Katarzyna Kieć-Kononowicz, 9 Medyczna Str., 30-688 Kraków, Phone: +12-620-55-80, e-mail: mfkonono@cyf-kr.edu.pl

Table of Contents

Table S1. Test results for selected compounds at cannabinoid receptors

	Compound	Structure	Human CB_1 receptor Radioligand binding *vs.* [^{3}H]CP55,940 (µM)	Human CB_2 receptor Radioligand binding *vs.* [^{3}H]CP55,940 (µM)
3	THC	-	**0.00387** ± 0.00091	**0.0716** ± 0.0024
5	PSB-KD107	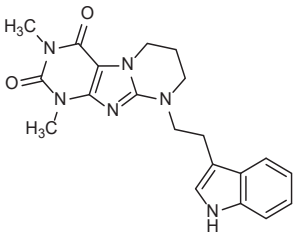	**>10** (11%)	**>10** (29%)
16	PSB-KD477	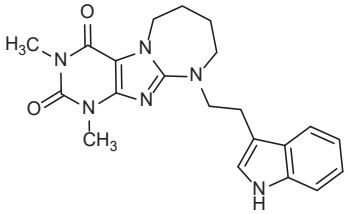	**>10** (24%)	**>10** (46%)
17		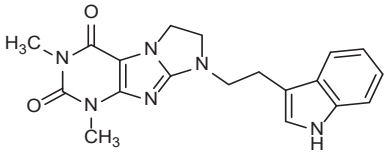	**>10** (30%)	**>10** (30%)

Table S2. EC_{50} values and maximal receptor activation for concentration-response curves of GPR18 **5** in the absence and presence of different concentrations of PSB-CB-27 (**20**).

Dose-response curve	EC_{50} ± SEM[a] (μM)	E_{max} (%)
5 alone	0.699 ± 0.125	100
5 + 3 μM **20**	0.554 ± 0.216	92
5 + 10 μM **20**	0.190 ± 0.058	75
5 + 15 μM **20**	0.171 ± 0.038	63
5 + 20 μM **20**	0.205 ± 0.034	53

[a]EC_{50} values are not significantly different from each other, ($p > 0.05$, unpaired t-test).

β-Arrestin recruitment assays at GPR18 and GPR55

ß-Arrestin recruitment assays were performed according to previously published procedures.[1, 2] Briefly, the Chinese hamster ovary (CHO) cell line expressed β-arrestin fused to a mutant of β-galactosidase (β-arrestin–EA, DiscoverX, Fremont, CA, USA) was stably expressing either the human GPR18-prolink1 or the human GPR55-prolink1 were prepared according to manufacturer protocol and previously described procedure.[1, 2] Briefly, the cells were kept in F-12 (Nutri-Mix) medium (Thermo Fisher Scientific, Waltham, MA, USA) supplemented with 10% Fetal Calf Serum (FCS, PANBiotech GmbH, Germany) 100 U/ml Penicillin, 100 µg/ml Streptomycin (Thermo Fisher Scientific, Waltham, MA, USA), 800 µg/ml Geneticin (Thermo Fisher Scientific, Waltham, MA, USA) and 300 µg Hygromycin (InvivoGen, San Diego, CA, USA). About 24h prior to the assay, the cells were seeded into 96-well plates (NUNClon™ Delta Surface, Thermo Fisher Scientific, Rosenkilde, Denmark) at the density of 200 000 cells per well in 90 µL of assay medium (Opti-Mem (Thermo Fisher Scientific, Waltham, MA, USA), supplemented with 2% FCS, 100 U/ml Penicillin, 100 µg/ml Streptomycin, 800 µg/ml Geneticin and 300 µg Hygromycin) and incubated for 24h at 37°C and 5-10% CO2. Test compounds were prepared as stock solution in dimethylsulfoxide (DMSO, 10 mM). Prior to assay, the test compounds were diluted in DMSO and subsequenty in PBS containing 0.1% bovine serum albumin (BSA, Carl Roth GmbH & Co. KG, Karlsruhe, Gemany) until the final concentration of DSMO is 1%. Compound dilutions (10 µL per well) at desired concentration were added into the plate and incubated for 90 min at 37 °C. About 50 µL of detection reagent was employed according to the previously described procedure[1, 2] and incubated for another 60 min at room temperature. Luminescence signals were subsequently measured in a TopCount NXT, Packard, Perkin-Elmer, for one second per well. Three to four independent experiments were performed, each in duplicate. All pharmacological data were analyzed using GraphPad Prism 7.0 or higher (GraphPad Inc., La Jolla, CA). For the human GPR18, Δ^9-THC as agonist was used in concentration of 10 µM to stimulate the receptor. As maximum response of the respective agonist Δ^9-THC was used at 30 µM. For the human GPR55, LPI was used as agonist in a concentration of 1 µM, as maximal response at 10 µM.

Radioligand binding studies at cannabinoid receptors

CHO stably transfected with human CB_1 or CB_2 receptors were grown and membrane preparations were prepared as previously described.[3] Competition binding assays using 30 µg of protein/well for CB_1 and 8 µg of protein/well for CB_2-receptors were performed employing the non-selective CB receptor agonist radioligand [^{3}H](−)-*cis*-3-[2-hydroxy-4-(1,1-dimethylheptyl)phenyl]-*trans*-4-(3-hydroxypropyl)cyclo-

hexanol ([^{3}H]CP55,940 (ARC American radiolabeled chemicals. St. Louis, MO, USA), final concentration 0.1 nM). All test compounds were dissolved and further diluted in 100% DMSO. Assay buffer (465 µL consisting of 50 mM tris(hydroxymethyl)-aminomethan (TRIS, Carl Roth GmbH & Co. KG, Karlsruhe, Gemany), 3 mM $MgCl_2$ (Carl Roth GmbH & Co. KG, Karlsruhe, Gemany), 0.1% BSA, pH 7.4) was added into the 96-well plate followed by the addition of 15 µL of the test compound in DMSO, 60 µL of [^{3}H]CP55,940 (in assay buffer), and 60 µL of membrane preparation (in 50 mM TRIS, pH 7.4). The mixture was then incubated for 2h at room temperature. The final DMSO concentration in the assay was 2.5%. Unlabeled CP55,940 (Sigma Aldrich Corp., St. Louis, MO, USA) at 10 µM was used to determine nonspecific binding while DMSO without test compound was used to measure total binding. Bound and unbound radioligand were separated by rapid filtration through glass fiber GF/C-filters (Perkin-Elmer, Waltham, MA, USA), presoaked for 0.5 h in 0.3% aq. polyethyleneimine (Fluka, Sigma Aldrich Corp., St. Louis, MO, USA) solution using a Brandel 96-well Harvester (Brandel, Gaithersburg, MD, USA). Filters were washed three times with ice-cold washing buffer (50 mM TRIS, 0.1% BSA, pH 7.4). Filter was then then dried for 1.5 h at 50 °C. The amount of radioactivity on the filters was determined using a liquid scintillation counter (Topcount NXT, Packard/Perkin-Elmer) after 10 h of preincubation with 50 µl of scintillation cocktail (Multiscint 25, Perkin-Elmer).

Experimental procedures for the synthesis of tricyclic xanthine derivatives

All starting materials, reagents and solvents were obtained from commercial suppliers (Sigma Aldrich, Alfa Aesar) and were used without further purification. Melting points were determined in open capillaries on a MEL-TEMP II apparatus (LD Inc., USA) and were not corrected. IR spectra were measured as KBr discs on an FT Jasco IR 410 spectrometer. UV spectra were recorded on a Jasco UV/Vis V-530 apparatus at a concentration of 10^{-5} mol/L in methanol. Elemental analysis was determined with an Elementar Vario-EL III apparatus and were within ± 0.4% of the theoretical value. Thin layer chromatography (TLC) was performed on Merck silica gel 60 F_{254} aluminium sheets. Spots were detected under UV light. ^{1}H NMR spectra were recorded on a Varian-Mercury-VX 300 MHz PFG (Varian, Palo Alto, CA, USA) or an FT NMR 500 MHz spectrometer (JNM-ECZ version ECZR) (Jeol LTD, Akishima, Tokyo, Japan) using the signal of the undeuterated solvent as an internal standard. If indicated, NMR data were collected on a Bruker Ascend 600 MHz NMR spectrometer at 600 MHz (^{1}H), or 151 MHz (^{13}C), respectively. Chemical shifts (δ) were expressed in parts per million (ppm). Data are reported as chemical shift, multiplicity (s, singlet; d, dublet; t, triplet; q, quartet; m, multiplet; br, broad; ind, indole). ^{13}C NMR data were recorded at 125 MHz. The purity of the final compounds was determined on a Waters TQD mass spectrometer coupled with a Waters ACQUITY UPLC or HPLC system or on an ESI-LCMS instrument from Applied Biosystems, API 2000 LCMS/MS, HPLC Agilent 1100.

Compound **5** (**PSB-KD107**)[4], compound **6**[5, 6], compound **7**[6], compound **8**[5], compound **9**[6], compound **11**[6], compound **12**[4], compound **13**[6], compound **14**[4], compound **15**[4], compound **18**[7], compound **19**[4] were synthesized as previously described.

9-(2-(Diethylamino)ethyl)-1,3-dimethyl-6,7,8,9-tetrahydropyrimido[2,1-*f*]purine-2,4(1*H*,3*H*)-dione (10)

A mixture of 9-(2-bromoethyl)-1,3-dimethyl-6,7,8,9-tetrahydropyrimido[2,1-*f*]purine-2,4(1*H*,3*H*)-dione (**V,** 1026 mg, 3 mmol) and diethylamine (6 ml, 57 mmol) in propanol (6 ml) was refluxed for 6 h. A small amount of formed precipitate was filtered off. The filtrate was evaporated in vacuo and the obtained residue was dissolved in 10 ml of H_2O, alkalized with 10% NaOH (till pH 10) and extracted

with dichloromethane. The organic phase was evaporated and the oily residue together with the filtered precipitate was crystallized from cyclohexane. The product (430 mg) was obtained as a white solid. Yield 43%. TLC: R_f = 0.44 (dichloromethane:acetone:propanol:aq. NH_3, 5:3:2:0.6). M.p. 164-166 °C; ^{1}H NMR (300 MHz, $CDCl_3$-*d*) δ ppm 1.02 (t, *J* = 7.18 Hz, 6H, 2x$CH_2C\underline{H}_3$) 2.19-2.17 (m, 2H, N5$CH_2C\underline{H}_2CH_2$N9) 2.57 (q, *J* = 7.05 Hz, 4H, 2x$CH_2C\underline{H}_3$) 2.65 (t, *J* = 6.92 Hz, 2H, N9$CH_2C\underline{H}_2$N) 3.36 (s, 3H, N3CH_3) 3.43 (t, *J* = 5.64 Hz, 2H, N9$C\underline{H}_2CH_2$N) 3.49 (s, 3H, N1CH_3) 3.58 (t, *J* = 6.92 Hz, 2H, CH_2N9) 4.20 (t, *J* = 6.03 Hz, 2H, N3CH_2); IR KBr (cm^{-1}): 2.966 CH_2, CH_3, 1698 CO(2), 1662 CO (4); UV λmax, logε: 301.0, 4.28. Anal Calcd for $C_{16}H_{26}N_6O_2$ (**10**) C, 57.47; H, 7.85; N, 25.13; Found: C, 57.16; H, 8.00; N, 25.09. Mol. wt. 334.42. LC/MS (m/z) positive mode 335 $[M + H]^{1+}$; purity by HPLC-UV (254 nm)-ESI: 99.0%.

10-(2-(1*H*-Indol-3-yl)ethyl)-1,3-dimethyl-7,8,9,10-tetrahydro-1*H*-[1,3]diazepino[2,1-*f*]purine-2,4(3*H*,6*H*)-dione (16, PSB-KD477)

A mixture of 8-bromo-7-(4-bromobutyl)-1,3-dimethyl-1*H*-purine-2,6(3*H*,7*H*)-dione (**VII**, 790 mg, 2 mmol) and tryptamine in 10 ml of 2-methoxyethanol (640 mg, 4mmol)) was refluxed for 12 h. The solvent was evaporated and the residue was crystallized from EtOH. The product (210 mg) was obtained as a white solid. Yield 27%. TLC: R_f = 0.69 (cyclohexane:dioxane, 1:1). M.p. 191-192°C; ^{1}H NMR (600 MHz, DMSO-d_6) δ 1.75 (tq, *J* = 8.8, 5.5, 4.3 Hz, 2H, CH_2), 1.80 (qt, *J* = 5.6, 2.3 Hz, 2H, CH_2), 3.18 (s, 3H, 3-NCH_3), 3.11 – 2.99 (m, 2H, CH_2, N-CH_2), 3.42 (s, 3H, 1-NCH_3), 3.40 – 3.34 (m, 2H, ind-CH_2), 3.87 – 3.62 (m, 2H, ind-CH_2), 4.36 – 4.04 (m, 2H, N-CH_2), 6.97 (ddd, *J* = 7.8, 6.9, 1.0 Hz, 1H, ind-H), 7.05 (ddd, *J* = 8.2, 6.9, 1.2 Hz, 1H, ind-H), 7.15 (d, *J* = 2.2 Hz, 1H, ind-H), 7.33 (dt, *J* = 8.1, 0.9 Hz, 1H, ind-H), 7.72 (dd, *J* = 8.0, 1.1 Hz, 1H, ind-H), 10.78 (d, *J* = 2.6 Hz, 1H, NH). ^{13}C NMR (151 MHz, DMSO) δ 23.35 (indCH_2), 25.97 (CH_2, 27.44 (N3CH_3), 28.42 (NCH_3), 29.44 16 (N1CH_3), 45.44 16 (C6), 51.17 (C7), 53.72 (N8C), 103.28 (C4a), 111.65 (C3ind), 118.34 (C7ind), 118.63 (C4ind), 121.07

(C6ind), 123.00 (C5ind), 127.49 (C3a ind), 136.40(C2 ind), 148.07 (C7a ind), 151.16 (C2153.45), (C4), 158.76. (C8a). $C_{21}H_{24}N_6O_2$ Mol. wt. 392.45. LC/MS (m/z) positive mode 393 $[M + H]^{1+}$; purity by HPLC-UV (254 nm)-ESI: 100%.

8-(2-(1*H*-Indol-3-yl)ethyl)-1,3-dimethyl-7,8-dihydro-1*H*-imidazo[2,1-*f*]purine-2,4(3*H*,6*H*)-dione (17)

A mixture of 8-bromo-7-(2-bromoethyl)-1,3-dimethyl-1*H*-purine-2,6(3*H*,7*H*)-dione (**VI**, 740 mg, 2 mmol) tryptamine (640 mg, 4mmol) of in 10 ml of DMF was refluxed for 10 h. The solvent was evaporated, and the residue was crystallized from EtOH. The product (220 mg) was obtained as a white solid. Yield 27%. TLC: R_f = 0.38 (cyclohexane:dioxane, 1:1). M.p. 218-220 ºC; ^{1}H NMR (500 MHz, DMSO-d_6) δ ppm: 2.99 (t, *J* = 7.45 Hz, 2H, indCH_2) 3.13 (s, 3H, N3CH_3) 3.28 (s, 3H, N1CH_3) 3.53 (t, *J* =7.45 Hz, 2H, CH_2N8) 3.85 (def t, 2H, N8CH_2) 4.02 (def t, 2H, N5CH_2) 6.96 (def t, 1H, C6H, ind) 7.04 (t, *J* = 7.16 Hz, 1H, C5H, ind) 7.18 (d, *J* = 2.01 Hz, 1H, C2H, ind) 7.30 (d, *J* = 8.02 Hz, 1H, C4H, ind) 7.55 (d, *J* = 7.73 Hz, 1H, C7H, ind) 10.82 (br.s. 1H,ind H); ^{13}C NMR (126 MHz, DMSO-d_6) δ ppm: 23.73(indCH_2), 27.87 (N3CH_3), 30.16 (N1CH_3), 43.77 (C6), 47.40 (C7), 52.61 (N8C) 102.22 (C4a), 111.55 (C3ind), 111.95 (C7ind), 118.74 (C4ind), 118.85 (C6ind)121.52 (C5ind), 123.48 (C2 ind), 127.61 (C3a ind), 136.76 (C7a ind), 151.45 (C2), 153.07 (C4), 161.30 (C8a). $C_{19}H_{20}N_6O_2$ Mol. wt. 364.40. LC/MS (m/z) positive mode 365 $[M + H]^{1+}$; purity by HPLC-UV (254 nm)-ESI: 98%.

References

(1) Rempel, V.; Atzler, K.; Behrenswerth, A.; Karcz, T.; Schoeder, C.; Hinz, S.; Kaleta, M.; Thimm, D.; Kiec-Kononowicz, K.; Müller, C. E. Bicyclic imidazole-4-one derivatives: a new class of antagonists for the orphan G protein-coupled receptors GPR18 and GPR55. *Med. Chem. Commun.* **2014**, *5*, 632-649.

(2) Schoeder, C. T.; Kaleta, M.; Mahardhika, A. B.; Olejarz-Maciej, A.; Łażewska, D.; Kieć-Kononowicz, K.; Müller, C. E. Structure-activity relationships of imidazothiazinones and analogs as antagonists of the cannabinoid-activated orphan G protein-coupled receptor GPR18. *Eur. J. Med. Chem.* **2018**, *155*, 381-397.

(3) Behrenswerth, A.; Volz, N.; Toräng, J.; Hinz, S.; Bräse, S.; Müller, C. E. Synthesis and pharmacological evaluation of coumarin derivatives as cannabinoid receptor antagonists and inverse agonists. *Bioorg. Med. Chem.* **2009**, *17*, 2842-2851.

(4) Drabczyńska, A.; Müller, C. E.; Schiedel, A.; Schumacher, B.; Karolak-Wojciechowska, J.; Fruziński, A.; Zobnina, W.; Yuzlenko, O.; Kieć-Kononowicz, K. Phenylethyl-substituted pyrimido[2,1-*f*]purinediones and related compounds: Structure–activity relationships as adenosine A1 and A2A receptor ligands. *Bioorg. Med. Chem.* **2007**, *15*, 6956-6974.

(5) Kieć-Kononowicz, K.; Drabczyńska, A.; Pękala, E.; Michalak, B.; Müller, C. E.; Schumacher, B.; Karolak-Wojciechowska, J.; Duddeck, H.; Rockitt, S.; Wartchow, R. New developments in A1 and A2 adenosine receptor antagonists. In *Pure and Applied Chemistry*, 2001; Vol. 73, p 1411.

(6) Drabczyńska, A.; Karcz, T.; Szymańska, E.; Köse, M.; Müller, C. E.; Paskaleva, M.; Karolak-Wojciechowska, J.; Handzlik, J.; Yuzlenko, O.; Kieć-Kononowicz, K. Synthesis, biological activity and molecular modelling studies of tricyclic alkylimidazo-, pyrimido- and diazepinopurinediones. *Purinergic Signal.* **2013**, *9*, 395-414.

(7) Drabczyńska, A.; Müller, C. E.; Lacher, S. K.; Schumacher, B.; Karolak-Wojciechowska, J.; Nasal, A.; Kawczak, P.; Yuzlenko, O.; Pękala, E.; Kieć-Kononowicz, K. Synthesis and biological activity of tricyclic aryloimidazo-, pyrimido-, and diazepinopurinediones. *Bioorg. Med. Chem.* **2006**, *14*, 7258-7281.

7.2. Appendix II
Supplementary information from publication II: Potent, selective agonists for the cannabinoid-like orphan G protein-coupled receptor GPR18: a promising drug target for cancer and immunity

The supplementary information of this publication is also available online at:

https://pubs.acs.org/doi/suppl/10.1021/acs.jmedchem.3c02423/suppl_file/jm3c02423_si_001.pdf

SUPPORTING INFORMATION

Potent, selective agonists for the cannabinoid-like orphan G protein-coupled receptor GPR18 – a promising drug target for cancer and immunity

Andhika B. Mahardhika,[1,3,4 ¥] Michal Załuski,[2 ¥] Clara T. Schoeder,[1,3 ¥] Nader M. Boshta,[1,§ ¥] Jakub Schabikowski,[2] Filomena Perri,[1,3], Dorota Łażewska,[2] Alexander Neumann,[1,3,χ] Sarah Kremers,[1] Angelo Oneto,[1] Anastasiia Ressemann,[1] Gniewomir Latacz,[2] Vigneshwaran Namasivayam,[1] Katarzyna Kieć-Kononowicz[2]* and Christa E. Müller[1,3,4] *

[1] Pharmaceutical Institute, Department of Pharmaceutical & Medicinal Chemistry, University of Bonn, Germany, An der Immenburg 4, D-53121 Bonn, Germany

[2] Department of Technology and Biotechnology of Drugs, Jagiellonian University Medical College, Faculty of Pharmacy, Pl 30-688 Kraków, Poland

[3] Research Training Group 1873, University of Bonn, 53127 Bonn, Germany

[4] Research Training Group 2873, University of Bonn, 53121 Bonn, Germany

Present address:

‡ C.T.S. Institute for Drug Discovery, Faculty of Medicine, Leipzig University, Liebigstr. 19, D-04103 Leipzig, Germany.

§ N.M.B. Chemistry Department, Faculty of Science, Manoufia University, Gamal Abdel-Nasser Street, Shebin El-Kom 32511, Egypt.

χ A.N. BioSolveIT, An der Ziegelei 79, 53757 Sankt Augustin, Germany

Corresponding Authors

Christa E. Müller, PharmaCenter Bonn, Pharmaceutical Institute, Department of Pharmaceutical & Medicinal Chemistry, University of Bonn, An der Immenburg 4, D-53121 Bonn, Germany. Phone: +49-228-73-2301. Fax: +49-228-73-2567. E-mail: christa.mueller@uni-bonn.de.

Katarzyna Kieć-Kononowicz, Department of Technology and Biotechnology of Drugs, 9 Medyczna Str., 30-688 Kraków, Phone: +12-620-55-80, e-mail: mfkonono@cyf-kr.edu.pl

Table of contents

Synthesis and characterization of products

*General method 1 (GP1): Synthesis of 8-bromo-1-alkyl/arylalkyl-3,7-dimethyl-3,7-dihydro-1H-purine-2,6-dione (**9a-g**)*

A mixture of 8-bromo-3,7-dimethyl-3,7-dihydro-1*H*-purine-2,6-dione **8** (1.04 g, 4 mmol), 6 mmol of alkyl or arylalkyl chloride, K_2CO_3 (1.38 g, 10 mmol), and DMF (10 ml) was heated at 70 °C for 4h. Water was added to the mixture and the formed precipitate was filtered off and used for the next reaction without further purification.

*General method 2 (GP2): Synthesis of 8-((2-(1H-indol-3-yl)ethyl)amino)-1-alkyl/arylalkyl-3,7-dimethyl-3,7-dihydro-1H-purine-2,6-diones (**10, 12-18**)*

A mixture of the appropriate 8-bromo-1- alkyl/arylalkyl -3,7-dimethyl-3,7-dihydro-1*H*-purine-2,6-dione ***(9a-g)*** (0.55 mmol), tryptamine (0.18 g, 1.1 mmol), TEA (0.16 g, 1.6 mmol), and 1 ml of propanol was heated in closed vessels in a microwave oven (300 W, 140 °C, 10 bar) for 1h. The solvent was removed and the residue was treated with ethanol. The products were purified by crystallization from ethanol or by flash column chromatography over silica gel with DCM : methanol (100 : 0 to 80 : 20) as eluent.

8-((2-(1*H*-Indol-3-yl)ethyl)amino)-3,7-dimethyl-3,7-dihydro-1*H*-purine-2,6-dione (10): Synthesized according to GP2; purification by column chromatography with eluent (DCM : methanol, 100 : 0 to 80 : 20); yield 66%; m.p. 262-265 °C; **^{1}H-NMR** (500 MHz, DMSO-d_6) δ 10.78 (br. s., 1H, NH $_{indole}$), 10.58 (s, 1H, NH $_{xanthine}$), 7.61 (d, J = 7.73 Hz, 1H, Ar-H), 7.30 (d, J = 8.31 Hz, 1H, Ar-H), 7.15 (s, J = 2.00 Hz, 1H, Ar-H), 7.11 (t, J = 5.73 Hz, 1H, *NH*-CH_2), 7.00 - 7.05 (m, 1H, Ar-H), 6.92 - 6.97 (m, 1H, Ar-H), 3.50 - 3.58 (m, 2H, NH-*CH_2*), 3.48 (s, 3H, N7-CH_3), 3.25 - 3.29 (m, 3H, N3-CH_3), 2.95 (t, J = 7.59 Hz, 2H, CH_2-indole); LC-MS

(*m/z*): 339.40 $[M+H]^+$; $C_{17}H_{18}N_6O_2$ (calculated MW: 338.37). Purity (HPLC-UV (220 – 400 nm)-ESI-MS): 100%.

8-((2-(1*H*-Indol-3-yl)ethyl)amino)-1-ethyl-3,7-dimethyl-3,7-dihydro-1*H*-purine-2,6-dione (12): Synthesized according to GP2; purification by column chromatography with eluent (DCM : methanol, 100 : 0 to 80 : 20); yield 45%; m.p. 264-266 °C; **^{1}H-NMR** (500 MHz, DMSO-d_6) δ 10.79 (br. s., 1H, NH $_{indole}$), 7.61 (d, J = 7.73 Hz, 1H, Ar-H), 7.30 (d, J = 8.02 Hz, 1H, Ar-H), 7.12 - 7.18 (m, 2H, Ar-H and *NH*-CH_2), 7.03 (t, J = 7.30 Hz, 1H, Ar-H), 6.95 (t, 1H, J = 7.30 Hz, 1H, Ar-H), 3.82 (q, J = 6.87 Hz, 2H, N1CH_2), 3.47 - 3.60 (m, 5H, N7-CH_3 and NH-*CH_2*), 3.35 (s, 3H, N3-CH_3), 2.96 (t, J = 7.59 Hz, 2H, CH_2-indole), 1.05 (t, J = 7.02 Hz, 3H, CH_3).). **^{13}C-NMR** (126 MHz, DMSO-$_6$) δ 154.6, 153.0, 151.1, 149.1, 136.8, 127.9, 123.3, 121.5, 118.9, 118.7, 112.2, 111.9, 102.4, 43.9, 35.6, 30.2, 29.7, 26.0, 13.9; LC-MS (*m/z*): 367.38 $[M+H]^+$; $C_{19}H_{22}N_6O_2$ (calculated MW: 366.42). Purity (HPLC-UV (220 – 400 nm)-ESI-MS): 95.3%.

8-((2-(1*H*-Indol-3-yl)ethyl)amino)-3,7-dimethyl-1-propyl-3,7-dihydro-1*H*-purine-2,6-dione (13): Synthesized according to GP2; purification by column chromatography with eluent (DCM : methanol, 100 : 0 to 80 : 20); yield 49%; m.p. 255-256 °C; **^{1}H-NMR** (500 MHz, DMSO-d_6) δ 10.79 (br. s., 1H, NH $_{indole}$), 7.61 (d, J = 7.73 Hz, 1H, Ar-H), 7.30 (d, J = 8.02 Hz, 1H, Ar-H), 7.11 - 7.20 (m, 2H, Ar-H and *NH*-CH_2), 7.03 (t, J = 7.30 Hz, 1H, Ar-H), 6.95 (t, J = 7.30 Hz, 1H, Ar-H), 3.74 (t, J = 7.45 Hz, 2H, N1-CH_2), 3.52 - 3.58 (m, 2H, NH-*CH_2*), 3.51 (s, 3H, N7-*CH_3*), 3.35 (s, 3H, N3-*CH_3*), 2.96 (t, J = 7.59 Hz, 2H, CH_2-indole), 1.42 - 1.55 (m, 2H, CH_2*CH_2*CH_3), 0.81 (t, J = 7.45 Hz, 3H, CH_2*CH_3*); **^{13}C-NMR** (126 MHz, DMSO-d_6) δ 154.6, 153.3, 151.3, 149.0, 136.8, 127.9, 123.3, 121.5, 118.9, 118.7, 112.2, 111.9, 102.4, 43.9,

42.0, 30.2, 29.7, 26.0, 21.5, 11.8; LC-MS (*m/z*): 381.41 $[M+H]^+$; $C_{20}H_{24}N_6O_2$ (calculated MW: 380.45). Purity (HPLC-UV (220 – 400 nm)-ESI-MS): 95.5%.

8-((2-(1*H*-Indol-3-yl)ethyl)amino)-1-butyl-3,7-dimethyl-3,7-dihydro-1*H*-purine-2,6-dione (14): Synthesized according to GP2; purification by column chromatography with eluent (DCM : methanol, 100 : 0 to 80 : 20); yield 44%; m.p.: 252-253 °C; **^{1}H-NMR** (500 MHz, DMSO-d_6) δ 10.78 (br. s., 1H, NH $_{indole}$), 7.61 (d, J = 7.73 Hz, 1H, Ar-H), 7.30 (d, J = 8.02 Hz, 1H, Ar-H), 7.11 - 7.18 (m, 2H, Ar-H and *NH*-CH_2), 7.03 (t, J = 7.45 Hz, 1H, Ar-H), 6.95 (t, J = 7.30 Hz, 1H, Ar-H), 3.77 (t, J = 7.30 Hz, 2H, N1-CH_2), 3.52 - 3.58 (m, 2H, NH-*CH_2*), 3.51 (s, 3H, N7-CH_3), 3.34 (s, 3H, N3-CH_3), 2.96 (t, J = 7.45 Hz, 2H, CH_2-indole), 1.45 – 1.51 (m, 2H, N1CH_2*CH_2*), 1.23 - 1.27 (m, 2H, *CH_2*CH_3), 0.85 (t, J = 7.45 Hz, 3H, CH_3); **^{13}C-NMR** (126 MHz, DMSO-d_6) δ 154.6, 153.2, 151.3, 149.0, 136.8, 127.9, 123.3, 121.5, 118.9, 118.7, 112.2, 111.9, 102.4, 43.9, 30.4, 30.2, 29.7, 26.0, 20.2, 14.3; LC-MS (*m/z*): 395.44 $[M+H]^+$; $C_{21}H_{26}N_6O_2$ (calculated MW: 394.47). Purity (HPLC-UV (220 – 400 nm)-ESI-MS): 95.0%.

8-((2-(1*H*-Indol-3-yl)ethyl)amino)-3,7-dimethyl-1-(prop-2-yn-1-yl)-3,7-dihydro-1*H*-purine-2,6-dione (15): Synthesized according to GP2; purification by column chromatography with eluent (DCM : methanol, 100 : 0 to 80 : 20); yield 41%; m.p.: 257-258 °C; **^{1}H-NMR** (500 MHz, DMSO-d_6) δ 10.79 (br. s., 1H, NH $_{indole}$), 7.60 (d, J = 7.73 Hz, 1H, Ar-H), 7.30 (d, J = 8.02 Hz, 1H, Ar-H), 7.24 (t, J = 5.58 Hz, 1H, *NH*-CH_2), 7.15 (s, 1H, Ar-H), 7.03 (t, J = 7.16 Hz, 1H, Ar-H), 6.91 - 6.98 (m, 1H, Ar-H), 4.51 (d, J = 2.00 Hz, 2H, N1CH_2), 3.52 - 3.59 (m, 2H, NH-*CH_2*), 3.49 - 3.52 (m, 3H, N7CH_3), 3.35 - 3.40 (m, 3H, N3CH_3), 3.01 (t, J = 2.29 Hz, 1H, C≡CH), 2.96 (t, J = 7.59 Hz, 2H, CH_2-indole); **^{13}C-NMR** (126 MHz, DMSO-d_6) δ 154.9, 152.1, 150.8, 149.5, 136.8, 127.8, 123.3 ,121.5, 118.9, 118.8, 112.2, 111.9, 102.2, 80.7, 73.0,

43.9, 30.3, 30.0, 29.8, 26.0; LC-MS (*m/z*): 377.36 $[M+H]^+$; $C_{20}H_{20}N_6O_2$ (calculated MW: 376.42) . Purity (HPLC-UV (220 – 400 nm)-ESI-MS): 95.1%.

8-((2-(1*H*-Indol-3-yl)ethyl)amino)-1-isobutyl-3,7-dimethyl-3,7-dihydro-1*H*-purine-2,6-dione (16): Synthesized according to GP2; purification by column chromatography with eluent (DCM : methanol, 100 : 0 to 80 : 20); yield 34%; m.p.: 224-225 °C; **^{1}H-NMR** (500 MHz, DMSO-d_6) δ 10.79 (br. s., 1H, NH $_{indole}$), 7.61 (d, *J* = 8.02 Hz, 1H, Ar-H), 7.30 (d, *J* = 8.02 Hz, 1H, Ar-H), 7.10 - 7.20 (m, 2H, *NH*-CH_2 + Ar-H), 7.03 (t, *J* = 7.30 Hz, 1H, Ar-H), 6.91 - 6.97 (m, 1H, Ar-H), 3.62 (d, *J* = 7.45 Hz, 2H, N1CH_2), 3.53 - 3.58 (m, 2H, NH-*CH_2*), 3.51 (s, 3H, N7CH_3), 3.35 (s, 3H, N3CH_3), 2.96 (t, *J* = 7.59 Hz, 2H, CH_2-indole), 1.99 (td, *J* = 6.87, 13.75 Hz, 1H, *CH*(CH_3)$_2$), 0.71 - 0.85 (m, 6H, 2CH_3); **^{13}C-NMR** (126 MHz, DMSO-d_6) δ 154.7, 153.5, 151.5, 149.1, 136.8, 127.9, 123.3, 121.5, 118.9, 118.7, 112.2, 111.9, 102.3, 47.3, 43.9, 30.2, 29.8, 27.3, 26.0, 20.5; LC-MS (*m/z*): 395.44 $[M+H]^+$; $C_{21}H_{26}N_6O_2$ (calculated MW: 394.47). Purity (HPLC-UV (220 – 400 nm)-ESI-MS): 96.1%.

8-((2-(1*H*-Indol-3-yl)ethyl)amino)-1-(cyclohexylmethyl)-3,7-dimethyl-3,7-dihydro-1*H*-purine-2,6-dione (17): Synthesized according to GP2; purification by column chromatography with eluent (DCM : methanol, 100 : 0 to 80 : 20); yield 28%; m.p.: 211-212 °C; **^{1}H-NMR** (500 MHz, DMSO-d_6) δ 10.79 (br. s., 1H, NH $_{indole}$), 7.61 (d, *J* = 7.73 Hz, 1H, Ar-H), 7.30 (d, *J* = 8.02 Hz, 1H, Ar-H), 7.09 - 7.21 (m, 2H, Ar-H), 7.02 (t, *J* = 7.59 Hz, 1H, Ar-H), 6.90 - 6.97 (m, 1H, Ar-H), 3.60 - 3.69 (m, 2H, N1-CH_2), 3.52 - 3.58 (m, 2H, NH-CH_2), 3.51 (s, 3H, N7-CH_3), 3.34 (s, 3H, N3-CH_3), 2.96 (t, *J* = 7.59 Hz, 2H, CH_2-indole), 1.56 - 1.71 (m, 3H, cyclohexane), 1.51 (br. s., 3H, cyclohexane), 1.07 (br. s., 3H, cyclohexane), 0.84 - 0.97 (m, 2H, cyclohexane); **^{13}C-NMR** (126 MHz, DMSO-d_6) δ 154.6, 153.5, 151.5, 149.0, 136.8, 127.9, 123.3, 121.4, 118.9, 118.7, 112.2, 111.9, 102.3, 56.6, 46.1, 43.9, 36.7, 30.9, 30.8, 30.2, 29.8, 26.6, 26.0, 25.9,

19.1; LC-MS (*m/z*): 435.46 $[M+H]^+$; $C_{24}H_{30}N_6O_2$ (calculated MW:434.54). Purity (HPLC-UV (220 – 400 nm)-ESI-MS): 95.4%.

8-((2-(1*H*-Indol-3-yl)ethyl)amino)-1-benzyl-3,7-dimethyl-3,7-dihydro-1*H*-purine-2,6-dione (18): Synthesized according to GP2; purification by column chromatography with eluent (DCM : methanol, 100 : 0 to 80 : 20); yield 53%; m.p.: 239-241 °C; **^{1}H-NMR** (500 MHz, DMSO-d_6) δ 10.79 (br. s., 1H, NH $_{indole}$), 7.62 (d, J = 7.73 Hz, 1H, Ar-H), 7.31 (d, J = 8.02 Hz, 1H, Ar-H), 7.13 - 7.27 (m, 7H, Ar-H), 7.03 (t, J = 7.16 Hz, 1H, Ar-H), 6.95 (m, 1H, J = 7.30 Hz, Ar-H), 4.98 (s, 2H, CH_2Ph), 3.54 - 3.60 (m, 2H, NH-CH_2), 3.52 (s, 3H, N7-CH_3), 3.35 - 3.38 (m, 3H, N3-CH_3), 2.97 (t, J = 7.59 Hz, 2H, CH_2-indole); **^{13}C-NMR** (126 MHz, DMSO-d_6) δ 154.8, 153.1, 151.4, 149.4, 138.8, 136.8, 128.7, 127.9, 127.9, 127.4, 123.3, 121.5, 118.9, 118.8, 112.2, 111.9, 102.4, 43.9, 43.6, 30.3, 29.8, 26.0; LC-MS (*m/z*): 429.41 $[M+H]^+$; $C_{24}H_{24}N_6O_2$ (calculated MW: 428.49). Purity (HPLC-UV (220 – 400 nm)-ESI-MS): 98.2%.

8-((2-(1*H*-Indol-3-yl)ethyl)amino)-1,3-dimethyl-7-(3-methylbut-2-en-1-yl)-3,7-dihydro-1*H*-purine-2,6-dione (25): Synthesized according to GP4; purification by column chromatography with eluent (DCM : methanol, 100 : 0 to 80 : 20); yield 43%; m.p.: 158-159 °C; **^{1}H-NMR** (500 MHz, DMSO-d6) δ 10.79 (s, 1H, NH $_{indole}$), 7.61 (d, J=7.45 Hz, 1H, Ar-H), 7.31 (d, J=8.02 Hz, 1H, Ar-H), 7.13 (d, J=2.29 Hz, 1 H, *NH*CH_2 and Ar-H), 7.00 - 7.07 (m, 2H, Ar-H), 6.92 - 6.97 (m, 1H, Ar-H), 5.07 - 5.12 (m, 1H, N7CH_2*CH*), 4.61 (d, J=6.30 Hz, 2H, N7CH_2), 3.53 - 3.59 (m, 2H, NHCH_2), 3.35 (s, 3H, N3CH_3), 3.13 (s, 3H, N1CH_3), 2.97 (t, J=7.16 Hz, 2H, NHCH$_2$$CH_2$), 1.67 (s, 3H, N7CH$_2$CHC($CH_3$)$_2$), 1.59 (s, 3H, N7CH$_2$CHC($CH_3$)$_2$); **^{13}C-NMR** (DMSO-$d_6$) δ ppm: 154.0, 153.2, 151.5, 149.3, 136.8, 135.8, 127.9, 123.3, 121.4, 120.0, 118.9, 118.8, 112.2, 111.9, 101.7, 43.9, 41.1, 29.8, 27.7, 25.9, 25.8,

18.4. UPLC-MS (*m/z*): 407.19 $[M+H]^+$; $C_{22}H_{26}N_6O_2$ (calculated MW: 406.49). Purity (UPLC-MS): 98.4%; t_R = 6.47;

8-((2-(1*H*-indol-3-yl)ethyl)amino)-7-(but-3-en-1-yl)-1,3-dimethyl-3,7-dihydro-1*H*-purine-2,6-dione (26): Synthesized according to GP4; purification by column chromatography with eluent (DCM : methanol, 100 : 0 to 80 : 20); yield 41%; m.p.: 148-149 °C; **^{1}H-NMR** (500 MHz, DMSO-d6) δ 10.80 (s, 1H, NH $_{indole}$), 7.61 (d, *J*=7.73 Hz, 1H, Ar-H), 7.31 (d, *J*=8.02 Hz, 1H, Ar-H), 7.17 (t, *J*=5.73 Hz, 1H, *NH*CH_2), 7.13 (d, *J*=2.01 Hz, 1H, Ar-H), 7.01 - 7.05 (m, 1H, Ar-H), 6.92 - 6.97 (m, 1H, Ar-H), 5.68 - 5.77 (m, 1H, N7CH_2CH_2*CH*CH_2), 4.92 - 4.98 (m, 2H, N7CH_2CH_2CH*CH*$_2$), 4.03 (t, *J*=7.16 Hz, 2H, N7CH_2), 3.52 - 3.58 (m, 2H, NH*CH*$_2$), 3.35 (s, 3H, N3CH_3), 3.14 (s, 3H, N1CH), 2.96 (t, *J*=7.45 Hz, 2H, NHCH_2*CH*$_2$), 2.32 (q, *J*=6.87 Hz, 2H, N7CH_2*CH*$_2$). UPLC-MS (*m/z*): 393.17 $[M+H]^+$; $C_{21}H_{24}N_6O_2$ (calculated MW: 392.46). Purity (UPLC-MS): 100.0%; t_R = 5.97;

4-((8-((2-(1*H*-indol-3-yl)ethyl)amino)-1,3-dimethyl-2,6-dioxo-1,2,3,6-tetrahydro-7*H*-purin-7-yl)methyl)benzoic acid (44): In a 50 mL round-bottom flask, **43** (33 mg, 0.68 mmol) was dissolved in 4 mL of THF, then an aqueous solution (50%) of LiOH · H_2O (0.12 g, 2.72 mmol) was added dropwise. The mixture was kept stirring overnight at RT. When no further progress was detected, water was added and the pH value was adjusted to 1-2 with 1N-HCl, which resulted in precipitation. The precipitate was filtered off under reduced pressure, and the residue was washed with Et_2O, then crystallized from methanol to yield the title compound. Yield 64%; m.p.: 221-223 °C; **^{1}H-NMR** (500 MHz, DMSO-d_6) δ 10.79 (s, 1H, NH $_{indole}$), 7.86 (d, *J* = 8.4 Hz, 1H, Ar-H), 7.63 (d, *J* = 7.9 Hz, 1H, Ar-H), 7.40 – 7.30 (m, 2H, *NH*CH_2 and Ar-H), 7.24 (d, *J* = 8.5 Hz, 2H, Ar-H), 7.11 (d, *J* = 2.3 Hz, 1H, Ar-H), 7.08 – 7.03 (m, 1H, Ar-H), 6.99 – 6.94 (m, 1H, Ar-H), 5.35 (s, 2H, N7CH_2), 3.63 – 3.58 (m, 2H, HN*CH*$_2$), 3.41 (s, 3H,

N3CH_3), 3.15 (s, 3H, N1CH_3), 3.00 – 2.96 (m, 2H, NHCH_2*CH_2*); **^{13}C-NMR** (126 MHz, DMSO) δ 166.85, 153.54, 152.41, 150.68, 148.62, 141.28, 135.93, 129.15, 126.93, 126.43, 122.46, 120.55, 117.96, 117.86, 111.18, 111.03, 100.93, 44.86, 43.00, 28.96, 26.84, 25.02; LC-MS (*m/z*): 473.0 $[M+H]^+$; $C_{25}H_{24}N_6O_4$ (calculated MW: 472.50). Purity (HPLC-UV (220 – 400 nm)-ESI-MS): 98.9%.

8-Chloro-7-(4-chlorobenzyl)-1-methyl-1*H*-purine-2,6(3*H*,7*H*)-dione (72): To a suspension of **68a** (5 g, 17.9 mmol) in water (50 ml) was added acetic acid (0.5 ml) followed by 4-chlorobenzaldehyde (6.75 g, 48.02 mmol) over 15 min at room temperature (RT). The solution was cooled, and the precipitate was filtered under vacuum, washed with cold water (50 ml) followed by cold acetonitrile to give **69** (6.67 g, 23.99 mmol, 75%). To a suspension of the product in DCM (50 ml) and methanol (50 ml) was added glacial acetic acid (1.46 g, 24.3 mmol) followed by $NaBH_3CN$ (1.6 g, 25.5 mmol). The reaction mixture was stirred at RT for 2h. Then, glacial acetic acid (0.146 g, 2.43 mmol) and $NaBH_3CN$ (0.16 g, 25.5 mmol) were added, the reaction mixture was further stirred overnight, and a TLC analysis was performed (eluent: DCM : ethyl acetate, 9:1) to check whether the reaction was completed. After completion, the reaction mixture was concentrated under reduced pressure, and the formed precipitate was filtered and washed with cold methanol to yield **70** (4.71 g, 70%). A suspension of **70** (4.7 g, 16.8 mmol) in triethyl orthoformate (50 ml) was heated to reflux for 5h. Then, it was cooled to RT, and the formed solid was filtered off, washed with diethyl ether (50 ml) and dried to give **71** (4.47 g, 92%). To a solution of **71** (4.5 g, 15.5 mmol) in THF (70 ml) was added *N*-chlorosuccinimide (2.7g, 20.22 mmol), and the mixture was stirred at RT for 16h. The reaction mixture was dried under vacuum, ice-water (100 ml) was added, and the precipitate was filtered off and washed with water (3x50 ml) under reduced pressure to give a white powder of **72.** Yield 81%; **^{1}H-NMR** (600 MHz, DMSO-d_6) δ 12.14 (s, 1H, NH $_{xanthine}$), 7.42

(d, *J* = 8.4 Hz, 2H, H-Ar), 7.30 (d, *J* = 8.4 Hz, 2H, H-Ar), 5.49 (s, 2H, N7CH_2), 3.17 (s, 3H, CH_3); ^{13}C-NMR (151 MHz, DMSO) δ 26.91, 47.55, 107.15, 128.78, 129.20, 132.69, 134.55, 137.97, 146.02, 150.65, 154.62; LC-MS (*m/z*)= 325.2 $[M+H]^+$; $C_{13}H_{10}Cl_2N_4O_2$ (calculated MW: 325.1)

8-((2-(1*H*-indol-3-yl)ethyl)amino)-7-(4-chlorobenzyl)-3-ethyl-1-methyl-3,7-dihydro-1*H*-purine-2,6-dione (75)

Step (a) A mixture of ethyl urea (3.96 g, 45 mmol) and cyanoacetic acid ethyl ester acid (3.78 g, 45 mmol) in 67 ml of sodium ethoxide was heated at 100 °C for 4h. Then the solvent was evaporated, and water was added to the residue. The resulting solution was adjusted to a pH value of 7 by addition of acetic acid. The resulting precipitate was filtered off and washed with acetone to afford 6-amino-1-ethyluracil**.** Yield: 2.65 g (38 %).

Step (b) A mixture of 6-amino-1-ethyluracil (3.10 g, 20 mmol) was heated in 45 ml of 50% aq. acetic acid at 60 °C until completely dissolved. Then approx. 1.40 g (20 mmol) of $NaNO_2$ was slowly added until brown fumes began to form. The resulting purple precipitate of 6-amino-1-ethyl-5-nitrosouracil was filtered off, washed with water and dried. The compound (1.84 g, 10 mmol) was subsequently suspended in 60 ml of an aq. NH_3 solution (12.5%), and the mixture was heated at 70 °C until a clear solution was obtained. Then, approx. 4.1 g of sodium dithionite was added over a period of 10 min until the color changed from red to yellow. The resulting solution was concentrated until the product started crystallize and then cooled to 4 °C. The resulting product 5,6-diamino-1-ethyluracil was filtered off, washed with water and used directly for the next step. Yield: 1.31 g (77 %).

Step (c) A mixture of 5,6-diamino-1-ethyluracil (1.70 g, 10 mmol) and 15 ml of formic acid (95-97%) was refluxed for 1h. Then, the excess formic acid was removed in a vacuum evaporator, and 10 ml of ethanol was added. The resulting precipitate was treated with 15 ml

of 10% aq. sodium hydroxide solution and refluxed for 45 min. The solution was then cooled and acidified with 10% aq. HCl solution to a pH value of 5. The formed precipitate of 3-ethylxanthine was filtered off and dried. Yield: 1.42 g (79 %).

Step (d) A mixture of 3-ethylxanthine (1.44 g, 8 mmol), 99.5% acetic acid (8.8 ml) and aq. HBr solution (40%, 1.22 ml) was heated in a water bath at 58 °C. After obtaining a clear mixture, an aq. solution of $NaClO_3$ (0.3 g $NaClO_3$ in 2 mL water) was added dropwise. The resulting mixture was heated for 2h. Then the precipitate of 8-bromo-3-ethylxanthine was filtered off, washed with water, and dried. Yield: 1.67 g (82%).

Step (e) A mixture of 8-bromo-3-ethylxanthine (1.04 g, 4 mmol), 4-chlorobenzyl chloride (0.97 g, 4.8 mmol), DIPEA (8 mmol), and DMF (8 ml) were heated at 40 °C for 4h. Then, water was added, and the resulting precipitate was filtered off, washed with water and dried. The obtained product (**8-**bromo-7-(4-chlorobenzyl)-3-ethylxanthine) was used directly for the next step. Yield: 1.12 g (73%).

Step (f) A mixture of 8-bromo-7-(4-chlorobenzyl)-3-ethylxanthine (0.91 g, 2.4 mmol), iodomethane (0.25 mL, 4 mmol), and K_2CO_3 (0.55 g, 4 mmol) in 4 ml DMF (4 mL) was heated at 40 °C for 4h. Then, 10 mL water was added, and the resulting precipitate was filtered off, washed with 5 mL water and dried. The obtained product (8-bromo-7-(4-chlorobenzyl)-3-ethyl-1-methylxanthine) was used in next step without further purification. Yield: 0.54 g (68%).

Step (g) Synthetic procedure according to method GP2 affording 8-((2-(1*H*-indol-3-yl)ethyl)amino)-7-(4-chlorobenzyl)-3-ethyl-1-methyl-3,7-dihydro-1*H*-purine-2,6-dione (**75**). Purification by column chromatography with eluent (DCM : methanol, 100 : 0 to 80 : 20); yield 46%; m.p.: 211-213 °C; **^{1}H-NMR** (300 MHz, DMSO-d_6) δ 10.81 (s, 1H, NH $_{indole}$), 7.66 (d, *J*=7.62 Hz, 1H, Ar-H), 7.40 (t, *J*=5.57 Hz, 1H, Ar-H), 7.31 - 7.36 (m, 3H, Ar-H and *NH*CH_2), 7.19 - 7.24 (m, 2H, Ar-H), 7.12 (d, *J*=2.34 Hz, 1H, Ar-H), 7.02 - 7.09 (m, 1H, Ar-H), 6.93 -

7.00 (m, 1H, Ar-H), 5.25 (s, 2H, N7CH_2), 4.00 (q, *J*=7.03 Hz, 2H, N3CH_2), 3.54 - 3.63 (m, 2H, NH*CH_2*), 3.15 (s, 3H, N1CH_3), 2.98 (t, *J*=7.33 Hz, 2H, NHCH_2*CH_2*), 1.23 (t, *J*=7.03 Hz, 3H, N3CH_2*CH_3*); **^{13}C-NMR** (DMSO-d_6) δ ppm: 154.2, 153.2, 150.9, 148.9, 136.7, 136.5, 132.5, 129.6, 128.9, 127.8, 123.3, 121.4, 118.8, 118.6, 112.0, 111.8, 101.7, 45.1, 43.8, 38.1, 27.6, 25.8, 13.7. UPLC-MS (*m/z*): 477.18 $[M+H]^+$; $C_{25}H_{25}ClN_6O_2$ (calculated MW: 476.97). Purity (UPLC-MS): 99.3%; t_R = 7.36. HR-MS (ESI-QTOF) calculated for $C_{25}H_{26}ClN_6O_2$ $[M+H]^+$: 477.1806; found: 477.1804.

8-((2-(1*H*-indol-3-yl)ethyl)amino)-7-(4-chlorobenzyl)-1-methyl-3-(prop-2-yn-1-yl)-3,7-dihydro-1*H*-purine-2,6-dione (77): Synthesized according to GP5; purification by column chromatography (DCM : methanol, 9.2 : 0.8), yield 32%; m.p.: 189-190 °C; **^{1}H-NMR** (500 MHz, DMSO-d_6) δ 10.79 (s, 1H, NH $_{indole}$), 7.67 (d, *J* = 7.8 Hz, 1H, Ar-H), 7.44 (t, *J* = 5.6 Hz, 1H, Ar-H), 7.35 – 7.33 (m, 3H, Ar-H and *NH*CH_2), 7.21 (d, *J* = 8.5 Hz, 2H, Ar-H), 7.13 (d, *J* = 2.2 Hz, 1H, Ar-H), 7.07 (t, *J* = 7.0 Hz, 1H, Ar-H), 6.99 (t, *J* = 7.9 Hz, 1H, Ar-H), 5.26 (s, 2H, N7CH_2), 4.71 (d, *J* = 2.4 Hz, 2H, N3CH_2), 3.65 – 3.56 (m, 2H, HN*CH_2*), 3.20 (t, *J* = 2.4 Hz, 1H, CH), 3.18 (s, 3H, N1CH_3), 3.03 – 2.98 (m, 2H, NHCH_2*CH_2*); **^{13}C-NMR** (126 MHz, DMSO-d_6) δ 153.7, 152.6, 150.1, 147.7, 136.2, 135.9, 132.1, 129.0, 128.4, 127.3, 122.8, 120.6, 118.4, 118.2, 111.45, 111.29, 101.6, 78.8, 73.9, 44.7, 43.3, 31.9, 27.2, 25.2; LC-MS (*m/z*): 487.0 $[M+H]^+$; $C_{26}H_{23}ClN_6O_2$ (calculated MW: 486.9). Purity (HPLC-UV (220 – 400 nm)-ESI-MS): 98.3%.

8-((2-(1*H*-indol-3-yl)ethyl)amino)-7-(4-chlorobenzyl)-1-methyl-3-propyl-3,7-dihydro-1*H*-purine-2,6-dione (78): Synthesized according to GP5; purification by column chromatography (DCM : methanol, 9.2 : 0.8), yield 19%; m.p.: 207-208 °C; **^{1}H-NMR** (600 MHz, DMSO-d_6) δ 10.80 (s, 1H, NH $_{indole}$), 7.65 (d, *J* = 7.9 Hz, 1H, Ar-H), 7.39 (t, *J* = 5.7 Hz,

1H, *NH*CH_2), 7.35 – 7.34 (m, 3H, Ar-H), 7.21 (d, *J* = 8.5 Hz, 2H, Ar-H), 7.12 (d, *J* = 2.2 Hz, 1H, Ar-H), 7.07 (t, *J* = 7.9 Hz, 1H, Ar-H), 6.97 (t, *J* = 7.8 Hz, 1H, Ar-H), 5.26 (s, 2H, N7CH_2), 3.97 – 3.91 (m, 2H, N3*CH_2*-CH_2), 3.61 – 3.55 (m, 2H, CH_2, HN*CH_2*), 3.16 (s, 3H, N1CH_3), 3.01 – 2.95 (m, 2H, NHCH$_2$*CH_2*), 1.71 – 1.68 (m, 2H, N3CH$_2$*CH_2*CH_3), 0.90 (t, *J* = 7.4 Hz, 3H, N3CH$_2$CH$_2$*CH_3*); **^{13}C-NMR** (151 MHz, DMSO-d_6) δ 153.7, 152.8, 150.7, 148.8, 136.30, 136.06, 132.1, 129.0, 128.5, 127.3, 122.9, 120.9, 118.3, 118.2, 111.5, 111.4, 101.1, 44.68, 44.08, 43.4, 27.2, 25.4, 20.9, 11.1; LC-MS (*m/z*): 491.3 $[M+H]^+$; $C_{26}H_{27}ClN_6O_2$ (calculated MW: 490.9). Purity (HPLC-UV (220 – 400 nm)-ESI-MS): 95.3%.

*General method 6 (GP6): Synthesis of compound **87**, **89,** and **91***

8-Bromotheobromine (5.18 g, 20 mmol) was refluxed for 15h in 80 mL of acetone with 22 mmol 4-chlorobenzyl bromide, or 2,4-dichlorobenzyl bromide, respectively, in the presence of K_2CO_3 (58 mmol) and TEBA (3 mmol). The formed precipitate was filtered off and washed with 50 ml 15% aq. NaOH solution and subsequently with 100 ml water. The residue was recrystallized from ethanol. Next, a mixture of 5 mmol of 8-bromo-7-(4-chloro)benzyl-1,3-dimethyl-3,7-dihydro-1*H*-purine-2,6-dione or 8-bromo-7-(3,4-dichloro)benzyl-1,3-dimethyl-3,7-dihydro-1*H*-purine-2,6-dione with 5.5 mmol of the appropriate amine (4-(2-aminoethyl)phenol (for **87)**, or 2-(3,4-dimethoxyphenyl)ethan-1-amine (for **89** and **91**))was refluxed for 11-16h in 2-methoxyethanol. Then, the solution was kept in a refrigerator for a few hours. The precipitated solid was crystallized from ethanol (**87**, **89**) or purified by column chromatography (DCM : methanol, 9.8 : 0.20) (**91**) yielding the final products.

7-(4-Chlorobenzyl)-8-((4-hydroxyphenylethyl)amino)-1,3-dimethyl-3,7-dihydro-1*H*-purine-2,6-dione (87): Synthesized according to GP6; crystallized from ethanol; yield 23%; m.p. 270-273 ºC; **^{1}H-NMR** (400 MHz, DMSO-d_6) δ 9.21 (br. s., 1H, OH), 7.37 (d, 2H, *J* = 8.6

Hz, Ar-H), 7.29 (t, 1H, *J* = 5.3 Hz, *NH*CH_2), 7.19 (d, 2H, *J* = 8.6 Hz, Ar-H), 6.97 (d, 2H, *J* = 8.2 Hz, Ar-H), 6.66 (d, 2H, *J* = 8.2 Hz, Ar-H), 5.26 (s, 2H, N7CH_2), 3.48 (q, 2H, *J* = 6.7 Hz, NH*CH_2*), 3.37 (br. s., 3H, N3CH_3), 3.16 (s, 3H, N1*CH_3*), 2.75 (t, 2H, *J* = 7.0 Hz, CH_2Ph); **^{13}C-NMR** (DMSO-d_6, 101 MHz) δ: 156.1, 154.0, 153.2, 151.4, 149.3, 136.5, 132.5, 130.1, 129.8, 129.5, 128.9, 115.5, 101.6, 45.1, 44.8, 34.8, 29.8, 27.7; LC-MS (*m/z*): 440.16 $[M+H]^+$; $C_{22}H_{22}ClN_5O_3$ (calculated MW: 439.90). Purity (HPLC-UV (220 – 400 nm)-ESI-MS): 100%. Elemental analysis calculated for $C_{22}H_{22}ClN_5O_3$: C (60.06%), H (5.04%), N (15.92%); found: C (59.60%), H (4.71%); N (15.77%).

7-(4-Chlorobenzyl)-8-((3,4-dimethoxyphenylethyl)amino)-1,3-dimethyl-3,7-dihydro-1*H*-purine-2,6-dione (89): Synthesized according to GP6; crystallized from ethanol; yield 35%; m.p. 197-200 °C; **^{1}H-NMR** (400 MHz, DMSO-d_6) δ 7.35 (d, 2H, *J* = 8.22 Hz, Ar-H), 7.28 (t, 1H, *J* = 5.28 Hz, *NH*CH_2), 7.17 (d, 2H, *J* = 8.61 Hz, Ar-H), 6.76 - 6.86 (m, 2H, Ar-H), 6.66 (d, 1H, *J* = 8.22 Hz, Ar-H), 5.26 (s, 2H, N7CH_2), 3.66 - 3.75 (m, 6H, 2OCH_3), 3.54 (q, 2H, *J* = 6.52 Hz, NH*CH_2*), 3.38 (s, 3H, N3CH_3), 3.16 (s, 3H, N1CH_3), 2.80 (t, 2H, *J* = 7.04 Hz, CH_2Ph); **^{13}C-NMR** (101 MHz, DMSO-d_6) δ 154.0, 153.2, 151.4, 149.1, 147.7, 136.5, 132.4, 132.2, 129.4, 128.9, 121.1, 113.0, 112.3, 101.6, 56.0, 55.8, 44.6, 35.1, 29.8 , 27.7; LC-MS (*m/z*): 484.16 $[M+H]^+$; $C_{24}H_{26}ClN_5O_4$ (calculated MW: 483.95). Purity (HPLC-UV (220 – 400 nm)-ESI-MS): 100%. Elemental analysis calculated for $C_{24}H_{26}ClN_5O_4$: C (59.56%), H (5.42%), N (14.47%); found: C (59.49%); H (5.14%); N (14.38%).

7-(2,4-Dichlorobenzyl)-8-((3,4-dimethoxyphenylethyl)amino)-1,3-dimethyl-3,7-dihydro-1*H*-purine-2,6-dione (91): Synthesized according to GP6; purification by column chromatography (DCM : methanol, 9.8 : 0.2); yield 25%; m.p. 155-157 °C; **^{1}H-NMR** (400 MHz, DMSO-d_6) δ 7.68 (d, 1H, *J* = 1.57 Hz, Ar-H), 7.32 (dd, 2H, *J* = 1.57, 8.22 Hz, Ar-H),

6.75 - 6.84 (m, 2H, Ar-H and *NH*CH_2), 6.67 (d, 1H, *J* = 7.83 Hz, Ar-H), 6.46 (d, 1H, *J* = 8.22 Hz, Ar-H), 5.30 (s, 2H, N7CH_2), 3.69 (d, 6H, *J* = 6.26 Hz, 2OCH_3), 3.53 (q, 2H, *J* = 6.65 Hz, NH*CH_2*), 3.42 (s, 3H, N3CH_3), 3.10 (s, 3H, N1CH_3), 2.80 (t, 2H, *J* = 7.04 Hz, CH_2Ph); **^{13}C-NMR** (101 MHz, DMSO-d_6) δ 154.4, 153.1, 151.4, 149.4, 149.0, 147.7, 134.3, 132.8, 132.4, 132.2, 129.2, 128.1, 127.6, 121.1, 113.0, 112.3 , 101.5, 55.9, 55.8, 44.6, 44.0, 35.0, 29.8, 27.6; LC-MS (*m/z*): 518.19 $[M+H]^+$; $C_{24}H_{25}Cl_2N_5O_4$ (calculated MW: 518.39). Purity (HPLC-UV (220 – 400 nm)-ESI-MS): 100%. Elemental analysis calculated for $C_{24}H_{25}Cl_2N_5O_4$: C (55.60%), H (4.86%), N (13.51%); found: C (55.36%), H (4.58%) N (13.42%).

*General method 7 (GP7): Synthesis of compounds **88** and **90***

3,4-Dimethoxyphenylethylamino derivative **89** or **91** (0.4 mmol) was refluxed for 30 min in 5 mL of 48% aq. hydrobromic acid. After cooling down to RT, saturated aq. sodium carbonate solution was added to obtain a basic pH value of 7. The precipitated solid was crystallized from ethanol-water (1:1) (**88**) or purified by column chromatography (DCM : methanol, 9.0 : 1.0; **90**) yielding the final products.

7-(4-Chlorobenzyl)-8-((3,4-dihydroxyphenylethyl)amino)-1,3-dimethyl-3,7-dihydro-1*H*-purine-2,6-dione (88): Synthesized according to GP7; crystallized from ethanol-water (1:1); yield 43%; m.p. 262-264 °C; **^{1}H-NMR** (400 MHz, DMSO-d_6) δ 8.74 (br. s., 1H, OH), 7.37 (d, 2H, *J* = 8.36 Hz, Ar-H), 7.29 (br. s., 1H, *NH*CH_2), 7.19 (d, 2H, *J* = 8.36 Hz, Ar-H), 6.58 - 6.67 (m, 2H, Ar-H), 6.43 (d, 1H, *J* = 7.92 Hz, Ar-H), 5.25 (s, 2H, PhCH_2), 3.46 (br. s., 5H, NH*CH_2* + N3CH_3), 3.16 (s, 3H, N1CH_3), 2.69 (t, 2H, *J* = 7.26 Hz, CH_2Ph); **^{13}C-NMR** (101 MHz, DMSO-d_6) δ 154.1, 153.2, 151.4, 149.4, 145.5, 144.0, 136.5, 132.5, 130.4, 129.5, 128.9, 119.8, 116.6, 115.9, 101.6, 45.1, 44.8, 35.0, 29.8, 27.7; LC-MS (*m/z*): 456.18 $[M+H]^+$; $C_{22}H_{22}ClN_5O_4$ (calculated MW: 455.89). Purity (HPLC-UV (220 – 400 nm)-ESI-MS): 99.4%. Elemental

analysis calculated for $C_{22}H_{22}ClN_5O_4$: C (57.96%), H (4.86%), N (15.36%); found: C (58.03%), H (4.78%), N (15.14%).

7-(2,4-Dichlorobenzyl)-8-((3,4-dihydroxyphenylethyl)amino)-1,3-dimethyl-3,7-dihydro-1*H*-purine-2,6-dione (90): Synthesized according to GP7; purification by column chromatography (DCM : methanol, 9.2 : 0.8), yield 24%; m.p. 277-279 °C; **^{1}H-NMR** (400 MHz, DMSO-d_6) δ 7.69 (d, 1H, *J* = 1.57 Hz, Ar-H), 7.35 (dd, 2H, *J* = 1.76, 8.41 Hz, Ar-H), 6.56 - 6.64 (m, 2H, Ar-H and *NH*CH_2), 6.50 (d, 1H, *J* = 8.22 Hz, Ar-H), 6.42 (d, 1H, *J* = 8.22 Hz, Ar-H), 5.31 (s, 2H, PhCH_2), 3.44 - 3.50 (m, 2H, NH*CH_2*), 3.43 (s, 3H, N3CH_3), 3.11 (s, 3H, N1CH_3), 2.68 (t, 2H, *J* = 7.04 Hz, CH_2Ph); **^{13}C-NMR** (101 MHz, DMSO-d_6) δ 154.4, 153.1, 151.5, 149.5, 145.5, 144.0, 134.3, 132.8, 132.4, 130.4, 129.2, 128.1, 127.7, 119.8, 116.5, 115.9, 101.5, 44.8, 44.0, 35.0, 29.8, 27.6; LC-MS (*m/z*): 490.14 $[M+H]^+$; $C_{22}H_{21}Cl_2N_5O_4$ (calculated MW: 490.34). Purity (HPLC-UV (220 – 400 nm)-ESI-MS): 100%. Elemental analysis calculated for $C_{22}H_{21}Cl_2N_5O_4$: C (53.88%), H (4.32%), N (14.28%); found: C (53.48%), H (4.14%), N (14.19%).

Table S1. Overview of the compounds' potencies at human and mouse GPR18, human GPR55, and human CB_1 and CB_2 receptors

Compound		β-arrestin-2 assay Human GPR18				β-arrestin-2 assay Mouse GPR18				β-arrestin-2 assay Human GPR55		Radioligand binding assays Human CB_1 receptor	Radioligand binding assays Human CB_2 receptor
		Agonistic activity			Antagonistic activity	Agonistic activity			Antagonistic activity	Agonistic activity	Antagonistic activity	Radioligand binding *vs.* $[^3H]$CP55,940	Radioligand binding *vs.* $[^3H]$CP55,940
		EC_{50} ± SEM (μM) (or percent receptor activation)[a] *[Efficacy][b]*	Global hill slope value	p-value (significance)[c]	IC_{50} ± SEM (μM) (or percent receptor inhibition)[d]	EC_{50} ± SEM (μM) (or percent receptor activation)[a] *[Efficacy][b]*	Global hill slope value	p-value (significance)[c]	IC_{50} ± SEM (μM) (or percent receptor inhibition)[d]	EC_{50} ± SEM (μM) (or percent receptor activation)[a] *[Efficacy][b]*	IC_{50} ± SEM (μM) (or percent receptor inhibition)[d]	K_i ± SEM (μM) or percent displacement of $[^3H]$CP55,940 (%)[e]	K_i ± SEM (μM) or percent displacement of $[^3H]$CP55,940 (%)[e]
1	NAGly	**>10** (10%)[f]	n.d	n.d	**>10** (15%)[f]	**>10** (4%)	n.d	n.d	**>10** (-1%)	n.d.[g]	n.d.	n.d	n.d
2	Abnormal cannabidiol	**>10** (-50%)[f]	n.d	n.d	**>10** (42%)[f]	**>10** (-5%)	n.d	n.d	**13.1** ± 1.6	**>10** (7%)[f]	**>10** (33%)[f]	n.d	n.d
3	THC	**3.37** ± 1.19[f] *[100%]*	1.1	0.90 (ns)	n.d.	**>10** (10%)	n.d	n.d	n.d	**>10** (-4%)[f]	**14.2** ± 5.2[f]	**0.00390** ± 0.0089	**0.00598** ± 0.0030
4	Resolvin D2	**>10** (26%)	n.d	n.d	n.d.	**>10** (4%)	n.d	n.d	n.d	n.d.	n.d.	n.d	n.d
5	PSB KD-107	**0.562** ± 0.113[f] *[191%]*	1.2	0.71 (ns)	n.d.	**1.78** ± 0.62 *[104%]*	1.2	0.52 (ns)	n.d	**>10** (-5%)[f]	**>10** (20%)[f]	**>10** (11%)[f]	**>10** (29%)[f]
6	PSB KD-477	**0.454** ± 0.156[f] *[171%]*	1.3	0.48 (ns)	n.d.	**0.583** ± 0.214 *[111%]*	1.3	0.44 (ns)	n.d	**>10** (38%)[f]	**>10** (21%)[f]	**>10** (24%)[f]	**>10** (46%)[f]
10		**>10** (14%)	n.d	n.d	**>10** (2%)	**>10** (12%)	n.d	n.d	**>10** (-3%)	**>10** (8%)	**>10** (3%)	**>10** (-6%)	**>10** (13%)
11		**0.902** ± 0.148 *[132%]*	1.0	0.95 (ns)	n.d	**2.97** ± 1.02 *[132%]*	1.3	0.61 (ns)	n.d	**>10** (-1%)	**>10** (36%)	**>10** (10%)	**>10** (15%)
12		**>10** (30%)	n.d	n.d	**>10** (-28%)	**>10** (35%)	n.d	n.d	**>10** (-8%)	**>10** (3%)	**>10** (11%)	**>10** (29%)	**>10** (16%)
13		**>10** (15%)	n.d	n.d	**>10** (-7%)	**>10** (23%)	n.d	n.d	**>10** (3%)	**>10** (-11%)	**>10** (22%)	**>10** (19%)	**>10** (21%)
14		**>10** (11%)	n.d	n.d	**>10** (-11%)	**>10** (11%)	n.d	n.d	**>10** (-8%)	**>10** (25%)	**>10** (-27%)	**>10** (20%)	**>10** (22%)
15		**>10** (18%)	n.d	n.d	**>10** (-5%)	**>10** (19%)	n.d	n.d	**>10** (-3%)	**>10** (-2%)	**>10** (-20%)	**>10** (-1%)	**>10** (17%)

16		**>10** (5%)	n.d	n.d	**>10** (-25%)	**>10** (16%)	n.d	n.d	**>10** (-6%)	**>10** (3%)	**>10** (35%)	**>10** (6%)	**>10** (29%)
17		**>10** (13%)	n.d	n.d	**>10** (3%)	**>10** (24%)	n.d	n.d	**>10** (-6%)	**>10** (10%)	**>10** (9%)	**>10** (29%)	**1.42** ± 0.42 *[66%]*
18		**>10** (37%)	n.d	n.d	**>10** (-45%)	**>10** (24%)	n.d	n.d	**>10** (-3%)	**>10** (14%)	**>10** (-55%)	**>10** (24%)	**>10** (31%)
21		**0.190** ± 0.043 *[113%]*	1.6	0.19 (ns)	n.d	**0.379** ± 0.055 *[85%]*	1.2	0.54 (ns)	n.d	**>10** (21%)	**>10** (-11%)	**>10** (11%)	**>10** (39%)
22		**0.196** ± 0.059 *[127%]*	1.0	0.98 (ns)	n.d	**0.299** ± 0.109 *[81%]*	1.2	0.75 (ns)	n.d	**>10** (48%)	**>10** (-9%)	**>10** (8%)	**>10** (42%)
23		**0.151** ± 0.045 *[103%]*	1.5	0.37 (ns)	n.d	**0.207** ± 0.038 *[111%]*	1.7	0.26 (ns)	n.d	**>10** (36%)	**>10** (18%)	**>10** (18%)	**8.14** ± 2.58 *[84%]*
24		**0.169** ± 0.041 *[80%]*	1.3	0.37 (ns)	n.d	**0.379** ± 0.079 *[84%]*	1.5	0.31 (ns)	n.d	**>1** (36%)	**>1** (-42%)	**>1** (-24%)	**>1** (3%)
25		**>10** (30%)	n.d	n.d	**>10** (-4%)	**>10** (37%)	n.d	n.d	n.d	**>10** (39%)	**>10** (-80%)	**>10** (20%)	**>10** (47%)
26		**0.111** ± 0.015 *[89%]*	1.3	0.57 (ns)	**>10** (30%)	**0.447** ± 0.119 *[80%]*	1.5	0.49 (ns)	n.d	**>10** (30%)	**>10** (-71%)	**>10** (23%)	**>10** (36%)
27		**0.247** ± 0.036 *[90%]*	1.0	0.87 (ns)	n.d	**0.318** ± 0.033 *[108%]*	1.4	0.06 (ns)	n.d	**>1** (25%)	**>1** (-18%)	>1 (23%)	>1 (12%)
28		**0.254** ± 0.010 *[90%]*	1.3	0.18 (ns)	n.d	**0.371** ± 0.102 *[102%]*	1.6	0.08 (ns)	n.d	**>10** (15%)	**>10** (-38%)	**>10** (45%)	**1.41** ± 0.13 *[72%]*
30		**1.39** ± 0.60 *[43%]*	1.0	0.87 (ns)	n.d	**2.64** ± 0.05 *[85%]*	1.5	0.36 (ns)	n.d	**>10** (-5%)	**>10** (6%)	**>10** (12)	**>10** (7)
31		**0.149** ± 0.056 *[134%]*	1.7	0.36 (ns)	n.d	**0.194** ± 0.053 *[116%]*	1.7	0.15 (ns)	n.d	**>10** (14%)	**>10** (41%)	**>10** (14%)	**3.06** ± 1.09 *[100%]*
32		**0.137** ± 0.032 *[123%]*	1.2	0.71 (ns)	n.d	**0.128** ± 0.018 *[106%]*	1.5	0.27 (ns)	n.d	**>10** (-8%)	**>10** (13%)	**>10** (40%)	**2.28** ± 0.89 *[100%]*
33		**0.0604** ± 0.0122 *[169%]*	1.1	0.58 (ns)	n.d	**0.157** ± 0.007 *[96%]*	1.2	0.51 (ns)	n.d	**>10** (-43%)	**>10** (10%)	**>10** (16%)	**>10** (47%)
34		**0.189** ± 0.027 *[148%]*	1.4	0.37 (ns)	n.d	**0.156** ± 0.013 *[92%]*	1.6	0.15 (ns)	n.d	**>10** (-48%)	**>10** (23%)	**>10** (34%)	**1.69** ± 0.91 *[72%]*
35		**0.115** ± 0.046 *[139%]*	1.0	0.90 (ns)	n.d	**0.301** ± 0.046 *[106%]*	1.5	0.13 (ns)	n.d	**>10** (46%)	**>10** (13%)	**>10** (35%)	**1.47** ± 0.04 *[100%]*
36	**PSB-KK1448**	**0.0711** ± 0.0174 *[85%]*	1.0	0.90 (ns)	n.d	**0.220** ± 0.062 *[134%]*	1.5	0.19 (ns)	n.d	**>10** (33%)	**>10** (13%)	**>10** (49%)	**0.896** ± 0.157 *[100%]*

37		**0.101** ± 0.013 *[134%]*	1.0	0.88 (ns)	n.d	**0.180** ± 0.033 *[101%]*	1.5	0.12 (ns)	n.d	**>10** (-27%)	**>10** (34%)	**3.48** ± 1.72 *[55%]*	**0.344** ± 0.104 *[100%]*
38		**0.166** ± 0.024 *[122%]*	1.4	0.15 (ns)	n.d	**0.245** ± 0.030 *[108%]*	1.5	0.21 (ns)	n.d	**>10** (-24%)	**>10** (36%)	**>10** (36%)	**1.62** ± 0.46 *[100%]*
39		**0.0246** ± 0.051 *[117%]*	1.0	0.92 (ns)	n.d	**0.0463** ± 0.0058 *[95%]*	1.2	0.56 (ns)	n.d	**>10** (-16%)	**>10** (35%)	**3.91** ± 1.08 *[58%]*	**0.827** ± 0.287 *[87%]*
40		**0.136** ± 0.017 *[111%]*	1.6	0.07 (ns)	n.d	**0.216** ± 0.066 *[112%]*	1.5	0.35 (ns)	n.d	**>10** (-6%)	**>10** (45%)	**>10** (35%)	**1.15** ± 0.48 *[85%]*
41		**0.138** ± 0.013 *[121%]*	1.1	0.77 (ns)	n.d	**0.171** ± 0.013 *[96%]*	1.2	0.42 (ns)	n.d	**>10** (-22%)	**>10** (3%)	**>10** (34%)	**1.41** ± 0.38 *[100%]*
42		**0.352** ± 0.096 *[111%]*	1.6	0.08 (ns)	n.d	**0.150** ± 0.019 *[87%]*	1.6	0.16 (ns)	n.d	**>10** (-10%)	**>10** (30%)	**6.28** ± 4.80 *[67%]*	**0.150** ± 0.019 *[100%]*
43		**0.469** ± 0.074 *[125%]*	1.5	0.11 (ns)	n.d	**0.488** ± 0.083 *[93%]*	1.4	0.18 (ns)	n.d	**>10** (3%)	**≈10** (49%)	**>10** (47%)	**>10** (47%)
44		**>10** (8%)	n.d	n.d	**>10** (4%)	**>10** (7%)	n.d	n.d	n.d	**>10** (1%)	**>10** (16%)	**>10** (13%)	**>10** (2%)
45		**3.60** ± 0.19 *[88%]*	1.8	0.07 (ns)	n.d	**4.00** ± 0.611 *[87%]*	2.3	<0.0001 (significant)	n.d	**>10** (2%)	**>10** (37%)	**>10** (22)	**>10** (20)
46		**1.41** ± 0.29 *[98%]*	1.3	0.22 (ns)	n.d	**1.27** ± 0.31 *[147%]*	1.5	0.66 (ns)	n.d	**>10** (6%)	**>10** (12%)	**>10** (13)	**>10** (36)
47		**6.64** ± 2.68 *[70%]*	1.8	0.07 (ns)	n.d	**10.9** ± 0.8 *[95%]*	2.0	0.0037 (significant)	n.d	**>10** (2%)	**>10** (32%)	**>10** (26)	**>10** (34)
48		**3.67** ± 1.07 *[116%]*	1.0	0.82 (ns)	n.d	**3.63** ± 0.24 *[99%]*	2.0	0.0106 (significant)	n.d	**>10** (19%)	**>10** (33%)	**>10** (16)	**>10** (48)
49		**0.584** ± 0.150 *[50%]*	1.2	0.53 (ns)	n.d	**1.30** ± 0.05 *[80%]*	1.6	0.16 (ns)	n.d	**>10 (6%)**	**>10 (23%)**	**3.01** ± 0.085 *[70%]*	**0.478** ± 0.069 *[97%]*
50	**PSB-KK1445**	**0.0454** ± 0.081 *[84%]*	1.7	0.11 (ns)	n.d	**0.124** ± 0.056 *[79%]*	1.7	0.36 (ns)	n.d	**>10 (-3%)**	**>10 (26%)**	**>10** (40%)	**>10** (48%)
51	**PSB-KK1415**	**0.0191** ± 0.0034 *[141%]*	1.6	0.36 (ns)	n.d	**0.0541** ± 0.0241 *[100%]*	1.2	0.20 (ns)	n.d	**>10 (8%)**	**>10 (43%)**	**1.18** ± 0.44 *[100%]*	**0.481** ± 0.104 *[100%]*
52		**0.0724** ± 0.547 *[65%]*	1.0	0.99 (ns)	n.d	**0.058** ± 0.008 *[105%]*	1.4	0.25 (ns)	n.d	**>10 (13%)**	**>10 (33%)**	**1.08** ± 0.47 *[70%]*	**0.749** ± 0.344 *[77%]*
53		**0.0426** ± 0.0155	1.0	0.98 (ns)	n.d	**0.280** ± 0.194 *[155%]*	1.2	0.58 (ns)	n.d	**>10 (-8%)**	**>10 (31%)**	**>10** (31%)	**4.89** ± 0.91 *[81%]*

S18

		[98%]											
54		**0.261** ± 0.041 *[112%]*	1.6	0.16 (ns)	n.d	**0.241** ± 0.032 *[110%]*	1.3	0.30 (ns)	n.d	**>10 (17%)**	**>10 (-7%)**	**>10** (24)	**4.58** ± 0.89 *[83%]*
55		**0.218** ± 0.008 *[109%]*	1.4	0.07 (ns)	n.d	**0.281**± 0.025 *[124%]*	1.9	0.16 (ns)	n.d	**>10 (8%)**	**>10 (15%)**	**>10** (14)	**2.32** ± 0.64 *[83%]*
56		**0.347** ± 0.0136 *[45%]*	1.9	0.35 (ns)	n.d	**0.559** ± 0.050 *[101%]*	1.8	0.25 (ns)	n.d	**>10 (15%)**	**>10 (24%)**	**>10** (45%)	**1.09** ± 0.24 *[79%]*
57		**0.0642** ± 0.0308 *[72%]*	1.2	0.67 (ns)	n.d	**0.244** ± 0.026 *[104%]*	1.2	0.57 (ns)	n.d	**>10 (-5%)**	**>10 (-4%)**	**>10** (2%)	**>10** (43%)
58		**0.0801** ± 0.0131 *[110%]*	1.3	0.30 (ns)	n.d	**0.121** ± 0.029 *[102%]*	1.7	0.12 (ns)	n.d	**>10 (-1%)**	**6.17** ± 0.75	**1.26** ± 1.07 *[82%]*	**2.56** ± 0.44 *[66%]*
59		**0.0741** ± 0.023 *[82%]*	1.2	0.64 (ns)	n.d	**0.0900** ± 0.0301 *[102%]*	1.4	0.37 (ns)	n.d	**>10** (4%)	**2.38** ± 0.65	**1.27** ± 0.87 *[44%]*	**0.999** ± 0.090 *[63%]*
60		**0.142** ± 0.019 *[113%]*	1.5	0.17 (ns)	n.d	**0.161** ± 0.039 *[122%]*	1.8	0.0294 (significant)	n.d	**>10** (6%)	**>10** (41%)	**>10** (43%)	**>10** (43%)
61		**0.193** ± 0.028 *[110%]*	1.2	0.48 (ns)	n.d	**0.251**± 0.042 *[122%]*	1.6	0.27 (ns)	n.d	**>10** (41%)	**7.87** ± 0.65	**>10** (45%)	**1.05** ± 0.08 *[87%]*
62		**0.102** ± 0.024 *[103%]*	1.6	0.13 (ns)	n.d	**0.127** ± 0.013 *[100%]*	1.5	0.17 (ns)	n.d	**>10** (-48%)	**>10** (38%)	**>10** (47%)	**0.786** ± 0.045 *[100%]*
63		**0.442** ± 0.152 *[155%]*	1.8	0.27 (ns)	n.d	**0.288** ± 0.071 *[108%]*	1.2	0.70 (ns)	n.d	**>10** (8%)	**>10** (45%)	**>10** (20%)	**2.16** ± 0.72 *[100%]*
64	**PSB-KK1418**	**0.120** ± 0.027 *[176%]*	1.7	0.34 (ns)	n.d	**0.223** ± 0.043 *[104%]*	1.3	0.68 (ns)	n.d	**>10** (4%)	**>10** (45%)	**>10** (37%)	**1.79** ± 0.55 *[100%]*
65		**0.229** ± 0.048 *[64%]*	1.4	0.52 (ns)	n.d	**0.334** ± 0.080 *[88%]*	1.6	0.41 (ns)	n.d	**>10** (-8%)	**>10** (11%)	**>10** (7%)	**>10** (30%)
66		**0.417** ± 0.173 *[64%]*	1.7	0.29 (ns)	n.d	**0.444** ± 0.084 *[84%]*	1.5	0.69 (ns)	n.d	**>10** (32%)	**>10** (17%)	**>10** (9%)	**>10** (44%)
74		**0.206** ± 0.023 *[100%]*	1.5	0.11 (ns)	**n.d**	**0.290** ± 0.019 *[93%]*	1.5	0.38 (ns)	n.d	**>10** (6%)	**>10** (23%)	**>10** (50%)	**>10** (45%)

75		**0.0950** ± 0.0069 *[85%]*	1.7	0.0381 (significant)	n.d	**0.297** ± 0.037 *[91%]*	1.2	0.63 (ns)	n.d	**>1** (29%)	**>1** (-55%)	**>1** (35%)	**>1** (44%)
76	**PSB-1846**	**1.22** ± 0.17 *[70%]*	1.8	0.0232 (significant)	n.d	**0.981** ± 0.242 *[97%]*	1.6	0.34 (ns)	n.d	**>10** (4%)	**0.884** ± 0.017	**>10** (52%)	**>10** (50%)
77		**>10** (18%)	n.d	n.d	**>10** (21%)	**>10** (14%)	n.d	n.d	n.d	**>10** (-10%)	**1.43** ± 0.28	**1.58** ± 1.35 *[69%]*	**0.586** ± 0.132 *[72%]*
78		**>10** (45%)	n.d	n.d	**>10** (46%)	**>10** (46%)	n.d	n.d	n.d	**>10** (-4%)	**1.99** ± 0.18	**0.551** ± 0.069 *[73%]*	**1.08** ± 0.01 *[79%]*
79		**0.486** ± 0.072 *[75%]*	1.8	0.0229 (significant)	n.d	**0.711** ± 0.101 *[83%]*	1.1	0.57 (ns)	n.d	**>10** (-6%)	**5.40** ± 0.62	**1.67** ± 0.95 *[73%]*	**1.38** ± 0.33 *[70%]*
80		**0.351** ± 0.017 *[78%]*	1.5	0.17 (ns)	n.d	**0.398** ± 0.089 *[93%]*	1.5	0.20 (ns)	n.d	**>10** (1%)	**2.64** ± 0.41	**0.983** ± 0.177 *[70%]*	**1.06** ± 0.01 *[67%]*
82	**PSB-1833**	**>10** (4%)	n.d	n.d	**>10** (5%)	**>10** (4%)	n.d	n.d	n.d	**>10** (-10%)	**1.74** ± 0.45	**≈10** (53%)	**>10** (37%)
83		**1.63** ± 0.13 *[80%]*	2.2	<0.0001 (significant)	n.d	**1.20** ± 0.54 *[103%]*	0.8	0.73 (ns)	n.d	**>10** (-4%)	**>10** (41%)	**>10** (46%)	**>10** (41%)
87		**>10** (3%)	n.d	n.d	**>10** (19%)	n.d	n.d	n.d	n.d	**>10** (15%)	**>10** (22%)	**>10** (45%)	**3.82** ± 0.71 *[100%]*
88		**>10** (4%)	n.d	n.d	**>10** (32%)	n.d	n.d	n.d	n.d	**>10** (3%)	**>10** (31%)	**>10** (45%)	**3.02** ± 0.38 *[90%]*
89		**>10** (4%)	n.d	n.d	**>10** (7%)	n.d	n.d	n.d	n.d	**>10** (-1%)	**>10** (-4%)	**>10** (26%)	**>10** (42%)
90		**>10** (-10%)	n.d	n.d	**>10** (31%)	n.d	n.d	n.d	n.d	**>10** (-14%)	**>10** (38%)	**>10** (-17%)	**>10** (42%)
91		**>10** (1%)	n.d	n.d	**>10** (13 %)	n.d	n.d	n.d	n.d	**>10** (2%)	**>10** (29%)	**>10** (31%)	**≈10** (50%)

[a] At the indicated concentration. Effects were normalized to the signal induced by 10 µM THC (human GPR18), or 0.3 µM of 51 (mouse GPR18), or 1 µM LPI (GPR55).

[b] Efficacy relative to the maximal effect of the standard agonist (30 µM THC for human GPR18 ,or 3 µM 51 for mouse GPR18, or 10 µM LPI for GPR55) set at 100%.

[c] Calculated using GraphPad Prism 10.2 using extra-sum-of-squares F test (embedded in GraphPad Prism); p-values were obtained by F test with a hypothetical Hill slope of 1 (unity), where "ns" indicates not significant. A "significant" result indicates that the Hill slope is significantly different from 1 (unity).[1]

[d] At the indicated concentration. Effects were normalized to the signal induced by an EC_{80} of a standard agonist at the corresponding receptor (10 µM THC (human GPR18), or 0.3 µM of 51 (mouse GPR18), or 1 µM LPI (GPR55)).

[e] At the indicated concentration. Determined vs. 0.1 nM [^{3}H]CP,55940

[f] Data from Schoeder et al. 2020[2]

[g] n.d = not determined

Table S2. Potency and activity of compound **51** at the human CB_1 receptor determined in different assays

Compd.	Human CB_1 receptor				
	Radioligand binding *vs.* [^{3}H]CP55,940	**cAMP accumulation assays**		**β-Arrestin assays**	
	K_i ± SEM (μM) [max. inhibition (%)]	**Agonistic** EC_{50} ± SEM (μM) (or percent receptor activation) *[Efficacy]*[a]	**Antagonistic** IC_{50} ± SEM (μM) (or percent receptor inhibition)[b]	**Agonistic** EC_{50} ± SEM (μM) (or percent receptor activation) *[Efficacy]*[c]	**Antagonistic** IC_{50} ± SEM (μM) (or percent receptor inhibition)[d]
3 (THC)	**0.00390** ± 0.0089 *[100%]*	**0.00321** ± 0.0015 *[49%]*	n.d[e]	**0.00673** ± 0.00174 *[22%]*	n.d.
51	**1.18** ± 0.44 *[100%]*	**>10** (30%)	**>10** (24%)	**0.0982** ± 0.0090 *[12%]*	**7.05** ± 0.76 (64% max inhibition)

[a] Efficacy relative to the maximal effect of the standard agonist CP55,940 at 1 μM set at 100%
[b] Compounds were tested at a concentration of 10 μM. Effects were normalized to the signal induced by 0.003 μM CP55940
[c] Compounds were tested at a concentration of 10 μM. Effect were normalized to the signal induced by CP55,940 at 0.1 μM set at 100%
[d] Inhibition compared to the EC_{80} of CP55,940 (0.001 μM) at the human CB_1 receptor, set at 100%
[e] not determined

Table S3. Potency and activity of compound **51** at the human CB_2 receptor determined in different assays

Compd.	Human CB_2 receptor				
	Radioligand binding *vs.* [^{3}H]CP55,940	**cAMP accumulation assay**		**β-Arrestin assay**	
	K_i ± SEM (μM) [max. inhibition (%)]	**Agonistic** EC_{50} ± SEM (μM) (or percent receptor activation) *[Efficacy]*[a]	**Antagonistic** IC_{50} ± SEM (μM) (or percent receptor inhibition)[b]	**Agonistic** EC_{50} ± SEM (μM) (or percent receptor activation) *[Efficacy]*[c]	**Antagonistic** IC_{50} ± SEM (μM) (or percent receptor inhibition)[d]
3 (THC)	**0.00598** ± 0.0030 *[100%]*	**0.00530** ± 0.0020 *[58%]*	n.d[e]	**0.00142** ± 0.00028 *[35%]*	n.d
51	**0.481** ± 0.104 *[100%]*	**>10** (34%)	**>10** (20%)	**0.0245** ± 0.0127 *[27%]*	**8.00** ± 1.03 (60% max. inhibition)

[a] Efficacy relative to the maximal effect of the standard agonist CP55,940 at 1 μM set at 100%
[b] Compounds were tested at a concentration of 10 μM. Effects were normalized to the signal induced by 0.003 μM CP55940
[c] Compounds were tested at a concentration of 10 μM. Effect were normalized to the signal induced by CP55,940 at 0.1 μM set at 100%
[d] Inhibition compared to the EC_{80} of CP55,940 (0.003 μM) at the human CB_2 receptor, set at 100%
[e] not determined

Table S4. Modeling observations of compound modifications and their effects on potencies.[a]

Compound(s)	Figure	Observation *[Effect]*
10-18	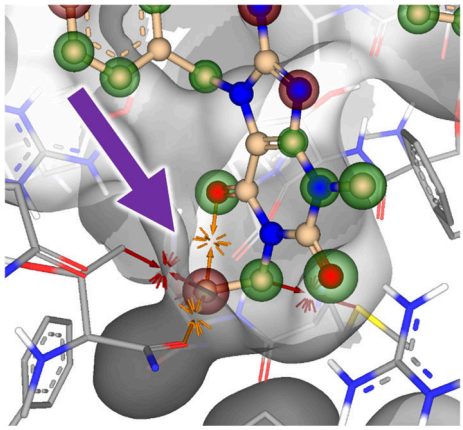	Intra- and inter-molecular clashes with Thr101$^{3.32}$ and Met275$^{7.42}$ for *N*1-xanthine substituents larger than methyl. Lacking H-bond interactions with backbone of Thr101$^{3.32}$ and Asn276$^{7.43}$. *[>10-fold decrease in potency compared to **51**]*
21-30	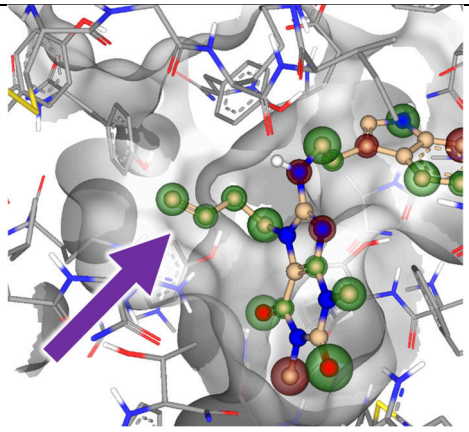	Absence of interacting functionalities for π-π stacking with Tyr21$^{1.31}$, Tyr81$^{2.63}$, Tyr82$^{2.64}$, and cation-π interactions with Lys161^{ECL2}. *[~10-fold decrease in potency compared to **51**]*
32-34	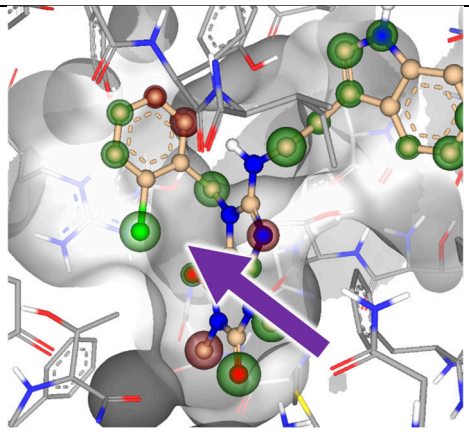	Binding of the *ortho*-halogen-substituted benzyl moiety (attached to xanthine-*N*7) in a sub-pocket formed by Arg78$^{2.60}$ and Thr101$^{3.32}$. *[modification tolerated]*

35-37	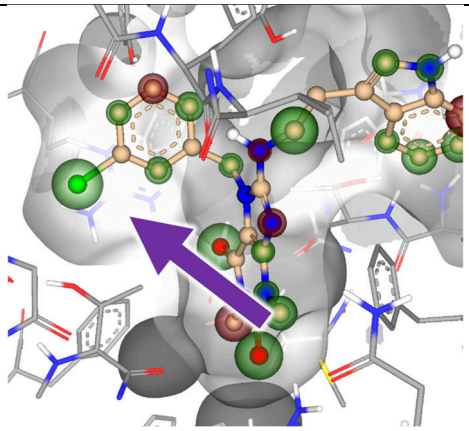	Binding of the *meta*-halogen-substituted benzyl (at xanthine-*N*7) in a sub-pocket formed by Arg78$^{2.60}$, Leu97$^{3.28}$, and Gly98$^{3.29}$. *[modification tolerated]*
40-48	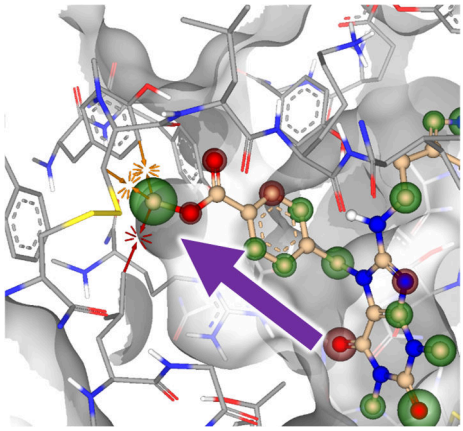	Potential clashes in a lipophilic sub-pocket formed by Tyr82$^{2.64}$, Leu97$^{3.28}$ and Cys172^{ECL2}. Challenging binding site topology for optimal H-bond interactions of investigated compounds. *[>10-fold decrease in potency compared to **51**]*
49	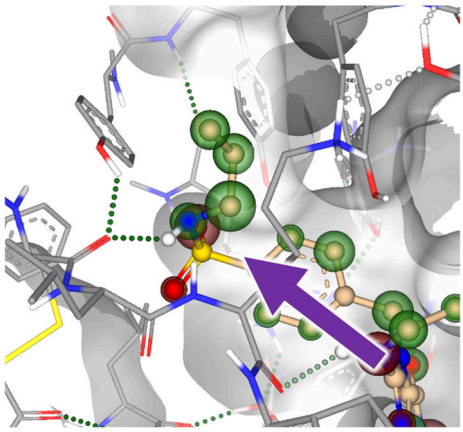	Binding at the halogen binding site is not possible due to limited space. Alkyl chain projects towards the extracellular lumen; may engage in lipophilic interactions with Tyr21$^{1.31}$, Tyr81$^{2.63}$, Tyr82$^{2.64}$ and Lys174 ^{ECL2}. H-bond interaction of sulfonamide with the backbone of Cys172^{ECL2} is feasible. *[decreased potency compared to **51**, but more potent than analogs of the series]*

50-53	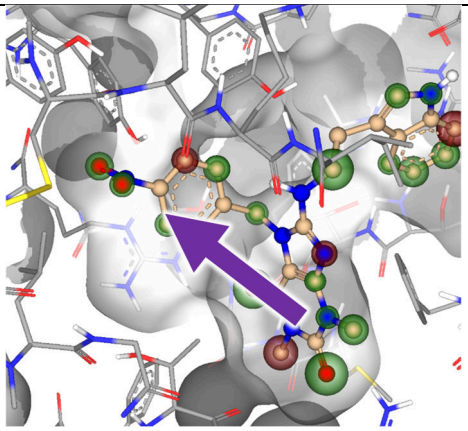	*para*-halogen and *p*-nitro-benzyl moieties bind in a lipophilic sub-pocket formed by Tyr82$^{2.64}$, Leu97$^{3.28}$ and Cys172^{ECL2}. *[most potent compounds of the series]*
54	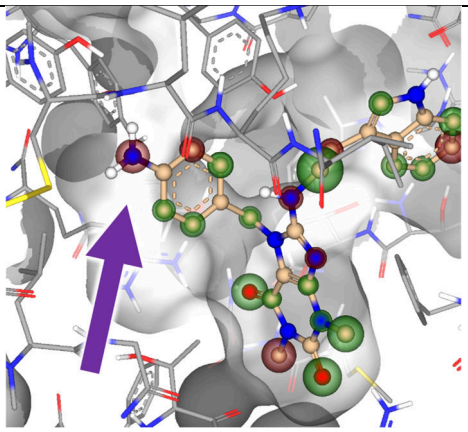	No optimal H-bond partners observed for the *p*-aminobenzyl residue. *[~10-fold decrease in potency compared to **51**]*
56-61	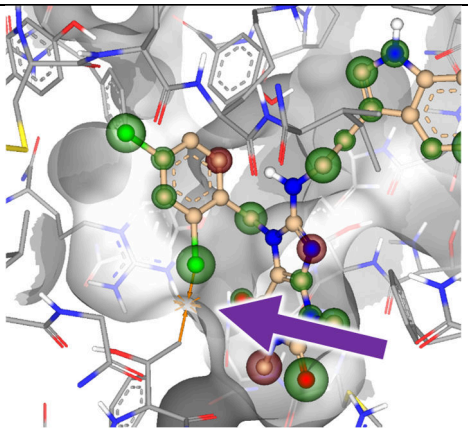	Potential clashes induced by the substitution pattern, leading to a shift of the position of the *para*-substituent compared to compound **51**. *[~2-fold decrease in potency compared to **51**]*

62	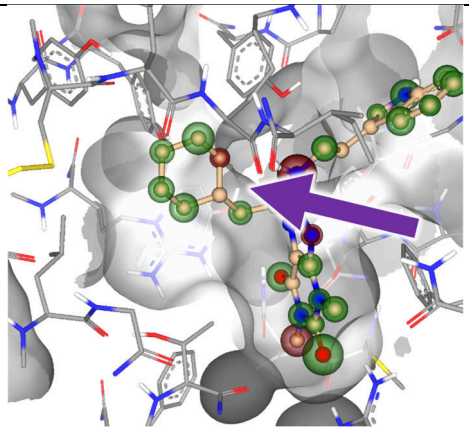	Potential lack of π-π interactions, good shape-complementation of the lipophilic surface. *[comparable potency to **31**]*
63-65	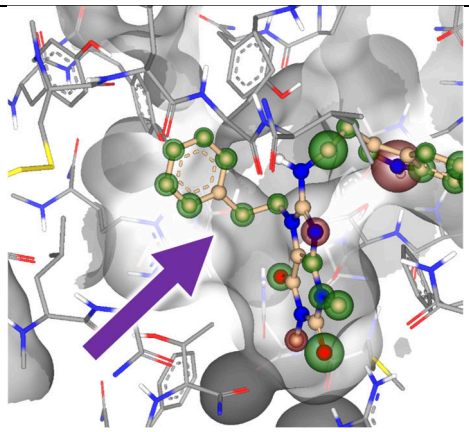	The proposed binding site can accommodate different linker lengths given the available space. *[benzyl group displays best linker length]*
66	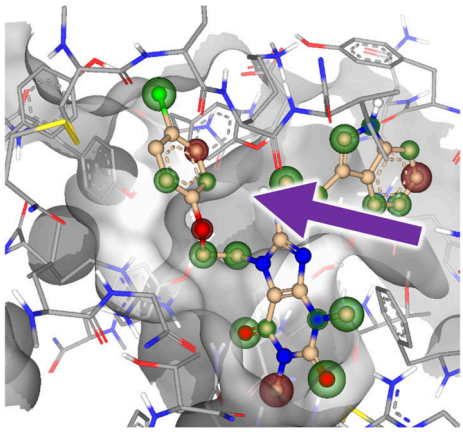	Alternating binding mode, similar to **49**, due to limited space in the lipophilic binding pocket. No interaction partners for the ether oxygen can be observed. *[linker length and presence of oxygen lead to a >20-fold decrease in potency compared to **51**]*

74	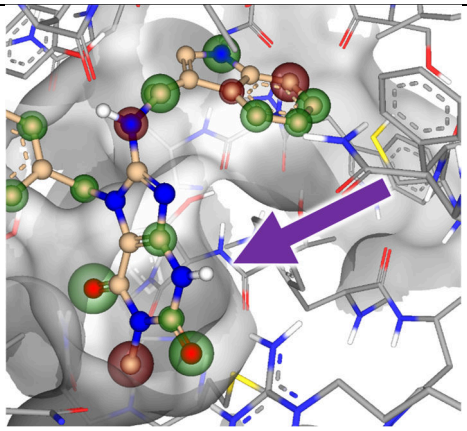	No scoring penalties for the unsubstituted *N*3. Methyl group with favorable binding score is absent. *[10-fold decrease in potency compared to **51**]*
75	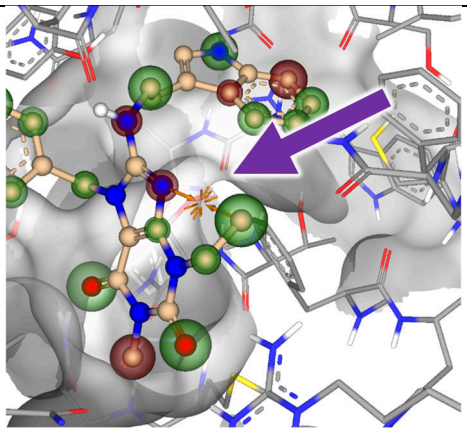	Intramolecular clash between the xanthine core and the *N*3-alkyl chain. *N*3-Ethyl substitution displays favorable binding scores. *[5-fold decrease in potency compared to **51**, but improved potency compared to **74**]*
76-83	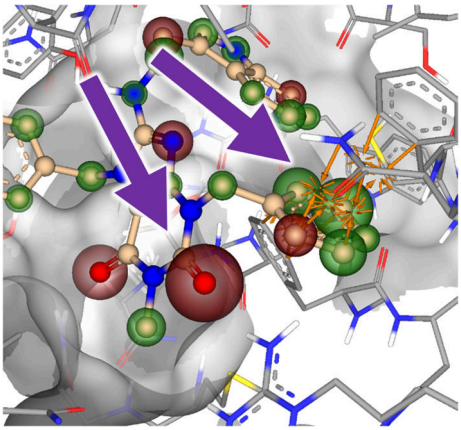	Space limitation by Arg191$^{5.42}$, as well as Asn188$^{5.39}$, Phe248$^{6.51}$ and Phe252$^{6.55}$ for larger *N*3-xanthine substituents. Required conformational change may lead to loss of optimal geometry for H-bond interactions between xanthine-O^{2} and Arg191$^{5.42}$. *[>10-fold decrease in potency compared to **51** or complete loss of potency]*

[a] The ligand complexes were evaluated using the HYDE scoring function of SeeSAR, where green spheres represent favorable contributions of individual atoms to the overall binding affinity, and red spheres indicate unfavorable contributions.

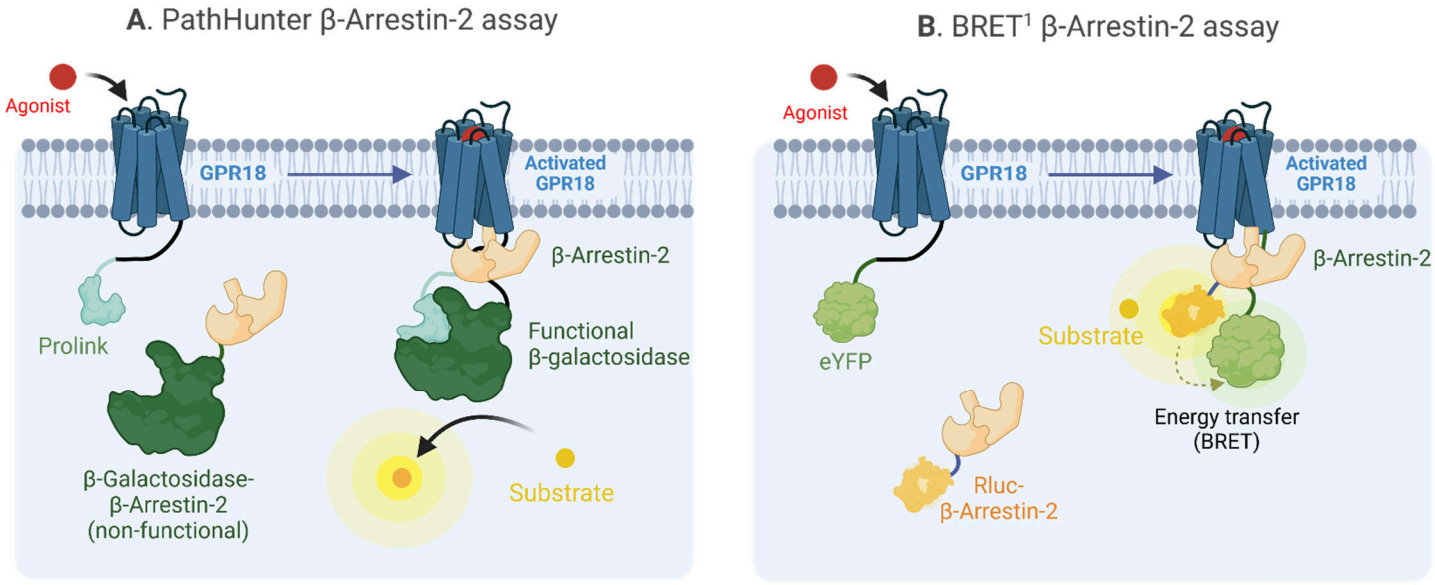

Figure S1. Principle of β-arrestin recruitment assay used for measuring GPR18 activation. The figure was created using Biorender®.

A. The PathHunter® assay is based on enzyme (β-galactosidase) complementation.[3, 4] Galactosidase is split into two fragments: a small part (called Prolink) and a complementary part. The Prolink is fused to the C-terminus of GPR18 (or another receptor) while the complementary part of galactosidase is attached to the N-terminus of β-arrestin-2. Upon addition of a GPR18 agonist, β-arrestin-2 is recruited, allowing Prolink1 and the complementary β-galactosidase fragment to interact, thereby activating the enzyme. The enzymatic activity can be measured by adding a substrate. The functional galactosidase will hydrolyze the substrate, producing luminescence. The amount of luminescence produced corresponds to the level of GPR18 activation.

B. Bioluminescence resonance energy transfer (BRET[1]) is based on the energy transfer from a donor protein (Renila luciferase, Rluc) to an acceptor protein (enhanced yellow fluorescent protein, eYFP) in the presence of the substrate coelenterazine h. In this assay system, eYFP is fused to the C-terminus of GPR18, whereas Rluc is attached to the N-terminus of β-arrestin2. Upon stimulation of GPR18 by an agonist, it induces the recruitment of β-arrestin-2, bringing eYFP and Rluc into close proximity. Energy transfer can only occur when eYFP and Rluc are in such proximity. Rluc oxidizes coelenterazine h, emitting luminescent light at 480 nm. This emission can then excite the eYFP protein, resulting in fluorescent emission at 530 nm. The BRET ratio is calculated by dividing the Rluc emission signal at 480 nm by the eYFP emission at 530 nm. The derived BRET ratio is directly proportional to the level of GPR18 activation.

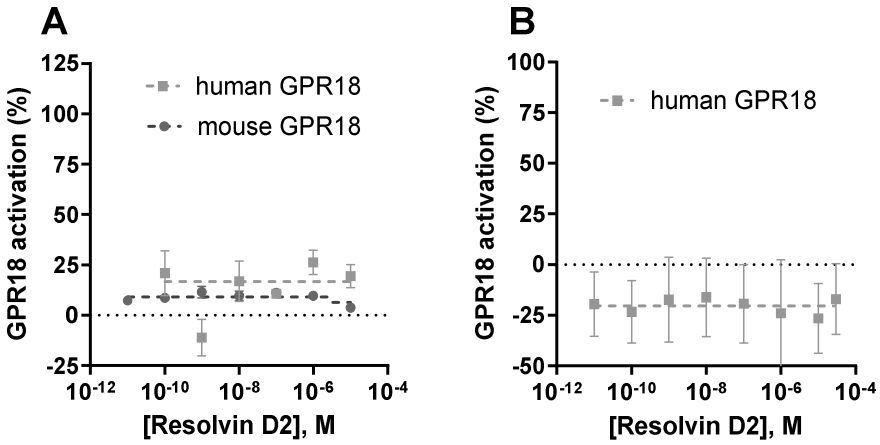

Figure S2. Concentration-dependent activation of human GPR18 or mouse GPR18 by Resolvin D2 (RvD2) in the presence of DMSO (**A**) or ethanol (**B**). A maximally effective concentration of THC (30 μM) was used for normalization at the human GPR18 (set at 100%), and compound **51** (3 μM) was utilized for normalization at the mouse GPR18 (set at 100%). All data are from β-arrestin recruitment assays. Data points represent means ± SEM of at least three independent (**A**) or two independent experiments (**B**).

- **A.** The experiments were performed in the presence of DMSO (final concentration of DMSO 1%). RvD2 solution in ethanol (Cayman Bioscience) was stored at -80°C. Solutions were freshly prepared for each experiment. Required RvD2 amounts were calculated to achieve the required final concentration of 0.1 – 10,000 nM, taken out of the vial, and subjected to gentle evaporation under a stream of nitrogen, followed by taking it up in DMSO and diluting it in assay buffer prior to the experiments.
- **B.** The experiments were performed in the presence of ethanol (final concentration of ethanol was 0.1%). The procedure was similar to that described in **A**, except that ethanol was used in place of DMSO.

The solvent had only minor effects on baseline luminescence.

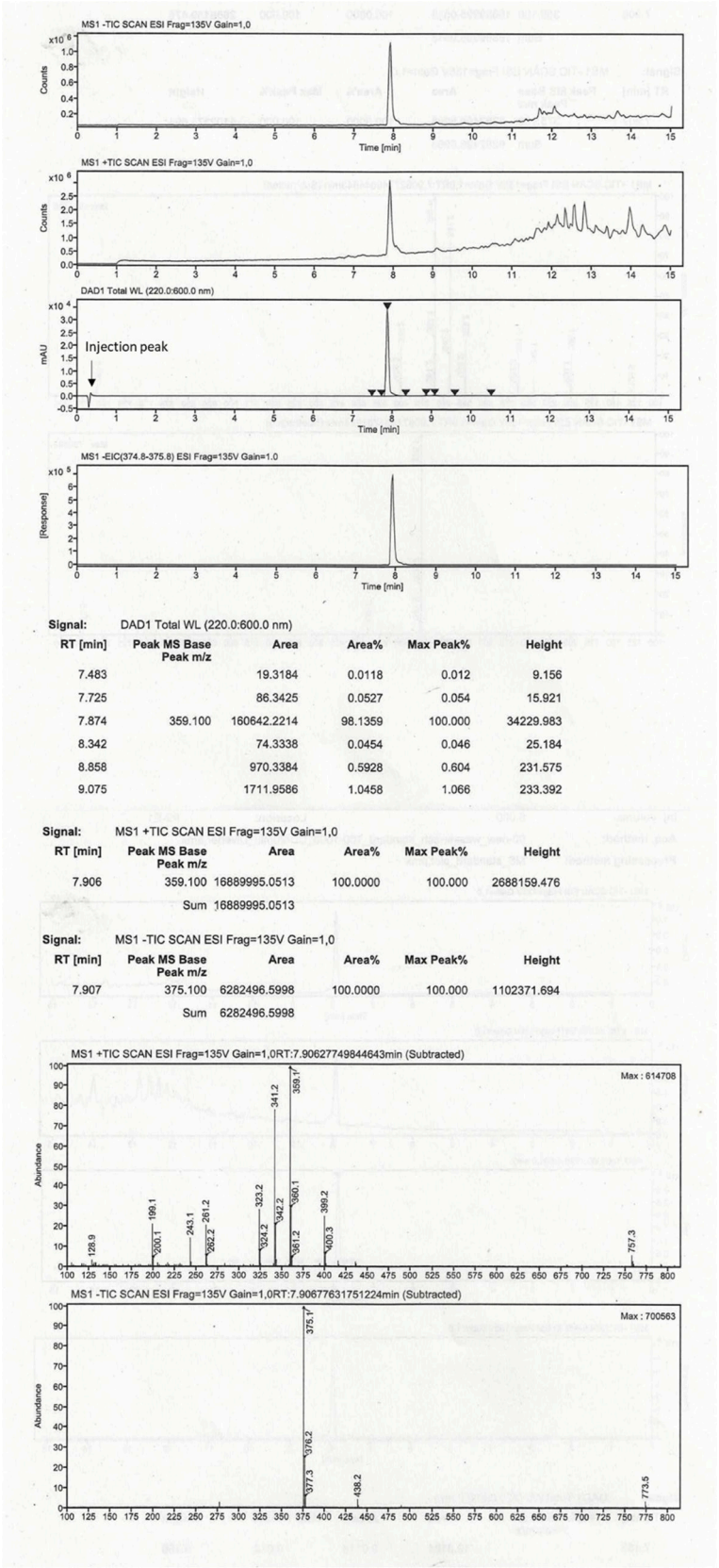

Figure S3. LC-MS assessment of purity of RvD2 (**4**) in ethanol. The purity of compound **4** is 98.1% (retention time at 7.88 min corresponds to the desired compound **4**).

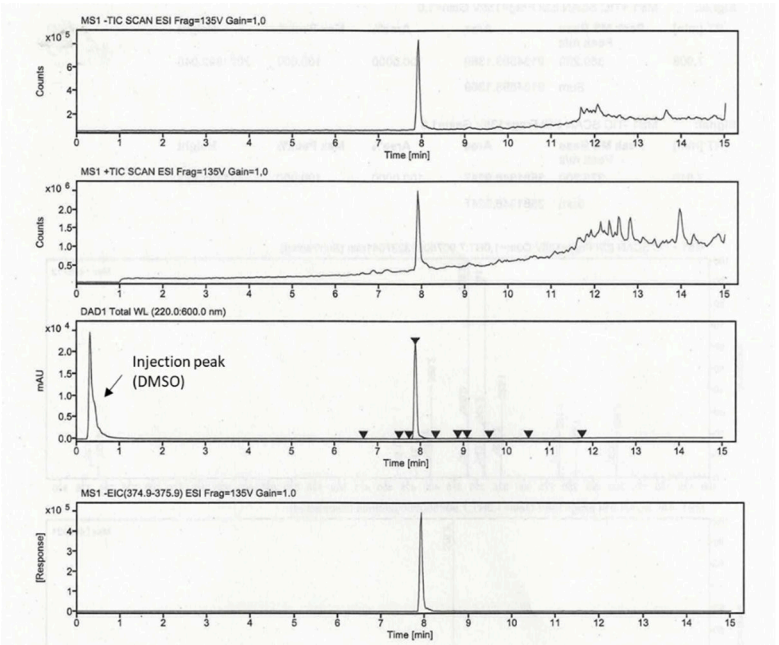

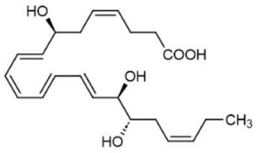

Chemical Formula: $C_{22}H_{32}O_5$
Exact Mass: 376.22
Molecular Weight: 376.49

Signal: DAD1 Total WL (220.0:600.0 nm)

RT [min]	Peak MS Base Peak m/z	Area	Area%	Max Peak%	Height
6.667		155.9494	0.1640	0.168	15.822
7.497		77.8324	0.0818	0.084	15.041
7.730		117.6666	0.1237	0.127	25.597
7.876		92850.6199	97.6148	100.000	21574.099
8.346		57.0171	0.0599	0.061	16.220
8.860		517.6938	0.5443	0.558	130.384

Signal: MS1 +TIC SCAN ESI Frag=135V Gain=1,0

RT [min]	Peak MS Base Peak m/z	Area	Area%	Max Peak%	Height
7.908	359.200	9134593.1369	100.0000	100.000	2024892.040
	Sum	9134593.1369			

Signal: MS1 -TIC SCAN ESI Frag=135V Gain=1,0

RT [min]	Peak MS Base Peak m/z	Area	Area%	Max Peak%	Height
7.910	375.200	3581346.9247	100.0000	100.000	777491.823
	Sum	3581346.9247			

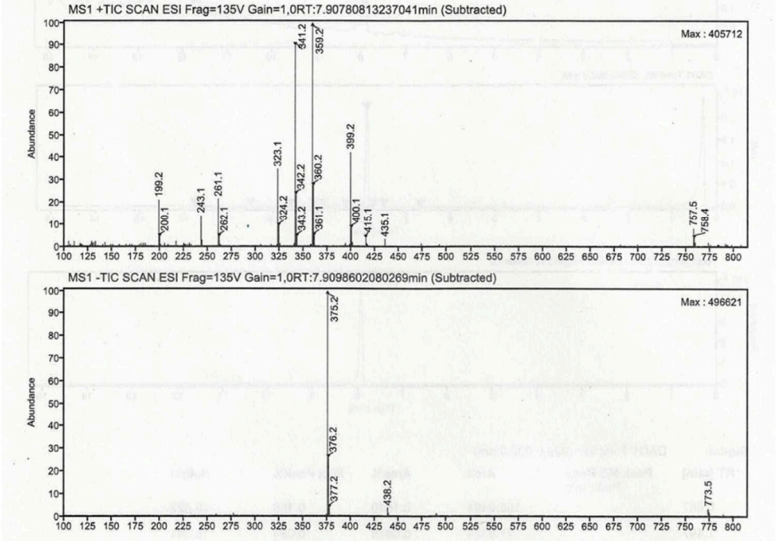

Figure S4. LC-MS assessment of purity of RvD2 (**4**) in DMSO. The purity of compound **4** is 97.6% (retention time at 7.88 min corresponds to the desired compound **4**).

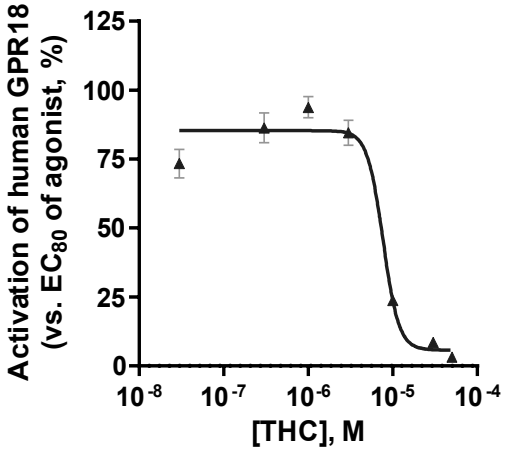

Figure S5. Concentration-dependent inhibition of compound **51**-induced mouse GPR18 activation by THC (**3**). Compound **51** was used at its EC_{80} concentration (0.3 μM). THC inhibits **51**-induced mouse GPR18 activation in a concentration-dependent manner with an IC_{50} value of 6.93 ± 0.28 μM. Data points represent means ± SEM of at least three independent experiments performed in duplicates.

```
GPR18_HUMAN     MITLNNQDQPVPFNSSHPDEYKIAALVFYSCIFIIGLFVNITALWVFSCTTKKRTTVTIY   60
GPR18_MOUSE     MATLSNHNQLDLSNGSHPEEYKIAALVFYSCIFLIGLFVNVTALWVFSCTTKKRTTVTIY   60
                * **.*::*    *.***:**************:******:********************

GPR18_HUMAN     MMNVALVDLIFIMTLPFRMFYYAKDEWPFGEYFCQILGALTVFYPSIALWLLAFISADRY  120
GPR18_MOUSE     MMNVALLDLVFILSLPFRMFYYAKGEWPFGEYFCHILGALVVFYPSLALWLLAFISADRY  120
                ******:**:**::**********.*********:*****.*****:*************

GPR18_HUMAN     MAIVQPKYAKELKNTCKAVLACVGVWIMTLTTTTPLLLLYKDPDKDSTPATCLKISDIIY  180
GPR18_MOUSE     MAIVQPKYAKELKNTGKAVLACGGVWVMTLTTTVPLLLLYEDPDKASSPATCLKISDITH  180
                *************** ****** ***:******.******:**** *:********** :

GPR18_HUMAN     LKAVNVLNLTRLTFFFLIPLFIMIGCYLVIIHNLLHGRTSKLKPKVKEKSIRIIITLLVQ  240
GPR18_MOUSE     LKAVNVLNFTRLIFFFLIPLFIMIGCYVVIIHSLLRGQTSKLKPKVKEKSIRIIMTLLLQ  240
                ********:*** **************:****.**:*:****************:***:*

GPR18_HUMAN     VLVCFMPFHICFAFLMLGTGENSYNPWGAFTTFLMNLSTCLDVILYYIVSKQFQARVISV  300
GPR18_MOUSE     VLVCFVPFHICFAVLMLQGQENSYSPWGAFTTFLMNLSTCLDVVLYYIVSKQFQARVISV  300
                *****:********.***   ****.******************:****************

GPR18_HUMAN     MLYRNYLRSMRRKSFRSGSLRSLSNINSEML          331
GPR18_MOUSE     MLYRNYLRSVRRKSVRSGSLRSLSNMNSEML          331
                *********:****.**********:*****
```

Figure S6. Sequence alignment of human GPR18 (GPR18_HUMAN; Uniprot ID Q14330) and mouse GPR18 (GPR18_mouse; Uniprot ID Q8K1Z6). Similar amino acids are highlighted by gray shading. Sequences were aligned with Clustal Omega. Blast of these two sequences showed 86% sequence identity and 90% sequence similarity.

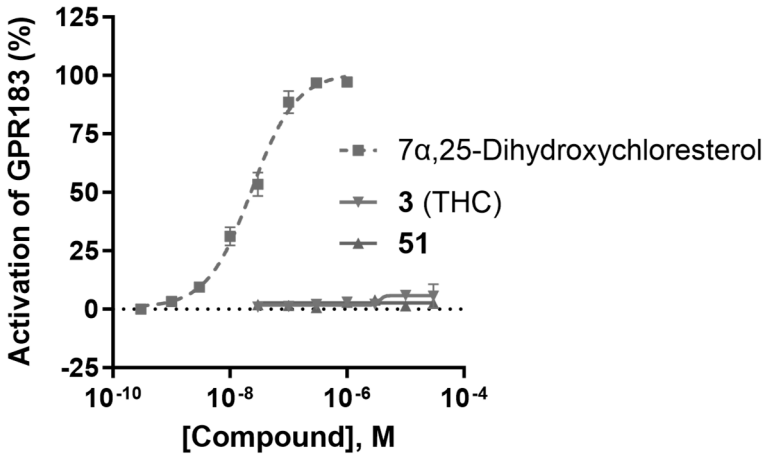

Figure S7. Concentration-dependent activation of GPR183 by **3** (THC) and by **51**. 7α,25-Dihydroxycholesterol was used for normalization (the maximal effect observed at 1 μM was set as 100%). All experiments were determined in β-arrestin recruitment assays. 7α,25-Dihydroxycholesterol was used as the cognate agonist of GPR183 (EC_{50} 0.0244 ± 0.0036 μM). Data points represent means ± SEM of at least three independent.

Stability of compound 51 in human and rat liver microsomes

Compound **51** (50 μM) was incubated with human or rat liver microsomes (1 mg/ml) in 10 mM Tris-HCl buffer (pH 7.4) for 5 min. The reaction was initiated by adding 50 μL of the NADPH Regeneration System into the mixture, and the mixture was further incubated for 120 min at 37 °C. The reaction was stopped by the addition of 200 μL of cold methanol, followed by 15 min of centrifugation at 14000 rpm. The supernatant was taken and subjected to analysis by LC/MS (Waters ACQUITY 8482 TQD).

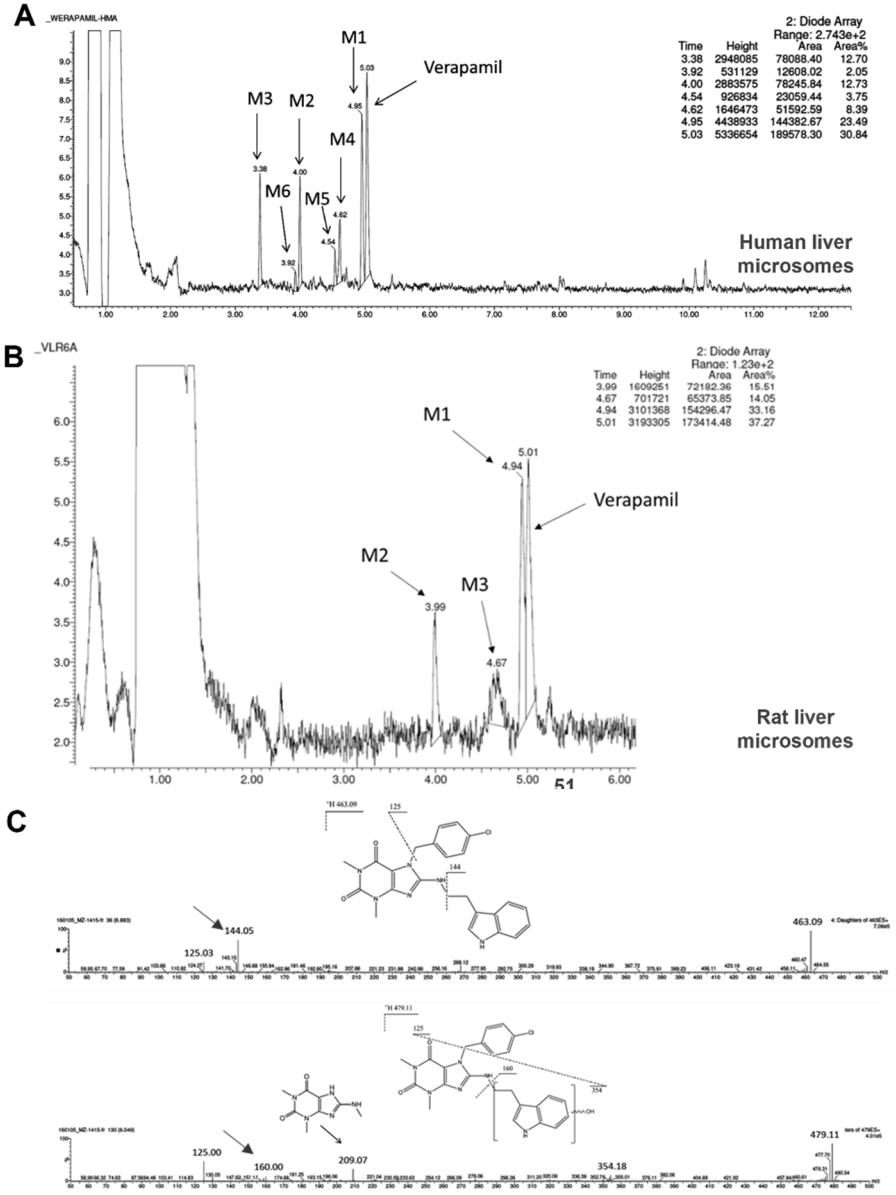

Figure **S8**. Metabolic stability of compound **51** determined in human (**A**) and rat liver microsomes (**B**). MS/MS analyses of **51** and its major metabolite (M1) found after incubation with human or rat liver microsomes. The ion fragment of indole moiety increased from *m/z* 144.05 to *m/z* 160.00 (red arrows) after incubation with microsomes.

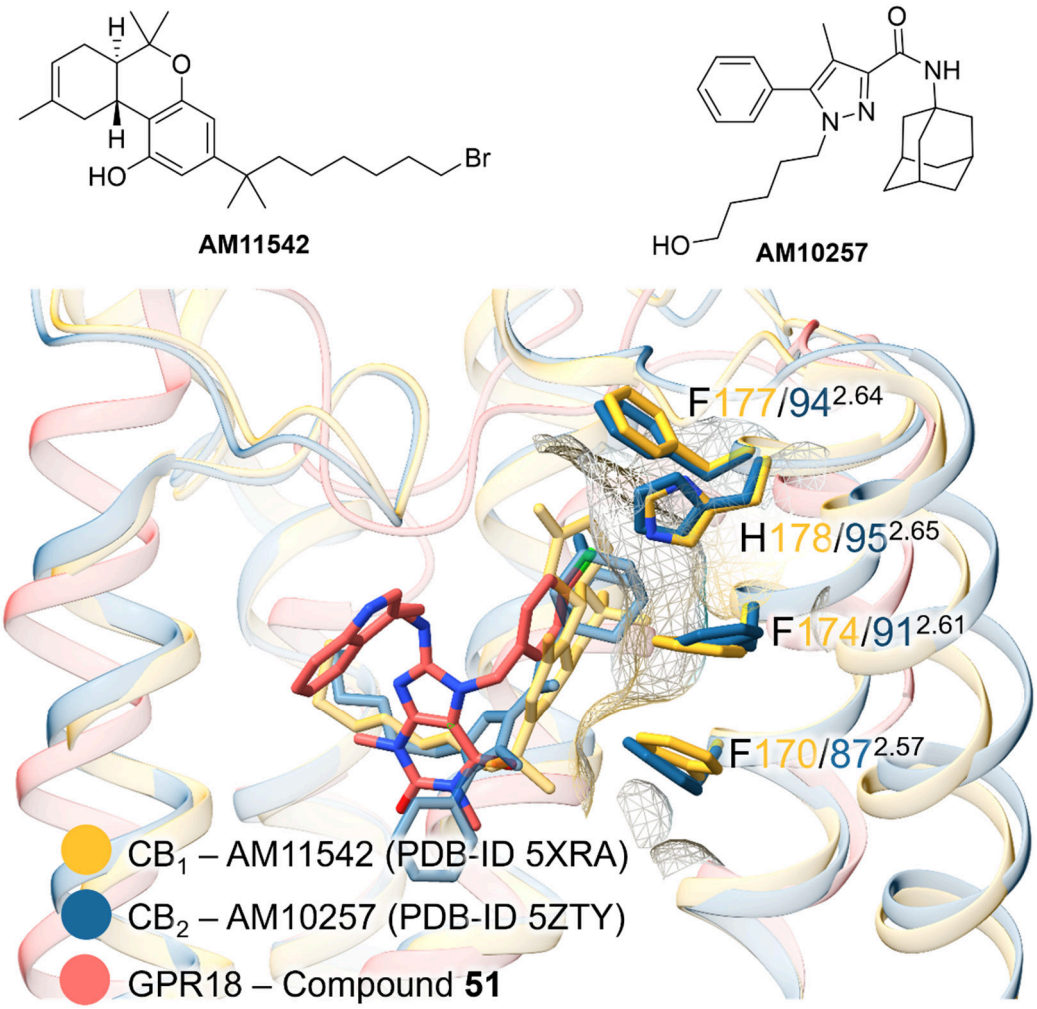

Figure **S9**. Comparison of the proposed binding mode of **51** at GPR18 with those of agonist-bound CB_1 (AM11542-CB_1 (PDB ID: 5XRA)[5] and antagonist-bound CB_2 receptor (PDB ID: 5ZTY)[6] crystal structures. GPR18 is denoted in red, while CB_1 and CB_2 are represented in yellow and blue color, respectively. Amino acid residues constituting the hydrophobic binding pocket are highlighted, and the hydrophobic surface area is illustrated in mesh form at the figure. Figure created using ChimeraX.[7]

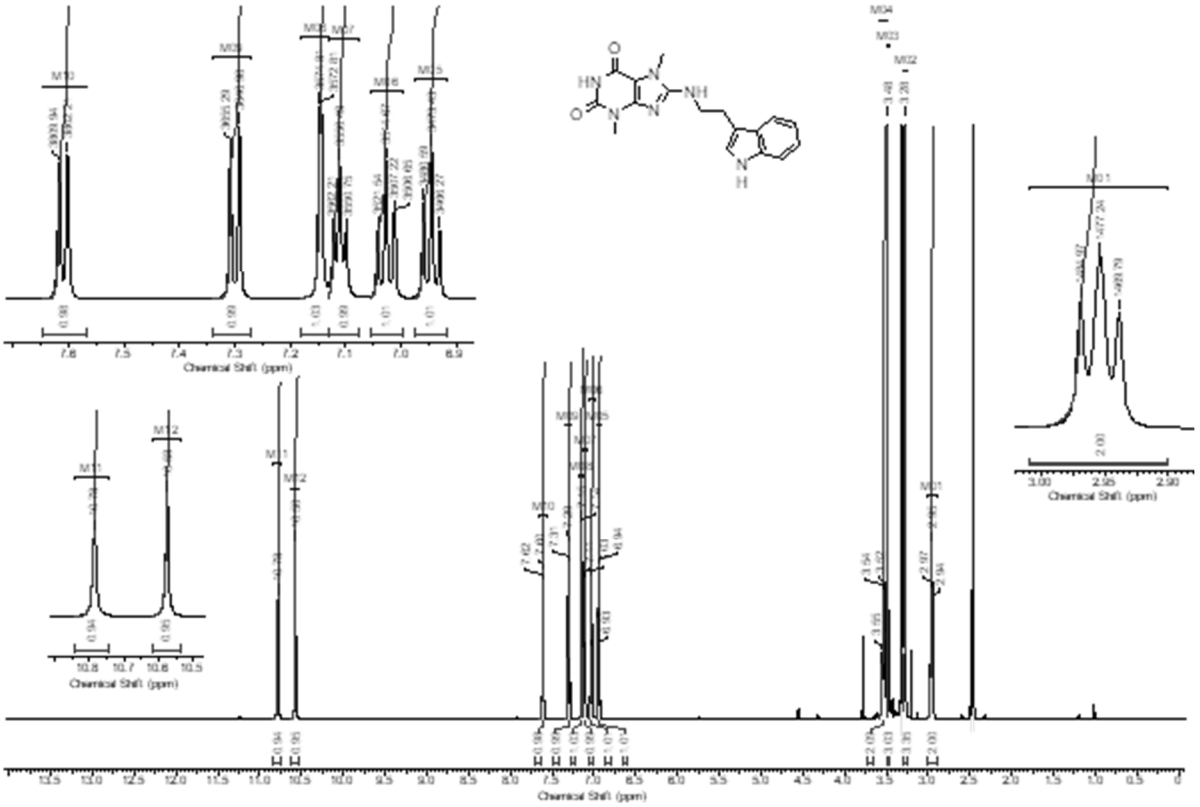

Figure S10. ^{1}H-NMR spectrum of compound **10**.

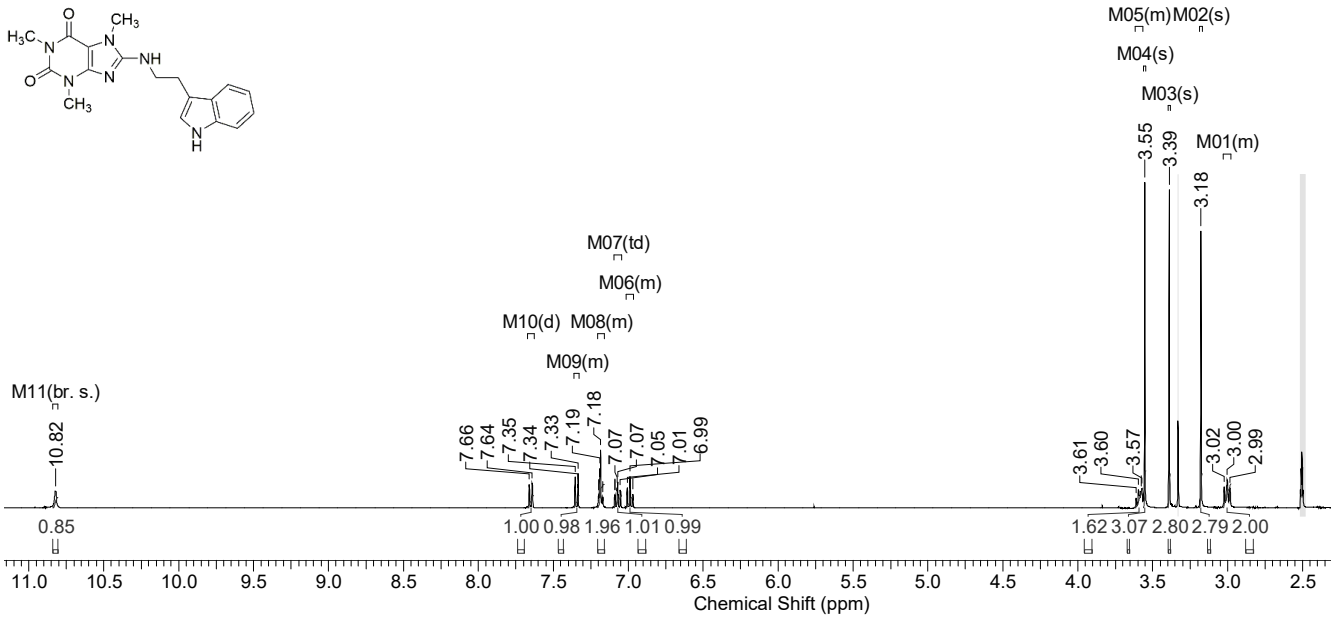

Figure S11. ^{1}H-NMR spectrum of compound **11**.

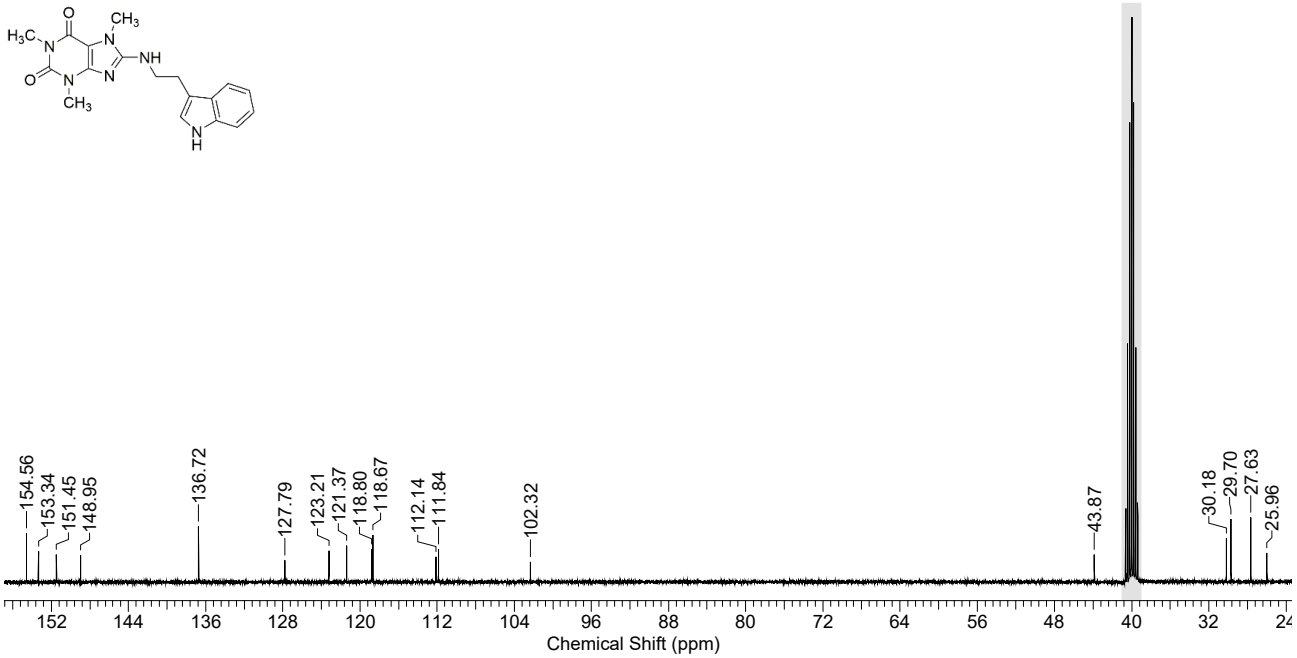

Figure S12. ^{13}C-NMR spectrum of compound **11**.

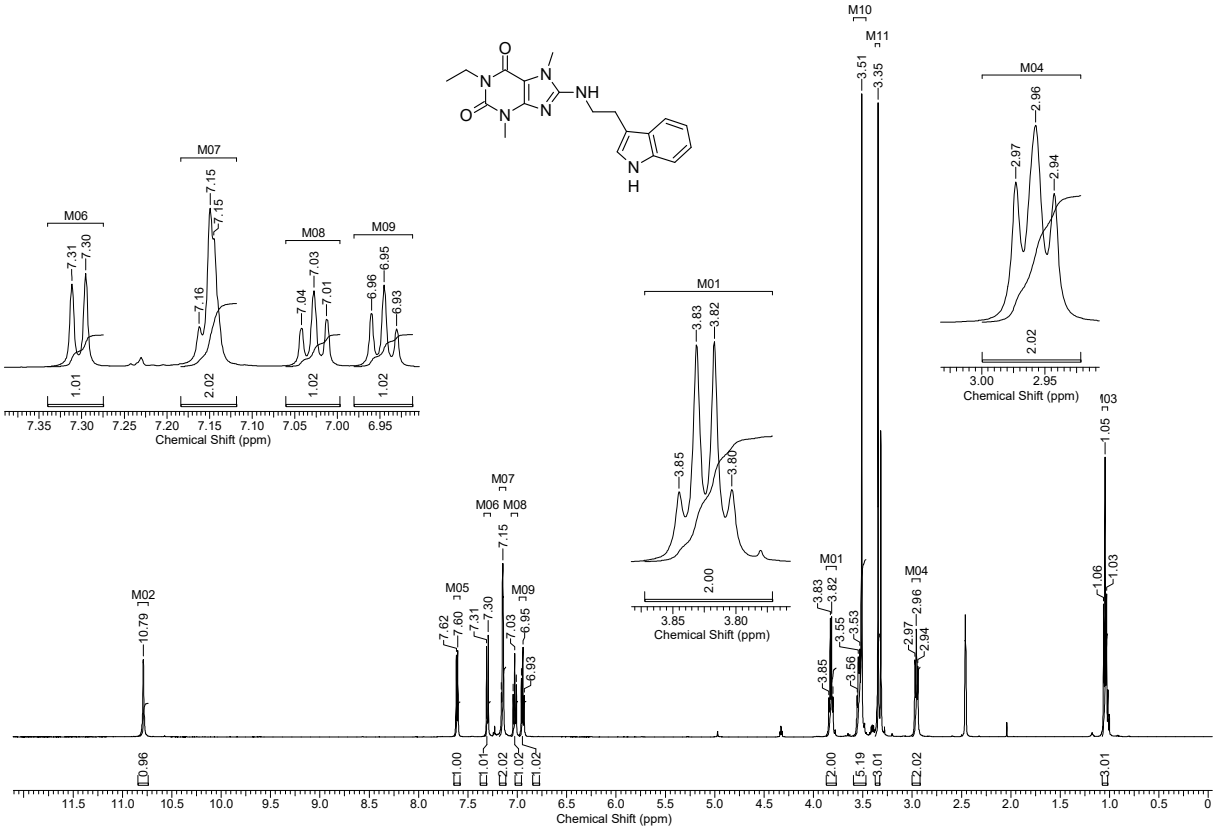

Figure S13. ^{1}H-NMR spectrum of compound **12**.

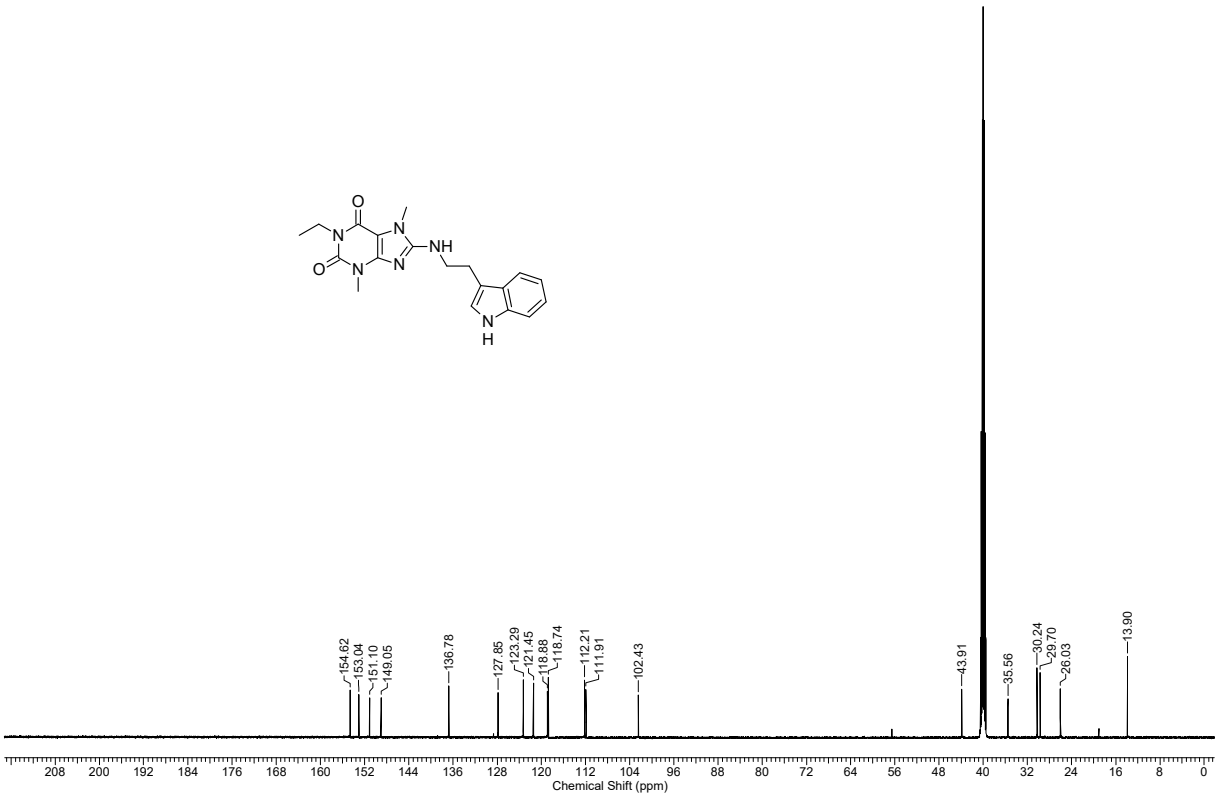

Figure S14. ^{13}C-NMR spectrum of compound **12**.

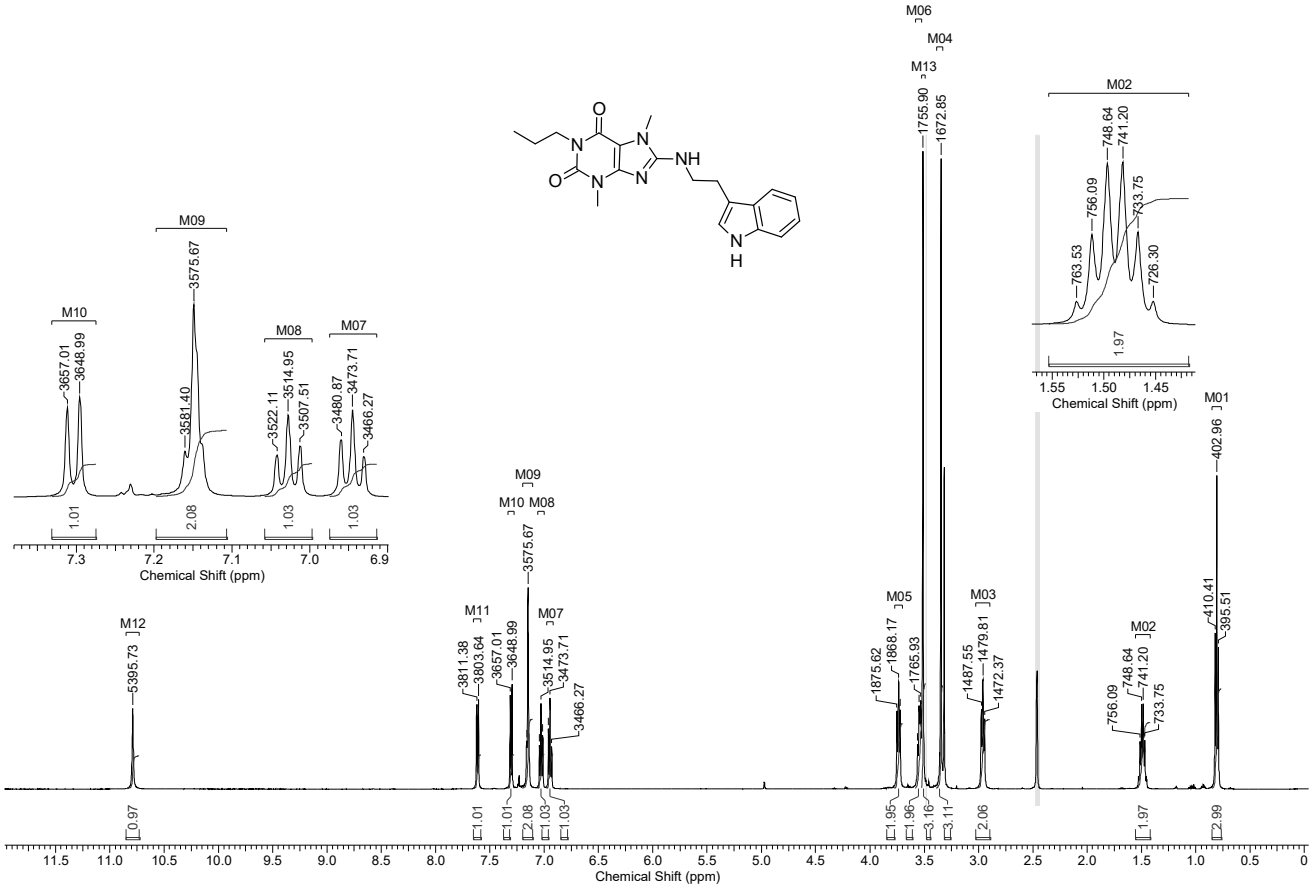

Figure S15. ^{1}H-NMR spectrum of compound **13**.

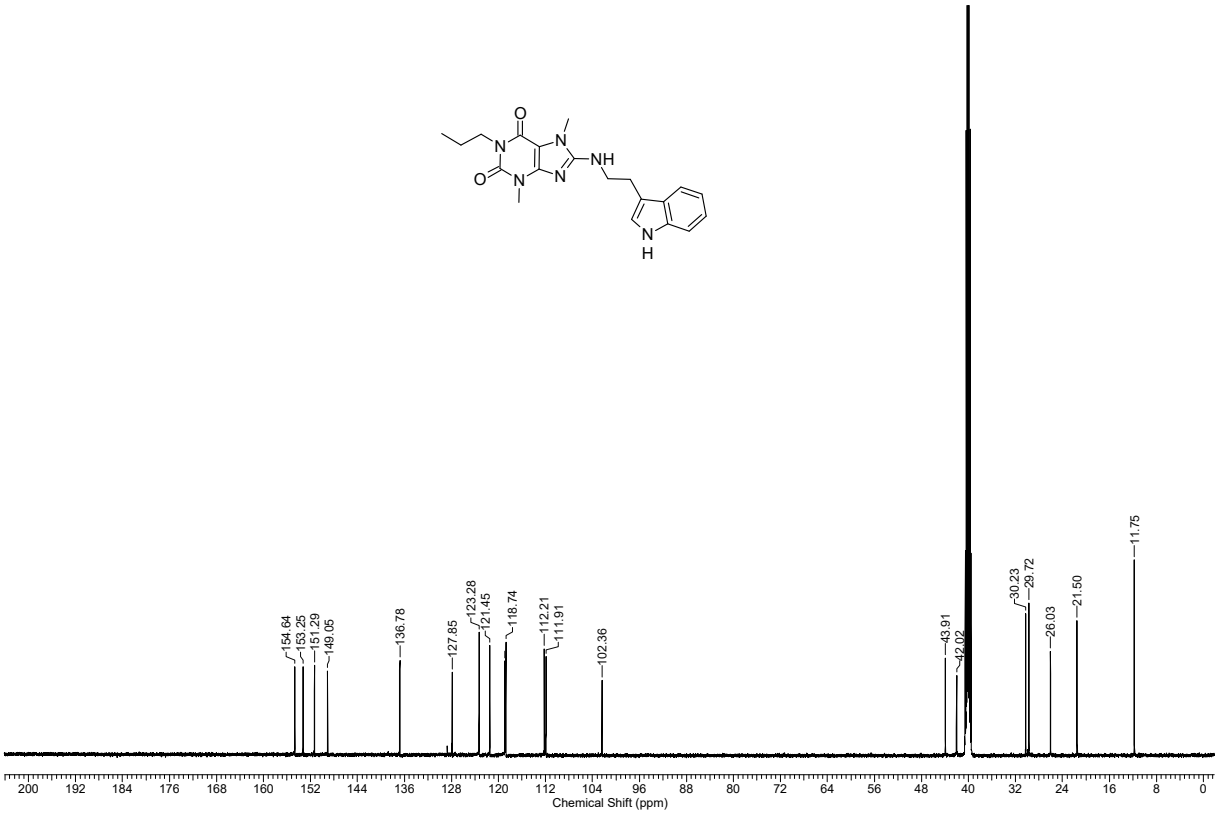

Figure S16. ^{13}C-NMR spectrum of compound **13**.

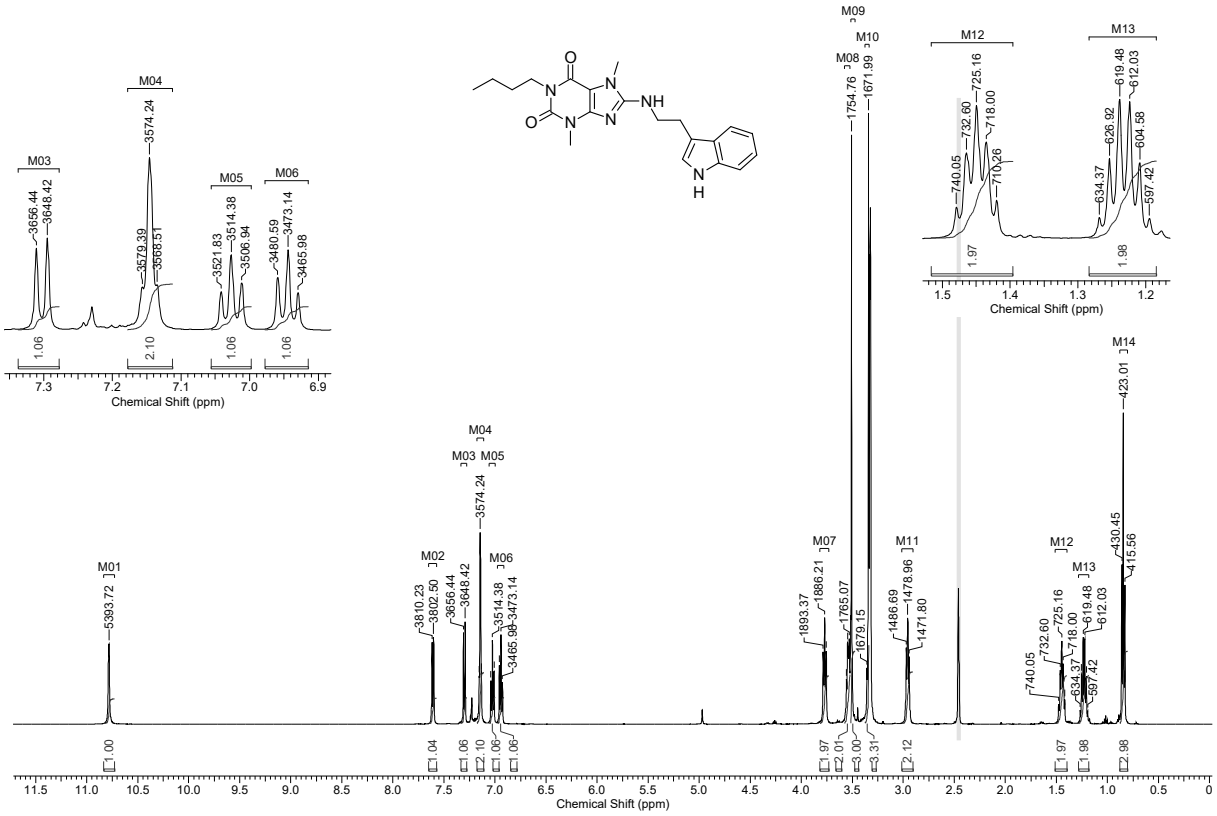

Figure S17. ^{1}H-NMR spectrum of compound **14**.

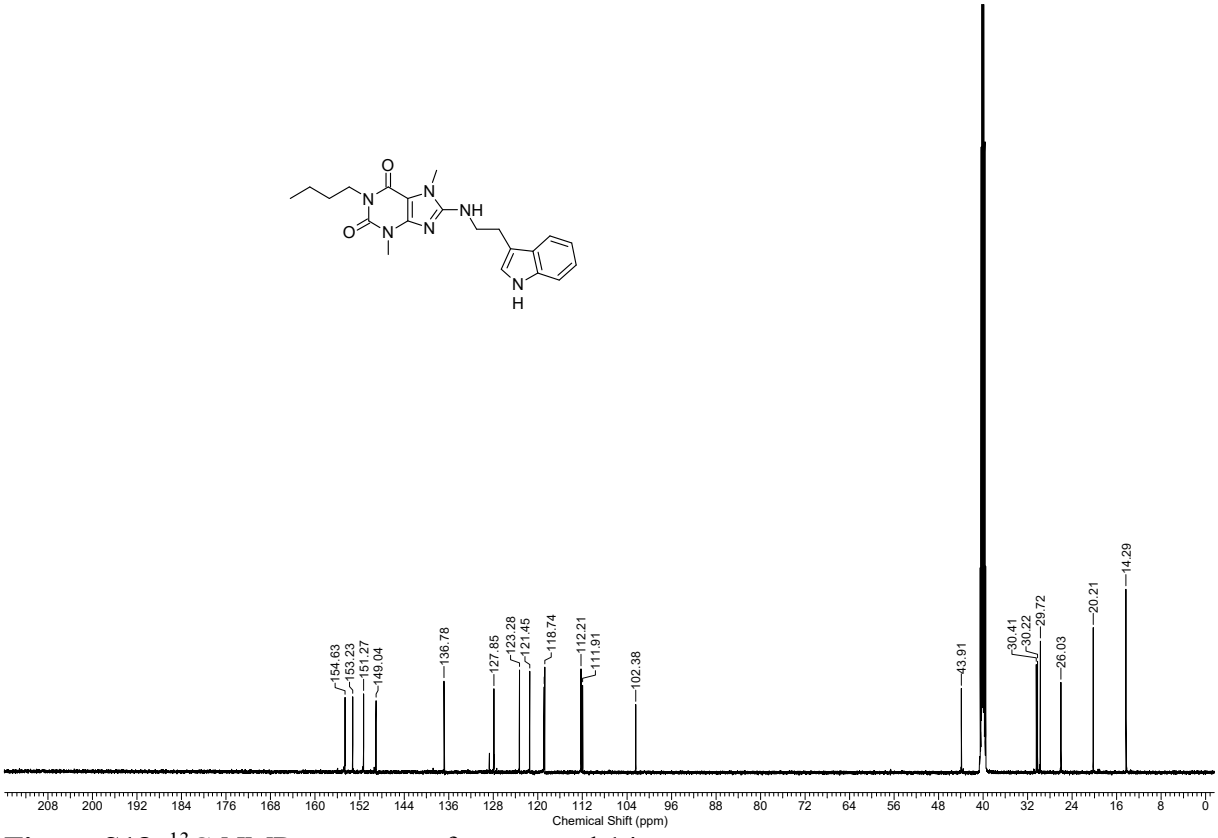

Figure S18. ^{13}C-NMR spectrum of compound **14**.

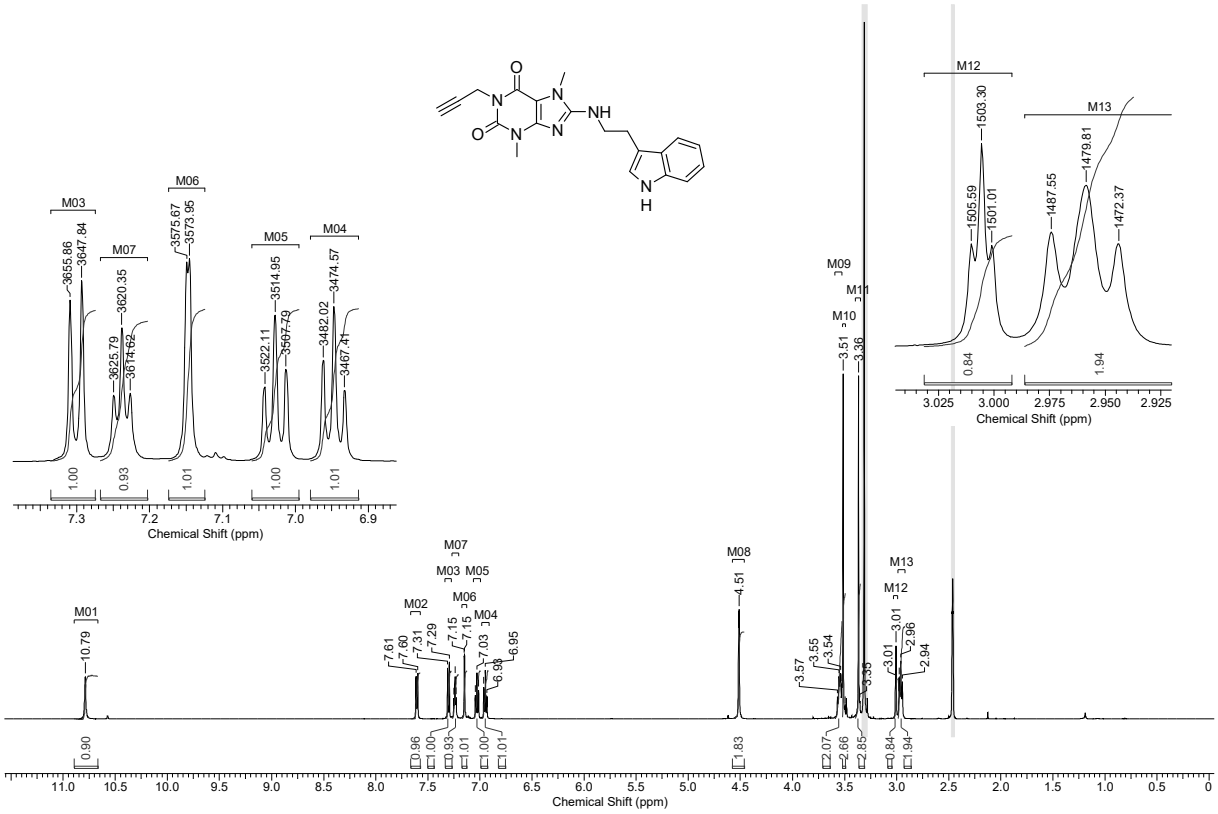

Figure S19. ^{1}H-NMR spectrum of compound **15**.

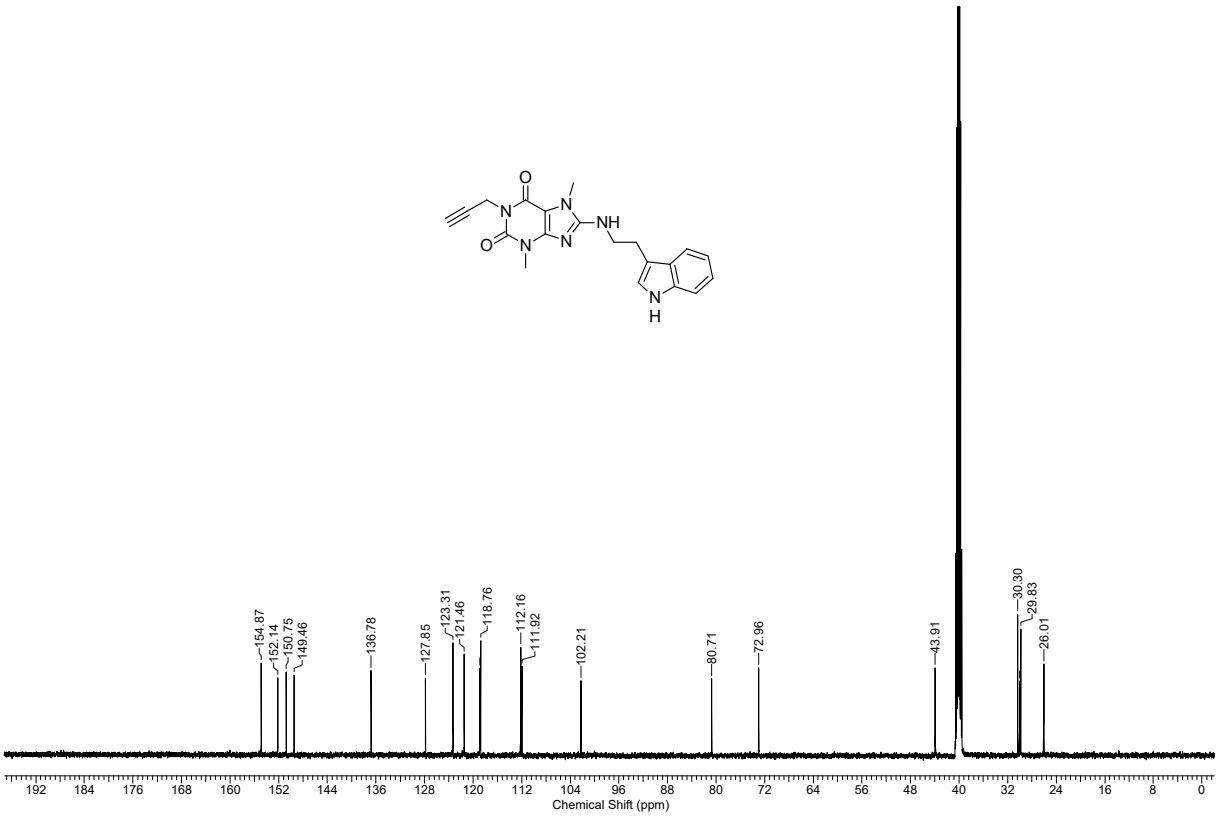

Figure S20. ^{13}C-NMR spectrum of compound **15**.

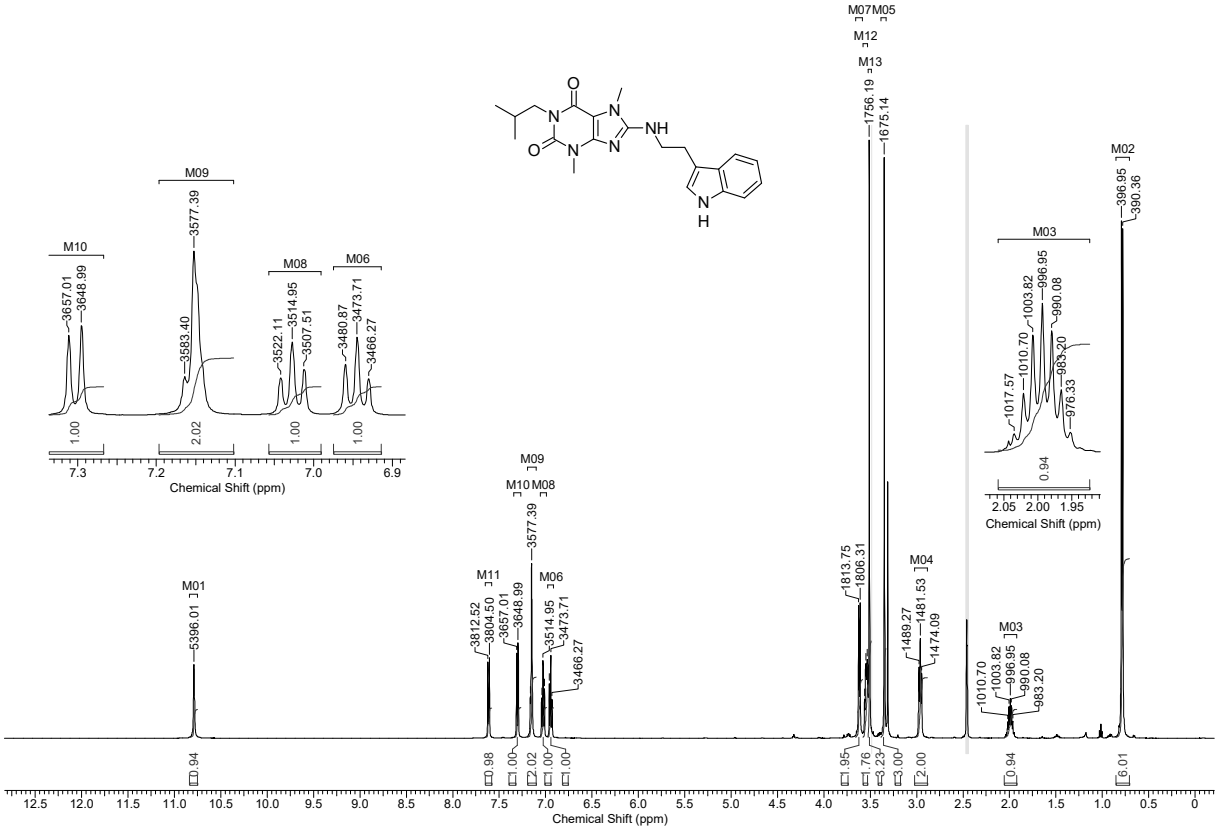

Figure S21. ^{1}H-NMR spectrum of compound **16**.

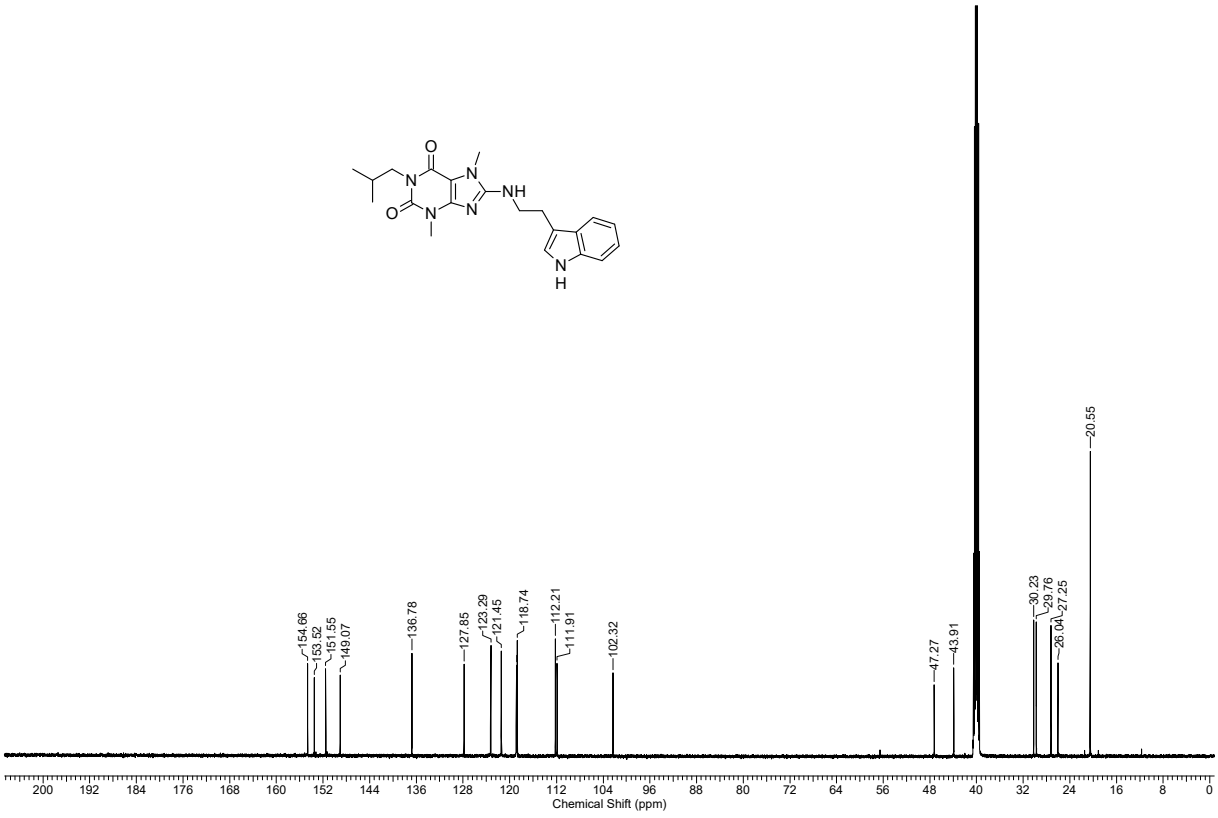

Figure S22. ^{13}C-NMR spectrum of compound **16**.

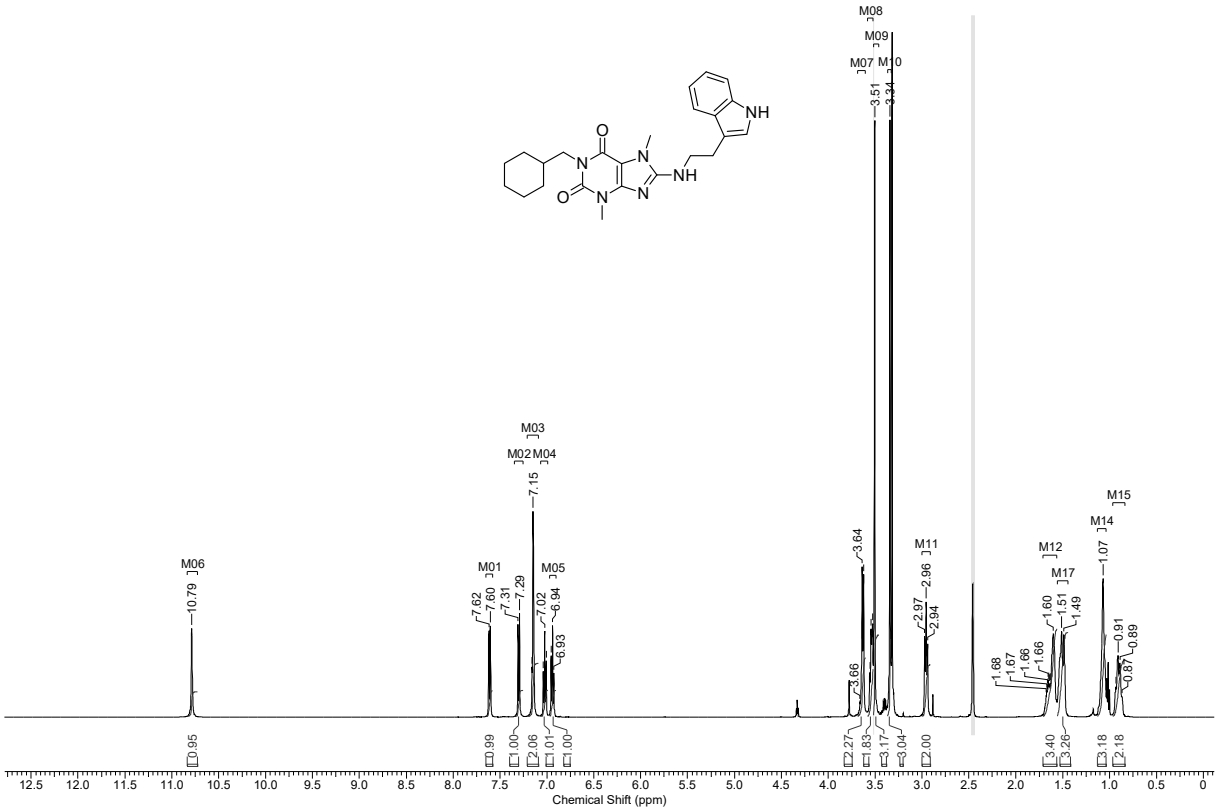

Figure S23. ^{1}H-NMR spectrum of compound **17**.

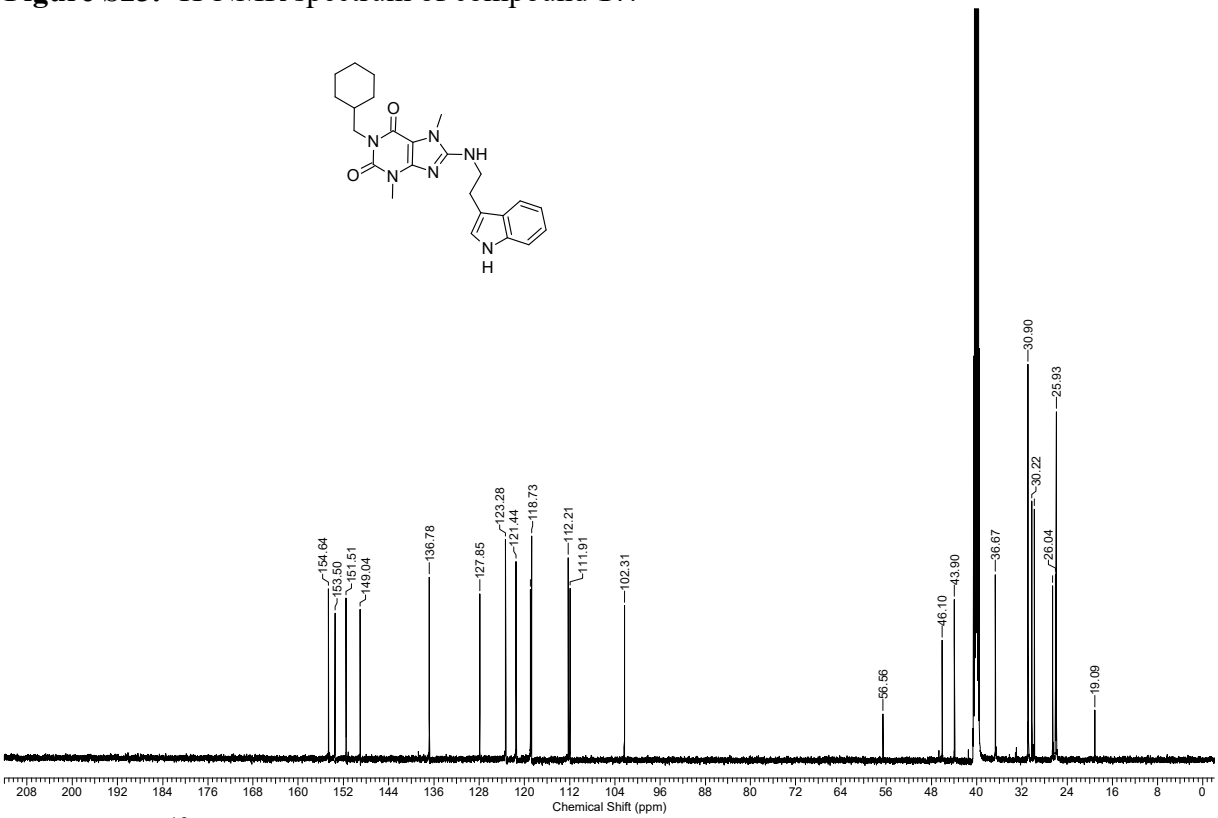

Figure S24. ^{13}C-NMR spectrum of compound **17**.

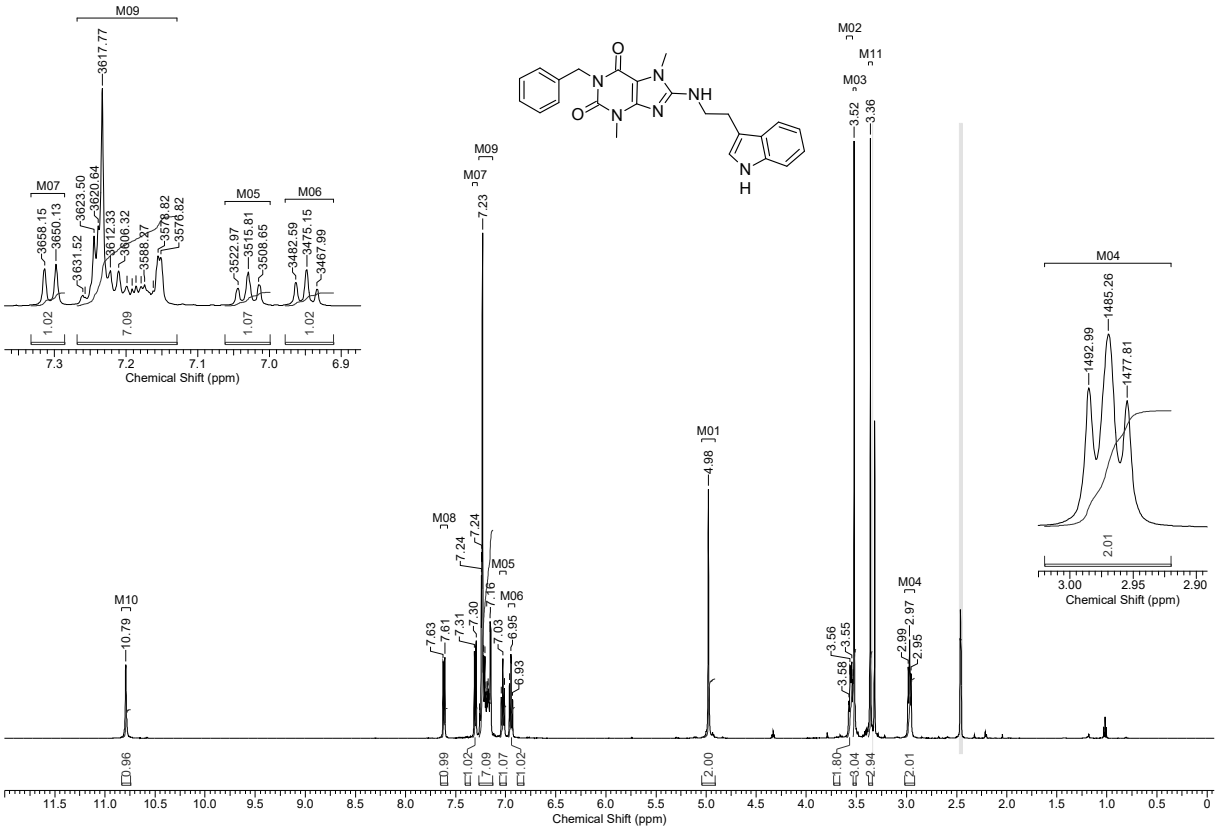

Figure S25. ^{1}H-NMR spectrum of compound **18**.

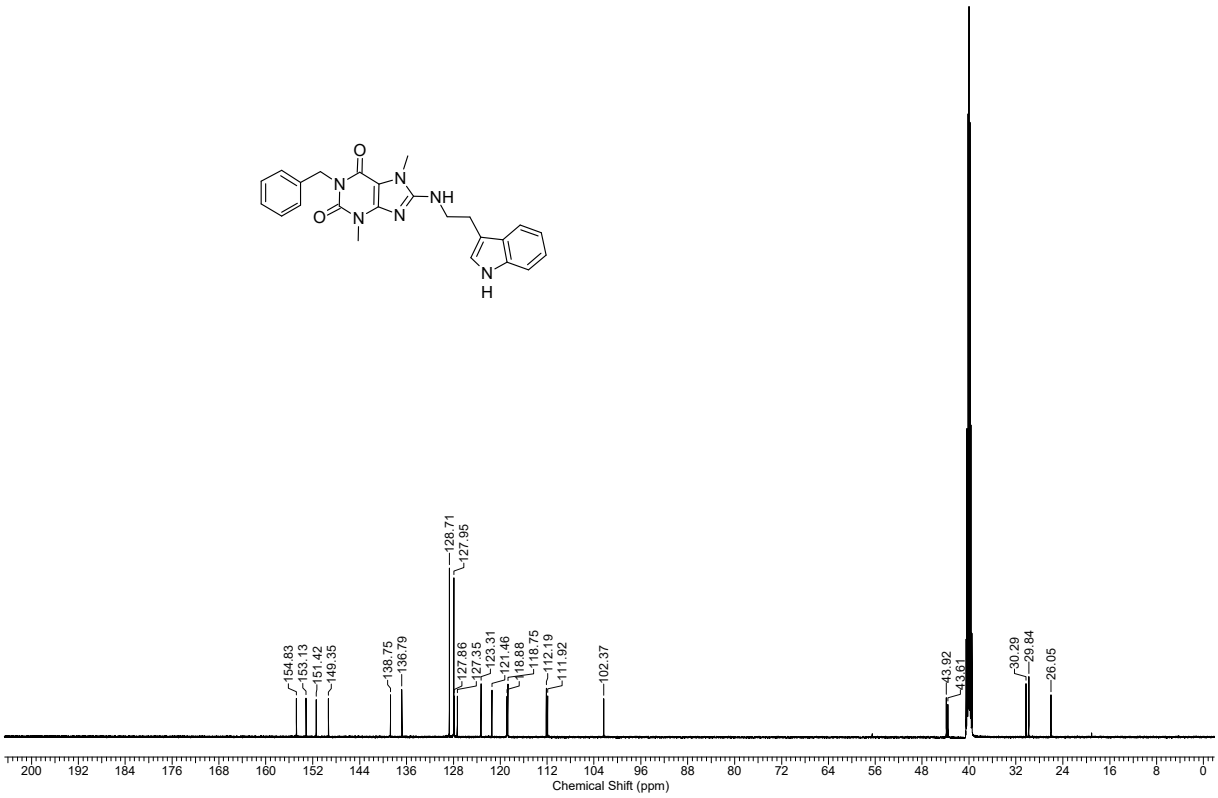

Figure S26. ^{13}C-NMR spectrum of compound **18**.

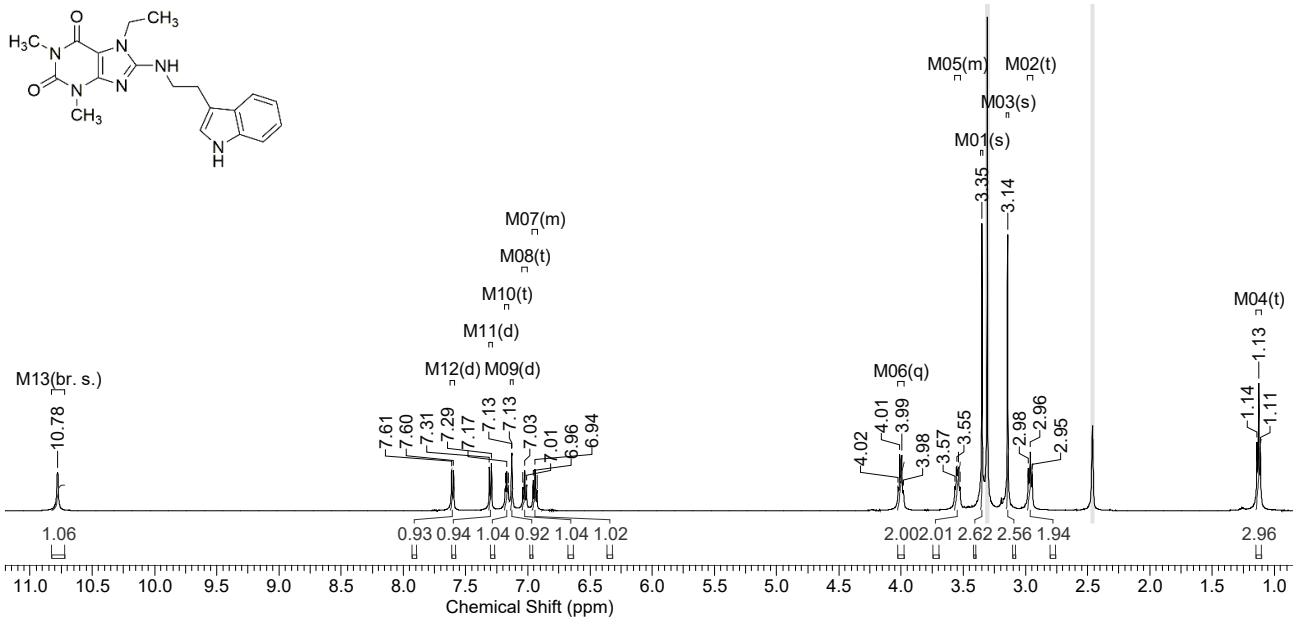

Figure S27. ^{1}H-NMR spectrum of compound **21.**

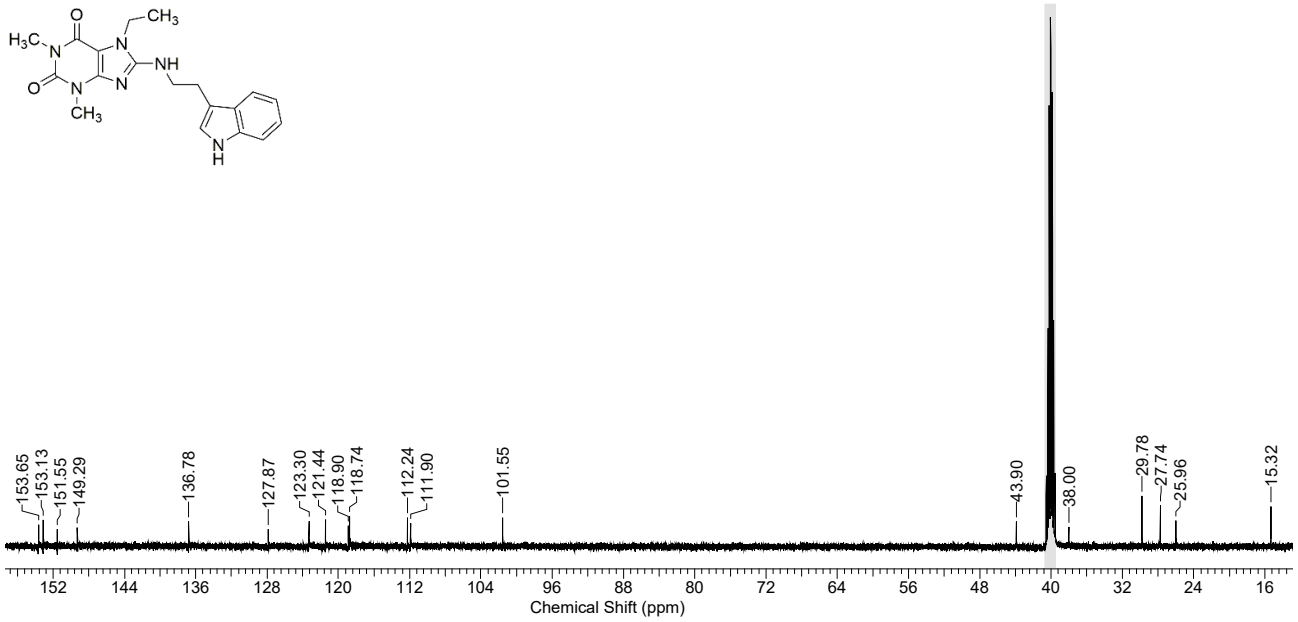

Figure S28. ^{13}C-NMR spectrum of compound **21.**

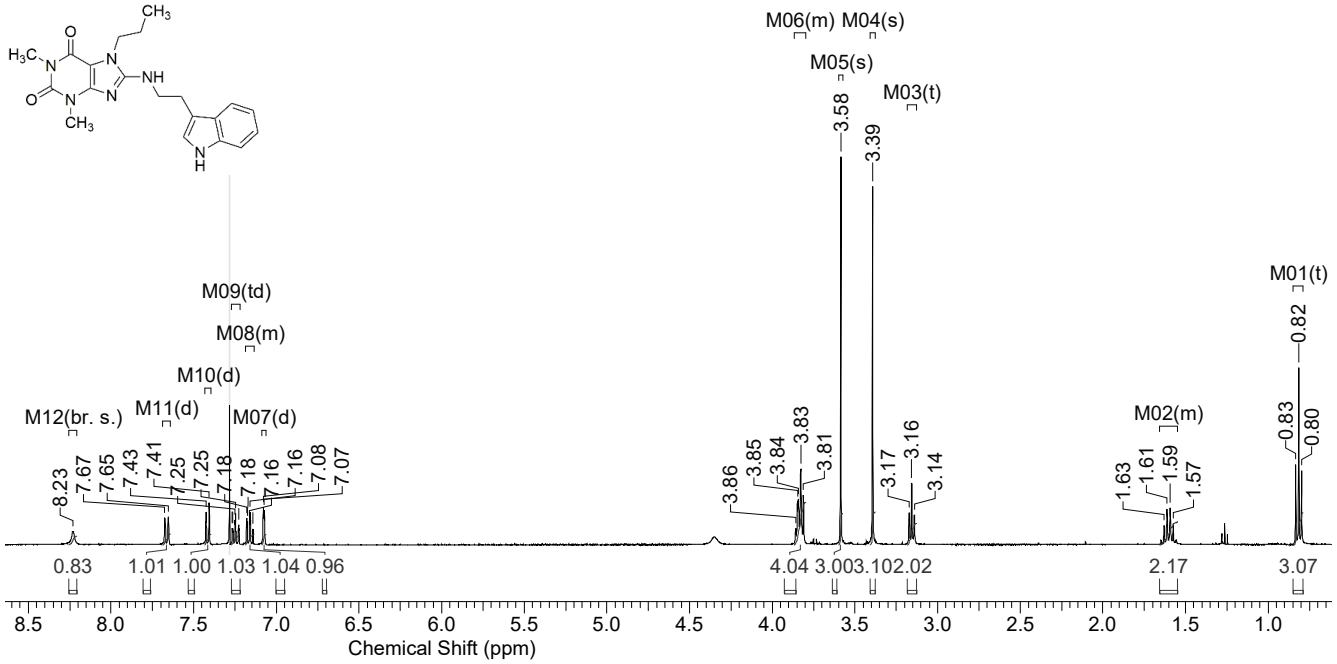

Figure S29. ^{1}H-NMR spectrum of compound **22**.

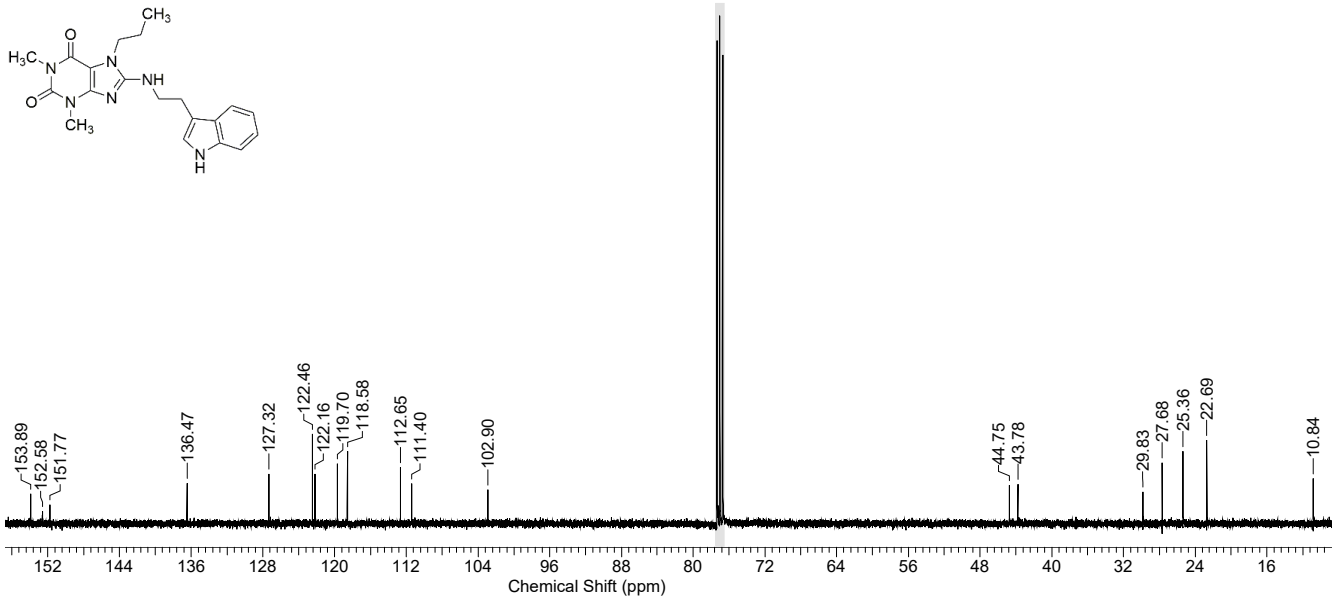

Figure S30. ^{13}C-NMR spectrum of compound **22**.

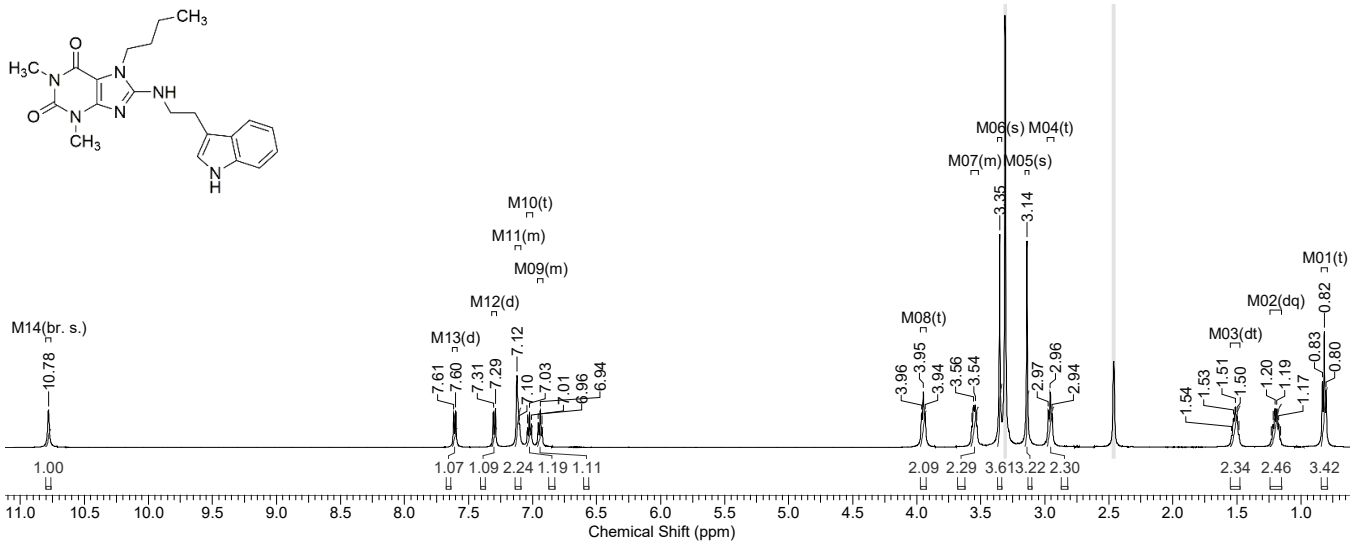

Figure S31. ^{1}H-NMR spectrum of compound **23**.

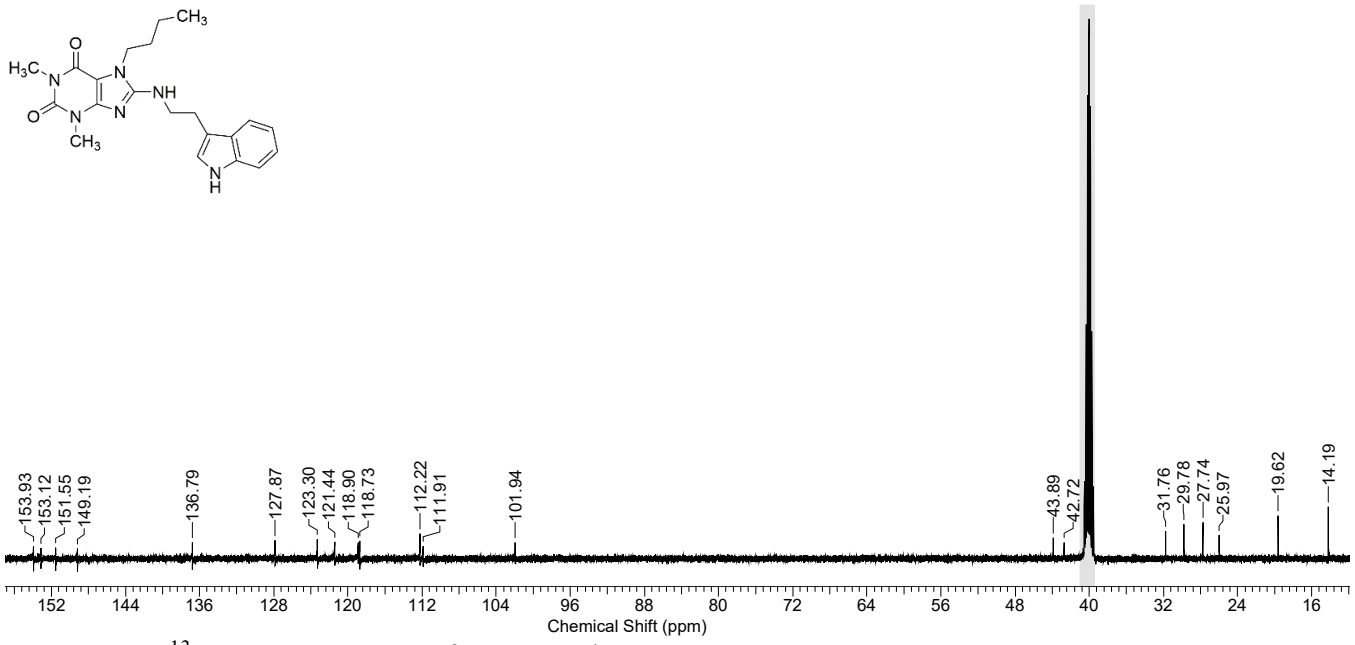

Figure S32. ^{13}C-NMR spectrum of compound **23**.

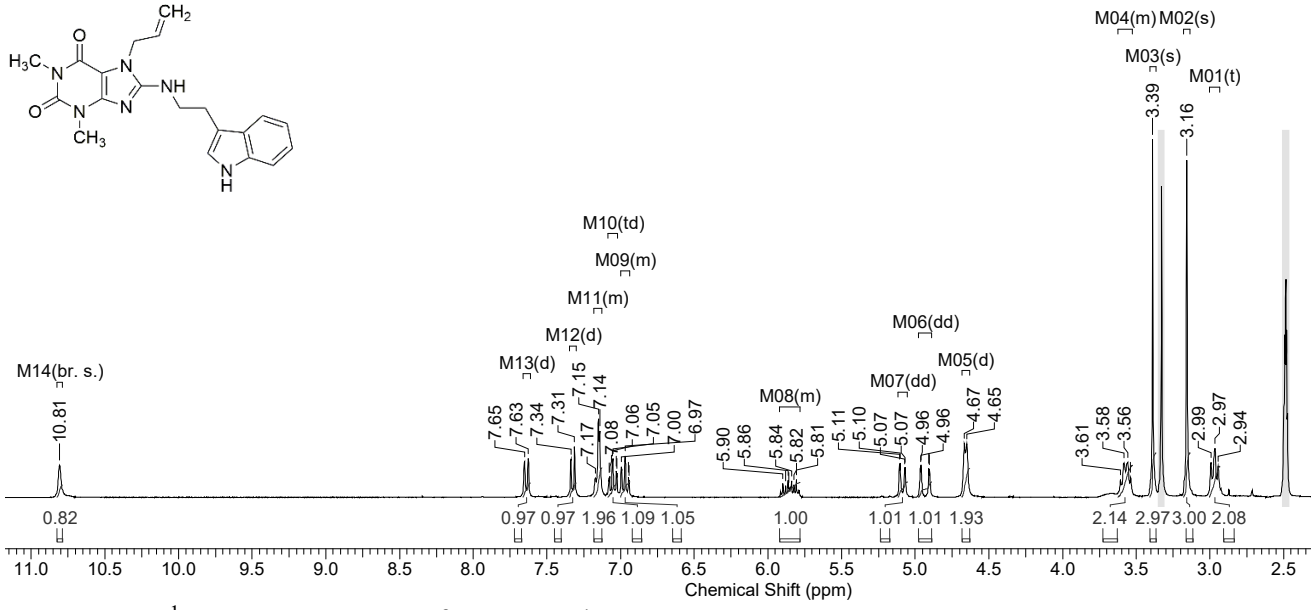

Figure S33. ^{1}H-NMR spectrum of compound **24**.

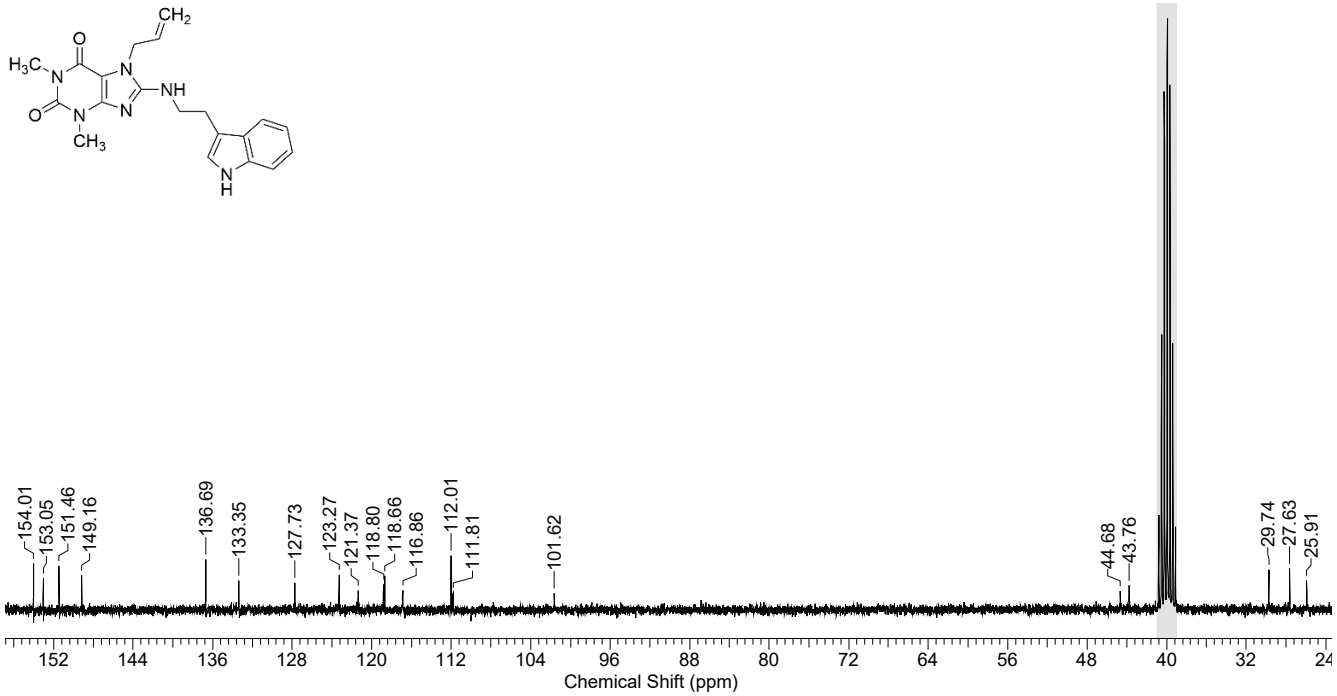

Figure S34. ^{13}C-NMR spectrum of compound **24**.

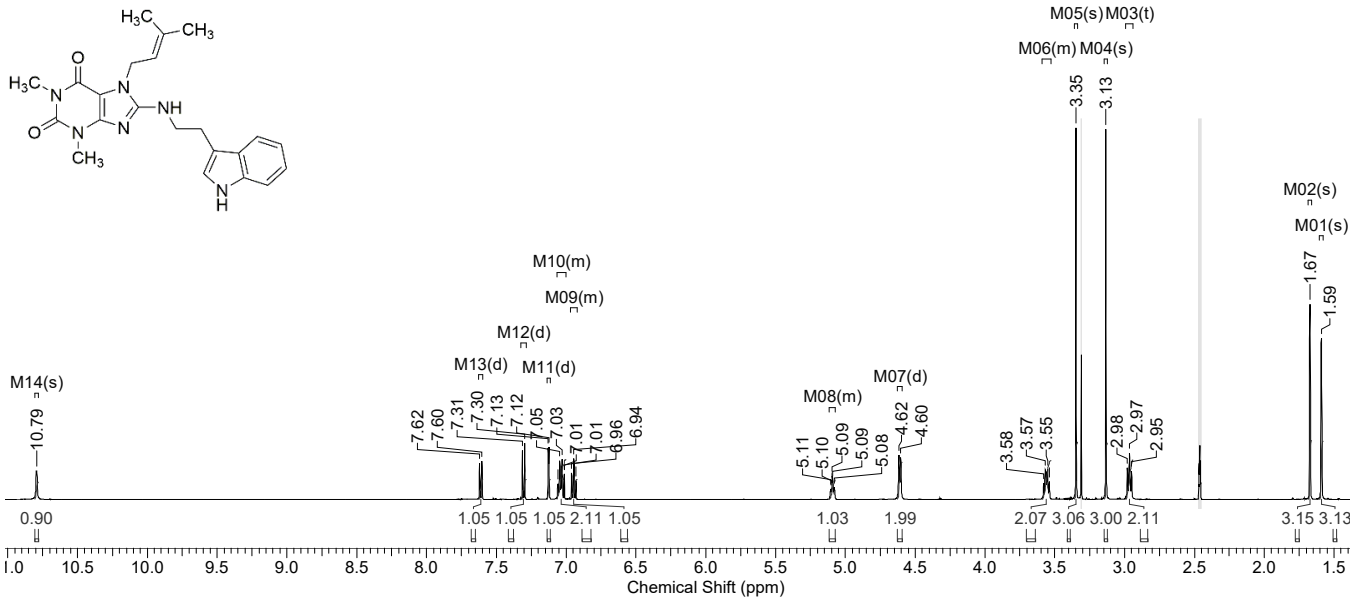

Figure S35. ^{1}H-NMR spectrum of compound **25**.

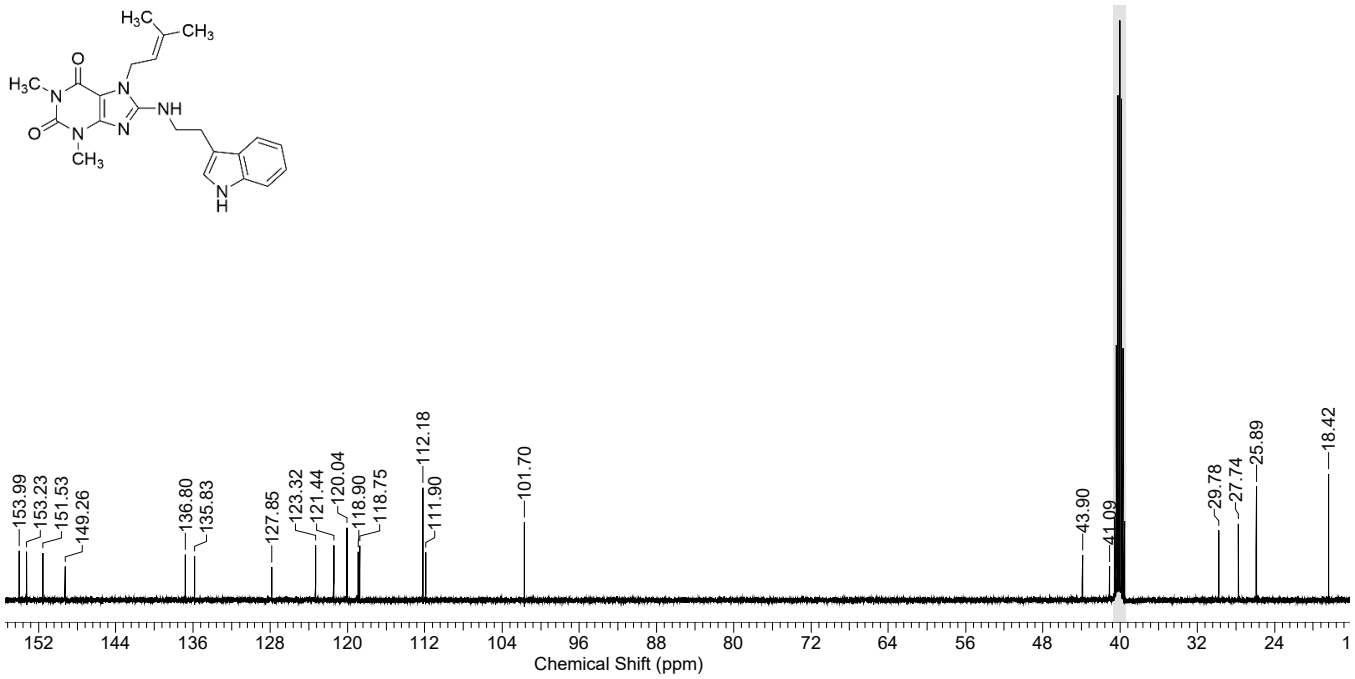

Figure S36. ^{13}C-NMR spectrum of compound **25**.

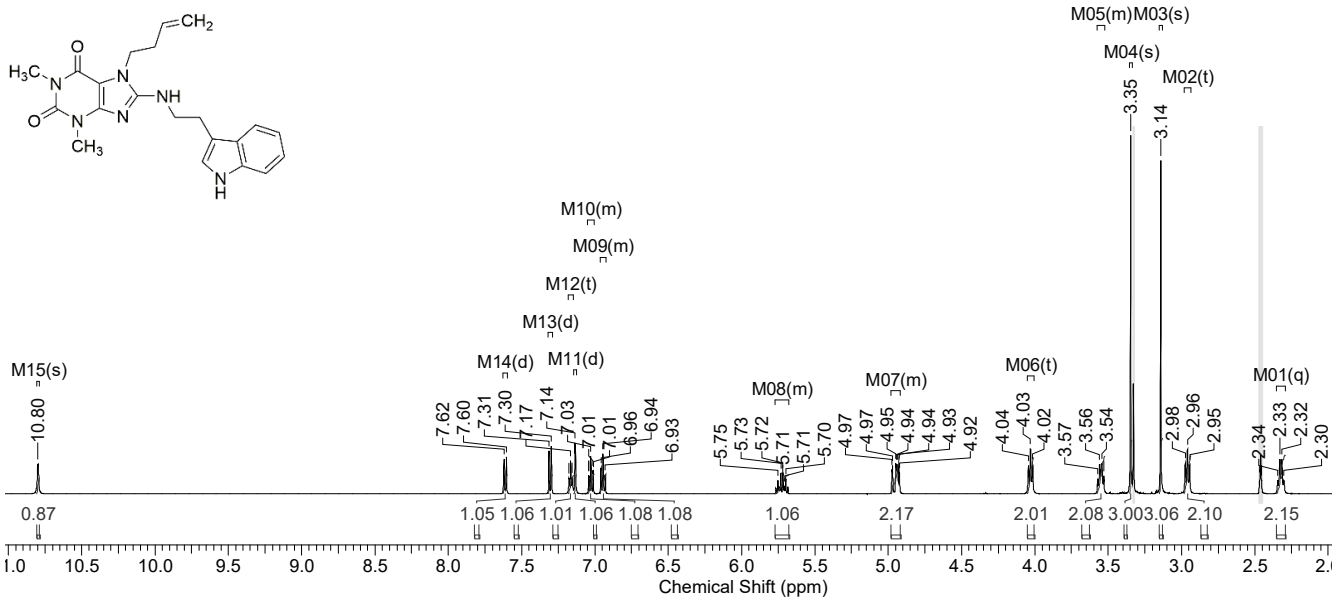

Figure S37. ^{1}H-NMR spectrum of compound **26**.

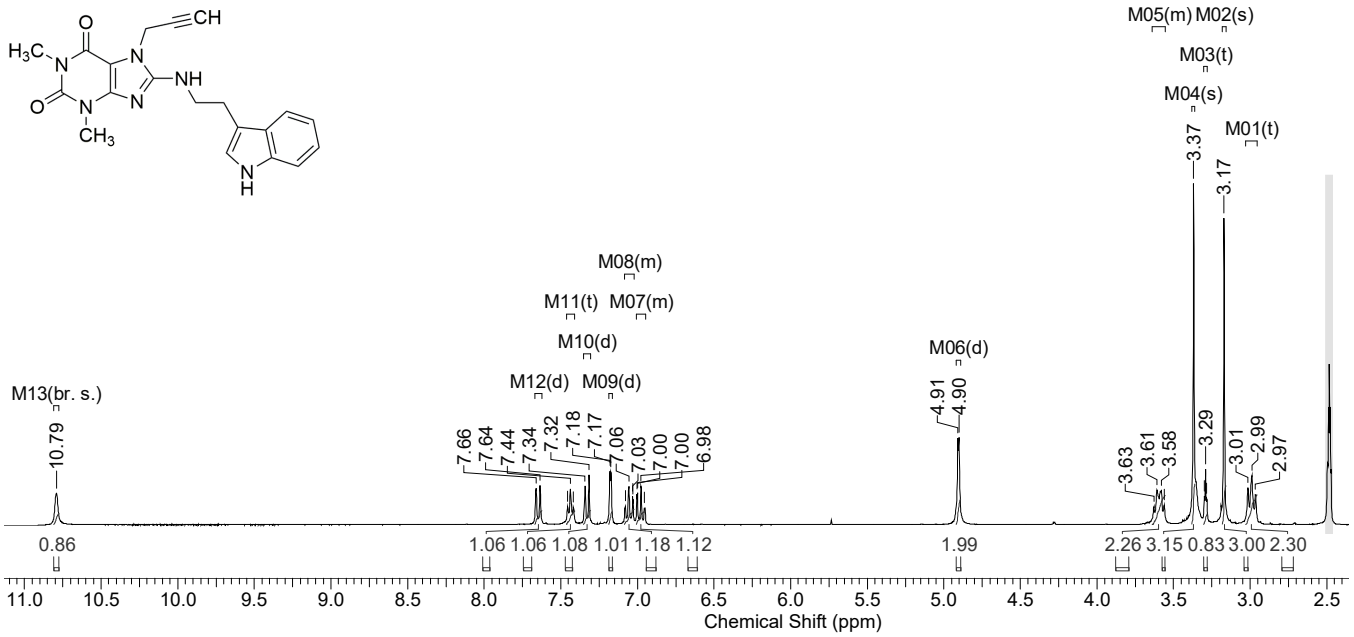

Figure S38. ^{1}H-NMR spectrum of compound **27**.

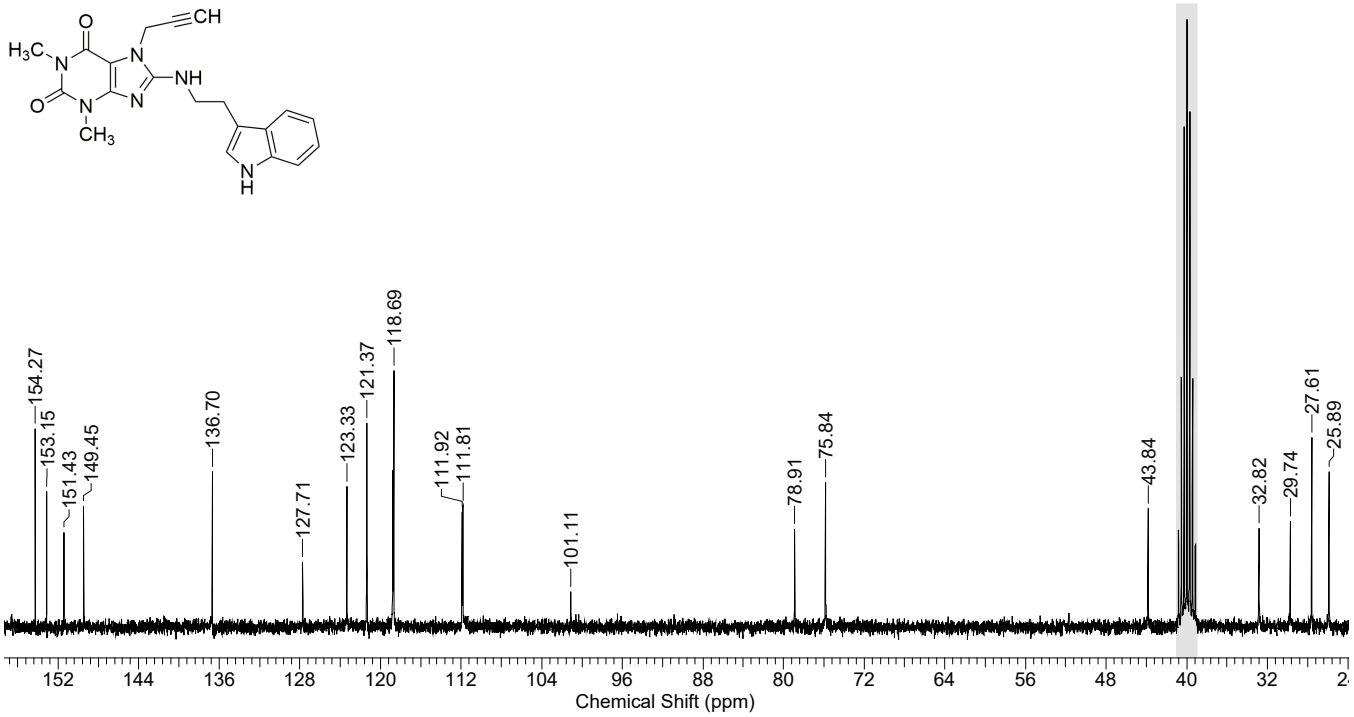

Figure S39. ^{13}C-NMR spectrum of compound **27**.

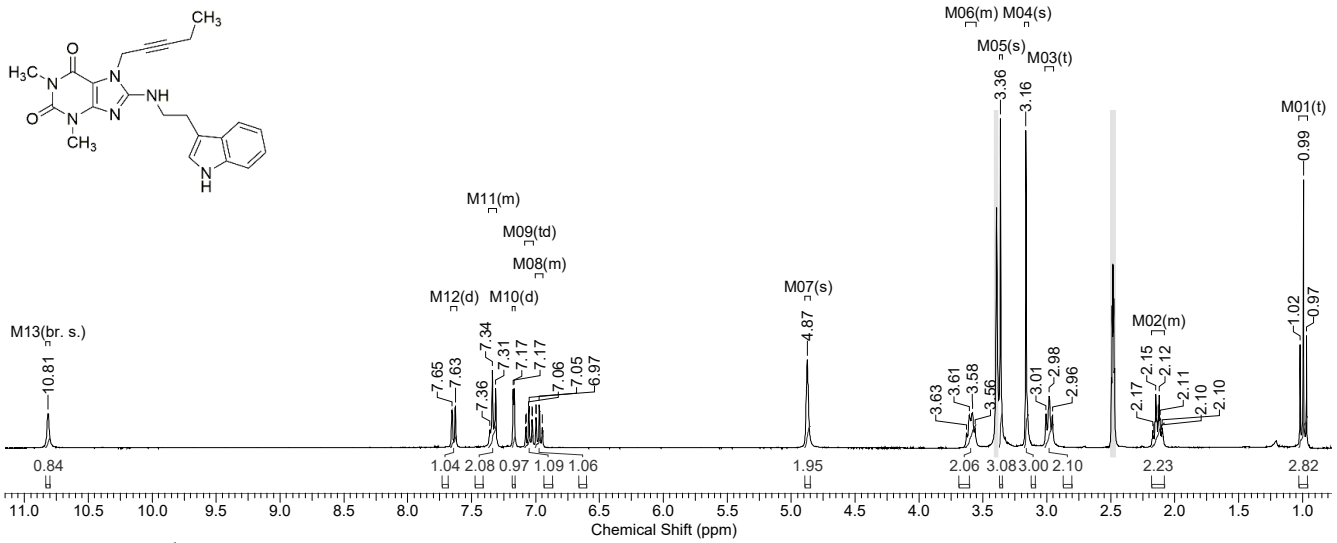

Figure S40. ^{1}H-NMR spectrum of compound **28**.

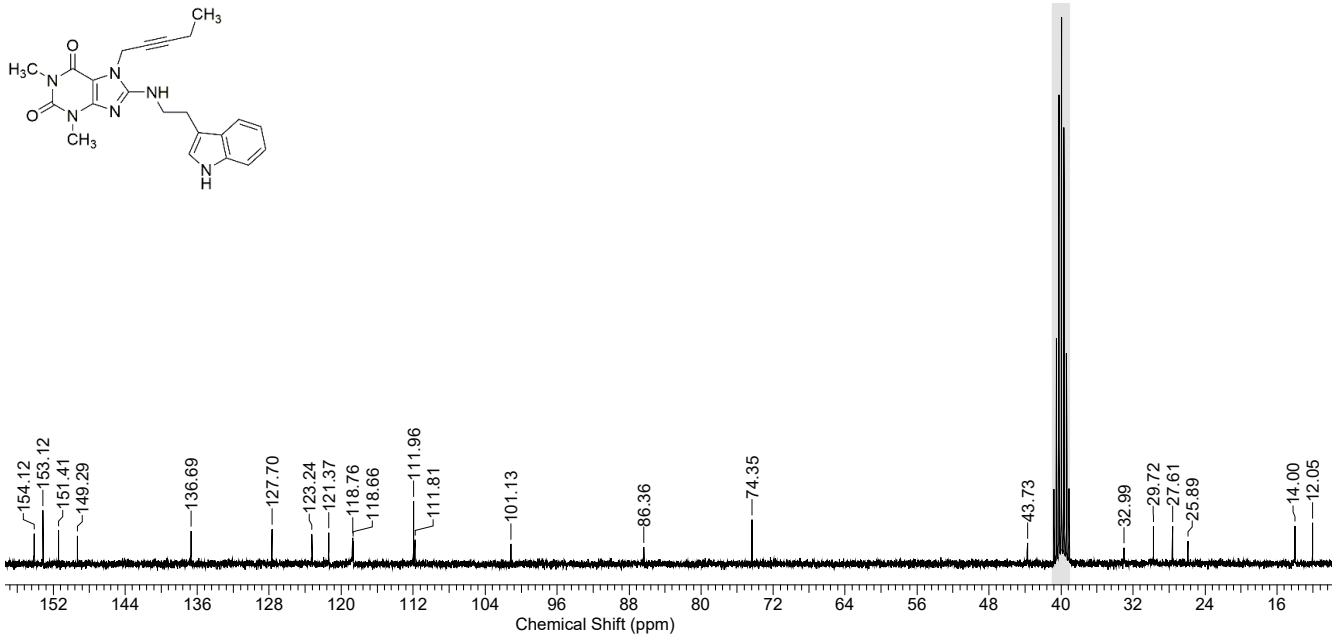

Figure S41. ^{13}C-NMR spectrum of compound **28**.

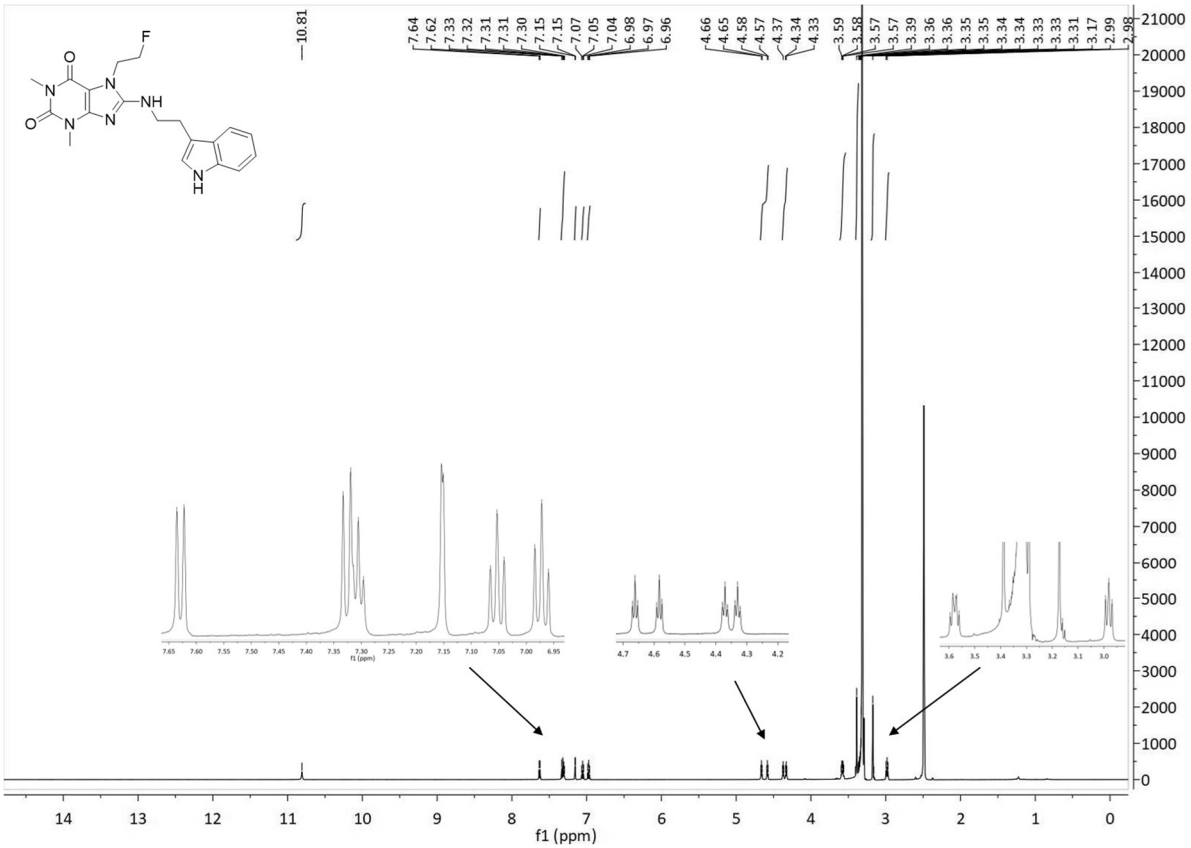

Figure S42. ^{1}H-NMR spectrum of compound **30**.

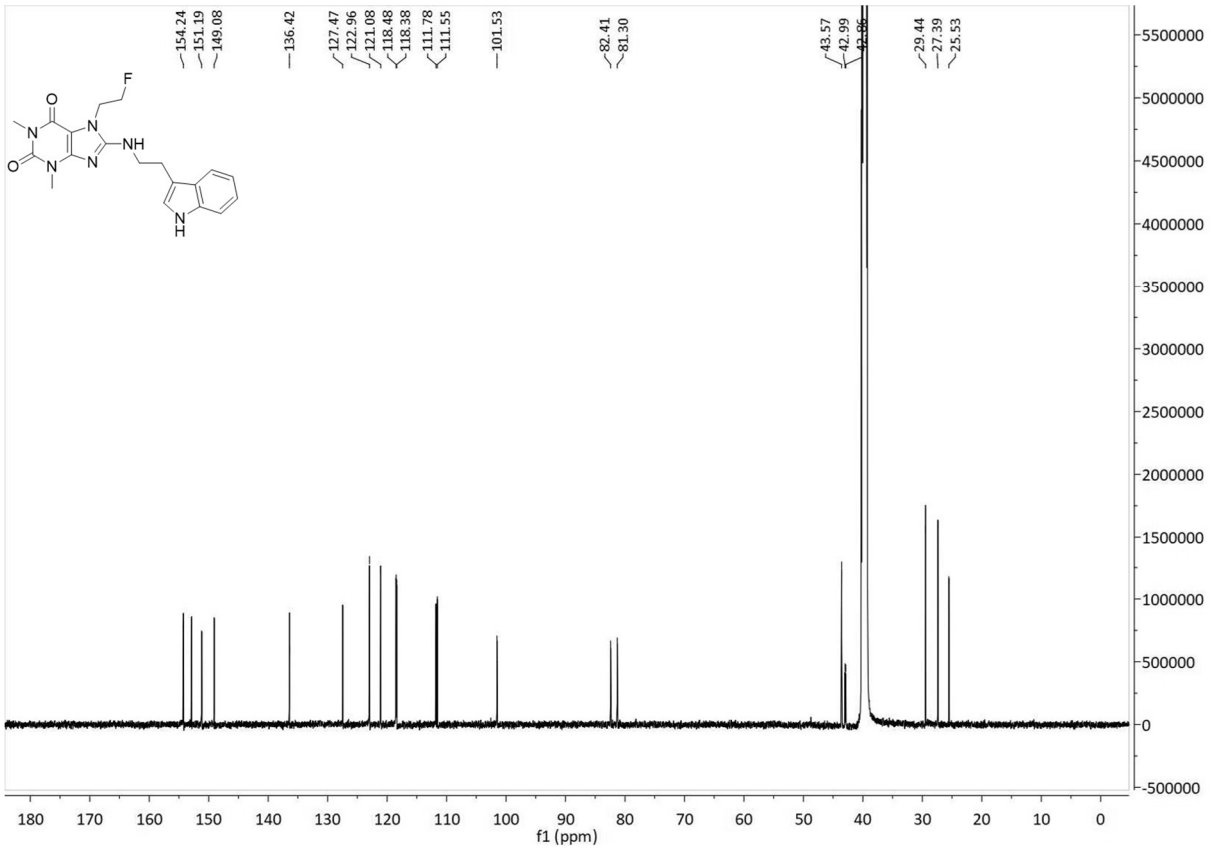

Figure S43. ^{13}C-NMR spectrum of compound **30**.

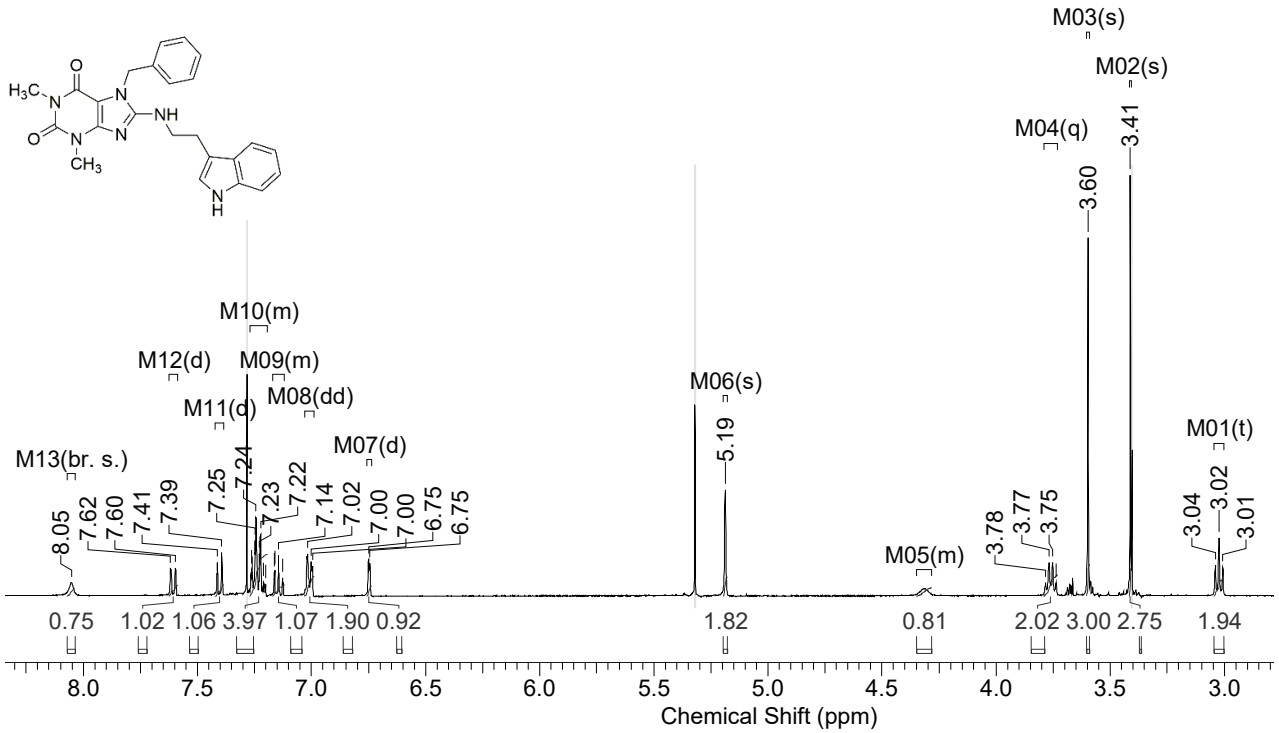

Figure S44. ^{1}H-NMR spectrum of compound **31.**

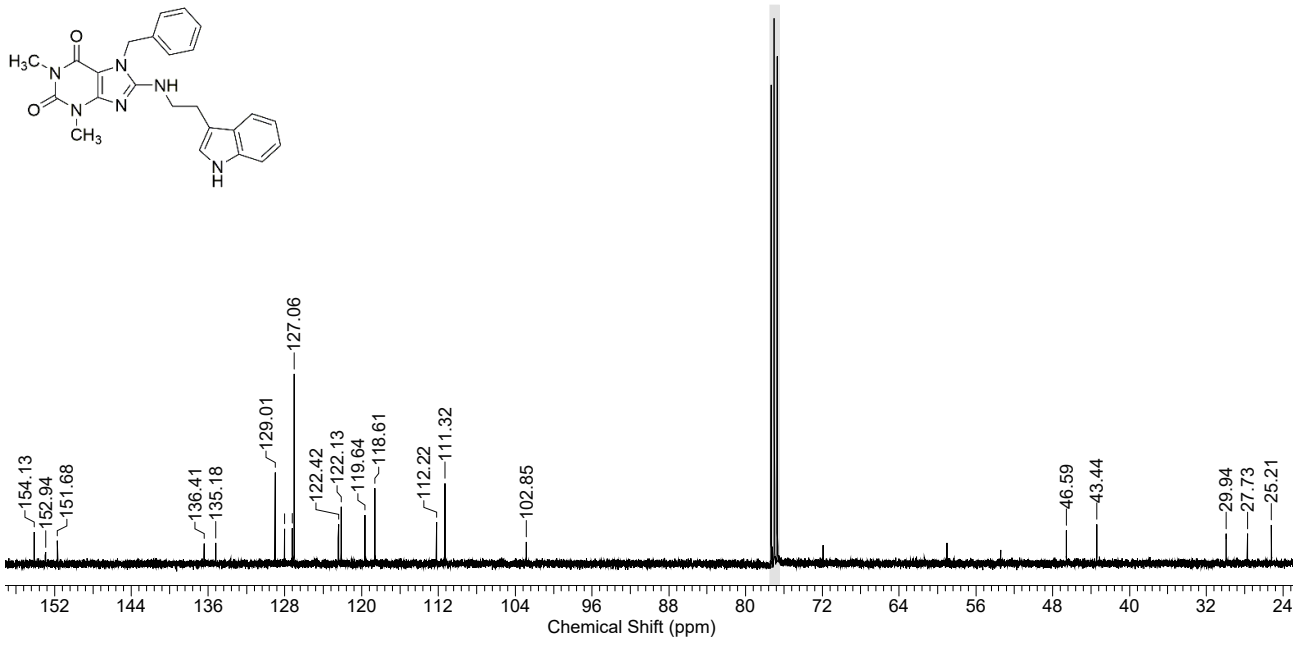

Figure S45. ^{13}C-NMR spectrum of compound **31.**

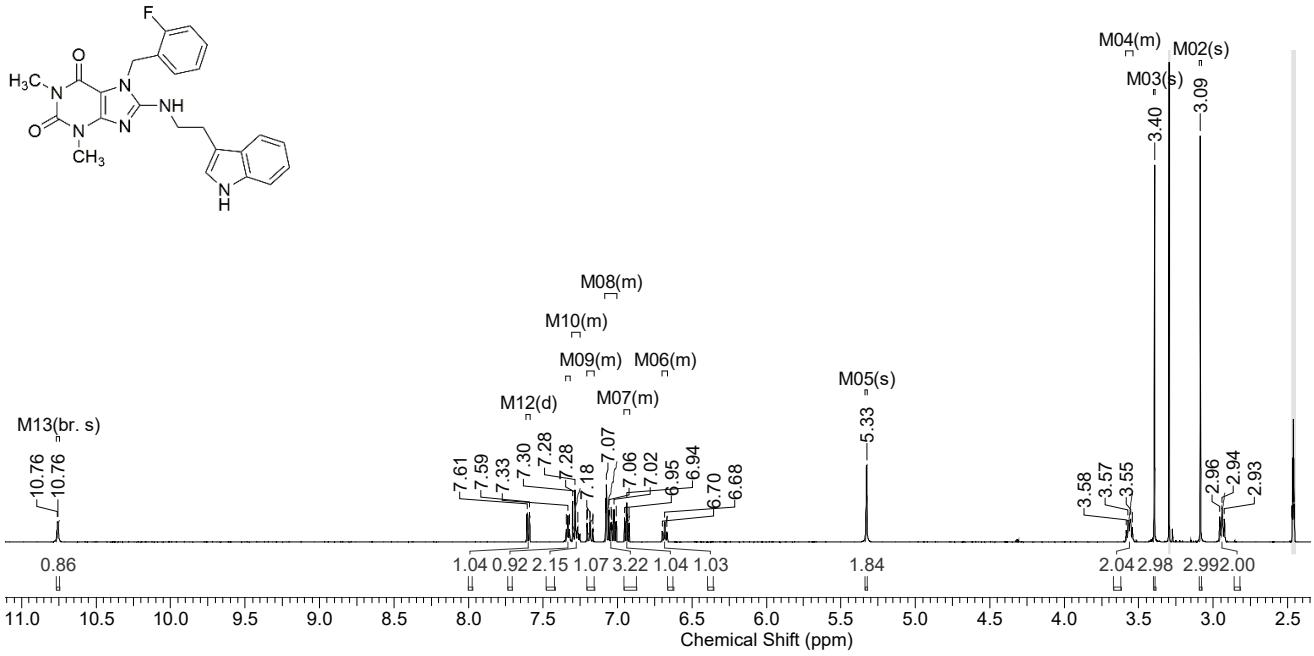

Figure S46. ^{1}H-NMR spectrum of compound **32**.

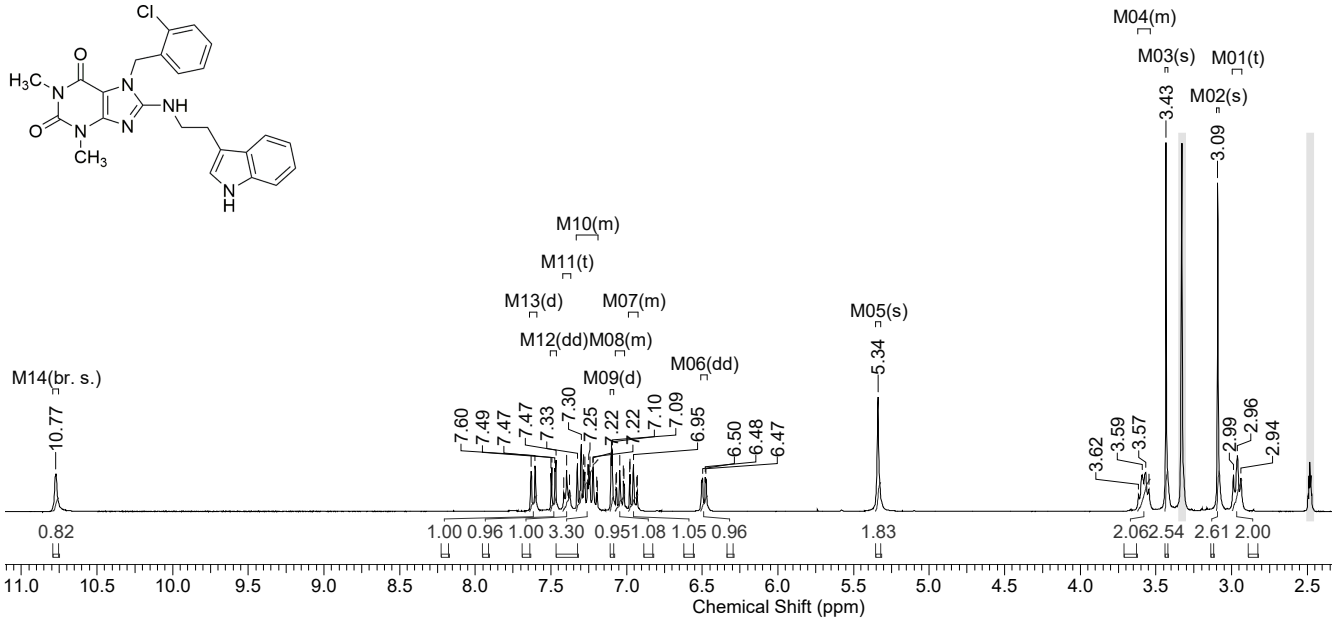

Figure S47. ^{1}H-NMR spectrum of compound **33**.

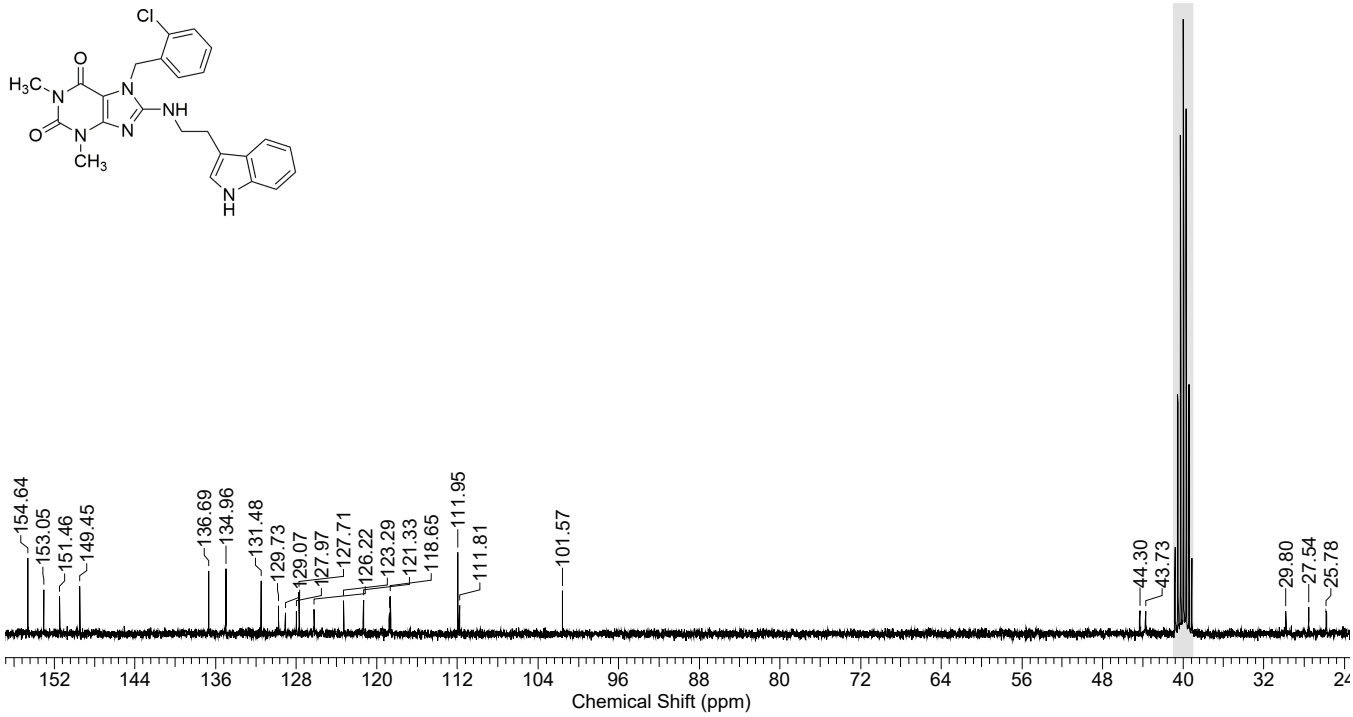

Figure S48. ^{13}C-NMR spectrum of compound **33**.

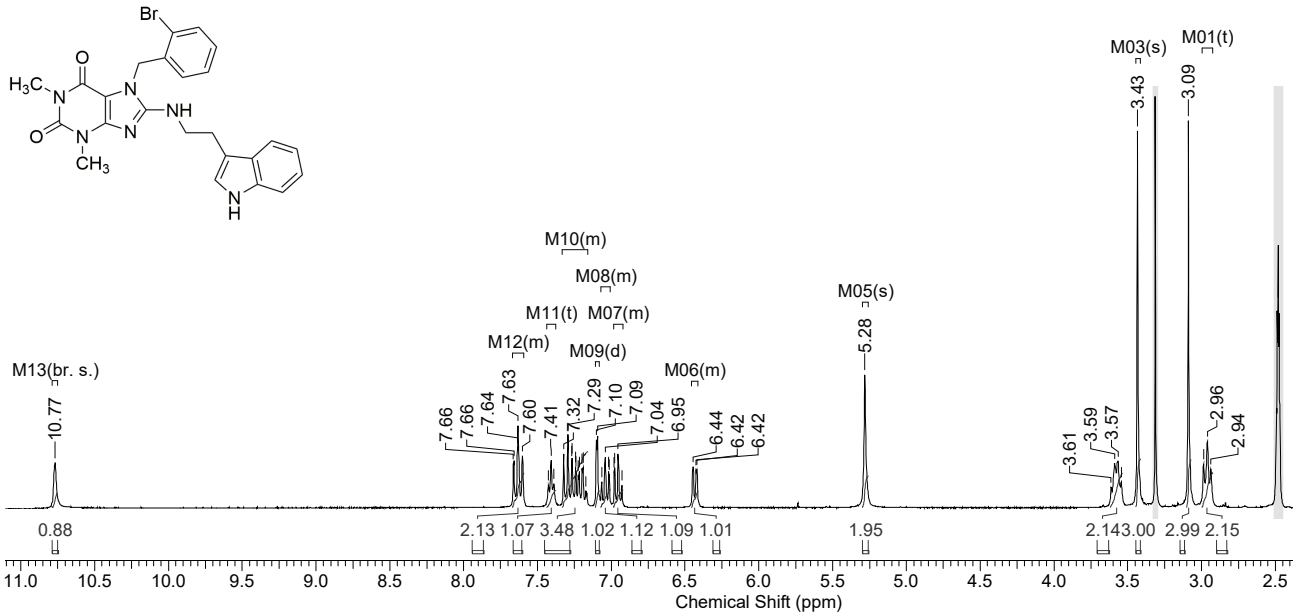

Figure S49. ^{1}H-NMR spectrum of compound **34**.

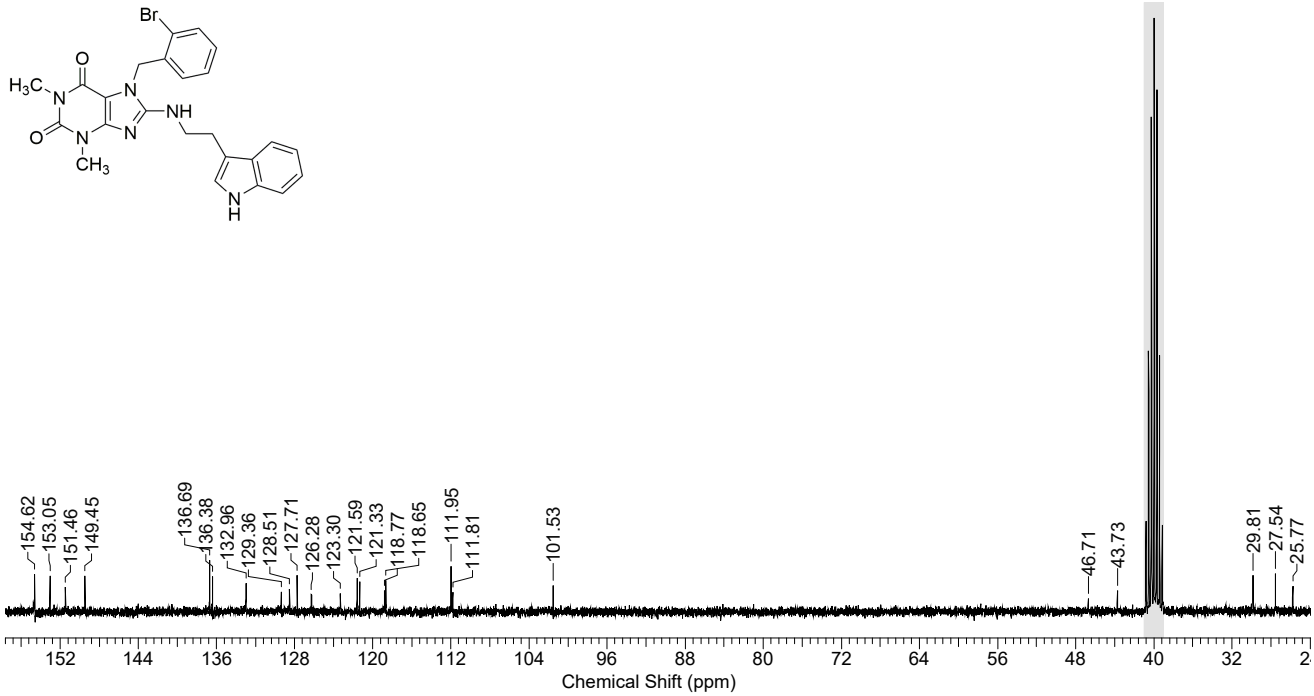

Figure S50. ^{13}C-NMR spectrum of compound **34**.

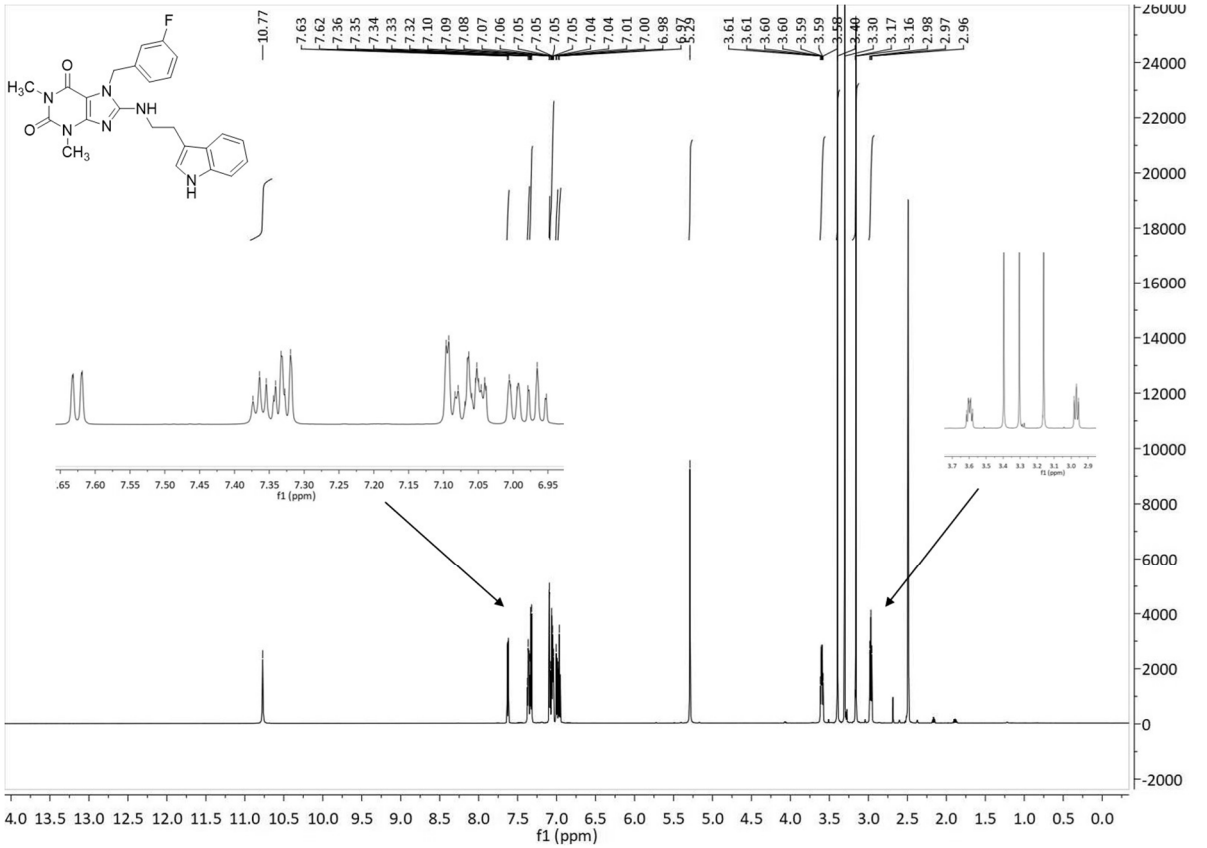

Figure S51. ^{1}H-NMR spectrum of compound **35**.

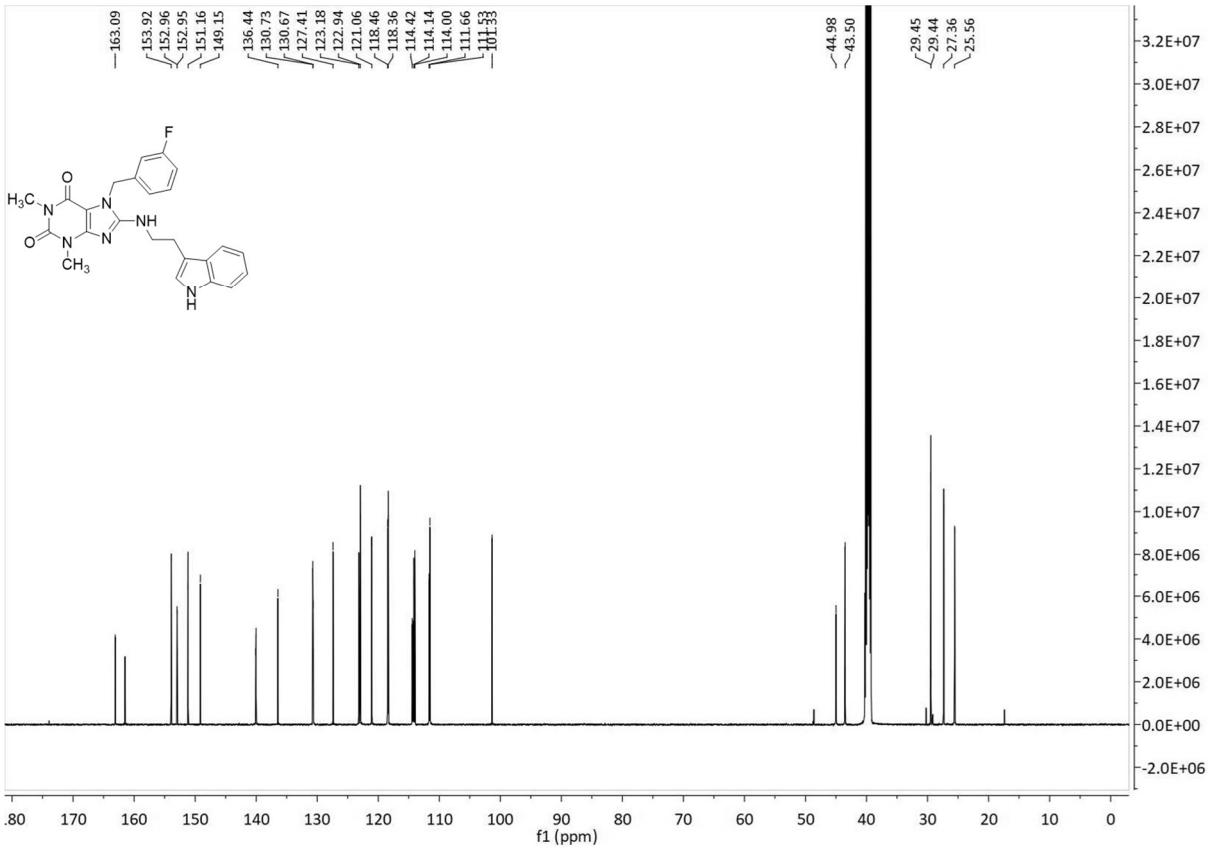

Figure S52. ^{13}C-NMR spectrum of compound **35**.

S58

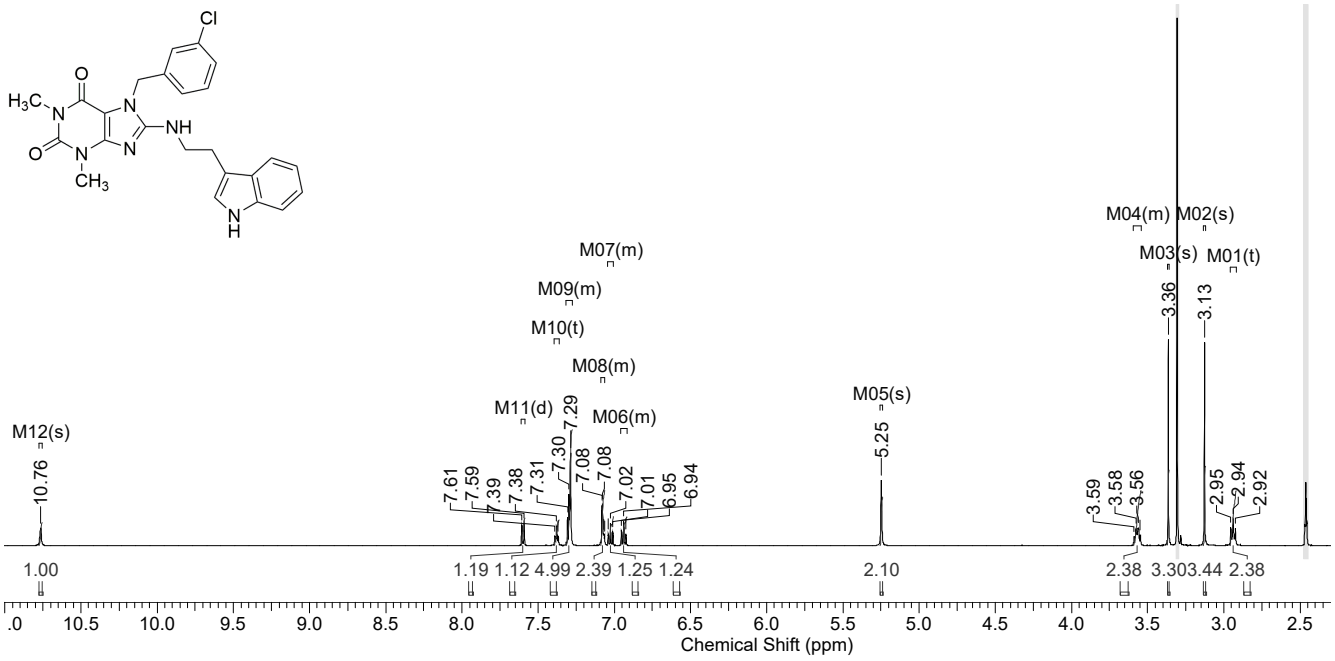

Figure S53.[1]H-NMR spectrum of compound **36** (PSB-KK1448)

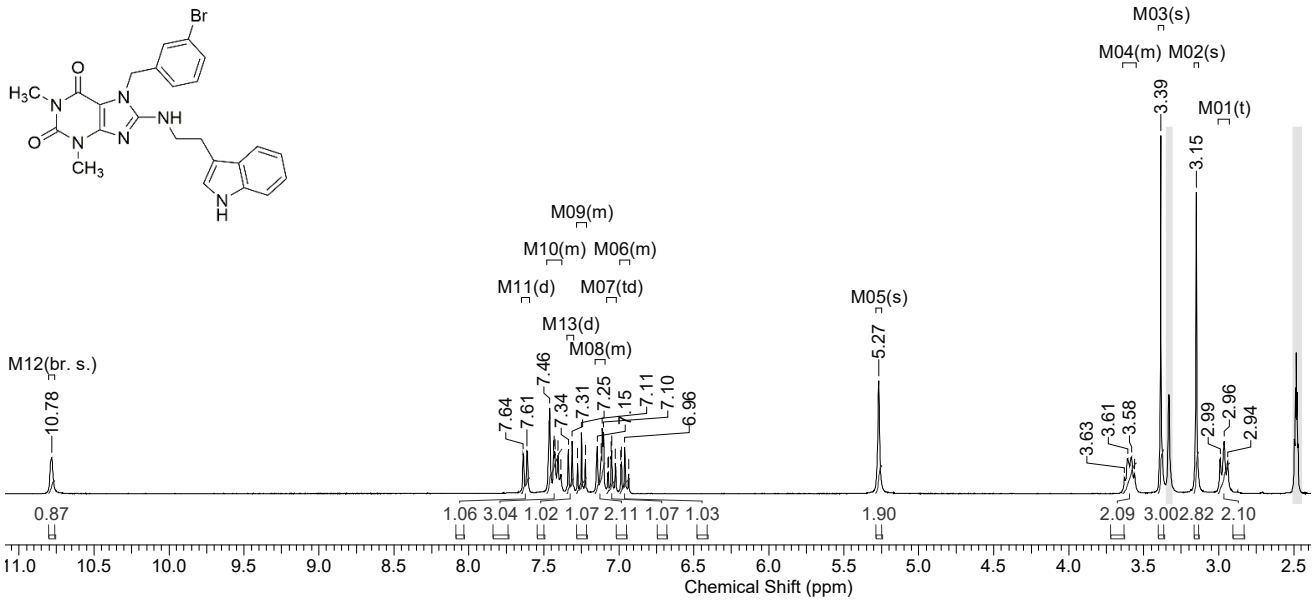

Figure S54. ^{1}H-NMR spectrum of compound **37**.

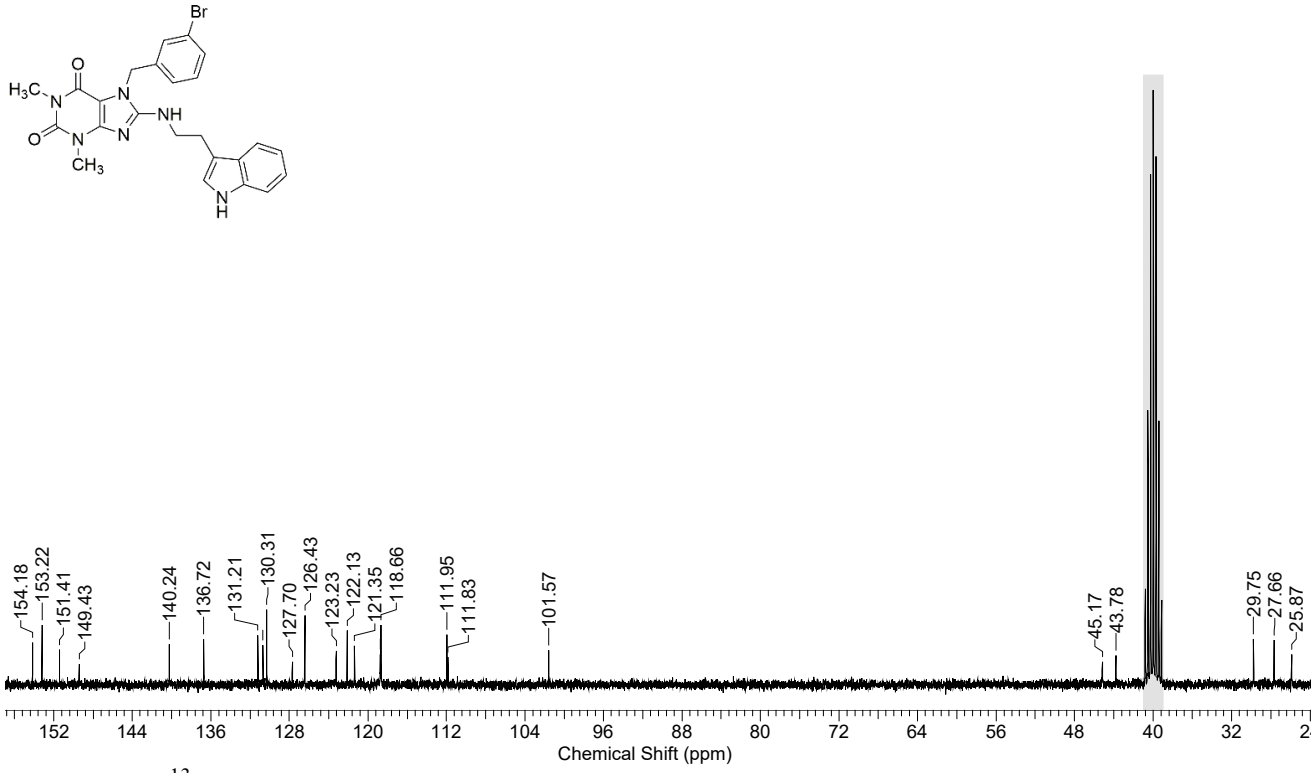

Figure S55. ^{13}C-NMR spectrum of compound **37**.

S60

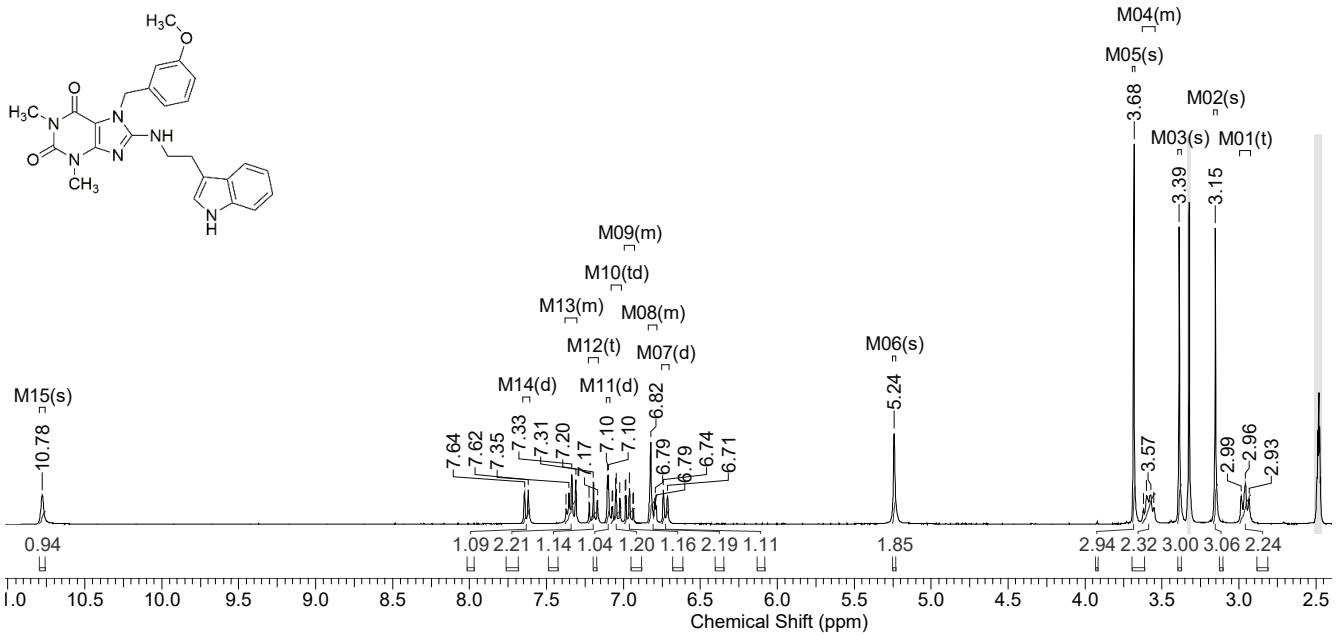

Figure S56. ^{1}H-NMR spectrum of compound **38**.

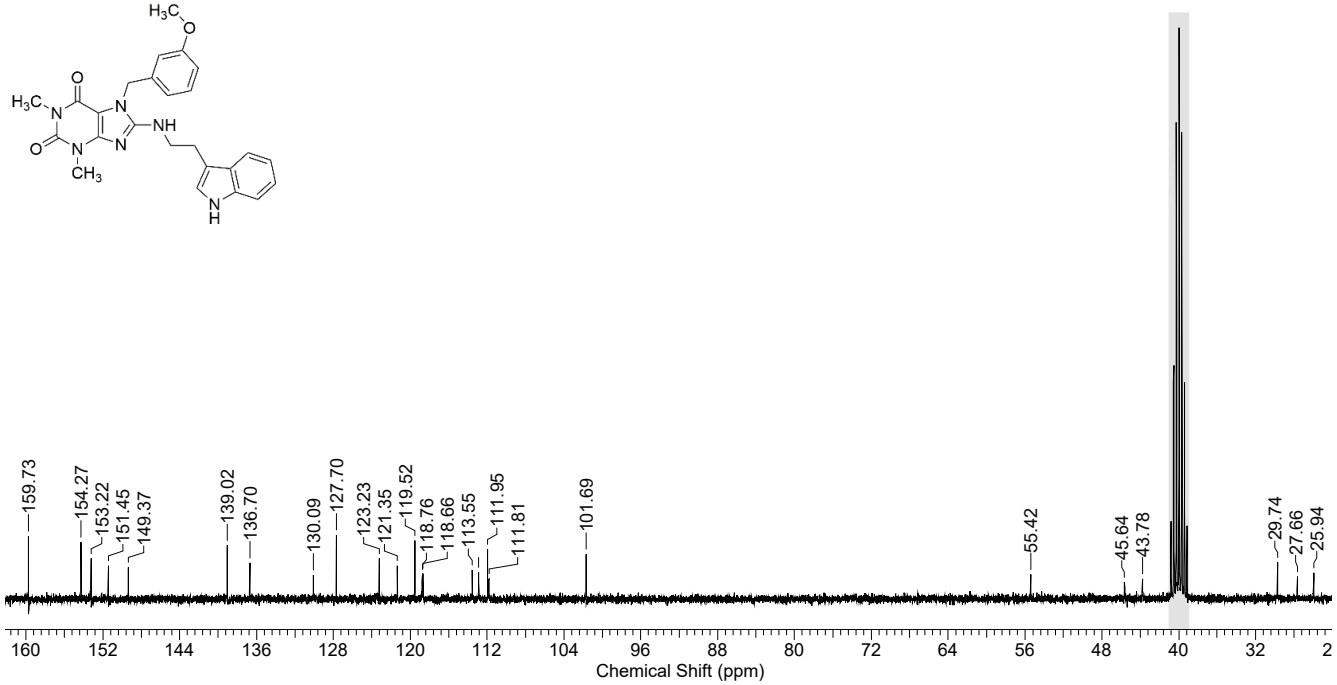

Figure S57. ^{13}C-NMR spectrum of compound **38**.

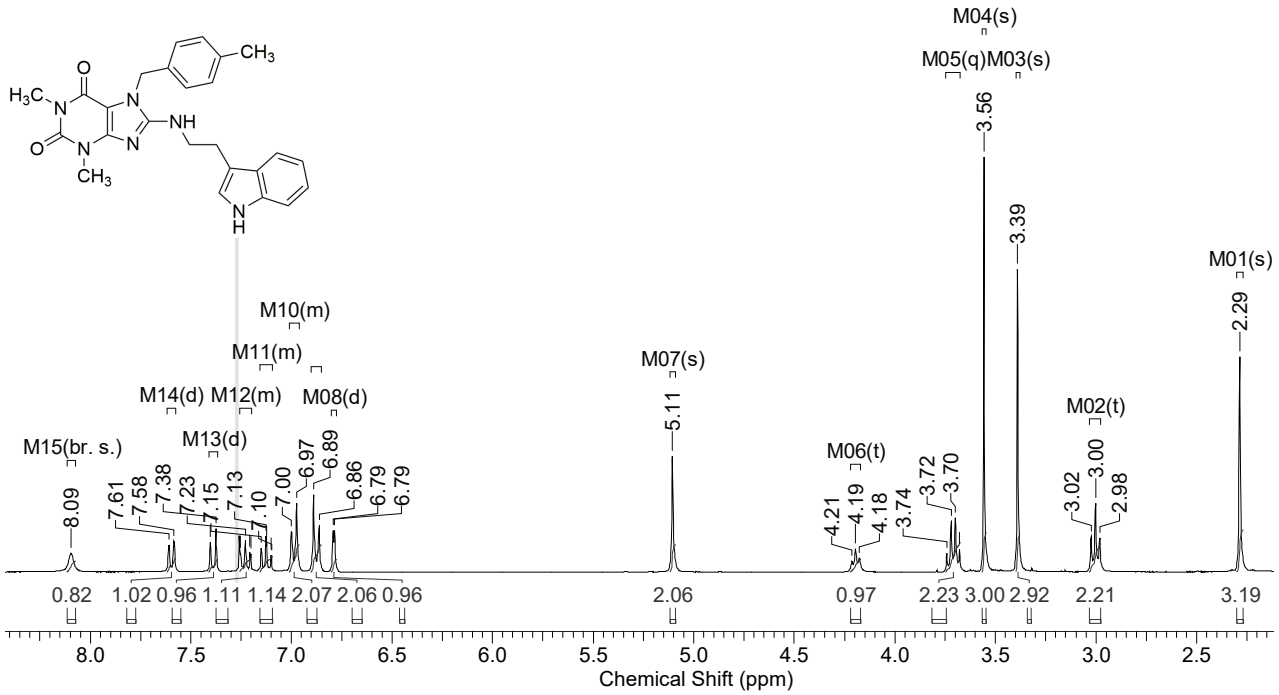

Figure S58. ^{1}H-NMR spectrum of compound **39**.

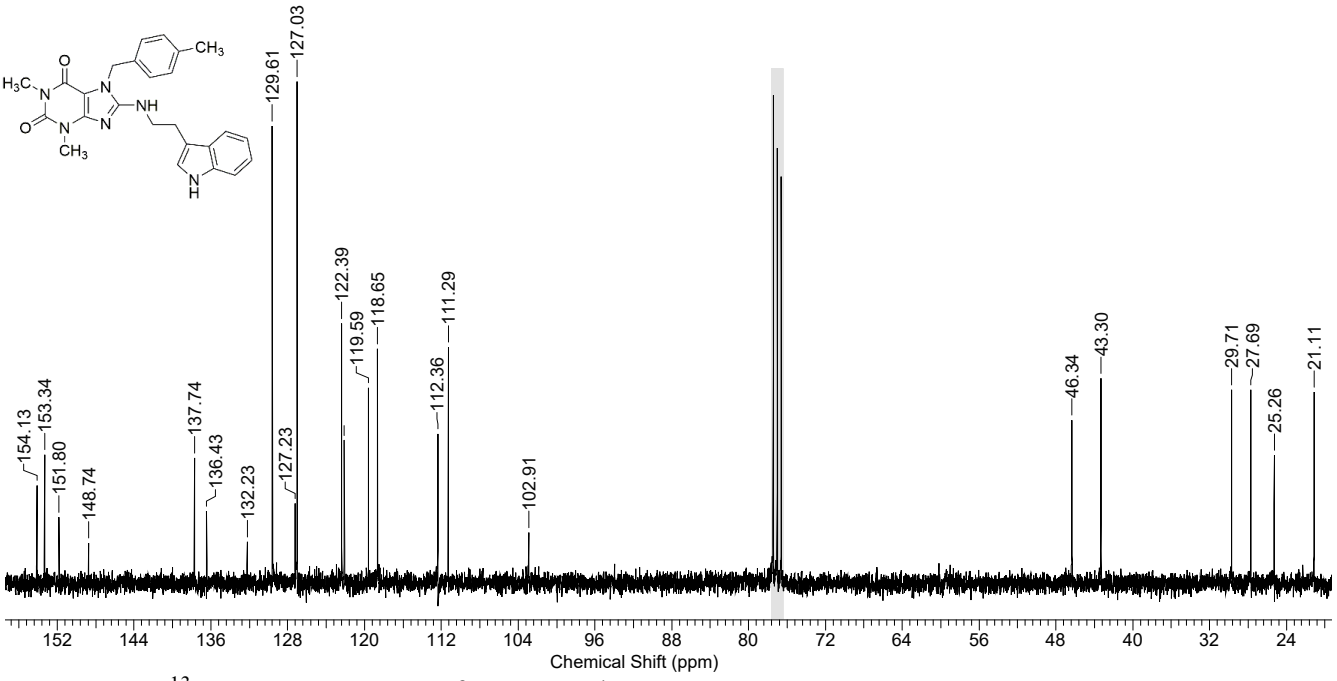

Figure S59. ^{13}C-NMR spectrum of compound **39**.

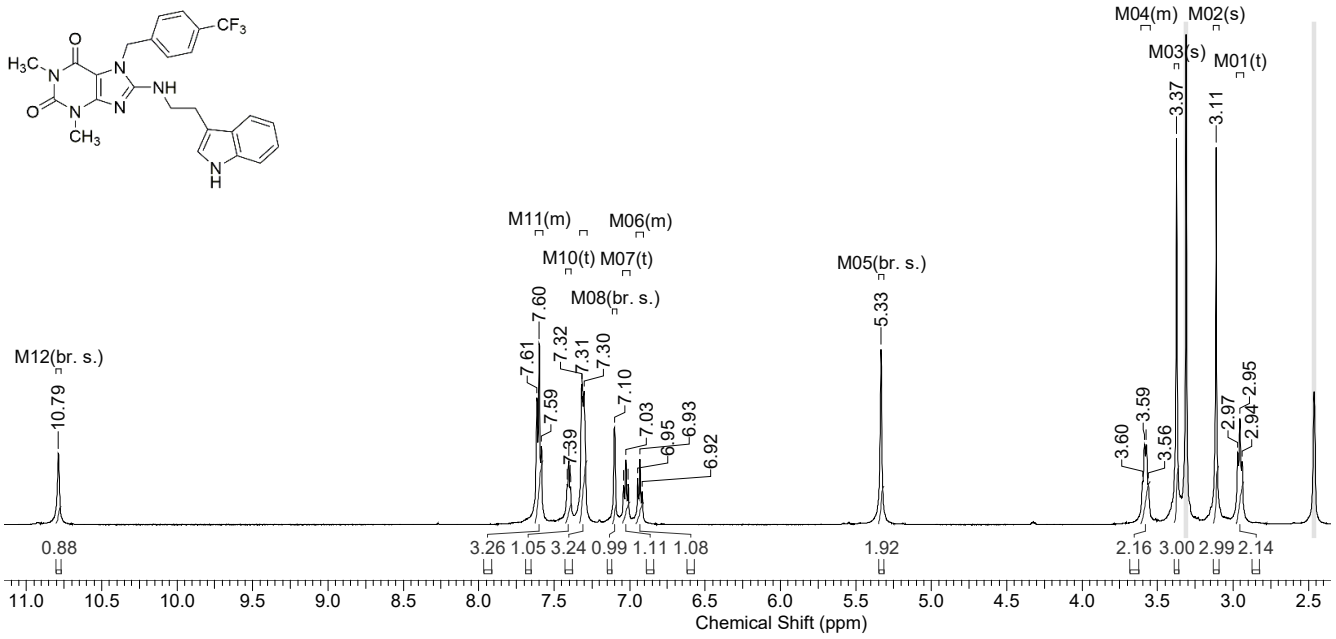

Figure S60. ^{1}H-NMR spectrum of compound **40**.

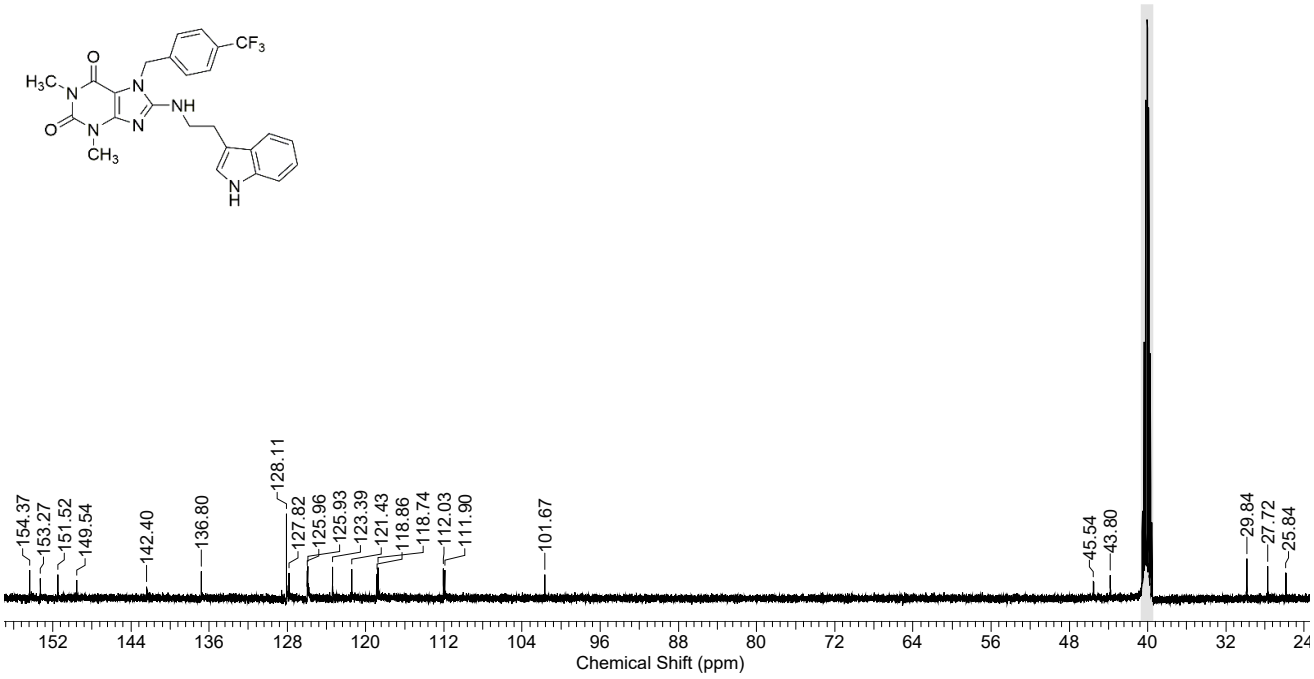

Figure S61. ^{13}C-NMR spectrum of compound **40**.

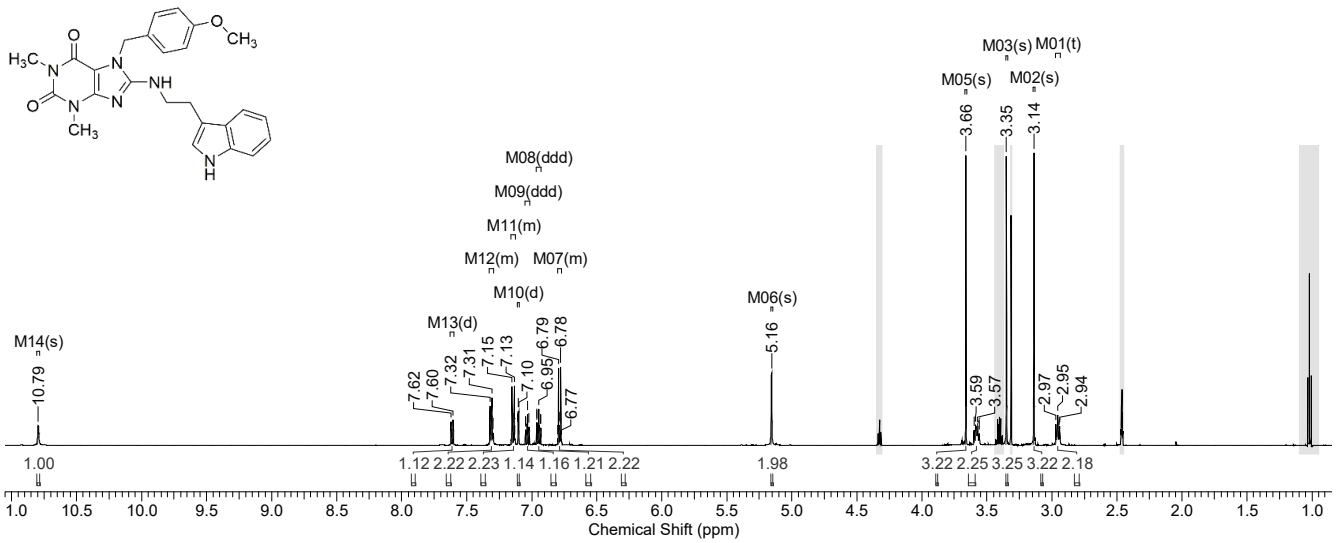

Figure S62. ^{1}H-NMR spectrum of compound **41**.

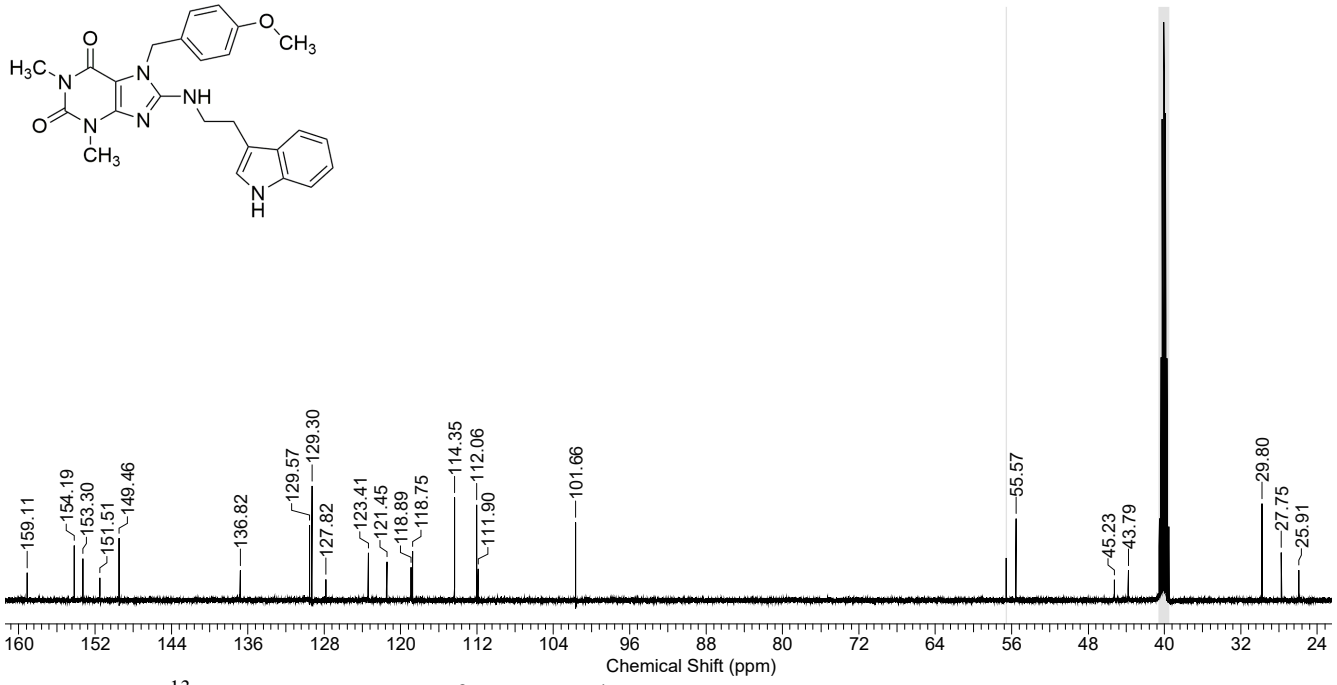

Figure S63. ^{13}C-NMR spectrum of compound **41**.

S64

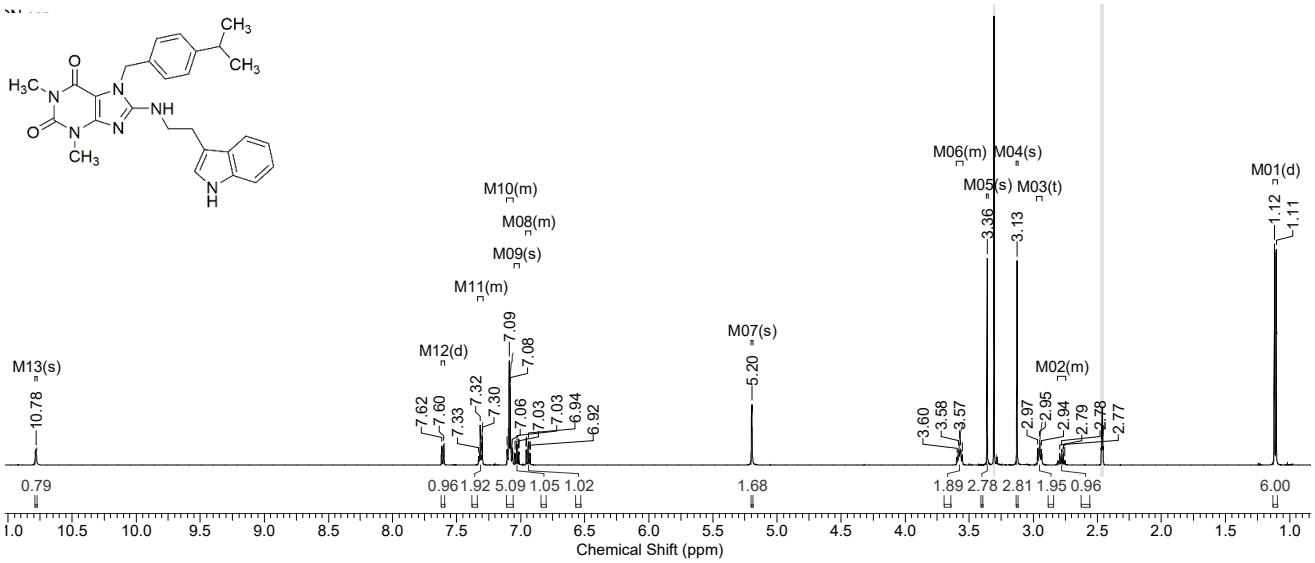

Figure S64. ^{1}H-NMR spectrum of compound **42**.

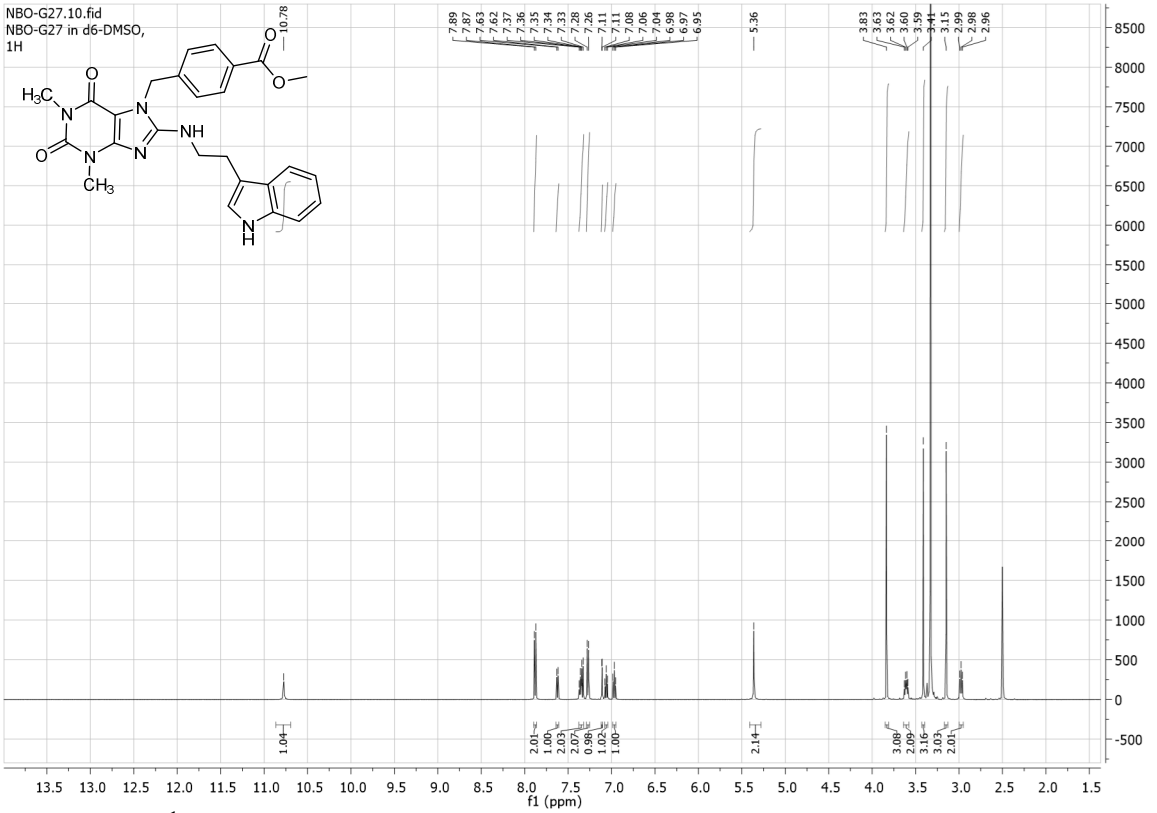

Figure S65. ^{1}H-NMR spectrum of compound **43**.

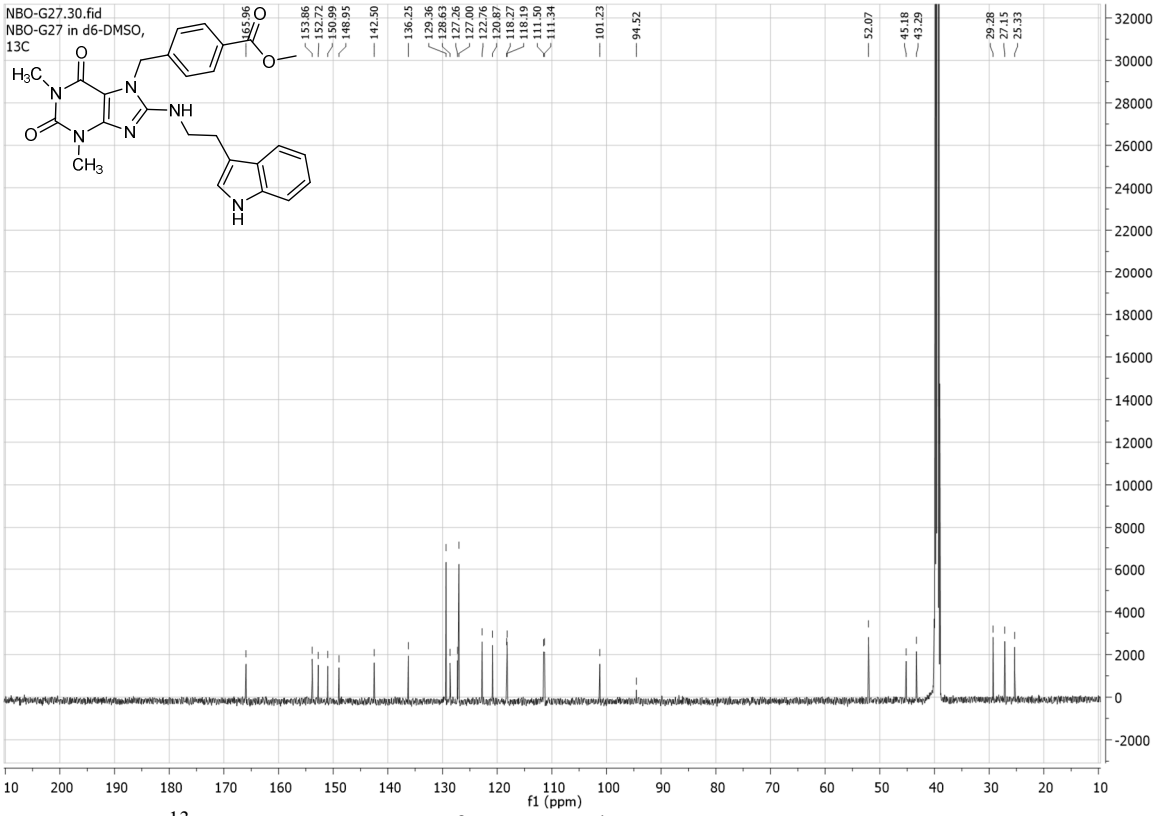

Figure S66. ^{13}C-NMR spectrum of compound **43**.

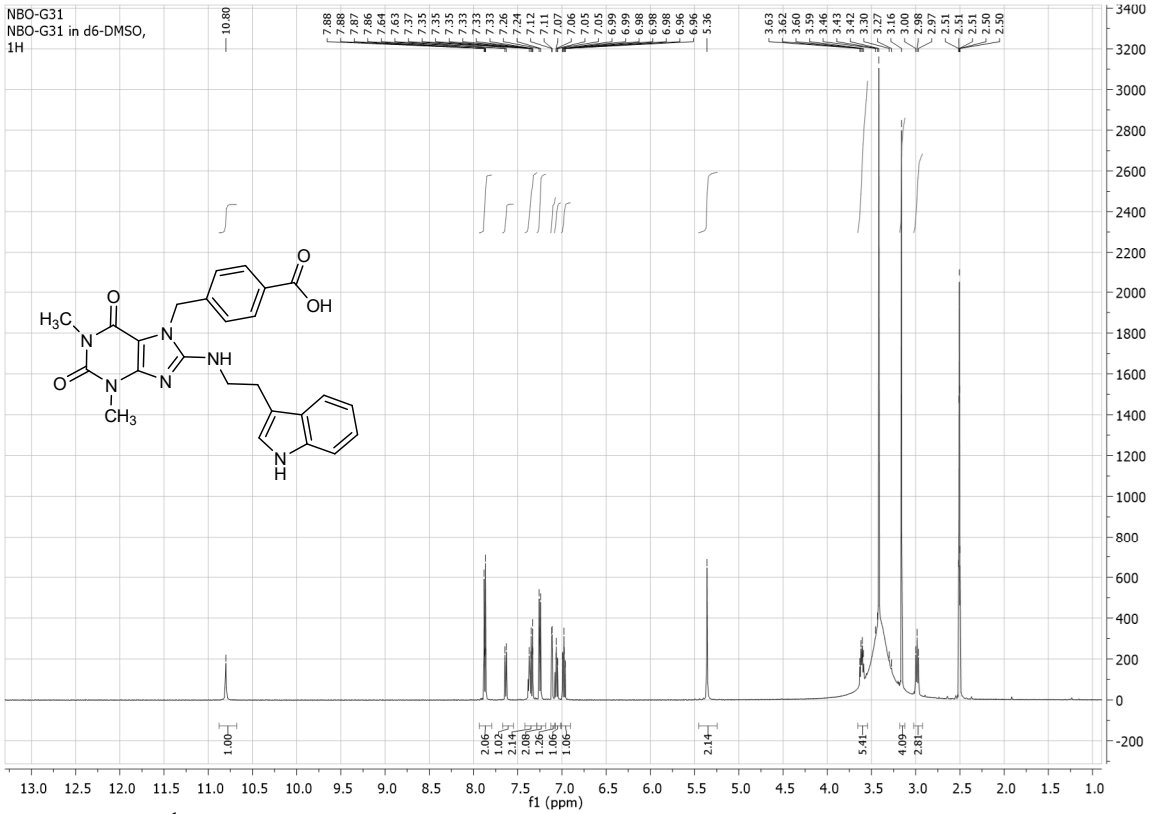

Figure S67. ^{1}H-NMR spectrum of compound **44**.

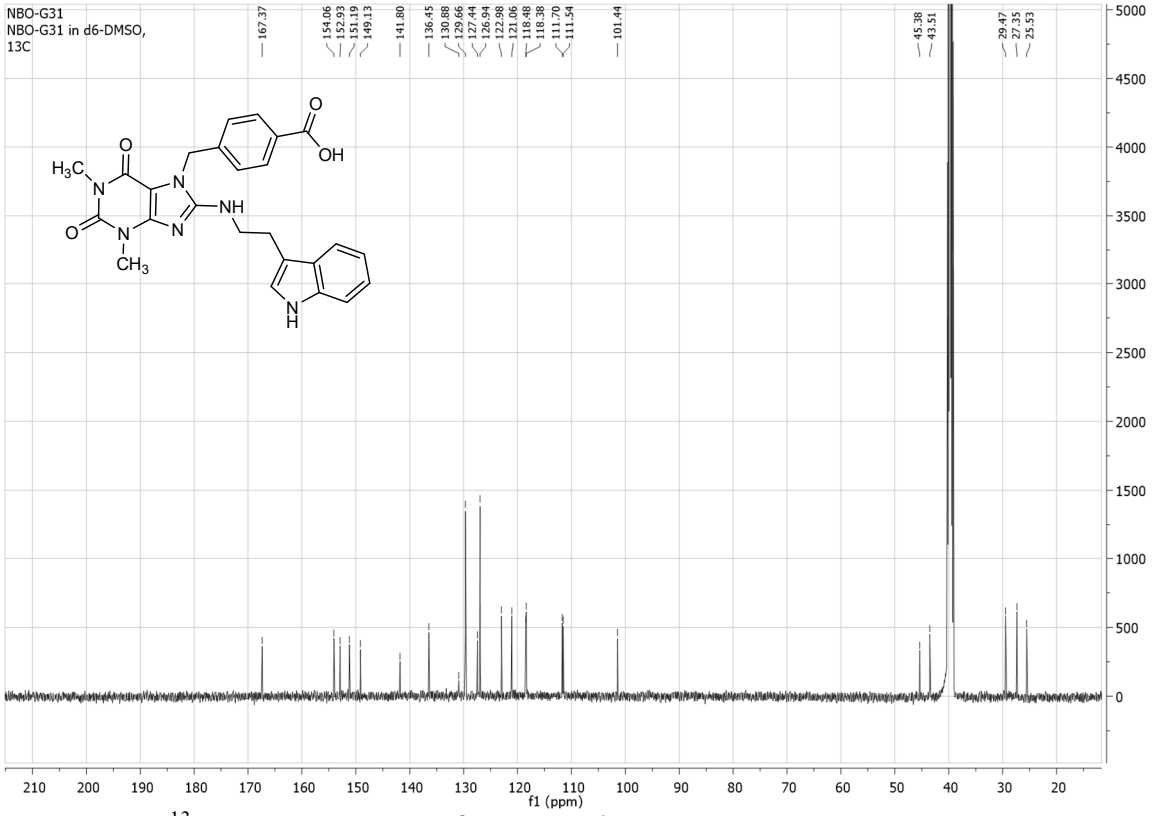

Figure S68. ^{13}C-NMR spectrum of compound **44**.

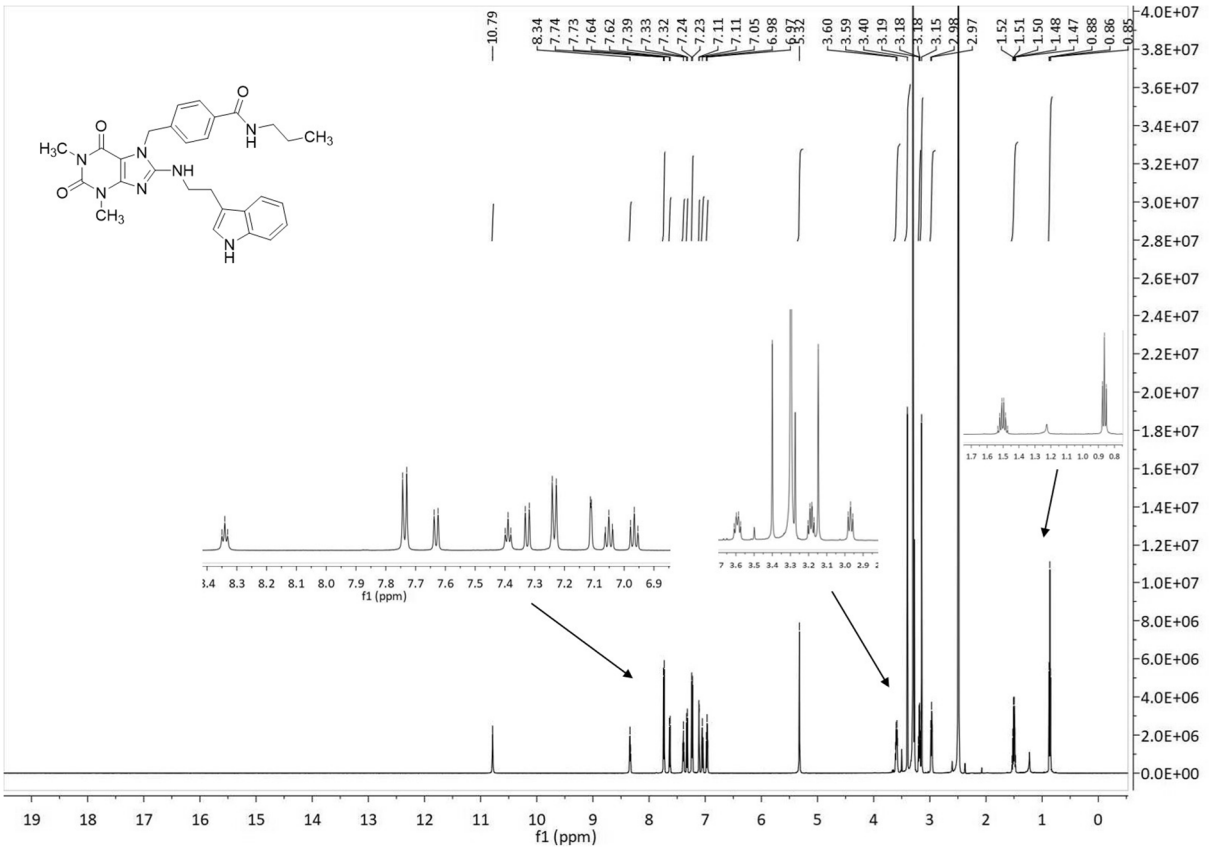

Figure S69. ^{1}H-NMR spectrum of compound **46**.

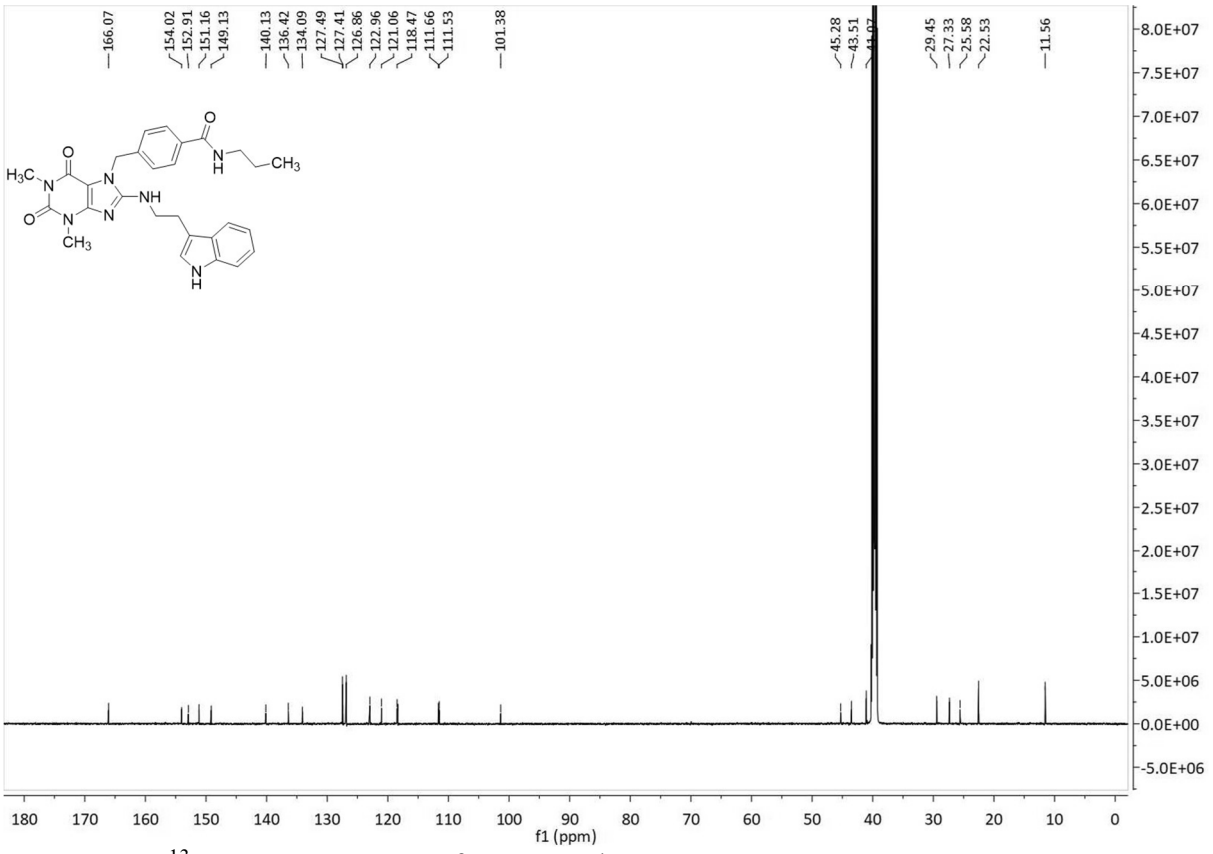

Figure S70. ^{13}C-NMR spectrum of compound **46**.

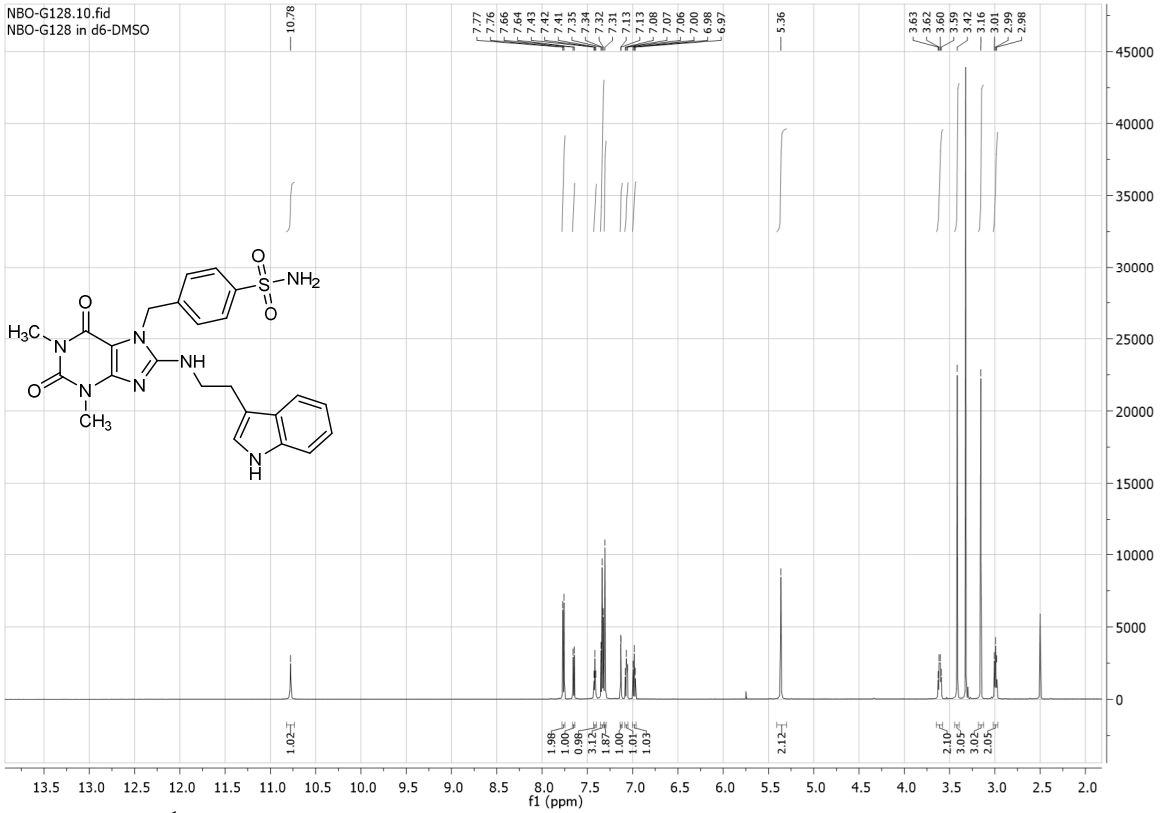

Figure S71. ^{1}H-NMR spectrum of compound **47**.

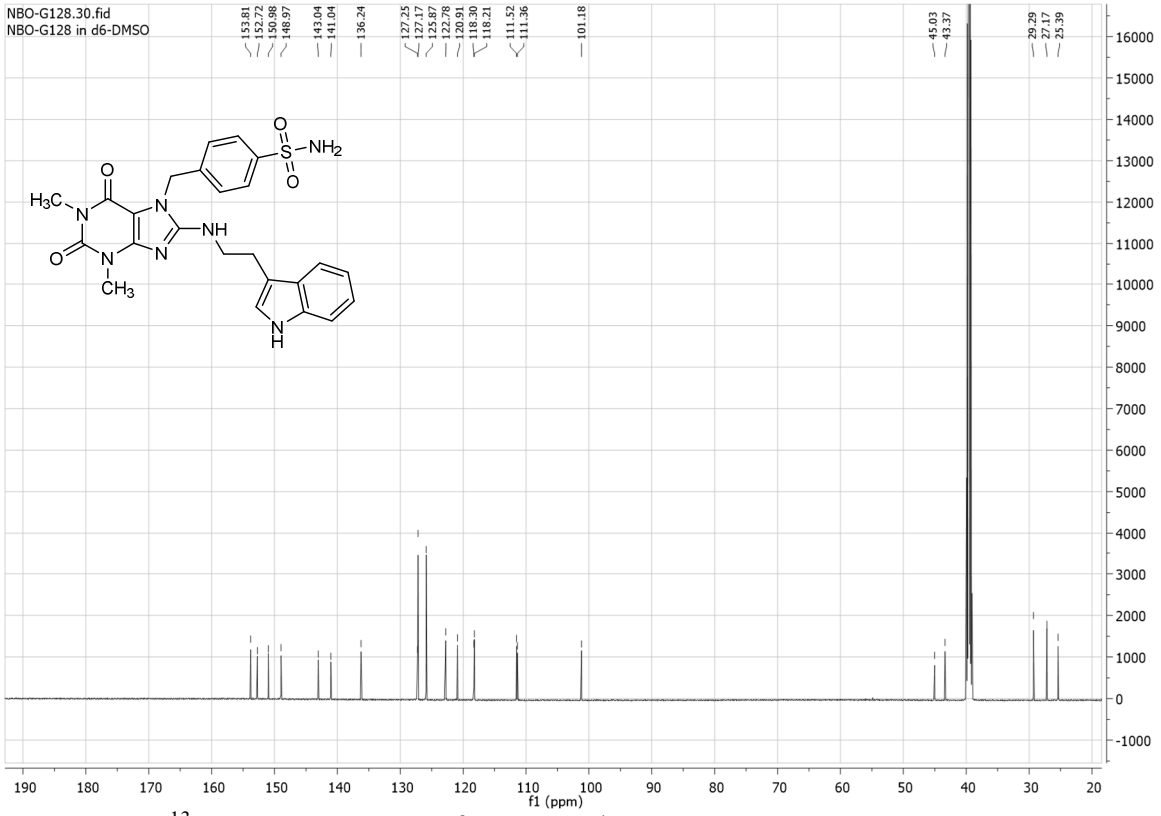

Figure S72. ^{13}C-NMR spectrum of compound **47**.

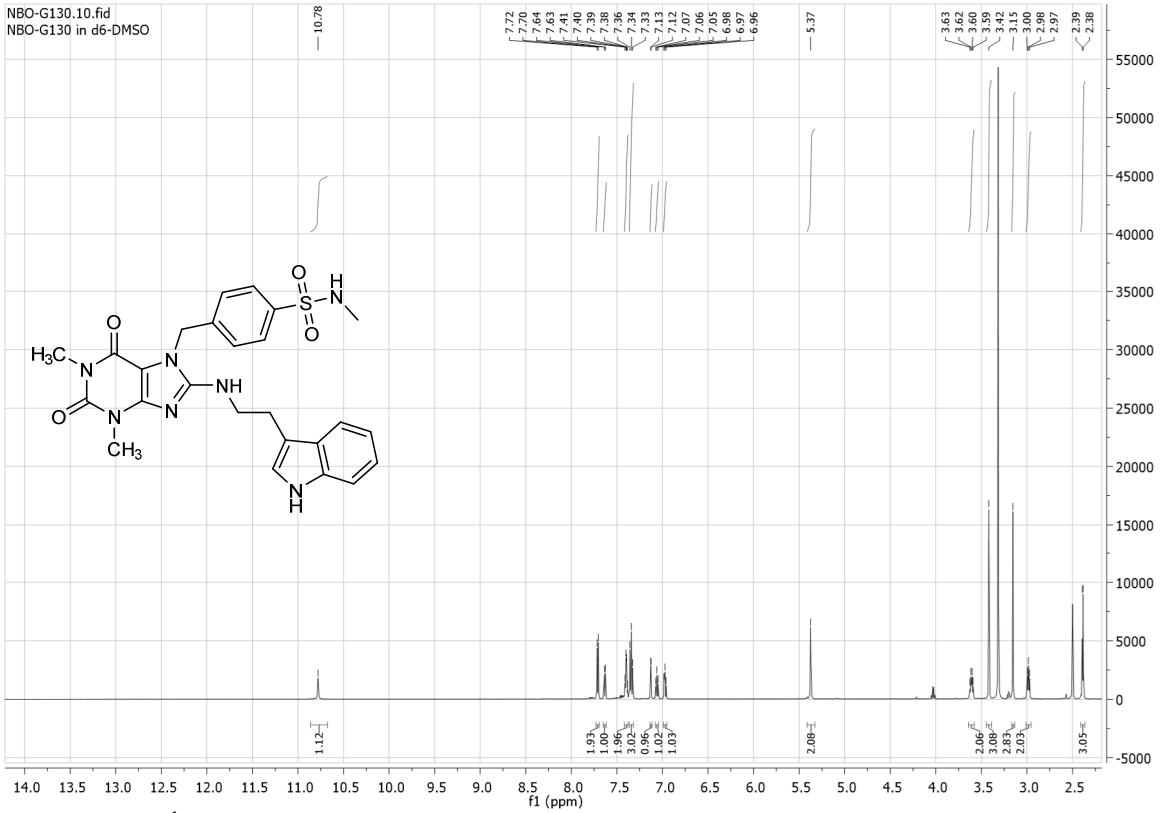

Figure S73. ^{1}H-NMR spectrum of compound **48**.

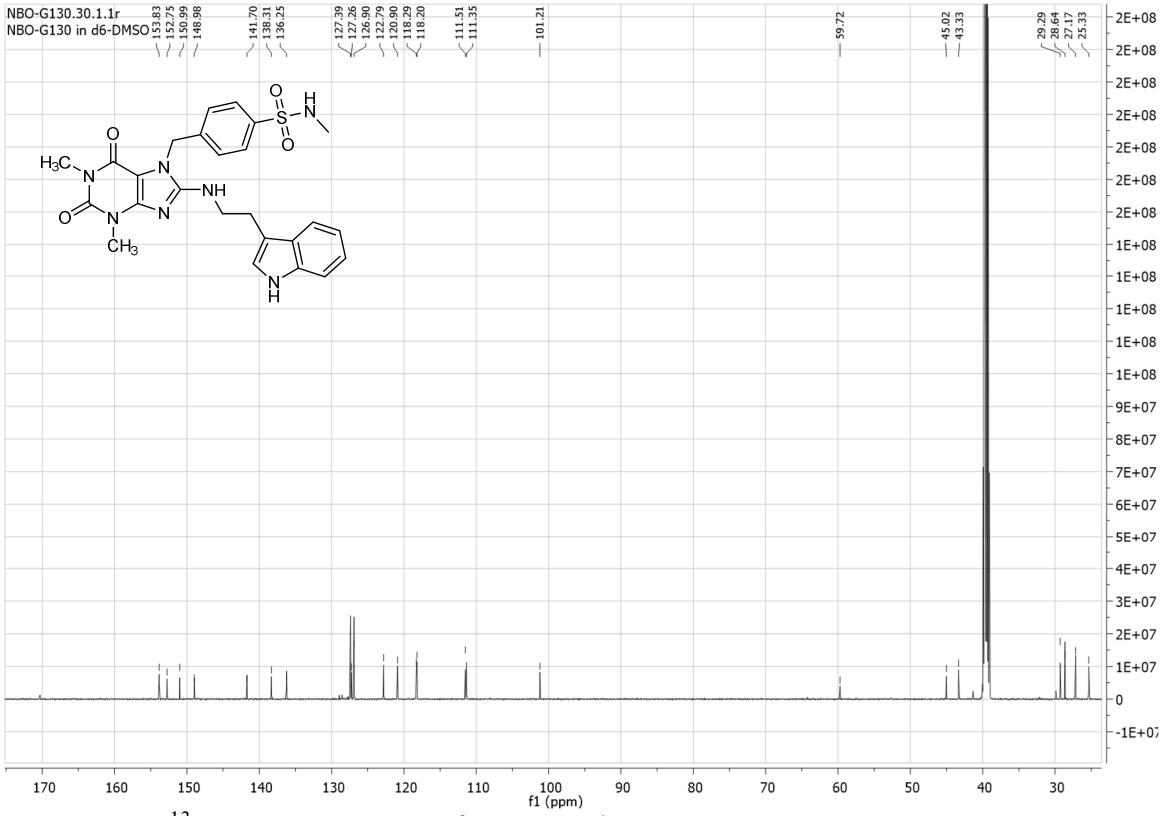

Figure S74. ^{13}C-NMR spectrum of compound **48**.

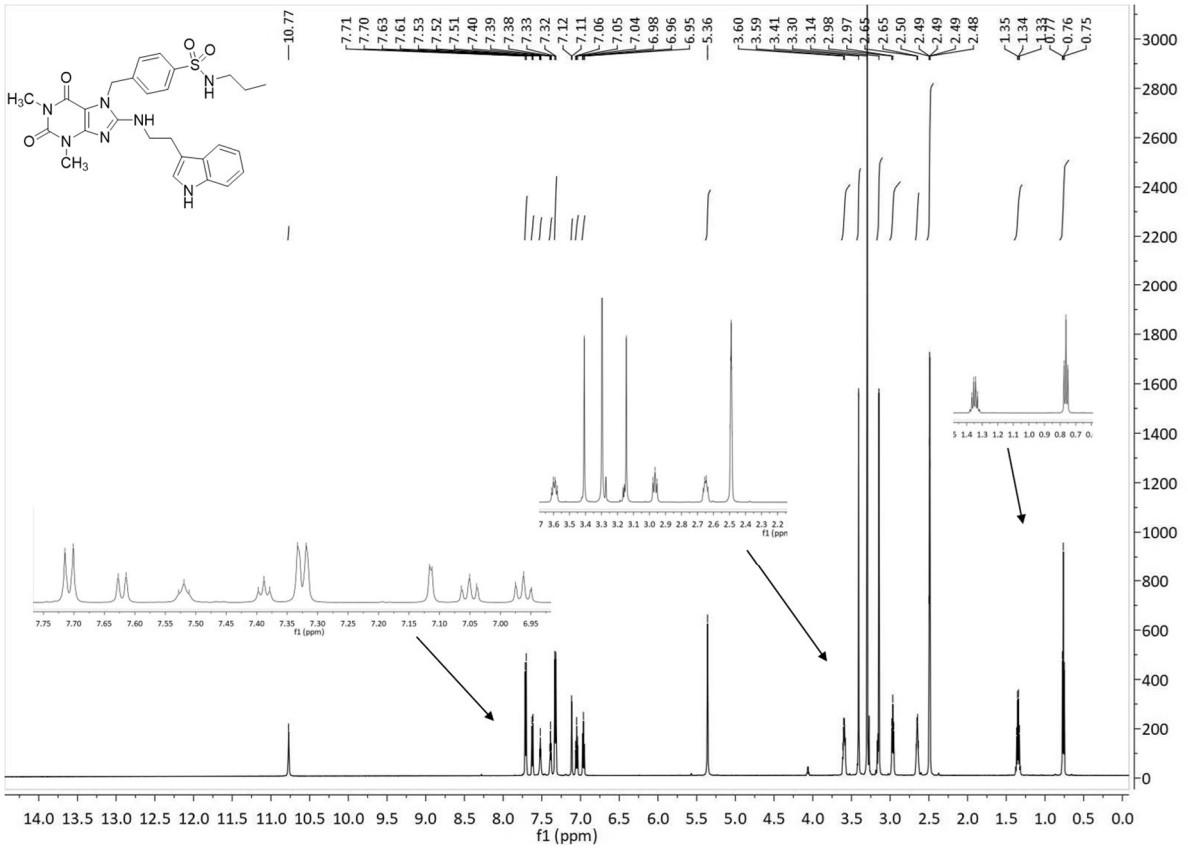

Figure S75. ^{1}H-NMR spectrum of compound **49**.

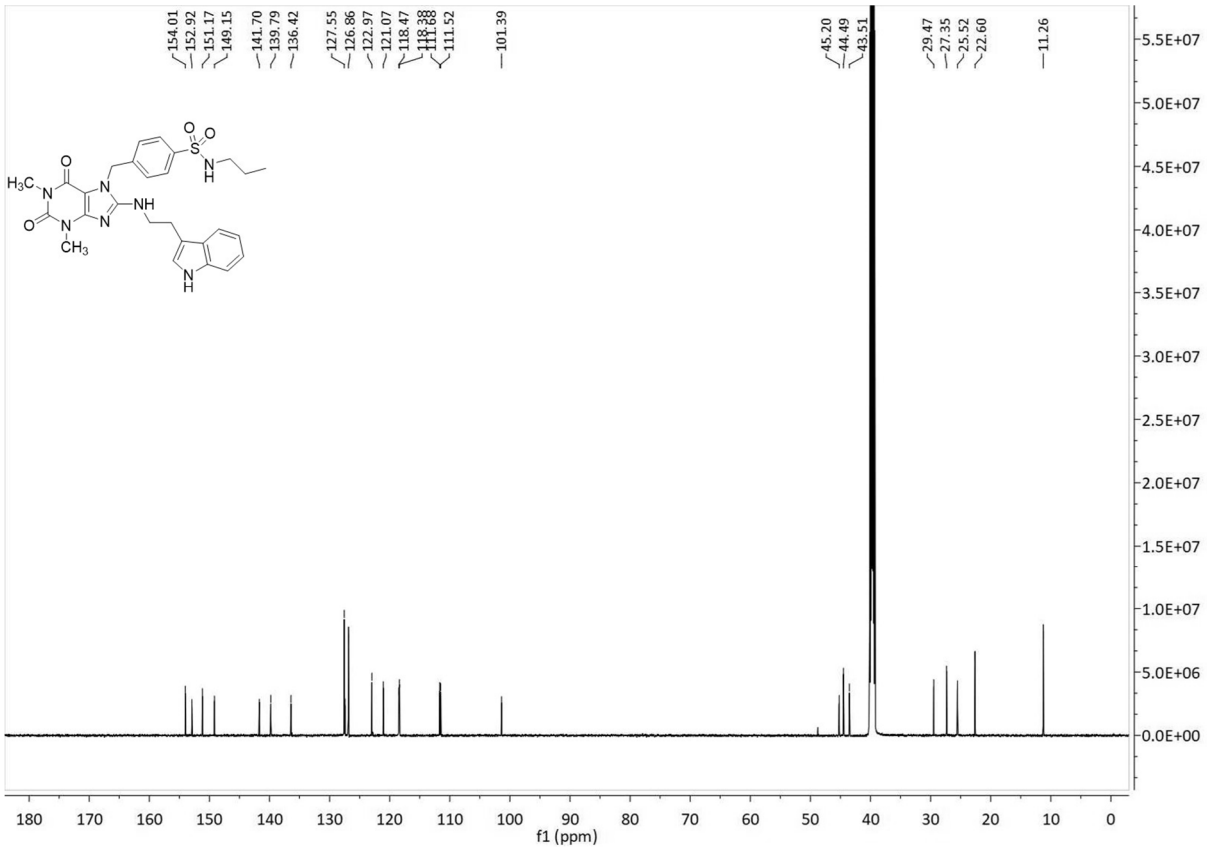

Figure S76. ^{13}C-NMR spectrum of compound **49**.

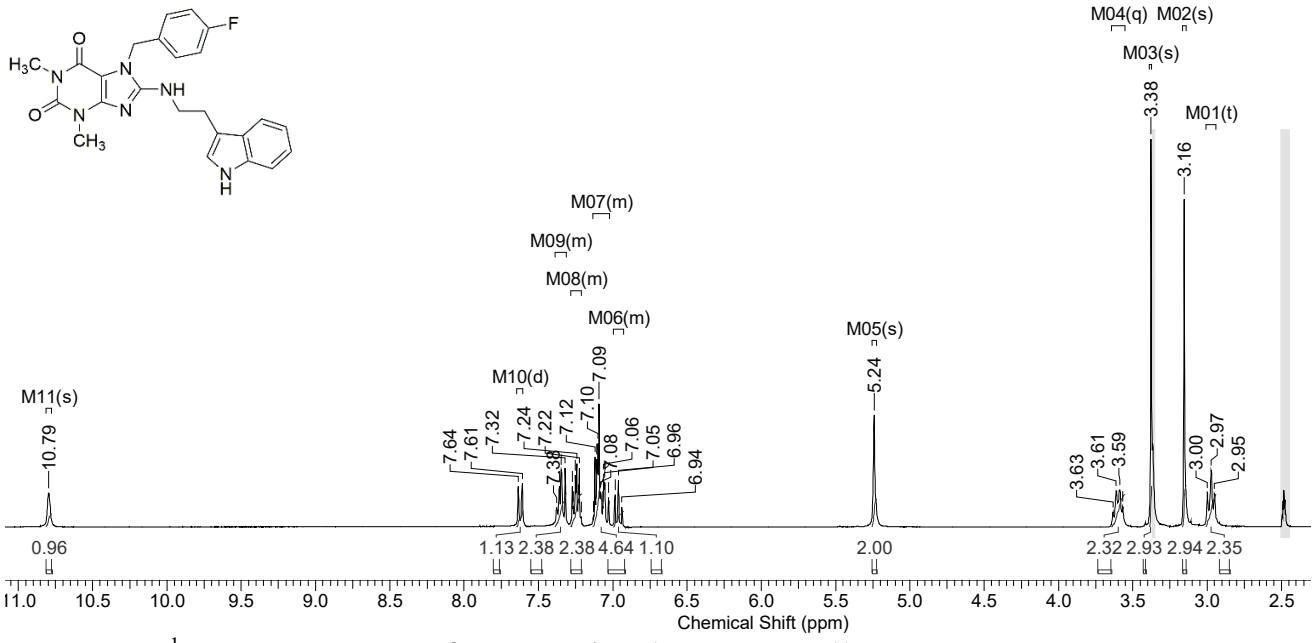

Figure S77. ^{1}H-NMR spectrum of compound **50** (PSB-KK1445))

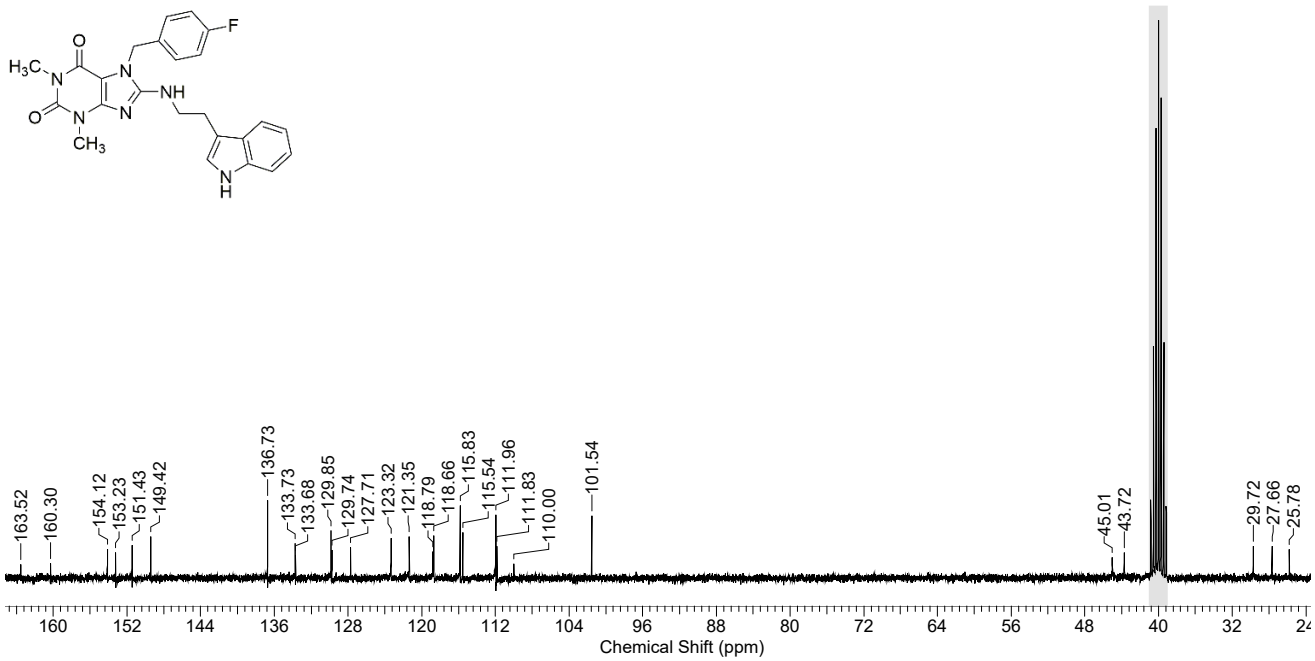

Figure S78. ^{13}C-NMR spectrum of compound **50** (PSB-KK1445)

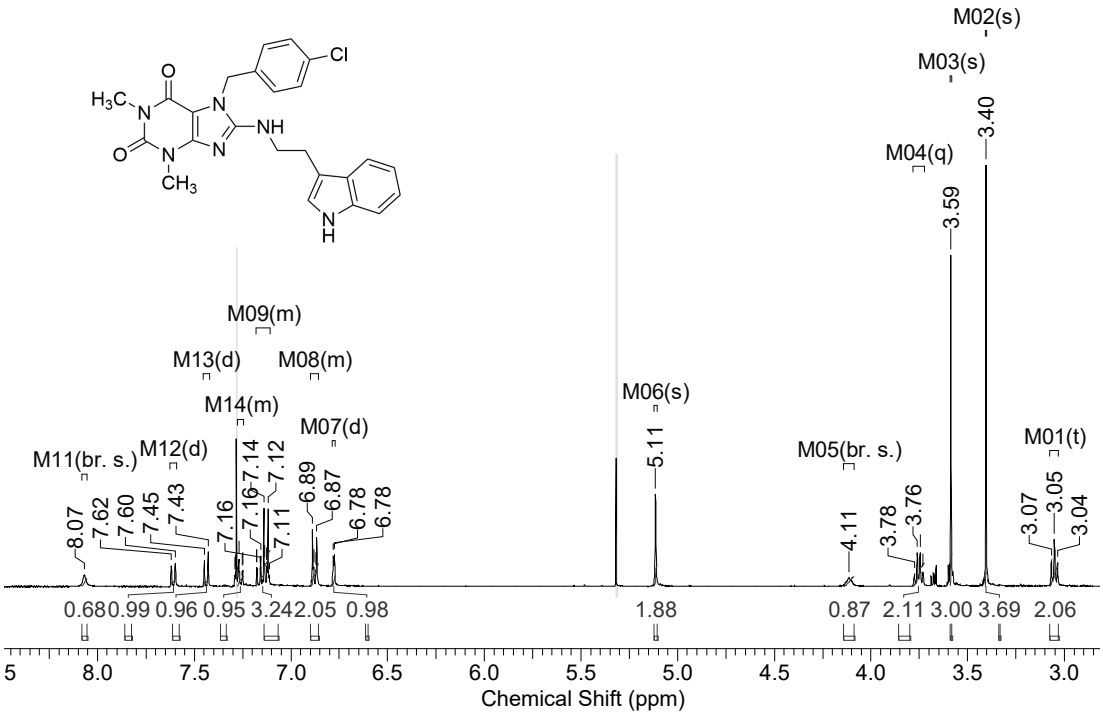

Figure S79. ^{1}H-NMR spectrum of compound **51** (PSB-KK1415).

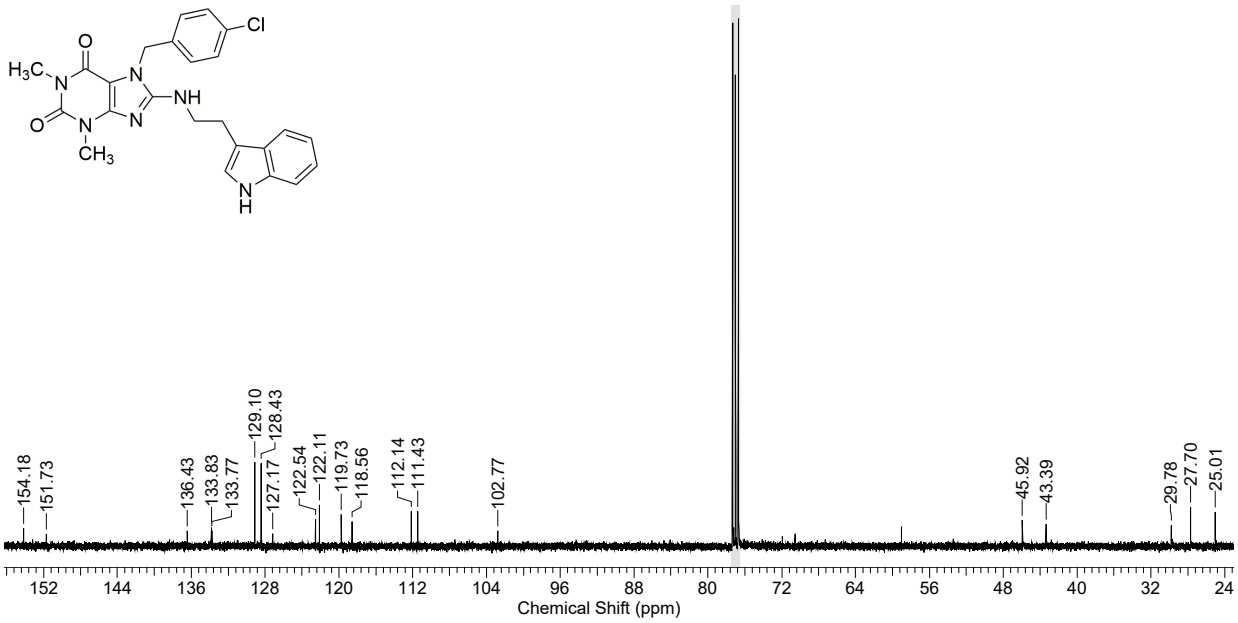

Figure S80. ^{13}C-NMR spectrum of compound **51** (PSB-KK1415).

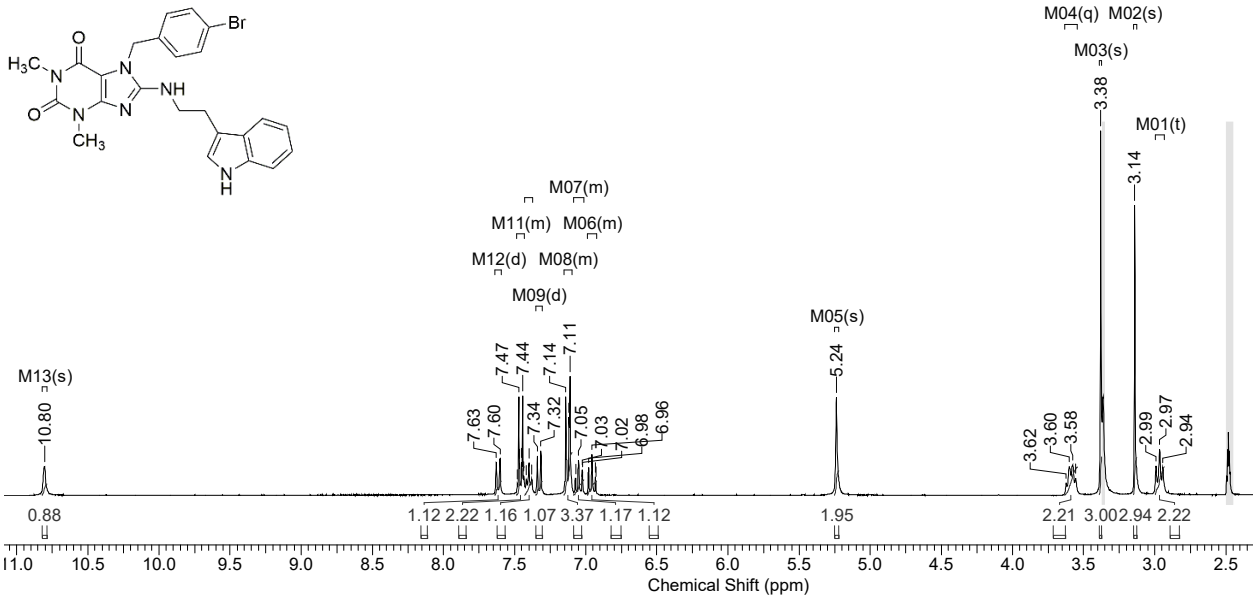

Figure S81. ^{1}H-NMR spectrum of compound **52**.

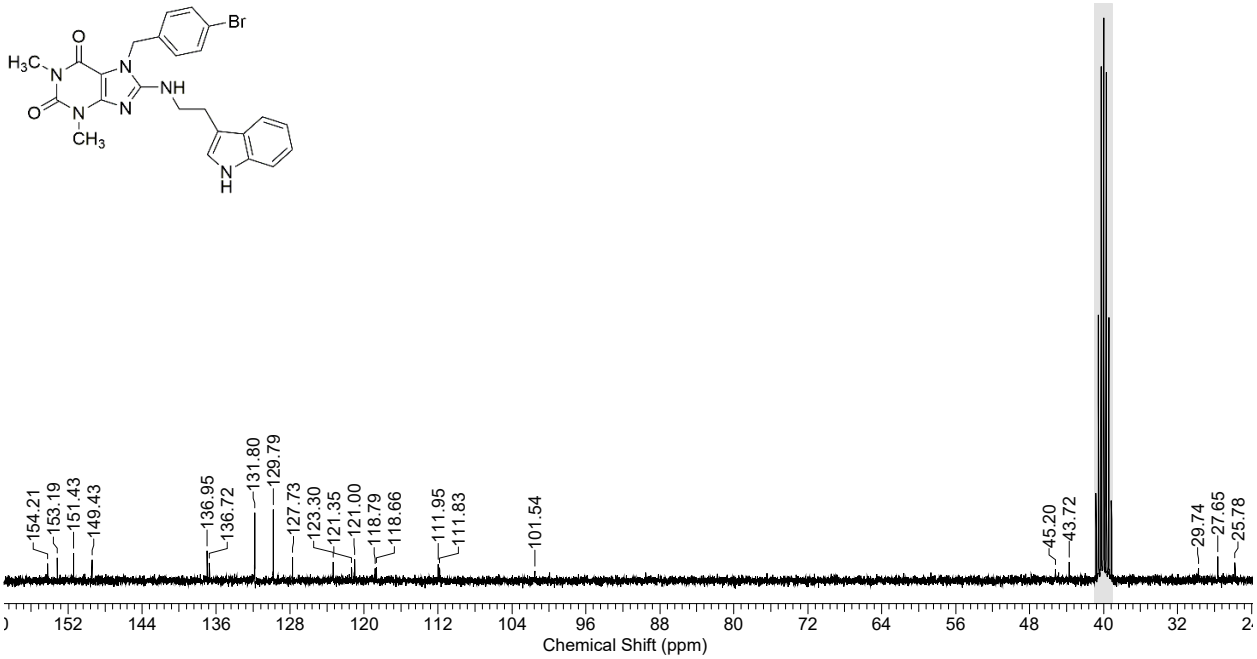

Figure S82. ^{13}C-NMR spectrum of compound **52**.

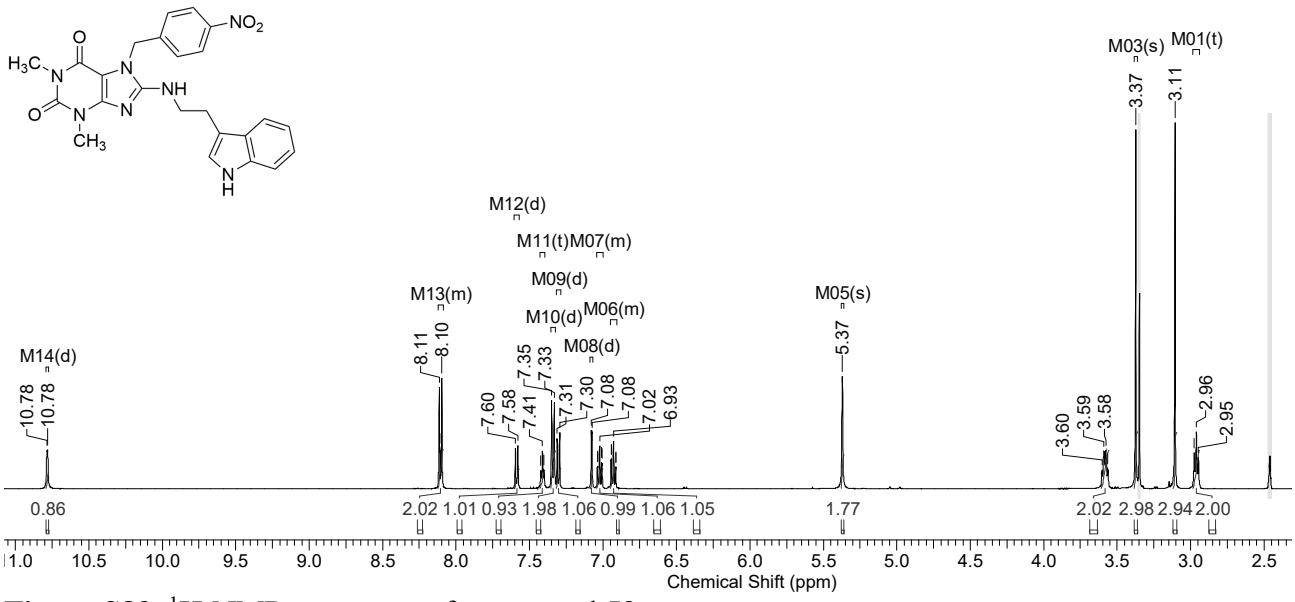

Figure S83. ^{1}H-NMR spectrum of compound **53**.

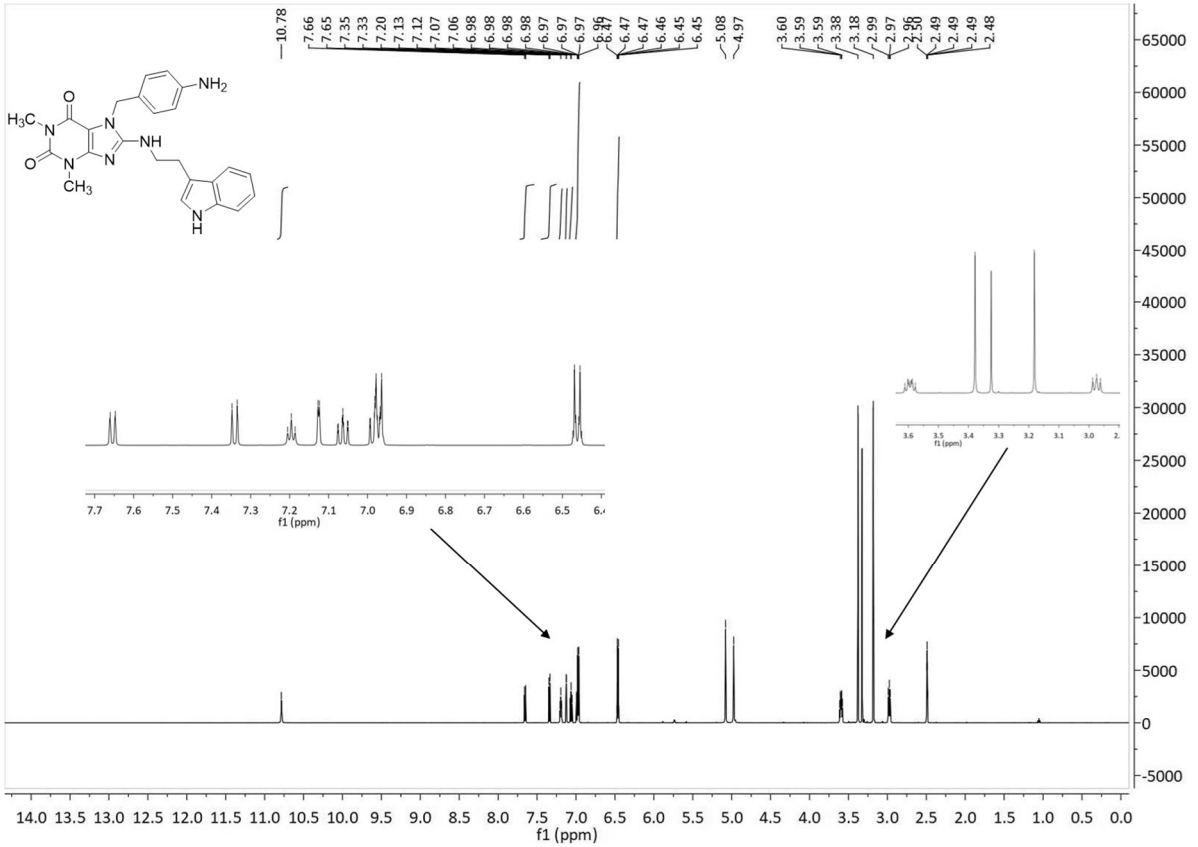

Figure S84. ^{1}H-NMR spectrum of compound **54**.

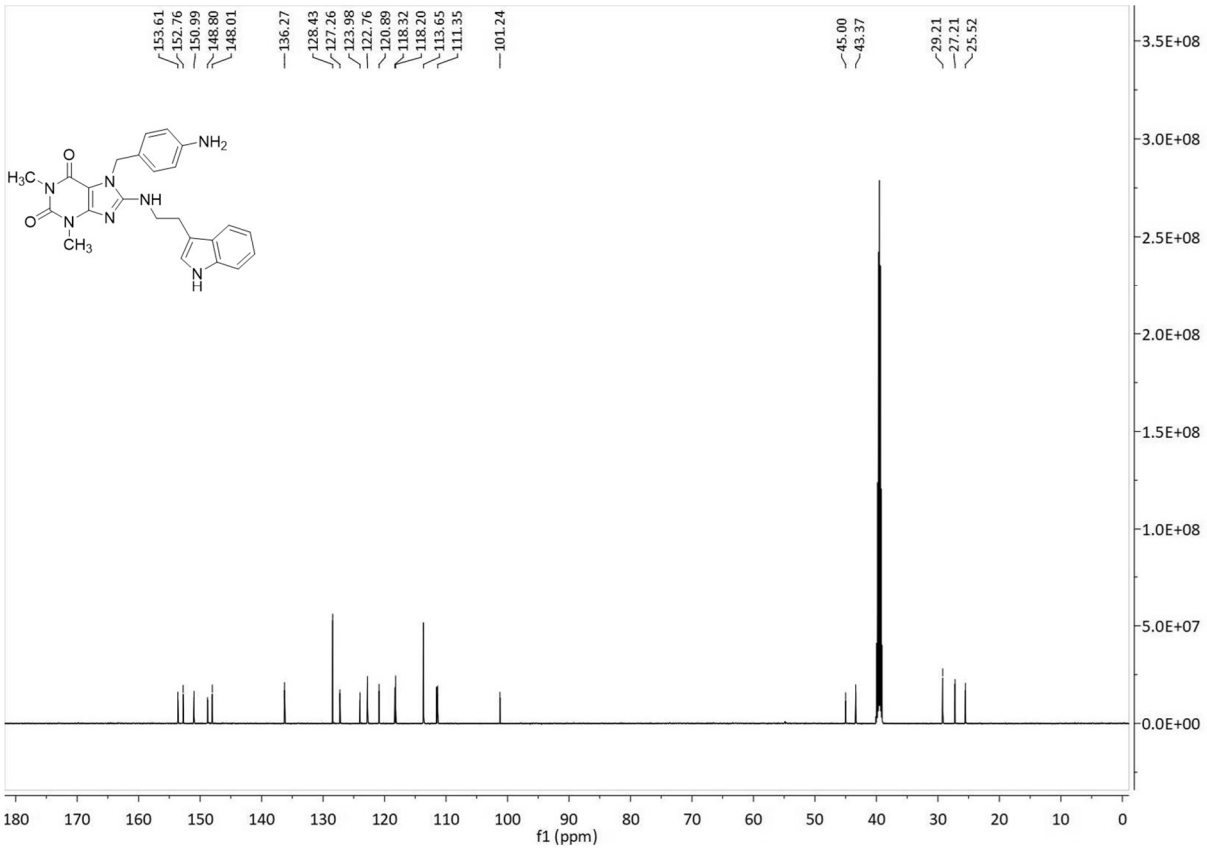

Figure S85. ^{13}C-NMR spectrum of compound **54**.

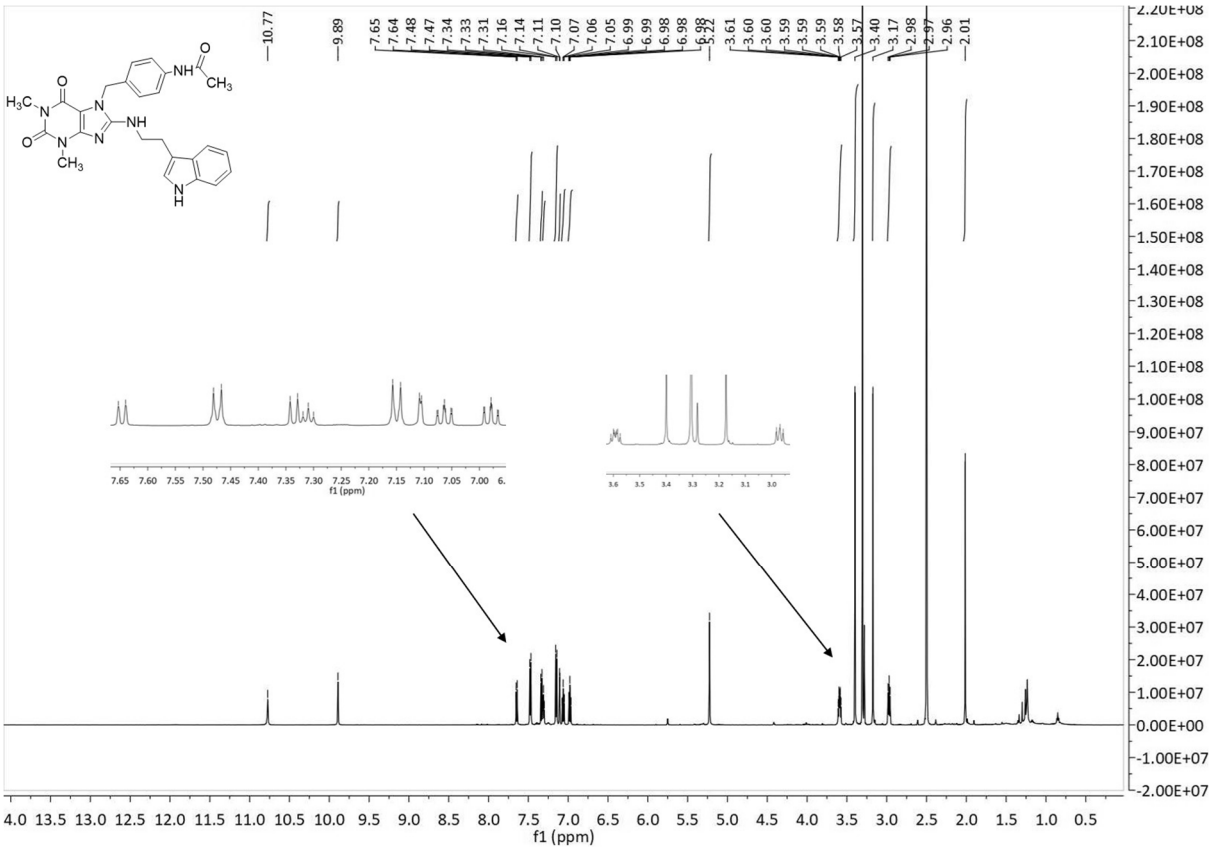

Figure S86. ^{1}H-NMR spectrum of compound **55**.

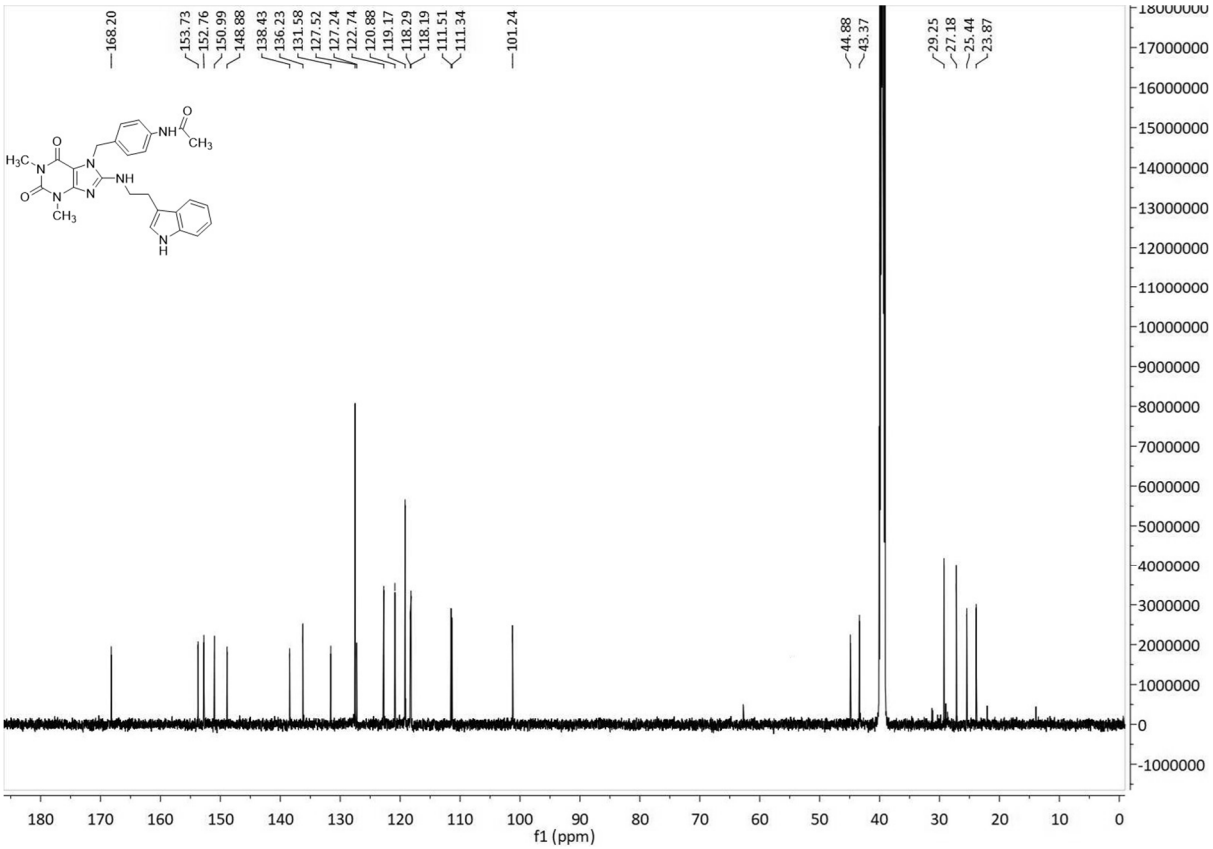

Figure S87. ^{13}C-NMR spectrum of compound **55**.

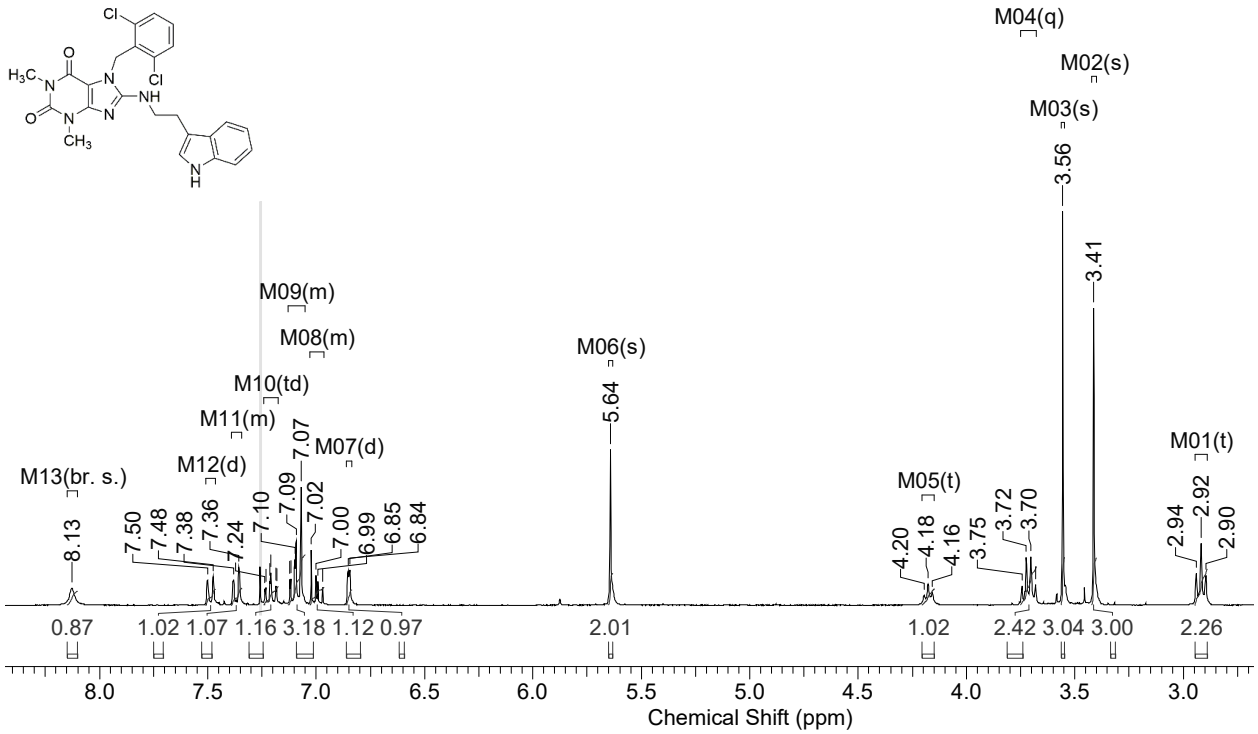

Figure S88. NMR spectrum of compound **56**.

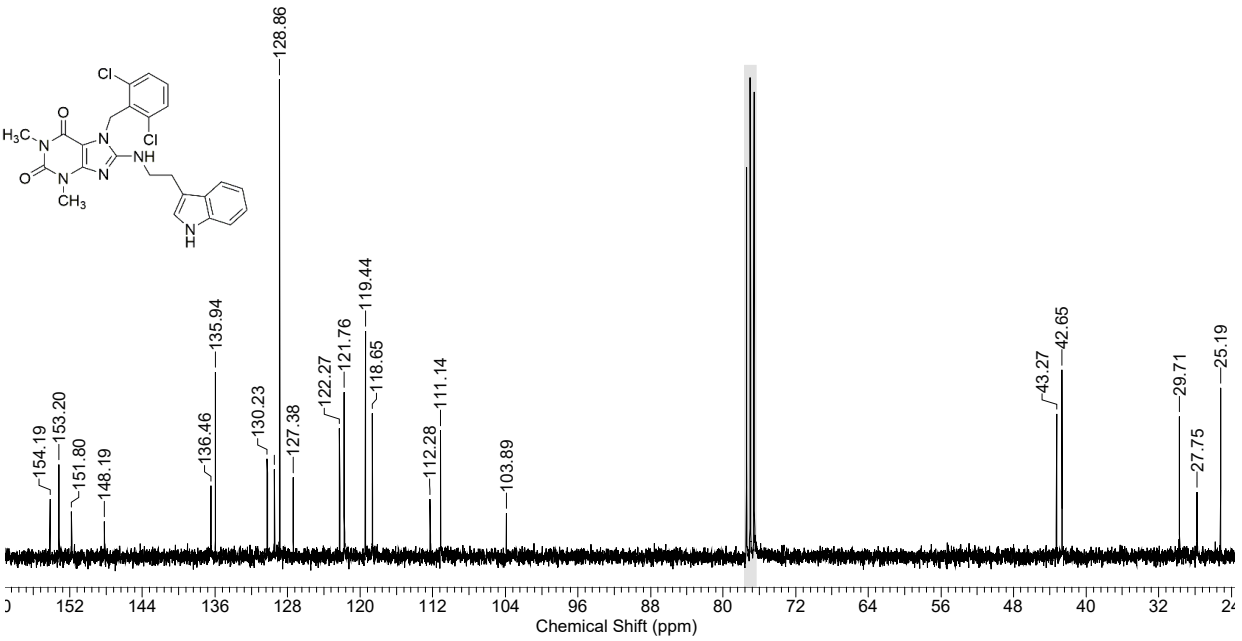

Figure S89. ^{13}C-NMR spectrum of compound **56**.

S78

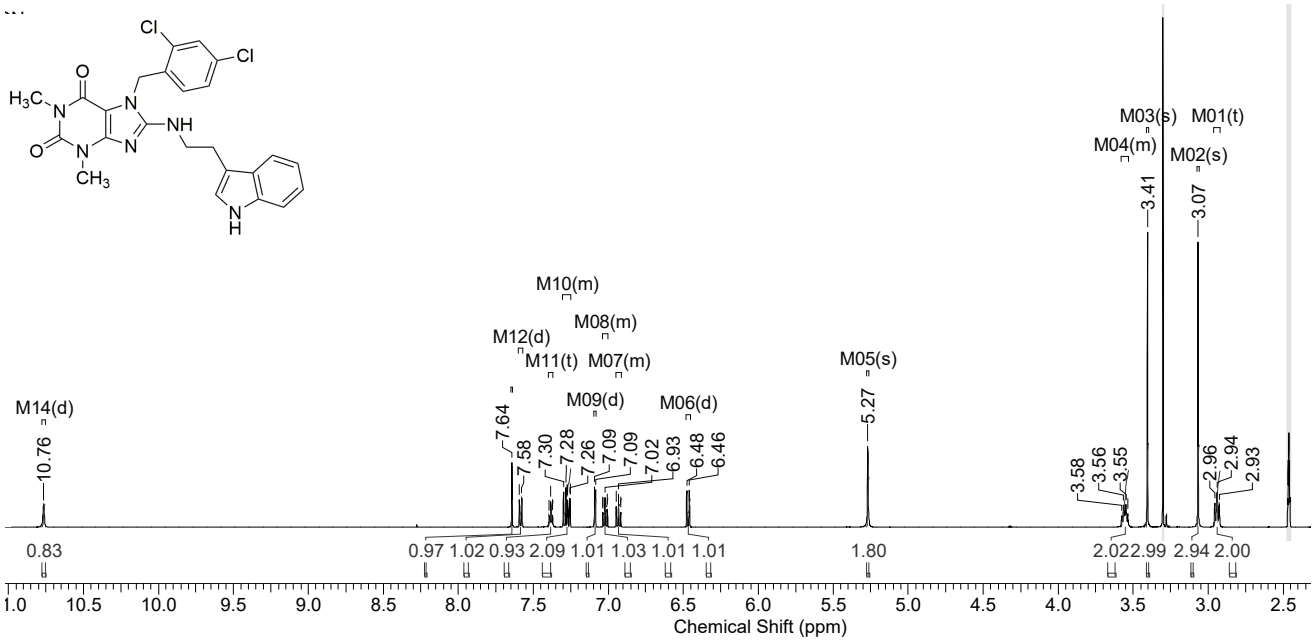

Figure S90. ^{1}H-NMR spectrum of compound **57**.

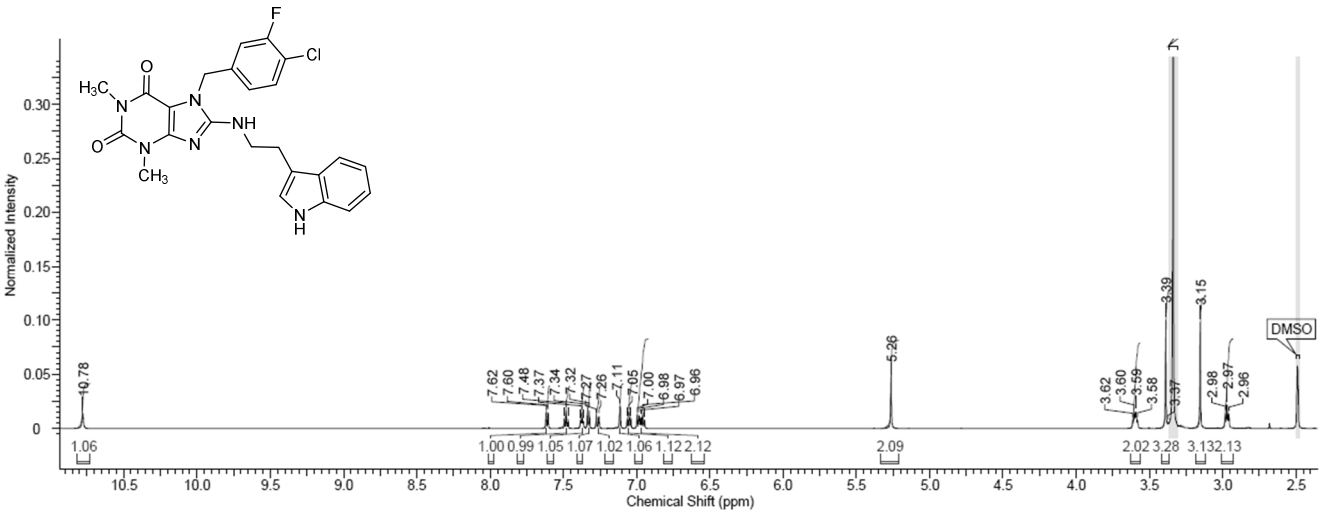

Figure S91. ^{1}H-NMR spectrum of compound **58**.

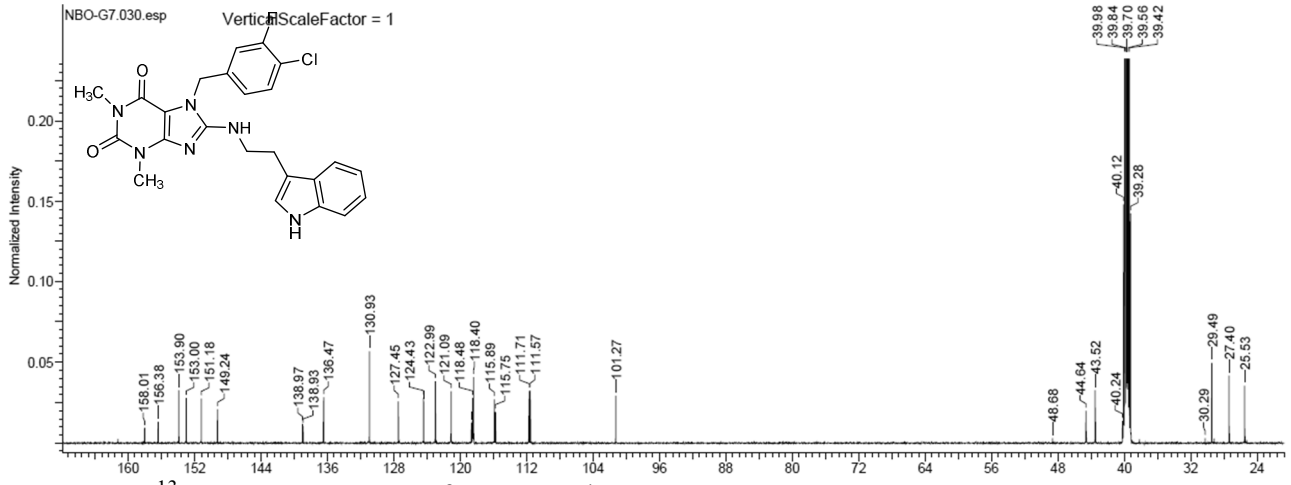

Figure S92. ^{13}C-NMR spectrum of compound **58**.

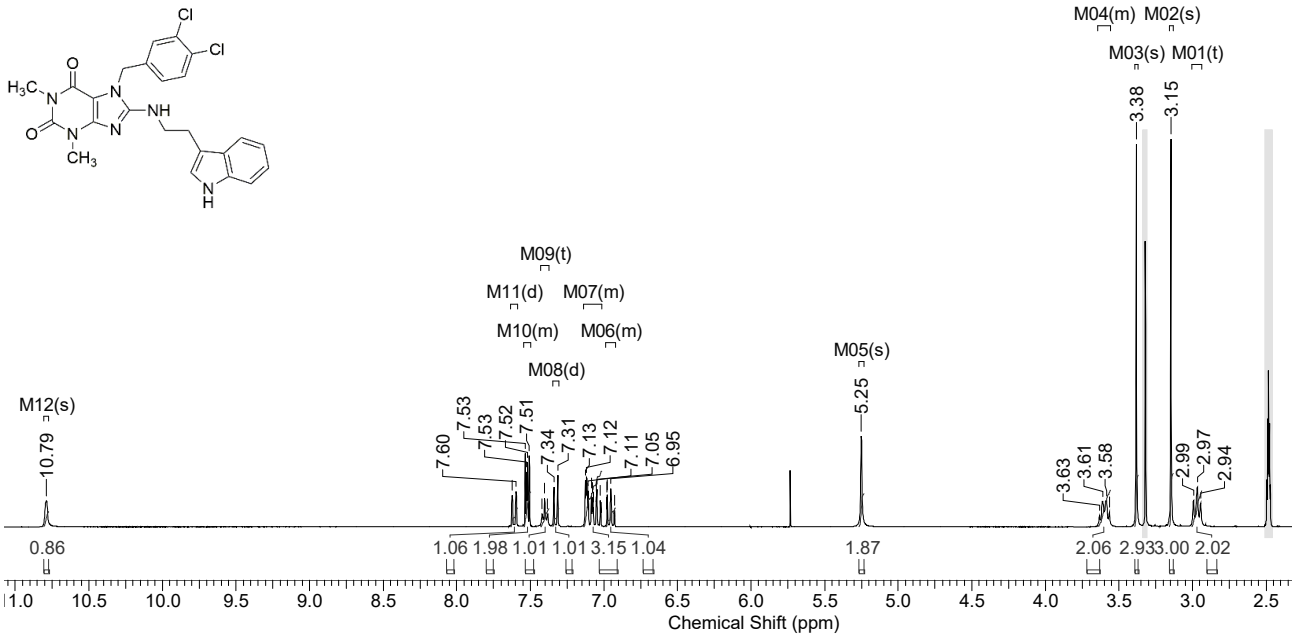

Figure S93. ^{1}H-NMR spectrum of compound **59**.

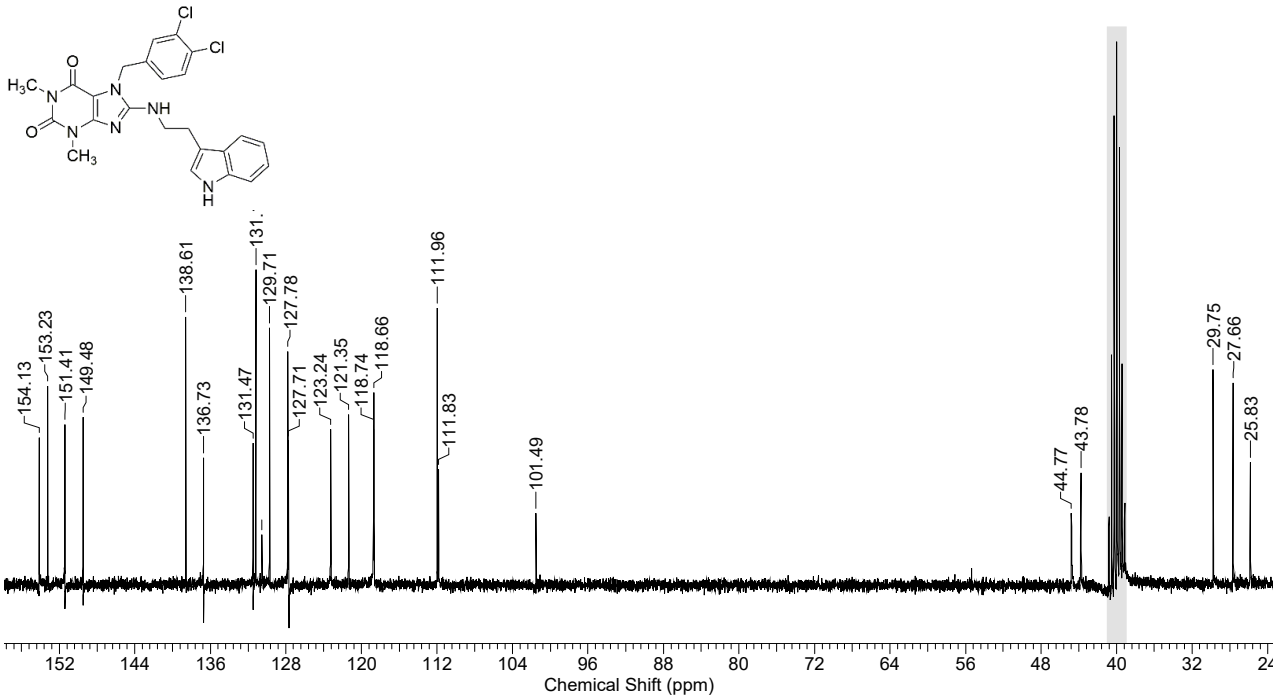

Figure S94. ^{13}C-NMR spectrum of compound **59**.

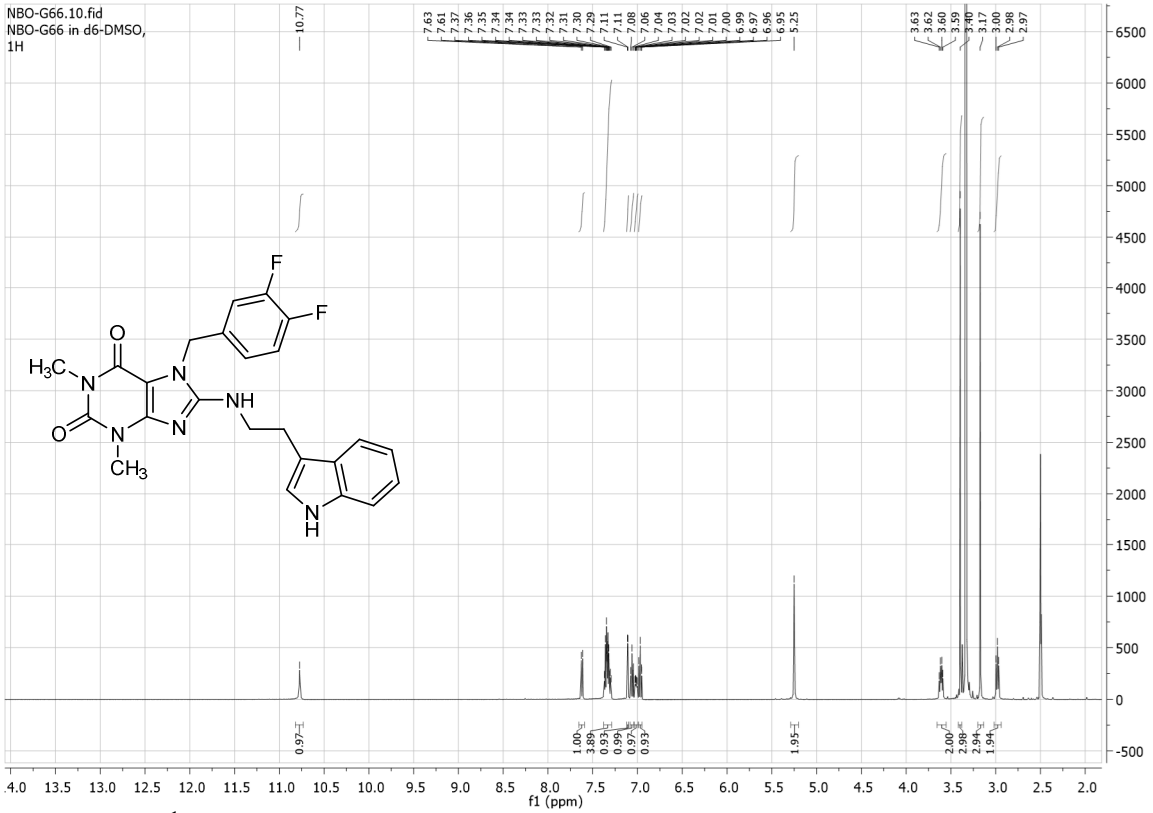

Figure S95. ^{1}H-NMR spectrum of compound **60**.

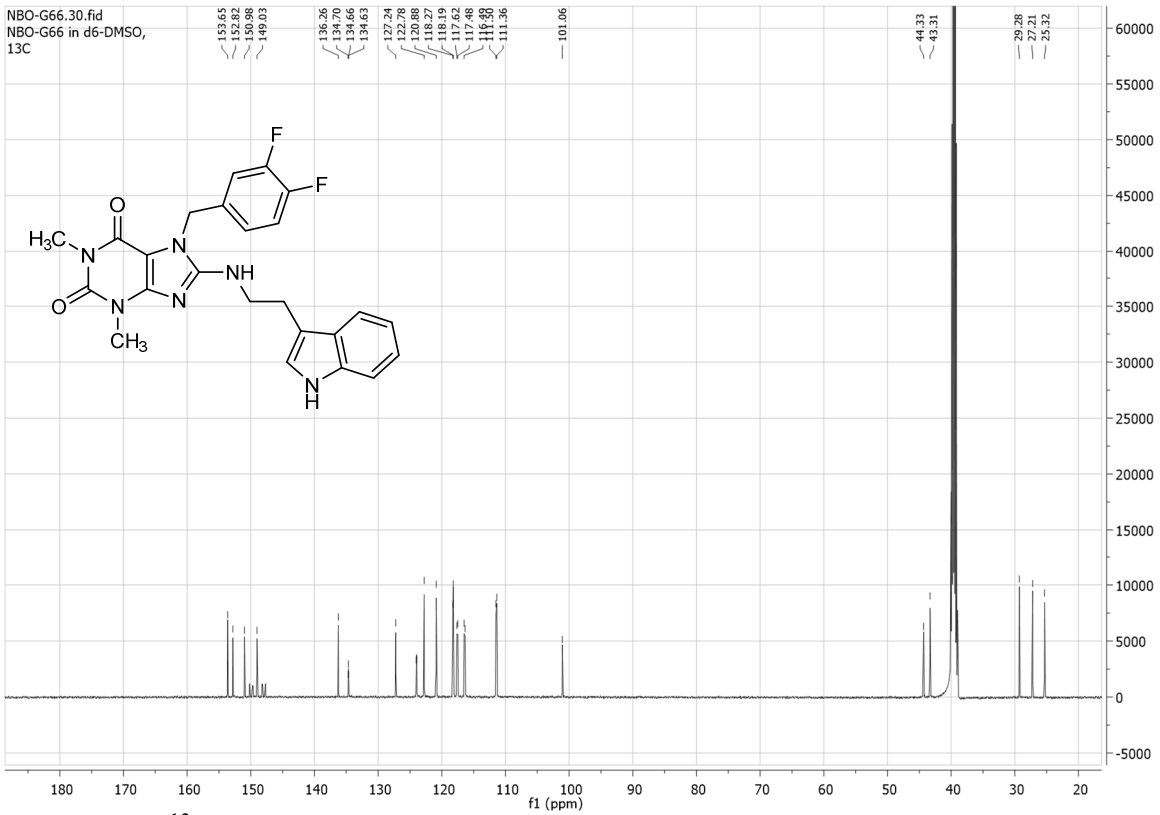

Figure S96. ^{13}C-NMR spectrum of compound **60**.

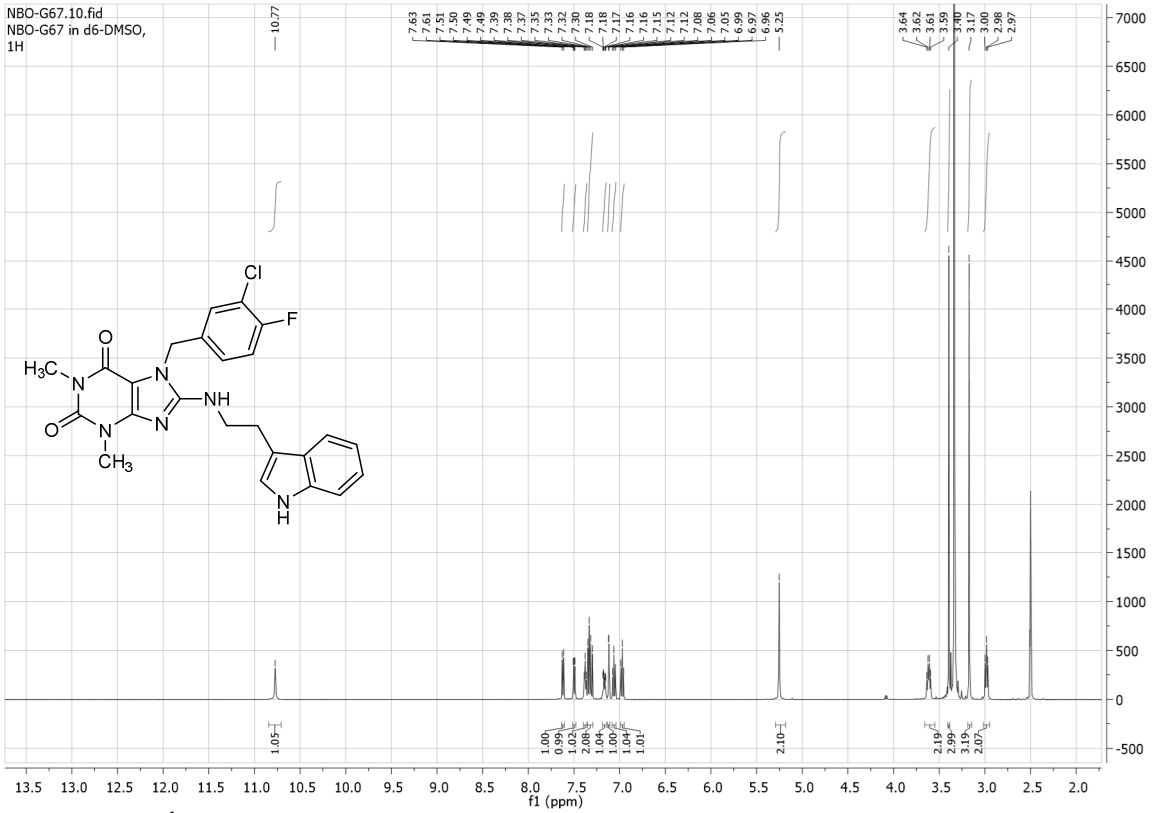

Figure S97. ^{1}H-NMR spectrum of compound **61**

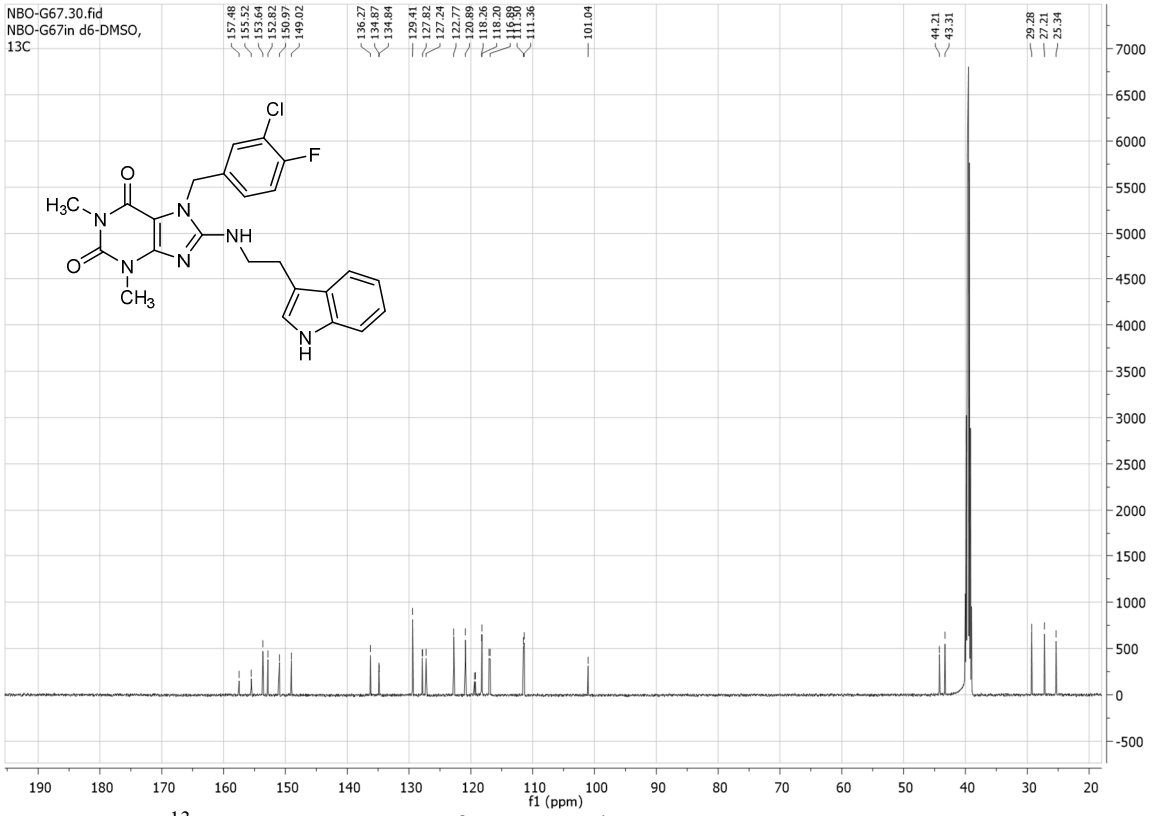

Figure S98. ^{13}C-NMR spectrum of compound **61**.

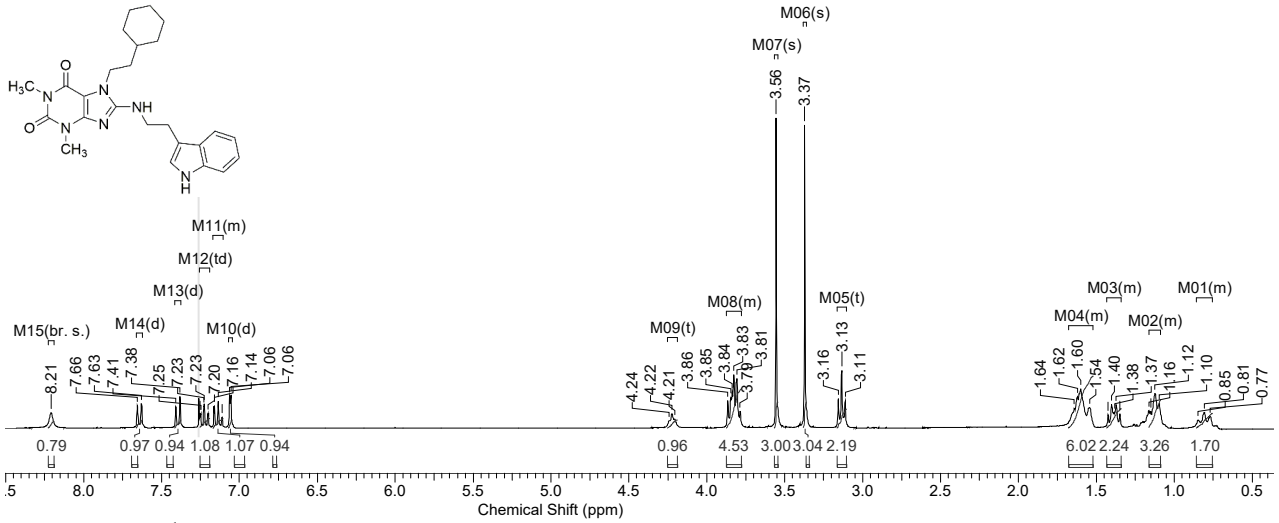

Figure S99. ^{1}H-NMR spectrum of compound **62**.

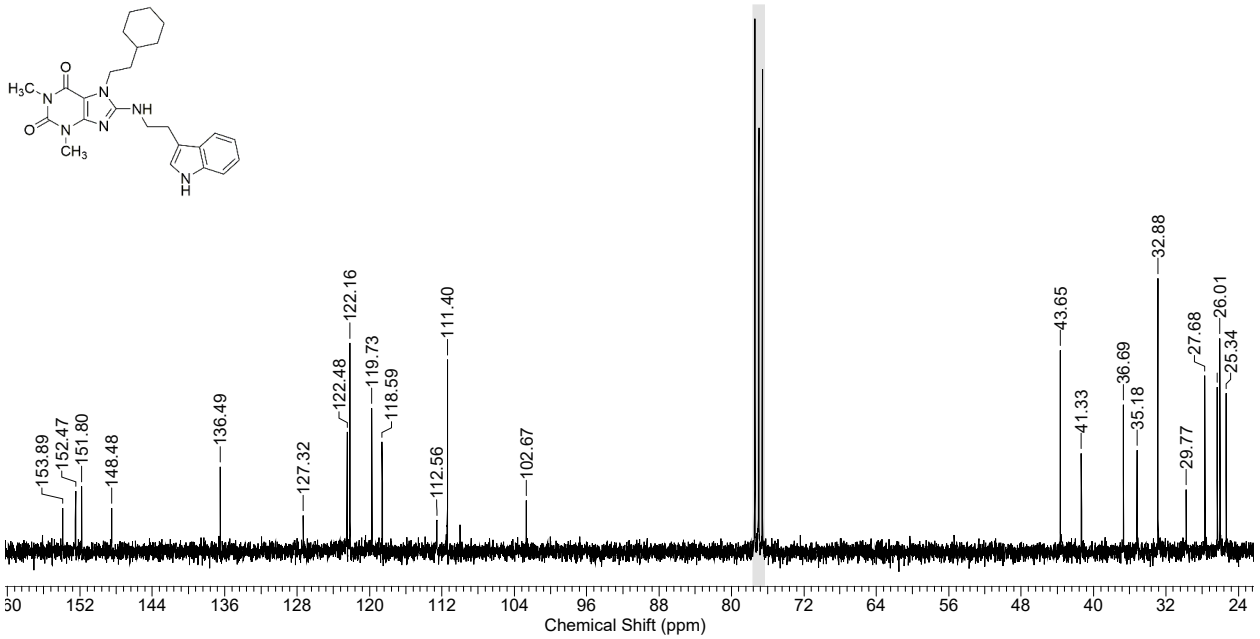

Figure S100. ^{13}C-NMR spectrum of compound **62**.

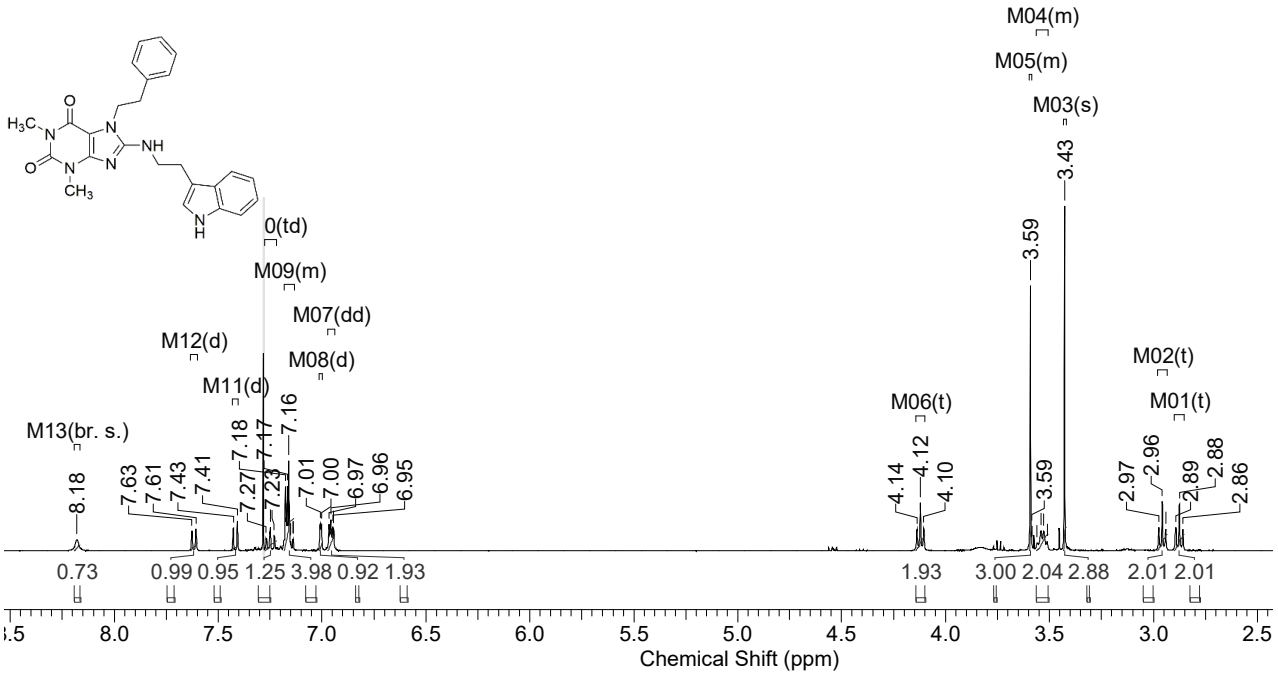

Figure S101. ^{1}H-NMR spectrum of compound **63**.

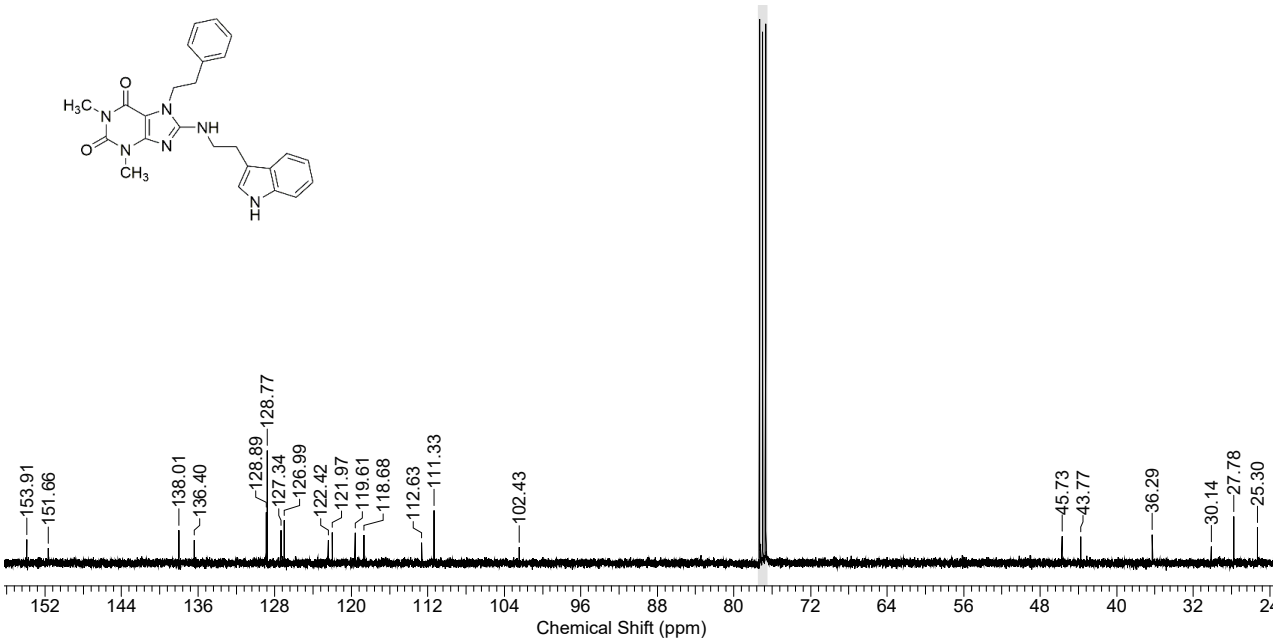

Figure S102. ^{13}C-NMR spectrum of compound **63**.

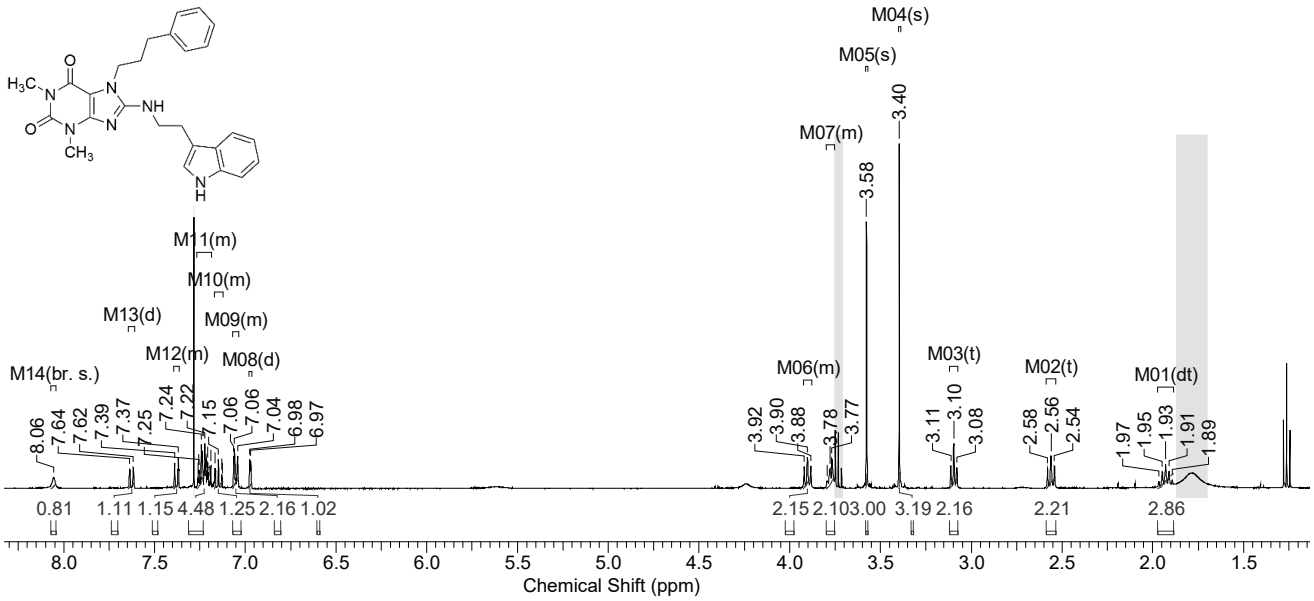

Figure S103. [1]H-NMR spectrum of compound **64** (PSB-KK1418).

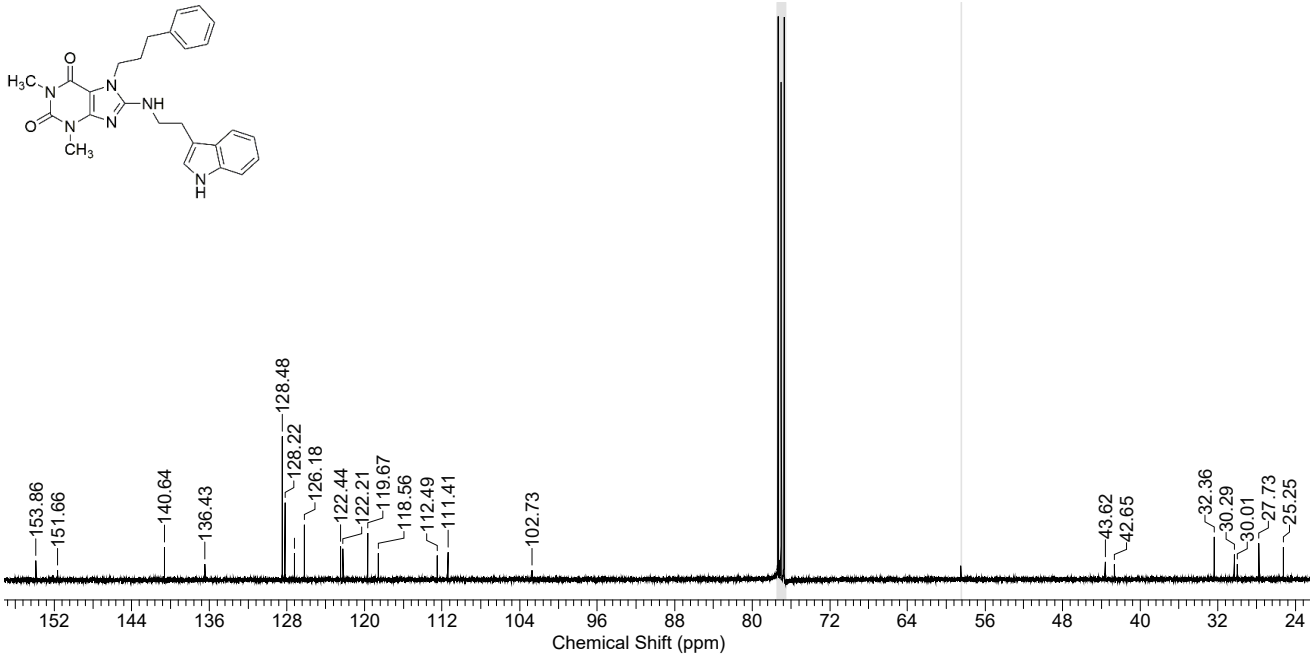

Figure S104. [13]C-NMR spectrum of compound **64** (PSB-KK1418).

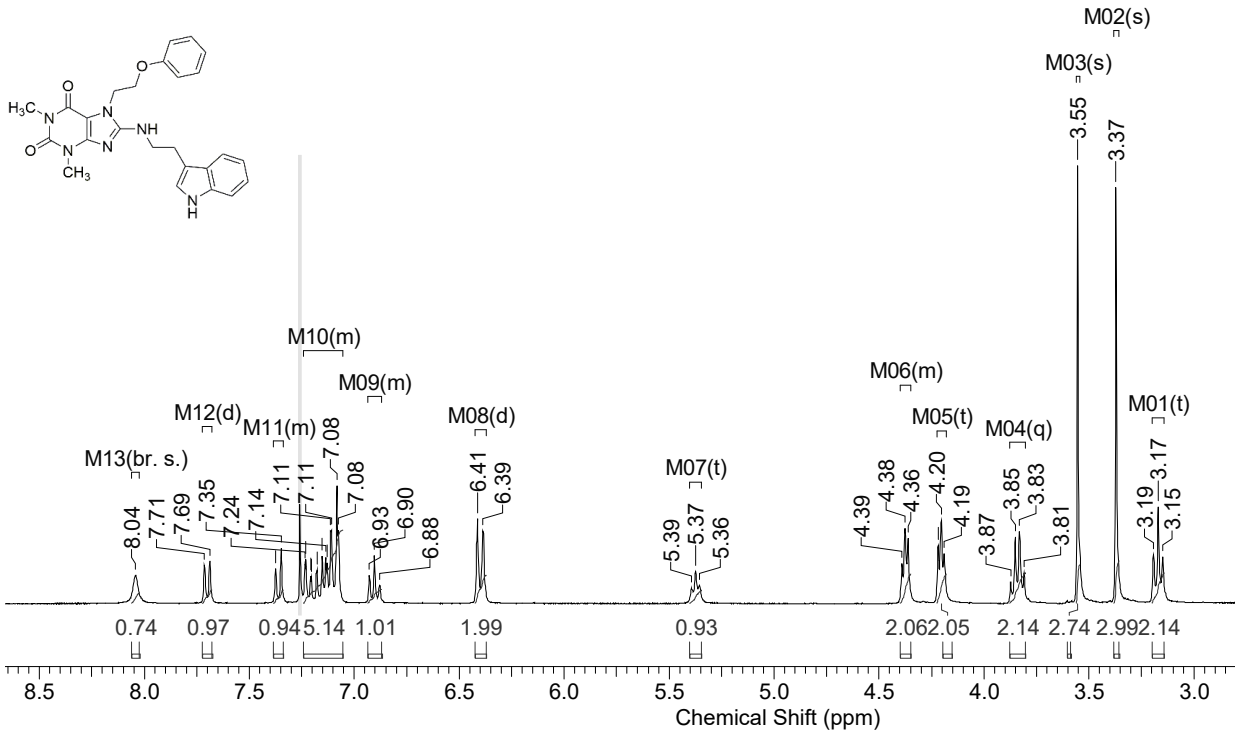

Figure S105. ^{1}H-NMR spectrum of compound **65.**

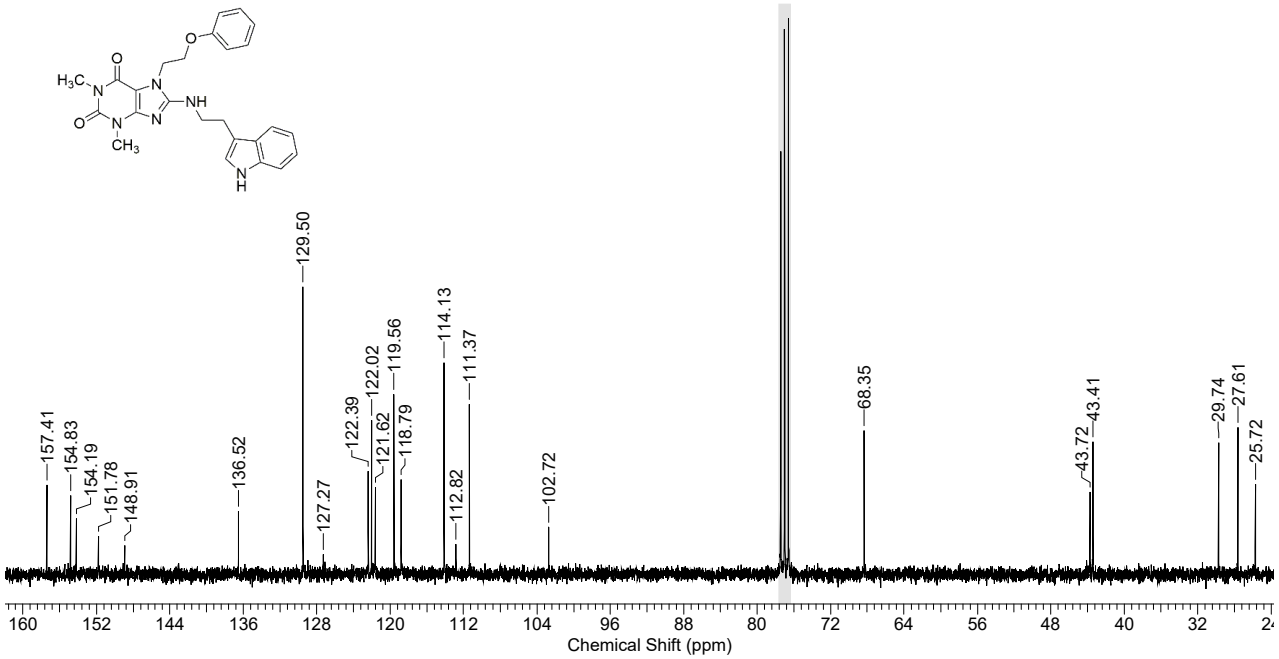

Figure S106. ^{13}C-NMR spectrum of compound **65**.

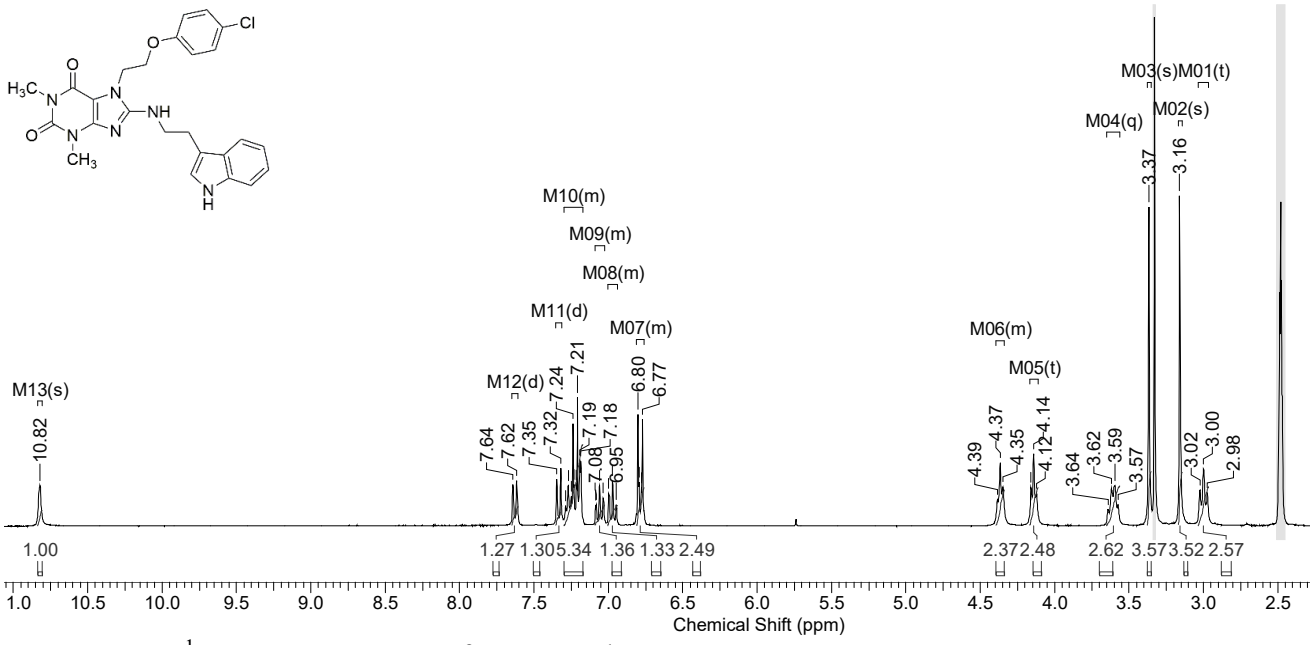

Figure S107. ^{1}H-NMR spectrum of compound **66**.

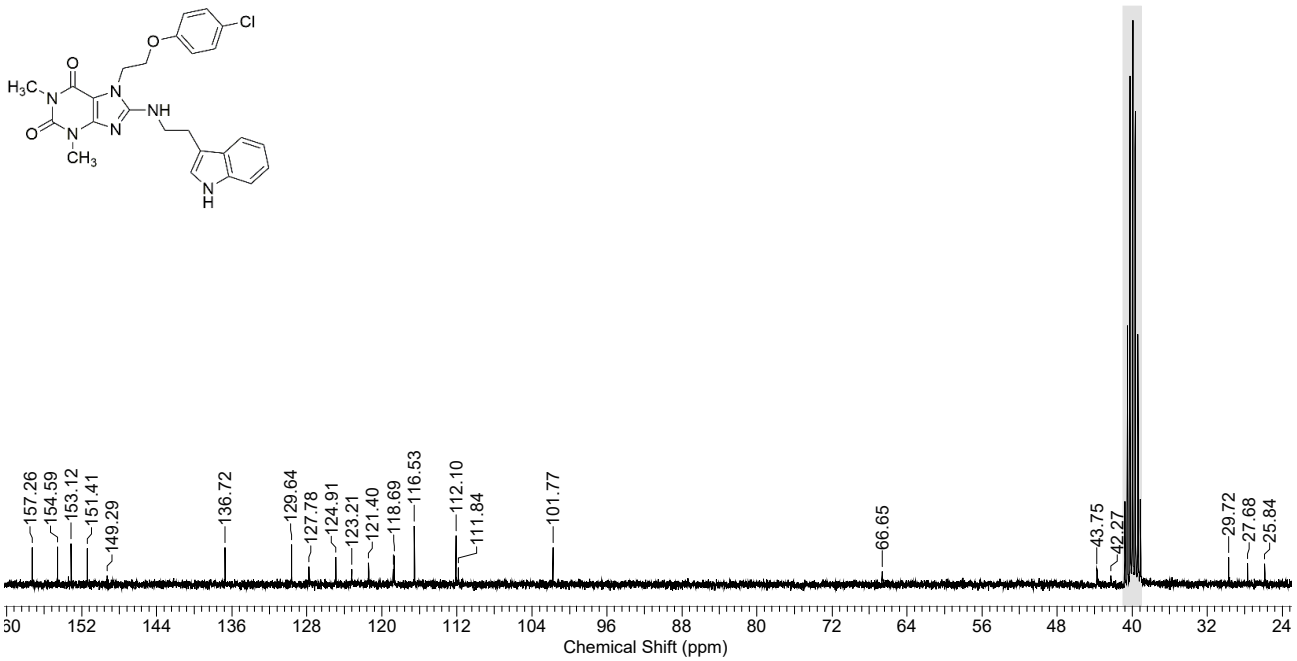

Figure S108. ^{13}C-NMR spectrum of compound **66**.

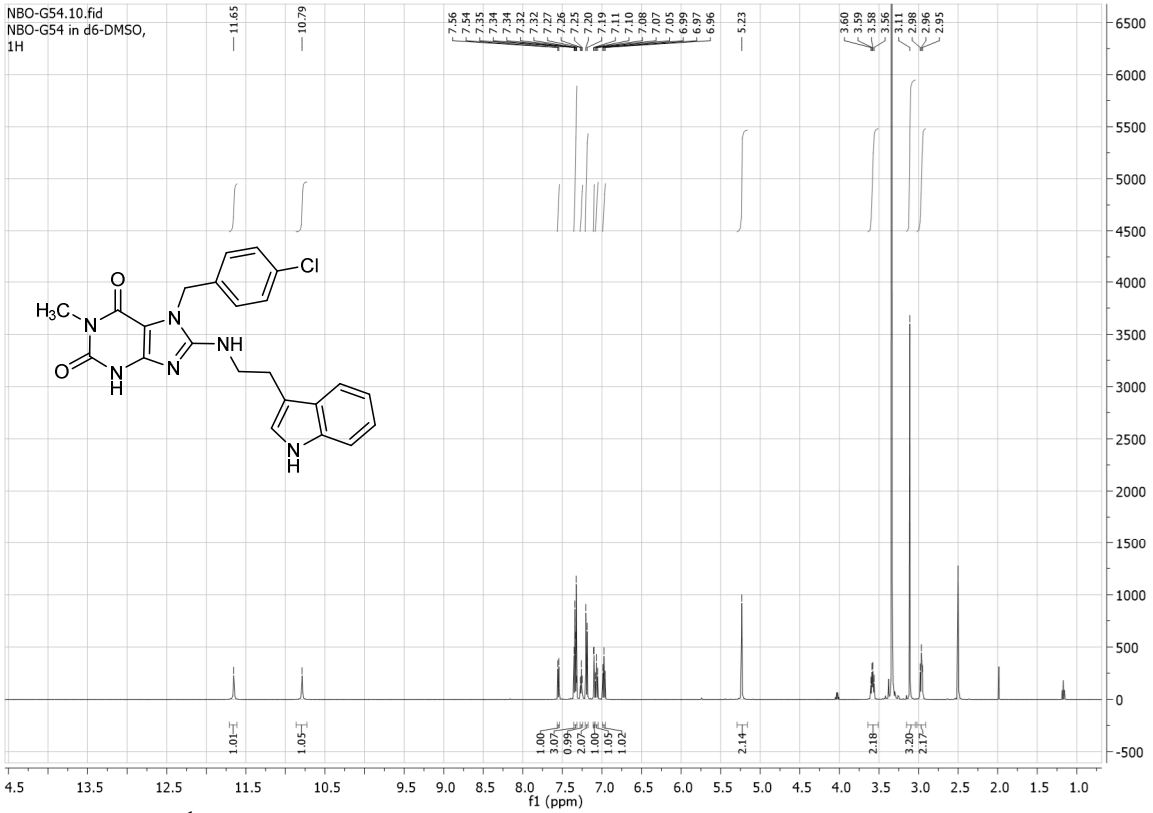

Figure S109. ^{1}H-NMR spectrum of compound **74**.

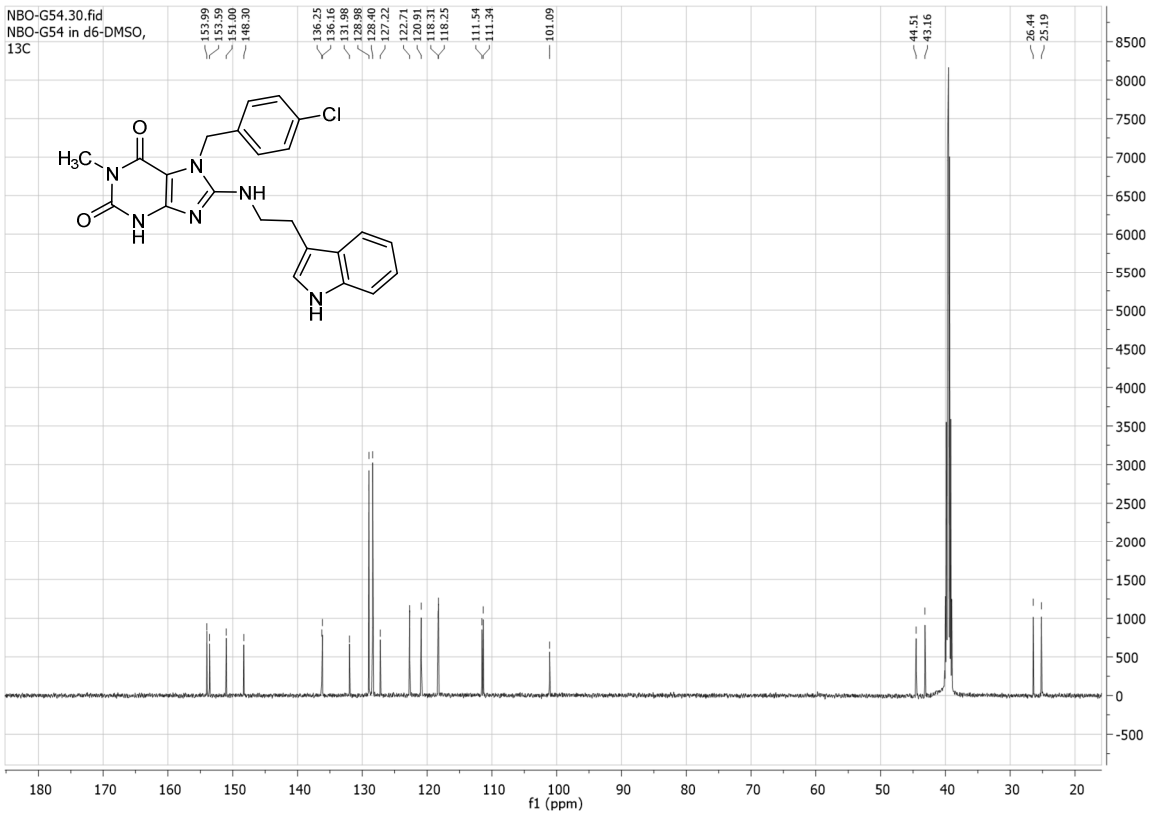

Figure S110. ^{13}C-NMR spectrum of compound **74**.

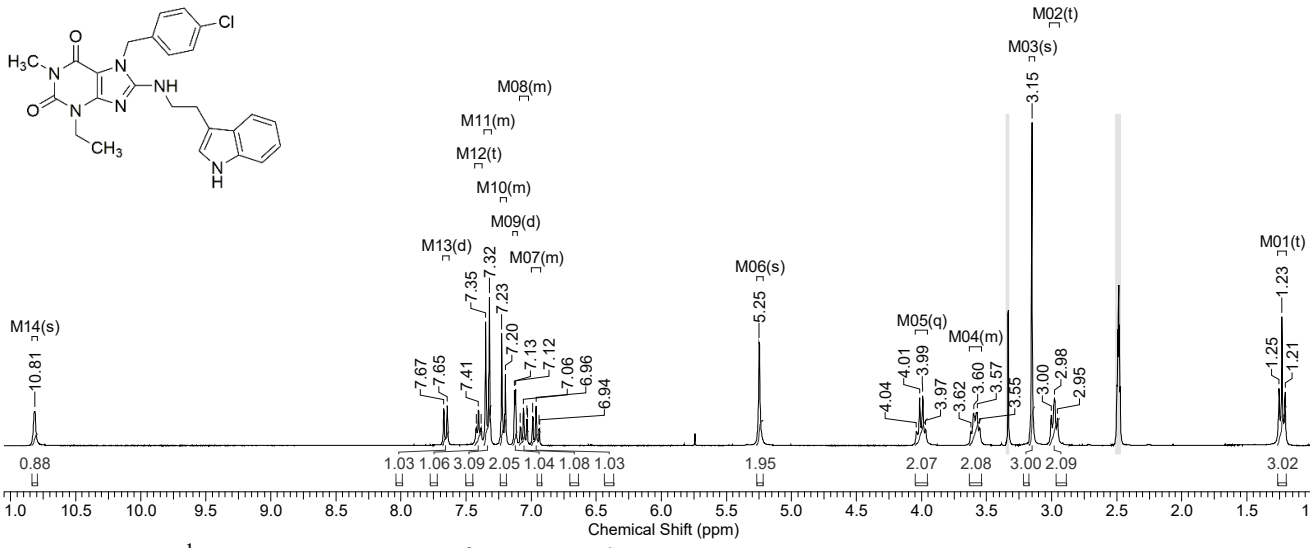

Figure S111. ^{1}H-NMR spectrum of compound **75**.

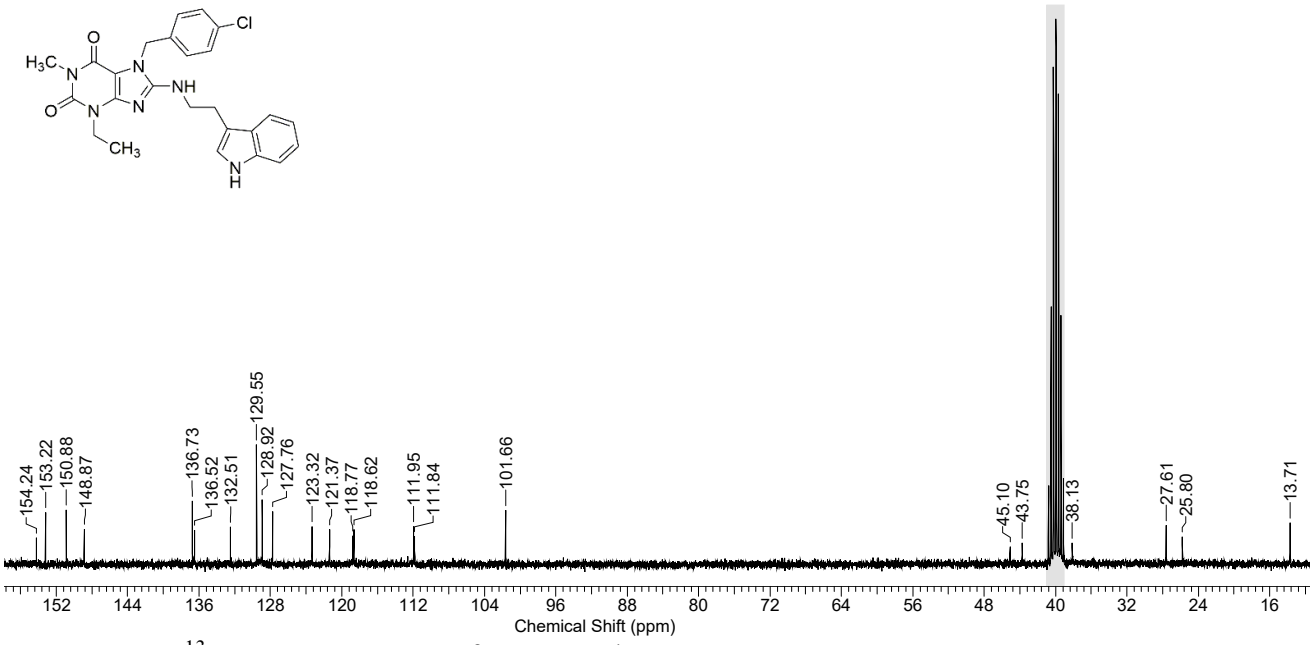

Figure S112. ^{13}C-NMR spectrum of compound **75**.

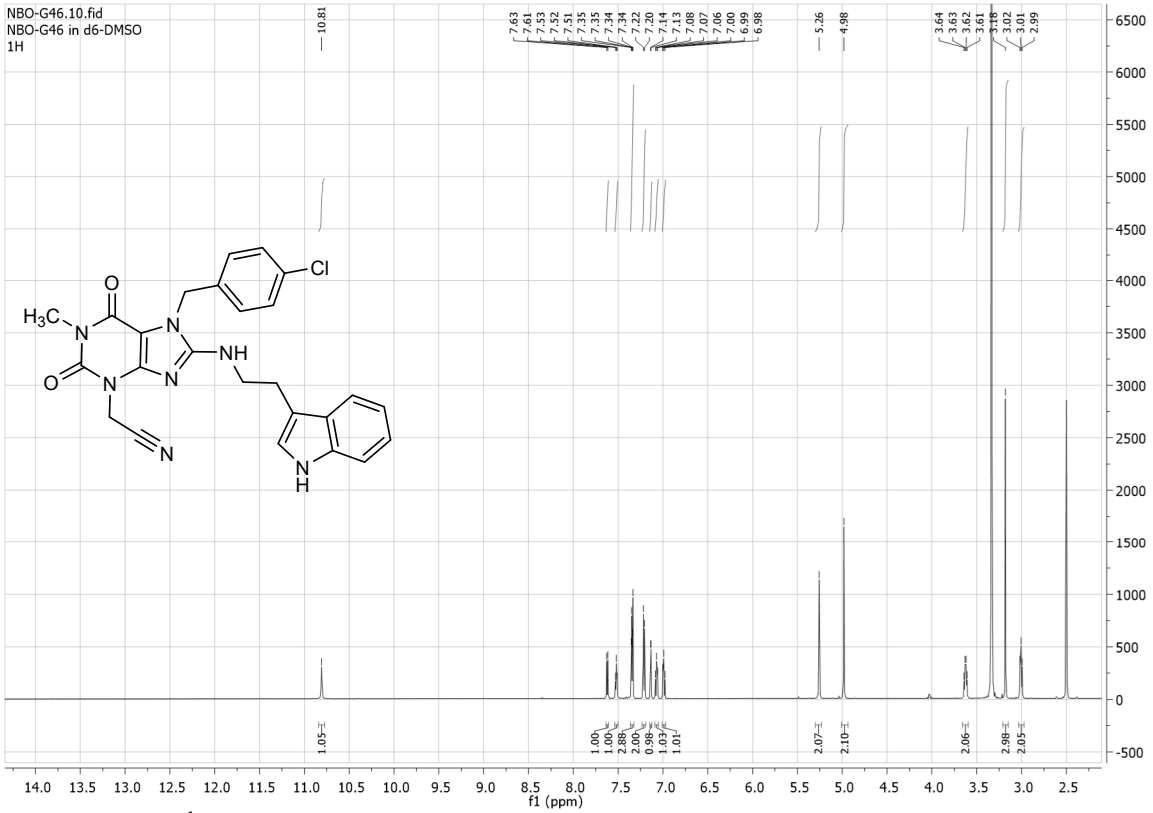

Figure S113. ^{1}H-NMR spectrum of compound **76** (PSB-1846).

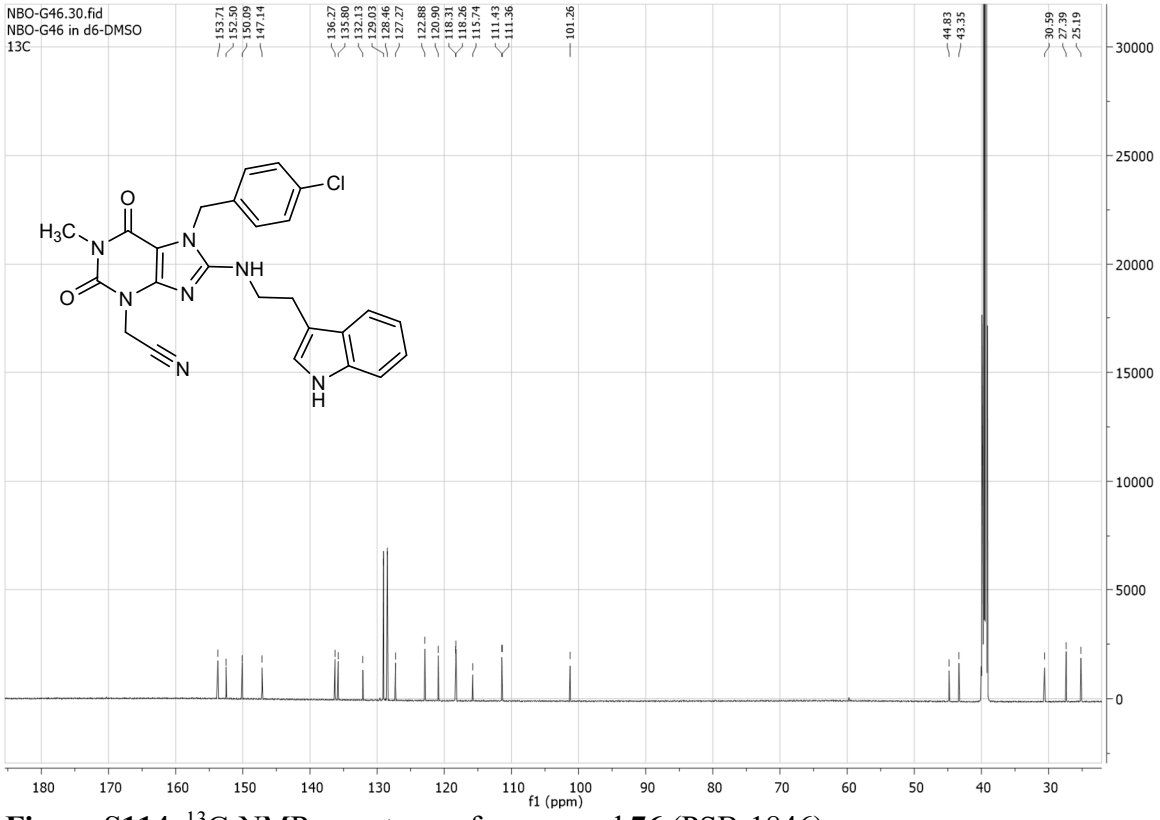

Figure S114. ^{13}C-NMR spectrum of compound **76** (PSB-1846).

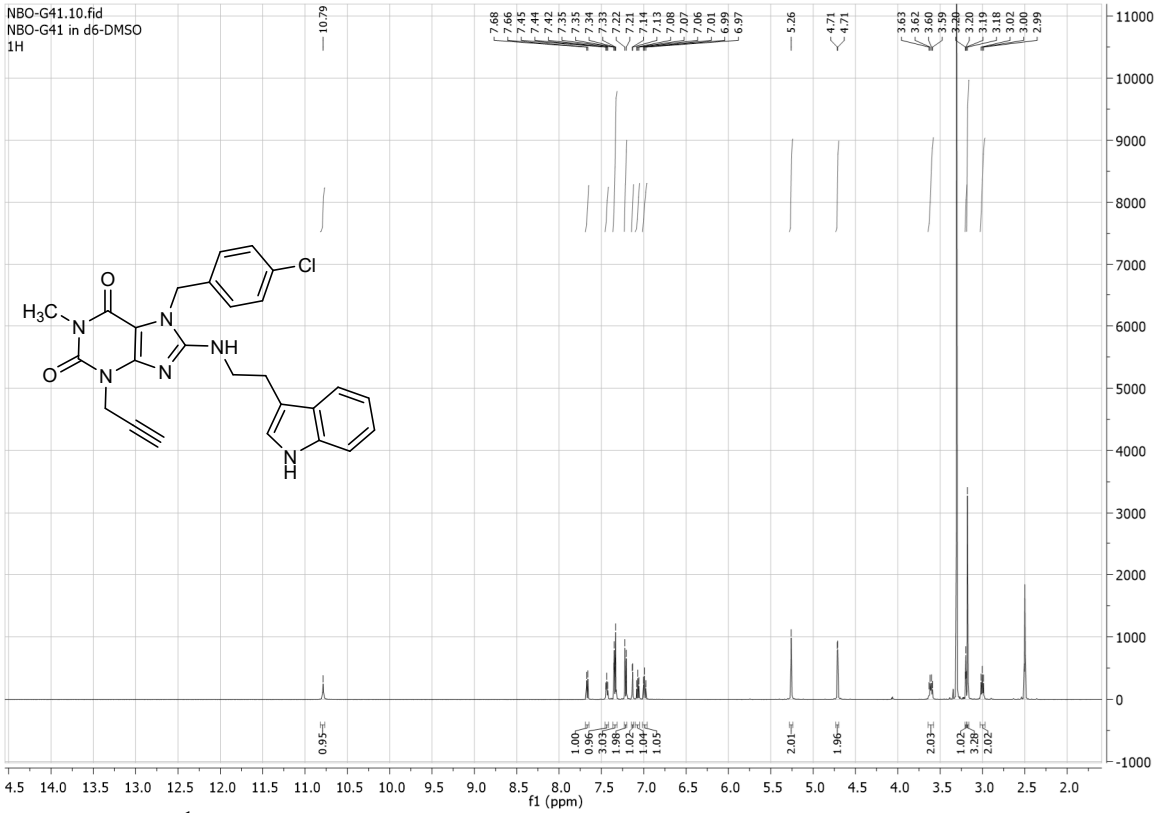

Figure S115. ^{1}H-NMR spectrum of compound **77**.

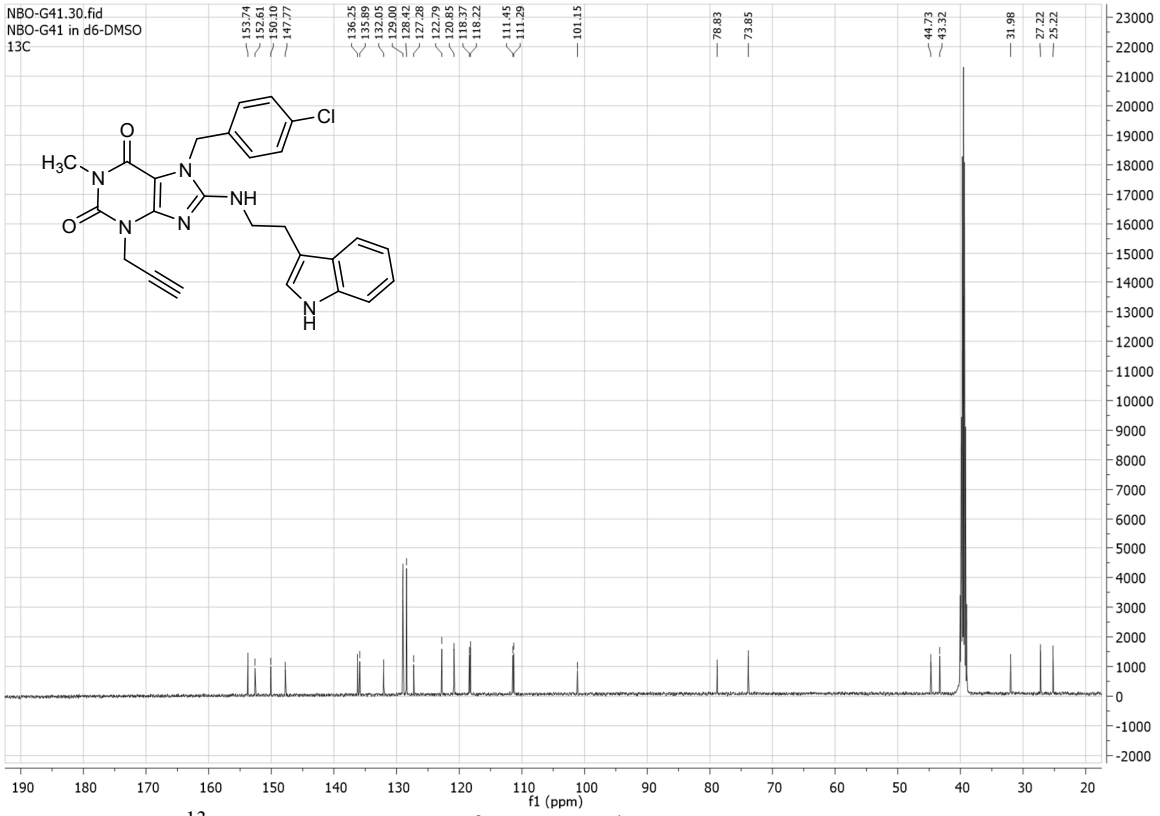

Figure S116. ^{13}C-NMR spectrum of compound **77**.

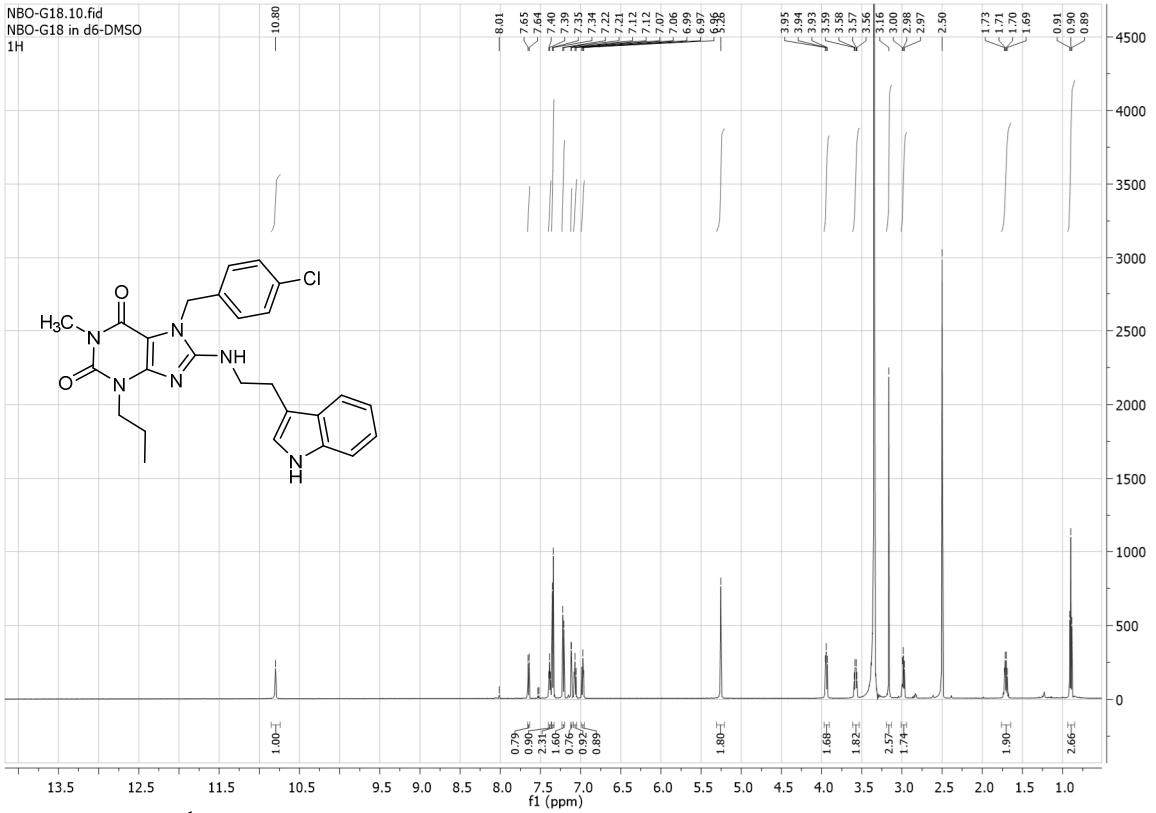

Figure S117. ^{1}H-NMR spectrum of compound **78**.

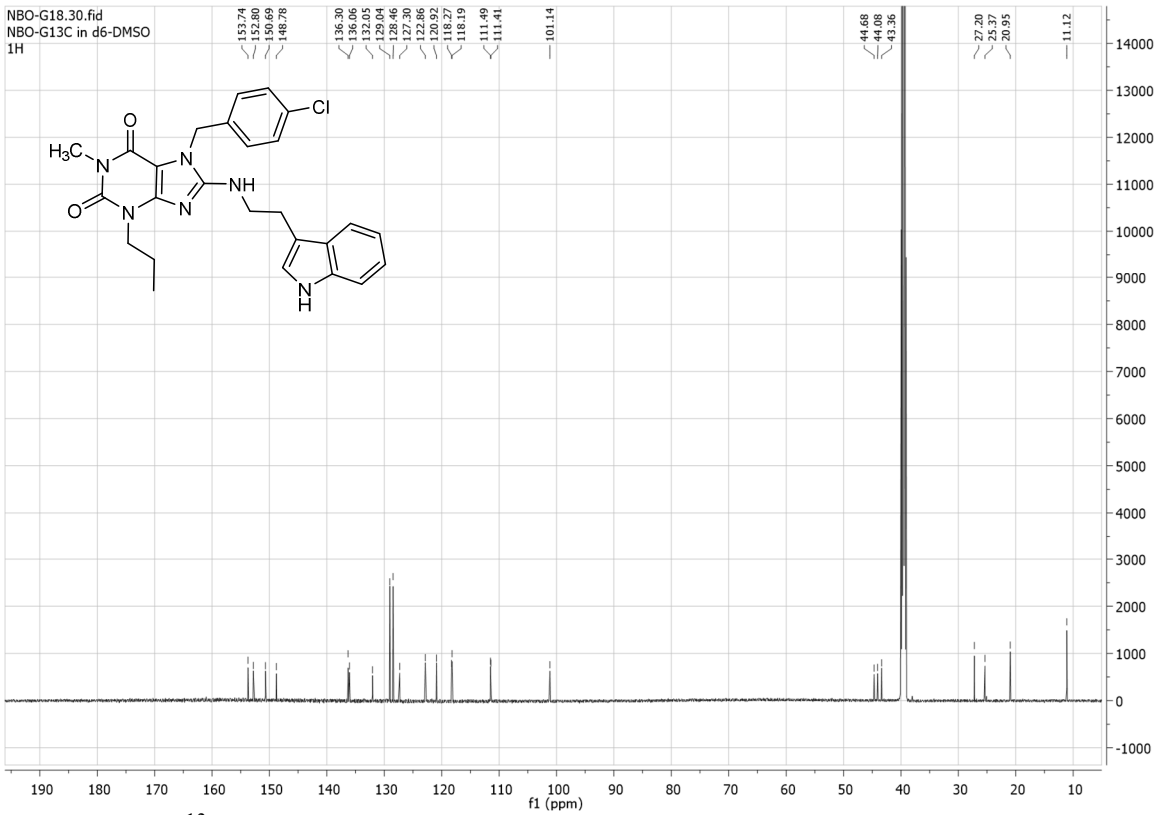

Figure S118. ^{13}C-NMR spectrum of compound **78**.

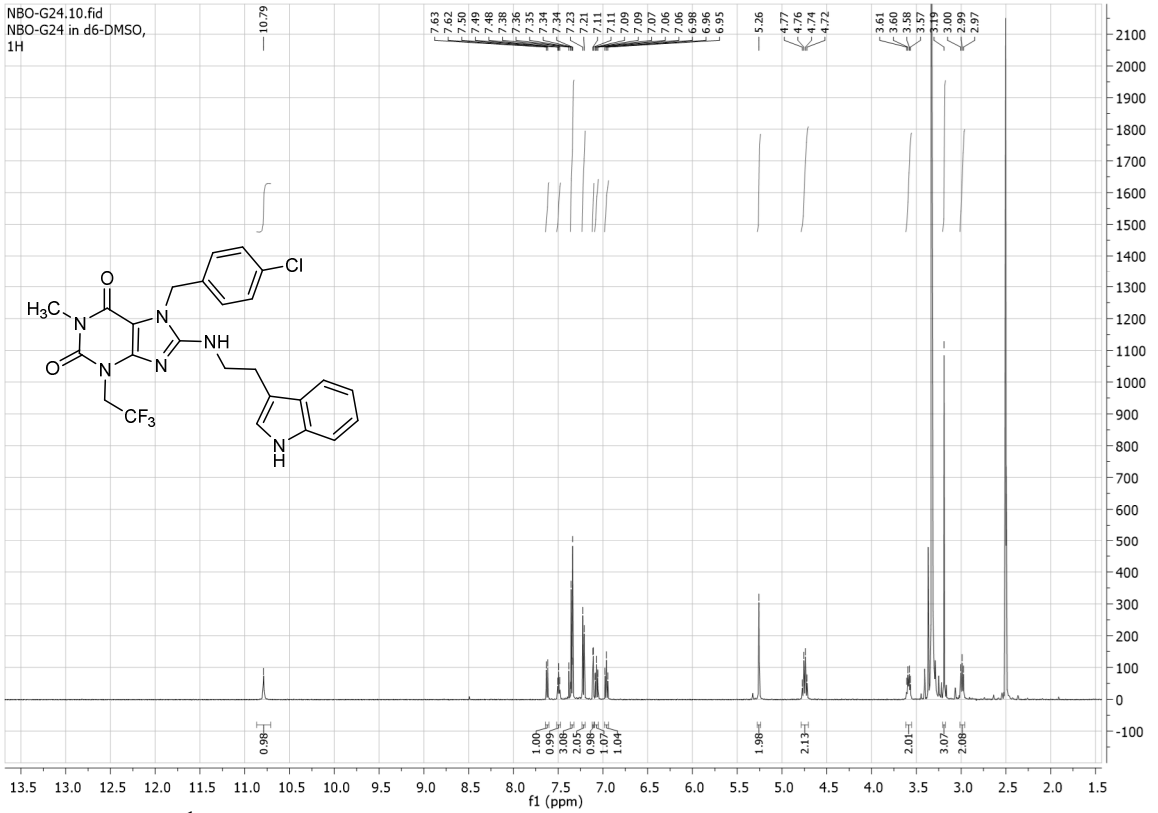

Figure S119. ^{1}H-NMR spectrum of compound **79**.

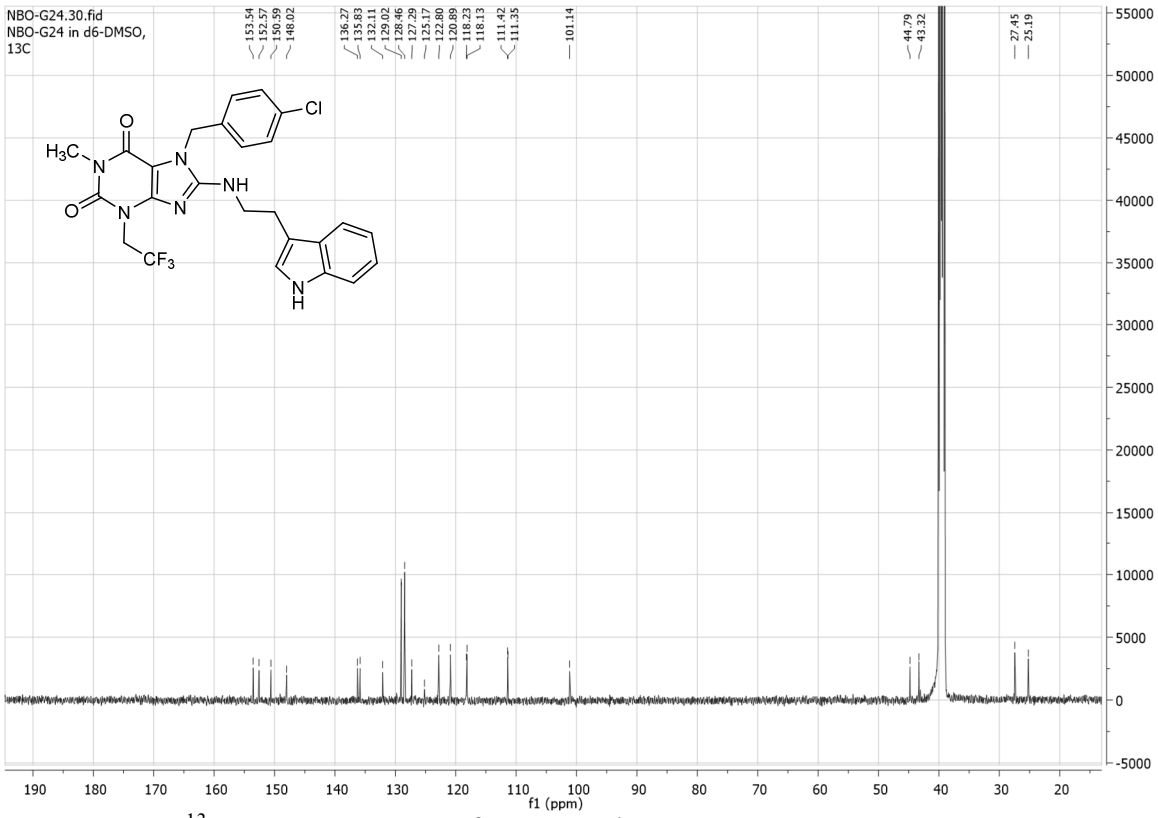

Figure S120. ^{13}C-NMR spectrum of compound **79**.

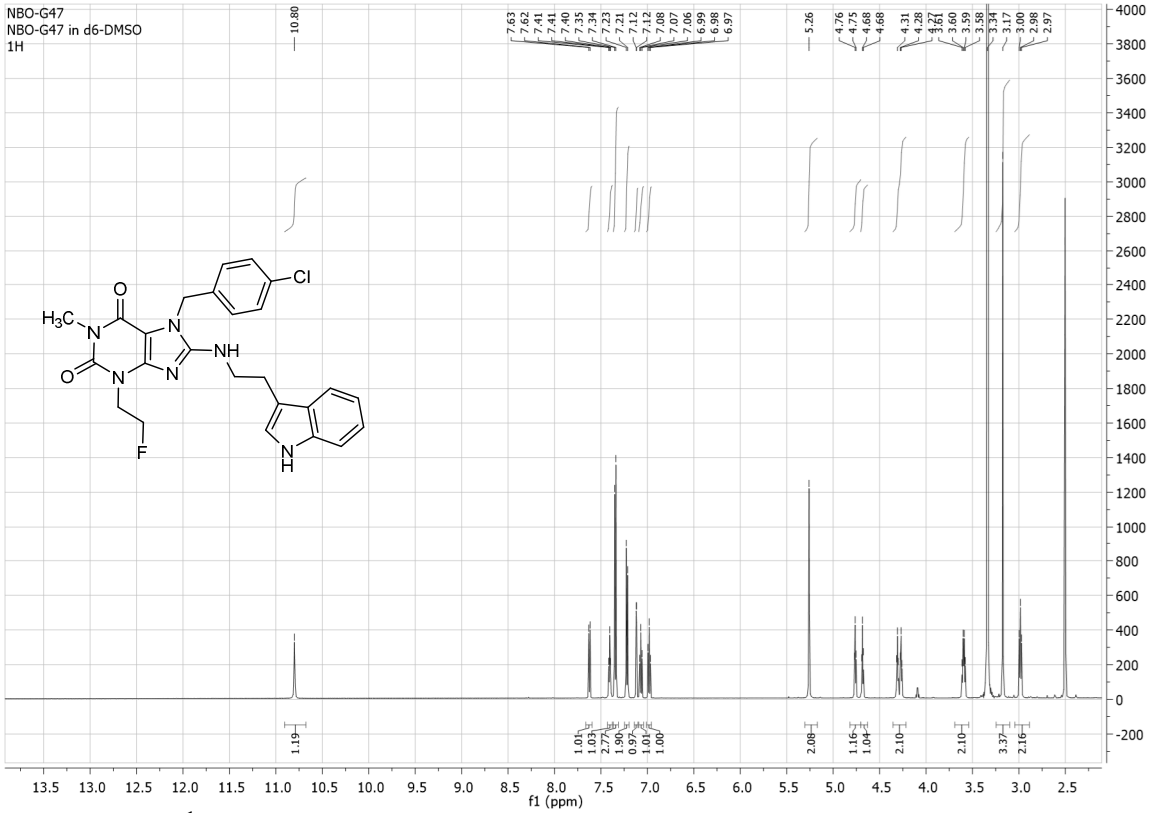

Figure S121. ^{1}H-NMR spectrum of compound **80**.

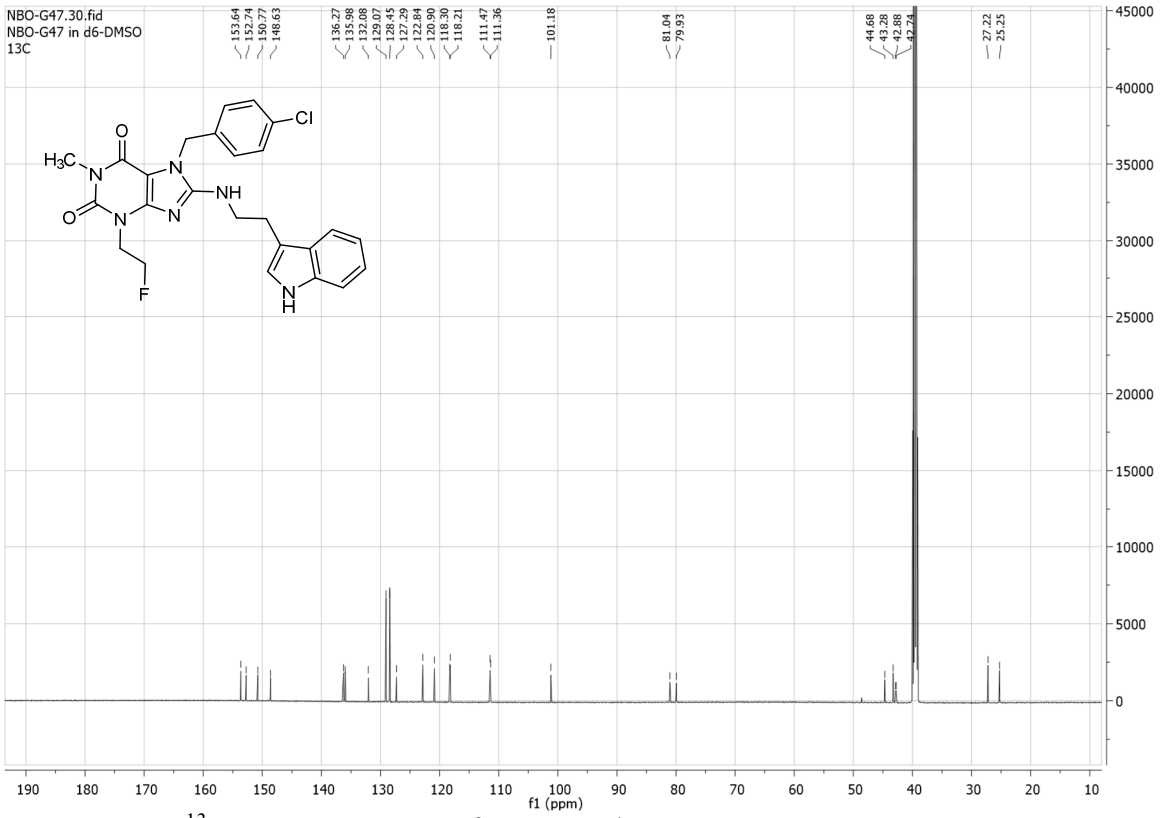

Figure S122. ^{13}C-NMR spectrum of compound **80**.

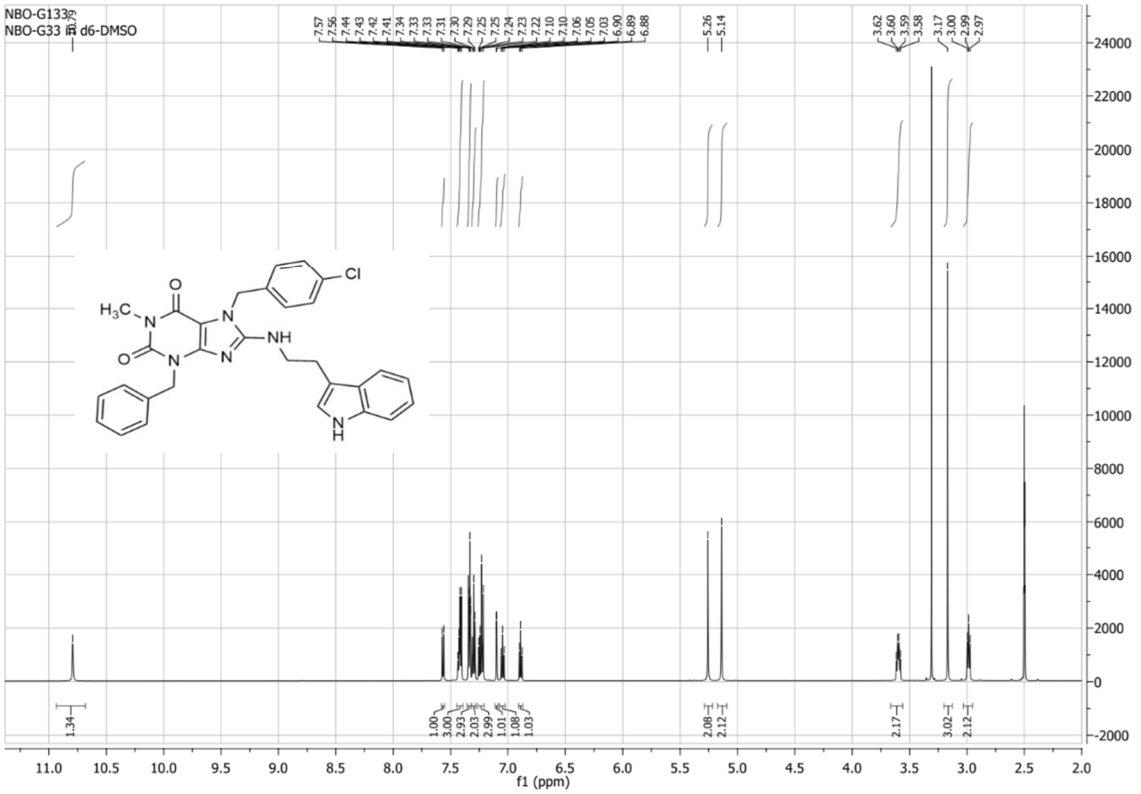

Figure S123. ^{1}H-NMR spectrum of compound **82** (PSB-1833).

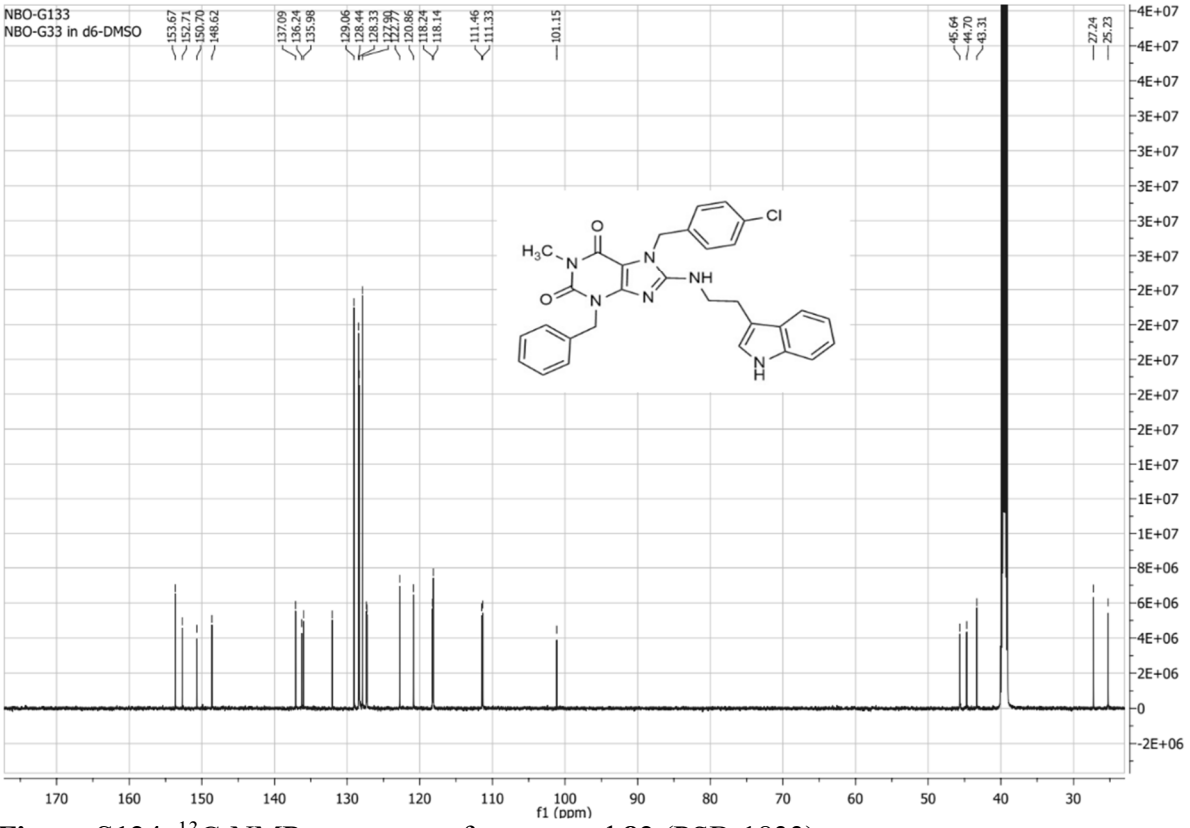

Figure S124. ^{13}C-NMR spectrum of compound **82** (PSB-1833).

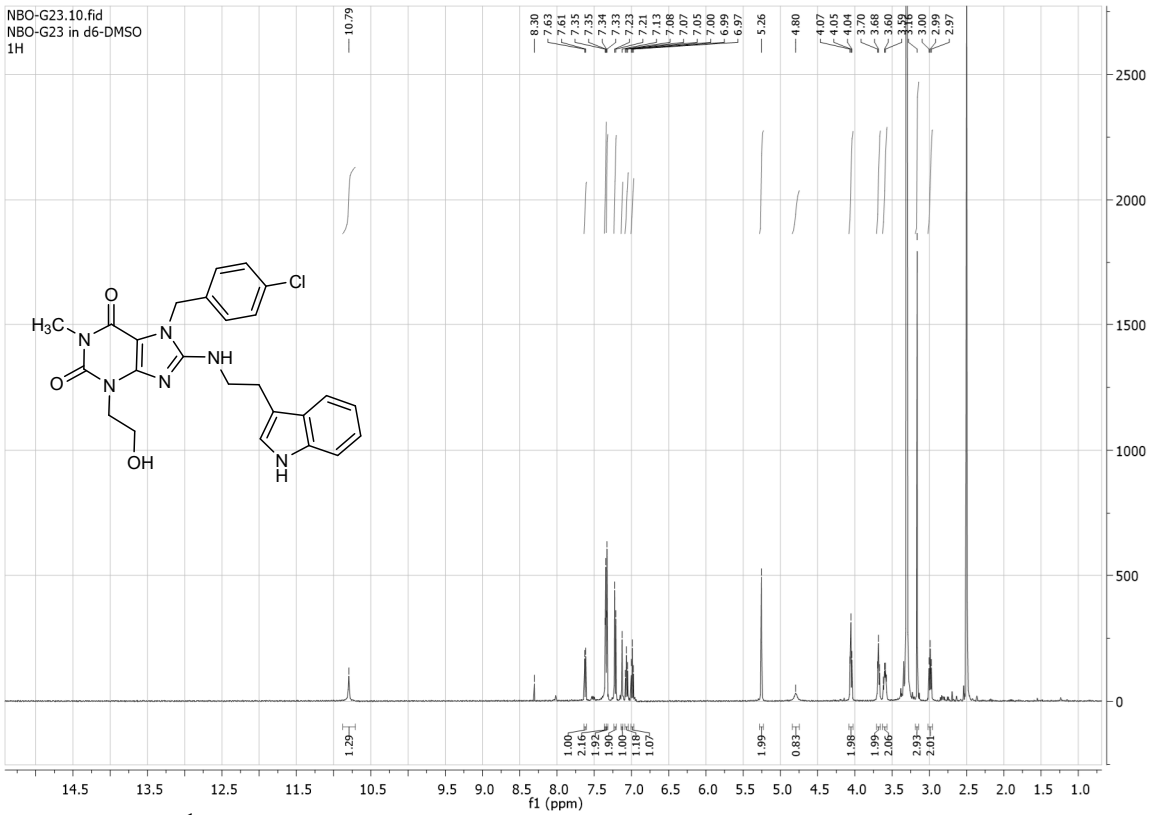

Figure S125. ^{1}H-NMR spectrum of compound **83**.

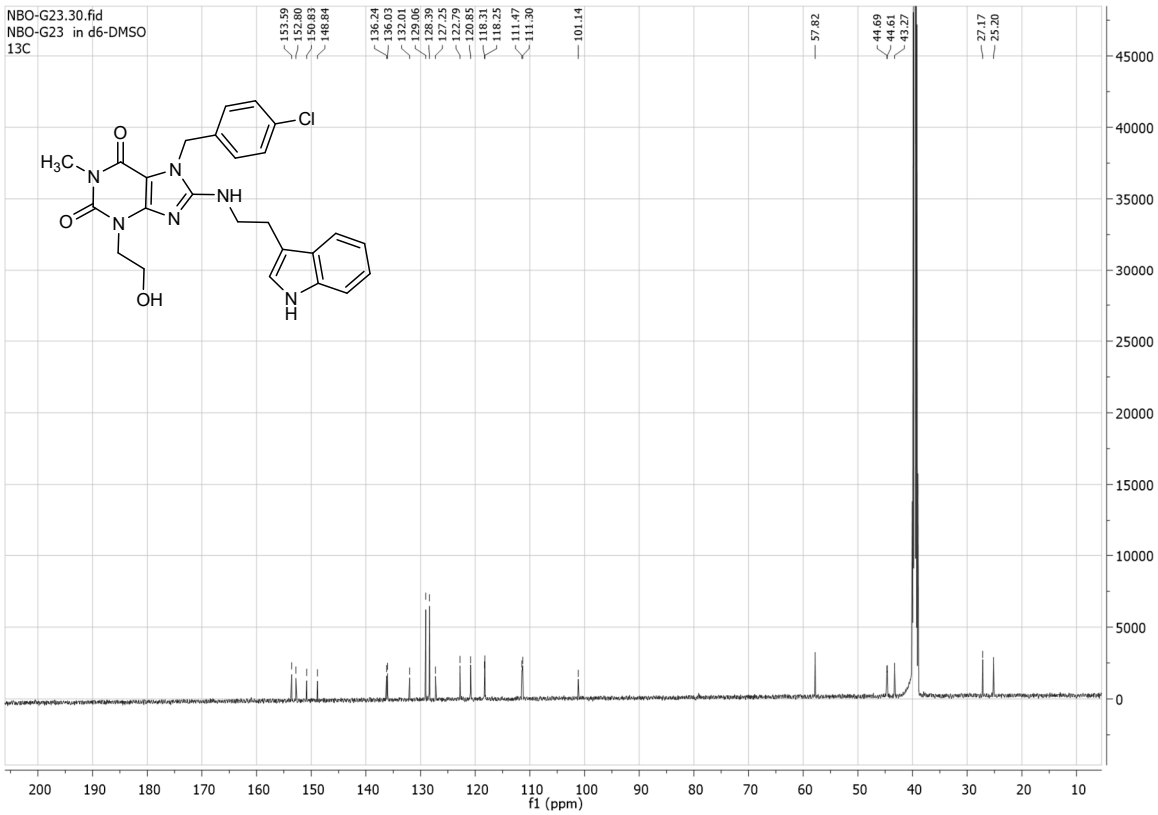

Figure S126. ^{13}C-NMR spectrum of compound **83**.

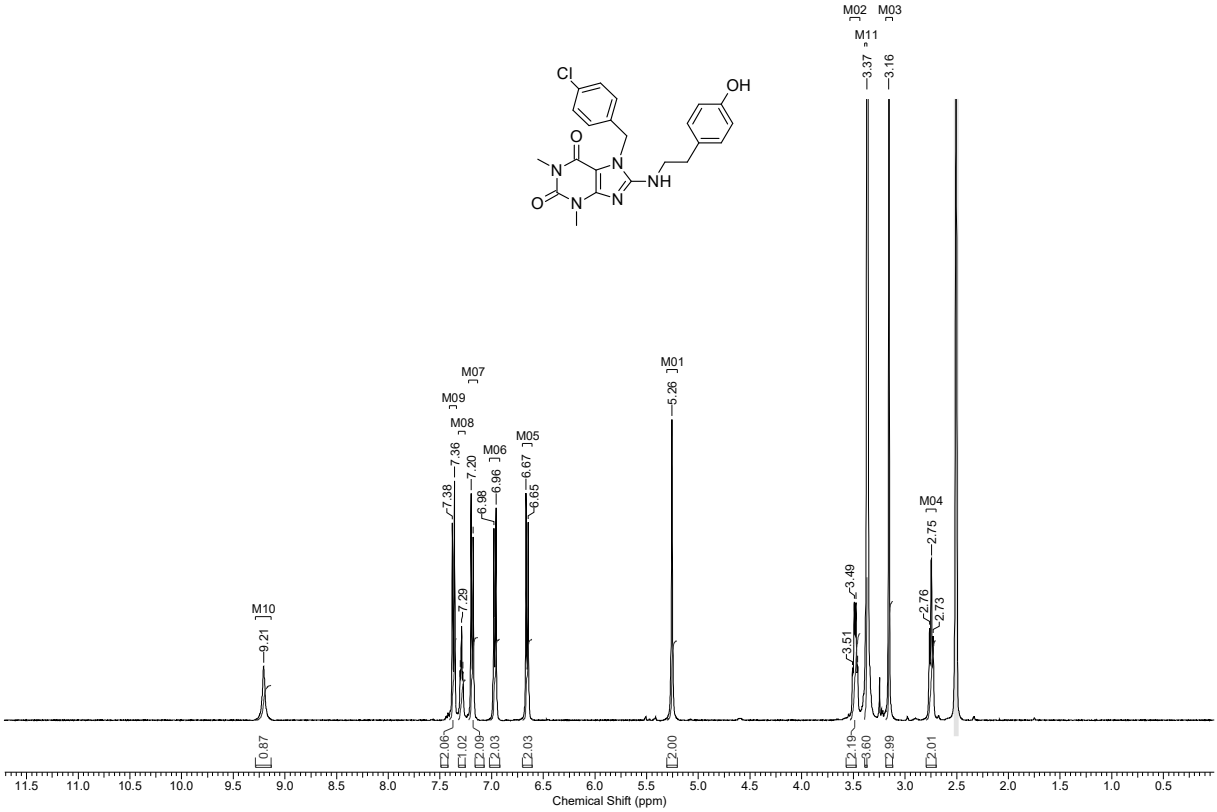

Figure S127. ^{1}H-NMR spectrum of compound **87.**

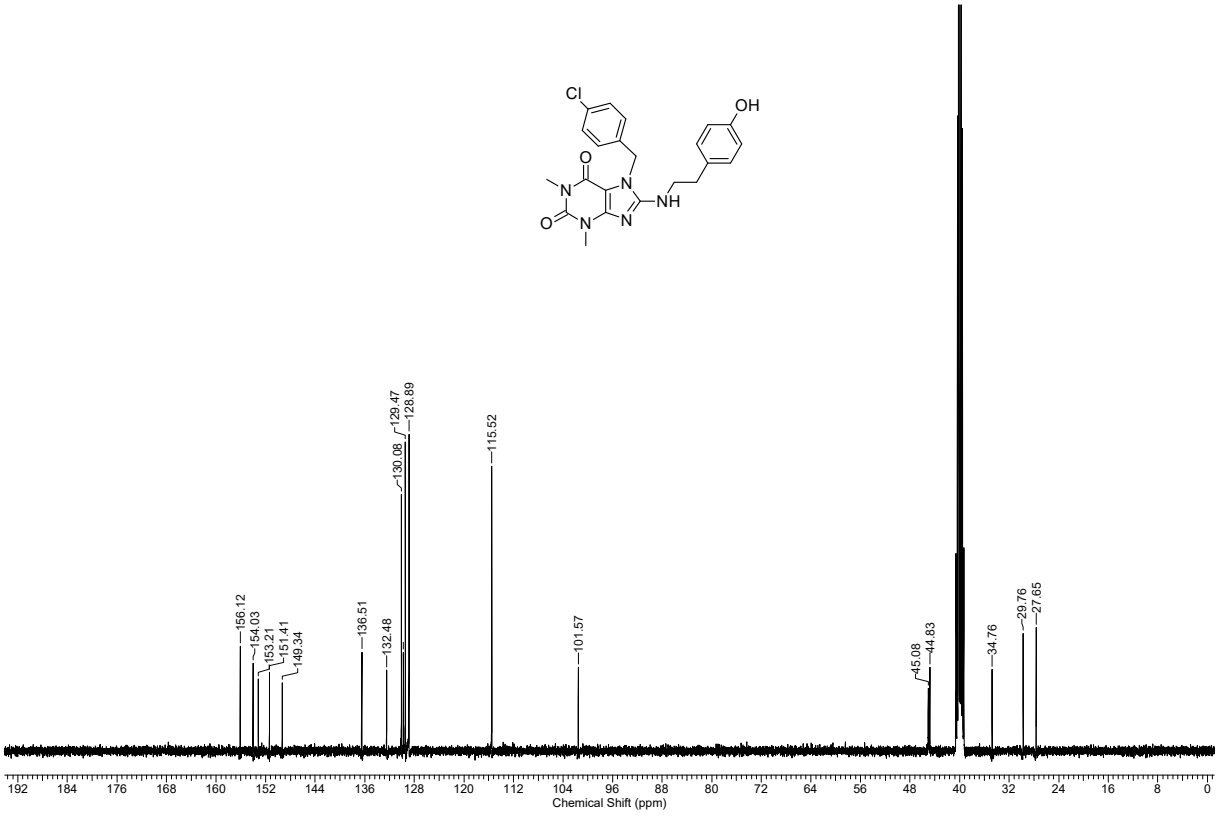

Figure S128. ^{13}C-NMR spectrum of compound **87.**

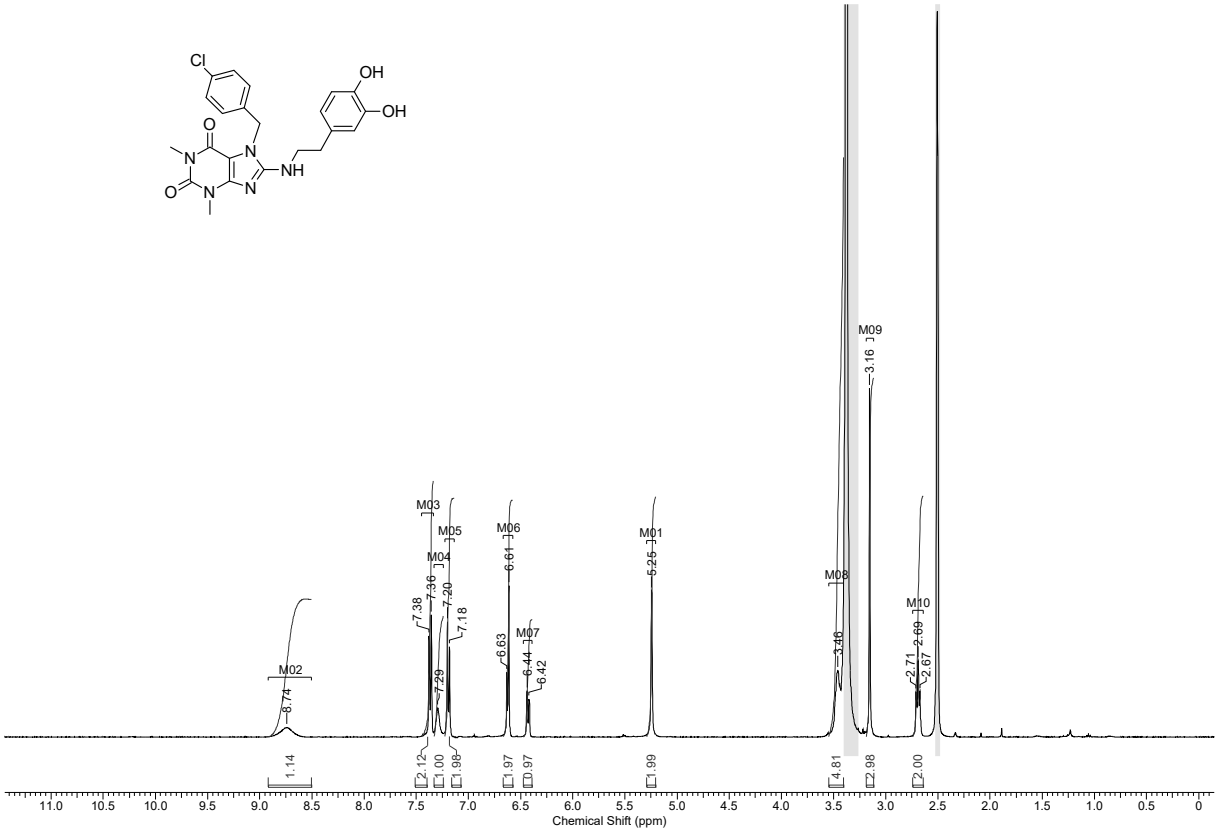

Figure S129. ^{1}H-NMR spectrum of compound **88**.

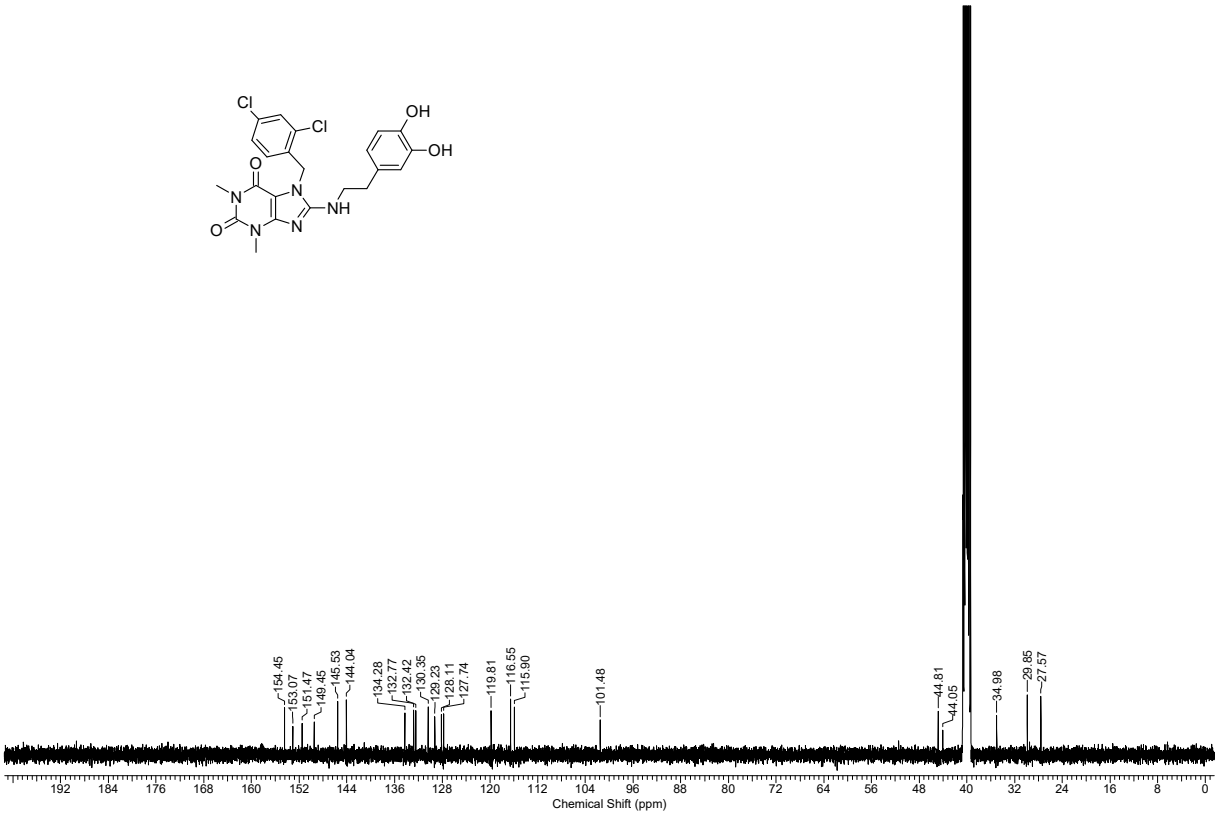

Figure S130. ^{13}C-NMR spectrum of compound **88**.

S99

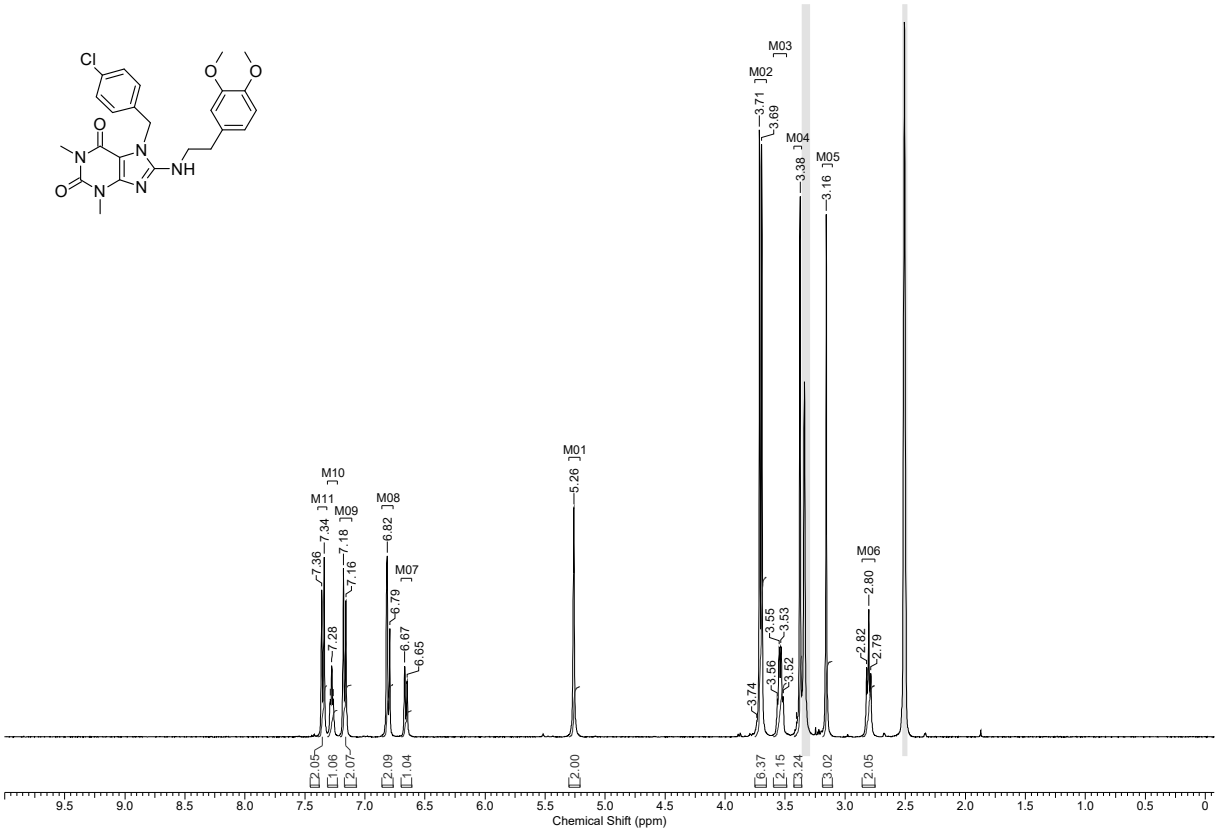

Figure S131. ^{1}H-NMR spectrum of compound **89**.

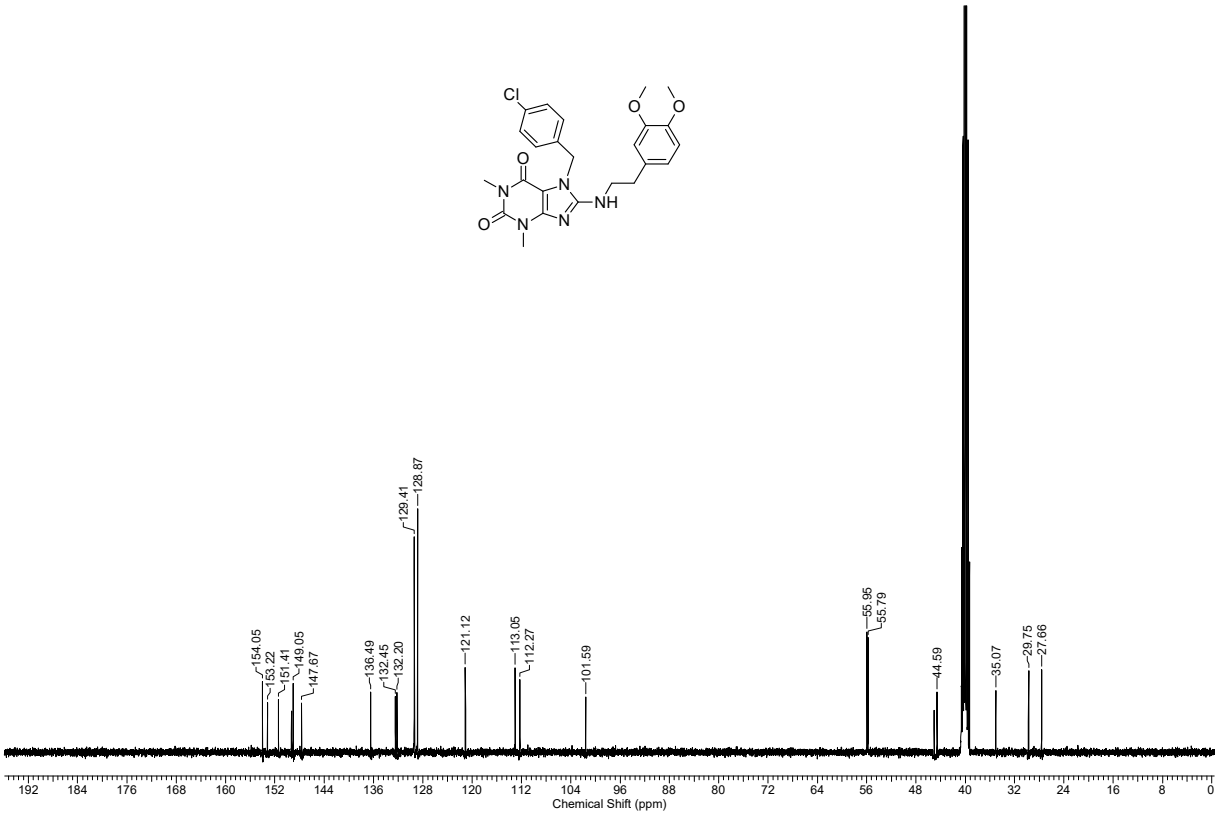

Figure S132. ^{13}C-NMR spectrum of compound **89**.

S100

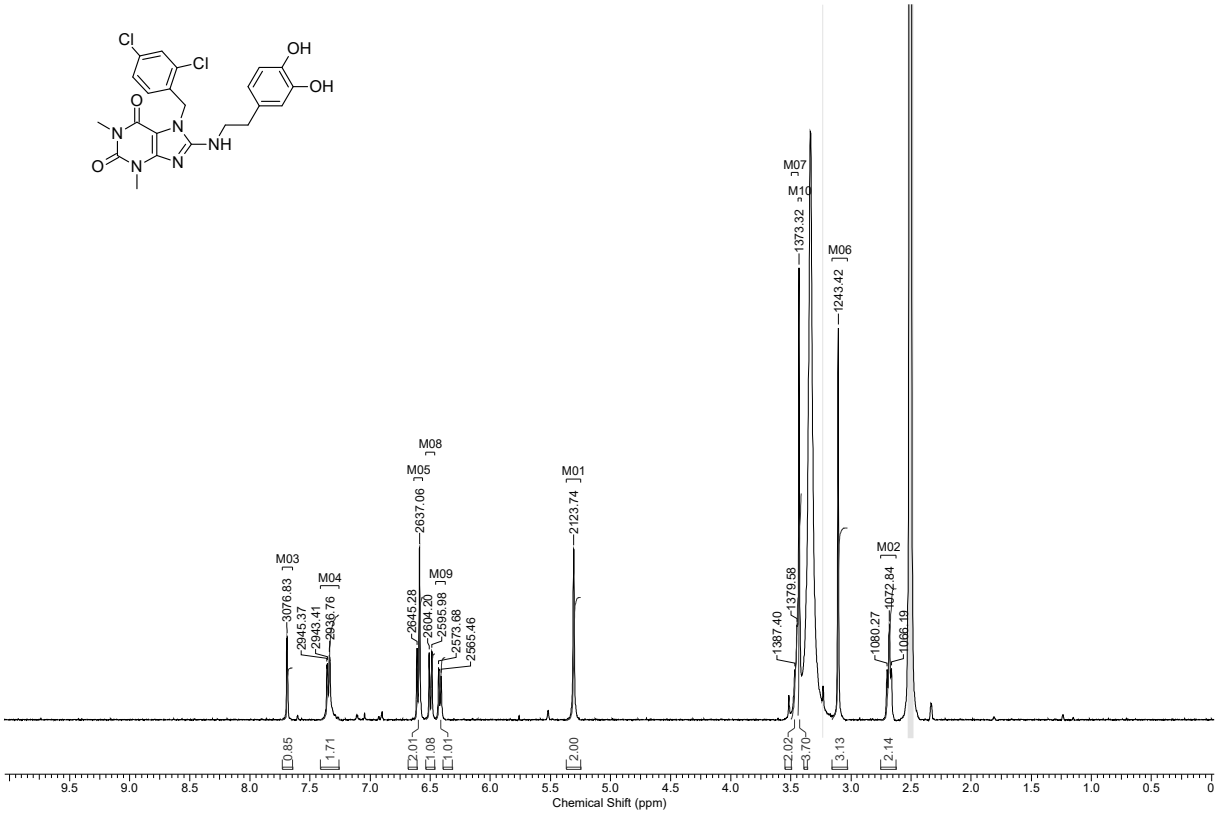

Figure S133.[1]H-NMR spectrum of compound **90**.

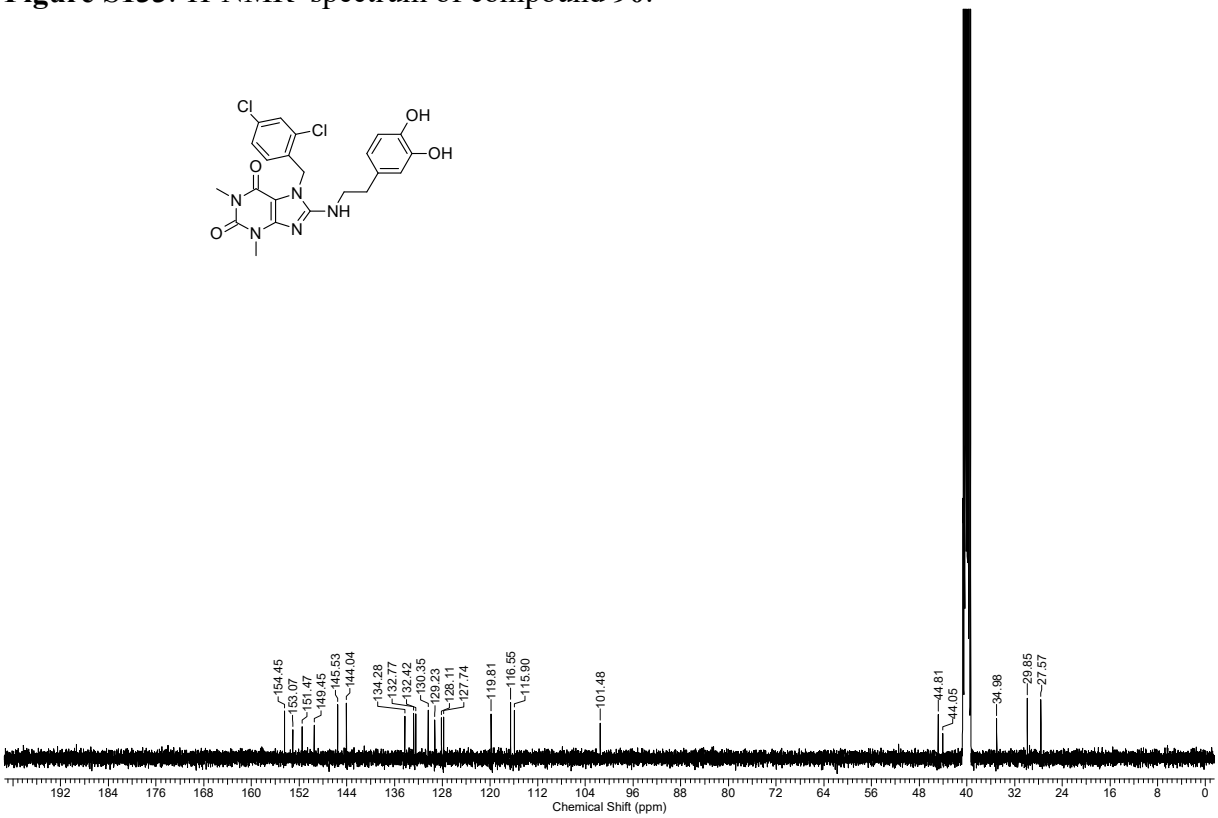

Figure S134. [13]C-NMR spectrum of compound **90**.

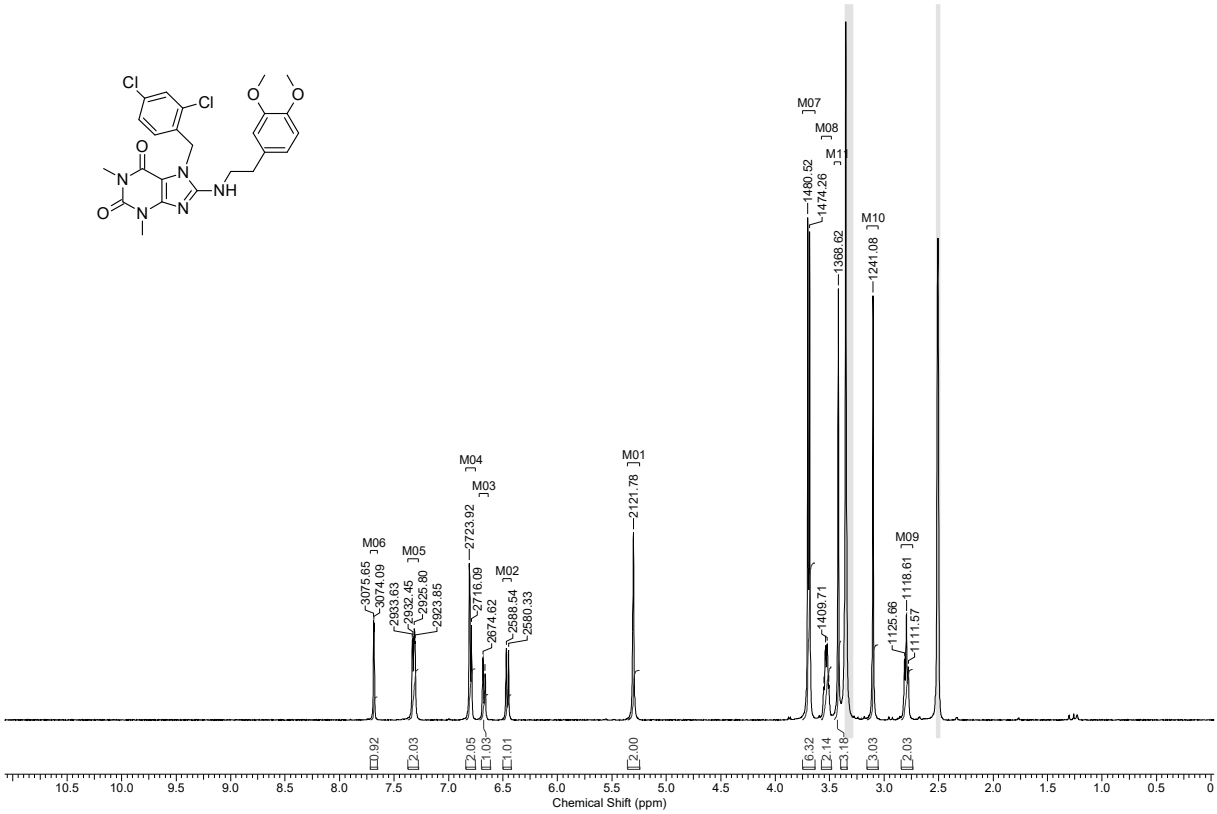

Figure S135. ^{1}H-NMR spectrum of compound **91**.

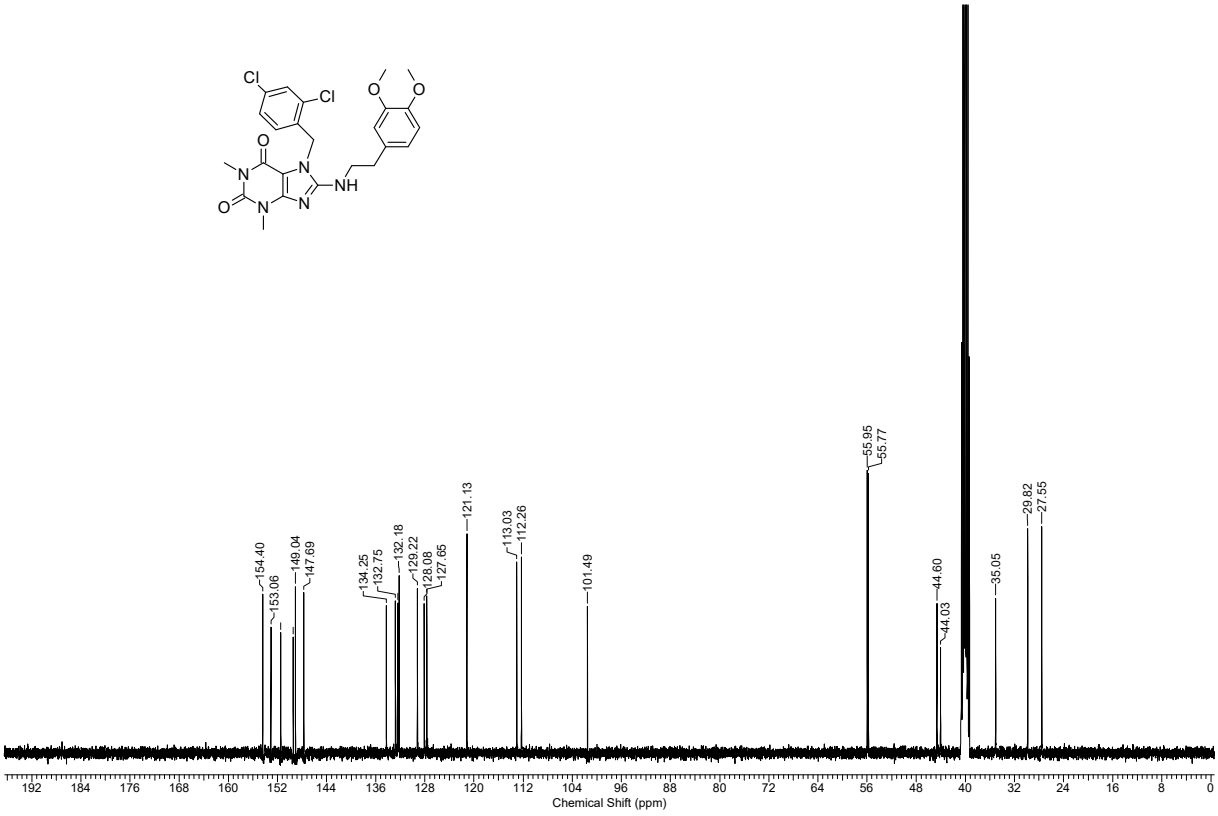

Figure S136. ^{13}C-NMR spectrum of compound **91**.

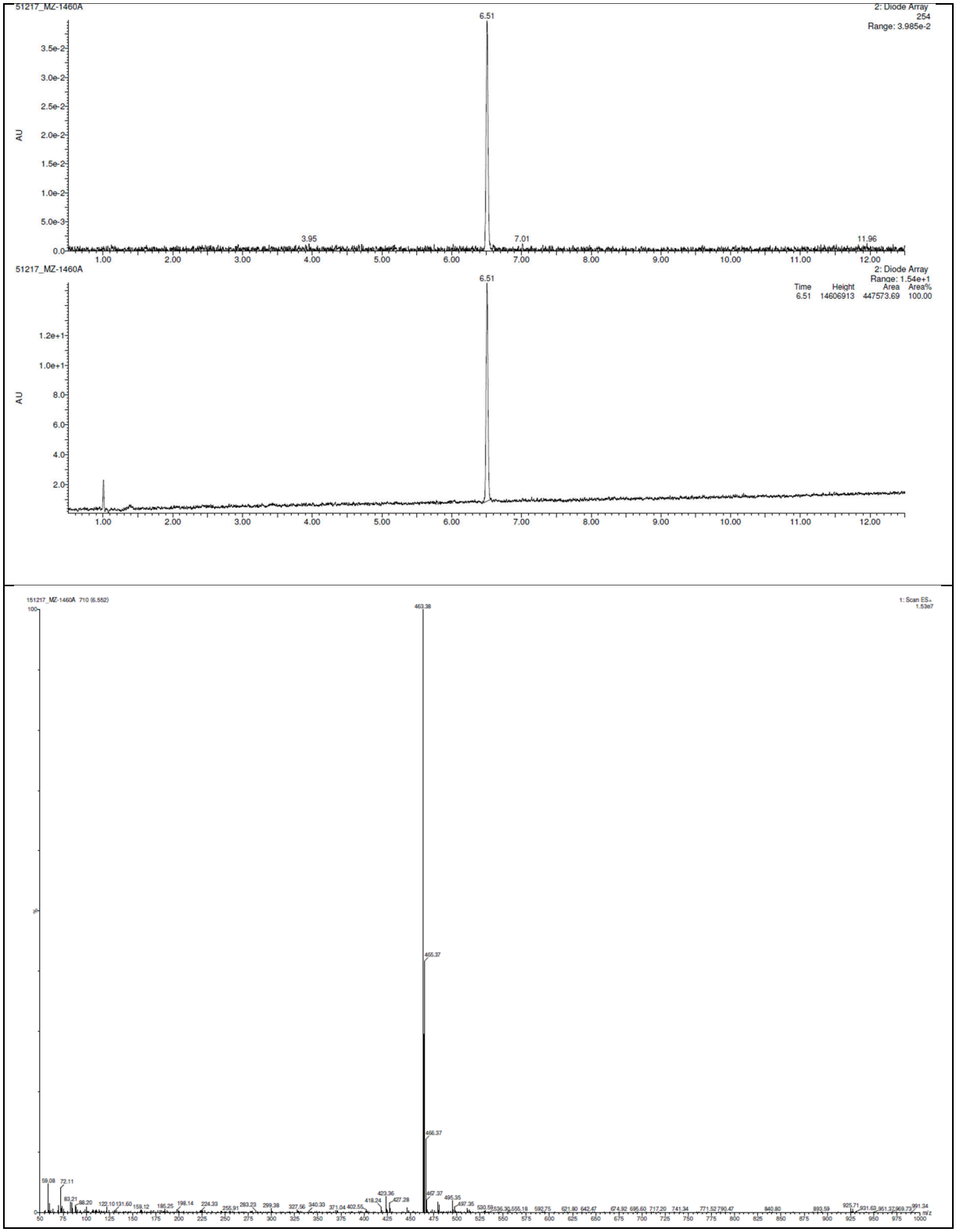

Figure S137. LC-MS assessment of the purity of compound **33**.
The purity of compound **33** is 100.0% (retention time: 6.51 min corresponds to the desired compound **33**)

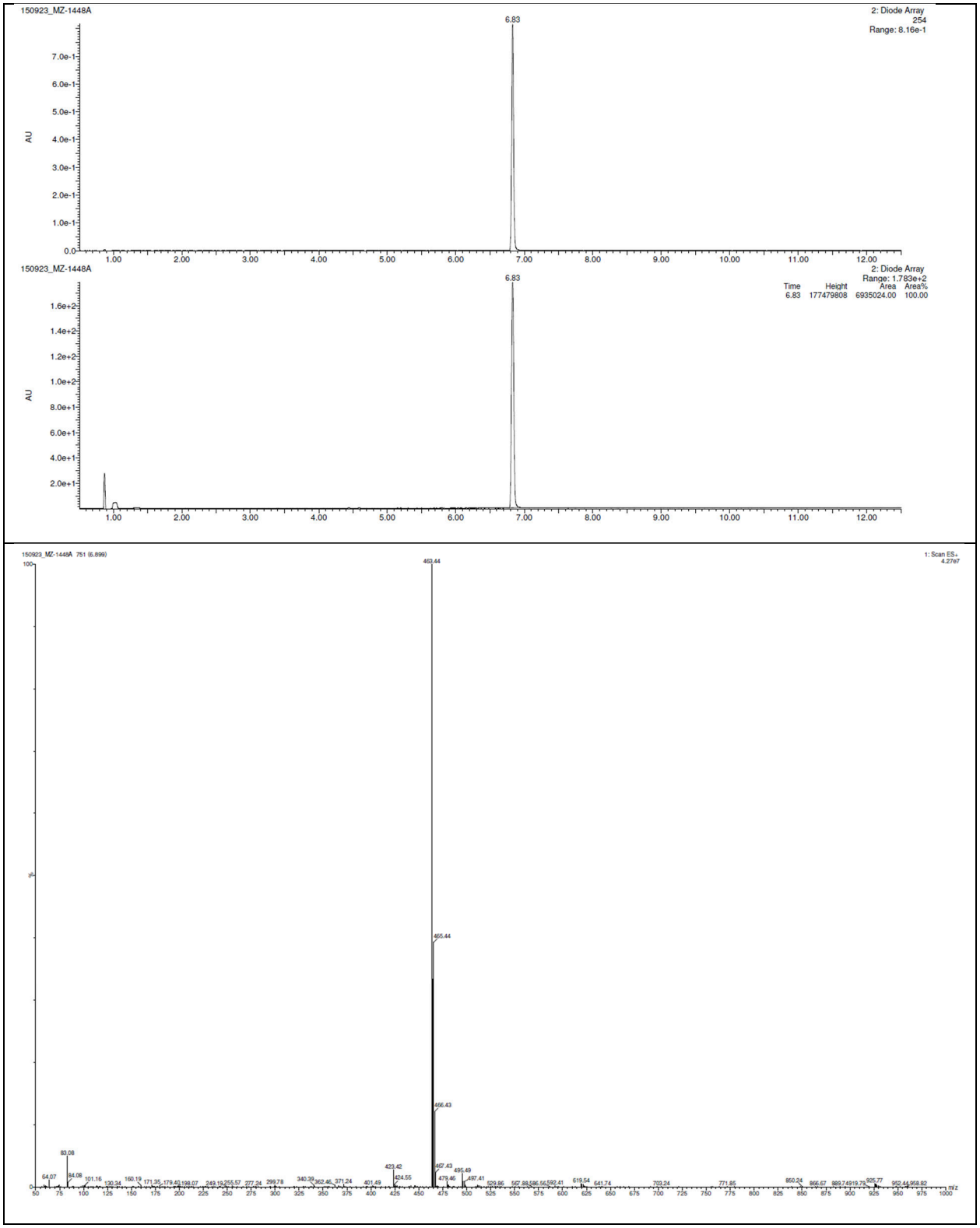

Figure S138. LC-MS assessment of purity of compound **36**.
The purity of compound **36** is 100.0% (retention time: 6.83 min corresponds to the desired compound **36**)

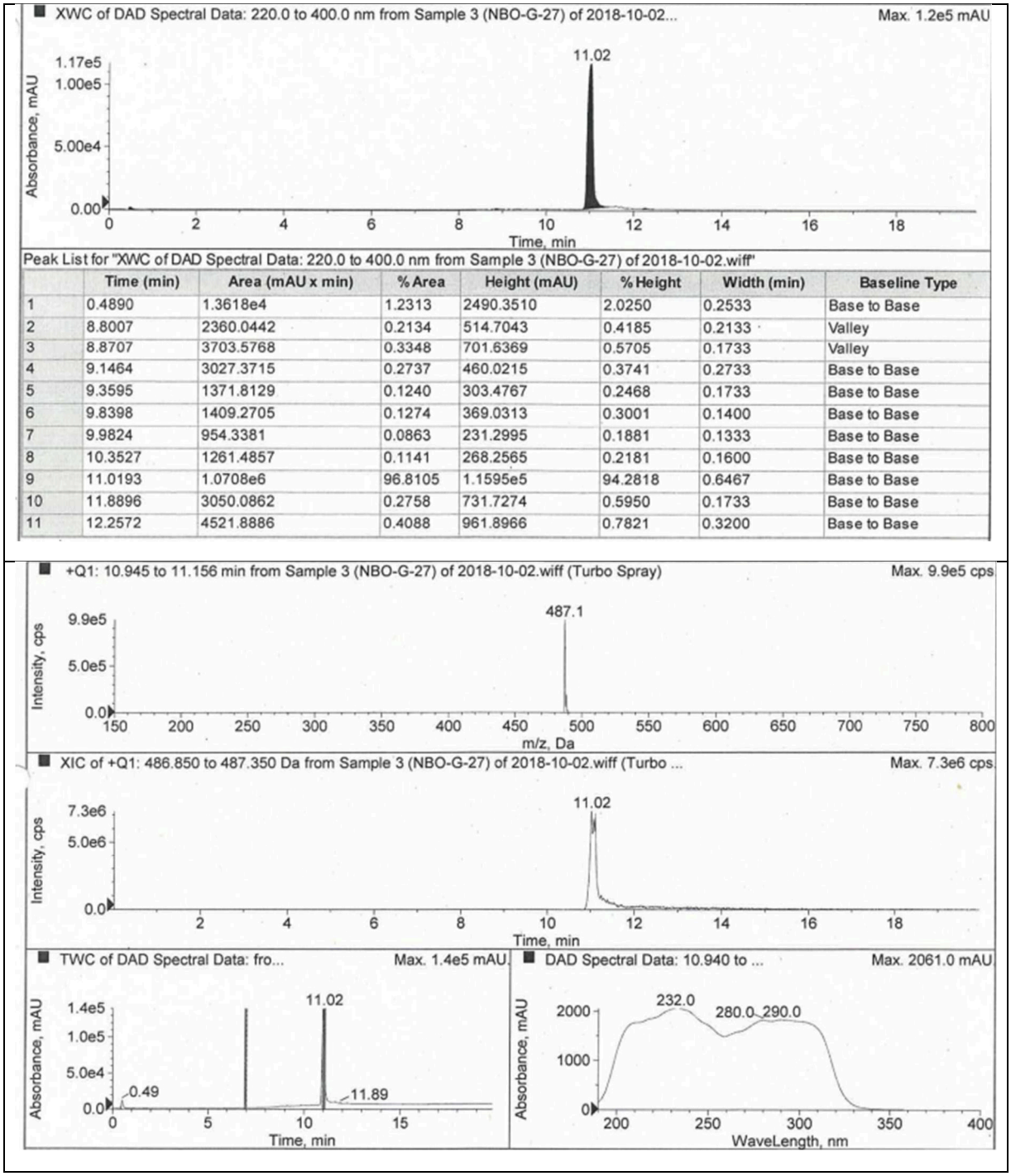

Peak List for "XWC of DAD Spectral Data: 220.0 to 400.0 nm from Sample 3 (NBO-G-27) of 2018-10-02.wiff"

	Time (min)	Area (mAU x min)	% Area	Height (mAU)	% Height	Width (min)	Baseline Type
1	0.4890	1.3618e4	1.2313	2490.3510	2.0250	0.2533	Base to Base
2	8.8007	2360.0442	0.2134	514.7043	0.4185	0.2133	Valley
3	8.8707	3703.5768	0.3348	701.6369	0.5705	0.1733	Valley
4	9.1464	3027.3715	0.2737	460.0215	0.3741	0.2733	Base to Base
5	9.3595	1371.8129	0.1240	303.4767	0.2468	0.1733	Base to Base
6	9.8398	1409.2705	0.1274	369.0313	0.3001	0.1400	Base to Base
7	9.9824	954.3381	0.0863	231.2995	0.1881	0.1333	Base to Base
8	10.3527	1261.4857	0.1141	268.2565	0.2181	0.1600	Base to Base
9	11.0193	1.0708e6	96.8105	1.1595e5	94.2818	0.6467	Base to Base
10	11.8896	3050.0862	0.2758	731.7274	0.5950	0.1733	Base to Base
11	12.2572	4521.8886	0.4088	961.8966	0.7821	0.3200	Base to Base

Figure S139. LC-MS assessment of purity of compound **43**.
The purity of compound **43** is 98.8% (retention time: 11.02 min corresponds to the desired compound **43**)

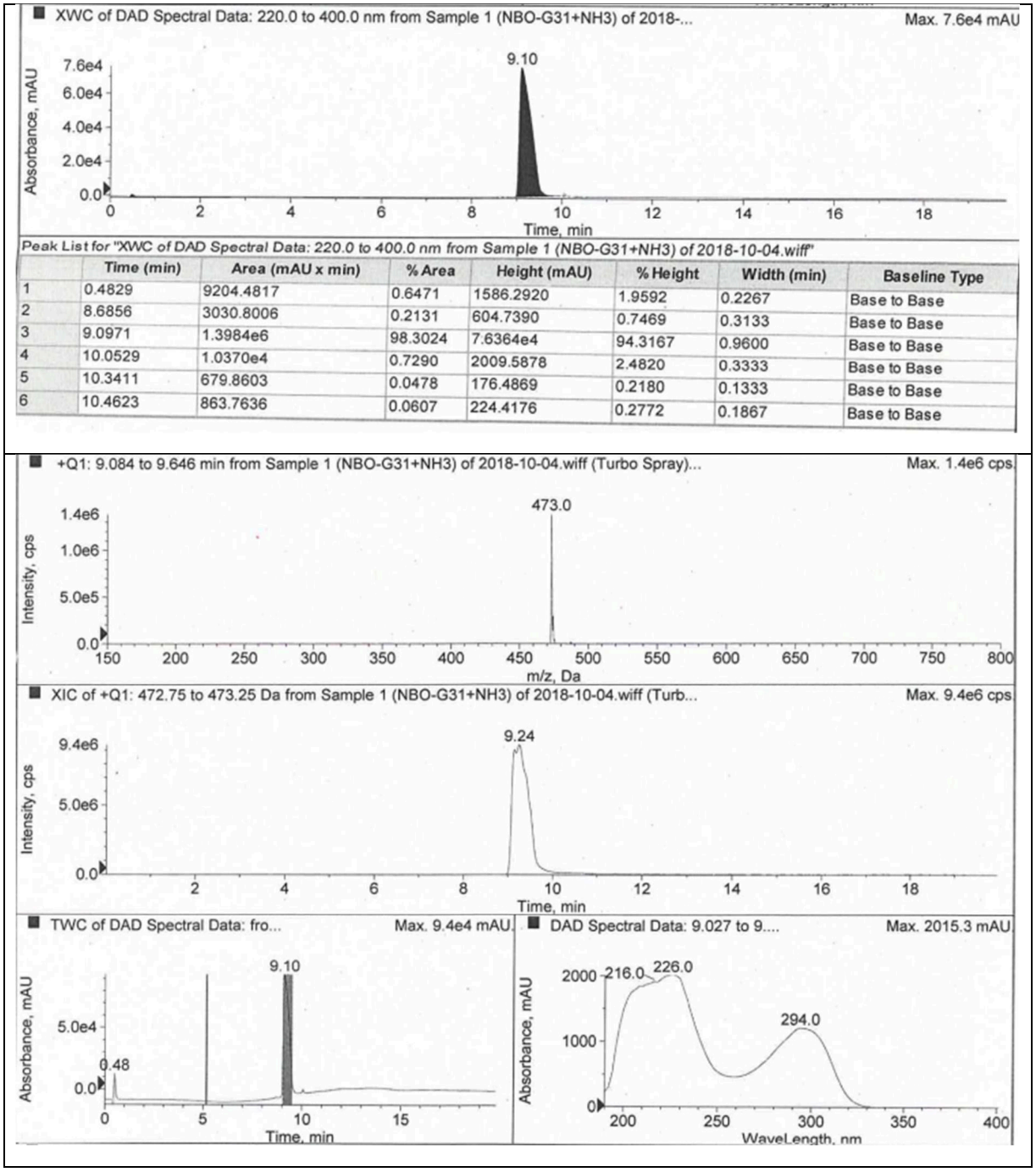

	Time (min)	Area (mAU x min)	% Area	Height (mAU)	% Height	Width (min)	Baseline Type
1	0.4829	9204.4817	0.6471	1586.2920	1.9592	0.2267	Base to Base
2	8.6856	3030.8006	0.2131	604.7390	0.7469	0.3133	Base to Base
3	9.0971	1.3984e6	98.3024	7.6364e4	94.3167	0.9600	Base to Base
4	10.0529	1.0370e4	0.7290	2009.5878	2.4820	0.3333	Base to Base
5	10.3411	679.8603	0.0478	176.4869	0.2180	0.1333	Base to Base
6	10.4623	863.7636	0.0607	224.4176	0.2772	0.1867	Base to Base

Figure S140. LC-MS assessment of purity of compound **44**.
The purity of compound **44** is 98.3% (retention time: 9.10 min corresponds to the desired compound **44**)

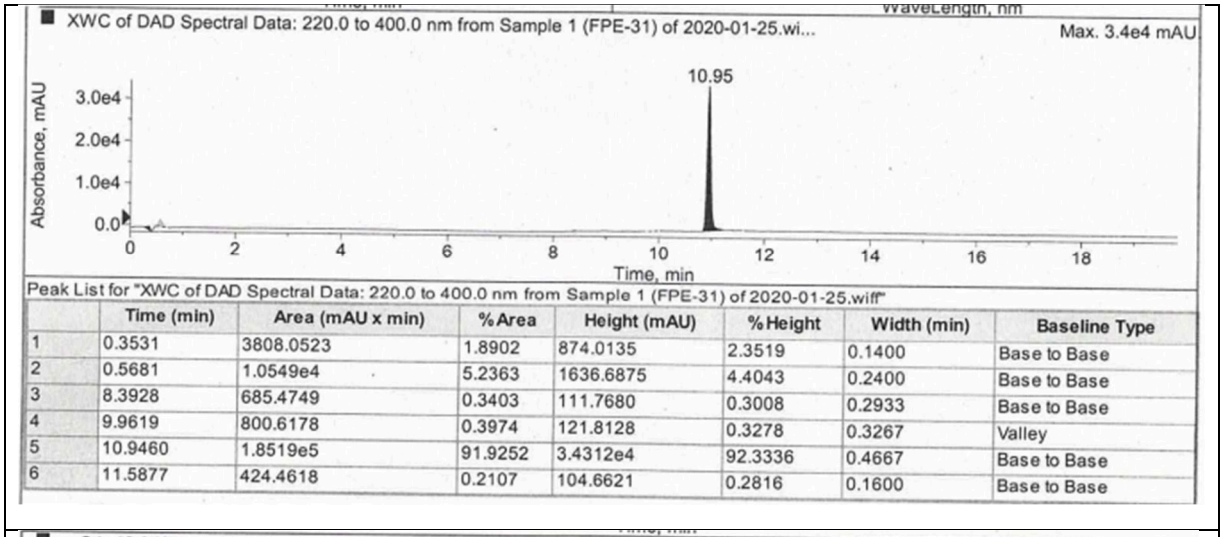

Peak List for "XWC of DAD Spectral Data: 220.0 to 400.0 nm from Sample 1 (FPE-31) of 2020-01-25.wiff"

	Time (min)	Area (mAU x min)	%Area	Height (mAU)	%Height	Width (min)	Baseline Type
1	0.3531	3808.0523	1.8902	874.0135	2.3519	0.1400	Base to Base
2	0.5681	1.0549e4	5.2363	1636.6875	4.4043	0.2400	Base to Base
3	8.3928	685.4749	0.3403	111.7680	0.3008	0.2933	Base to Base
4	9.9619	800.6178	0.3974	121.8128	0.3278	0.3267	Valley
5	10.9460	1.8519e5	91.9252	3.4312e4	92.3336	0.4667	Base to Base
6	11.5877	424.4618	0.2107	104.6621	0.2816	0.1600	Base to Base

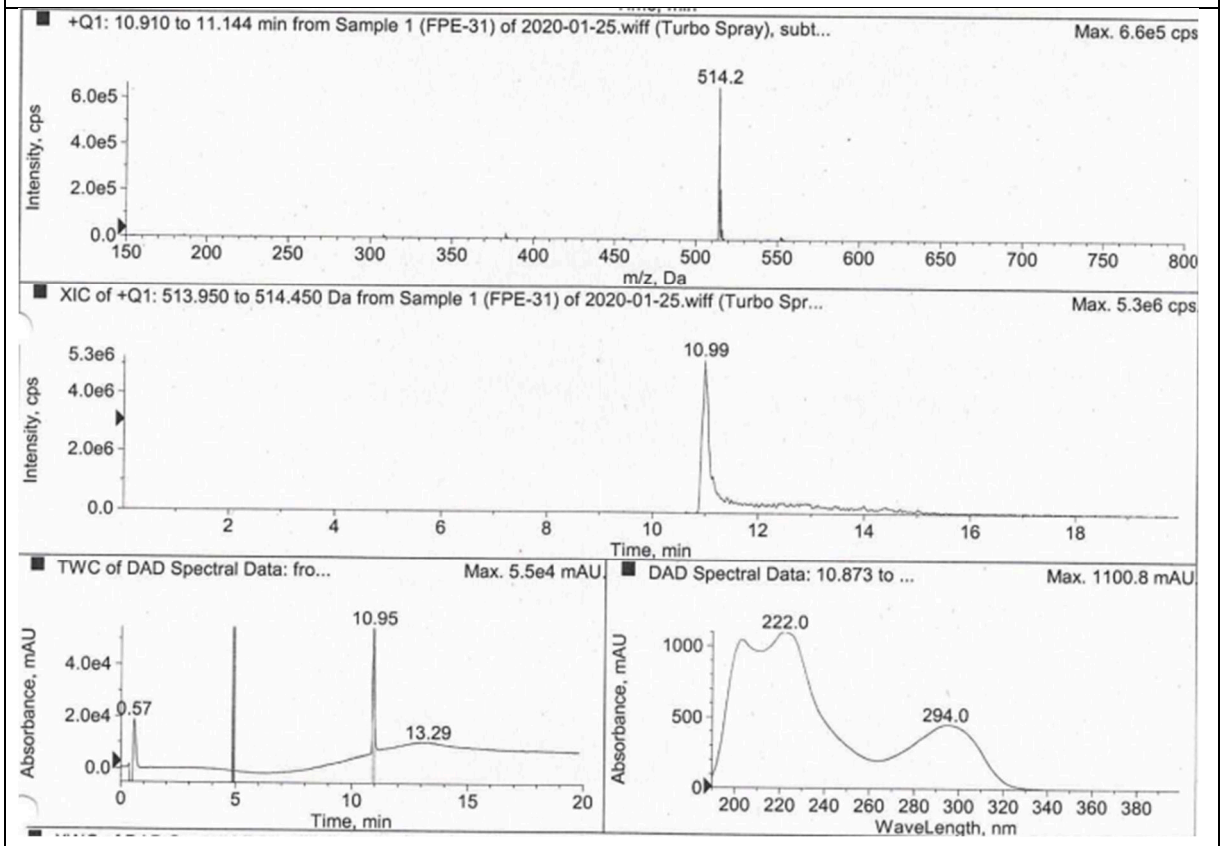

*The purity of compound **46** is 94%

Figure S141. LC-MS assessment of purity of compound **46**.
The purity of compound **46** is 94% (retention time: 10.95 min corresponds to the desired compound **46**; 2% injection peak; also see NMR spectra, Figure S64 – S65).

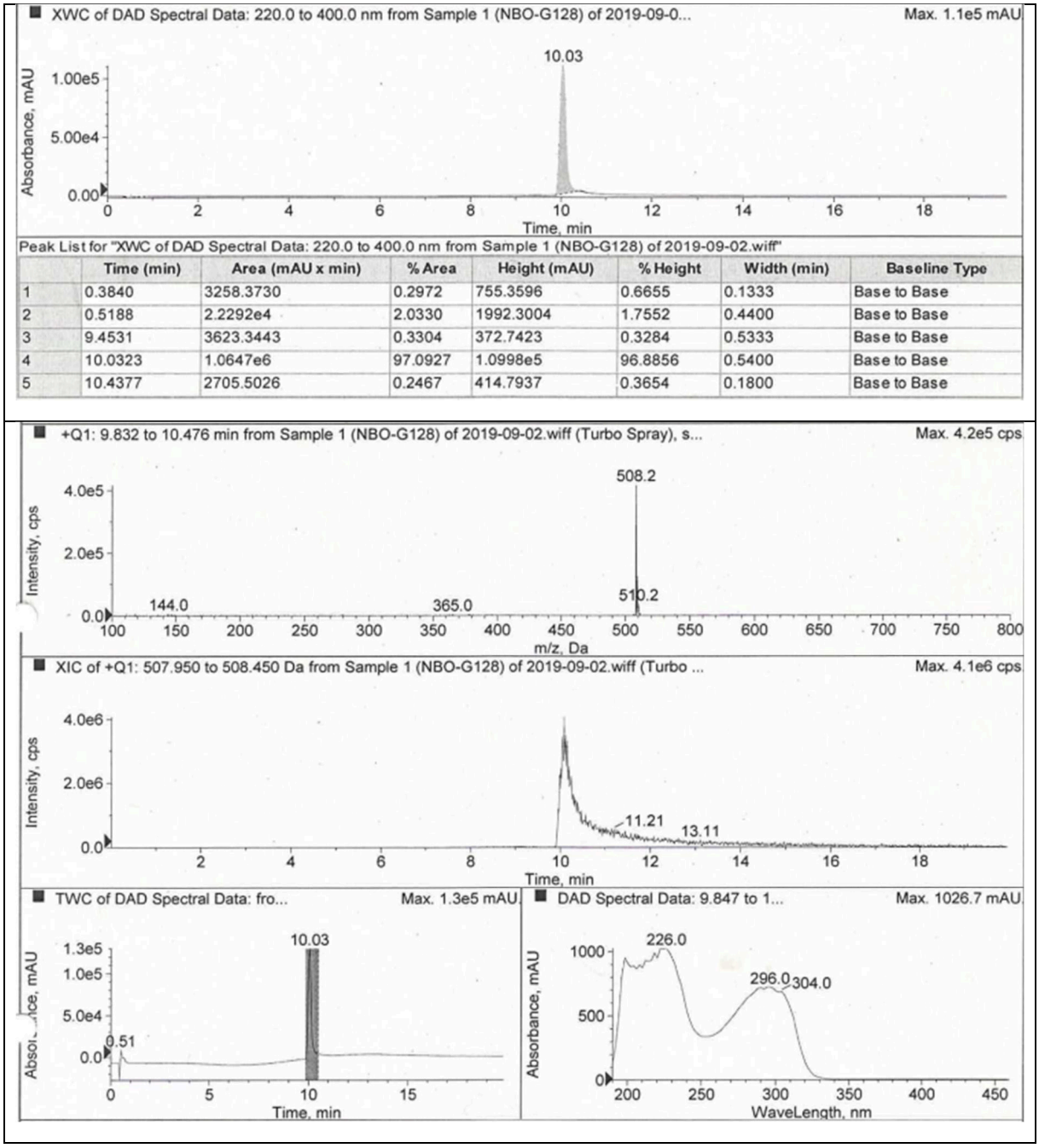

Peak List for "XWC of DAD Spectral Data: 220.0 to 400.0 nm from Sample 1 (NBO-G128) of 2019-09-02.wiff"

	Time (min)	Area (mAU x min)	% Area	Height (mAU)	% Height	Width (min)	Baseline Type
1	0.3840	3258.3730	0.2972	755.3596	0.6655	0.1333	Base to Base
2	0.5188	2.2292e4	2.0330	1992.3004	1.7552	0.4400	Base to Base
3	9.4531	3623.3443	0.3304	372.7423	0.3284	0.5333	Base to Base
4	10.0323	1.0647e6	97.0927	1.0998e5	96.8856	0.5400	Base to Base
5	10.4377	2705.5026	0.2467	414.7937	0.3654	0.1800	Base to Base

Figure S142. LC-MS assessment of purity of compound **47**.
The purity of compound **47** is 97.1% (retention time: 10.03 min corresponds to the desired compound **47**)

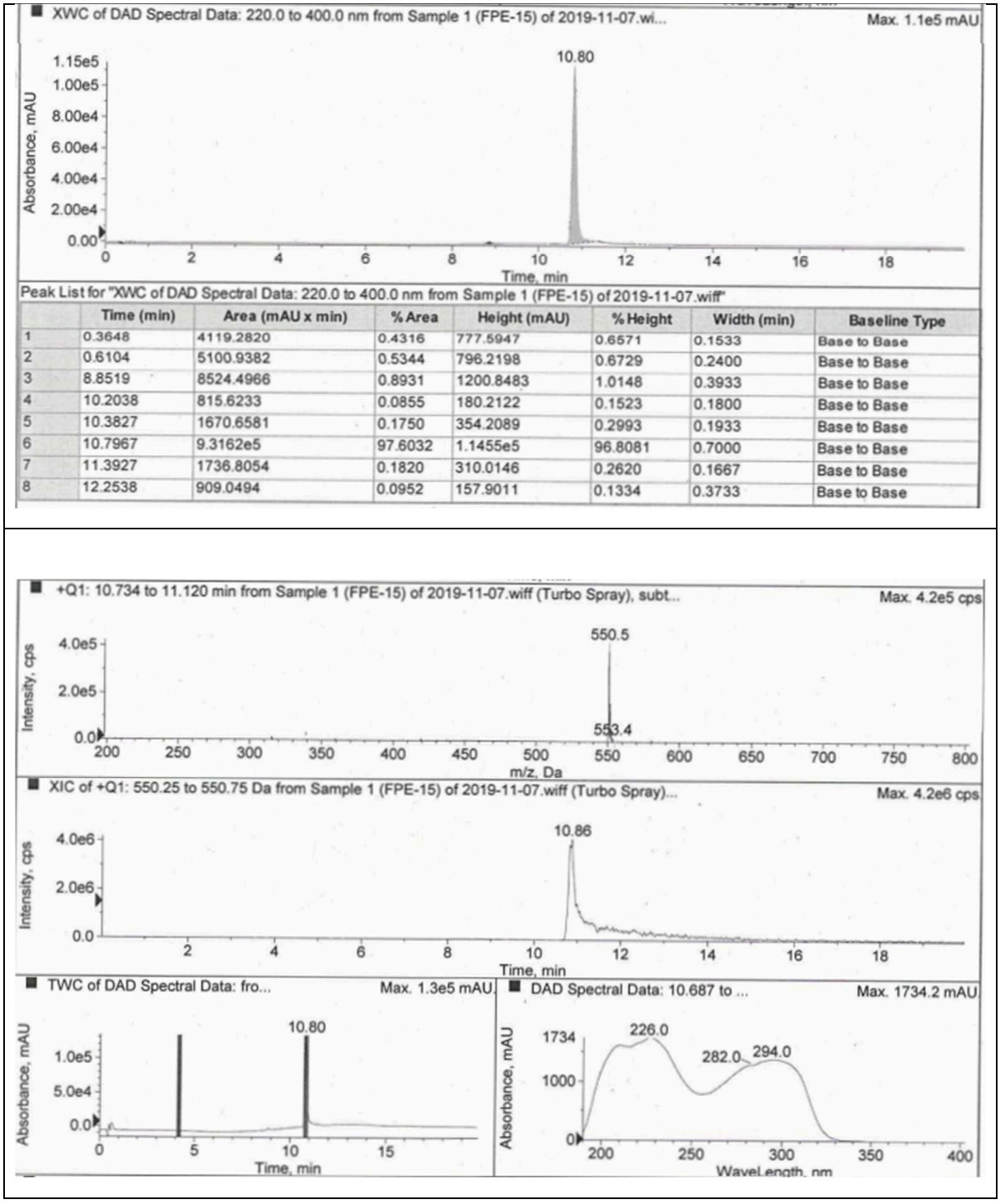

	Time (min)	Area (mAU x min)	% Area	Height (mAU)	% Height	Width (min)	Baseline Type
1	0.3648	4119.2820	0.4316	777.5947	0.6571	0.1533	Base to Base
2	0.6104	5100.9382	0.5344	796.2198	0.6729	0.2400	Base to Base
3	8.8519	8524.4966	0.8931	1200.8483	1.0148	0.3933	Base to Base
4	10.2038	815.6233	0.0855	180.2122	0.1523	0.1800	Base to Base
5	10.3827	1670.6581	0.1750	354.2089	0.2993	0.1933	Base to Base
6	10.7967	9.3162e5	97.6032	1.1455e5	96.8081	0.7000	Base to Base
7	11.3927	1736.8054	0.1820	310.0146	0.2620	0.1667	Base to Base
8	12.2538	909.0494	0.0952	157.9011	0.1334	0.3733	Base to Base

Figure S143. LC-MS assessment of purity of compound **49**.
The purity of compound **49** is 97.6% (retention time: 10.79 min corresponds to the desired compound **49**)

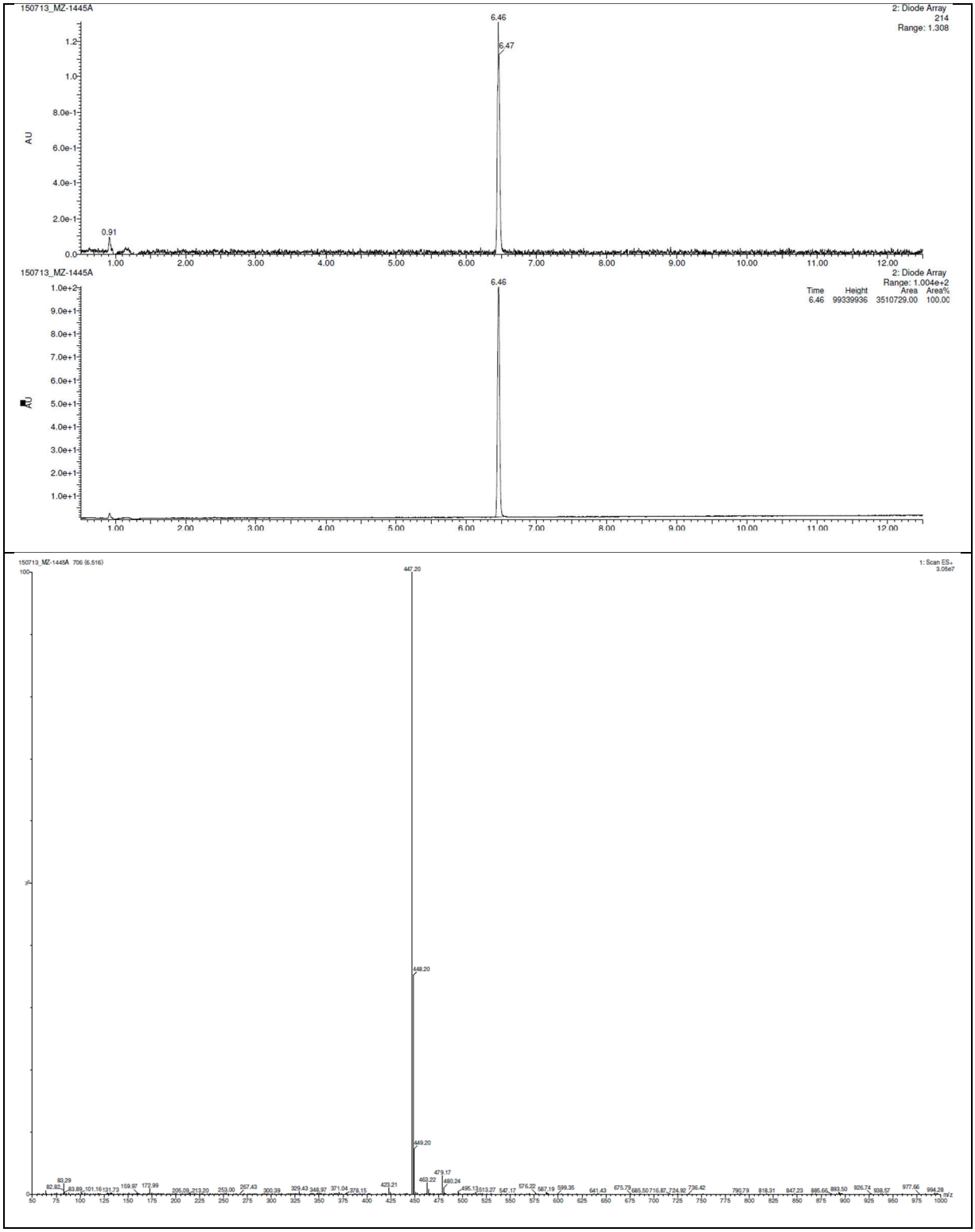

Figure S144. LC-MS assessment of purity of compound **50**.
The purity of compound **50** is 100.0% (retention time: 6.46 min corresponds to the desired compound **50**)

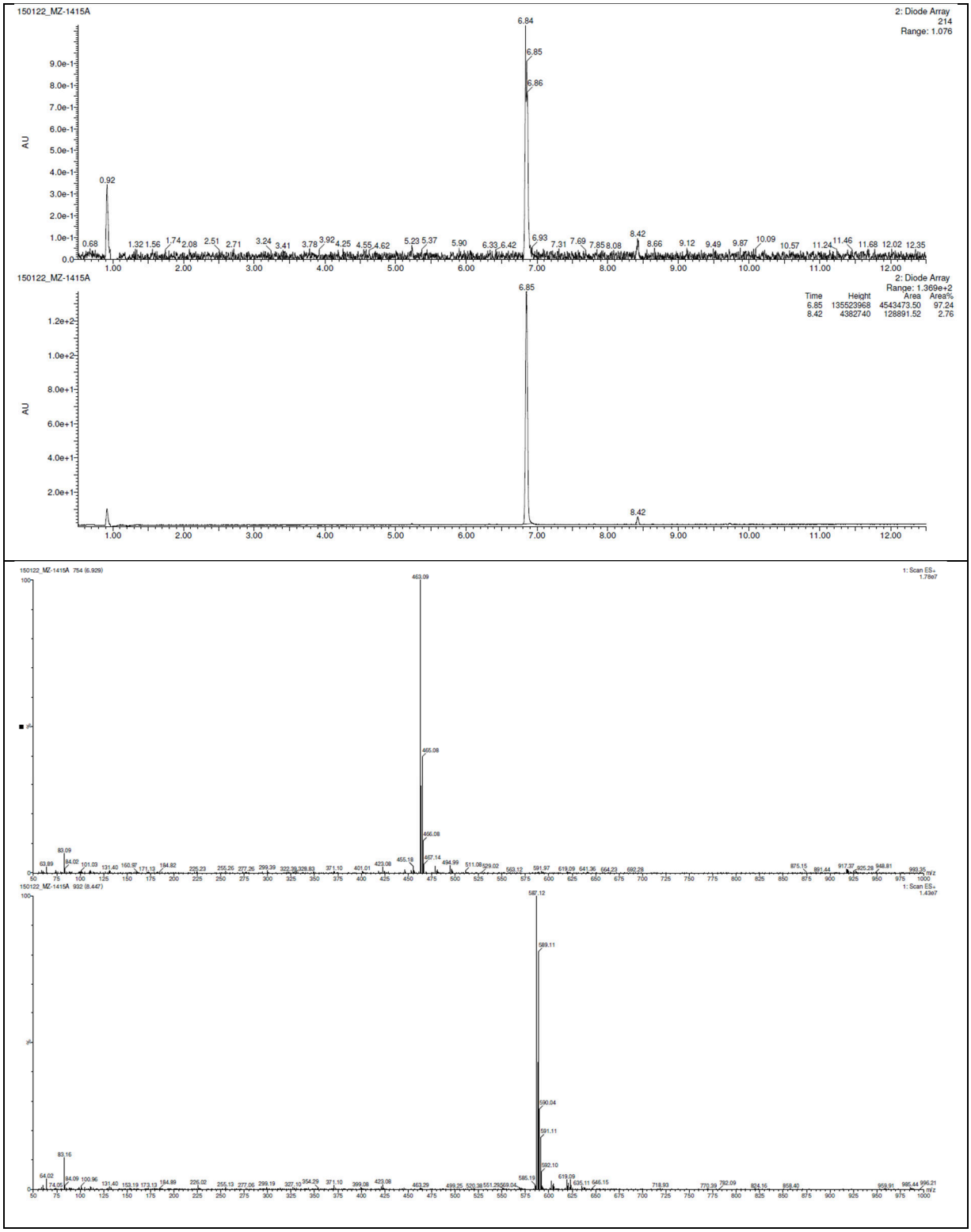

Figure S145. LC-MS assessment of purity of compound **51**.
The purity of compound **51** is 97.2% (retention time: 6.85 min corresponds to the desired compound **51**)

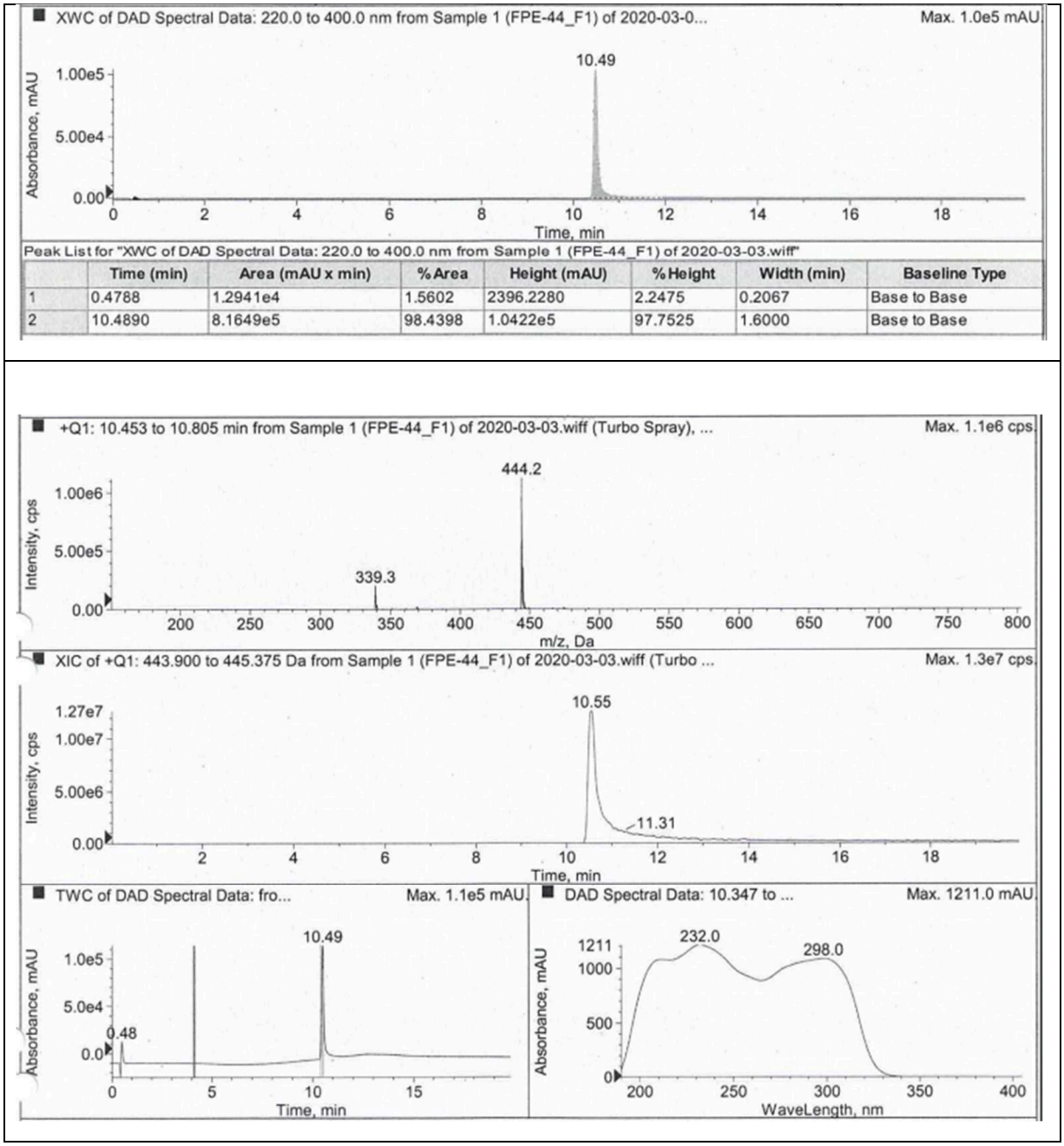

	Time (min)	Area (mAU x min)	% Area	Height (mAU)	% Height	Width (min)	Baseline Type
1	0.4788	1.2941e4	1.5602	2396.2280	2.2475	0.2067	Base to Base
2	10.4890	8.1649e5	98.4398	1.0422e5	97.7525	1.6000	Base to Base

Figure S146. LC-MS assessment of purity of compound **54**.
The purity of compound **54** is 98.4% (retention time: 10.49 min corresponds to the desired compound **54**)

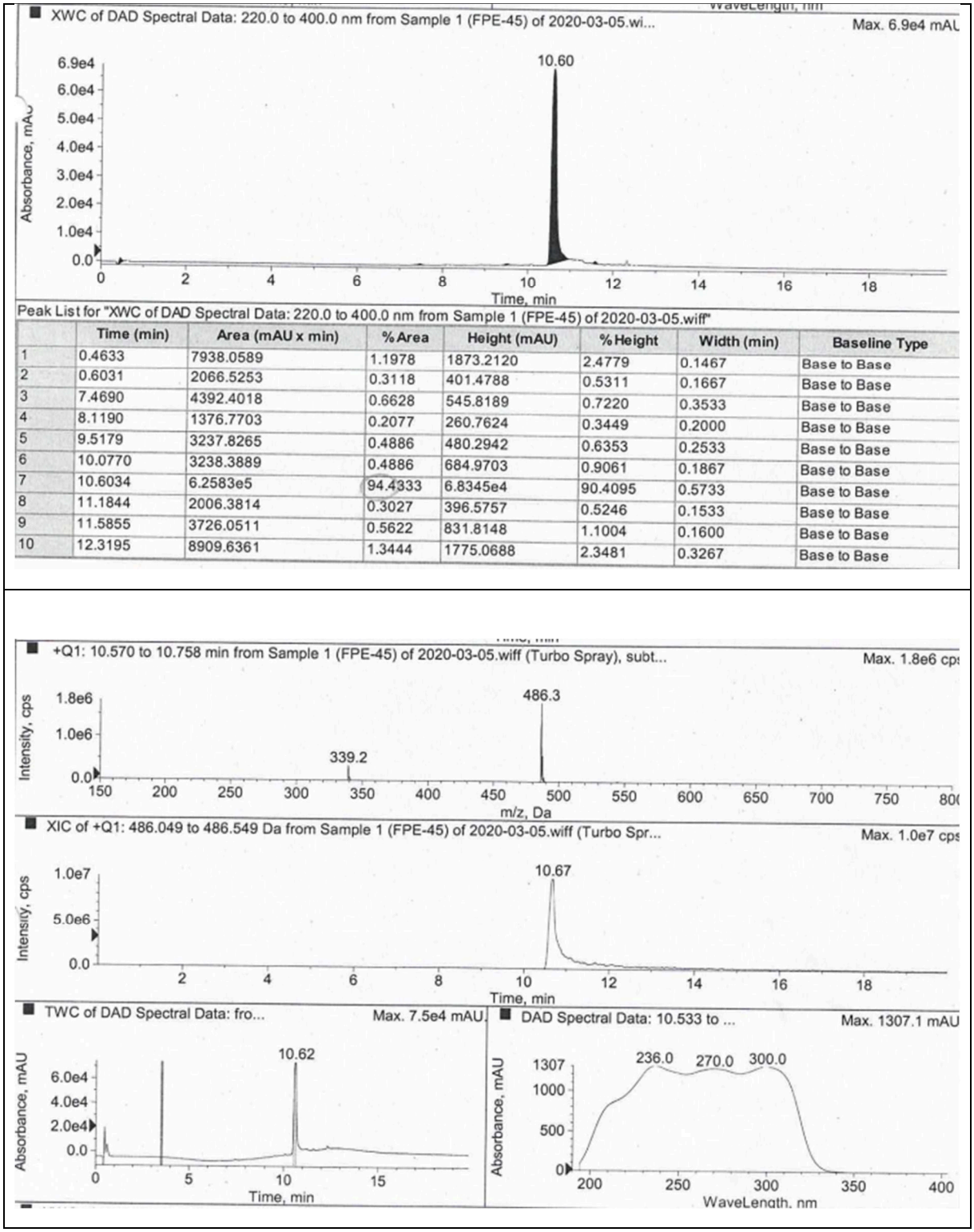

	Time (min)	Area (mAU x min)	% Area	Height (mAU)	% Height	Width (min)	Baseline Type
1	0.4633	7938.0589	1.1978	1873.2120	2.4779	0.1467	Base to Base
2	0.6031	2066.5253	0.3118	401.4788	0.5311	0.1667	Base to Base
3	7.4690	4392.4018	0.6628	545.8189	0.7220	0.3533	Base to Base
4	8.1190	1376.7703	0.2077	260.7624	0.3449	0.2000	Base to Base
5	9.5179	3237.8265	0.4886	480.2942	0.6353	0.2533	Base to Base
6	10.0770	3238.3889	0.4886	684.9703	0.9061	0.1867	Base to Base
7	10.6034	6.2583e5	94.4333	6.8345e4	90.4095	0.5733	Base to Base
8	11.1844	2006.3814	0.3027	396.5757	0.5246	0.1533	Base to Base
9	11.5855	3726.0511	0.5622	831.8148	1.1004	0.1600	Base to Base
10	12.3195	8909.6361	1.3444	1775.0688	2.3481	0.3267	Base to Base

Figure S147. LC-MS assessment of purity of compound **55**.
The purity of compound **55** is 94.4% (retention time: 10.60 min corresponds to the desired compound **55**)

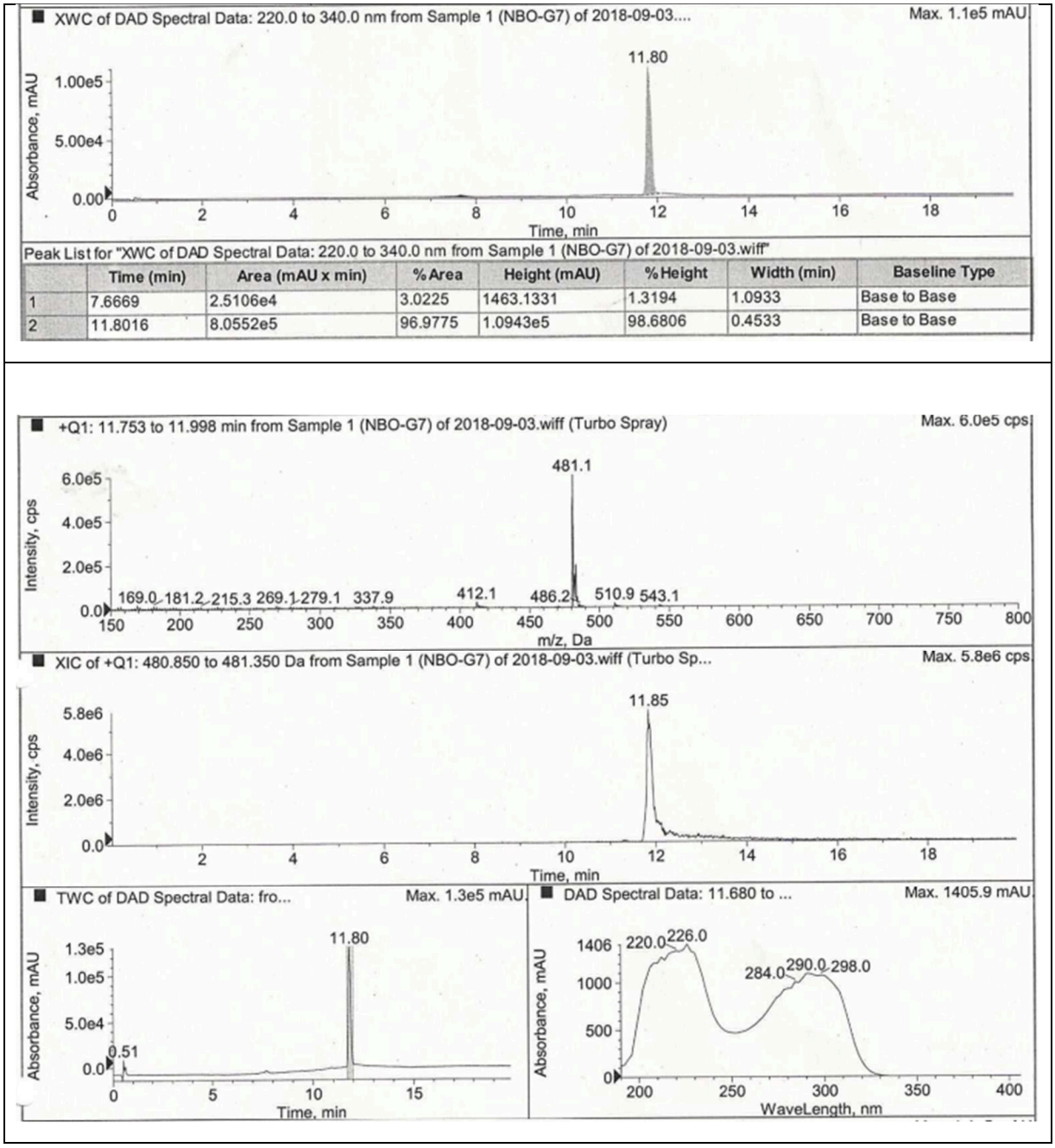

	Time (min)	Area (mAU x min)	% Area	Height (mAU)	% Height	Width (min)	Baseline Type
1	7.6669	2.5106e4	3.0225	1463.1331	1.3194	1.0933	Base to Base
2	11.8016	8.0552e5	96.9775	1.0943e5	98.6806	0.4533	Base to Base

Figure S148. LC-MS assessment of purity of compound **58**.
The purity of compound **58** is 96.9% (retention time: 11.80 min corresponds to the desired compound **58**)

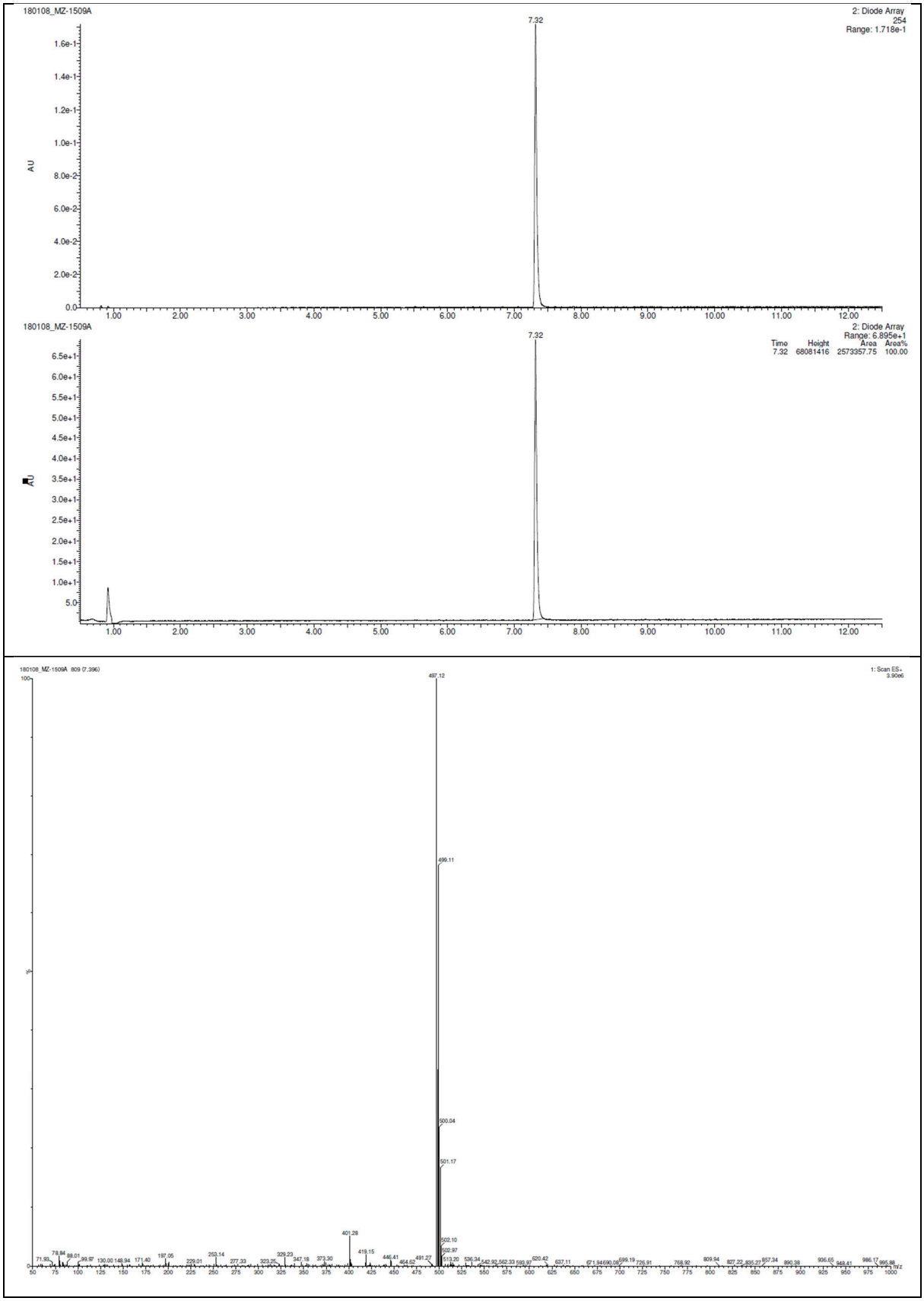

Figure S149. LC-MS assessment of purity of compound **59**.
The purity of compound **59** is 100.0% (retention time: 7.32 min corresponds to the desired compound **59**)

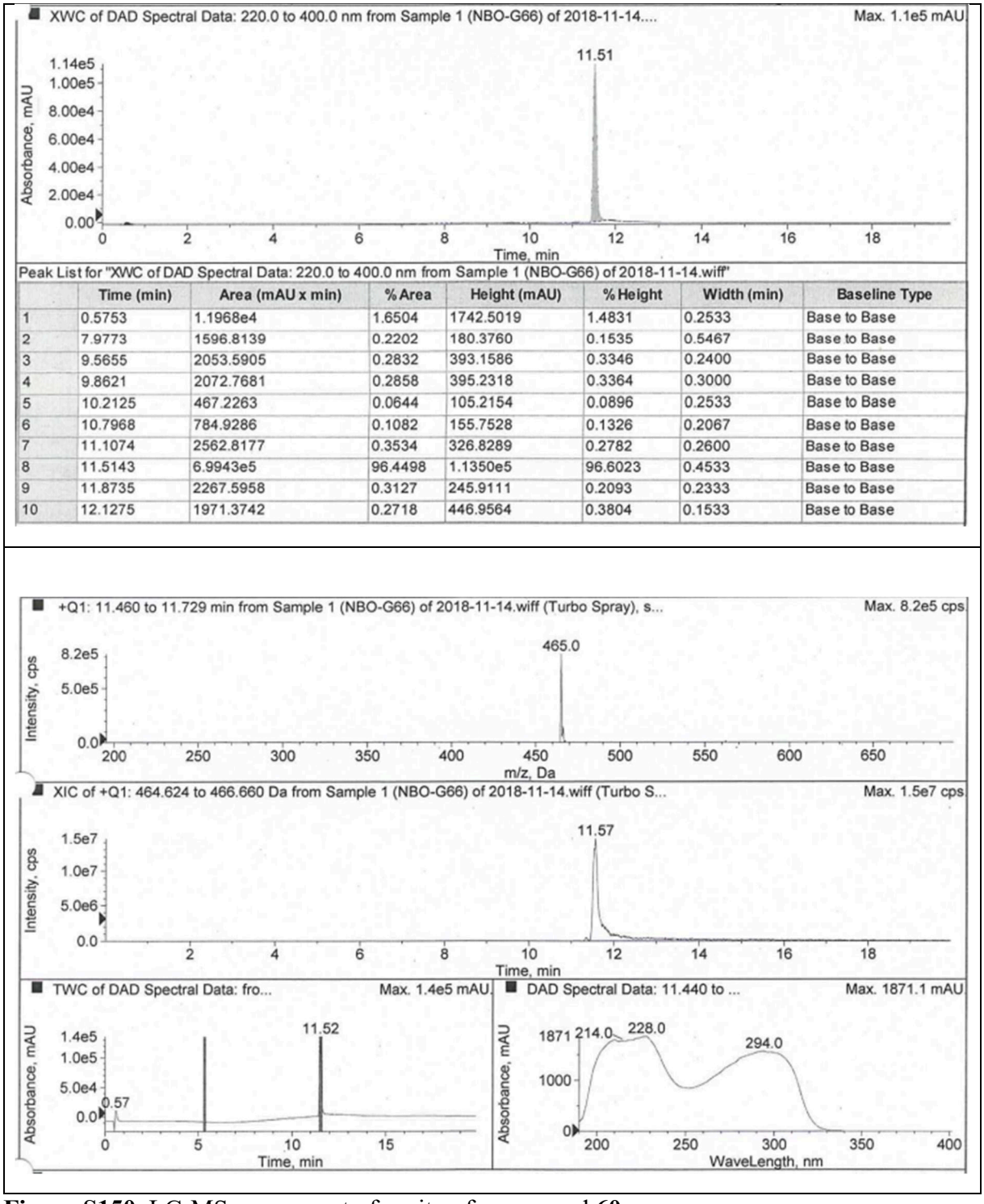

Peak List for "XWC of DAD Spectral Data: 220.0 to 400.0 nm from Sample 1 (NBO-G66) of 2018-11-14.wiff"

	Time (min)	Area (mAU x min)	% Area	Height (mAU)	% Height	Width (min)	Baseline Type
1	0.5753	1.1968e4	1.6504	1742.5019	1.4831	0.2533	Base to Base
2	7.9773	1596.8139	0.2202	180.3760	0.1535	0.5467	Base to Base
3	9.5655	2053.5905	0.2832	393.1586	0.3346	0.2400	Base to Base
4	9.8621	2072.7681	0.2858	395.2318	0.3364	0.3000	Base to Base
5	10.2125	467.2263	0.0644	105.2154	0.0896	0.2533	Base to Base
6	10.7968	784.9286	0.1082	155.7528	0.1326	0.2067	Base to Base
7	11.1074	2562.8177	0.3534	326.8289	0.2782	0.2600	Base to Base
8	11.5143	6.9943e5	96.4498	1.1350e5	96.6023	0.4533	Base to Base
9	11.8735	2267.5958	0.3127	245.9111	0.2093	0.2333	Base to Base
10	12.1275	1971.3742	0.2718	446.9564	0.3804	0.1533	Base to Base

Figure S150. LC-MS assessment of purity of compound **60**.
The purity of compound **60** is 96.4% (retention time: 11.51 min corresponds to the desired compound **60**)

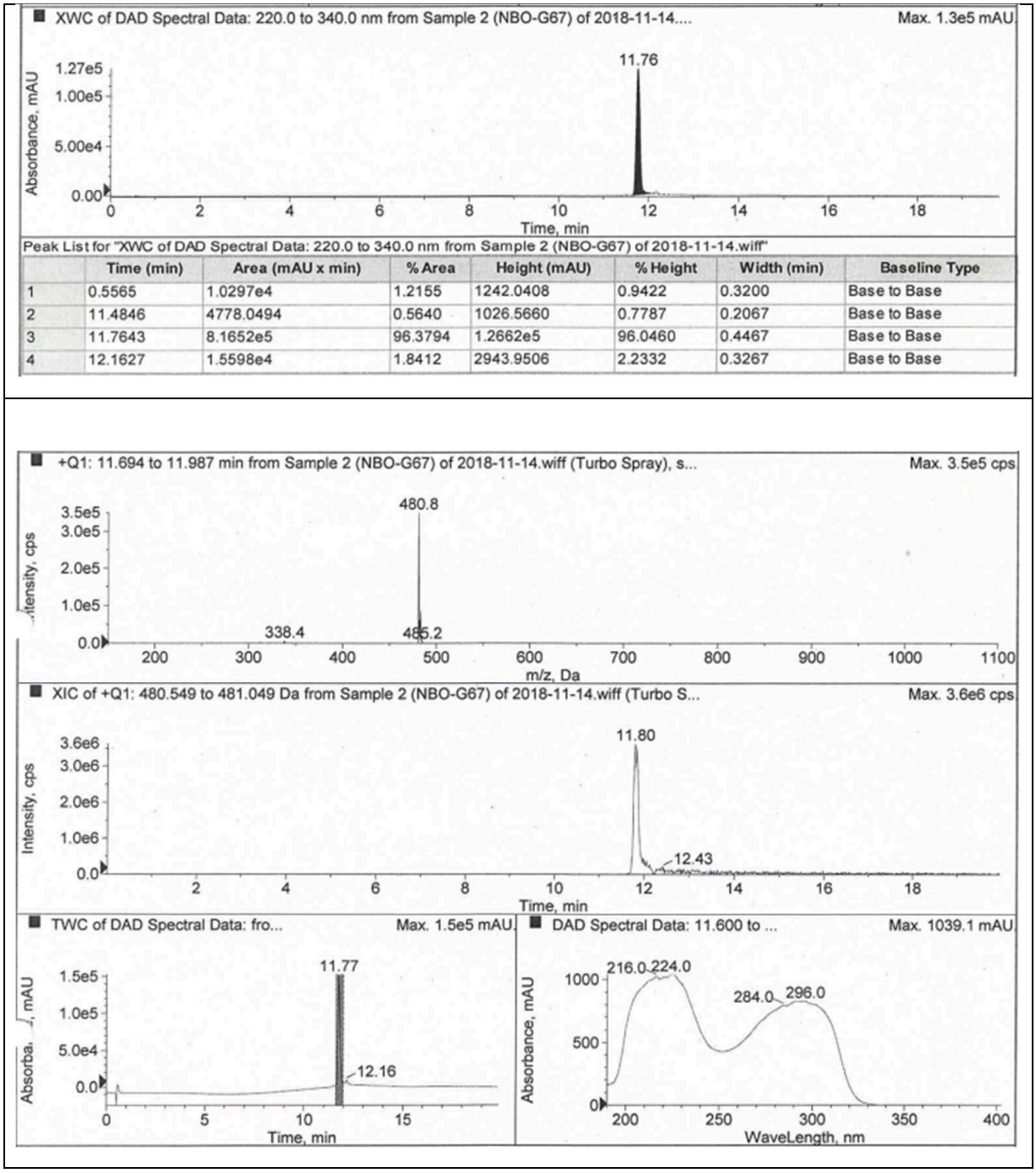

	Time (min)	Area (mAU x min)	% Area	Height (mAU)	% Height	Width (min)	Baseline Type
1	0.5565	1.0297e4	1.2155	1242.0408	0.9422	0.3200	Base to Base
2	11.4846	4778.0494	0.5640	1026.5660	0.7787	0.2067	Base to Base
3	11.7643	8.1652e5	96.3794	1.2662e5	96.0460	0.4467	Base to Base
4	12.1627	1.5598e4	1.8412	2943.9506	2.2332	0.3267	Base to Base

Figure S151. LC-MS assessment of purity of compound **61**.
The purity of compound **61** is 96.4% (retention time: 11.76 min corresponds to the desired compound **61**)

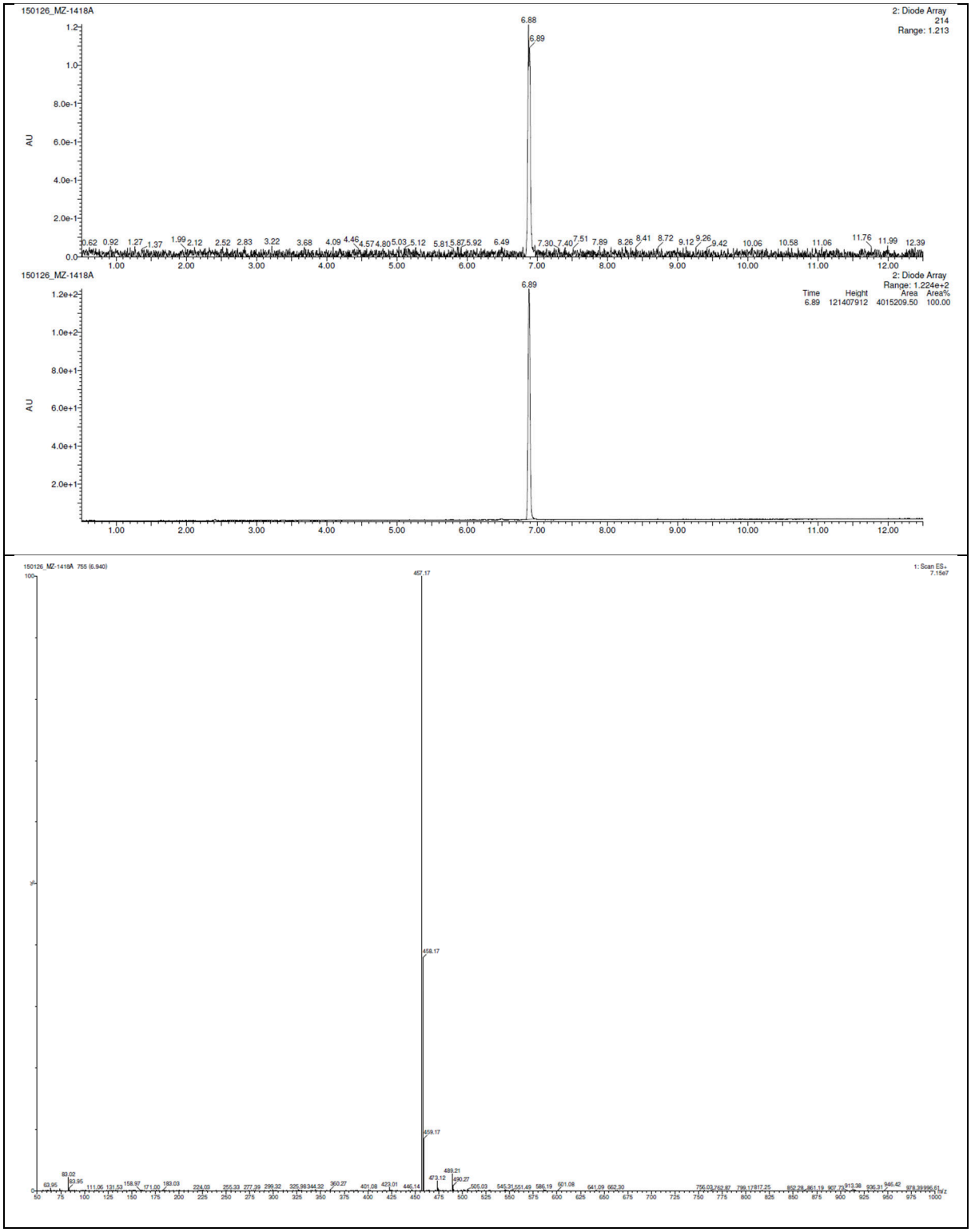

Figure S152. LC-MS assessment of purity of compound **64**.
The purity of compound **64** is 100.0% (retention time: 6.89 min corresponds to the desired compound **64**)

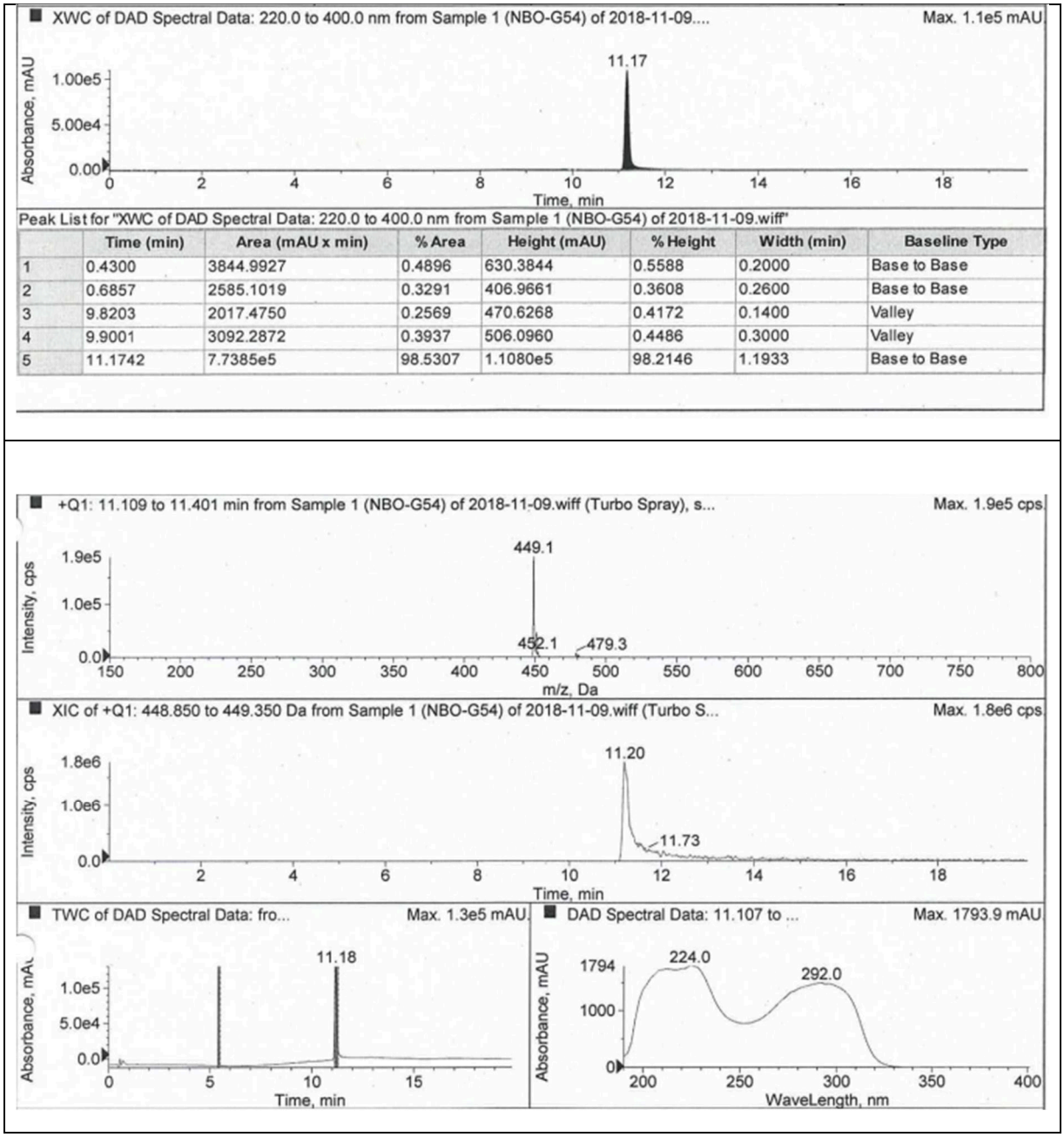

	Time (min)	Area (mAU x min)	% Area	Height (mAU)	% Height	Width (min)	Baseline Type
1	0.4300	3844.9927	0.4896	630.3844	0.5588	0.2000	Base to Base
2	0.6857	2585.1019	0.3291	406.9661	0.3608	0.2600	Base to Base
3	9.8203	2017.4750	0.2569	470.6268	0.4172	0.1400	Valley
4	9.9001	3092.2872	0.3937	506.0960	0.4486	0.3000	Valley
5	11.1742	7.7385e5	98.5307	1.1080e5	98.2146	1.1933	Base to Base

Figure S153. LC-MS assessment of purity of compound **74**.
The purity of compound **74** is 98.5% (retention time: 11.17 min corresponds to the desired compound **74**)

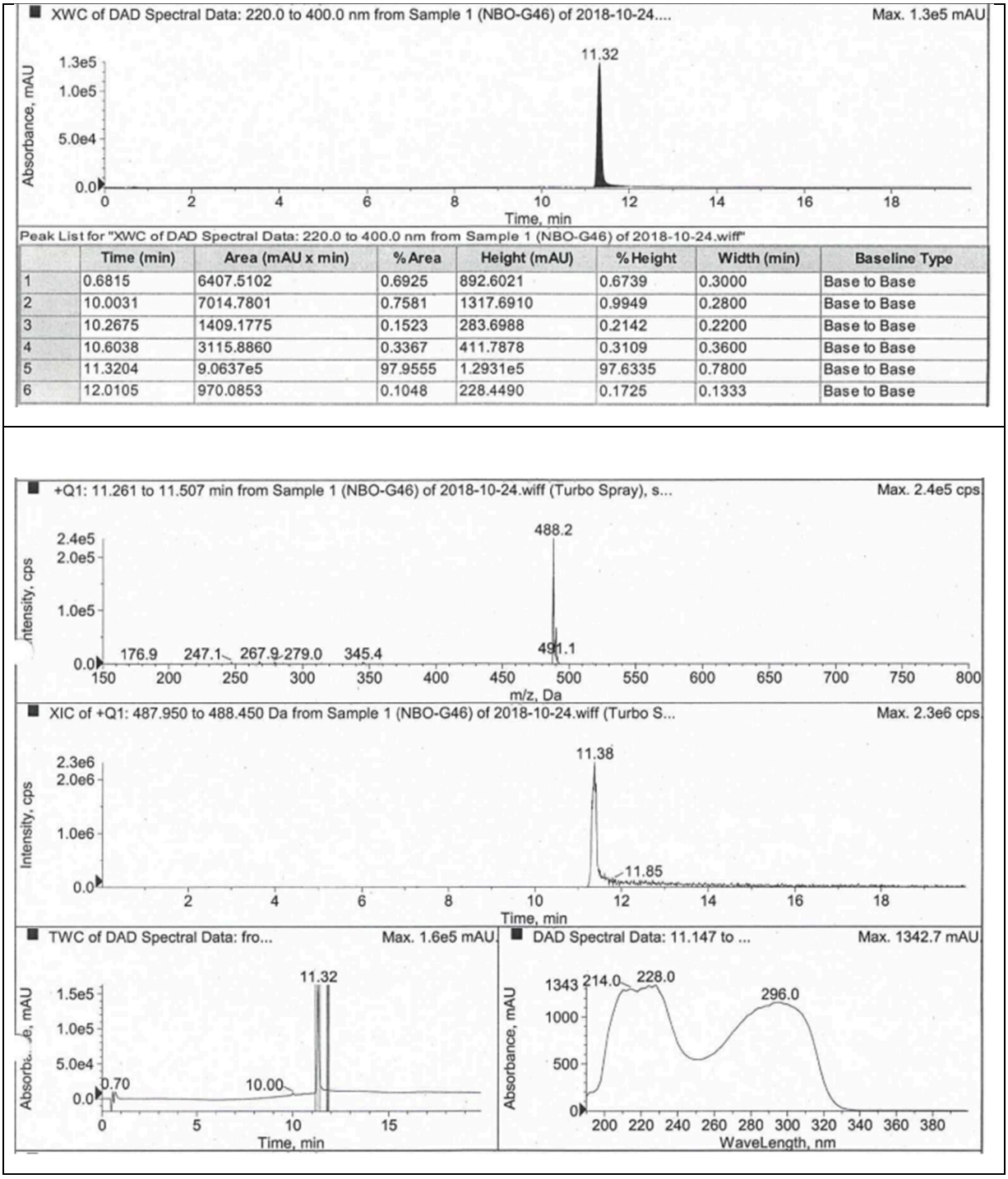

Peak List for "XWC of DAD Spectral Data: 220.0 to 400.0 nm from Sample 1 (NBO-G46) of 2018-10-24.wiff"

	Time (min)	Area (mAU x min)	% Area	Height (mAU)	% Height	Width (min)	Baseline Type
1	0.6815	6407.5102	0.6925	892.6021	0.6739	0.3000	Base to Base
2	10.0031	7014.7801	0.7581	1317.6910	0.9949	0.2800	Base to Base
3	10.2675	1409.1775	0.1523	283.6988	0.2142	0.2200	Base to Base
4	10.6038	3115.8860	0.3367	411.7878	0.3109	0.3600	Base to Base
5	11.3204	9.0637e5	97.9555	1.2931e5	97.6335	0.7800	Base to Base
6	12.0105	970.0853	0.1048	228.4490	0.1725	0.1333	Base to Base

Figure S154. LC-MS assessment of purity of compound **76**.
The purity of compound **76** is 97.9% (retention time: 11.32 min corresponds to the desired compound **76**)

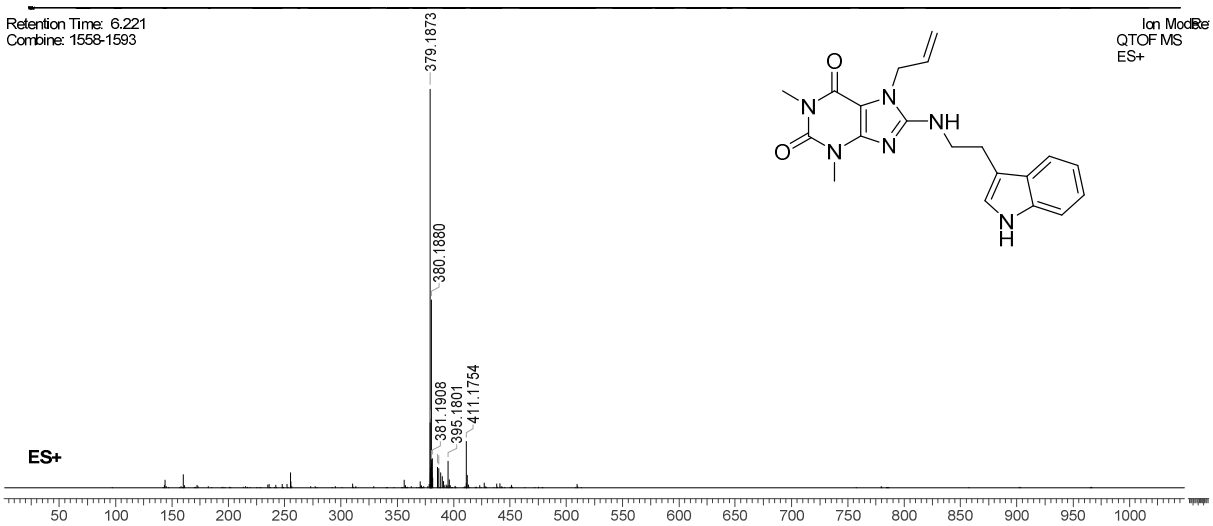

Figure **S155.** HR-MS assessment of purity of compound **24**. HR-MS (ESI-QTOF) calculated for $C_{20}H_{23}N_6O_2$ $[M+H]^+$: 379.1882; found: 379.1873.

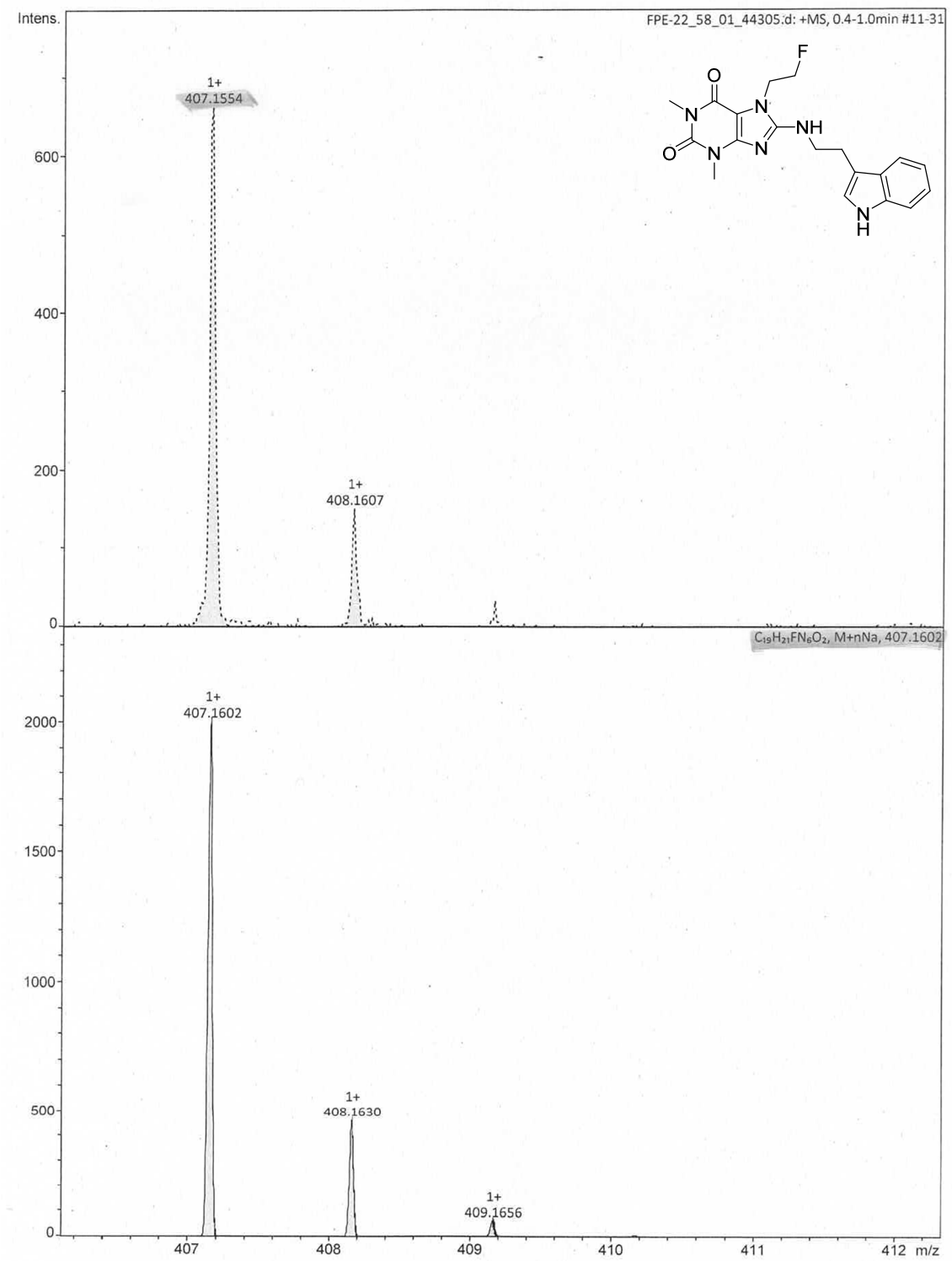

Figure **S156.** HR-MS assessment of purity of compound **30**. HR-MS (ESI-QTOF) calculated for $C_{19}H_{21}FN_6O_2Na$ $[M+Na]^+$: 407.1608; found: 407.1602.

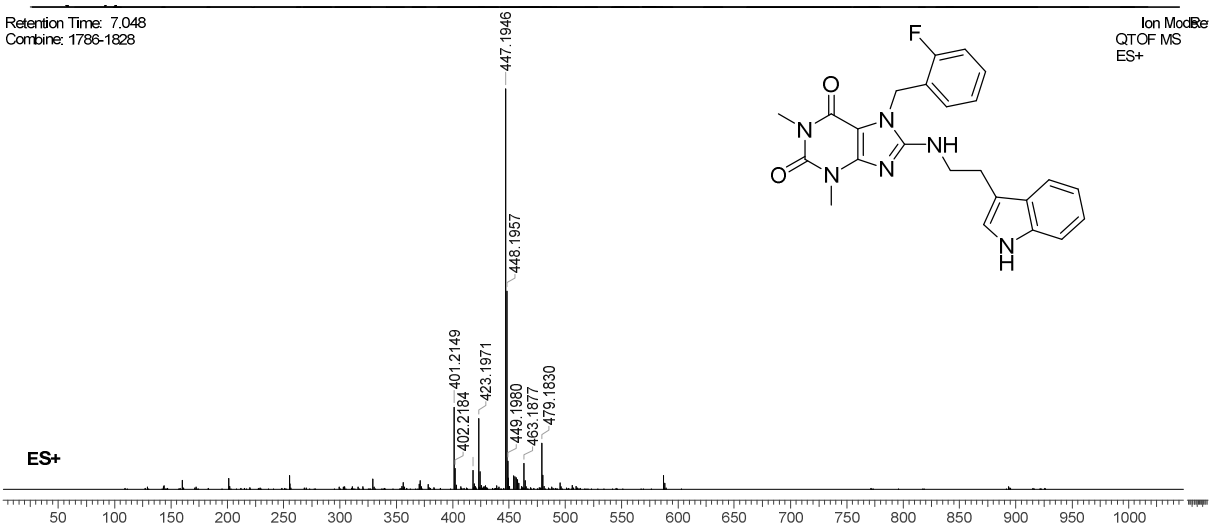

Figure **S157.** HR-MS assessment of purity of compound **32**. HR-MS (ESI-QTOF) calculated for $C_{24}H_{24}FN_6O_2$ $[M+H]^+$: 447.1945; found: 447.1946.

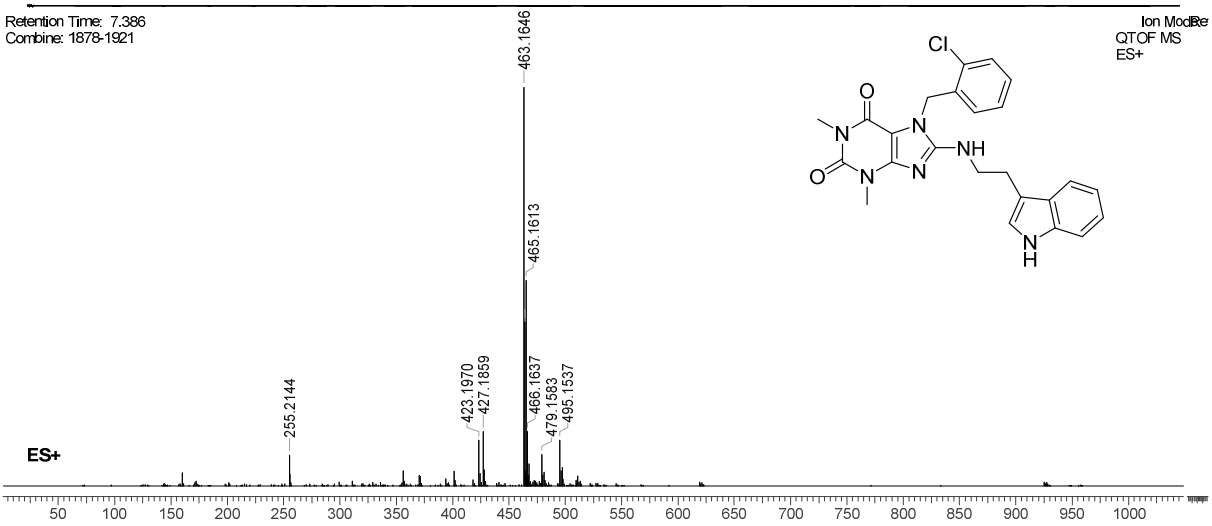

Figure **S158.** HR-MS assessment of purity of compound **33.** HR-MS (ESI-QTOF) calculated for $C_{24}H_{24}ClN_6O_2$ $[M+H]^+$: 463.1649; found: 463.1646.

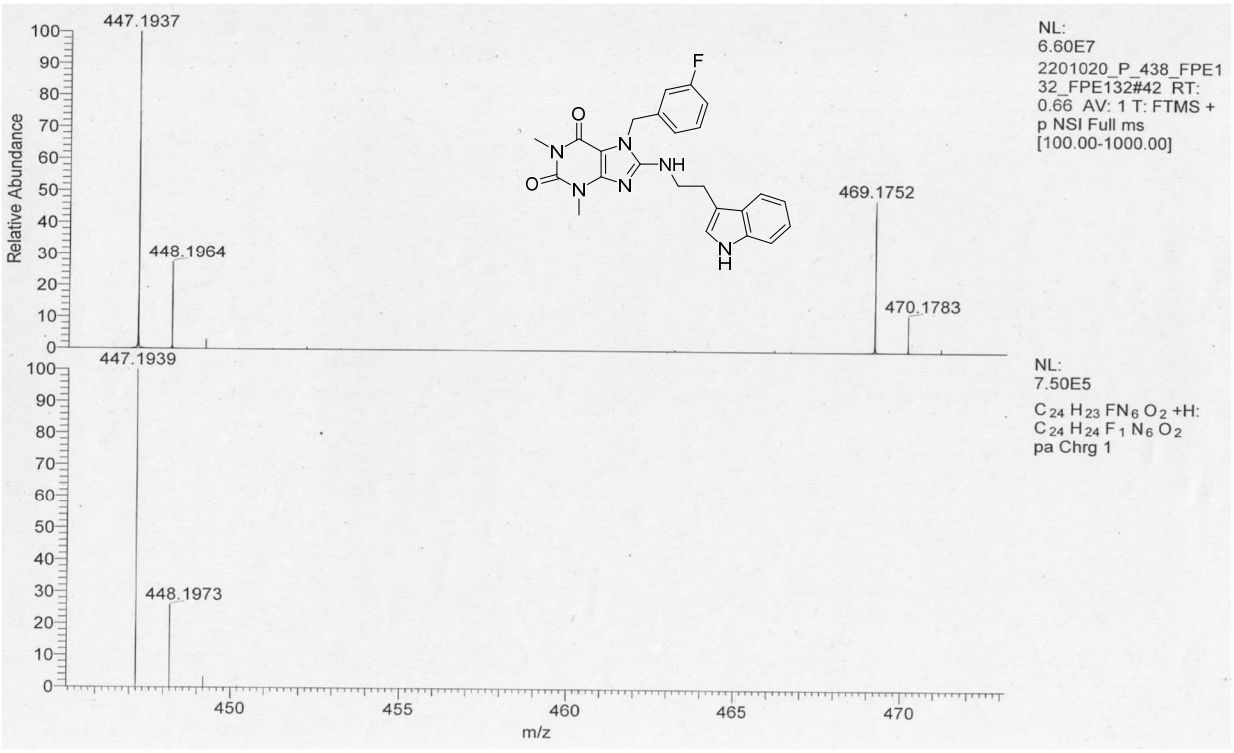

Figure **S159**. HR-MS assessment of purity of compound **35**. HR-MS (ESI-QTOF) calculated for $C_{24}H_{24}FN_6O_2$ $[M+H]^+$: 447.1945; found: 447.1937.

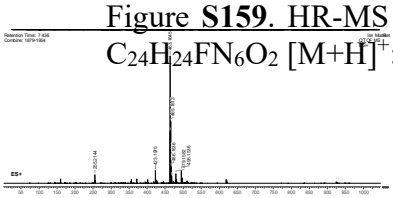

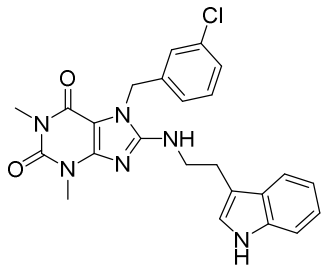

Figure **S160**. HR-MS assessment of purity of compound **36.** HR-MS (ESI-QTOF) calculated for $C_{24}H_{24}ClN_6O_2$ $[M+H]^+$: 463.1649, found: 463.1645.

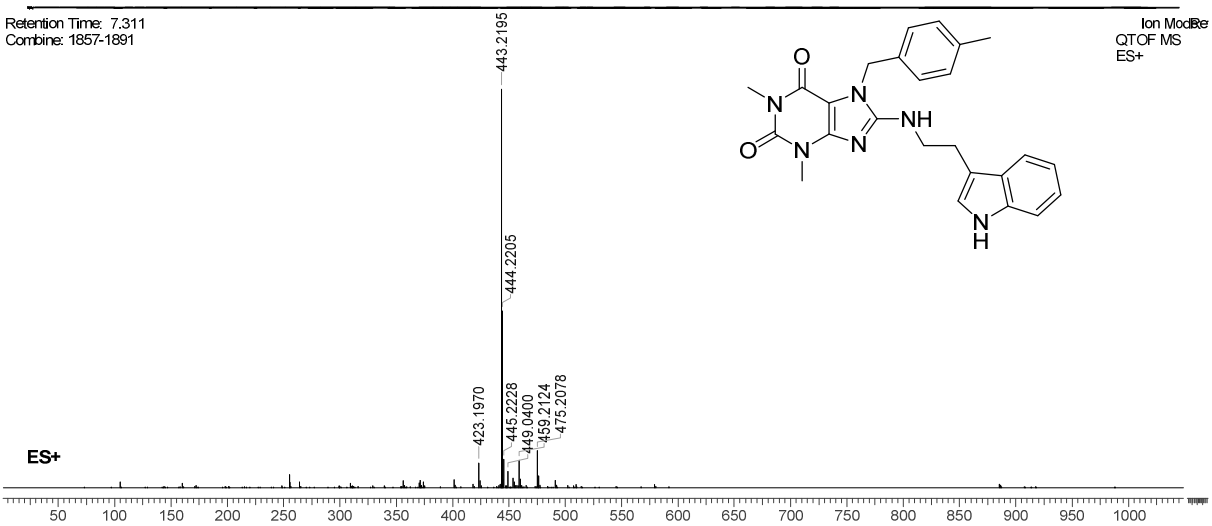

Figure **S161.** HR-MS assessment of purity of compound **39**. HR-MS (ESI/Q-TOF): m/z calcd for $C_{25}H_{27}N_6O_2$ $[M+H]^+$ 443.2195, found 443.2195

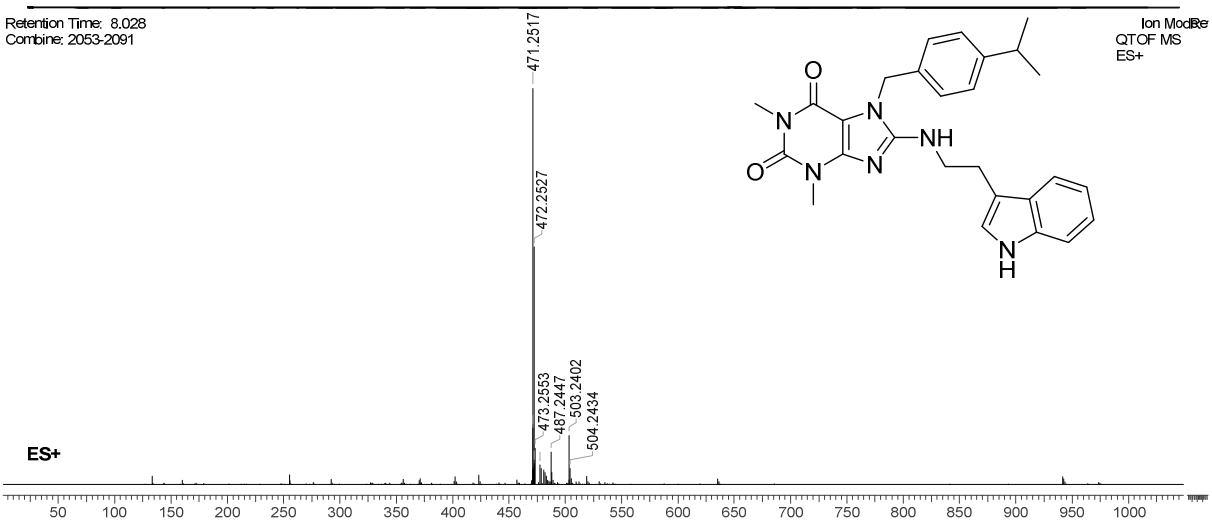

Figure **S162**. HR-MS assessment of purity of compound **42**. HR-MS (ESI-QTOF) calculated for $C_{27}H_{31}N_6O_2$ $[M+H]^+$: 471.2508, found: 471.2517.

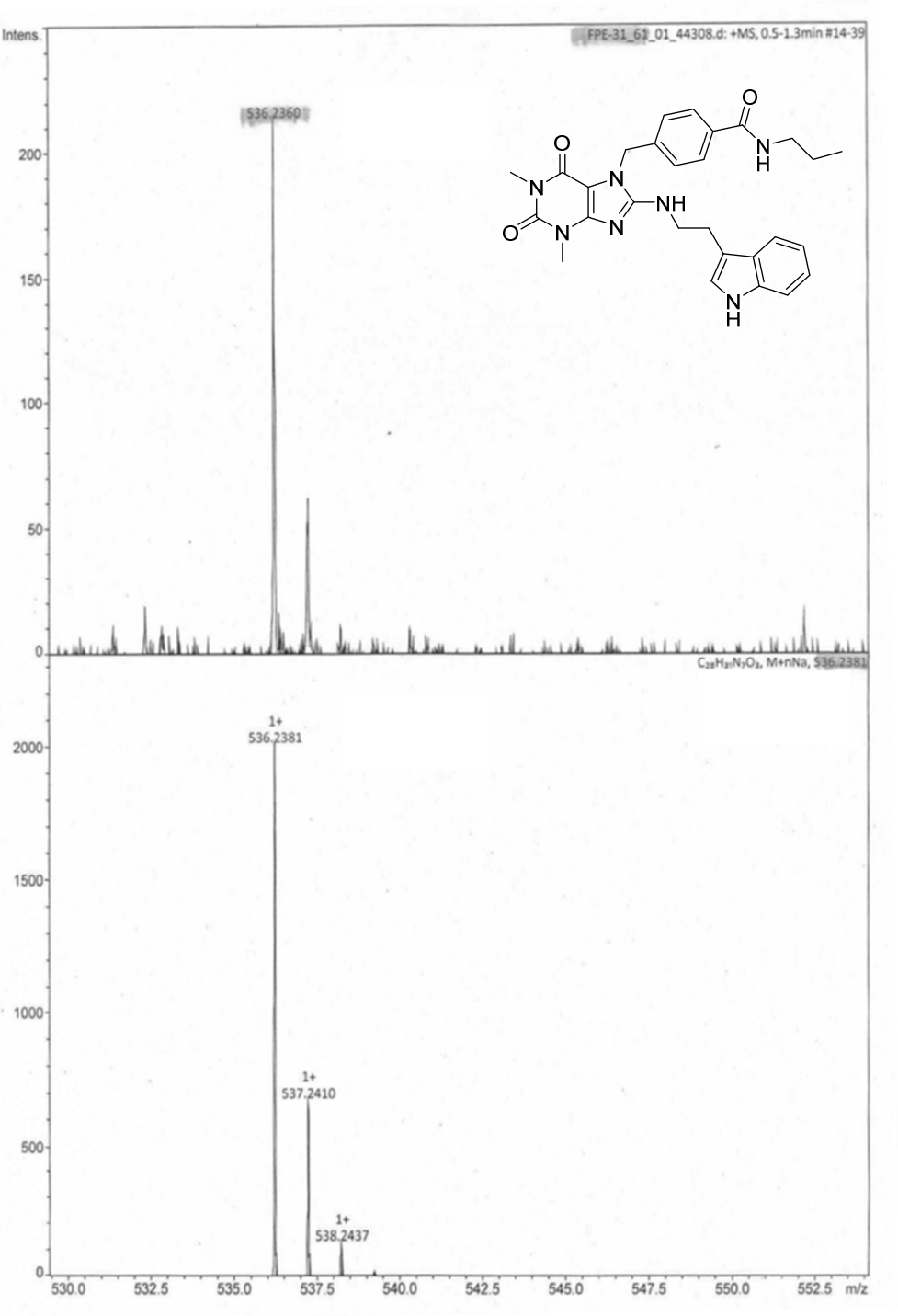

Figure **S163.** HR-MS assessment of purity of compound **46**. HR-MS (ESI-QTOF) calculated for $C_{28}H_{31}N_7O_3Na$ $[M+Na]^+$: 536.2381, found: 536.2360.

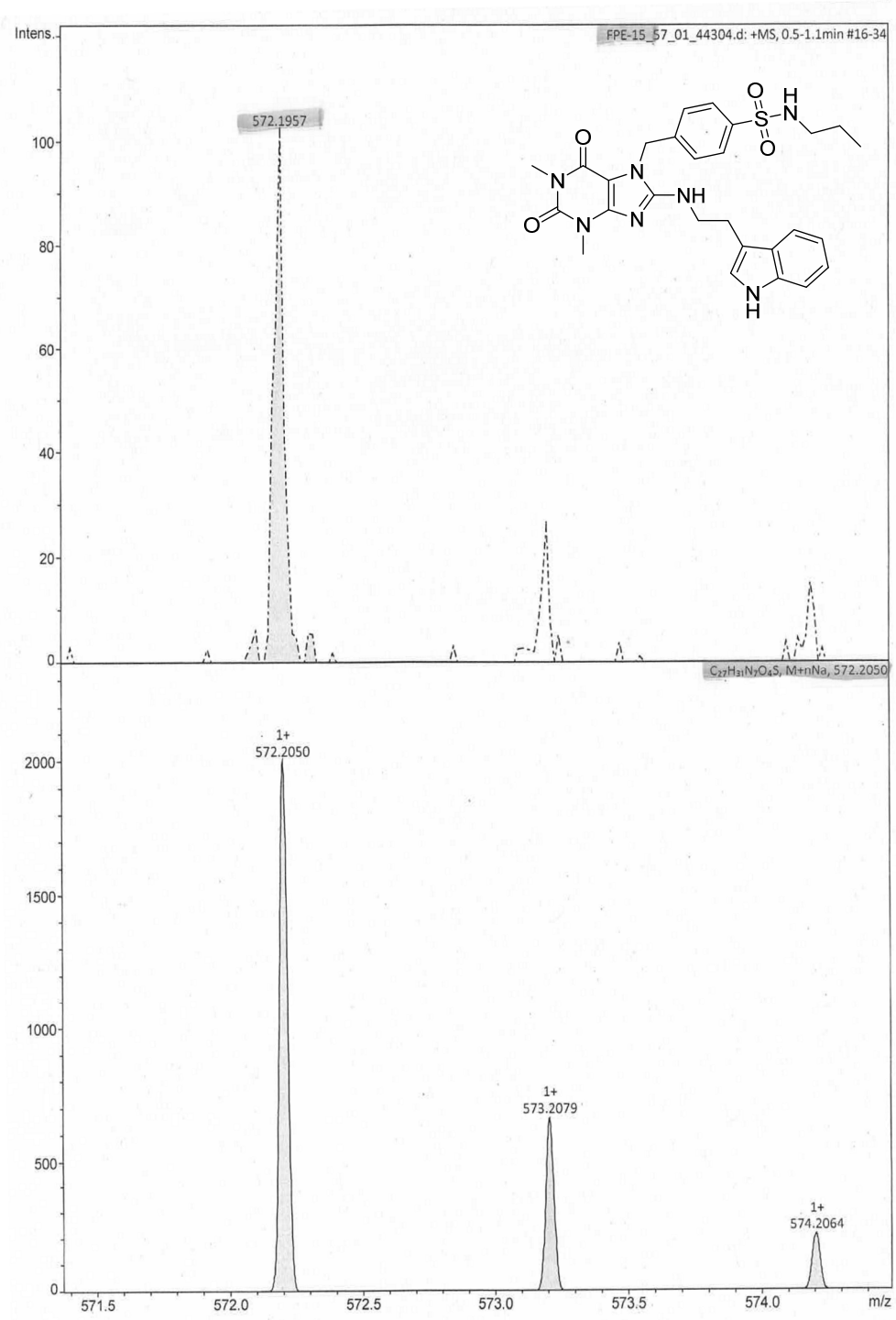

Figure **S164.** HR-MS assessment of purity of compound **49**. HR-MS (ESI-QTOF) calculated for $C_{27}H_{31}N_7O_4SNa$ $[M+Na]^+$: 572.2050, found: 572.1957.

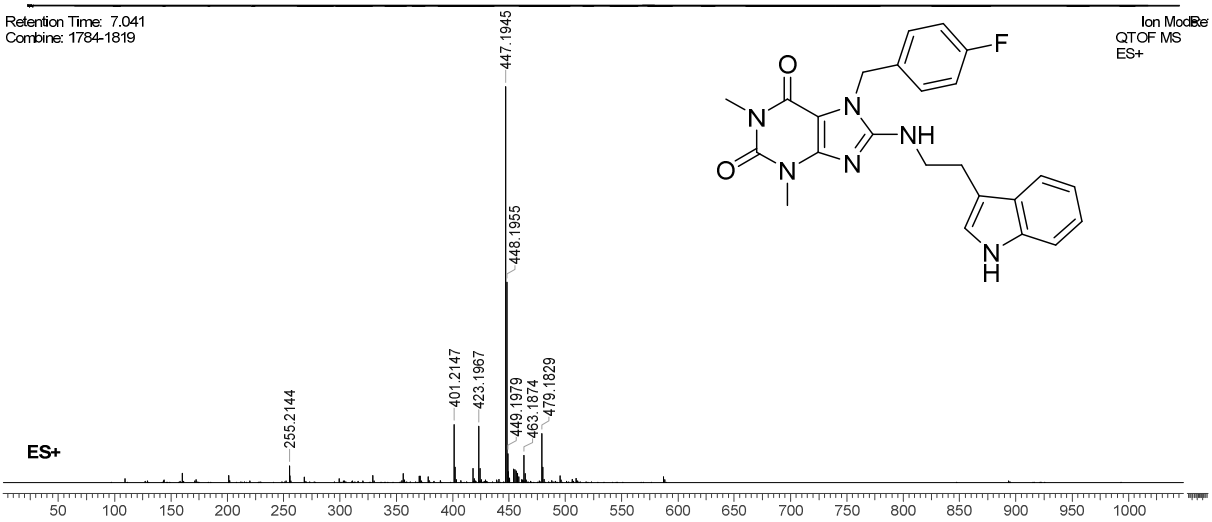

Figure **S165.** HR-MS assessment of purity of compound **50**. HR-MS (ESI-QTOF) calculated for $C_{24}H_{24}FN_6O_2$ $[M+H]^+$: 447.1945, found: 447.1945.

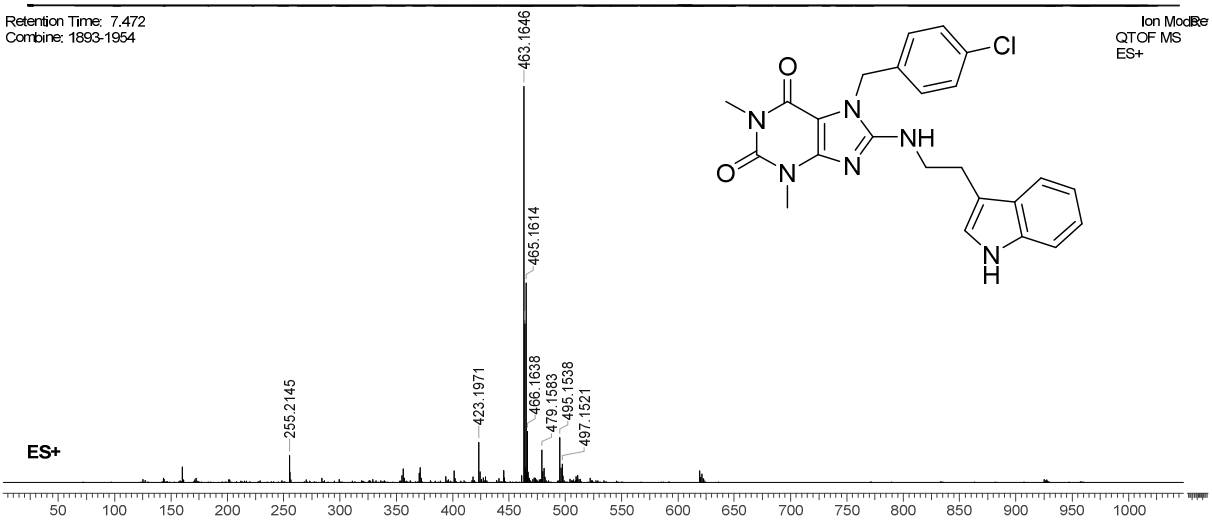

Figure **S166.** HR-MS assessment of purity of compound **51**. HR-MS (ESI-QTOF) calculated for $C_{24}H_{24}ClN_6O_2$ $[M+H]^+$: 463.1649, found: 463.1646.

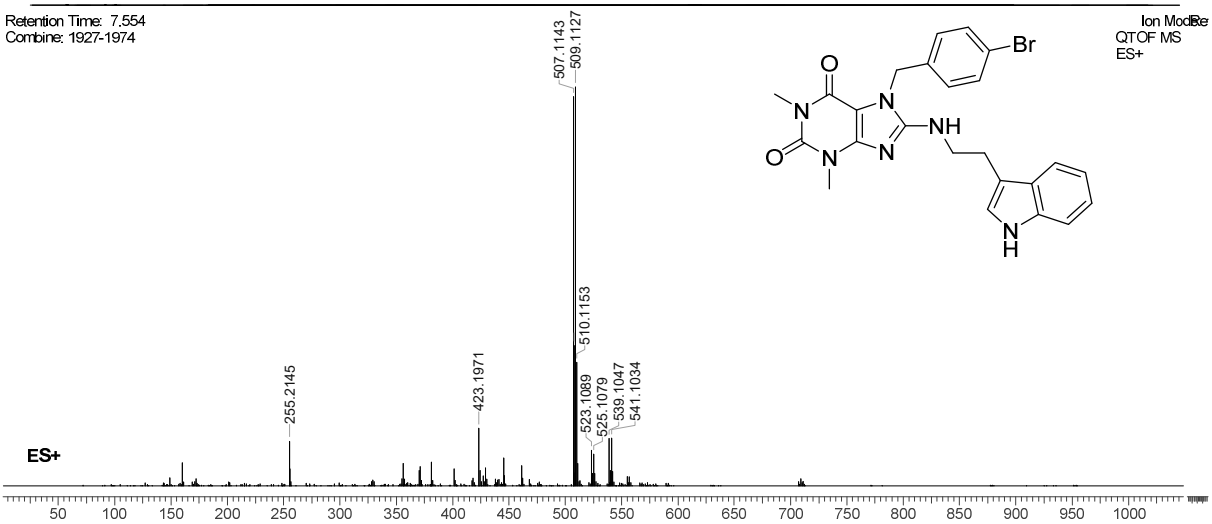

Figure **S167**. HR-MS assessment of purity of compound **52**. HR-MS (ESI-QTOF) calculated for $C_{24}H_{24}BrN_6O_2$ $[M+H]^+$: 507.1144, found: 507.1143.

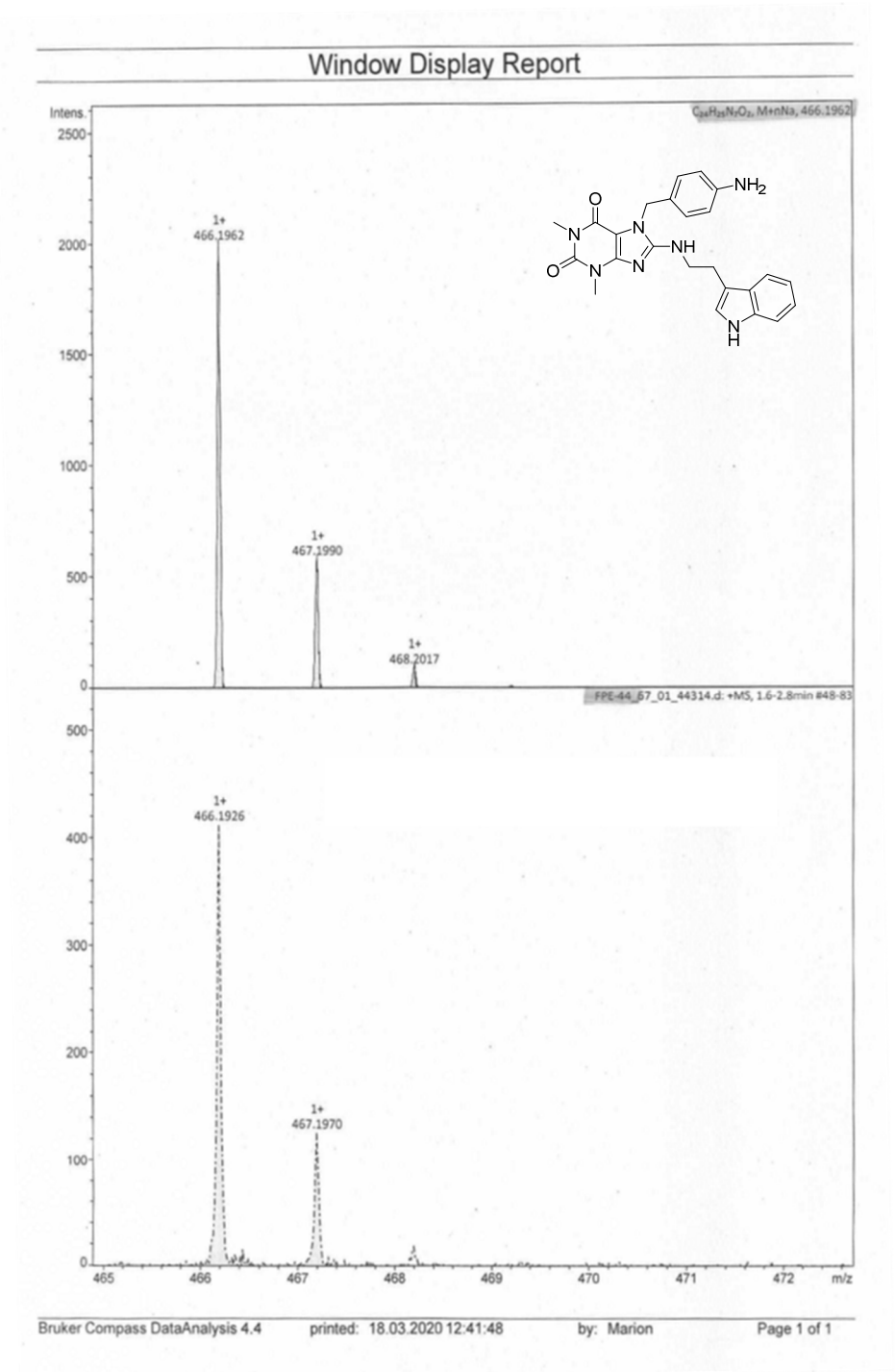

Figure **S168.** HR-MS assessment of purity of compound **54**. HR-MS (ESI-QTOF) calculated for $C_{24}H_{25}N_7O_2Na$ $[M+Na]^+$: 466.1962, found: 466.1926.

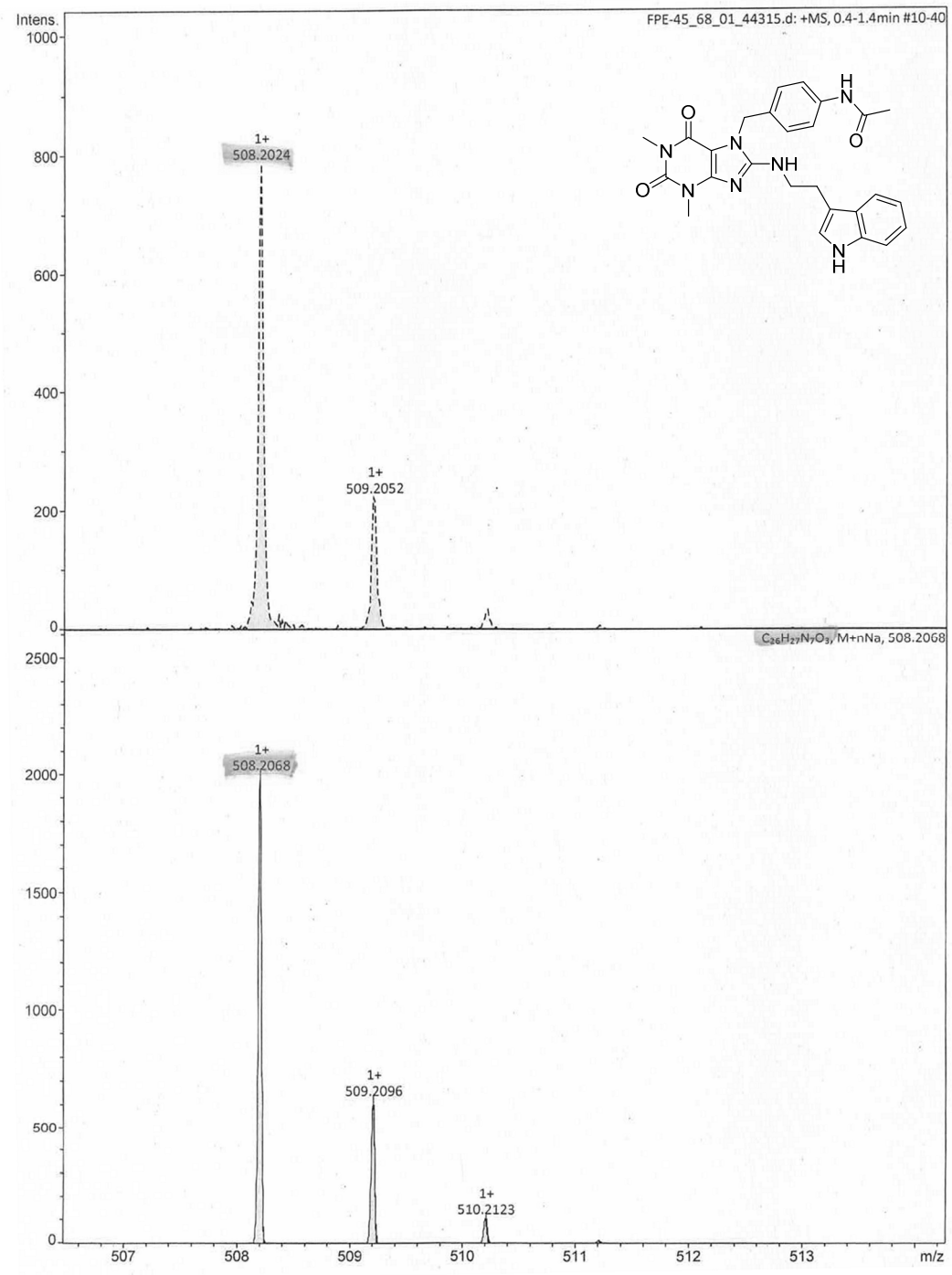

Figure **S169.** HR-MS assessment of purity of compound **55**. HR-MS (ESI-QTOF) calculated for $C_{26}H_{27}N_7O_3Na$ $[M+Na]^+$: 508.2024; found: 508.2068.

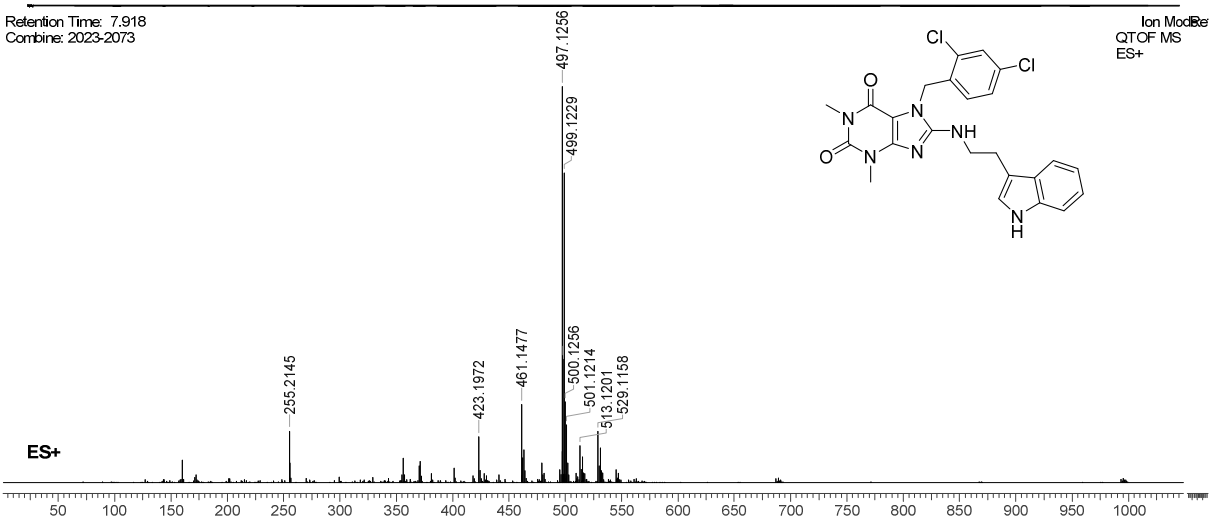

Figure **S170.** HR-MS assessment of purity of compound **57**. HR-MS (ESI-QTOF) calculated for $C_{24}H_{23}Cl_2N_6O_2$ $[M+H]^+$: 497.1260, found: 497.1256.

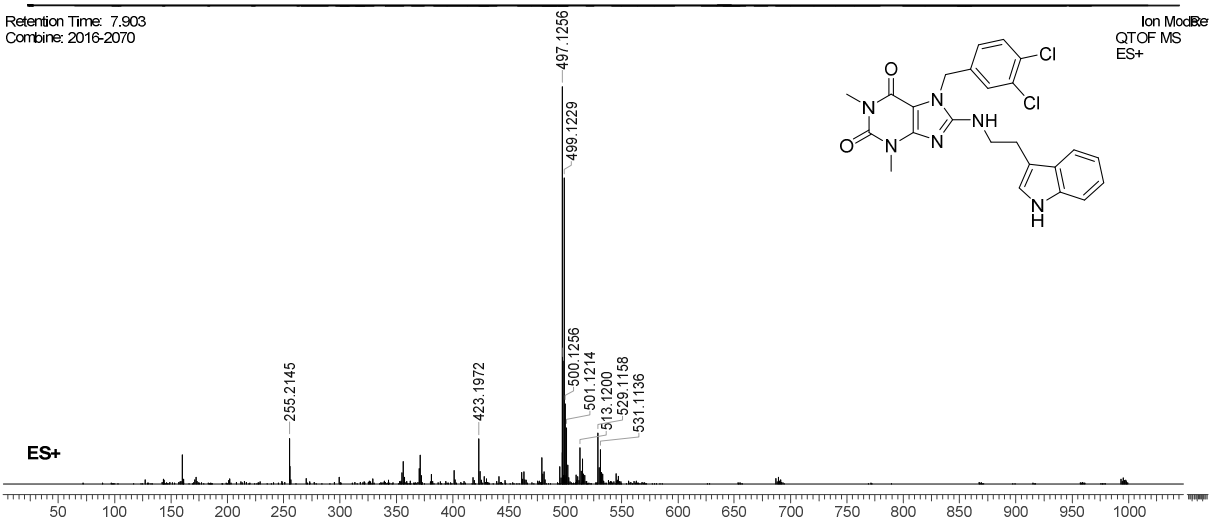

Figure **S171.** HR-MS assessment of purity of compound **59**. HR-MS (ESI-QTOF) calculated for $C_{24}H_{23}Cl_2N_6O_2$ $[M+H]^+$: 497.1260, found: 497.1256.

7.3. Appendix III
Supplementary information from publication III: Development of high-affinity fluorinated ligands for cannabinoid subtype 2 receptor, and in vitro evaluation of a radioactive tracer for imaging

The supplementary information of this publication is also available online at:

https://ars.els-cdn.com/content/image/1-s2.0-S022352342200040X-mmc1.docx

Supporting Information

Table S1: Activities of investigated compounds at human GPR18 and human GPR55 determined in ß-arrestin recruitment assays[a].

Comp.	Human GPR18		Human GPR55	
	Agonistic activity (% activation)	Antagonistic activity (% inhibition)	Agonistic activity (% activation)	Antagonistic activity (% inhibition)
5	>10 (−4%)	>10 (−8%)	>10 (−3%)	>10 (11%)
6	>10 (−7%)	>10 (27%)	>10 (−8%)	>10 (45)
7 (DM102)	>10 (2%)	>10 (16%)	>10 (−6%)	>10 (−2%)
8	>10 (−6%)	>10 (42%)	>10 (−6%)	>10 (31%)
9	>10 (−9%)	>10 (46%)	>10 (−9%)	>10 (44%)
10	>10 (−6%)	>10 (45%)	>10 (−17%)	>10 (32%)
14	>10 (1%)	>10 (21%)	>10 (−4%)	>10 (9%)
15	>10 (1%)	>10 (8%)	>10 (−12%)	>10 (32%)
12	>10 (−1%)	>10 (5%)	>10 (−1%)	>10 (0%)
16	>10 (0%)	>10 (43%)	>10 (−16%)	>10 (20%)
18	>10 (−5%)	>10 (28%)	>10 (−1%)	>10 (−4%)

[a] Compounds were tested at a concentration of 10 µM as described in the Experimental Section.

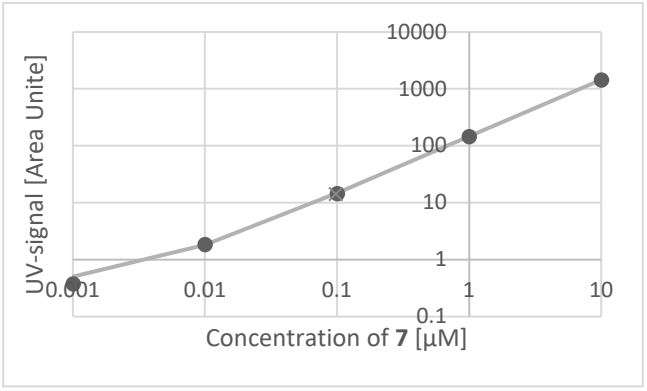

Figure S1: HPLC calibration of compound **7** concentration vs. UV-signal for determination of molar activity. Measurement of 1500 GBq/µmol is marked.

Purity by HPLC

The purity of the compounds investigated in biological assays was determined by HPLC-UV (Agilent, column by Macherey-Nagel EC 150/3 Nucleodur 100-3 C18ec). Gradient elution was applied using a mobile phase A of water containing 0.1% of trifluoroacetic acid (TFA) and mobile phase B of acetonitrile containing 0.1% TFA. The flow was adjusted to 0.6 mL/min, from 0–10 min with 70% mobile phase B, 30% A. From 10–15 min the percentage of mobile phase B was increased to 100%. The wavelength of the UV detector was adjusted to 305 nm. The compounds were dissolved in 50% mobile phase A and 50% mobile phase B at a concentration of 1 mM, and the injection volume was 10 µL.

In the top right corner of the chromatogram an overview is depicted, which is scaled to the maximum. The red lines in the overview show the zoom of the chromatogram. The measured purity values correspond to the UV absorbance of the product peak divided by that of the summed impurities.

HPLC Blank measurement

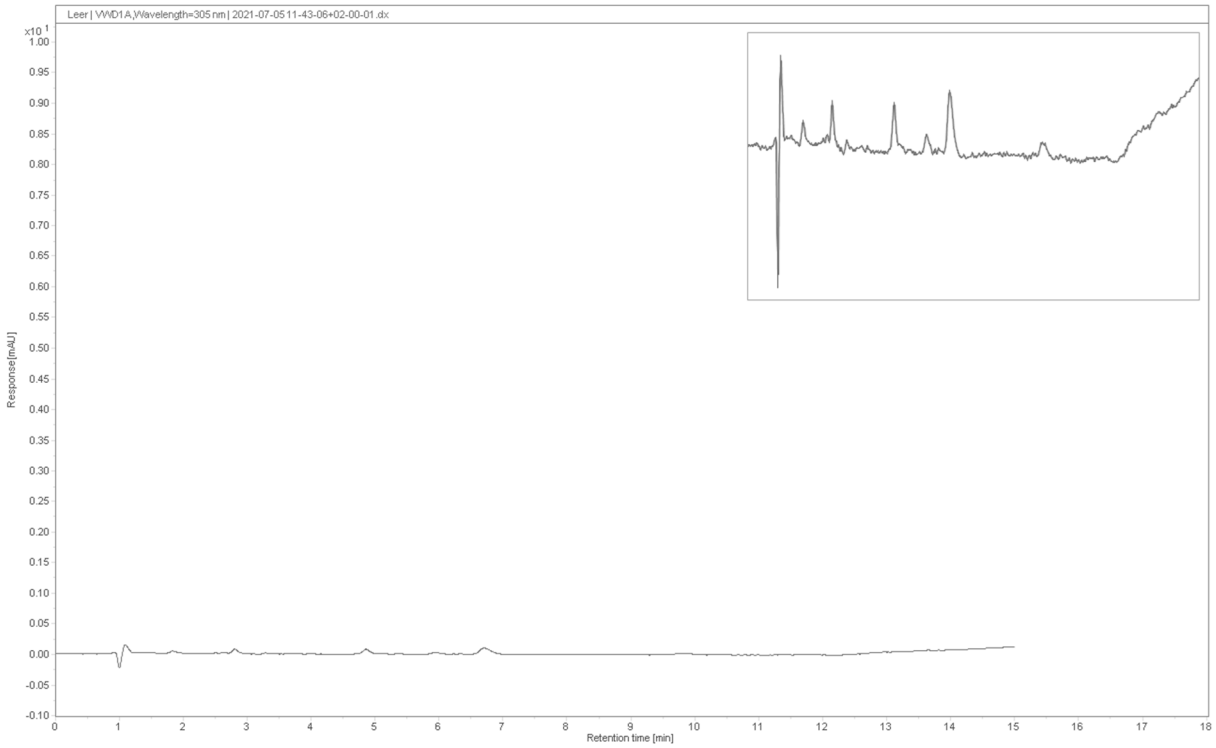

HPLC Thiourea 1.146 min

Thiourea was used to measure column dead time (t_0), due to the poor retention on a C18-Phase.

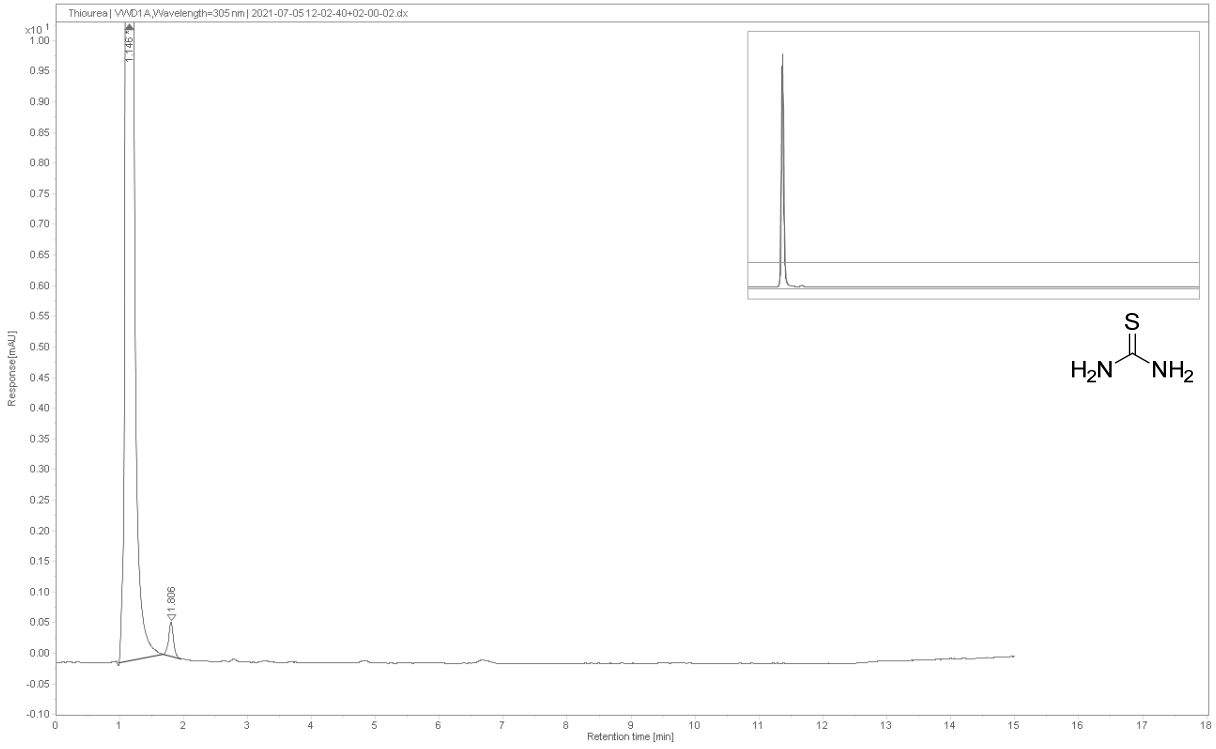

Compound 5

HPLC 4.692 min (k: 3.1) 99.78%

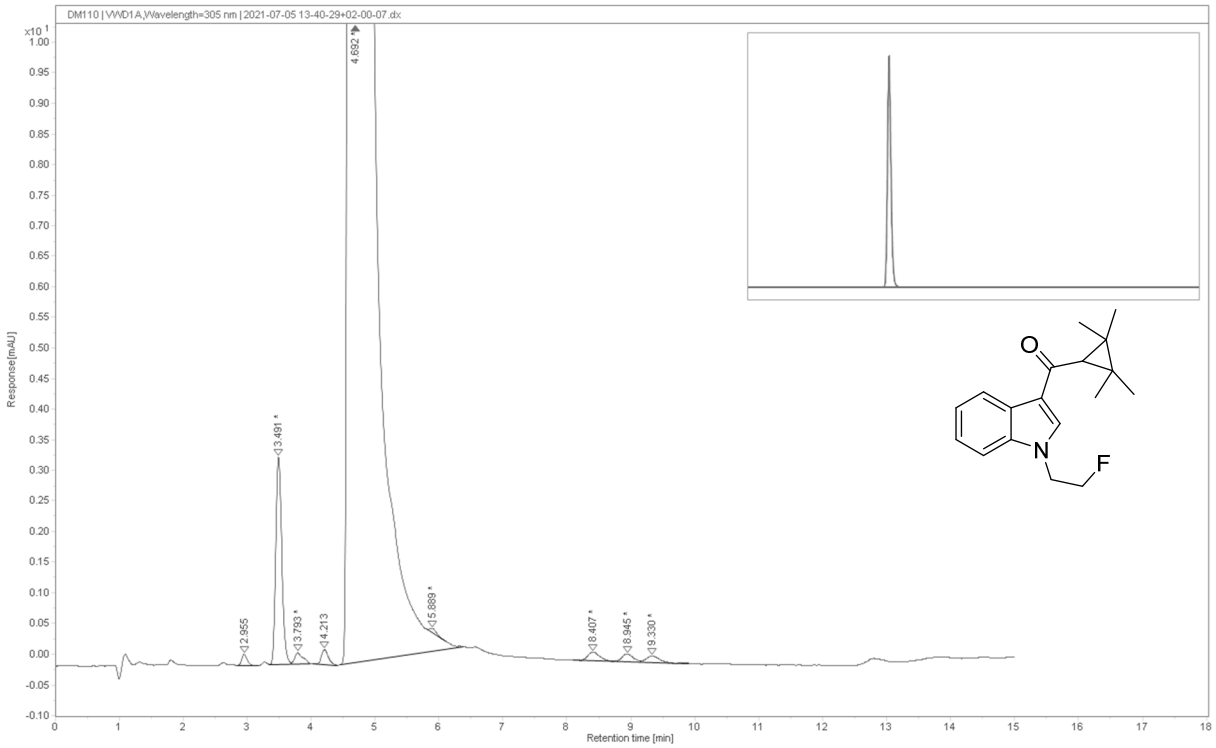

^{1}H-NMR

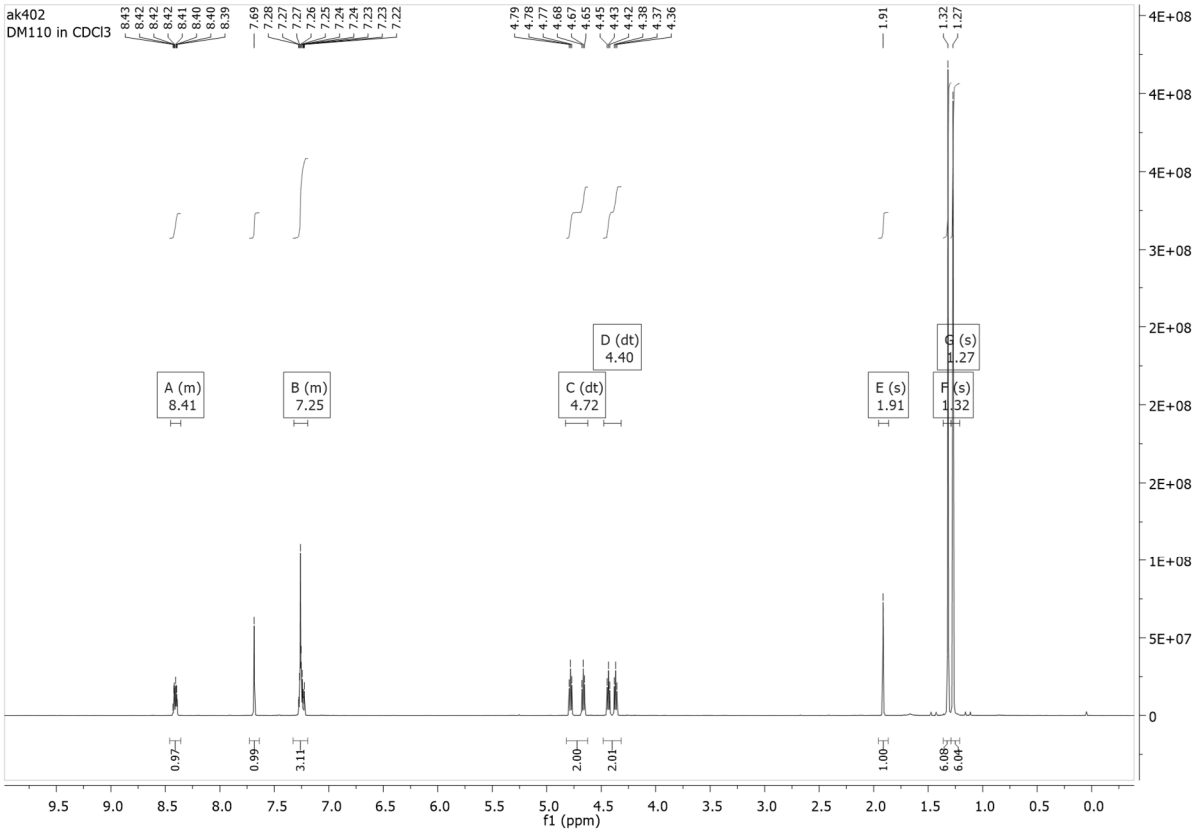

^{13}C-NMR (APT)

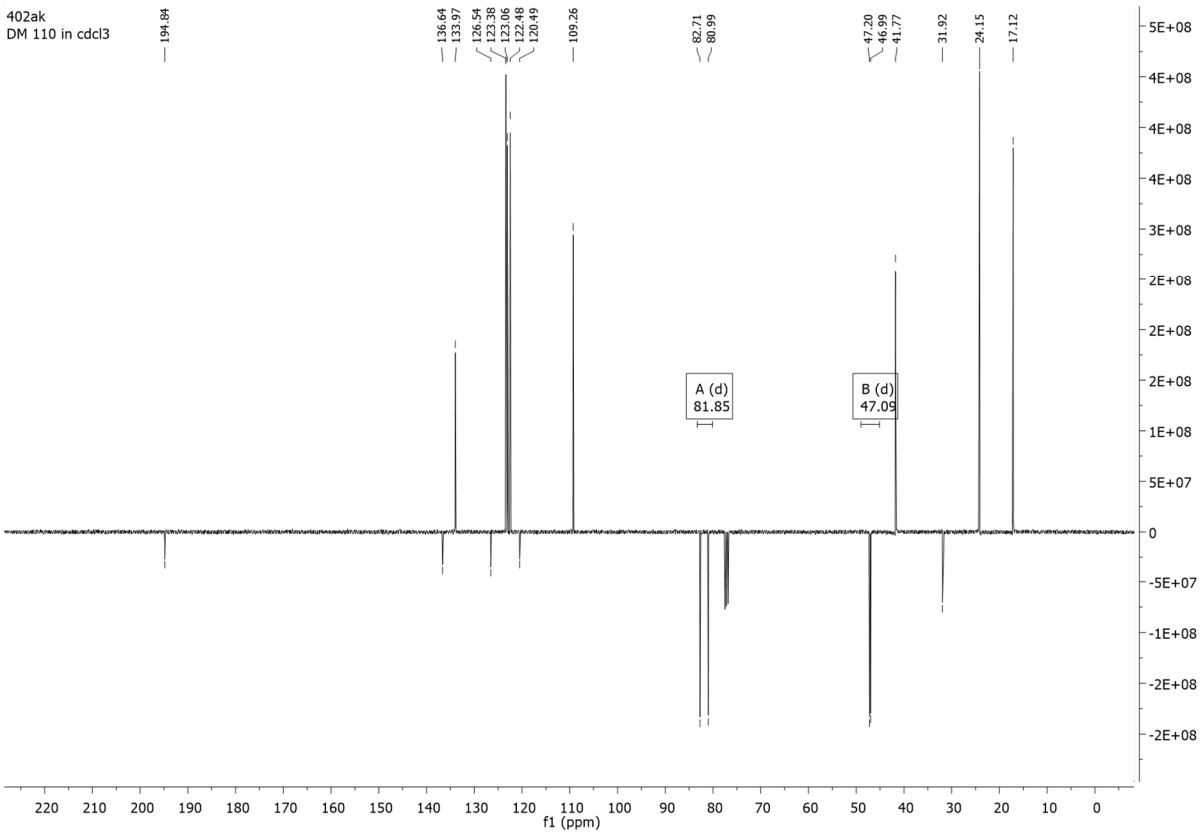

^{19}F-NMR

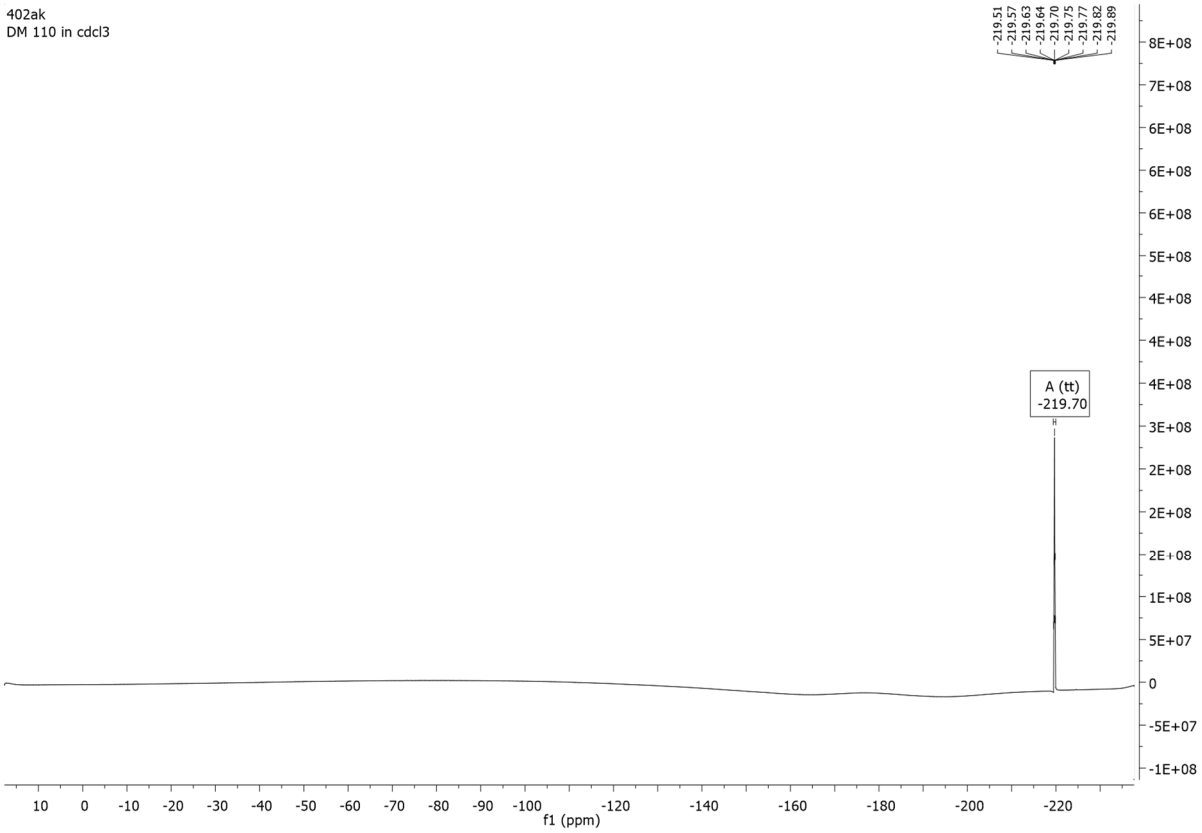

Compound 6

HPLC: 6.428 min (k: 4.6) 99.02%

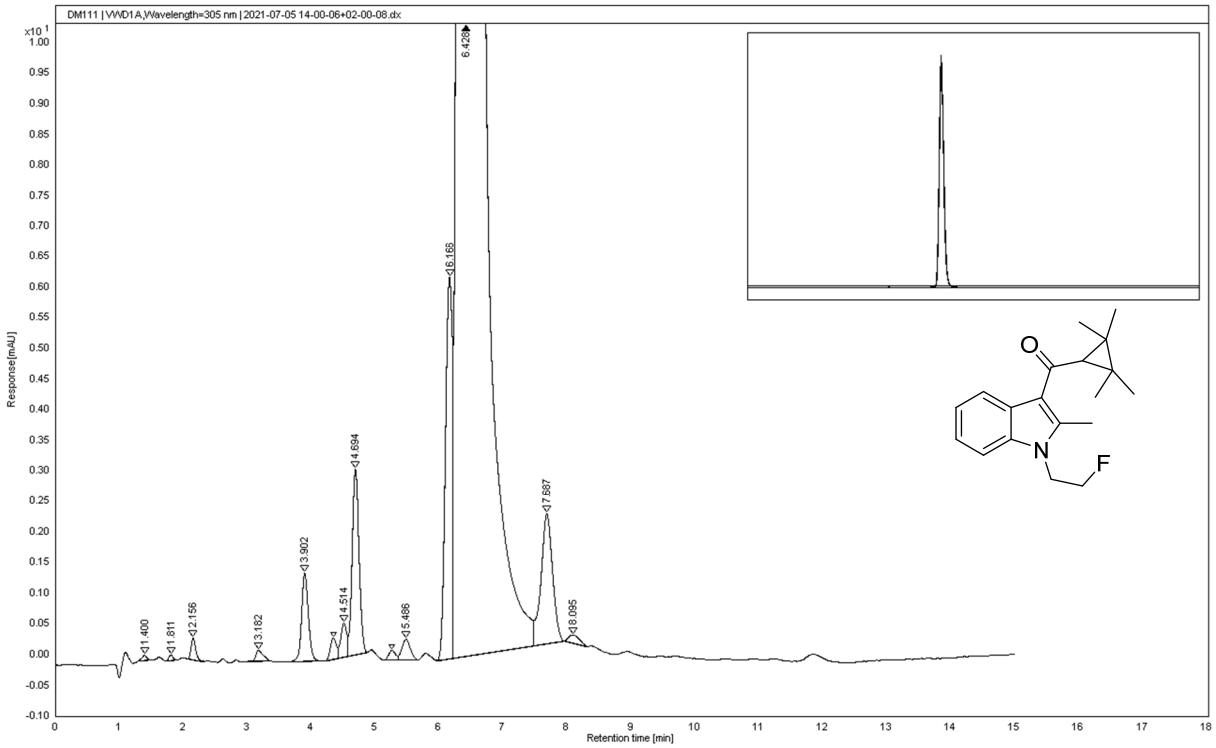

^{1}H-NMR

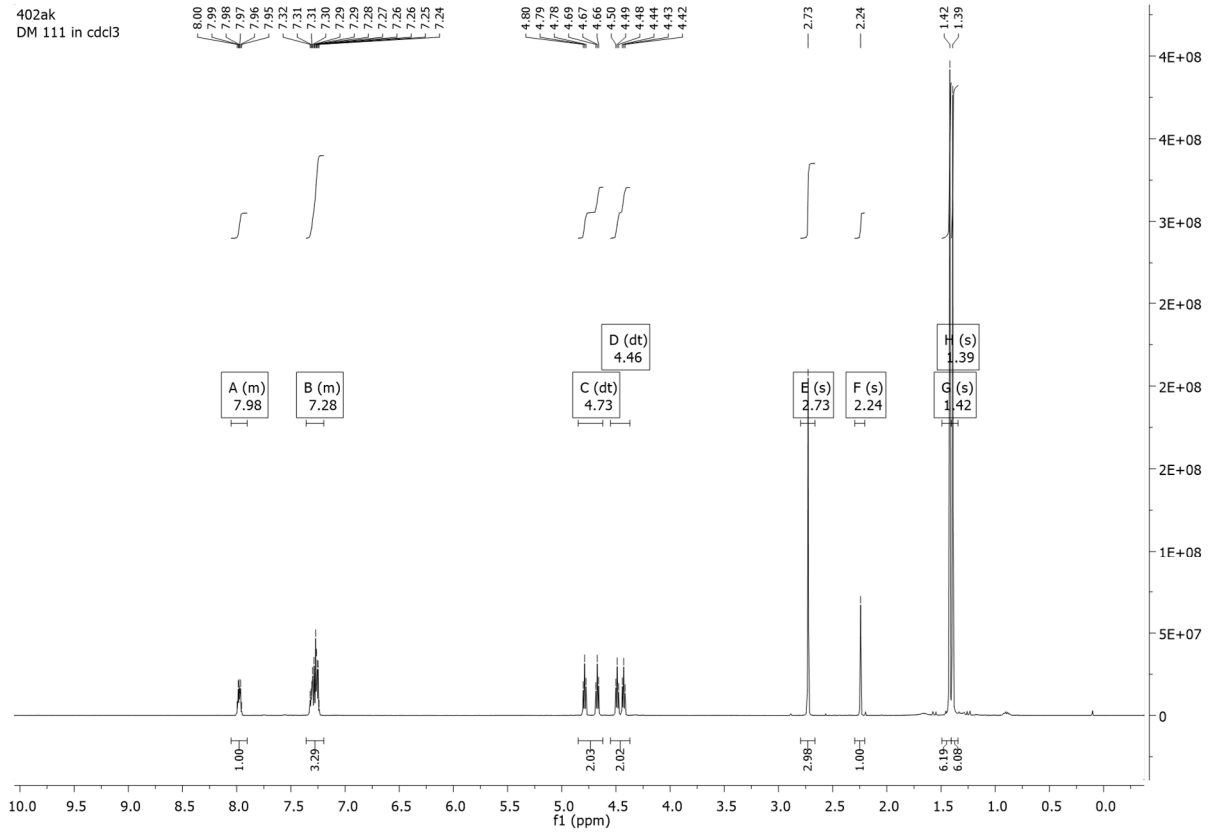

^{13}C-NMR (APT)

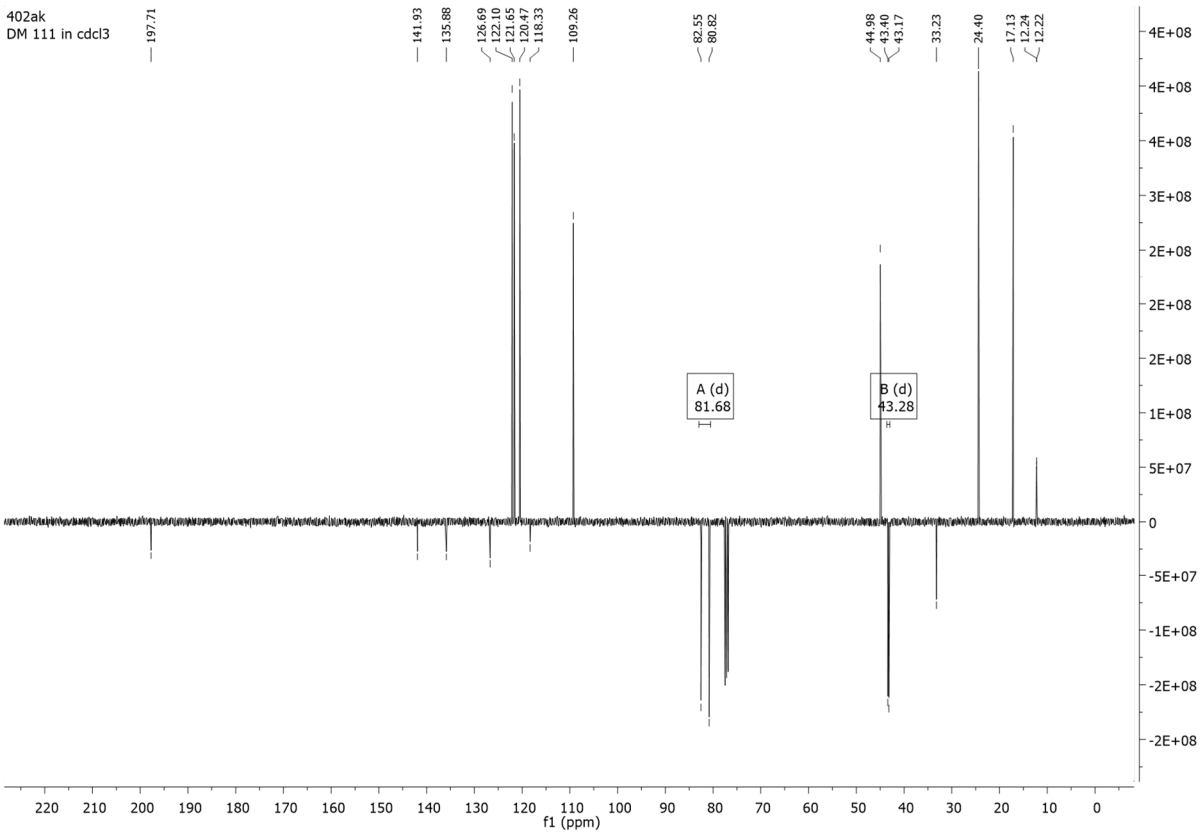

^{19}F-NMR

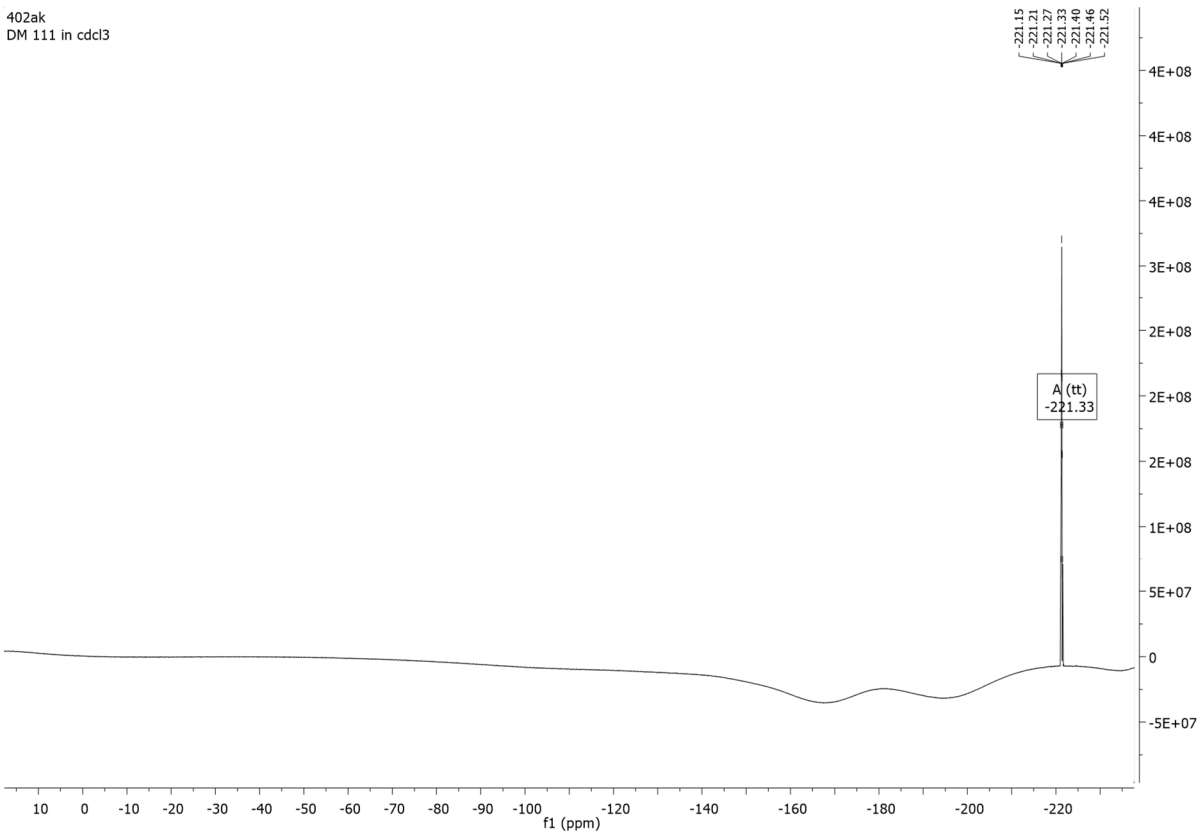

Compound 7

HPLC 5.905 min (k: 4.2) 99.75%

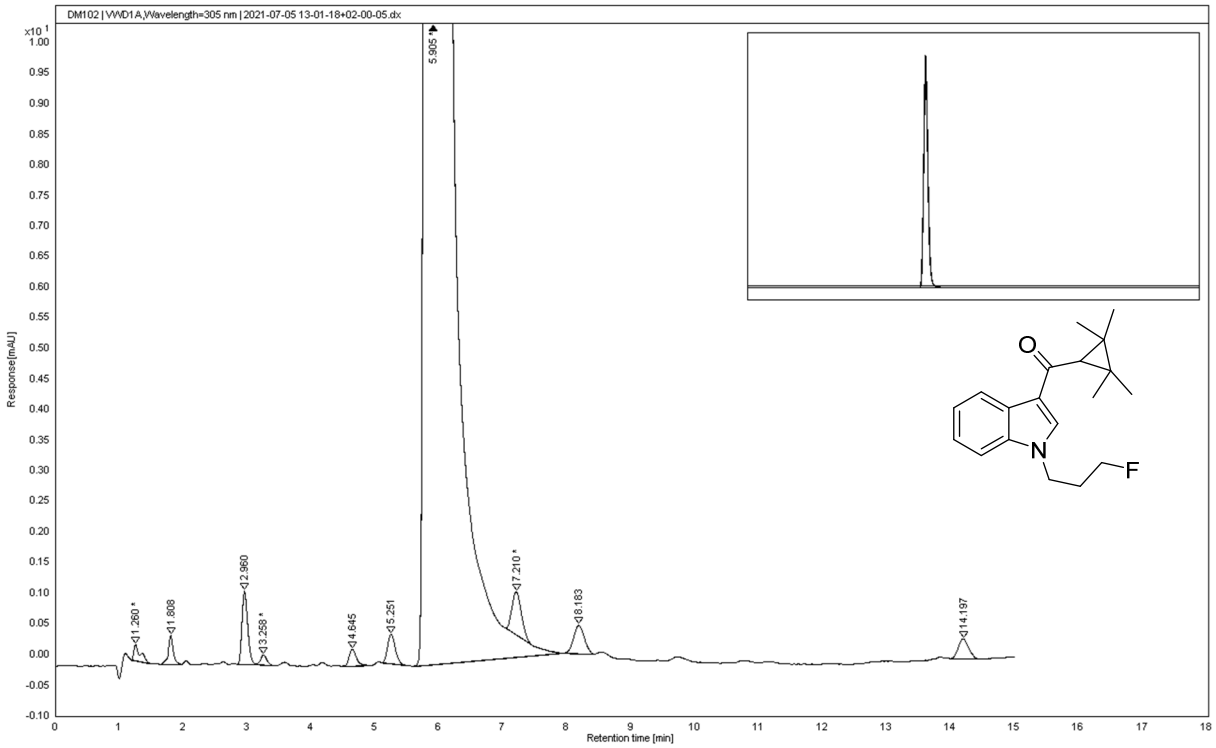

^{1}H-NMR

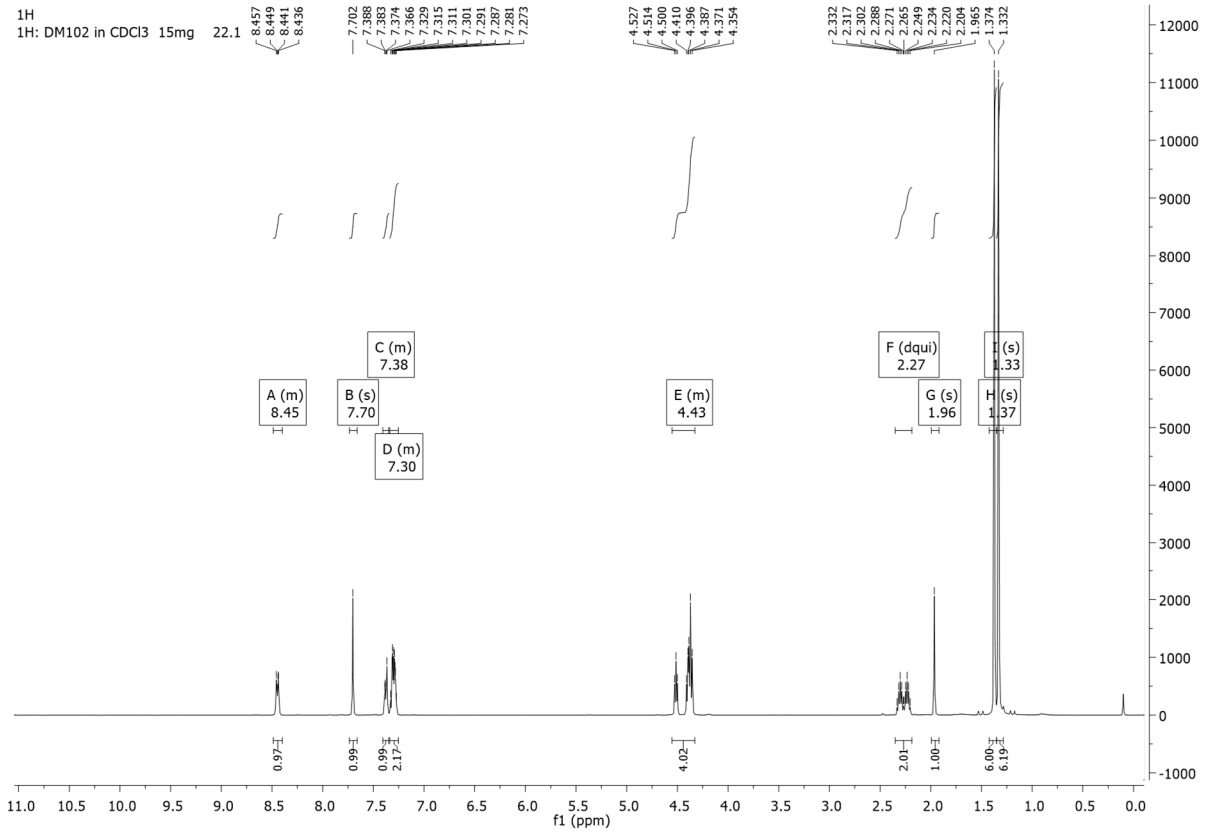

^{13}C-NMR (APT)

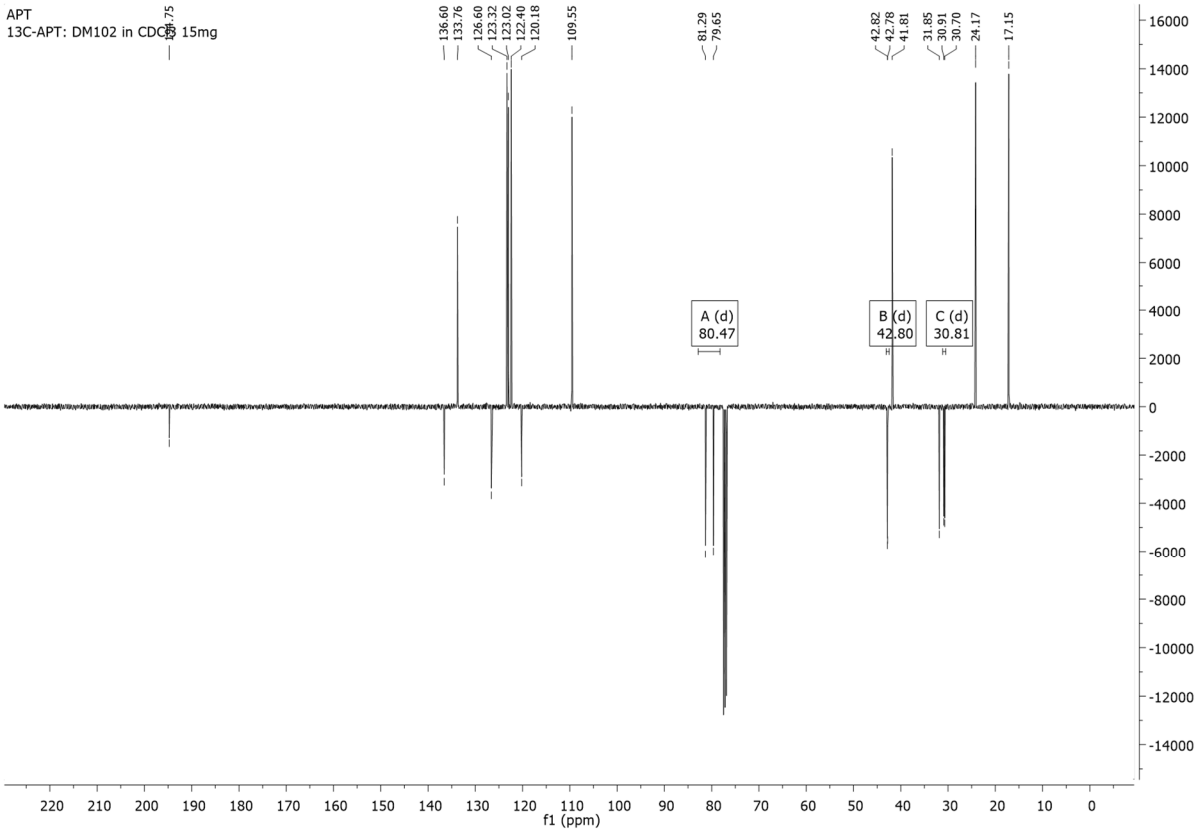

^{19}F-NMR

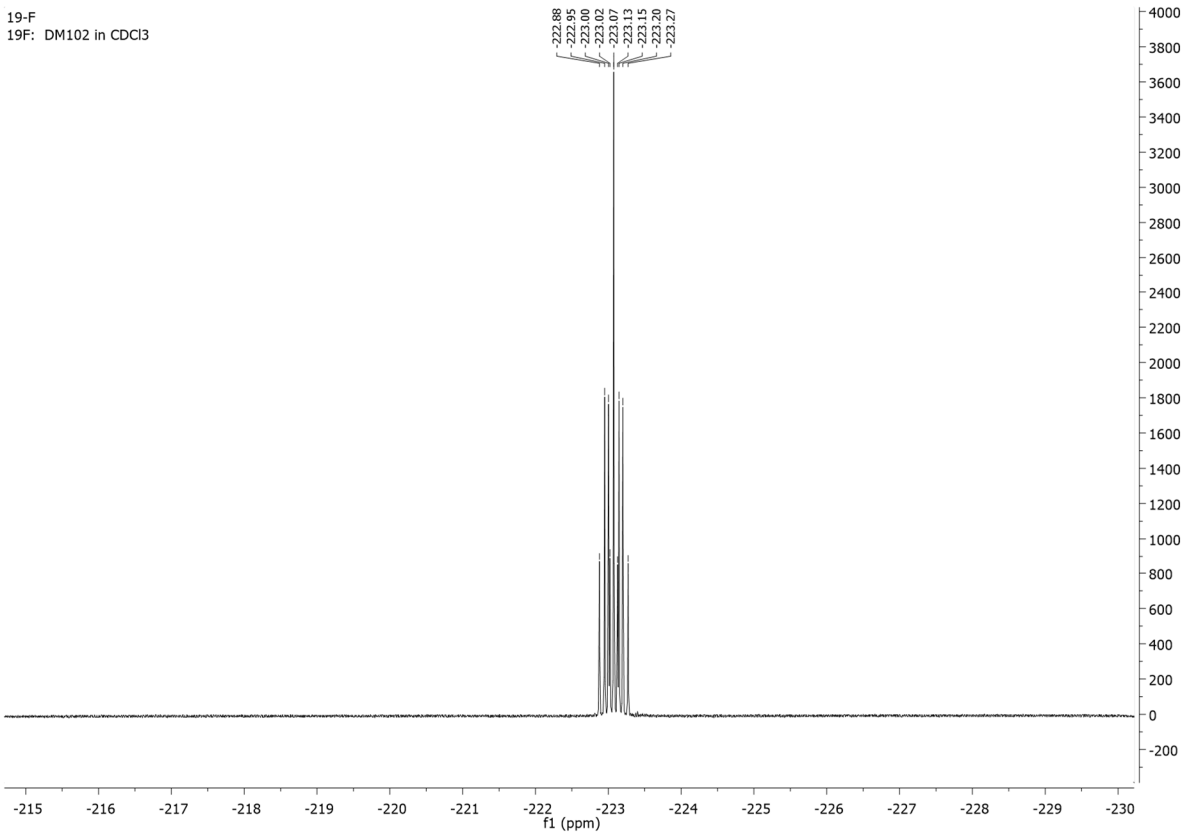

Compound 8

HPLC 9.411 min (k: 6.3) 98.23%

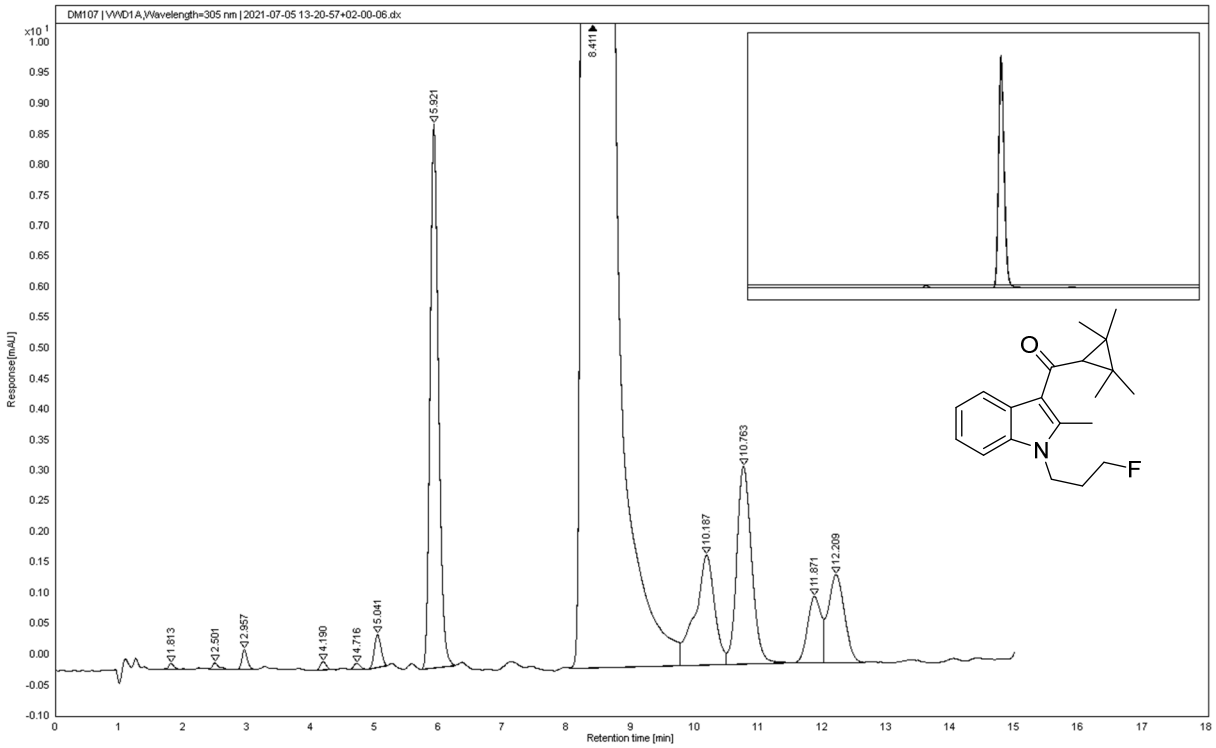

^{1}H-NMR

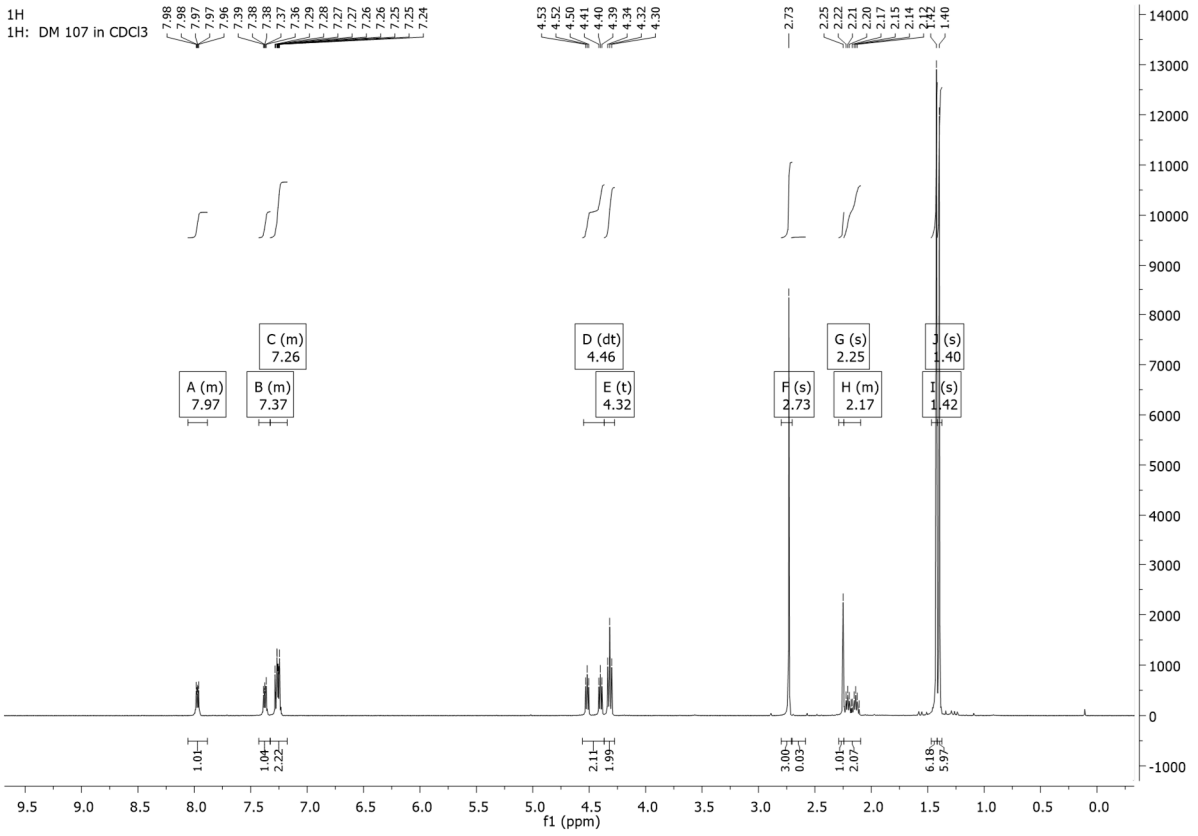

^{13}C-NMR (APT)

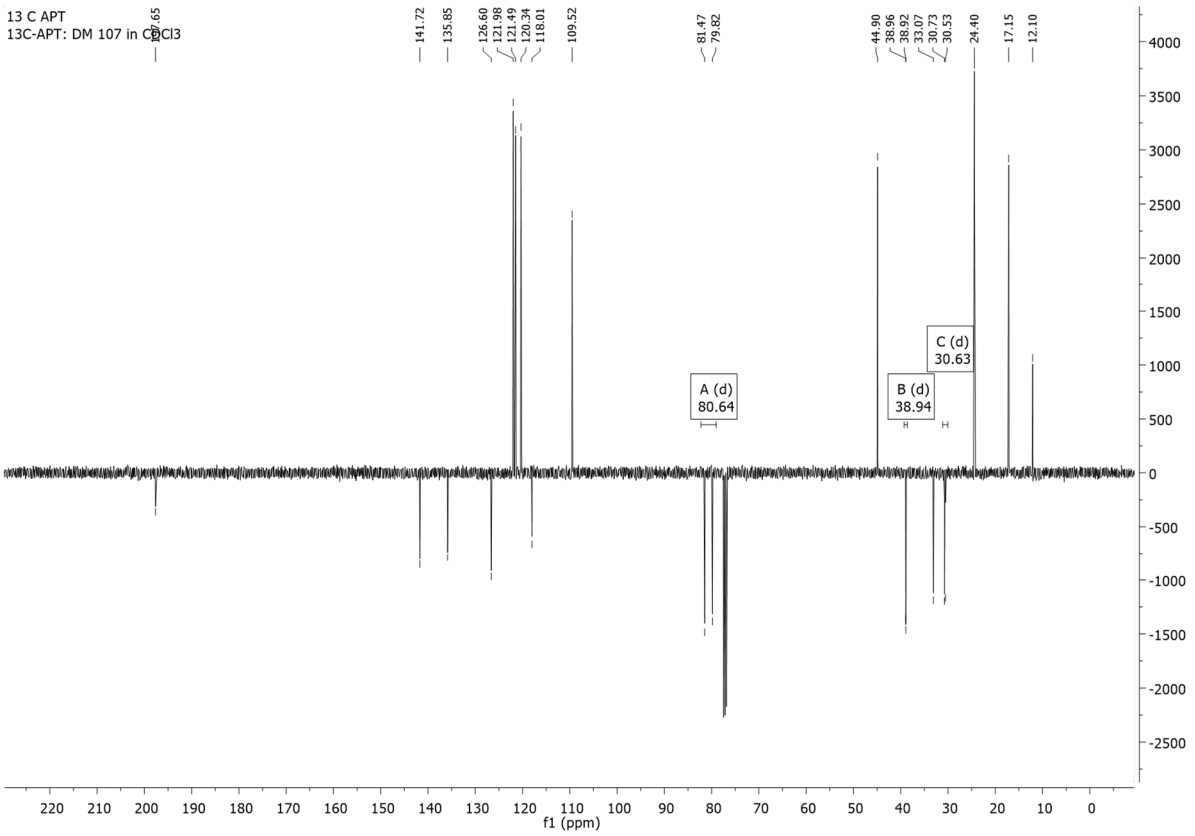

^{19}F-NMR

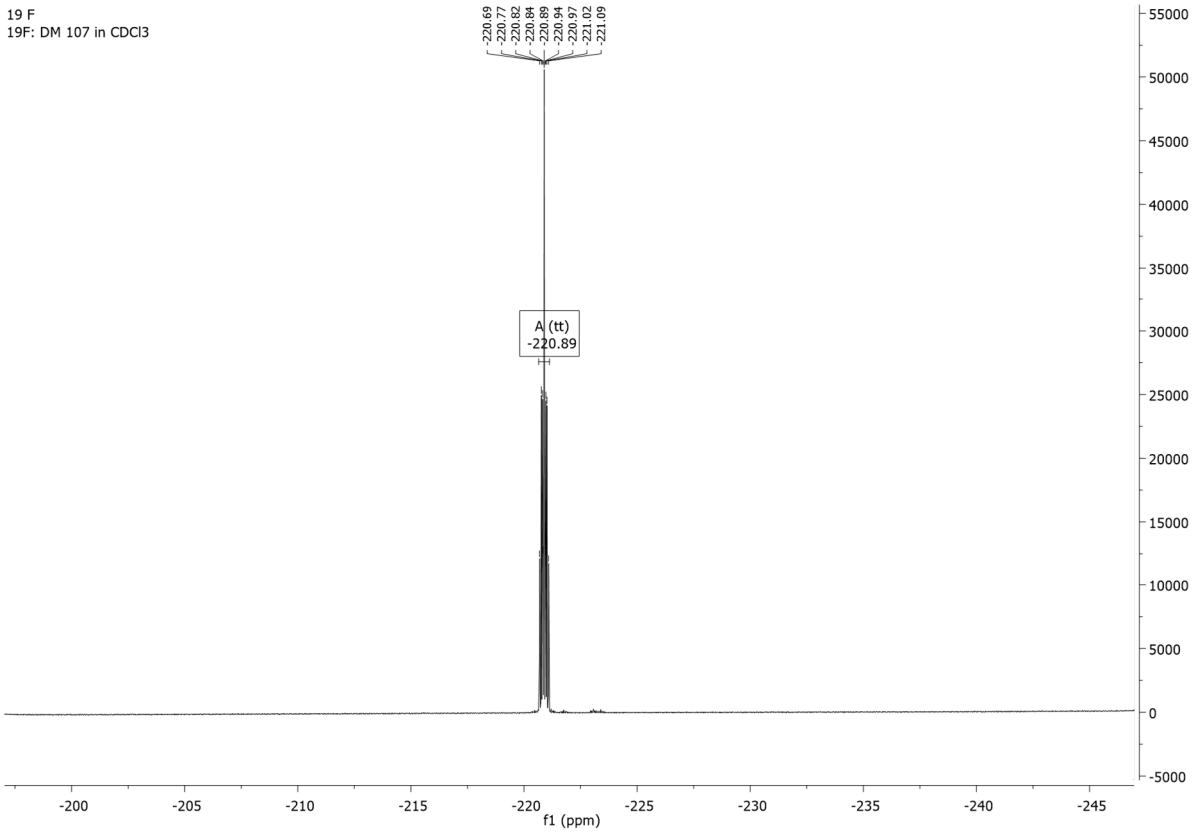

Compound 9

HPLC 6.728 min (k: 4.9) 99.77%

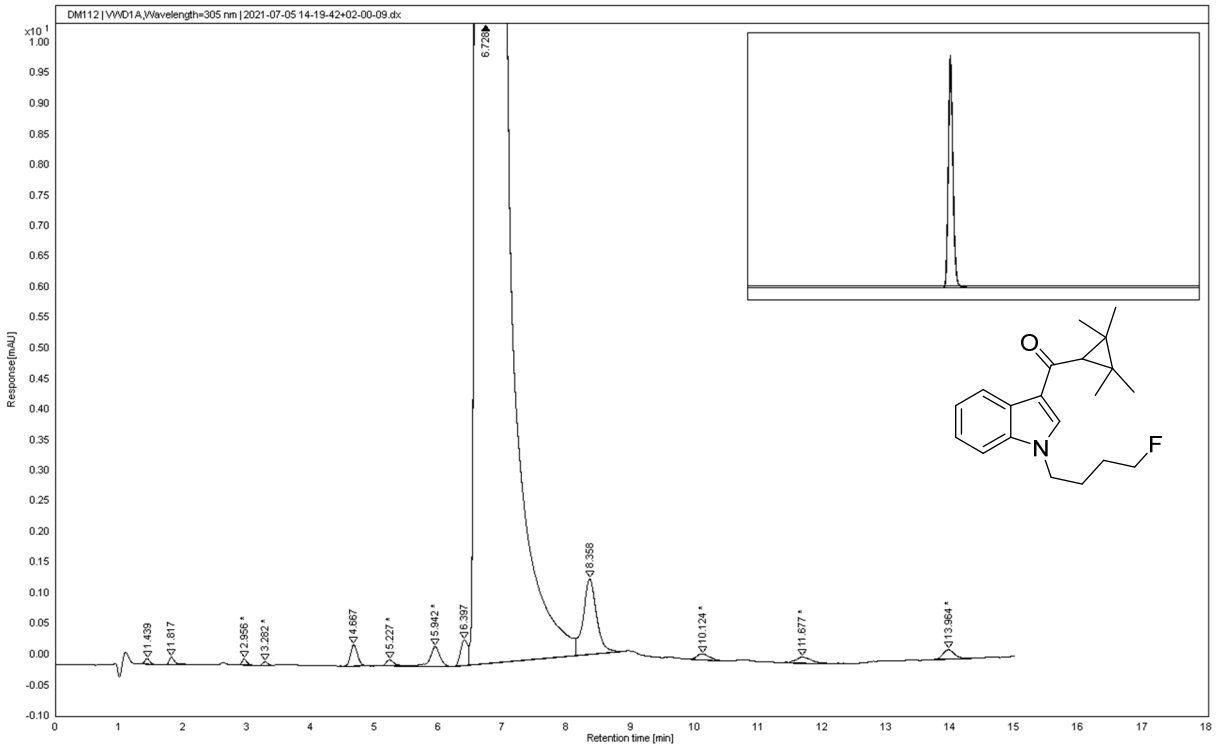

^{1}H-NMR

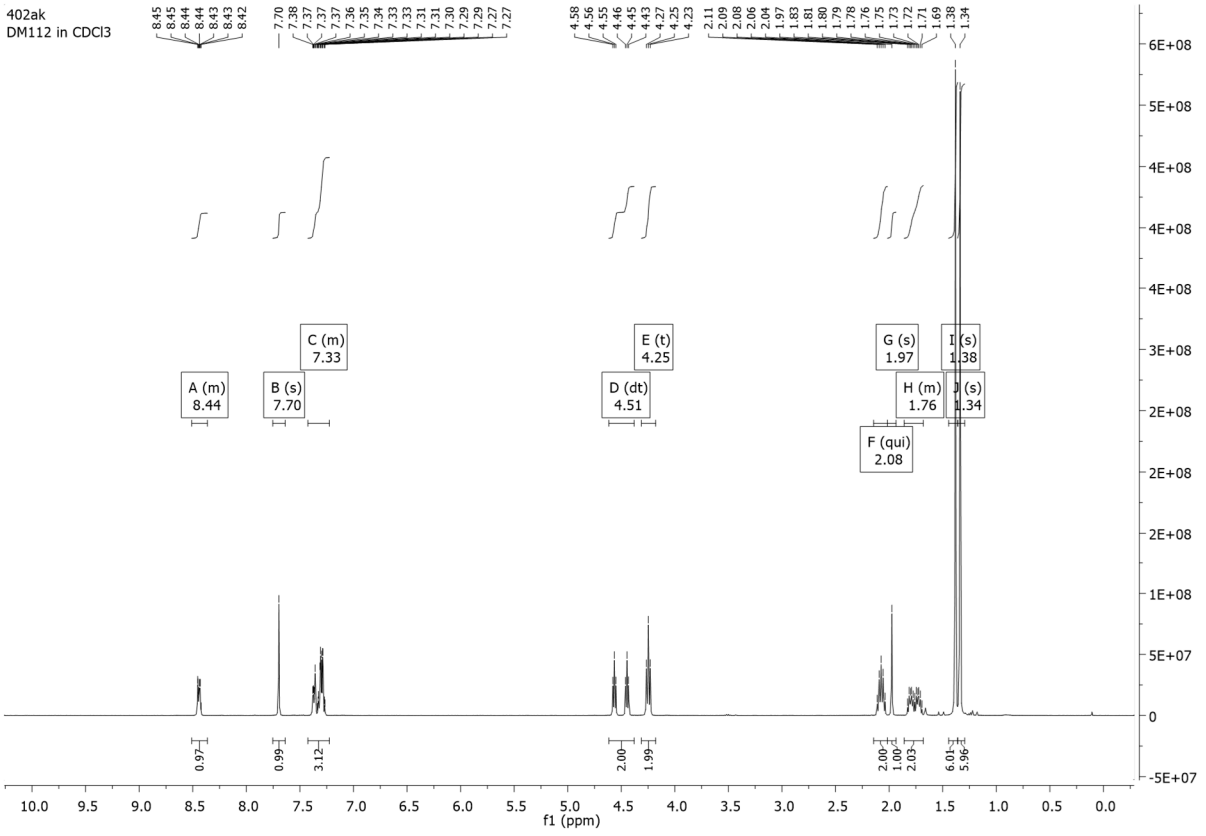

^{13}C-NMR (APT)

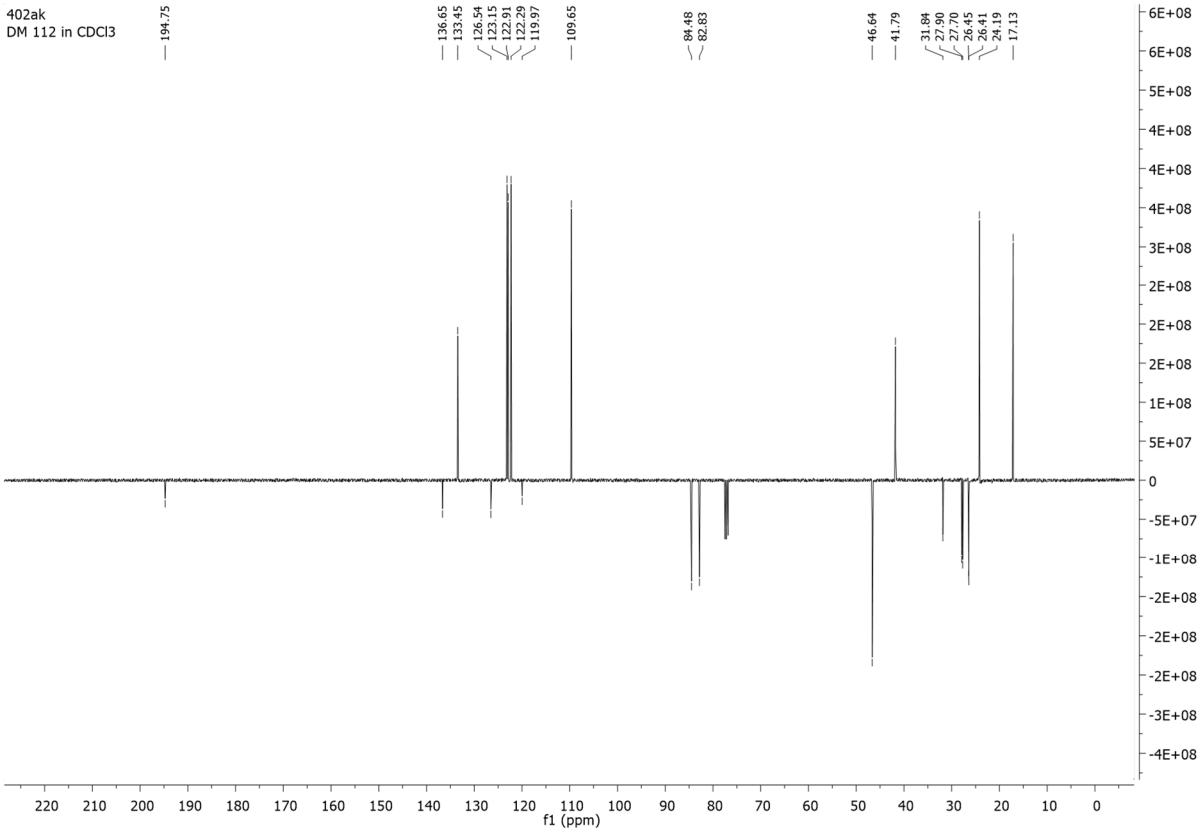

^{19}F-NMR

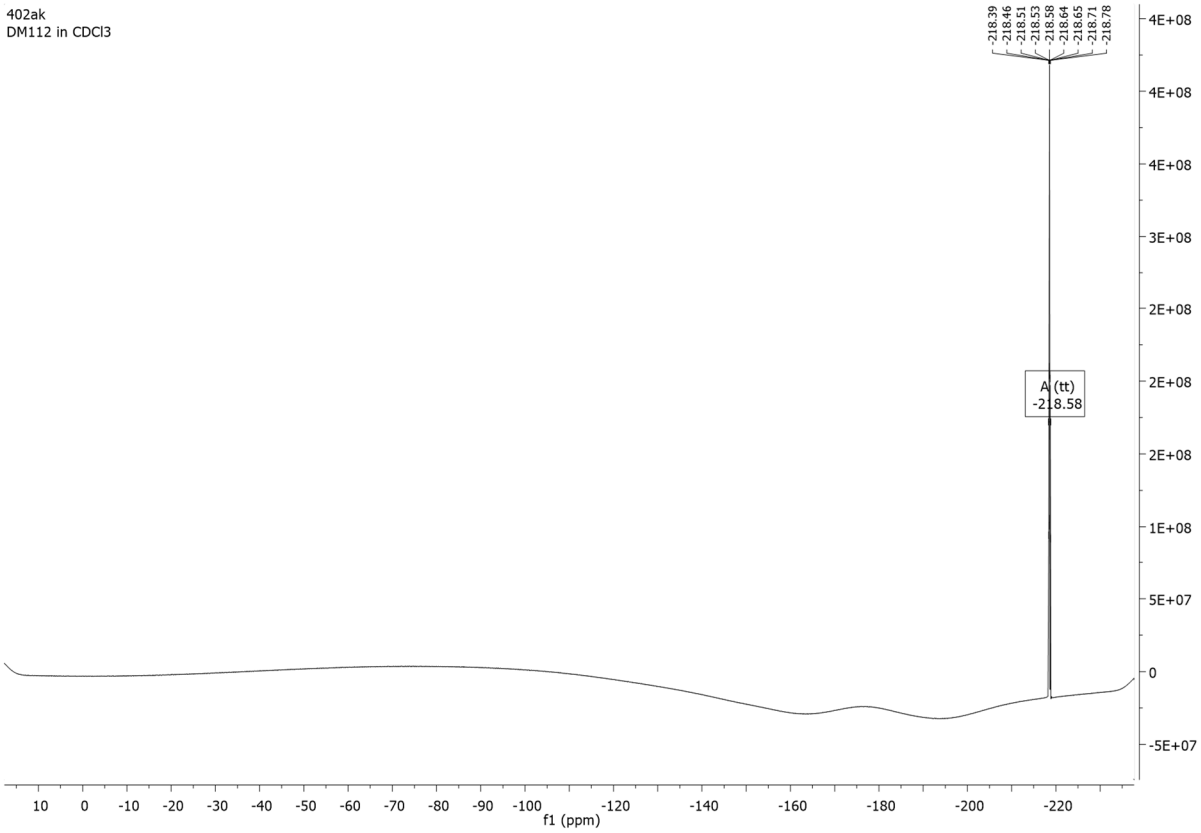

Compound 10

HPLC 9.701 min (k: 7.5) 99.73%

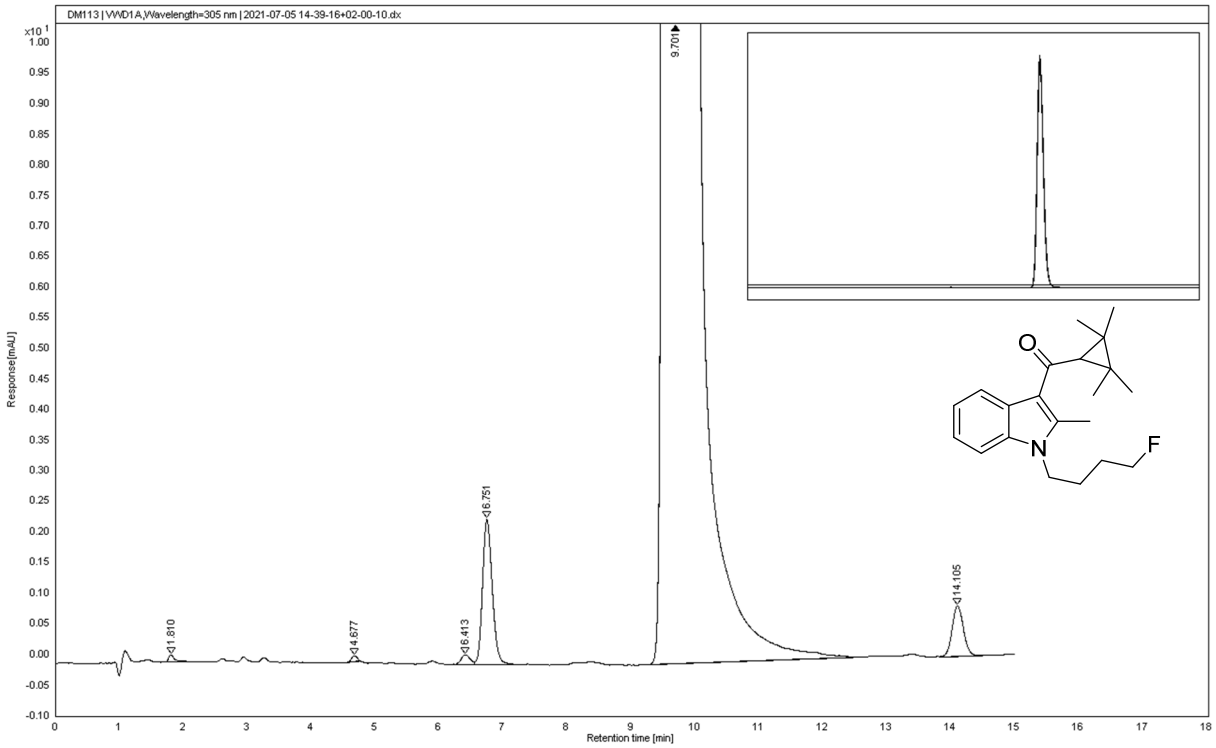

^{1}H-NMR

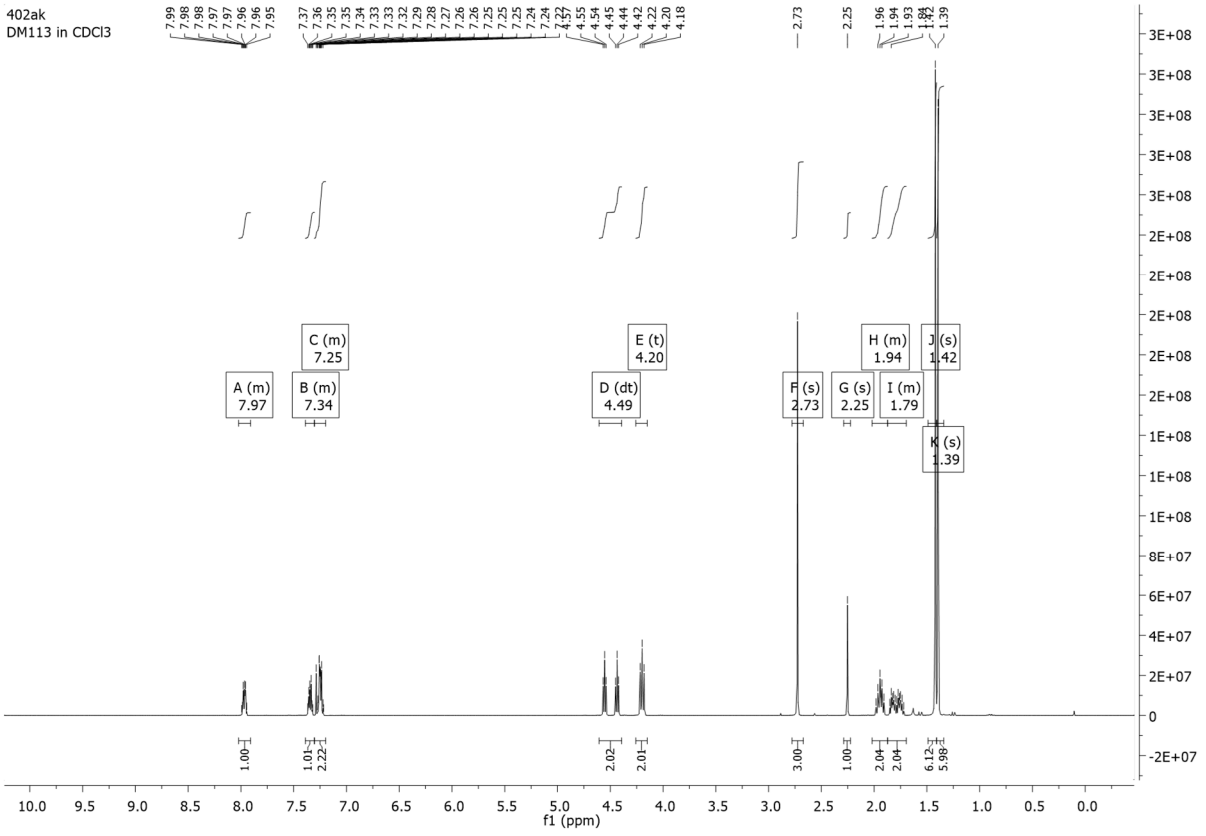

^{13}C-NMR (APT)

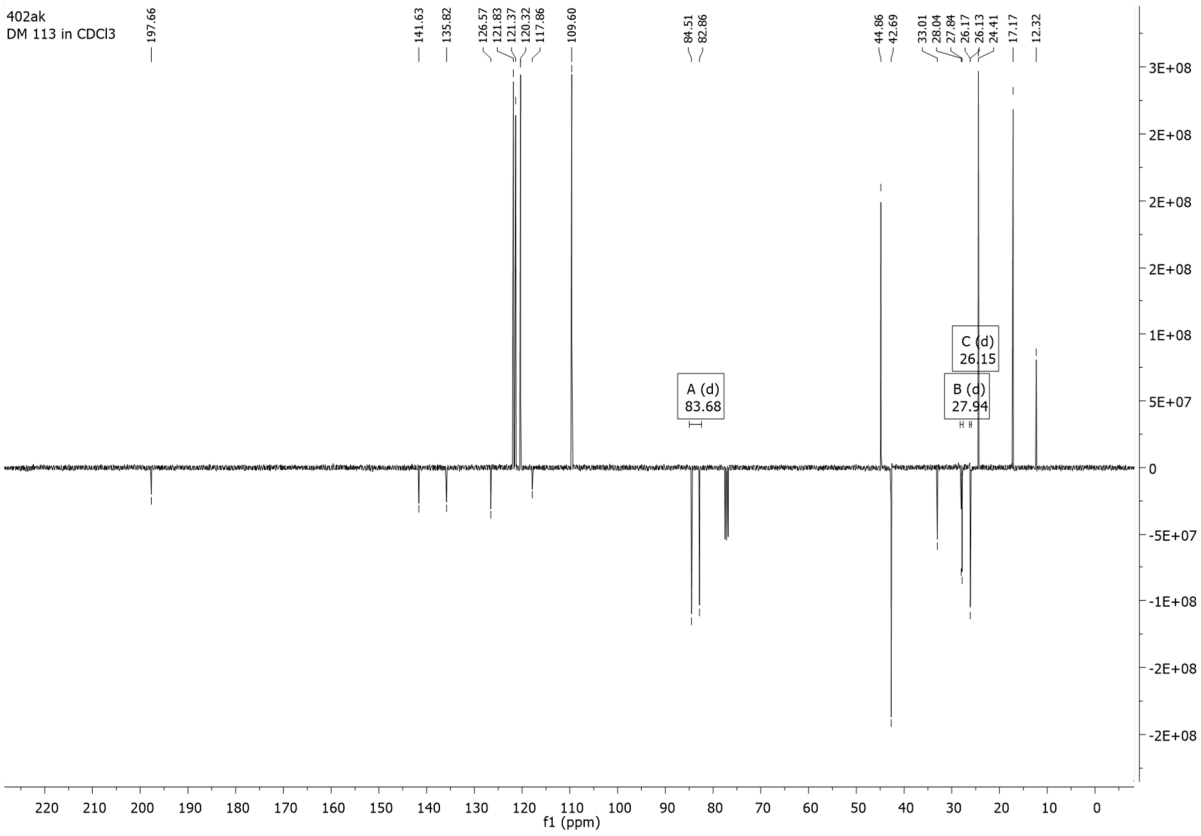

^{19}F-NMR

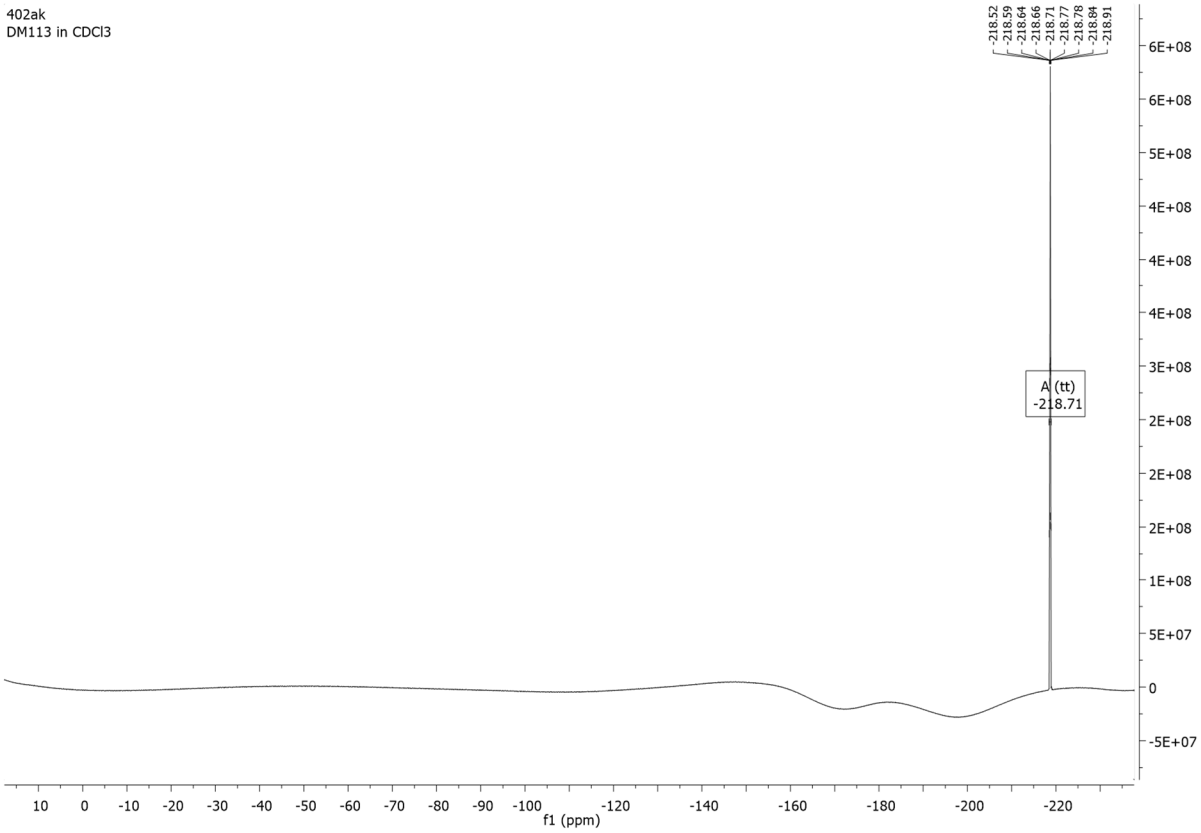

Compound 12

HPLC 2.777 min (k: 1.4) 99.92%

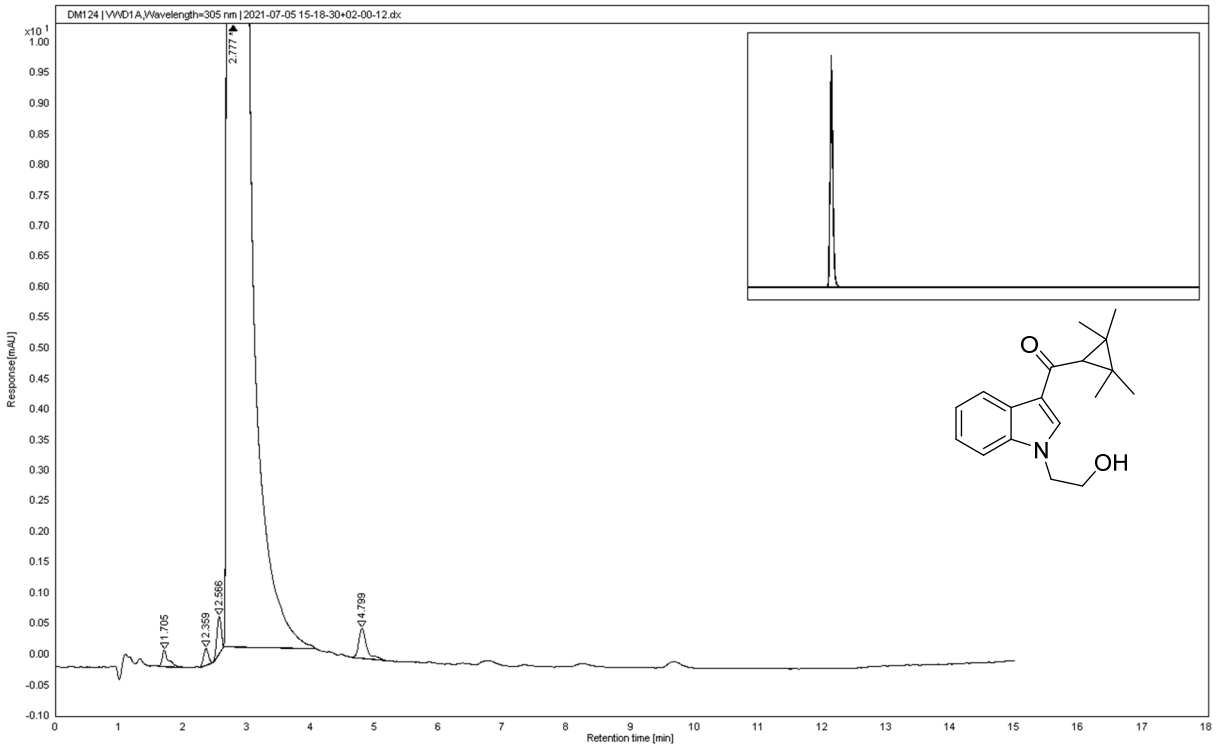

^{1}H-NMR

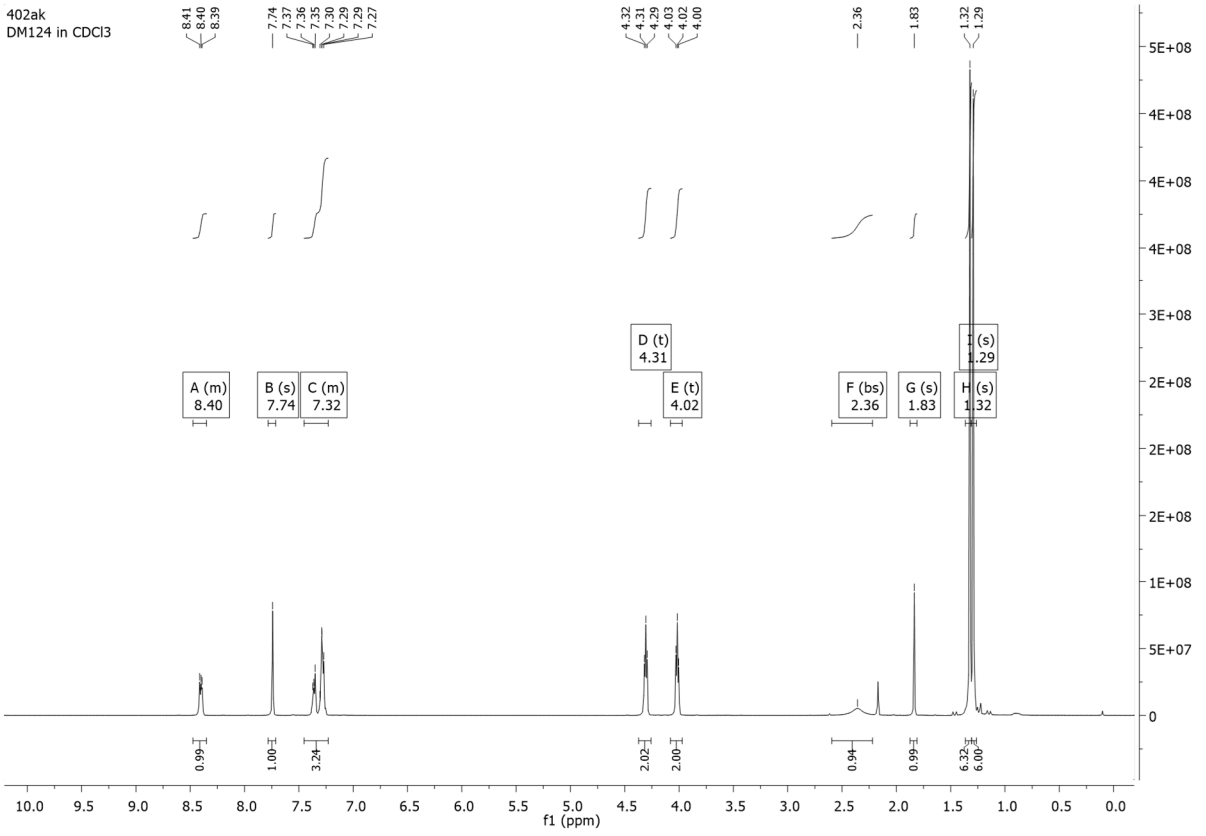

^{13}C-NMR (APT)

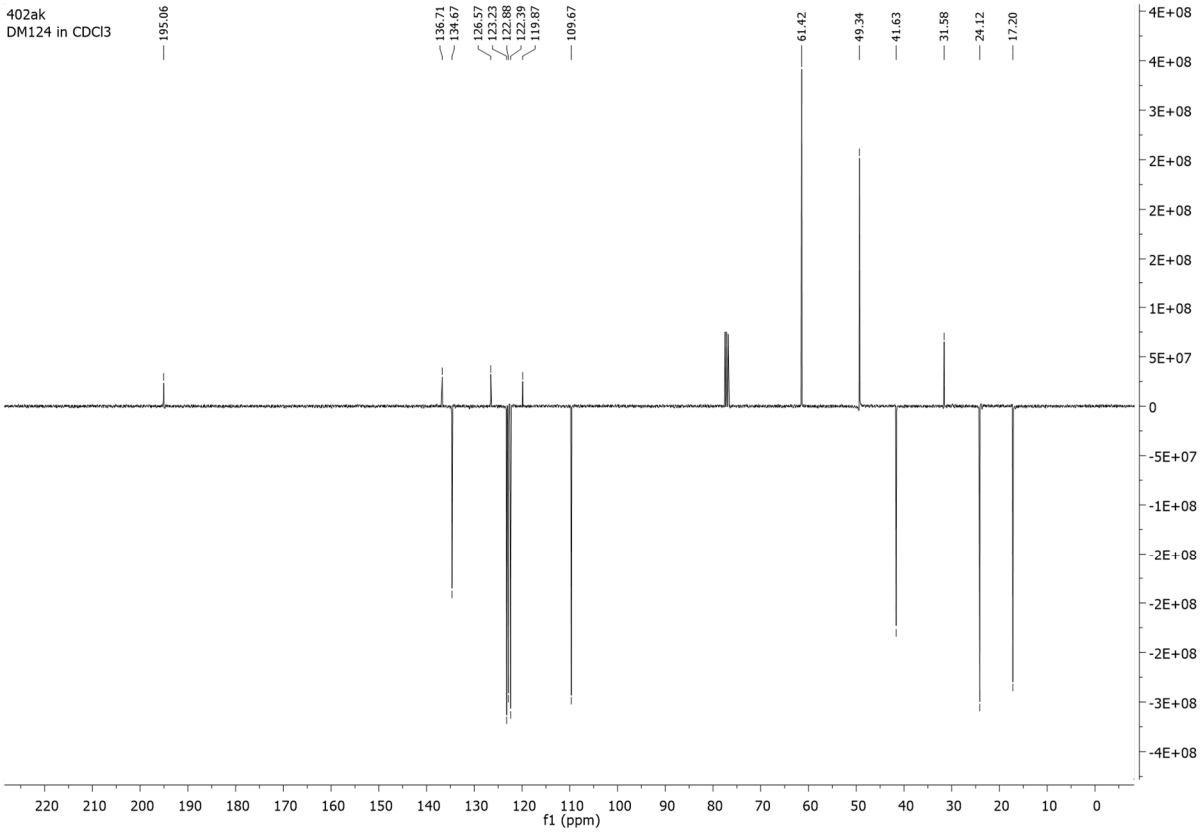
402ak
DM124 in CDCl3
195.06
136.71
134.67
126.57
123.23
122.88
122.39
119.87
109.67
61.42
49.34
41.63
31.58
24.12
17.20
4E+08
4E+08
3E+08
2E+08
2E+08
2E+08
1E+08
5E+07
0
-5E+07
-1E+08
-2E+08
-2E+08
-2E+08
-3E+08
-4E+08
220 210 200 190 180 170 160 150 140 130 120 110 100 90 80 70 60 50 40 30 20 10 0
f1 (ppm)

Compound 14

HPLC 4.816 min (k: 3.2) 98.07%

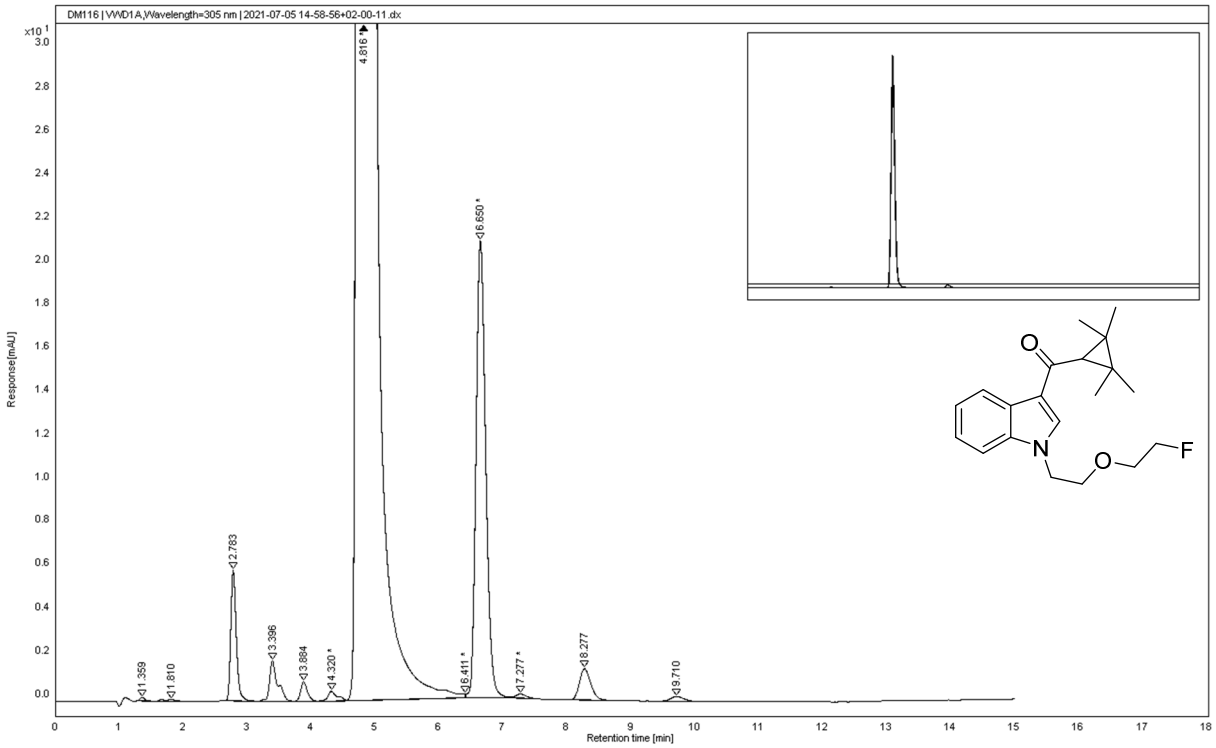

^{1}H-NMR

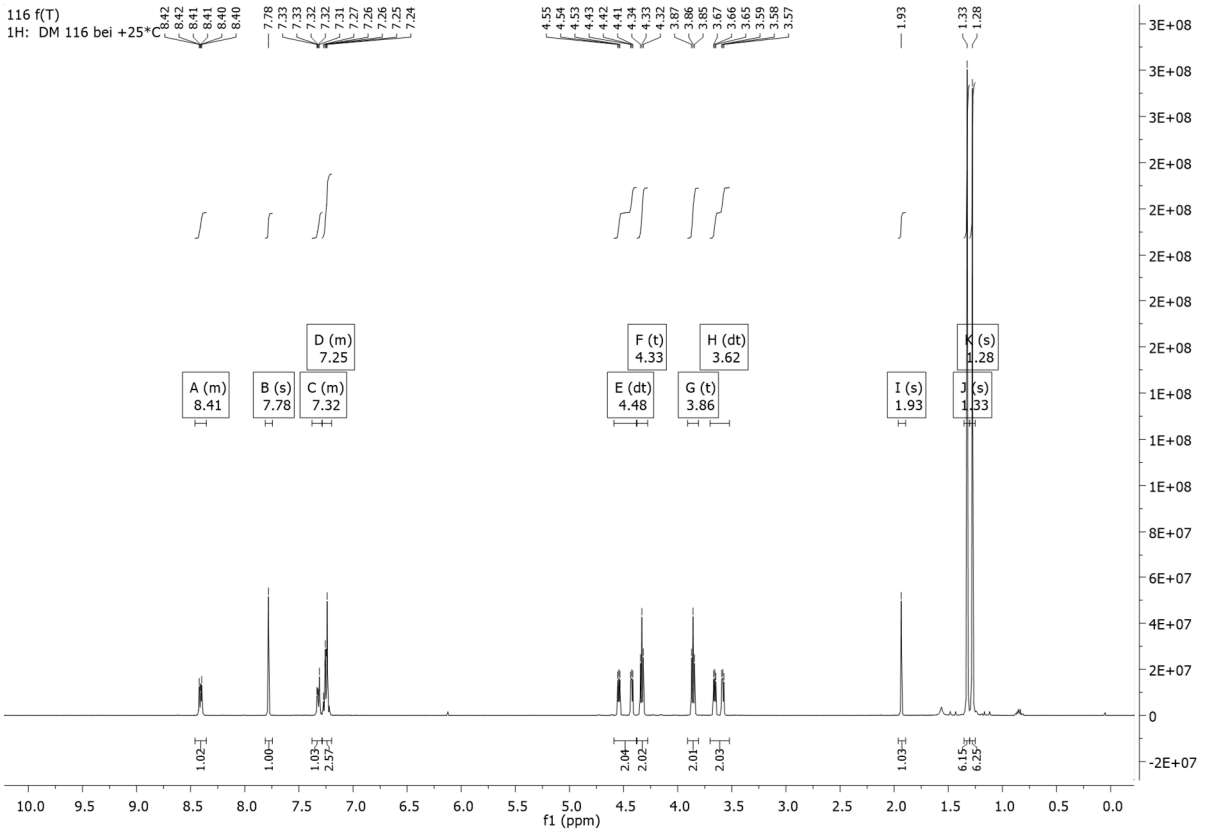

^{13}C-NMR (APT)

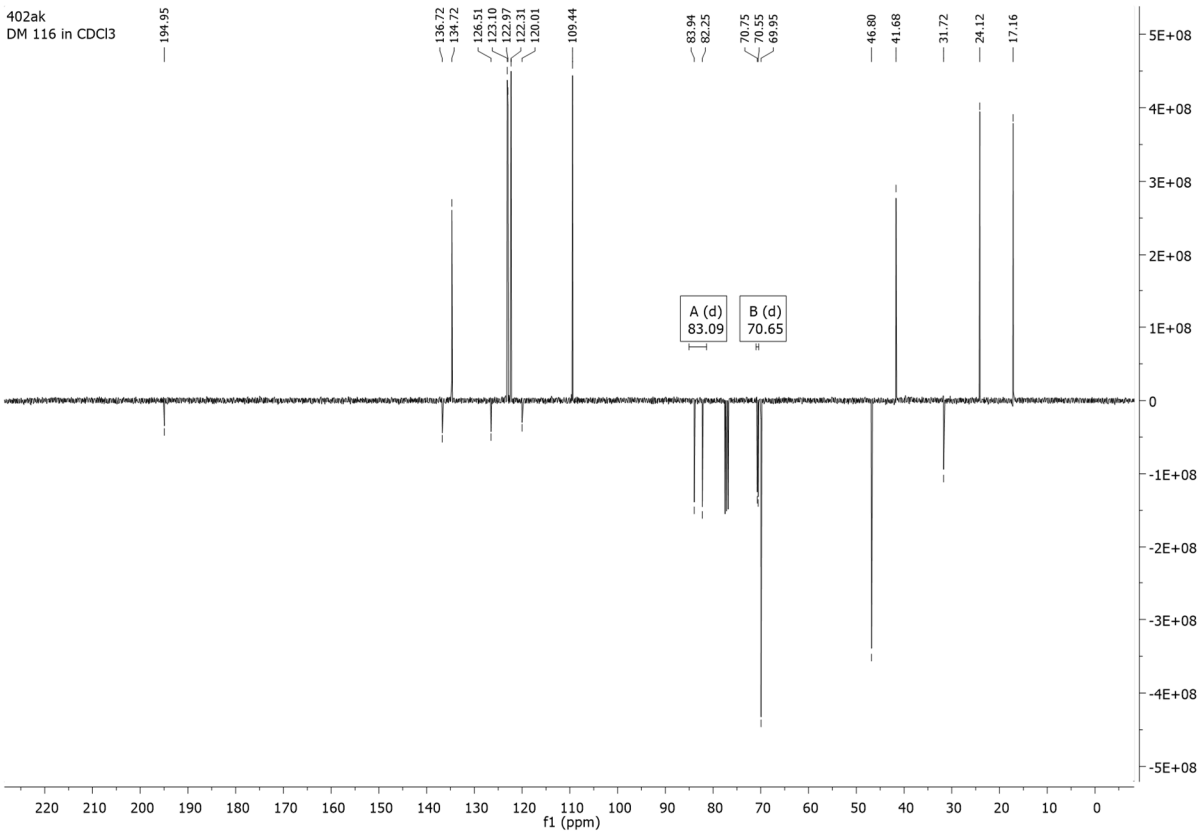

^{19}F-NMR

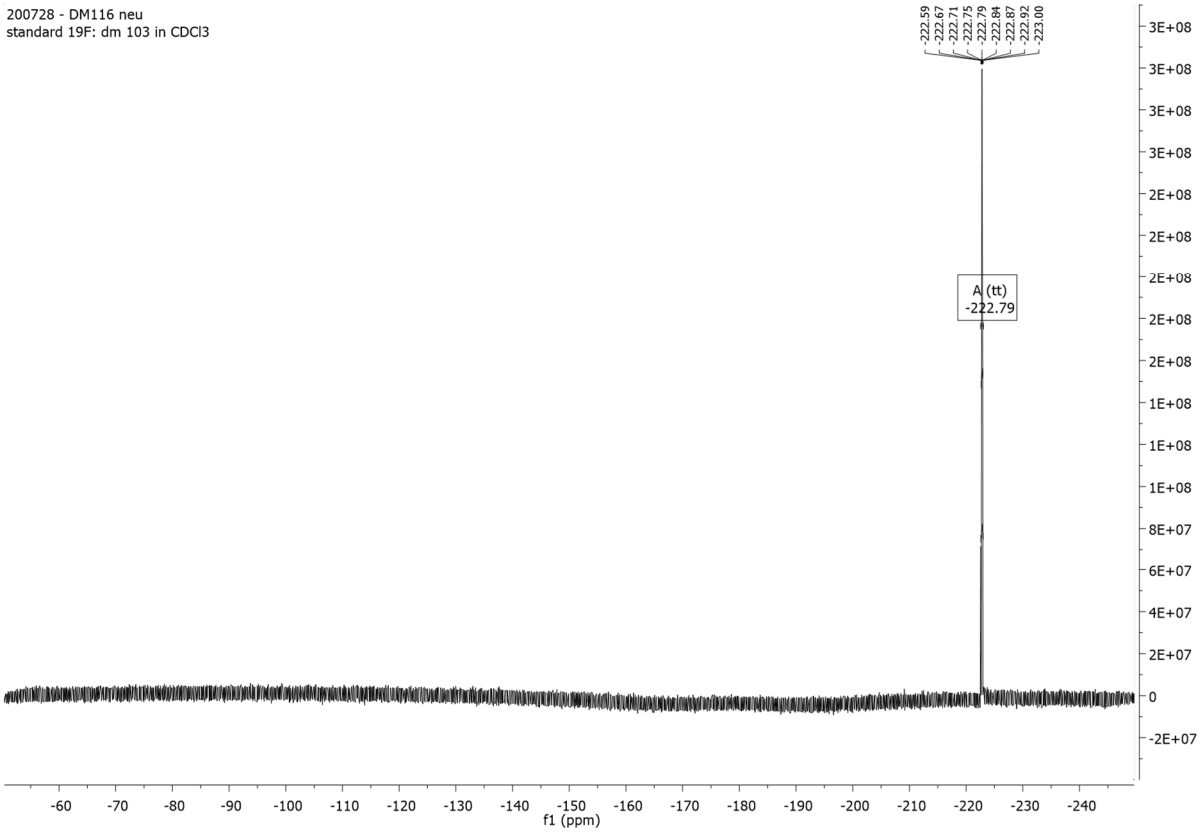

Compound 15

HPLC 6.621 min (k: 4.2) 98.73%

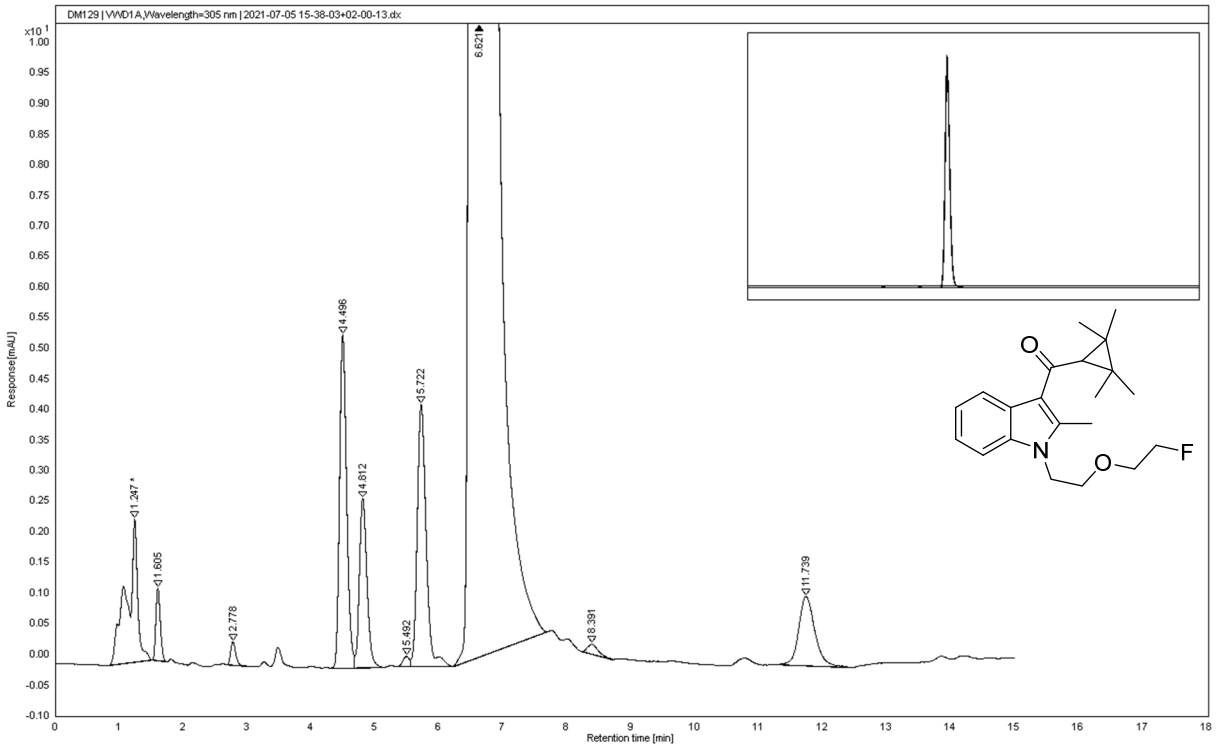

^{1}H-NMR

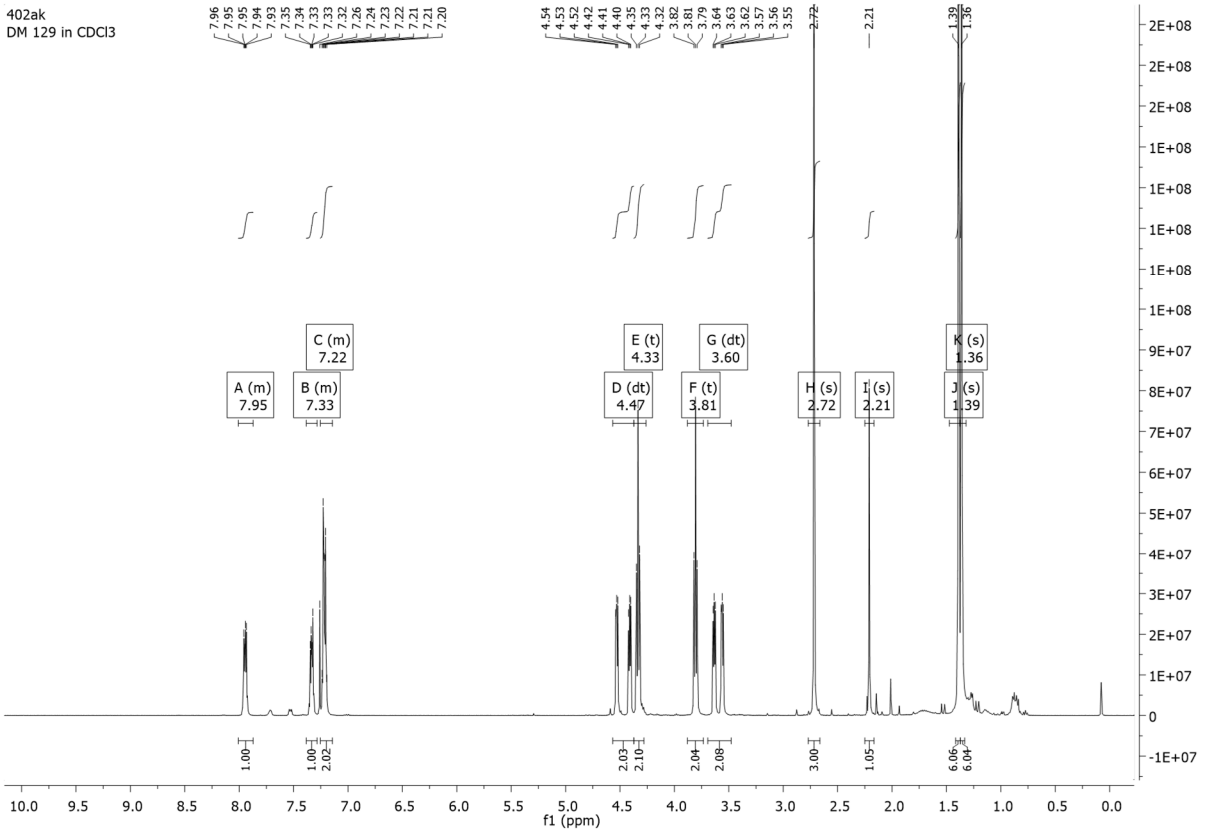

^{13}C-NMR (APT)

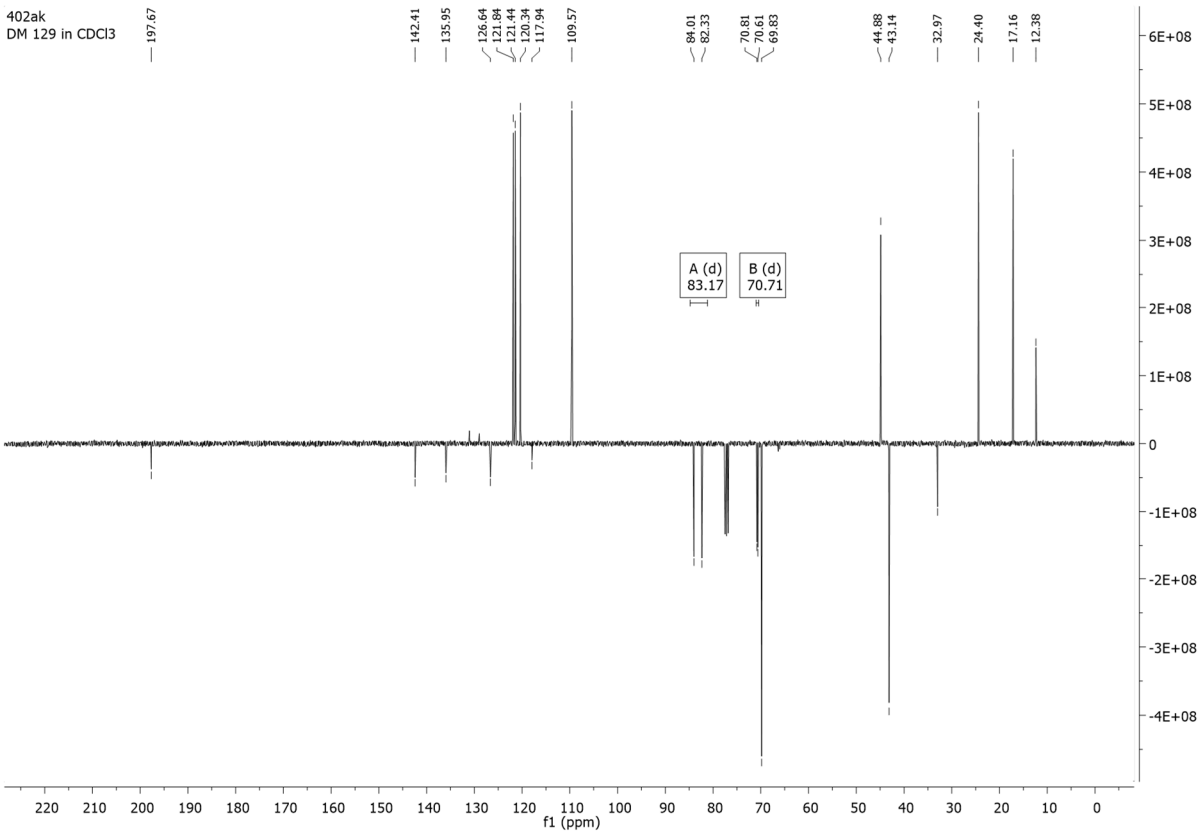

^{19}F-NMR

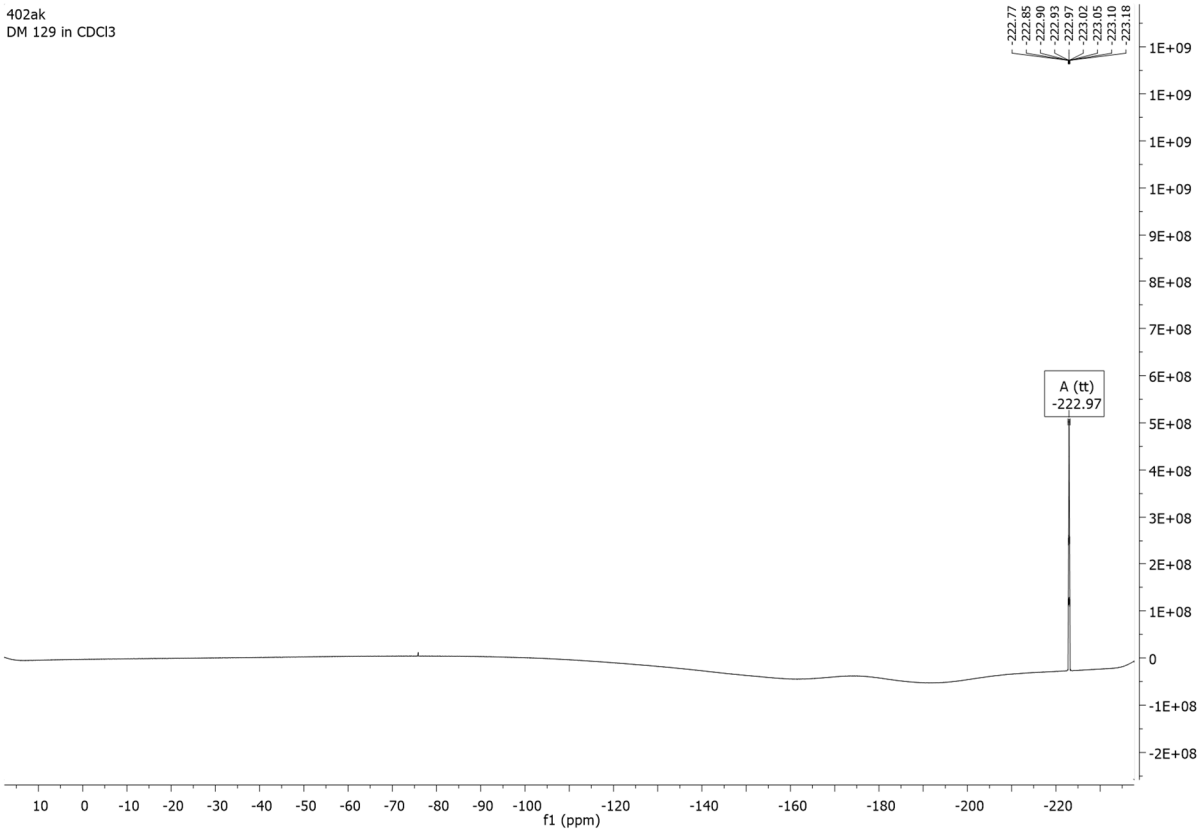

Compound 16

HPLC 8.570 min (k: 6.5) 99.96%

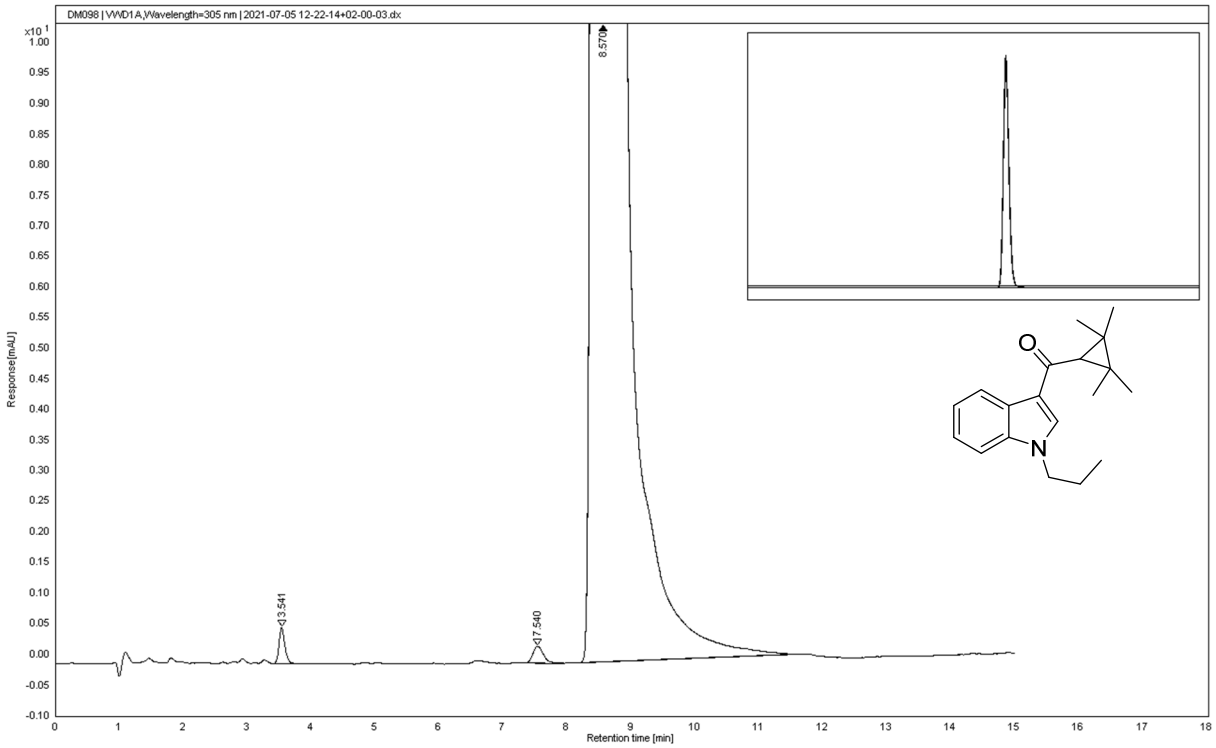

^{1}H-NMR

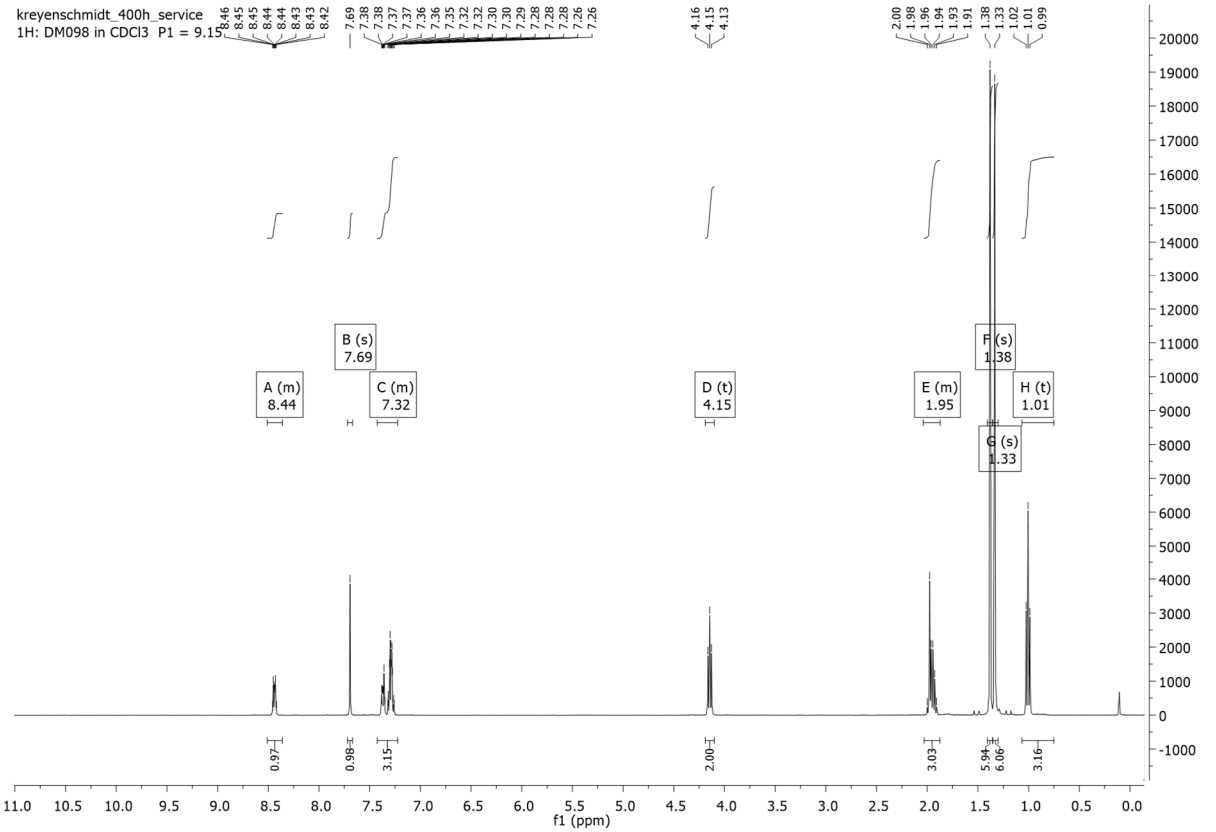

^{13}C-NMR (APT)

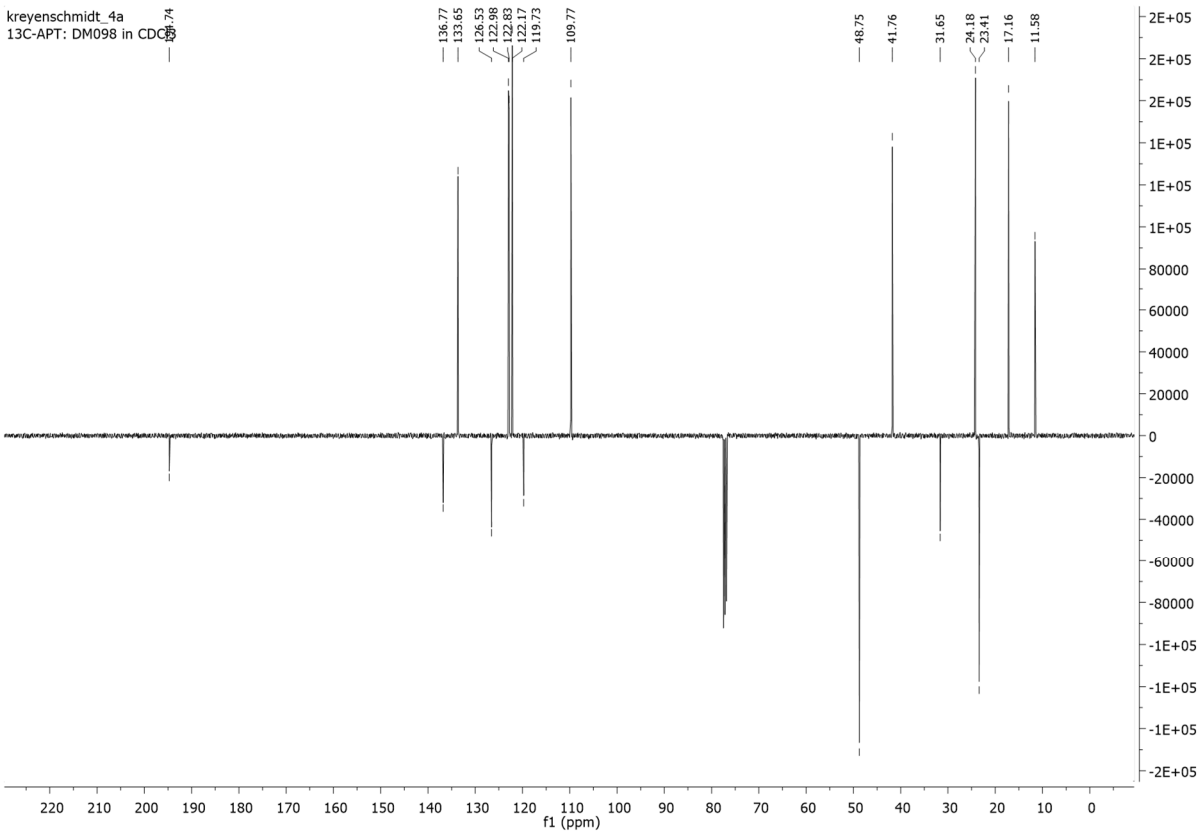
kreyenschmidt_4a
13C-APT: DM098 in CDCl3
194.74
136.77
133.65
126.53
122.98
122.83
122.17
119.73
109.77
48.75
41.76
31.65
24.18
23.41
17.16
11.58
2E+05
2E+05
2E+05
1E+05
1E+05
1E+05
80000
60000
40000
20000
0
-20000
-40000
-60000
-80000
-1E+05
-1E+05
-1E+05
-2E+05
220 210 200 190 180 170 160 150 140 130 120 110 100 90 80 70 60 50 40 30 20 10 0
f1 (ppm)

Compound 18

HPLC 2.957 min (k: 1.6) 99.23%

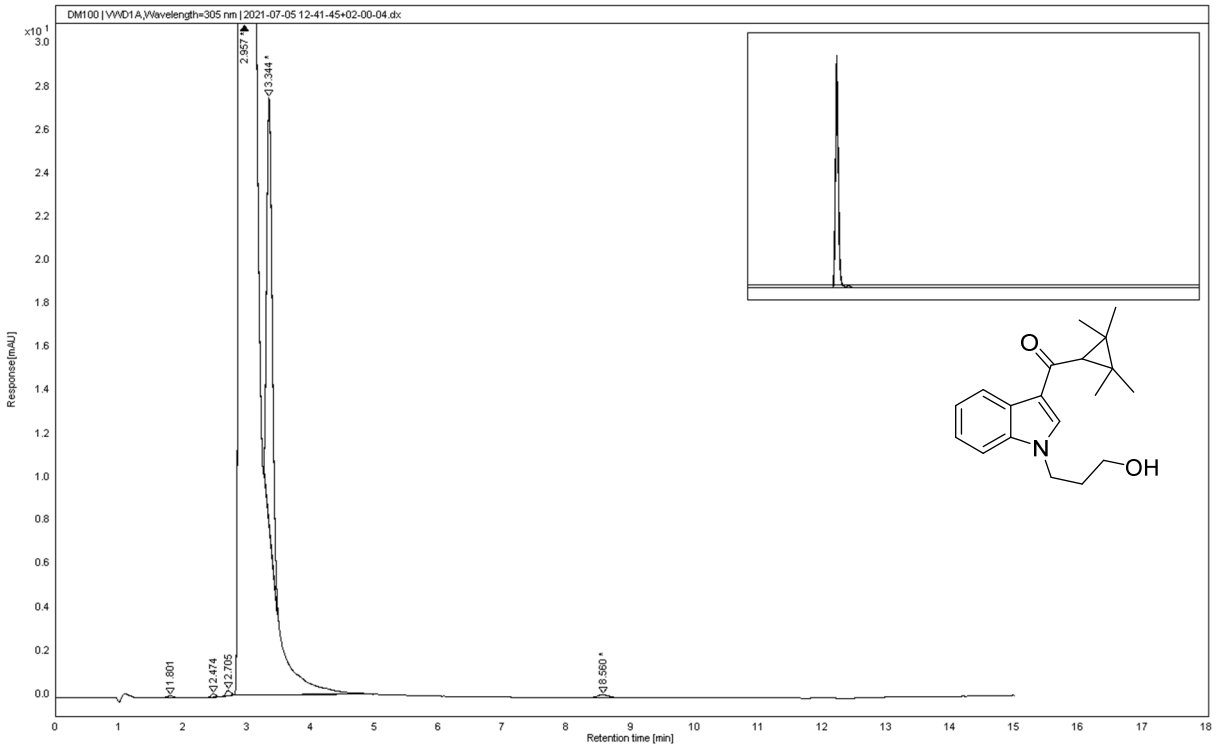

^{1}H-NMR

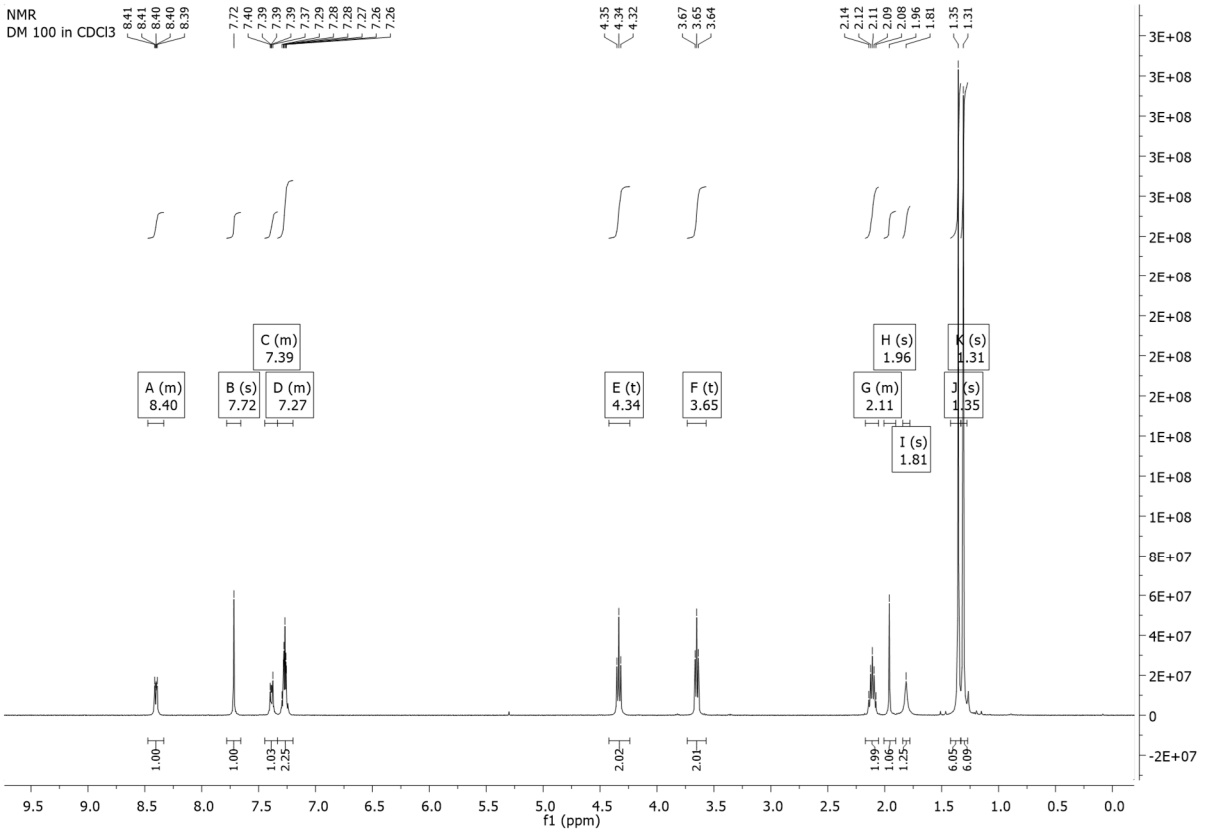

^{13}C-NMR (APT)

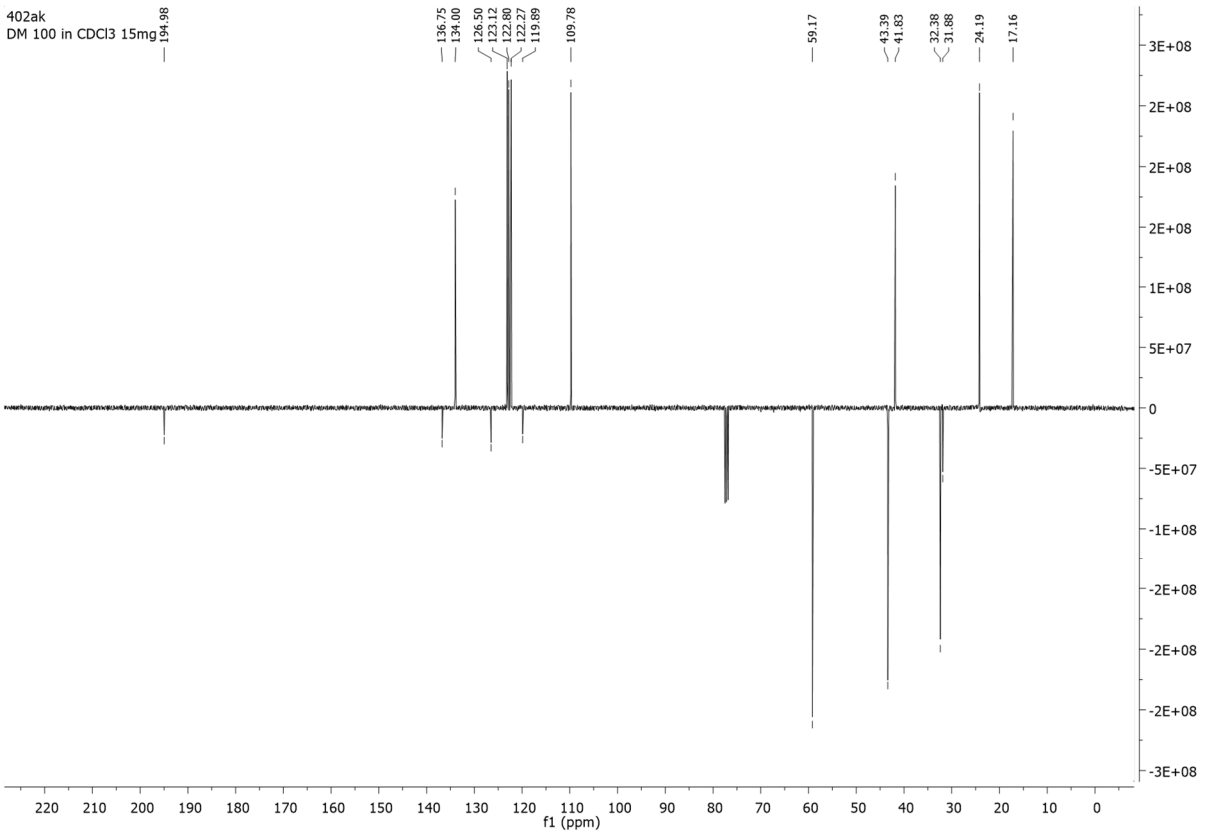
402ak
DM 100 in CDCl3 15mg
194.98
136.75
134.00
126.50
123.12
122.80
122.27
119.89
109.78
59.17
43.39
41.83
32.38
31.88
24.19
17.16
3E+08
2E+08
2E+08
2E+08
1E+08
5E+07
0
-5E+07
-1E+08
-2E+08
-2E+08
-2E+08
-3E+08
220 210 200 190 180 170 160 150 140 130 120 110 100 90 80 70 60 50 40 30 20 10 0
f1 (ppm)

Compound 19

^{1}H-NMR

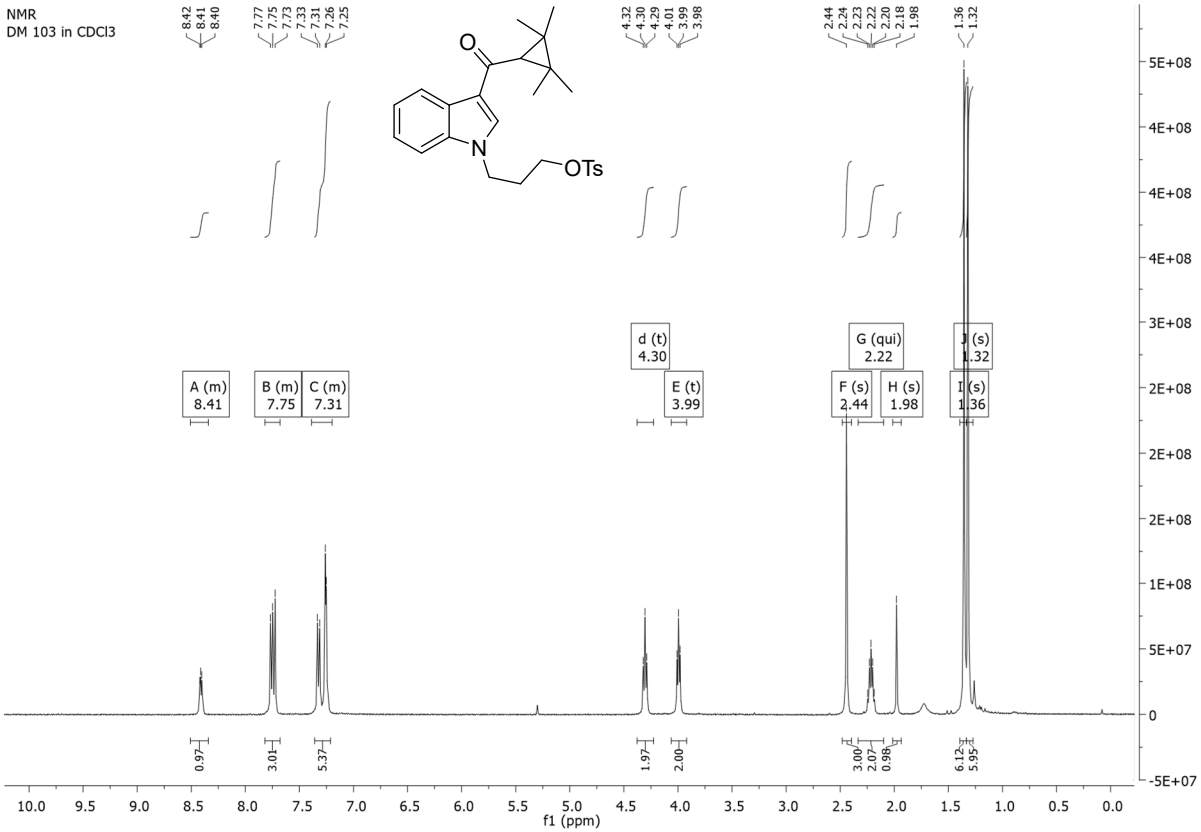

^{13}C-NMR (APT)

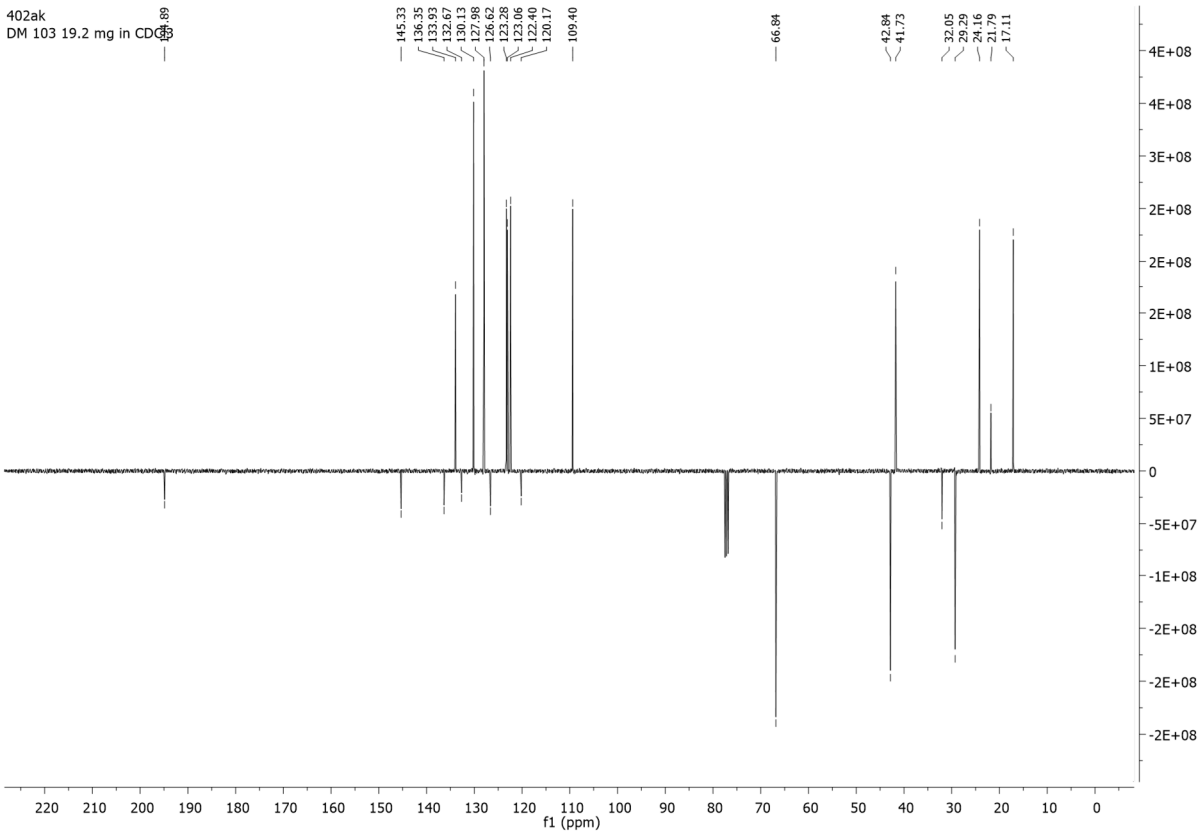

7.4. Appendix IV
Supplementary information from publication IV: Design, synthesis, and structure-activity relationships of diindolylmethane derivatives as cannabinoid CB_2 receptor agonists

The supplementary information of this publication is also available online at:

https://onlinelibrary.wiley.com/action/downloadSupplement?doi=10.1002%2Fardp.202200493&file=ardp202200493-sup-0001-ArchPharm_Supplementary_Information.docx

ARCH PHARM
Archiv der Pharmazie

Supporting Information

Design, synthesis and structure-activity relationships of diindolylmethane derivatives as cannabinoid receptor agonists

Andhika B. Mahardhika[1,2], Anastasiia Ressemann[1], Sarah E. Kremers[1], Mariana S. Gregório Castanheira[1], Clara T.Schoeder[1,2], Christa E. Müller[1,2,*], Thanigaimalai Pillaiyar[1,3,*]

1 PharmaCenter Bonn, Pharmaceutical Institute (Department of Pharmaceutical & Medicinal Chemistry, University of Bonn, An der Immenburg 4, D-53121 Bonn, Germany)
2 Research Training Group 1873 (University of Bonn, 53127 Bonn, Germany)
3 Institute of Pharmacy, Pharmaceutical/Medicinal Chemistry and Tübingen Center for Academic Drug Discovery, Eberhard Karls University, D-72076 Tübingen, Germany

*Correspondence:
Prof. Dr. Christa Müller, PharmaCenter Bonn, Pharmaceutical Institute, Pharmaceutical & Medicinal Chemistry, An der Immenburg 4, D-53121 Bonn, Germany. Phone: +49-228-73-2301. Fax: +49-228-73-2567.
E-mail: christa.mueller@uni-bonn.de
Dr. Thanigaimalai Pillaiyar, Institute of Pharmacy, Pharmaceutical/Medicinal Chemistry and Tübingen Center for Academic Drug Discovery, Eberhard Karls University, D-72076 Tübingen, Germany.
E-mail: thanigaimalai.pillaiyar@uni-tuebingen.de

Table of content

ARCH PHARM
Archiv der Pharmazie

Supplemental Material: Novel Compounds and Biological Screening Results

Table S1. InChi keys of Diindolylmethane derivatives and their activtiy at cannabinoid receptors

Compound number	InChI string	Human CB_2 receptor	Human CB_1 receptor	Human CB_2 receptor	Human CB_1 receptor		Human CB_2 receptor	Human CB_1 receptor	
		Radioligand binding assay		**cAMP assay**			**β-Arrestin recruitment assay**		
		***K*i ± SEM** (μM) (or percent inhibition of [^{3}H]CP55,940 at 5 μM) *[Maximal inhibition (%)]*	***K*i ± SEM** (μM) (or percent inhibition of [^{3}H]CP55,940 at 5 μM) *[Maximal inhibition (%)]*	EC_{50} ± SEM (μM) (or percent receptor activation at 10 μM) [*efficacy*] [a] **(Agonistic activity)**	EC_{50} ± SEM (μM) (or percent receptor activation at 10 μM) [*efficacy*] [a] **(Agonistic activity)**	IC_{50} ± SEM (μM) (or percent receptor activation at 10 μM) [b] **(Antagonistic activity)**	EC_{50} ± SEM (μM) (or percent receptor activation at 10 μM) [*efficacy*] [c] **(Agonistic activity)**	EC_{50} ± SEM (μM) (or percent receptor activation at 10 μM) [*efficacy*] [d] **(Agonistic activity)**	IC_{50} ± SEM (μM) (or percent receptor activation at 10 μM) [e] **(Antagonistic activity)**
1 (THC)	InChI=1S/C21H30O2/c1-5-6-7-8-15-12-18(22)20-16-11-14(2)9-10-17(16)21(3,4)23-19(20)13-15/h11-13,16-17,22H,5-10H2,1-4H3/t16-,17-/m1/s1	**0.00595** ± 0.0027 *[100 %]*	**0.00387** ± 0.0091	0.00527 ± 0.0019 *[59 %]*	**0.00326** ± 0.0017 *[51 %]*	n.d [f]	0.00142 ± 0.00003 *[32 %]*	n.d	n.d
2 (CP55940)	InChI=1S/C24H40O3/c1-4-5-6-7-14-24(2,3)19-11-13-21(23(27)16-19)22-17-20(26)12-10-18(22)9-8-15-25/h11,13,16,18,20,22,25-27H,4-10,12,14-15,17H2,1-3H3/t18-,20?,22+/m1/s1	**0.000293** ± 0.0008 *[100 %]*	**0.00192** ± 0.00140 *[100 %]*	**0.00320** ± 0.0068 *[100 %]*	**0.00336** ± 0.00057 *[100 %]*	n.d	**0.00262** ± 0.00003 *[100 %]*	n.d	n.d
4 (DIM)	InChI=1S/C17H14N2/c1-3-7-16-14(5-1)12(10-18-16)9-13-11-19-17-8-4-2-6-15(13)17/h1-8,10-11,18-19H,9H2	**0.690** ± 0.159 *[98 %]* (**1.1**) [a]	**5.42** ± 1.00 *[86 %]* (**4.3**) [a]	**0.334** ± 0.174 *[65 %]*	n.d	n.d	**0.562** ± 0.195 *[63 %]*	n.d	n.d
40	InChI=1S/C19H18N2/c1-12-5-3-7-16-18(12)14(10-20-16)9-15-11-21-17-8-4-6-13(2)19(15)17/h3-8,10-11,20-21H,9H2,1-2H3	**0.845** ± 0.086 *[81 %]*	**>5** (4 %)	n.d	n.d	n.d	n.d	n.d	n.d
41	InChI=1S/C19H18N2O2/c1-22-16-7-3-5-14-18(16)12(10-20-14)9-13-11-21-15-6-4-8-17(23-	**0.579** ± 0.157 *[94 %]*	**5.03** ± 2.29 *[79 %]*	n.d	n.d	n.d	n.d	n.d	n.d

ARCH PHARM
Archiv der Pharmazie

	2)19(13)15/h3-8,10-11,20-21H,9H2,1-2H3								
42 (PSB-16357)	InChI=1S/C17H12F2N2/c18-12-3-1-5-14-16(12)10(8-20-14)7-11-9-21-15-6-2-4-13(19)17(11)15/h1-6,8-9,20-21H,7H2	**0.279** ± 0.056 *[99 %]*	**>5** (28 %)	**0.0551** ± 0.0189 *[80 %]*	n.d	n.d	**0.290** ± 0.148 *[70 %]*	n.d	n.d
43	InChI=1S/C17H12Cl2N2/c18-12-3-1-5-14-16(12)10(8-20-14)7-11-9-21-15-6-2-4-13(19)17(11)15/h1-6,8-9,20-21H,7H2	**0.332** ± 0.230 *[93 %]*	**0.753** ± 0.048 *[61 %]*	n.d	**>10** (2 %)	**>10** (-22 %)	n.d	**>10** (5 %)	**>10** (43 %)
44 (PSB-19571)	InChI=1S/C17H12Br2N2/c18-12-3-1-5-14-16(12)10(8-20-14)7-11-9-21-15-6-2-4-13(19)17(11)15/h1-6,8-9,20-21H,7H2	**0.374** ± 0.074 *[100 %]*	**7.27** ± 0.45 *[99 %]*	**0.509** ± 0.100 *[85 %]*	n.d	n.d	**0.0450** ± 0.0189 *[61 %]*	n.d	n.d
45	InChI=1S/C17H12N4O4/c22-20(23)14-5-1-3-12-16(14)10(8-18-12)7-11-9-19-13-4-2-6-15(17(11)13)21(24)25/h1-6,8-9,18-19H,7H2	**>5** (29 %)	**>5** (6 %)	n.d	n.d	n.d	n.d	n.d	n.d
46 (PSB-19837)	InChI=1S/C19H12N4/c20-8-12-3-1-5-16-18(12)14(10-22-16)7-15-11-23-17-6-2-4-13(9-21)19(15)17/h1-6,10-11,22-23H,7H2	**0.339** ± 0.061 *[99 %]*	**≥10** (47%)	**0.0144** ± 0.0023 *[95 %]*	n.d	n.d	**0.0149** ± 0.0021 *[67 %]*	n.d	n.d
47	InChI=1S/C19H18N2/c1-12-3-5-18-16(7-12)14(10-20-18)9-15-11-21-19-6-4-13(2)8-17(15)19/h3-8,10-11,20-21H,9H2,1-2H3	**2.78 ±** 1.36 *[86 %]*	**>5** (26 %)	n.d	n.d	n.d	n.d	n.d	n.d
48 (PSB-16105)	InChI=1S/C19H18N2O2/c1-22-14-3-5-18-16(8-14)12(10-20-18)7-13-11-21-19-6-4-15(23-2)9-17(13)19/h3-6,8-11,20-21H,7H2,1-2H3	**2.84** ± 1.51 *[83 %]*	**5.89** ± 1.28 *[62 %]*	n.d	n.d	n.d	n.d	n.d	n.d
49	InChI=1S/C17H12F2N2/c18-12-1-3-16-14(6-12)10(8-20-16)5-	**1.17** ± 0.33	**4.08** ± 0.22	n.d	n.d	n.d	n.d	n.d	n.d

ARCH PHARM
Archiv der Pharmazie

(PSB-15160)	11-9-21-17-4-2-13(19)7-15(11)17/h1-4,6-9,20-21H,5H2	*[100 %]*	*[96 %]*						
50	InChI=1S/C19H12F6N2/c20-18(21,22)12-1-3-16-14(6-12)10(8-26-16)5-11-9-27-17-4-2-13(7-15(11)17)19(23,24)25/h1-4,6-9,26-27H,5H2	**1.98** ± 0.140 *[100 %]*	**9.94** ± 3.86 *[100 %]*	n.d	n.d	n.d	n.d	n.d	n.d
51	InChI=1S/C17H12Cl2N2/c18-12-1-3-16-14(6-12)10(8-20-16)5-11-9-21-17-4-2-13(19)7-15(11)17/h1-4,6-9,20-21H,5H2	**0.747 ±** 0.067 *[73 %]*	**>5** (6 %)	n.d	n.d	n.d	n.d	n.d	n.d
52	InChI=1S/C17H12Br2N2/c18-12-1-3-16-14(6-12)10(8-20-16)5-11-9-21-17-4-2-13(19)7-15(11)17/h1-4,6-9,20-21H,5H2	**1.27** ± 0.226 *[100 %]*	**>5** (34 %)	n.d	n.d	n.d	n.d	n.d	n.d
53	InChI=1S/C19H12N4/c20-8-12-1-3-18-16(5-12)14(10-22-18)7-15-11-23-19-4-2-13(9-21)6-17(15)19/h1-6,10-11,22-23H,7H2	**>5** (30 %)	**>5** (35 %)	n.d	n.d	n.d	n.d	n.d	n.d
54	InChI=1S/C17H12N4O4/c22-20(23)12-1-3-16-14(6-12)10(8-18-16)5-11-9-19-17-4-2-13(21(24)25)7-15(11)17/h1-4,6-9,18-19H,5H2	**≥5** (45 %)	**>5** (30 %)	n.d	n.d	n.d	n.d	n.d	n.d
55	InChI=1S/C21H18N2O4/c1-26-20(24)12-3-5-18-16(8-12)14(10-22-18)7-15-11-23-19-6-4-13(9-17(15)19)21(25)27-2/h3-6,8-11,22-23H,7H2,1-2H3	**2.99** ± 0.029 *[71 %]*	**>5** (19 %)	n.d	n.d	n.d	n.d	n.d	n.d
56	InChI=1S/C19H14N2O2/c22-10-12-1-3-18-16(5-12)14(8-20-18)7-15-9-21-19-4-2-13(11-23)6-17(15)19/h1-6,8-11,20-21H,7H2	**7.25** ± 1.39 *[71 %]*	**>5** (23 %)	n.d	n.d	n.d	n.d	n.d	n.d
57	InChI=1S/C19H14N2O4/c22-18(23)10-1-3-16-14(6-10)12(8-20-16)5-13-9-21-17-4-2-	**>5** (34 %)	**>5** (-17 %)	n.d	n.d	n.d	n.d	n.d	n.d

ARCH PHARM
Archiv der Pharmazie

	11(19(24)25)7-15(13)17/h1-4,6-9,20-21H,5H2,(H,22,23)(H,24,25)								
58	InChI=1S/C31H26N2O2/c1-3-7-22(8-4-1)20-34-26-11-13-30-28(16-26)24(18-32-30)15-25-19-33-31-14-12-27(17-29(25)31)35-21-23-9-5-2-6-10-23/h1-14,16-19,32-33H,15,20-21H2	**>5** (37 %)	**2.95** ± 0.749 *[88 %]*	n.d	n.d	n.d	n.d	n.d	n.d
59	InChI=1S/C19H18N2/c1-12-3-5-16-14(10-20-18(16)7-12)9-15-11-21-19-8-13(2)4-6-17(15)19/h3-8,10-11,20-21H,9H2,1-2H3	**0.504** ± 0.252 *[76 %]*	**>5** (30 %)	n.d	n.d	n.d	n.d	n.d	n.d
60	InChI=1S/C19H18N2O2/c1-22-14-3-5-16-12(10-20-18(16)8-14)7-13-11-21-19-9-15(23-2)4-6-17(13)19/h3-6,8-11,20-21H,7H2,1-2H3	**>5** (32 %)	**>5** (26 %)	n.d	n.d	n.d	n.d	n.d	n.d
61 (PSB-16358)	InChI=1S/C17H12F2N2/c18-12-1-3-14-10(8-20-16(14)6-12)5-11-9-21-17-7-13(19)2-4-15(11)17/h1-4,6-9,20-21H,5H2	**0.985** ± 0.094 *[90 %]*	**>5** (27 %)	n.d	n.d	n.d	n.d	n.d	n.d
62	InChI=1S/C17H12ClN2/c18-12-1-3-14-10(8-20-16(14)6-12)5-11-9-21-17-7-13(19)2-4-15(11)17/h1-4,6-9,20-21H,5H2	**0.911** ± 0.105 *[84 %]*	**0.820** ± 0.385 *[59 %]*	n.d	**>10** (11 %)	**>10** (13 %)	**>10** (2 %)	**>10** (35 %)	n.d
63	InChI=1S/C17H12BrN2/c18-12-1-3-14-10(8-20-16(14)6-12)5-11-9-21-17-7-13(19)2-4-15(11)17/h1-4,6-9,20-21H,5H2	**3.44** ± 0.56 *[100 %]*	**5.28** ± 2.02 *[100 %]*	n.d	n.d	n.d	n.d	n.d	n.d
64 (PSB-16381)	InChI=1S/C17H12F2N2/c18-14-5-1-3-12-10(8-20-16(12)14)7-11-9-21-17-13(11)4-2-6-15(17)19/h1-6,8-9,20-21H,7H2	**≥5** (49 %)	**>5** (18 %)	n.d	n.d	n.d	n.d	n.d	n.d
65	InChI=1S/C19H18N2O2/c1-22-16-7-3-5-14-12(10-20-18(14)16)9-13-11-21-19-	**≥5** (48 %)	**>5** (30 %)	n.d	n.d	n.d	n.d	n.d	n.d

ARCH PHARM
Archiv der Pharmazie

	15(13)6-4-8-17(19)23-2/h3-8,10-11,20-21H,9H2,1-2H3								
66	InChI=1S/C17H10Cl4N2/c18-10-2-12(20)16-8(6-22-14(16)4-10)1-9-7-23-15-5-11(19)3-13(21)17(9)15/h2-7,22-23H,1H2	**0.626 ±** 0.22 *[90 %]*	**1.68** ± 0.32 *[68 %]*	n.d	n.d	n.d	n.d	n.d	n.d
67	InChI=1S/C17H10Cl2F2N2/c18-12-4-16-10(2-14(12)20)8(6-22-16)1-9-7-23-17-5-13(19)15(21)3-11(9)17/h2-7,22-23H,1H2	>5 (36 %)	**>5** (25 %)	n.d	n.d	n.d	n.d	n.d	n.d
68	InChI=1S/C17H10F4N2/c18-10-1-3-12-14(16(10)20)8(6-22-12)5-9-7-23-13-4-2-11(19)17(21)15(9)13/h1-4,6-7,22-23H,5H2	**3.04** ± 0.781 *[90 %]*	**5.34** ± 1.81 *[70 %]*	n.d	n.d	n.d	n.d	n.d	n.d
69 (PSB-16586)	InChI=1S/C17H10F4N2/c18-12-2-10-8(6-22-16(10)4-14(12)20)1-9-7-23-17-5-15(21)13(19)3-11(9)17/h2-7,22-23H,1H2	≈5 (59 %)	**>5** (39 %)	n.d	n.d	n.d	n.d	n.d	n.d
70 (PSB-16671)	InChI=1S/C17H10F4N2/c18-10-2-12-8(6-22-16(12)14(20)4-10)1-9-7-23-17-13(9)3-11(19)5-15(17)21/h2-7,22-23H,1H2	**1.10** ± 0.19 *[100 %]*	**2.64** ± 0.28 *[100 %]*	n.d	n.d	n.d	n.d	n.d	n.d
71	InChI=1S/C19H18N2/c1-20-12-14(16-7-3-5-9-18(16)20)11-15-13-21(2)19-10-6-4-8-17(15)19/h3-10,12-13H,11H2,1-2H3	**3.39** ± 1.14 *[68 %]*	**>5** (35 %)	n.d	n.d	n.d	n.d	n.d	n.d
72	InChI=1S/C19H18N2/c1-12-16(14-7-3-5-9-18(14)20-12)11-17-13(2)21-19-10-6-4-8-15(17)19/h3-10,20-21H,11H2,1-2H3	**≥ 5** (48 %)	**>5** (45 %)	n.d	n.d	n.d	n.d	n.d	n.d
73	InChI=1S/C15H12N4/c1-3-12-10(8-18-14(12)16-5-1)7-11-9-	**>5** (3 %)	**>5** (20 %)	n.d	n.d	n.d	n.d	n.d	n.d

ARCH PHARM
Archiv der Pharmazie

	19-15-13(11)4-2-6-17-15/h1-6,8-9H,7H2,(H,16,18)(H,17,19)								
100	InChI=1S/C18H16N2/c1-12(15-10-19-17-8-4-2-6-13(15)17)16-11-20-18-9-5-3-7-14(16)18/h2-12,19-20H,1H3	**5.74** ± 0.30 *[77 %]*	**8.15** ± 2.40 *[71 %]*	n.d	n.d	n.d	n.d	n.d	n.d
101	InChI=1S/C19H18N2/c1-2-13(16-11-20-18-9-5-3-7-14(16)18)17-12-21-19-10-6-4-8-15(17)19/h3-13,20-21H,2H2,1H3	**0.804** ± 0.25 *[97 %]*	**2.70** ± 1.86 *[90 %]*	n.d	n.d	n.d	n.d	n.d	n.d
102	InChI=1S/C20H20N2/c1-2-7-14(17-12-21-19-10-5-3-8-15(17)19)18-13-22-20-11-6-4-9-16(18)20/h3-6,8-14,21-22H,2,7H2,1H3	**>5** (33 %)	**>5** (45 %)	n.d	n.d	n.d	n.d	n.d	n.d
103	InChI=1S/C21H22N2/c1-2-3-8-15(18-13-22-20-11-6-4-9-16(18)20)19-14-23-21-12-7-5-10-17(19)21/h4-7,9-15,22-23H,2-3,8H2,1H3	**>5** (36 %)	**>5** (-2 %)	n.d	n.d	n.d	n.d	n.d	n.d
104	InChI=1S/C24H20N2/c1-16-10-12-17(13-11-16)24(20-14-25-22-8-4-2-6-18(20)22)21-15-26-23-9-5-3-7-19(21)23/h2-15,24-26H,1H3	**2.55** ± 0.28 *[98 %]*	**2.51** ± 0.40 *[100 %]*	n.d	n.d	n.d	n.d	n.d	n.d
105	InChI=1S/C24H20N2/c1-16-7-6-8-17(13-16)24(20-14-25-22-11-4-2-9-18(20)22)21-15-26-23-12-5-3-10-19(21)23/h2-15,24-26H,1H3	**1.79** ± 0.36 *[79 %]*	**3.56** ± 1.47 *[74 %]*	n.d	n.d	n.d	n.d	n.d	n.d
106	InChI=1S/C24H20N2/c1-16-8-2-3-9-17(16)24(20-14-25-22-12-6-4-10-18(20)22)21-15-26-23-13-7-5-11-19(21)23/h2-15,24-26H,1H3	**4.55** ± 1.52 *[59 %]*	**2.98** ± 1.76 *[58 %]*	n.d	n.d	n.d	n.d	n.d	n.d
107	InChI=1S/C25H22N2/c1-2-17-11-13-18(14-12-17)25(21-15-26-23-9-5-3-7-19(21)23)22-16-	**1.35** ± 0.56 *[95 %]*	**4.44** ± 2.16 *[100 %]*	n.d	n.d	n.d	n.d	n.d	n.d

ARCH PHARM
Archiv der Pharmazie

	27-24-10-6-4-8-20(22)24/h3-16,25-27H,2H2,1H3								
108	InChI=1S/C26H24N2/c1-17(2)18-11-13-19(14-12-18)26(22-15-27-24-9-5-3-7-20(22)24)23-16-28-25-10-6-4-8-21(23)25/h3-17,26-28H,1-2H3	**1.55** ± 0.41 *[85 %]*	**0.832** ± 0.281 *[82 %]*	n.d	n.d	n.d	n.d	n.d	n.d
109	InChI=1S/C24H20N2O/c1-27-17-12-10-16(11-13-17)24(20-14-25-22-8-4-2-6-18(20)22)21-15-26-23-9-5-3-7-19(21)23/h2-15,24-26H,1H3	**2.41** ± 0.02 *[73 %]*	**0.774** ± 0.169 *[71 %]*	n.d	**>10** (1 %)	**>10** (10 %)	**>10** (1 %)	**6.09** ± 0.50	n.d
110	InChI=1S/C24H20N2O/c1-27-17-8-6-7-16(13-17)24(20-14-25-22-11-4-2-9-18(20)22)21-15-26-23-12-5-3-10-19(21)23/h2-15,24-26H,1H3	**2.07** ± 0.75 *[96 %]*	**3.04** ± 1.16 *[91 %]*	n.d	n.d	n.d	n.d	n.d	n.d
111	InChI=1S/C24H20N2O/c1-27-23-13-7-4-10-18(23)24(19-14-25-21-11-5-2-8-16(19)21)20-15-26-22-12-6-3-9-17(20)22/h2-15,24-26H,1H3	**2.72** ± 2.02 *[59 %]*	**1.70** ± 0.41 *[84 %]*	n.d	n.d	n.d	n.d	n.d	n.d
112	InChI=1S/C24H18N2O2/c1-3-9-20-15(6-1)18(12-25-20)23(17-8-5-11-22-24(17)28-14-27-22)19-13-26-21-10-4-2-7-16(19)21/h1-13,23,25-26H,14H2	**3.04** ± 0.22 *[84 %]*	**1.19** ± 0.102 *[84 %]*	n.d	n.d	n.d	n.d	n.d	n.d
113	InChI=1S/C29H22N2O/c1-2-8-21(9-3-1)32-22-16-14-20(15-17-22)29(25-18-30-27-12-6-4-10-23(25)27)26-19-31-28-13-7-5-11-24(26)28/h1-19,29-31H	**>5** (41 %)	**0.402** ± 0.306 *[80 %]*	n.d	**>10** (0 %)	**>10** (-3 %)	**>10** (1 %)	**4.43** ± 0.61	n.d
114	InChI=1S/C23H18N2O/c26-16-11-9-15(10-12-16)23(19-13-24-21-7-3-1-5-17(19)21)20-14-25-22-8-4-2-6-18(20)22/h1-14,23-26H	**7.13** ± 0.617 *[60 %]*	**>5** (43 %)	n.d	n.d	n.d	n.d	n.d	n.d
115	InChI=1S/C23H17ClN2/c24-16-11-9-15(10-12-16)23(19-13-25-	**3.06** ± 0.90	**1.24** ± 0.398	n.d	n.d	n.d	n.d	n.d	n.d

ARCH PHARM
Archiv der Pharmazie

	21-7-3-1-5-17(19)21)20-14-26-22-8-4-2-6-18(20)22/h1-14,23,25-26H	*[94 %]*	*[92 %]*						
116	InChI=1S/C23H17FN2/c24-16-11-9-15(10-12-16)23(19-13-25-21-7-3-1-5-17(19)21)20-14-26-22-8-4-2-6-18(20)22/h1-14,23,25-26H	**>5** (44 %)	**3.54** ± 1.49 *[88 %]*	n.d	n.d	n.d	n.d	n.d	n.d
117	InChI=1S/C23H17N3O2/c27-26(28)16-11-9-15(10-12-16)23(19-13-24-21-7-3-1-5-17(19)21)20-14-25-22-8-4-2-6-18(20)22/h1-14,23-25H	**1.57** ± 0.04 *[80 %]*	**0.596** ± 0.240 *[78 %]*	n.d	n.d	n.d	n.d	n.d	n.d
118	InChI=1S/C29H24N2O2/c1-32-25-14-6-12-23-28(25)21(16-30-23)27(20-11-5-9-18-8-3-4-10-19(18)20)22-17-31-24-13-7-15-26(33-2)29(22)24/h3-17,27,30-31H,1-2H3	**>5** (9 %)	**>5** (7 %)	n.d	n.d	n.d	n.d	n.d	n.d
119	InChI=1S/C28H22N2O/c1-31-21-13-12-18-14-20(11-10-19(18)15-21)28(24-16-29-26-8-4-2-6-22(24)26)25-17-30-27-9-5-3-7-23(25)27/h2-17,28-30H,1H3	**>5** (36 %)	**0.983** ± 0.463 *[69 %]*	n.d	n.d	n.d	n.d	n.d	n.d
120	InChI=1S/C25H19N3/c1-4-10-22-16(7-1)19(13-26-22)25(20-14-27-23-11-5-2-8-17(20)23)21-15-28-24-12-6-3-9-18(21)24/h1-15,25-28H	**>5** (9 %)	**>5** (18 %)	n.d	n.d	n.d	n.d	n.d	n.d
121	InChI=1S/C25H22N2O2/c1-28-21-12-6-10-19-24(21)17(14-26-19)23(16-8-4-3-5-9-16)18-15-27-20-11-7-13-22(29-2)25(18)20/h3-15,23,26-27H,1-2H3	**>5** (35 %)	**>5** (44 %)	n.d	n.d	n.d	n.d	n.d	n.d
122	InChI=1S/C26H24N2O3/c1-29-17-12-10-16(11-13-17)24(18-14-27-20-6-4-8-22(30-2)25(18)20)19-15-28-21-7-5-9-	**>5** (26 %)	**0.541** ± 0.173 *[88 %]*	n.d	**>10** (0 %)	**>10** (31 %)	**>10** (1 %)	**3.06** ± 0.29	n.d

ARCH PHARM
Archiv der Pharmazie

	23(31-3)26(19)21/h4-15,24,27-28H,1-3H3								
123	InChI=1S/C26H24N2O2/c1-16-4-6-17(7-5-16)26(22-14-27-24-10-8-18(29-2)12-20(22)24)23-15-28-25-11-9-19(30-3)13-21(23)25/h4-15,26-28H,1-3H3	**>5** (42 %)	**0.414** ± 0.26 *[68 %]*	n.d	**>10** (-10 %)	**>10** (32 %)	**>10** (0 %)	**6.43** ± 0.45	n.d
124	InChI=1S/C25H21FN2O2/c1-29-17-7-9-23-19(11-17)21(13-27-23)25(15-3-5-16(26)6-4-15)22-14-28-24-10-8-18(30-2)12-20(22)24/h3-14,25,27-28H,1-2H3	**>5** (18 %)	**>5** (34 %)	n.d	n.d	n.d	n.d	n.d	n.d
125	InChI=1S/C26H24N2O3/c1-29-17-6-4-16(5-7-17)26(22-14-27-24-10-8-18(30-2)12-20(22)24)23-15-28-25-11-9-19(31-3)13-21(23)25/h4-15,26-28H,1-3H3	**2.04** ± 0.37 *[91 %]*	**0.176** ± 0.649 *[83 %]*	n.d	n.d	n.d	n.d	n.d	n.d
126	InChI=1S/C25H22N2/c1-16-8-10-23-19(12-16)21(14-26-23)25(18-6-4-3-5-7-18)22-15-27-24-11-9-17(2)13-20(22)24/h3-15,25-27H,1-2H3	**>5** (-8 %)	**>5** (-31 %)	n.d	n.d	n.d	n.d	n.d	n.d
127	InChI=1S/C26H24N2O/c1-16-4-10-24-20(12-16)22(14-27-24)26(18-6-8-19(29-3)9-7-18)23-15-28-25-11-5-17(2)13-21(23)25/h4-15,26-28H,1-3H3	**1.30** ± 0.45 *[79 %]*	**2.34** ± 0.172 *[76 %]*	n.d	n.d	n.d	n.d	n.d	n.d
128	InChI=1S/C25H21FN2/c1-15-3-9-23-19(11-15)21(13-27-23)25(17-5-7-18(26)8-6-17)22-14-28-24-10-4-16(2)12-20(22)24/h3-14,25,27-28H,1-2H3	**2.18** ± 0.29 *[87 %]*	**2.69** ± 0.60 *[92 %]*	n.d	n.d	n.d	n.d	n.d	n.d
129	InChI=1S/C27H18F2N2/c28-19-7-9-25-21(12-19)23(14-30-25)27(18-6-5-16-3-1-2-4-17(16)11-18)24-15-31-26-10-8-	**2.35** ± 0.19 *[71 %]*	**2.79** ± 0.61 *[80 %]*	n.d	n.d	n.d	n.d	n.d	n.d

ARCH PHARM
Archiv der Pharmazie

	20(29)13-22(24)26/h1-15,27,30-31H								
130	InChI=1S/C22H15F2N3/c23-16-3-1-5-18-21(16)14(11-26-18)20(13-7-9-25-10-8-13)15-12-27-19-6-2-4-17(24)22(15)19/h1-12,20,26-27H	**5.42** ± 0.22 *[92 %]*	**4.96** ± 0.17 *[82 %]*	n.d	n.d	n.d	n.d	n.d	n.d
131	InChI=1S/C22H15F2N3/c23-14-1-3-20-16(9-14)18(11-26-20)22(13-5-7-25-8-6-13)19-12-27-21-4-2-15(24)10-17(19)21/h1-12,22,26-27H	**>5** (28 %)	**>5** (47 %)	n.d	n.d	n.d	n.d	n.d	n.d
132	InChI=1S/C22H15F2N3/c23-14-1-3-16-18(11-26-20(16)9-14)22(13-5-7-25-8-6-13)19-12-27-21-10-15(24)2-4-17(19)21/h1-12,22,26-27H	**>5** (29 %)	**5.03** ± 1.40 *[79 %]*	n.d	n.d	n.d	n.d	n.d	n.d
133	InChI=1S/C22H15F2N3/c23-18-5-1-3-14-16(11-26-21(14)18)20(13-7-9-25-10-8-13)17-12-27-22-15(17)4-2-6-19(22)24/h1-12,20,26-27H	**>5** (14 %)	**>5** (23 %)	n.d	n.d	n.d	n.d	n.d	n.d
134	InChI=1S/C22H15Cl2N3/c23-14-1-3-20-16(9-14)18(11-26-20)22(13-5-7-25-8-6-13)19-12-27-21-4-2-15(24)10-17(19)21/h1-12,22,26-27H	**>5** (9 %)	**>5** (9 %)	n.d	n.d	n.d	n.d	n.d	n.d
135	InChI=1S/C25H22N2/c1-17-11-13-18(14-12-17)25(2,21-15-26-23-9-5-3-7-19(21)23)22-16-27-24-10-6-4-8-20(22)24/h3-16,26-27H,1-2H3	**0.674** ± 0.529 *[53 %]*	≥5 (44 %)	n.d	n.d	n.d	n.d	n.d	n.d
136	InChI=1S/C25H22N2O/c1-25(17-11-13-18(28-2)14-12-17,21-15-26-23-9-5-3-7-19(21)23)22-16-27-24-10-6-4-8-20(22)24/h3-16,26-27H,1-2H3	**>5** (35%)	**2.84** ± 0.171 *[73%]*	n.d	n.d	n.d	n.d	n.d	n.d
149	InChI=1S/C18H16N2/c1-12-5-4-8-17-18(12)14(11-20-17)9-13-	**0.498** ± 0.176	**>10** (35 %)	**0.0652** ± 0.0112	n.d	n.d	**1.08** ± 0.37	n.d	n.d

ARCH PHARM
Archiv der Pharmazie

(PSB-18691)	10-19-16-7-3-2-6-15(13)16/h2-8,10-11,19-20H,9H2,1H3	*[98 %]*		*[89 %]*			*[93 %]*		
150	InChI=1S/C17H13FN2/c18-14-5-3-7-16-17(14)12(10-20-16)8-11-9-19-15-6-2-1-4-13(11)15/h1-7,9-10,19-20H,8H2	**0.758** ± 0.178 *[98 %]*	**6.09** ± 1.78 *[100 %]*	n.d	n.d	n.d	n.d	n.d	n.d
151	InChI=1S/C17H13BrN2/c18-14-5-3-7-16-17(14)12(10-20-16)8-11-9-19-15-6-2-1-4-13(11)15/h1-7,9-10,19-20H,8H2	**0.944** ± 0.106 *[99 %]*	**31.1** ± 7.4 *[97 %]*	n.d	n.d	n.d	n.d	n.d	n.d
152	InChI=1S/C18H16N2O/c1-21-14-6-7-18-16(9-14)13(11-20-18)8-12-10-19-17-5-3-2-4-15(12)17/h2-7,9-11,19-20H,8H2,1H3	**2.32** ± 0.71 *[87 %]*	**>5** (33 %)	n.d	n.d	n.d	n.d	n.d	n.d
153	InChI=1S/C17H13FN2/c18-13-5-6-17-15(8-13)12(10-20-17)7-11-9-19-16-4-2-1-3-14(11)16/h1-6,8-10,19-20H,7H2	**3.78** ± 0.30 *[85 %]*	**>5** (20 %)	n.d	n.d	n.d	n.d	n.d	n.d
154	InChI=1S/C17H13ClN2/c18-13-5-6-17-15(8-13)12(10-20-17)7-11-9-19-16-4-2-1-3-14(11)16/h1-6,8-10,19-20H,7H2	**1.21** ± 0.05 *[93 %]*	**4.40** ± 0.40 *[91 %]*	n.d	n.d	n.d	n.d	n.d	n.d
155	InChI=1S/C19H16N2O2/c1-23-19(22)12-6-7-18-16(9-12)14(11-21-18)8-13-10-20-17-5-3-2-4-15(13)17/h2-7,9-11,20-21H,8H2,1H3	n.d [a]	**>5** (41 %)	n.d	n.d	n.d	n.d	n.d	n.d
156	InChI=1S/C18H14N2O3/c21-18(23-22)11-5-6-17-15(8-11)13(10-20-17)7-12-9-19-16-4-2-1-3-14(12)16/h1-6,8-10,19-20,22H,7H2	**>5** (20 %)	**>5** (-7 %)	n.d	n.d	n.d	n.d	n.d	n.d
157	InChI=1S/C17H12BrClN2/c18-12-3-1-5-14-16(12)10(8-20-14)7-11-9-21-15-6-2-4-13(19)17(11)15/h1-6,8-9,20-21H,7H2	**0.237** ± 0.006 *[98 %]*	**4.07** ± 1.36 *[92 %]*	**0.237** ± 0.081 *[87 %]*	n.d	n.d	**0.0385** ± 0.0125 *[69 %]*	n.d	n.d

ARCH PHARM
Archiv der Pharmazie

158	InChI=1S/C18H15ClN2/c1-11-4-2-6-15-17(11)12(9-20-15)8-13-10-21-16-7-3-5-14(19)18(13)16/h2-7,9-10,20-21H,8H2,1H3	**0.536** ± 0.058 *[96 %]*	**7.13** ± 1.68 *[89 %]*	**0.281** ± 0.109 *[110 %]*	n.d	n.d	**0.120** ± 0.045 *[51 %]*	n.d	n.d
159	InChI=1S/C18H15FN2O/c1-22-13-5-6-16-14(8-13)11(9-20-16)7-12-10-21-17-4-2-3-15(19)18(12)17/h2-6,8-10,20-21H,7H2,1H3	**1.17** ± 0.136 *[97 %]*	**>5** (39 %)	n.d	n.d	n.d	n.d	n.d	n.d
160	InChI=1S/C18H15FN2O/c1-22-14-3-5-18-16(8-14)12(10-21-18)6-11-9-20-17-4-2-13(19)7-15(11)17/h2-5,7-10,20-21H,6H2,1H3	**2.44** ± 0.267 *[88 %]*	**>5** (49 %)	n.d	n.d	n.d	n.d	n.d	n.d
161	InChI=1S/C18H15FN2O/c1-22-13-5-6-17-15(8-13)12(9-20-17)7-11-10-21-18-14(11)3-2-4-16(18)19/h2-6,8-10,20-21H,7H2,1H3	**2.82** ± 0.09 *[91 %]*	**>5** (31 %)	n.d	n.d	n.d	n.d	n.d	n.d
162	InChI=1S/C18H14F2N2O/c1-23-12-2-4-15-13(7-12)10(8-21-15)6-11-9-22-16-5-3-14(19)18(20)17(11)16/h2-5,7-9,21-22H,6H2,1H3	**3.74** ± 0.14 *[98 %]*	**>5** (36 %)	n.d	n.d	n.d	n.d	n.d	n.d
163	InChI=1S/C18H14F2N2O/c1-23-13-2-3-16-14(7-13)10(8-21-16)4-11-9-22-17-6-12(19)5-15(20)18(11)17/h2-3,5-9,21-22H,4H2,1H3	**1.64** ± 0.15 *[98 %]*	**>5 (**44 %)	n.d	n.d	n.d	n.d	n.d	n.d
164	InChI=1S/C19H18N2O/c1-12-3-5-18-16(7-12)13(10-20-18)8-14-11-21-19-6-4-15(22-2)9-17(14)19/h3-7,9-11,20-21H,8H2,1-2H3	**1.20** ± 0.28 *[95 %]*	**>5** (48 %)	n.d	n.d	n.d	n.d	n.d	n.d
165	InChI=1S/C17H13FN2O/c18-12-1-3-14-10(8-20-17(14)6-12)5-11-9-19-16-4-2-13(21)7-15(11)16/h1-4,6-9,19-21H,5H2	**12.0** ± 3.2 *[80 %]*	**26.5** ± 12.4 *[82 %]*	n.d	n.d	n.d	n.d	n.d	n.d

ARCH PHARM
Archiv der Pharmazie

166	InChI=1S/C19H15F3N2O/c1-25-14-3-5-17-16(8-14)12(10-23-17)6-11-9-24-18-7-13(19(20,21)22)2-4-15(11)18/h2-5,7-10,23-24H,6H2,1H3	**8.93** ± 1.10 *[82 %]*	**>5** (44 %)	n.d	n.d	n.d	n.d	n.d	n.d
167	InChI=1S/C23H17FN2O/c24-17-6-8-20-15(13-26-23(20)11-17)10-16-14-25-22-9-7-19(12-21(16)22)27-18-4-2-1-3-5-18/h1-9,11-14,25-26H,10H2	**1.99** ± 0.39 *[96 %]*	**1.40** ± 0.07 *[100 %]*	n.d	n.d	n.d	n.d	n.d	n.d
168	InChI=1S/C24H17F3N2O/c25-24(26,27)17-6-8-20-15(13-29-23(20)11-17)10-16-14-28-22-9-7-19(12-21(16)22)30-18-4-2-1-3-5-18/h1-9,11-14,28-29H,10H2	**4.12** ± 0.49 *[94 %]*	**2.87** ± 0.93 *[100 %]*	n.d	n.d	n.d	n.d	n.d	n.d
169	InChI=1S/C18H16N2/c1-20-12-14(16-7-3-5-9-18(16)20)10-13-11-19-17-8-4-2-6-15(13)17/h2-9,11-12,19H,10H2,1H3	**>5** (30 %)	**>5** (16 %)	n.d	n.d	n.d	n.d	n.d	n.d
170	InChI=1S/C19H18N2/c1-13-6-5-8-17-19(13)14(11-20-17)10-15-12-21(2)18-9-4-3-7-16(15)18/h3-9,11-12,20H,10H2,1-2H3	**0.716** ± 0.001 [99 %]	**≈ 10** (53 %)	**0.228** ± 0.030 *[89 %]*	n.d	n.d	**0.0803** ± 0.0340 *[70 %]*	n.d	n.d
175	InChI=1S/C18H14N2O2/c1-22-12-6-7-16-14(9-12)11(10-19-16)8-15-13-4-2-3-5-17(13)20-18(15)21/h2-10,19H,1H3,(H,20,21)/b15-8-	**>5** (28 %)	**>5** (38 %)	n.d	n.d	n.d	n.d	n.d	n.d
176	InChI=1S/C17H10F2N2O/c18-10-1-3-15-12(6-10)9(8-20-15)5-14-13-7-11(19)2-4-16(13)21-17(14)22/h1-8,20H,(H,21,22)/b14-5-	**3.42** ± 0.22 *[100 %]*	**4.72** ± 0.143 *[100 %]*	n.d	n.d	n.d	n.d	n.d	n.d
177	InChI=1S/C18H13FN2O2/c1-23-12-3-5-16-13(8-12)10(9-20-16)6-15-14-7-11(19)2-4-	**>5** (39 %)	**9.14** ± 0.87 *[100 %]*	n.d	n.d	n.d	n.d	n.d	n.d

ARCH PHARM
Archiv der Pharmazie

	17(14)21-18(15)22/h2-9,20H,1H3,(H,21,22)/b15-6-								
178	InChI=1S/C18H16N2O2/c1-22-12-6-7-16-14(9-12)11(10-19-16)8-15-13-4-2-3-5-17(13)20-18(15)21/h2-7,9-10,15,19H,8H2,1H3,(H,20,21)	**>5** (33 %)	**>5** (33 %)	n.d	n.d	n.d	n.d	n.d	n.d
179	InChI=1S/C17H12F2N2O/c18-10-1-3-15-12(6-10)9(8-20-15)5-14-13-7-11(19)2-4-16(13)21-17(14)22/h1-4,6-8,14,20H,5H2,(H,21,22)	**>5** (20 %)	**>5** (33 %)	n.d	n.d	n.d	n.d	n.d	n.d
180	InChI=1S/C18H15FN2O2/c1-23-12-3-5-16-13(8-12)10(9-20-16)6-15-14-7-11(19)2-4-17(14)21-18(15)22/h2-5,7-9,15,20H,6H2,1H3,(H,21,22)	**>5** (41 %)	**>5** (16 %)	n.d	n.d	n.d	n.d	n.d	n.d

[a] Efficacy relative to the maximal effect of the standard agonist CP55,940 at 1 μM set at 100 %. [b] Efficacy relative to the maximal effect of the standard agonist CP55,940 at 0.1 μM set at 100 %. [c] Compounds were tested at a concentration of 10 μM. Effects were normalized to the signal induced by 0.003 μM CP55,940. [d] Efficacy relative to the maximal effect of the standard agonist CP55,940 (0.1 μM) set at 100 %
[e] Compounds were tested at a concentration of 10 μM. Effects were normalized to the signal induced by 0.001 μM CP55,940. [f] not determined

ARCH PHARM
Archiv der Pharmazie

Supplemental Material

Table S2. Comparison of activities of selected DIM derivatives at human cannabinoid receptors

Compd.		Human CB_2 receptor			Human CB_1 receptor
		Radioligand binding assay	**cAMP assay**	**β-Arrestin recruitment assay**	**Radioligand binding assay**
		K_i ± SEM (μM) (or percent inhibition [^{3}H]CP55,940 at 5 μM) *[maximal inhibition (%)]*	**EC_{50} ± SEM** (μM) (or percent receptor activation at 10 μM) **[*efficacy*] [a]**	**EC_{50} ± SEM** (μM) (or percent receptor activation at 10 μM) **[*efficacy*] [b]**	**K_i ± SEM** (μM) (or percent inhibition [^{3}H]CP55,940 at 5 μM) *[maximal inhibition (%)]*
1	THC	**0.00595** ± 0.0027 *[100 %]*	**0.00527** ± 0.0019 *[59 %]*	**0.0142** ± 0.0003 *[32 %]*	**0.00387 ±** 0.0091 [c]
2	CP55,940	**0.000293** ± 0.0008 *[100 %]*	**0.000320** ± 0.00068 *[100 %]*	**0.000262** ± 0.00003 *[100 %]*	**0.001916** ± 0.0014 *[100 %]*
4 DIM	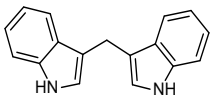 DIM	**0.690** ± 0.159 *[98 %]*	**0.334** ± 0.174 *[65 %]*	**0.562** ± 0.195 *[63 %]*	**5.42** ± 1.00 *[86 %]*
42	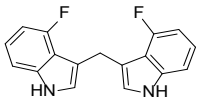	**0.279** ± 0.056 *[99 %]*	**0.0551** ± 0.0189 *[80 %]*	**0.290** ± 0.148 *[70 %]*	**>5** (28 %)
44	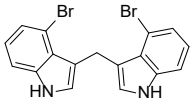	**0.374** ± 0.074 *[100 %]*	**0.509** ± 0.100 *[85 %]*	**0.0450** ± 0.0189 *[61 %]*	**7.27** ± 0.45 *[99 %]*
46	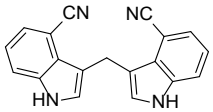	**0.339** ± 0.061 *[99 %]*	**0.0144** ± 0.0023 *[95 %]*	**0.0149** ± 0.0021 *[67 %]*	**≥10** (47 %)
149	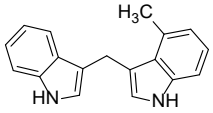	**0.498** ± 0.176 *[98 %]*	**0.0652** ± 0.0112 *[89 %]*	**1.08** ± 0.37 *[93 %]*	**>10** (35 %)

ARCH PHARM
Archiv der Pharmazie

157	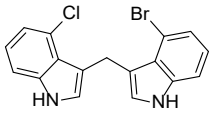	**0.237** ± 0.006 *[98 %]*	**0.237** ± 0.081 *[87 %]*	**0.0385** ± 0.0125 *[69 %]*	**4.07** ± 1.36 *[92 %]*
158	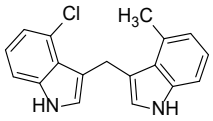	**0.536** ± 0.058 *[96 %]*	**0.281** ± 0.109 *[110 %]*	**0.120** ± 0.045 *[51 %]*	**7.13** ± 1.68 *[89 %]*
170	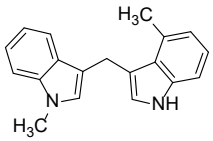	**0.716** ± 0.001 *[99 %]*	**0.228** ± 0.030 *[89 %]*	**0.0803** ± 0.0340 *[70 %]*	≈ **10** (53 %)

[a] Efficacy relative to the maximal effect of the standard agonist CP55,940 (1 μM) set at 100 %. [b] Efficacy relative to the maximal effect of the standard agonist CP55,940 (0.1 μM) set at 100 %. [c] Data from Schoeder, et al., 2018

ARCH PHARM
Archiv der Pharmazie

Table S3. Potency of diindolylmethane derivatives as agonists and antagonist at the human CB_1 receptor

Compd.	Human CB_1 receptor				
	Radioligand binding assay	**cAMP assay (agonistic assay)**	**cAMP assay (antagonistic assay)**	**β-Arrestin recruitment assay (agonistic assay)**	**β-Arrestin recruitment assay (antagonistic assay)**
	K_i ± SEM (μM) (or percent inhibition [^{3}H]CP55,940 at 5 μM) *[maximal inhibition (%)]*	**EC_{50} ± SEM** (μM) (or percent receptor activation at 10 μM) **[*efficacy*]** [a]	**IC_{50} ± SEM** (μM) (or percent receptor inhibition at 10 μM) [b]	**EC_{50} ± SEM** (μM) (or percent receptor activation at 10 μM) **[*efficacy*]** [c]	**IC_{50} ± SEM** (μM) (or percent receptor activation at 10 μM) [d]
43	**0.753** ± 0.048 *[61 %]*	**>10** (2 %)	**>10** (-22 %)	**>10** (5 %)	**>10** (43 %)
62	**0.820** ± 0.385 *[59 %]*	**>10** (11 %)	**>10** (13 %)	**>10** (2 %)	**>10** (35 %)
109	**0.774** ± 0.169 *[71 %]*	**>10** (1 %)	**>10** (10 %)	**>10** (1 %)	**6.09** ± 0.50
113	**0.402** ± 0.306 *[8 0%]*	**>10** (0 %)	**>10** (-3 %)	**>10** (1 %)	**4.43** ± 0.61
122	**0.541** ± 0.173 *[88 %]*	**>10** (0 %)	**>10** (31 %)	**>10** (1 %)	**3.06** ± 0.29
123	**0.414** ± 0.26 *[68 %]*	**>10** (-10 %)	**>10** (32 %)	**>10** (0 %)	**6.43** ± 0.45

[a] Efficacy relative to the maximal effect of the standard agonist CP55,940 (1 μM) set at 100 %. [b] Compounds were tested at a concentration of 10 μM. Effects were normalized to the signal induced by 0.003 μM CP55,940. [c] Efficacy relative to the maximal effect of the standard agonist CP55,940 (0.1 μM) set at 100 %. [d] Compounds were tested at a concentration of 10 μM. Effects were normalized to the signal induced by 0.001 μM CP55,940.

ARCH PHARM
Archiv der Pharmazie

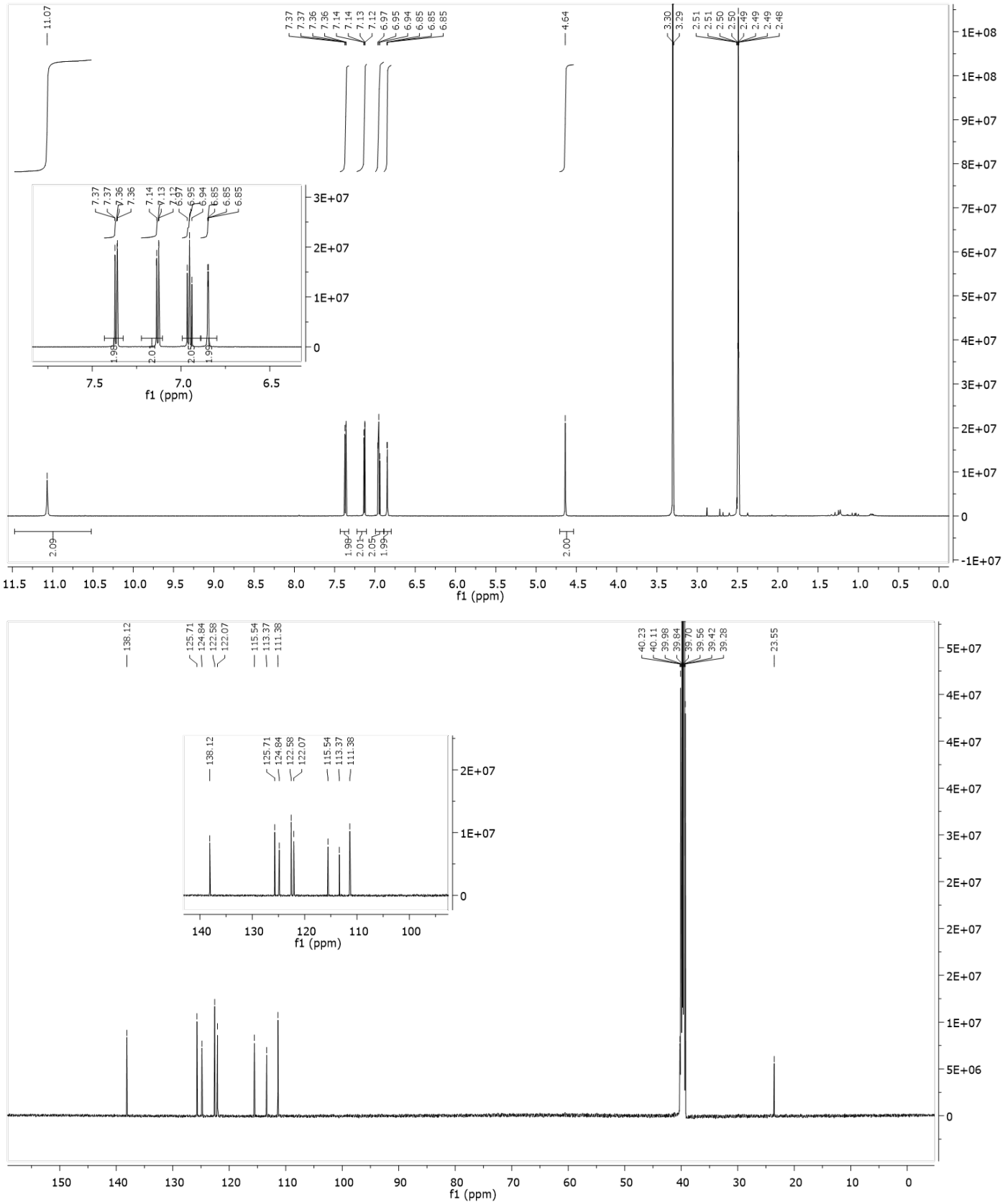

Figure S1. ^{1}H (500 MHz) & ^{13}C (126 MHz) NMR (DMSO-d_6) spectra of di(4-bromo-1*H*-indole-3-yl)methane (**44**)

ARCH PHARM
Archiv der Pharmazie

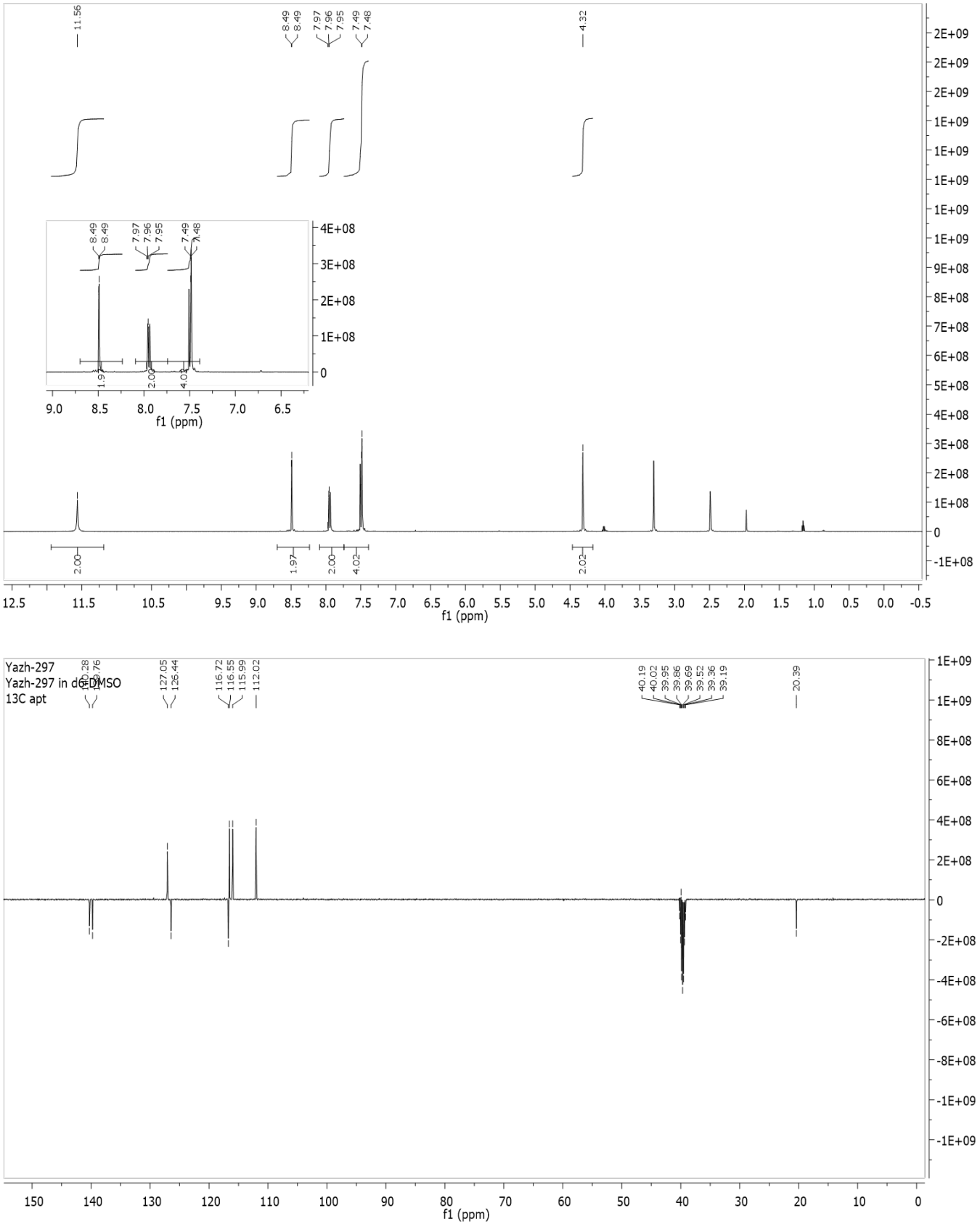

Figure S2. ^{1}H (500 MHz) & ^{13}Capt (126 MHz) NMR (DMSO-d_6) spectra of di(4-nitro-1*H*-indole-3-yl)methane (**45**)

ARCH PHARM
Archiv der Pharmazie

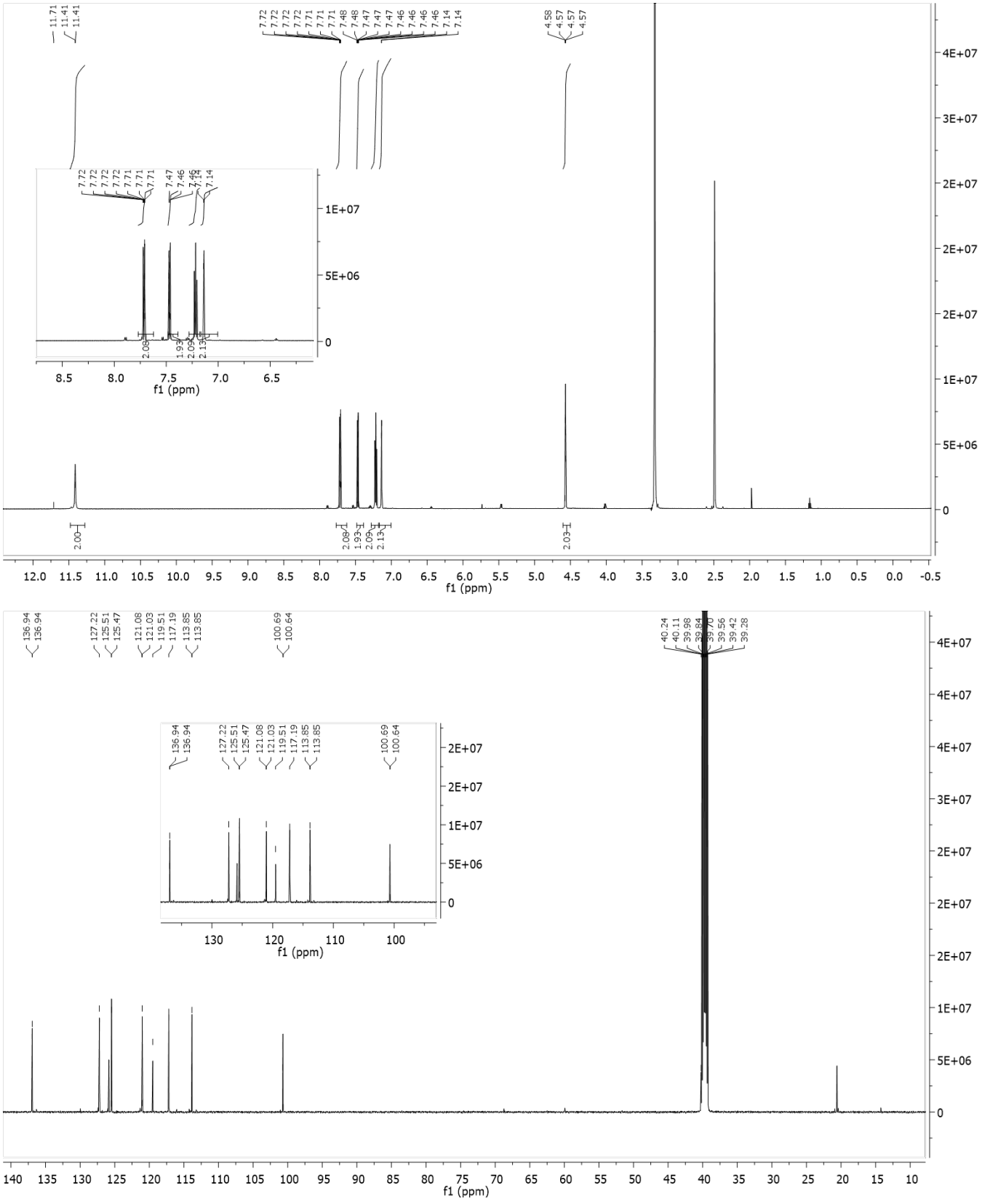

Figure S3. ^{1}H (500 MHz) & ^{13}C (126 MHz) NMR (DMSO-d_6) spectra of di(4-cyano-1*H*-indole-3-yl)methane (**46**)

ARCH PHARM
Archiv der Pharmazie

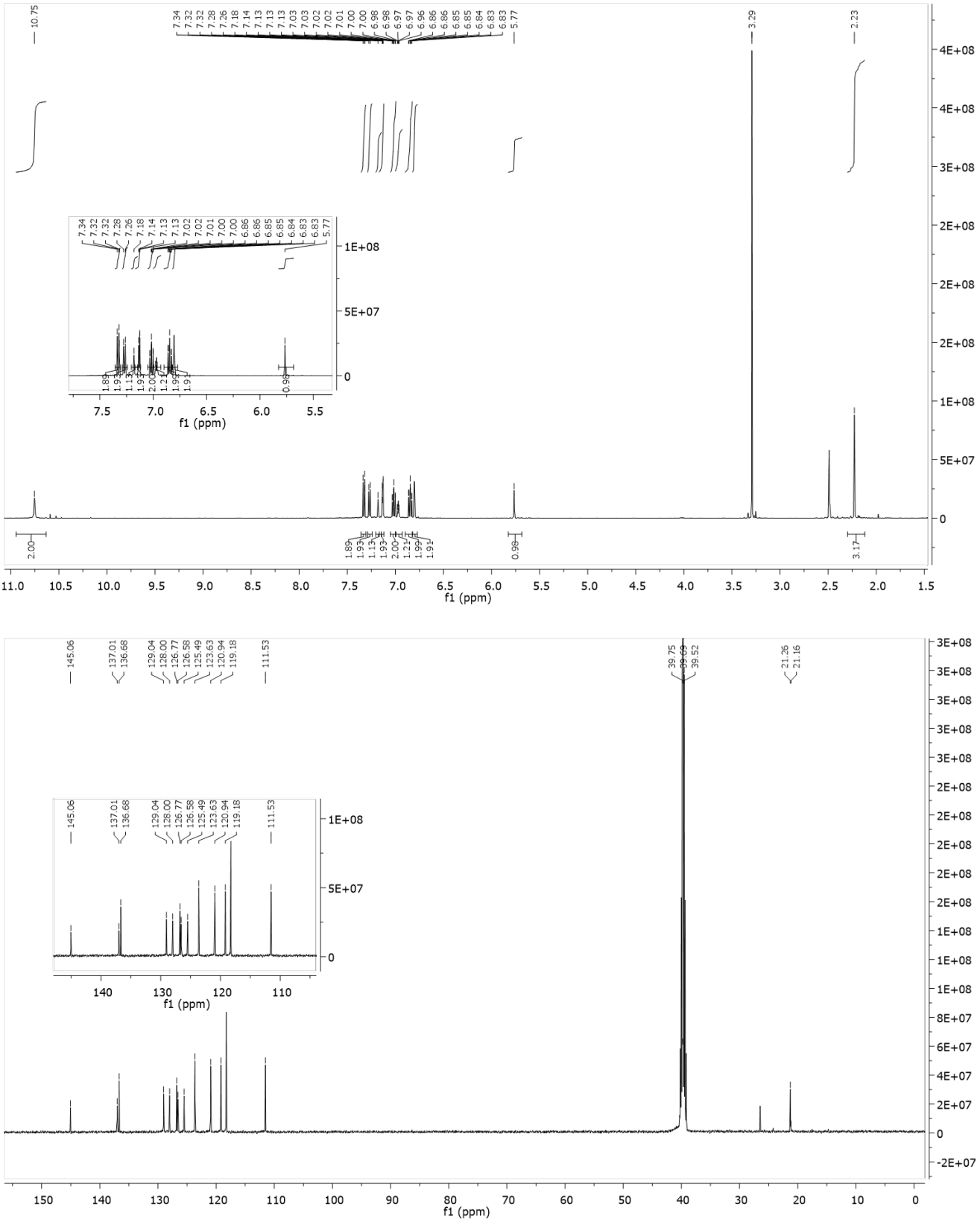

Figure S4. ^{1}H (500 MHz) & ^{13}C (126 MHz) NMR (DMSO-d_6) spectra of 3,3'-(*m*-tolylmethylene)di(1*H*-indole) (**105**)

ARCH PHARM
Archiv der Pharmazie

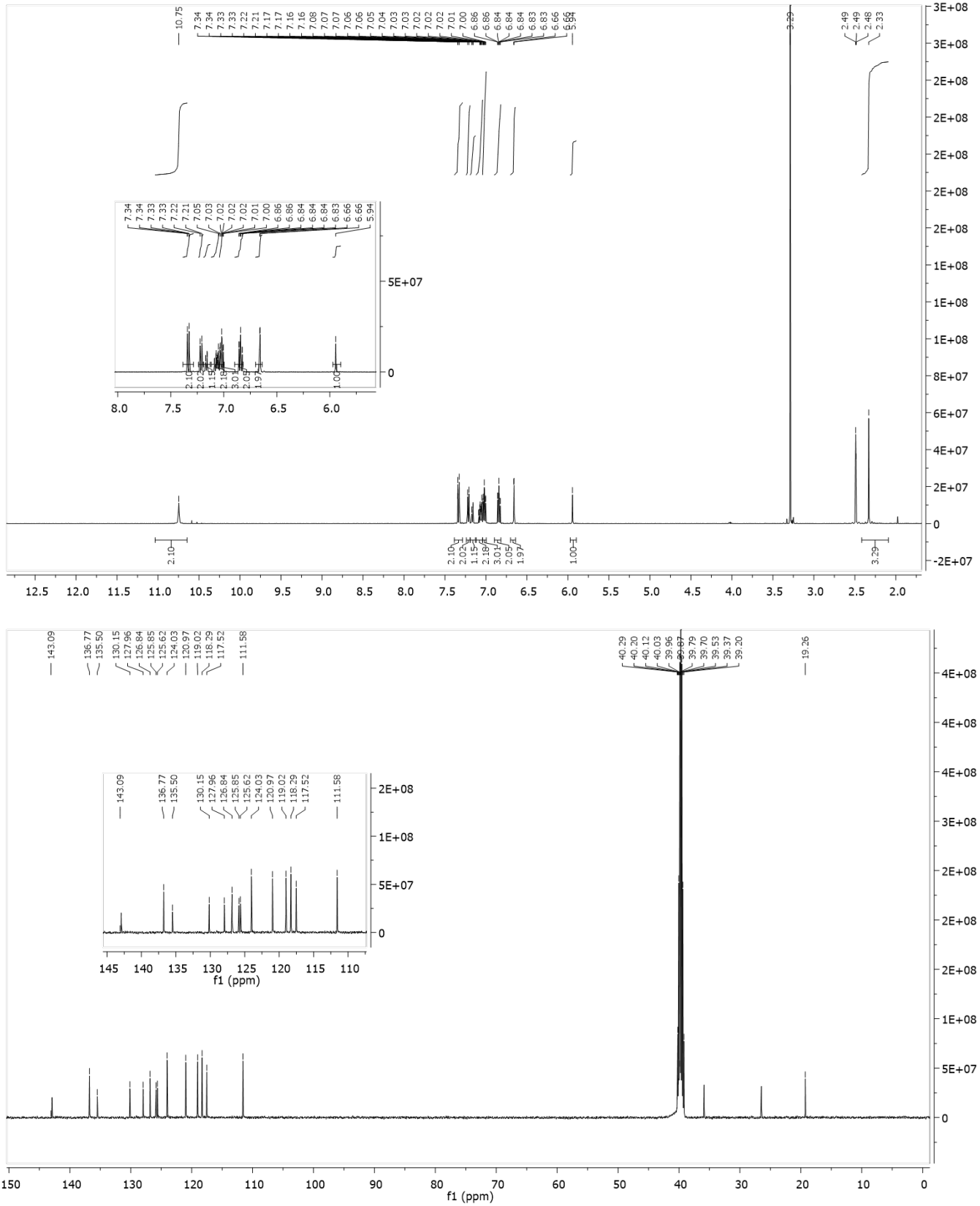

Figure S5. ^{1}H (500 MHz) & ^{13}C (126 MHz) NMR (DMSO-d_6) spectra of 3,3'-(*o*-tolylmethylene)di(1*H*-indole) (**106**)

ARCH PHARM
Archiv der Pharmazie

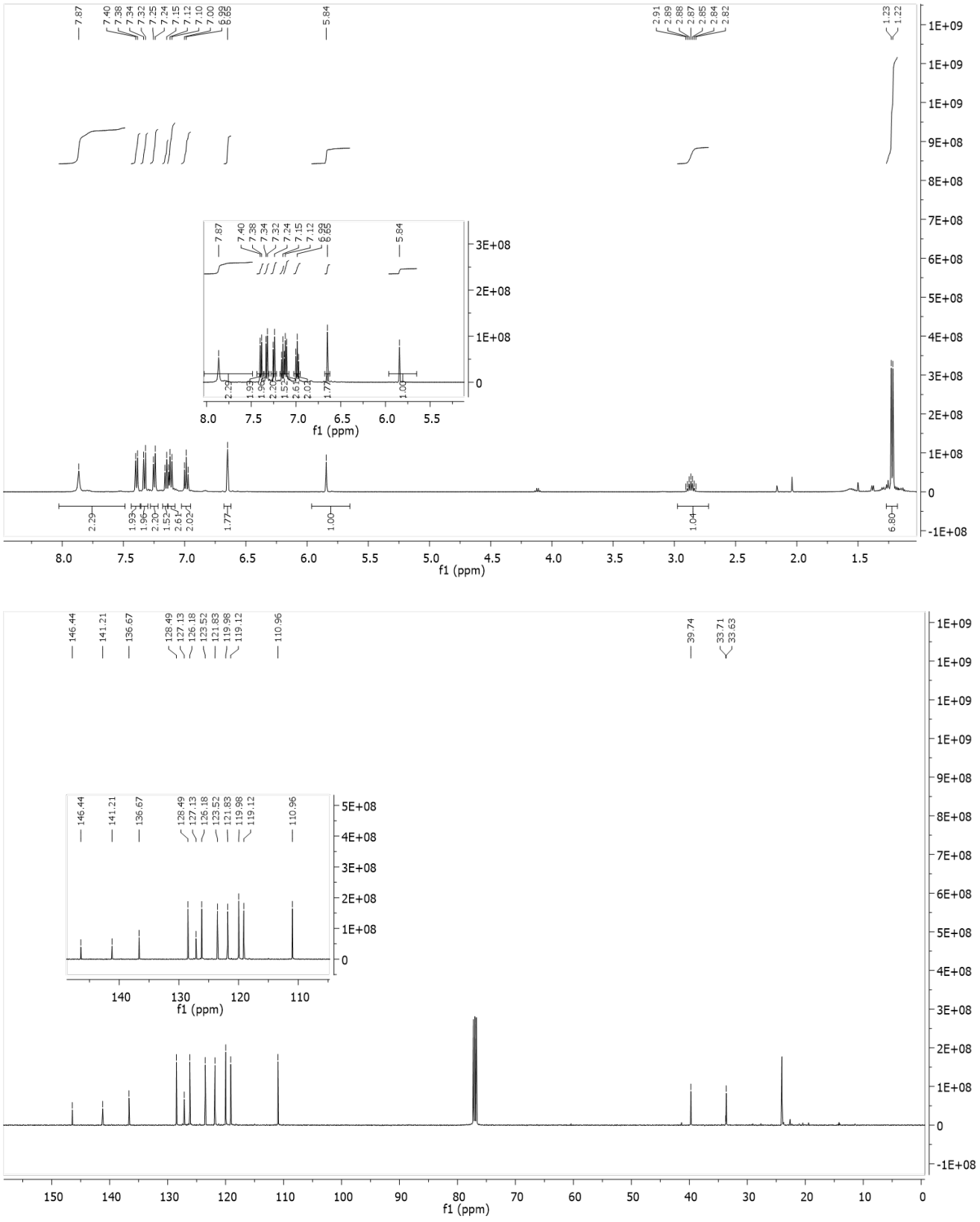

Figure S6. ^{1}H (500 MHz) & ^{13}C (126 MHz) NMR ($CDCl_3$) spectra of 3,3'-((4-iso-propylphenyl)methylene)di(*1H*-indole) (**108**)

ARCH PHARM
Archiv der Pharmazie

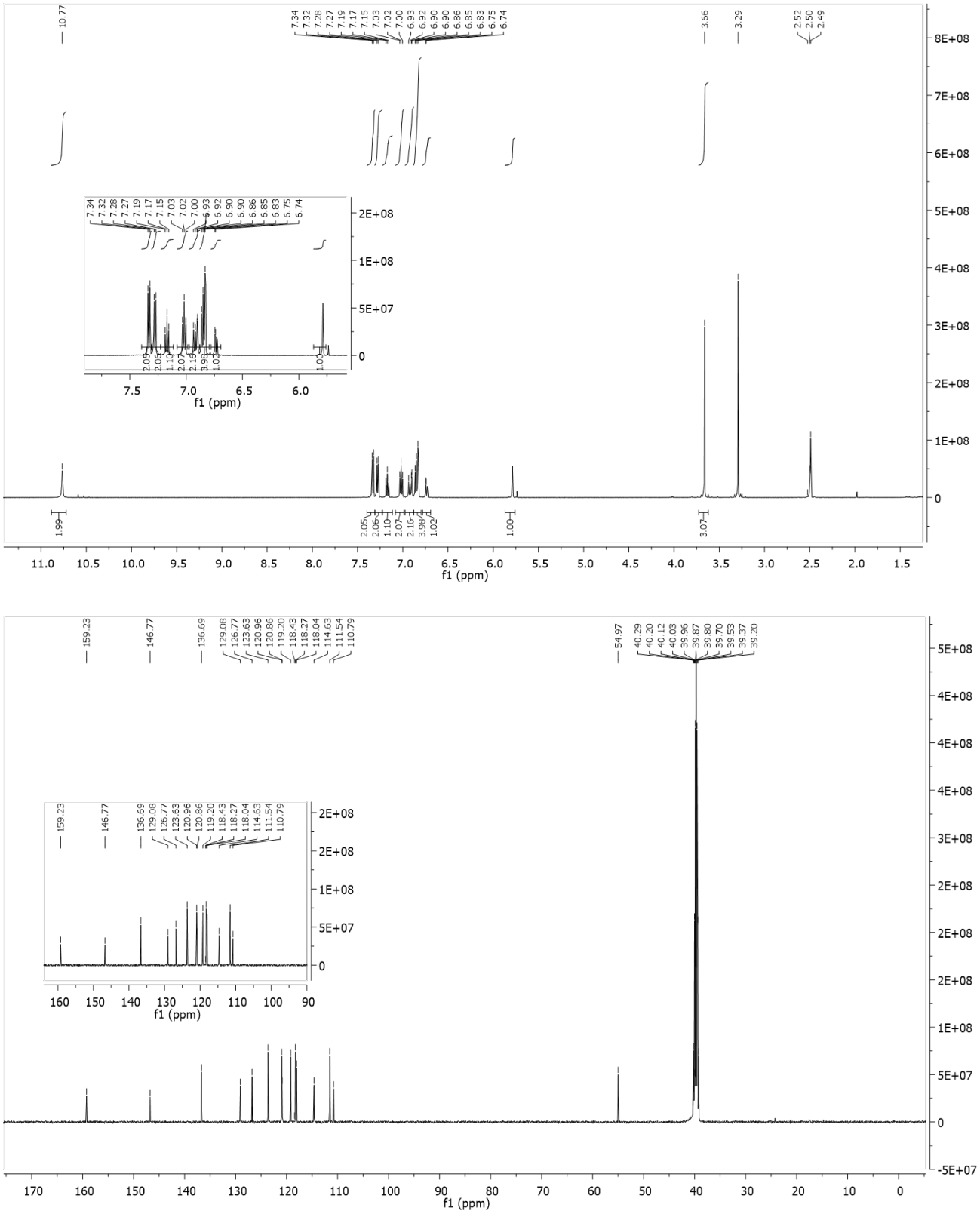

Figure S7. ^{1}H (500 MHz) & ^{13}C (126 MHz) NMR (DMSO-d_6) spectra of 3,3'-((3-methoxyphenyl)methylene)di(1*H*-indole)(**110**)

ARCH PHARM
Archiv der Pharmazie

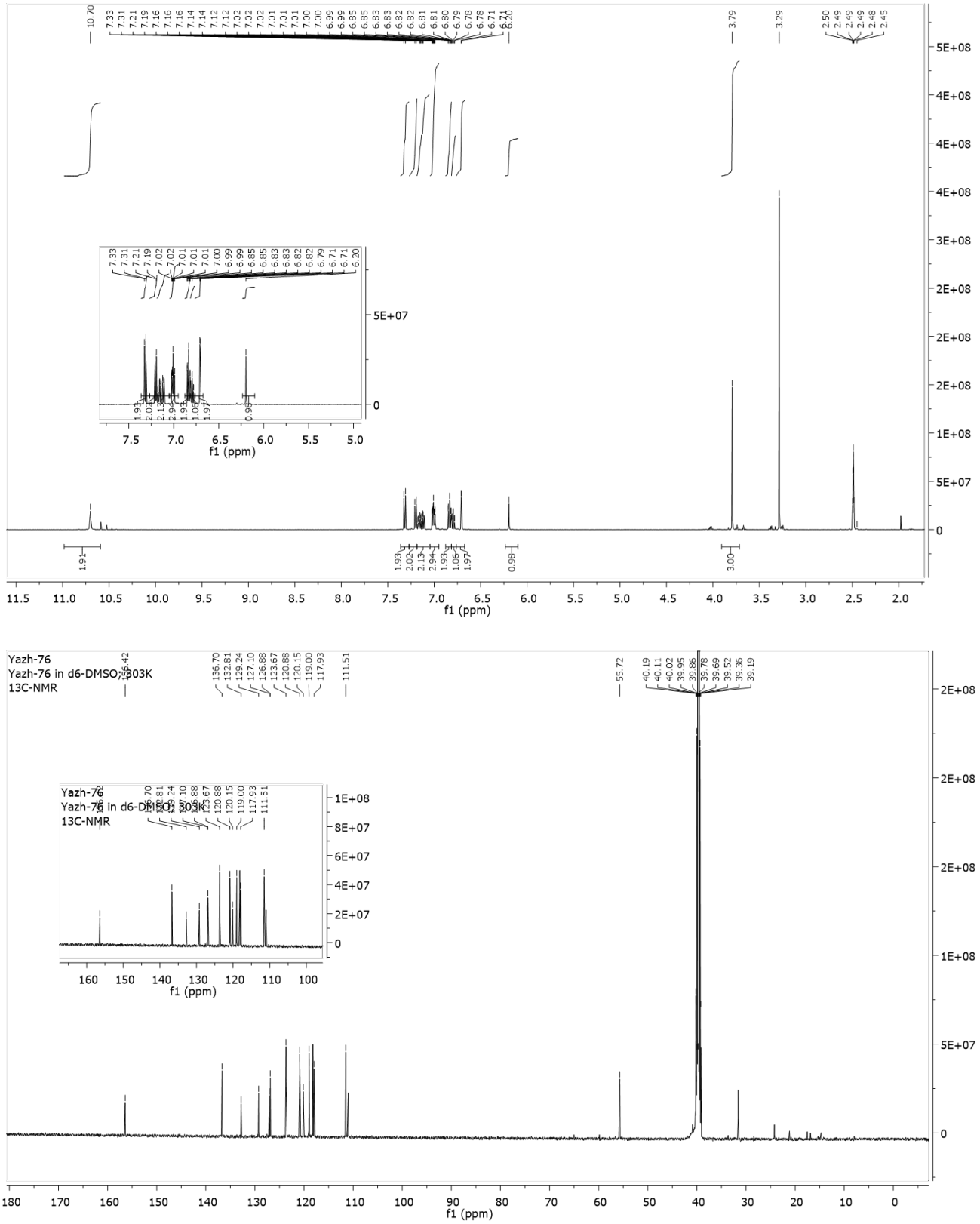

Figure S8. ^{1}H (500 MHz) & ^{13}C (126 MHz) NMR (DMSO-d_6) spectra of 3,3'-((2-methoxyphenyl)methylene)di(1*H*-indole) (**111**)

8. ACKNOWLEDGMENTS

Words cannot fully express how grateful I am to be a part of the AK Müller group.

First and foremost, I would like to express my deepest gratitude to Prof. Christa E. Müller, my mentor and also my supervisor. Thank you for accepting me into your wonderful group, for your patience with my occasional carelessness, and for supporting me in every possible way to become a better scientist. Your tireless guidance, encouragement, and generosity in sharing your knowledge have shaped my journey. Thank you for giving me the opportunity to learn and explore various techniques in your laboratory.

I am also deeply grateful to my thesis committee, PD Dr. Anke C. Schiedel, Prof. Dr. Finn Hansen, and Prof. Dr. Ivar von Kügelgen, for their time and willingness to serve on my PhD examination committee.

Special thanks to Lembaga Pengelola Dana Pendidikan (LPDP – Indonesia) for funding my PhD and to RTG 1873 and RTG 2783 for their invaluable support throughout my research.

My sincere appreciation goes to Beate Ponatowski and Dr. Amelie Fiene for their tremendous help with paperwork and administrative processes—especially the seemingly never-ending immigration office matters.

I am also grateful to Dr. Clara Schoeder for introducing me to the fascinating and challenging world of GPR18 research. It has been an exciting journey, and I have enjoyed every step along the way.

To my fellow researchers and collaborators in GPR18: Dr. Nader Bostha, Filomena Perri, Dr. Alexander Neumann, Dr. Robin Geschold, Dr. Thanigaimalai Pillaiyar, and Dr. Vignesh Namasivayam - thank you for the time and effort we shared working on this project. A special thanks to Nader, Filo, and Malai for not only synthesizing compounds for my receptors but also patiently answering my endless chemistry-related questions. Thank you for the "Synthetic Chemistry for Dummies" crash course—even though I still don't fully understand it, I truly enjoyed every discussion over coffee and sweets in your offices.

Thank you, Dr. Dominik Thimm, for the time we spent together on practical courses. While we were supposed to teach students, I often found myself learning great things from you!

To my former office mates (Dr. Sonja Hinz, Dr. Isaac Attah, Dr. Jonathan Schlegel, Dr. Yvonne Riedel) and my current office mates (Dr. Victoria Vaaßen, Haneen Al-Hroub, Sana Mulani)—thank you for always listening to my complaints, for your support during my most fragile moments, and for reminding me that everything will eventually be "fineeee". Thank you, Vicky, for your cooking and cleaning tips and for always being so helpful in the lab and beyond. And thank you, Sana, for helping me achieve 10,000 steps per day!

A big thanks to Jessica Nagel, my next-door office buddy, for all the laughter and tears, the countless cups of coffee, the everyday memes, the shared struggles with molecular biology, and even the little things like filling pipette tip boxes together. Thank you Jessi, Vicky, and Sana, for always checking up on me.

I am also grateful to our amazing technical assistants: Katharina Silvester, Christiane Bous, Christin Vielmuth, Marion Schneider, and Nicole Florin for teaching me various laboratory assays and techniques (and of course the tricks in the lab).

ACKNOWLEDGMENTS

To all the members of AK Müller—thank you for creating such a warm and supportive environment.

Angelo Oneto and Luca Svolacchia, for every phone call and the support along the way; Dr. Ahmed Elgokha and Dr. Ahmed Temirak, for your invaluable help with all things chemistry-related; Franka Westermann, for introducing me to the wonderfully diverse world of German cakes; Ghazl Al-Hamwi, for always cheering me up and giving me a positive perspective; Hashem Al-Musawi, for our parent-to-parent talks; Helay Baburi, for your cheerful greetings and for always bringing joy to the lab; Dr. Jan Voß, for providing various protocols, and also for the new plasmids; Dr. Jonathan Schlegel (and Paulina), for always helping me with complex regulations in Germany and for consistently correcting my German writing. Laila Akdidach, for your inspiring work in creating new molecules and helping me gain new insights into GPR18; Michel Lewash, my buddy for the CO_2 bottle duty.

Dr. Tobias Claff, for the time we shared in the lab (and coffee, and lunch, and sweets!), for teaching me new molecular biology techniques, and for all the new ideas and assistance with the projects, both in the lab and outside the lab, and thank you for always checking up on me.

And of course, to all the other wonderful members of AK Müller—Albert, Ali, Ahmed Ismail, Bea, Carolin, Constantin, Eugen, Fabian, Florian, Jianyu, Julia, Leon, Riham, Salahuddin, Patrick, Sophie, Sarah, and Marianna—thank you for being part of this journey!

Each and every one of you has contributed in some way to making my PhD journey possible. The challenges were many, but the environment you created gave me the strength to keep moving forward.

To the little princess, Cahaya, and the little dragon (and sometimes Paw Patrol), Rafael - your presence is my greatest gift. You keep me grounded and give me the strength to keep moving forward, no matter the challenges.

Terima kasih untuk Bapak, Ibu, Aki, Enin, Mbak Wulan, Mas Toni, Chandra, Ivani, Neira, dan seluruh keluarga di Indonesia atas setiap doa dan dukungan yang tak henti-hentinya.

Terima kasih juga untuk Jeffry dan Adi untuk dukungan dan hiburan di sela-sela perjalanan panjang ini.

And finally, sayangku, Nana terima kasih atas kesabaran dan keteguhanmu dalam menghadapi segala hal bersamaku. Terima kasih untuk setiap senyuman, teguran, perhatian, tawa, kepercayaan, dan pengorbananmu. Terima kasih telah selalu percaya padaku dan memberikan semangat tanpa henti. Terima kasih sudah mengasihi dan mencintaiku apa adanya.